

**INTERNATIONAL COUNCIL FOR RESEARCH AND INNOVATION  
IN BUILDING AND CONSTRUCTION**

**WORKING COMMISSION W18 - TIMBER STRUCTURES**

# **CIB - W18**

**MEETING FORTY-FIVE**

**VÄXJÖ**

**SWEDEN**

**AUGUST 2012**

Ingenieurholzbau und Baukonstruktionen  
Karlsruhe Institute of Technology  
Germany  
Compiled by Rainer Görlacher  
2012

ISSN 1864-1784

## CONTENTS

1. Chairman's Introduction
2. General Topics
3. Structural Design Code
4. Test Methods
5. Fire
6. Structural Stability
7. Trussed Rafters
8. Laminated Members
9. Environmental Conditions
10. Timber Joints and Fasteners
11. Stress Grading
12. Columns
13. Notes
14. Any Other Business
15. Venue and Program for Next Meeting
16. Close
17. Peer Review of Papers for the CIB-W18 Proceedings
18. List of CIB-W18 Papers Växjö, Sweden 2012
19. Current List of CIB-W18 Papers

CIB-W18 Papers 45-2-1 up to 45-102-1



## **0 List of Participants**



**INTERNATIONAL COUNCIL FOR RESEARCH AND INNOVATION  
IN BUILDING AND CONSTRUCTION  
WORKING COMMISSION W18 - TIMBER STRUCTURES**

**MEETING FORTY-FIVE**

**VÄXJÖ, SWEDEN**

**27 AUGUST –30 AUGUST 2012**

**LIST OF PARTICIPANTS**

**AUSTRALIA**

K Crews  
University of Technology, Sydney

**AUSTRIA**

T Bader  
Vienna University of Technology  
R Brandner  
Institute of Timber Engineering and Wood Technology, Graz  
J Denzler  
Holzforschung Austria  
G Hochreiner  
Vienna University of Technology  
G Schickhofer  
Institute of Timber Engineering and Wood Technology, Graz

**CANADA**

G Doudak  
University of Ottawa  
F Lam  
University of British Columbia, Vancouver  
M Popovski  
FPInnovations, Vancouver  
I Smith  
University of New Brunswick

**CROATIA**

V Rajcic  
University of Zagreb, Faculty of Civil Engineering

**DENMARK**

H J Larsen  
Copenhagen  
J Munch-Andersen  
Danish Timber Information, Lyngby

**FINLAND**

J Hakkarainen  
METSÄ WOOD, Building Products  
A Kevarinmäki  
VTT Expert Services Ltd  
T Poutanen  
Tampere University of Technology

**FRANCE**

C Barthram  
LERMAB Laboratory, Epinal  
J-F Bocquet  
LERMAB Laboratory, Epinal  
E Leroy  
ITECH, Montreuil  
D Quidet  
ITECH Montreuil

**GERMANY**

S Aicher  
MPA University Stuttgart  
H J Blaß  
Karlsruhe Institute of Technology (KIT)  
F Brühl  
University Stuttgart  
P Dietsch  
TU München  
M Frese  
Karlsruhe Institute of Technology (KIT)  
A Gamper  
TU München

R Görlacher	Karlsruhe Institute of Technology (KIT)
U Kuhlmann	University Stuttgart
W Seim	University Kassel
P Stapel	TU München
G Stapf	MPA University Stuttgart
S Winter	TU München

### **ITALY**

A Ceccotti	IVALSA-CNR
A Polastri	IVALSA-CNR
L Pozza	University of Padova
R Tomasi	University of Trento

### **JAPAN**

K Kobayashi	Shizuoka University
M Yasumura	Shizuoka University

### **NEW ZEALAND**

W van Beerschoten	University of Canterbury, Christchurch
P Quenneville	University of Auckland
P Zarnani	University of Auckland

### **NORWAY**

S Eide	Norwegian Institute of Wood Technology, Oslo
G Glasø	Norwegian Institute of Wood Technology, Oslo
J Köhler	NTNU, Trondheim
K A Malo	NTNU, Trondheim
K Nore	Norwegian Institute of Wood Technology, Oslo

### **SLOWENIA**

B Dujic	Contemporary building design, Celje
I Sustersic	Contemporary building design, Celje
R Zarnic	University of Ljubljana

### **SWEDEN**

C Bengtsson	SP Wood Technology
M Dorn	Linnéuniversitetet
P-E Eriksson	SP Wood Technology
E Frühwald Hansson	Lunds Universitet
U A Girhammar	Luleå tekniska universitet
M Johansson	Linnéuniversitetet
A Just	SP Wood Technology
B Källsner	Linnéuniversitetet
J König	SP Wood Technology
E Lukaszewska	SWECO AB
H Movaffaghi	Linnéuniversitetet
I Näslund	Luleå tekniska universitet
A Olsson	Linnéuniversitetet
H Pettersson	Linnéuniversitetet
A Pousette	SP Wood Technology
J Schmid	SP Wood Technology
E Serrano	Linnéuniversitetet
J Vessby	Linnéuniversitetet

**SWITZERLAND**

A Frangi	ETH Zürich
R Jockwer	EMPA Dübendorf
M Klippel	ETH Zürich
P Kobel	ETH Zürich
P Palma	ETH Zürich
C Sigrist	Berner Fachhochschule, Biel
R Steiger	EMPA Dübendorf
T Theiler	ETH Zürich
F Wanninger	ETH Zürich

**THE NETHERLANDS**

A Jorissen	TU Eindhoven
------------	--------------

**UNITED KINGDOM**

K K Ranasinghe	TRADA, High Wycombe
----------------	---------------------

**USA**

T Skaggs	American Plywood Association, Tacoma
B Yeh	American Plywood Association, Tacoma



- 1. Chairman's Introduction**
- 2. General Topics**
- 3. Structural Design Code**
- 4. Test Methods**
- 5. Fire**
- 6. Structural Stability**
- 7. Trussed Rafters**
- 8. Laminated Members**
- 9. Environmental Conditions**
- 10. Timber Joints and Fasteners**
- 11. Stress Grading**
- 12. Columns**
- 13. Notes**
- 14. Any Other Business**
- 15. Venue and Program for Next Meeting**
- 16. Close**



**INTERNATIONAL COUNCIL FOR RESEARCH AND INNOVATION  
IN BUILDING AND CONSTRUCTION**

**WORKING COMMISSION W18 - TIMBER STRUCTURES**

**MEETING FORTY-FIVE**

**VÄXJÖ, SWEDEN**

**27 AUGUST –30 AUGUST 2012**

**M I N U T E S  
(F Lam)**

**1 CHAIRMAN'S INTRODUCTION**

Prof. Hans Blass welcomed the delegates to the 45th CIB W18 Meeting in Växjö, Sweden. He thanked C Bengtsson (SP Boras) and E Serrano (Linnaeus University) for cohosting the meeting. This is the third meeting in Sweden; the first and second meetings took place in Stockholm (1977) and Åhus (1992), respectively.

Over 80 participants are attending the meeting. There are 23 papers and 8 notes accepted for this meeting. Papers brought directly to the meeting would not be accepted for presentation, discussions, or publication. The same applies to papers where none of the authors is present or papers which are not defended by one of the authors. The papers were selected based on the new review process for abstracts. The four acceptance criteria are: state of the art; originality; content; and relation to codes or standards. Each criterion was judged with a scale of 0 (bad) to 5 (very good) leading to an overall grade. In total 10 submitted abstracts were not accepted.

The presentations are limited to 20 minutes each, allowing time for meaningful discussions after each paper. The Chair asked the presenters to conclude the presentation with a general proposal or statements concerning impact of the research results on existing or future potential application and development in codes and standards. R Görlacher will deal with questions regarding the meeting proceedings.

There are 10 topics covered in this meeting: Timber Columns (1), Stress grading (2), Timber joints and fasteners (5), Environmental conditions (1), Laminated members (4), Trussed rafters (1), Structural stability (6), fire (1) Test methods (1), Structural design codes (1).

**2 GENERAL TOPICS**

The Chair discussed recent issues on the conduction of this working commission raised in complaint letters to CIB by T Van der Put. The chair asked the participants to consider the following issues during the next three days of the meeting: 1) the issue of the chairmanship on whether they wish to have a change in chairmanship and the terms of the chairmanship; and 2) should there be the possibility of publishing in the meeting proceedings a) papers not presented in the meeting or b) written comments to papers presented in the meeting. This is in reference to the desire of T Van der Put to have his contributions included in the proceedings even though his health conditions prevented him from attending the meeting.

The chairman noted that the number of pages involved in T Van der Put's contributions exceeded the maximum allowed. Furthermore the issue of appointing coauthors who could not defend the paper was discussed. The question of whether the proceedings should stay as meeting proceedings or be changed to a kind of a Journal was also raised. The issues will be discussed and voted on during the last day of this meeting.

E Serrano and C Bengtsson welcomed the participants and presented information about Linnaeus University and SP. They also discussed organizational matters for the meeting.

### 3. STRUCTURAL DESIGN CODES

*45 - 102 - 1 Assessment of Relevant Eurocode Based Design Equations in Regard to Structural Reliability - J Köhler, R Steiger, G Fink, R Jockwer*

Presented by J Köhler

T Poutanen received clarification that the Beta values calculated in the paper are based on one year maximum snow load. He commented that the Eurocode is based on snow load with a 50 year return period. He also commented that loads were combined independently. J Köhler responded that this issue was covered extensively in the past year and would further discuss with T Poutanen during break. J Munch Andersen questioned the calculations based on "optimized" beta values of finding the partial safety factors from minimization of error between calculated and target beta. One should look into cases that lied below the target beta. J Köhler agreed that it could be done and perhaps with consideration weighing different cases. J König commented that the EN1990 noted that the target beta was based on assuming normally distributed loads. External loads that are based on Gumbel distribution will give different results. J Köhler responded that different load models were also considered. S Aicher stated that target beta of 4.7 was used in the Eurocode and asked whether the results were showing that the partial safety factors in the code were too low. He also asked whether the difference was due to the use of Gumbel distribution only. J Köhler stated that the choice of Weibull distribution for the resistance might also make a difference as beta values were sensitive to the lower tail of the distribution. U Kuhlmann stated that one should consider different target beta for different failure modes, and stiffness dependence should also be considered where not only simple structures are studied. J Köhler agreed. J Munch Andersen commented that it didn't make sense to use different distributions for different strengths and compare the results. J Köhler agreed. T. Poutanen further commented that target beta values for one year and 50 year were 4.7 and 3.6, respectively. F Lam received confirmation that the resistance distributions were not based on real data. He commented that in Canada by fitting to the lower tails of the strength data more consistent results were obtained where the beta values were less sensitive to the choice of strength distribution. S Winter commented that more transparent strength data were needed; e.g. new material strength data in the code is based on test data and also may consider test data from worldwide sources. J Köhler commented different partial safety factors for different strengths might add complications to design and agreed on the need to use transparent test data. S. Aicher commented that the partial safety factors would always reflect the COV of the material; therefore, one should have groupings with COV.

#### 4. TEST METHODS

45 - 21 - 1 *Evaluation of Shear Modulus of Structural Timber Utilizing Dynamic Excitation and FE Analysis - A Olsson, B Källsner*

Presented by A Olsson

R Görlacher asked whether the data from a 1994 CIBW18 paper with more than 1000 specimens were compared. A Olsson responded that they were not compared but would look into it. R Brandner asked whether static shear modulus rather than dynamic G should be compared. A Olsson responded that there were no test results. R Brandner stated that since there was difference between E static and E dynamic, one should also expect differences between G static and G dynamics. A Olsson agreed with R Görlacher that the ratio between E and G was not constant and grade dependent. R Steiger asked whether the mass of the accelerometer was considered. A Olsson said no but thinks he should.

#### 5. FIRE

45 - 16 - 1 *The Reduced Cross Section Method for Timber Members Subjected to Compression, Tension and Bending in Fire - M Klippel, J Schmid, A Frangi*

Presented by M Klippel

S Winter asked which strength values were considered. M Klippel responded mean strength values from Eurocode were considered. S Winter asked whether solid timber or glulam. M Klippel stated it did not matter as the study considered the reduction. Also the member was considered as stub column i.e. no buckling. They will study intermediate and long columns later. S Winter commented that information on the temperature to strength relationship was weak and we had to try and make new tests and one to one scale test to establish more reliable data on temperature to strength relationship. M Klippel agreed. J Schmid clarified that on slide 20 EN1995-1-2 for small members the zero strength layer was much larger. Also as far as temperature strength curves, they were doing full scale tests. J König stated that according EC5 strength did not have to be reduced for temperature increase until after 60°C which applied to continuous heating of members e.g. in roof attic. The fire situation is transient and the EC5 provisions derived from fire tests include load duration, moisture effect etc. A Jorissen stated that EC5 had two methods i.e. also the reduced properties method. He asked if there would be agreement if the results from this study were compared to the reduced properties method. M Klippel stated that they had not yet done so. A Frangi stated that there was background information that the reduced properties method was inaccurate and should be deleted. J König stated that there would be a difference between the methods as we knew the reduced properties method was incorrect. The fire people are still working on this issue. S Winter stated that with the adoption of fire design method since the last decade there had not been reports of serious fire damage based on this method. We have to look into the design principle versus outcome. Simplicity for designer and impact to designs should be considered and one should not make the work too theoretical. The issue of the validity of the properties reduction method for small cross section versus large cross section is an issue. J Schmid responded that the likelihood of fire was not a subject of this paper. S Aicher commented that the results showed we were unsafe for stub columns. J König stated that what the safety was in case of fire was an important issue that required more studies.

## 6. STRUCTURAL STABILITY

### *45 - 15 - 1 Performance Based Design and Force Modification Factors for CLT Structures - S Pei, M Popovski, J van de Lindt*

Presented by M Popovski

M Yasumura asked about the failure criteria for hold-down. M Popovski responded that the hold-downs took vertical uplift forces while shear connectors took shear forces. In CLT hold-downs contribute to shear response. B Dujic commented about openings in the assembly and asked how the step joints affected the results. M Popovski stated that the building was designed with step joints in openings and there was no special consideration of the influence of openings. B Dujic commented that in performance based design you did not need the R or Q factor. M Popovski stated that they did performance based design to show that it worked for CLT and R factors were chosen based on drift limits. I Smith asked what was the status of discussion on performance based design in US. M Popovski stated that the performance objectives in FEMA were used and they were considered to be conservative. I Smith commented that he wondered whether steel and concrete people were in agreement with performance based design principles. T Skaggs commented that the results show CLT without hold-down had higher R factors than cases with hold-down. M Popovski responded that hold-downs were desirable but there were trade-offs. BJ Yeh received confirmations that R factors were only applicable to the connectors. R Tomasi asked about the contribution of the corners. M Popovski stated that it was not studied but would consider it in the future. W Seim stated that forced based design was used by engineers and they would stay with this approach for a long while yet. He received confirmation that the study considered symmetrical conditions only. M Yasumura received confirmation about the rocking of the shear wall where vertical loading was included in the analysis. G Schickhofer commented that CLT element concept was originally based on the use of large panels as full elements and asked why so many small elements were used. M Popovski stated that small panels were used in building and this was a trade off between resistance and ductility. F Lam asked whether acceleration in the floors were checked. M Popovski responded that ~ 1.6 g was observed in the model. P Quenneville commented about one full panel versus many smaller panels that in US 1.2 m wide panels were produced. B Dujic stated that this was a production capacity and transportation issue.

### *45 - 15 - 2 Seismic Behaviour of Wood-Concrete Frame Shear-wall System and Comparison with Code Provisions - L Pozza, R Scotta, A Polastri, A Ceccotti*

Presented by L Pozza

F Lam commented that 50% non exceedance at 4% drift corresponded to a beta of zero. In FEMA 80% non exceedance at 4% drift was recommended. B Dujic commented that the infill was connected to the timber frame and a rigid diaphragm but connected to the frame with ductile screws. He asked if there was any restriction to wood design of hybrid system as in this case there was lower q factor. He asked whether these procedures for these buildings should be used in the scope of EC5. L Pozza stated that these buildings were specific to Italy as a solution to the hot climate and the external concrete skin could also provide stiffness required to resist earthquakes. They agreed that such procedures were suitable for EC5. However the durability of the connection must be considered carefully. W Seim asked for the clarification of the definition of code related design and asked whether the same q factor could be used for taller structures such as a 4 story building. L

Pozza responded that q factor might depend on the number stories and if we considered 3 d response. More work will need to be done. Code related design was referenced to  $q=1$ . Two different masses were considered so that one building was on the plateau while the second one exceeded the plateau. S Winter asked why the ventilation area was needed and asked whether the concrete was needed for weather protection. L Pozza explained that the plastic bushing reduced the clearance between the wood and the concrete and the concrete slab was the final facade. S Winter stated that the durability performance against weather was doubtful.

45 - 15 - 3 *Determination of Failure Mechanism of CLT Shear Walls Subjected to Seismic Action* - **M Yasumura**

Presented by M Yasumura

B Dujic commented that the stiffness of connection rather than the load capacity of the connection might be important as the study dealt with connection. B Dujic also asked why determined the joint first then worked on the shear wall. M Yasumura stated that the work dealt with capacity first then would focus on other aspects. R Žarnić commented that energy dissipation devices could be used in this system. M Yasumura responded that this was an interesting topic but the energy dissipation should take place at a location away from failure. B Dujic commented that such a system must consider but energy dissipation and strength; couldn't ignore either.

45 - 15 - 4 *Seismic Response of Timber Frames with Laminated Glass Infill* - **V Rajčić, R Žarnić**

Presented by R Žarnić

B Dujic commented that the hysteresis loops indicate large residual deformation from wood crushing. R Žarnić responded that the building could be pushed back after deformation. B Dujic commented that the literature review was incomplete in this paper. R Žarnić responded that the paper described research in progress. H Blass stated that was not the interest of this working commission. C Sigrist asked about the details of how the connection looked like between the glass and the wood and received confirmation that it was based on classical window technology and they were not glued. He asked why not gluing. R Žarnić responded that the idea was not to damage the glass but to have damage in wood. F Lam commented that as a lateral load resistant system it would need to carry seismic as well as wind loads. In high winds there is a risk of projectiles that can damage the glass. R Žarnić responded that this system might not be suitable for all cases. Also he pointed out that even without glass the system had some capacity left. P Quenneville received clarification about the contact surface between the glass and wood and vertical load that there was enough surface not to damage the wood but enough to promote friction.

45 - 15 - 5 *Modeling Wood Structural Panel Portal Frame Response* - **T Skaggs, B Yeh**

Presented by T Skaggs

G Doudak asked about other possible failure modes such as sill plate or header beam failures. T Skaggs responded that they were not observed except rare cases of strap failures. G Doudak asked about that testing with straps but without sheathing could be conducted to evaluate the cumulative effects. T Skaggs responded they were not done and the straps might be bending but modeled as pure moment couple. G Doudak asked if there was any limit on horizontal deformation. T Skaggs stated there was no drift limits for wind.

H Larsen questioned the scientific content of the work. T Skaggs and BJ Yeh responded that the work provided engineers answers to problems that currently did not have readily available solutions. It is a justification to confirm engineering mechanics approach with data to support the case. I Smith asked why there was no drift limit for wind in codes. T Skaggs clarified that drift limits or wind were more relaxed compared to seismic.

45 - 15 - 6 *Simplified Cross-laminated Timber Wall Modeling for Linear-elastic Seismic Analysis* - **I Sustersic, B Dujic**

Presented by I Sustersic

P Quenneville asked whether the corners would be relied upon for horizontal shear and the shear connectors were needed for wind and they should be considered along with the hold-downs. I Sustersic responded that the corners would not be relied on for shear resistance and their formulation considered every connection. R Žarnić received clarification about the contribution of the paper towards code. W Seim asked and received clarification of the spring element. He commented the bending was translated into shear in the model and asked whether uplift was considered. I Sustersic responded that the model did not consider uplift. W Seim received further clarification that the diaphragm was considered rigid in the model. W Seim stated that there was a string statement of the potential application of the model in analysis; however, this depended on the details and limitation of the model; ie. if you were not real exact in the model one must be careful with the claims. I Sustersic agreed and stated the model must be verified.

## 7. LAMINATED MEMBERS

45 - 12 - 1 *Asymmetrically Combined Glulam - Simplified Verification of the Bending Strength* - *M Frese, H J Bläß*

Presented by M Frese

J Köhler commented that not enough samples were considered in the simulation as the results seem to be unstable. M Frese stated that 1000 replicates were considered in the simulation and one could smooth the results with regression. He clarified also that E1 and E2 ratio was the ratio of the E of the outer and intermediate zone. Higher ratios imply more loads and stresses are attached to the higher grade lumber. S Aicher commented that as the results were based on 600 mm deep beam, would the same results apply to 2 m deep beams. M Frese responded that yes they had to take into account of the percentage of the different grades. G Stapf asked what assumptions were made for the laminates. M. Frese would look into the details and discuss with G Stapf. G Stapf asked why only considered MOE in compression and not the MOE in tension for moisture content adjustment. M Frese stated that there was no moisture adjustment method for MOE in tension and engineers in general did not consider this. T Poutanen stated that one option was to consider proof loading of the bottom chord. M Frese will discuss with T Poutanen directly. A Jorissen asked and received clarification of the glulam grades and moisture content adjustment procedures where moisture content was considered in the regression equations with E and compression strength. I Smith commented that the use of different seeds in the random number generator might solve the sample size stability issue. T Poutanen received clarification that 100% failure was in the bottom chord as this was the failure criterion chosen and plastic deformation zone did not stop the calculations. A Olsson stated that experience with solid boards failure initiate in compression and then tension fracture. He

asked whether there was a coupling effect. M Frese and H Blass responded that there were differences between the failure modes of high grade timber and glulam.

*45 - 12 - 2 Determination of Shear Strength of Structural and Glued Laminated Timber - R Brandner, W Gattermig, G Schickhofer*

Presented by R Brandner

F Lam stated that it was good to see data from Europe indicating size effect in shear strength of wood that agreed with Canadian results. F Lam questioned the influence of overhang on shear strength of beams and whether the reinforcing self-tapping screws against bearing failure might influence the shear strength. R Brandner stated that past results from Graz indicated that there was no overhang effect and explained that the self-tapping screws did not influence shear failure. F Lam received confirmation that shear failures initiated in the zone between the support and the loading head. BJ Yeh stated that overhang could serve as reinforcement and there were limits specified in ASTM test method. BJ Yeh felt that difference from Canadian approach the results seemed to indicate that it was only a depth effect on shear and not a volume effect as there wasn't any influence of specimen width. J Denzler commented that couldn't explain why small specimens had these low strength values especially for the low strength class. S Aicher commented that length of the constant shear stress and not only depth should have an influence on shear strength. He further stated that ASTM 4 point bending test procedures for estimating shear strength might be better since in the 3 point bending tests used in this study where the influence of decreasing shear length as the beam deflects was an issue. P Dietsch received confirmation that shear failure near the top of the screws were not observed. He questioned whether the self-tapping screws needed to be that long. R Brandner stated based on test experience, the length of the screws could be reduced but not based on calculations. K Malo received confirmation that the shear area was defined as the product between specimen depth and length of constant stress zone. He asked whether one would use this data directly in FEM simulation. R Brandner stated that it should not be used in FEM analysis directly.

*45 - 12 - 3 Shear Resistance of Glulam Beams with Cracks - A Pousette, M Ekevad*

Presented by A Pousette

There was discussion that natural cracks, artificial cracks and artificial grooves were different. Natural crack could be a release of strain. In terms of shear area and shear strength issue, cracks occur due to tension perpendicular to grain stress and not by shear; therefore, the remaining area should not have higher shear strength! Consideration of varying indoor climate conditions in real buildings is important. S Winter asked for information on the international standard for the reference beam grade. Also moisture measurements in the beams and on the surface during wetting and drying should be done to quantify these as the moisture treatment. A Pousette responded that this was done and the beam grades were GL28 to GL32. She stated that the results were not too bad and seemed to be sensible. For example Type II has approximately 2/3 of the strength. Irrespective of how you make the cracks, the results make engineering sense. S. Winter stated that the question was when you had natural cracks they didn't have the same behaviour as artificial cracks. Also the natural cracks induced in this study were not representative of the extreme cases that he saw in practice. Here, the width effect was important. A Jorissen stated that it seemed problematic to get shear failure unless the span to depth ratio is ~7:1. For real roof structures, the span to depth ratio is larger; therefore he questioned the application of

the findings. A Pousette stated that there were situations such as curved cambered beams where this could be important and also in short deep beams. J Köhler stated that the issue of production of natural cracks and the issue of internal stresses from moisture loads during conditioning are important. I Smith commented on stable crack and unstable crack development in relationship with volume effect.

45 - 12 - 4 *Experimental Investigation on in-plane Behaviour of Cross-laminated Timber Elements* - **M Andreolli, A Polastri, R Tomasi**

Presented by R Tomasi

G Schickhofer stated that the test configuration should be compliant to the loading condition of the building and the model should be consistent. He stated that satisfying equilibrium condition only was not enough as kinematic conditions needed to be considered also. Also the diagonal shear test configuration could have compression failure; therefore, there could be an interaction effect. Diagonal shear test configuration which puts the panel in tension needs to be used. R Tomasi agreed that the model only considered equilibrium and these were their assumptions. He also agreed that the diagonal test configuration did not yield a pure shear case. The TU Graz diagonal shear device is the only tension shear apparatus that gives stiffness measurement. I Sustersic asked if there was any observed difference in results between panels produced with hydraulic and vacuum presses. R Tomasi stated that conclusion could not be drawn on this issue. F Lam asked for clarification on how many specimens were studied. R Tomasi agreed that the number of specimens were limited and would consider more next time.

## 8. TRUSSED RAFTERS

45 - 14 - 1 *Robustness Analysis of Timber Truss Systems* - *D Čizmar, V Rajčić*

(presented by V Rajčić)

H Larsen commented that the only thing done correctly in the Ballerup Super Arena building was robustness in that the secondary beams were designed such that if one truss failed it did not cause damage to its neighbours. In this case only two trusses failed in the structure. J Munch Andersen stated that the building had basic design errors where members were undersized. V Rajčić stated that with gross design error robustness could not be calculated. U Kuhlmann stated that concerning robustness there were two approaches. The approach of redundancy and ductility is more suitable to steel structures. Here separation of damage of members is a good means perhaps for this type of timber structure where robustness can be improved. U Kuhlmann commented that some of the tables in the presentation were interesting but missing in the paper. H Blass suggested that the presentation could be put on the CIB W18 home page. I Smith asked about wind loading where damage was also a response to the system properties. V Rajčić stated that they were waiting for information on wind loading.

## 9. ENVIRONMENTAL CONDITIONS

45 - 11 - 1 *Building Climate – Long-term Measurements to Determine the Effect on the Moisture Gradient in Large-span Timber Structures* - **P Dietsch, A Gamper, M Merk, S Winter**

Presented by P Dietsch

J Köhler commented that the work was useful and had agreement with his own results. G Schickhofer commented that the work was important and asked about using different kmod factors for different cases. He also asked for comments on the use of reinforcement. P Dietsch responded that this was a balance between scientific knowledge. This was important for large span glulam structures with beams of large widths. The type of reinforcement must consider its suitability in high moisture conditions. S Aicher questioned the conclusion that the timber should be produced to the moisture condition of use. This point is already in the code but never followed in practice. F Lam asked why correction to low moisture contents were not done as the study had such information. P Dietsch replied that the data was not suitable for this consideration because different types of wood were involved. S Winter stated that in combination with precipitation the erection time of the building was also important.

## 10. TIMBER JOINTS AND FASTENERS

45 - 7 - 1 *A Stiffness-based Analytical Model for Wood Strength in Timber Connections loaded Parallel to Grain: Riveted Joint Capacity in Brittle and Mixed Failure Modes* - **P Zarnani, P Quenneville**

Presented by P Zarnani

C Sigrist asked about the purpose to study these failure modes as we had to avoid them. P Zarnani responded that the model provided a means to predict in order to avoid the brittle failure mode. I Smith asked whether the EC approach was more conservative than the Canadian approach. P Zarnani responded yes because effective thickness rather than entire thickness was used therefore more conservative. R Steiger asked about the specimens whether the analysis considered one side versus two side failures and whether the study accounts for series systems. P Zarnani responded that this was not considered. F Lam stated that you could use MLE procedure to account for this. S Aicher and P Quenneville discussed strain in the front plane is within the limit of the shearing strain in the side block. S Aicher stated that these should be compatible. P Quenneville stated that the block moved as a solid block. A Jorissen asked what happened when the bottom and side blocks were thin. P Zarnani stated that the model considered this. H Blass stated that net tension failure could happen. I Smith asked how many additional pages in the code were needed. P Zarnani stated three pages.

45 - 7 - 2 *Beams Loaded Perpendicular to Grain by Connections – Combined Effect of Edge and End Distance* - **J L Jensen, P Quenneville, U A Girhammar, B Källsner**

Presented by P Quenneville

A Frangi asked whether cross banded LVL could be made to address this issue. P Quenneville responded that yes we had done this but there was a limit. I Smith asked how this work compared to other species and tests. P Quenneville said that other tests were done mostly at midpoint and could not be compared. Also extrapolation to multi bolt cases was quite a step away. A Jorissen asked and received clarification about the definition of parameters in slide 27.

45 - 7 - 3 *L Block Failure of Dowelled Connections Subject to Bending Reinforced with Threaded Rods* - **J-F Bocquet, C Barthram, A Pineur**

Presented by J-F Bocquet

H Blass asked why there was not a kbending. J-F Bocquet stated that data did not support kbending >1 as values were near bending capacity of beam. P Zarnani received confirmation that the distribution of stresses inside the joint was not discussed even though different detailed analyses were made where it was important to take into account the elastic properties of the material. They also discussed the contribution of shear from the screw reinforcements. K Malo asked whether the normal stresses were caused by applied axial forces. J-F Bocquet stated that external normal forces were not used in the tests.

45 - 7 - 4 *Block Shear Failure of Wooden Dowel Connections* - **G Stapf, S Aicher, N Zisi**

Presented by G Stapf

I Smith commented that in Canada we did not believe the simple model could explain the complicated stress state. It was a fitting exercise. F Lam commented that the real stress state is complicated with the non-homogeneous and orthogonal elastic properties of wood as well as the possible occurrence of tensile stresses perpendicular to grain even from slight misalignment of the connectors. W Seim stated the FE model used was plane stress and isotropic. He questioned how 3 D model could affect the results. G Stapf stated that a non-isotropic 3 D model would show bending of the dowel was important. P Quenneville commented that what we had was not perfect but added to our understanding. P Zarnani commented on the cases of large dowels and more dowels in a row. F Stapf agreed that the load distribution between the dowels was important and wider connections were being considered. A Jorissen asked and received clarification on the comparison to code that there could be unsafe cases. M Yasumura received clarification of the observed failure mode was due to the oak glulam with high density. H Blass suggested also the quality of steel in dowels were usually higher than specification which could help to explain the failure mode.

45 - 7 - 5 *Requirements on Ductility in Timber Structures* - **F Brühl, U Kuhlmann**

Presented by F Brühl

W van Beerschoten commented about the assumed shape of the stress distribution that triangular stress distribution might be more appropriate. He also commented on the over strength factor. F Brühl agreed that the over strength factor was a driving factor. K Malo asked and received clarification on the characteristic strength of the connection. T Poutanen asked about the benefit in terms of numerical value. F Brühl stated that they did not have a number. P Quenneville questioned whether this connection was the most effective as plates with inclined wood screw underneath was also an option. W van Beerschoten questioned about damage after a big earthquake as large deformation might lead to non-repairable problems. F Brühl stated that in case of Europe this should be okay. I Smith commented and discussed the analog of links in a chain versus link in a double chain and practical achievement of ductility was difficult. K Malo discussed alternative of using the steel bracket. J Munch Andersen stated if you followed P Quenneville's suggestion of the alternative connection it would not be good for fire performance. M

Frese asked why put a gap between screws and dowel. F Brühl stated that this was a practical approach and contact was not doable on site.

## 11. STRESS GRADING

45 - 5 - 1 *Harmonised Tensile Strength Classes* - **J K Denzler**

Presented by J Denzler

H Blass stated that the study is proposing to lower the density which would penalize connection design. He suggested that a  $\Delta\rho$  for pine could be used to account for its higher density. J Denzler agreed. G Schickhofer stated that proof loading concept could help in terms of density. J Denzler agreed but not all companies had such equipment.

45 - 5 - 2 *Visual Strength Grading in Europe* - **P Stapel, J W G van de Kuilen, O Strehl**

Presented by P Stapel

S Winter commented that one of the reasons for the observed difference could be related to the type of harvesting. P Stapel responded that they did not observe any clear sawn damage and do not believe problems with machine parts. F Lam asked did you observe compression wood. P Stapel responded no. J Denzler asked whether bending values were corrected. P Stapel responded yes  $k_h$  was used and the possible influence of thickness was discussed. A Jorissen asked for clarification of slide 17 regarding C18 and C16 grades. Total KAR for DIN C18 was 0.43 and BS C16 was 0.36. R Steiger commented on Swiss visual grading standard and reasons to change to DIN standard. There is one for grading of laminates and one for grading of solid timber. There are additional grading rules for laminates which can be tried and one might get better results. P Stapel stated that they did not use laminates for this analysis. J Köhler stated that deviation from nominal value was a concern. The occurrence of structural failure did not seem to agree with the observed results.

J Denzler stated in central Europe C30 was not produced. Without the high grades C24 might get a better fit. J Munch Andersen commented about the small difference from different strength classes. R Steiger commented on the amount of rejects experienced with the Swiss AS standard.

## 12. TIMBER COLUMNS

45 - 2 - 1 *Design of Timber Columns Based on 2nd Order Structural Analysis* - **M Theiler, A Frangi, R Steiger**

Presented by M Theiler

G Schickhofer asked if there was any allowance for out of plane torsional buckling. M Theiler responded no. H Larsen stated that it was a déjà vu and test results should be compared to theoretical value at the mean level. M Theiler stated that they used mean values for comparison to test results and Monte Carlo simulations to obtain characteristic values. J Köhler commented about the sensitivity and importance of representing stiffness especially in the slender column. M Theiler agreed and stated that the test columns were

not slender as they have a slenderness ratio of 60 to 70. J Malo received clarification that the models were based on measurements performed by H Blass. Material variability within the column is assumed to be taken by variability in the strength data. F Lam received clarification of the difference in definition of slenderness ratio between N. America and Europe. G Doudak received clarification on the grading rule issues and simulation process.

### 13. NOTES

*Block Shear* - **H J Larsen**

*Single Shearing Properties on Various Types of Screwed Joints Tested According to ISO16670* - **K Kobayashi, M Yasumura**

*Failure Criteria for Post-tensioned Timber Beams* - **W van Beerschoten, A Palermo, D Carradine, A Buchanan**

*Some comments on CIB-W18 paper 45-102-1 by J. Köhler, R. Steiger, G. Fink and R. Jockwer* - **T Poutanen**

*The withdrawal strength of 8 threaded nails types* - **J Munch-Andersen, S Svensson**

*Simulation of Bottom Rail Fracture in Partially Anchored Shear Walls Using XFEM* - **J Vessby, E Serrano, A Olsson, U A Girhammar, B Källsner**

*Some Comments on the Sugiyama Opening Coefficient method and lower-bound solutions for shear walls* - **J L Jensen, Xi'an Jiaotong, B Källsner, P Quenneville, U A Girhammar**

*A note on surface scanning and stress grading based on fracture mechanics* - **H Petersson**

### 14. ANY OTHER BUSINESS

J Munch Andersen presented the CIB W18 website. Chairman thanked HJ Larsen for his contribution to the CIBW18 homepage.

CIB W18 Chairmanship: Extensive discussion on CIB W18 chairmanship took place. The options of affirming the current chairman, electing a new chairman, or adopting a rotating chairmanship were discussed by the participants. The participants agreed that the CIB W18 chairmanship position provides an important service to the timber engineering community. They expressed strong interest of having continuity. The motion to affirm the current chairmanship for a period of 5 year was voted on and unanimously approved by the participants.

Publication of proceedings: Extensive discussion on the procedure, format and content of CIB W18 proceedings took place. Participants agreed that 1) current procedure, format and content of the publication of the CIB W18 proceeding is appropriate and should be maintained. 2) Outside comments should not be included in the proceedings. 3) Email comments should be sent to the chair and the chair will evaluate its relevance before making a decision to circulate to the members of CIB W18.

**15. VENUE AND PROGRAMME FOR NEXT MEETING**

F Lam invited the colleagues to come to 2013 CIB W18 in Vancouver Canada.

Bath UK will host the 2014 CIB W18 meeting.

Croatia will host the 2015 CIB W18 meeting.

**16. CLOSE**

Chairman thanked C Bengtsson and E Serrano and the supporting group for hosting and organizing an excellent meeting.



**17. Peer Review of Papers for the  
CIB-W18 Proceedings**



## **17. Peer review of papers for the CIB-W18 Proceedings**

Experts involved:

Members of the CIB-W18 “Timber Structures” group are a community of experts in the field of timber engineering.

Procedure of peer review

- Submission of manuscripts: all members of the CIB-W18 group attending the meeting receive the manuscripts of the papers at least four weeks before the meeting. Everyone is invited to read and review the manuscripts especially in their respective fields of competence and interest.
- Presentation of the paper during the meeting by the author
- Comments and recommendations of the experts, discussion of the paper
- Comments, discussion and recommendations of the experts are documented in the minutes of the meeting and are printed on the front page of each paper.
- Final acceptance of the paper for the proceedings with
  - no changes
  - minor changes
  - major changes
  - or reject
- Revised papers are to be sent to the editor of the proceedings and the chairman of the CIB-W18 group
- Editor and chairman check, whether the requested changes have been carried out.



**18. List of CIB-W18 Papers,  
Växjö, Sweden 2012**



## List of CIB-W18 Papers, Växjö, Sweden 2012

- 45 - 2 - 1 Design of Timber Columns Based on 2<sup>nd</sup> Order Structural Analysis - **M Theiler, A Frangi, R Steiger**
- 45 - 5 - 1 Harmonised Tensile Strength Classes - **J K Denzler**
- 45 - 5 - 2 Visual Strength Grading in Europe - **P Stapel, J W G van de Kuilen, O Strehl**
- 45 - 7 - 1 A Stiffness-based Analytical Model for Wood Strength in Timber Connections loaded Parallel to Grain: Riveted Joint Capacity in Brittle and Mixed Failure - **P Zarnani, P Quenneville**
- 45 - 7 - 2 Beams Loaded Perpendicular to Grain by Connections – Combined Effect of Edge and End Distance - **J L Jensen, P Quenneville, U A Girhammar, B Källsner**
- 45 - 7 - 3 L Block Failure of Dowelled Connections Subject to Bending Reinforced with Threaded Rods - **J-F Bocquet, C Barthram, A Pineur**
- 45 - 7 - 4 Block Shear Failure of Wooden Dowel Connections - **G Stapf, S Aicher, N Zisi**
- 45 - 7 - 5 Requirements on Ductility in Timber Structures - **F Brühl, U Kuhlmann**
- 45 - 11 - 1 Building Climate – Long-term Measurements to Determine the Effect on the Moisture Gradient in Large-span Timber Structures - **P Dietsch, A Gamper, M Merk, S Winter**
- 45 - 12 - 1 Asymmetrically Combined Glulam - Simplified Verification of the Bending Strength - **M Frese, H J Blaß**
- 45 - 12 - 2 Determination of Shear Strength of Structural and Glued Laminated Timber - **R Brandner, W Gatterig, G Schickhofer**
- 45 - 12 - 3 Shear Resistance of Glulam Beams with Cracks - **A Pousette, M Ekevad**
- 45 - 12 - 4 Experimental Investigation on in-plane Behaviour of Cross-laminated Timber Elements - **M Andreolli, A Polastri, R Tomasi**
- 45 - 14 - 1 Robustness Analysis of Timber Truss Systems - **D Čizmar, V Rajčić**
- 45 - 15 - 1 Performance Based Design and Force Modification Factors for CLT Structures - **S Pei, M Popovski, J van de Lindt**
- 45 - 15 - 2 Seismic Behaviour of Wood-Concrete Frame Shear-wall System and Comparison with Code Provisions - **L Pozza, R Scotta, A Polastri, A Ceccotti**
- 45 - 15 - 3 Determination of Failure Mechanism of CLT Shear Walls Subjected to Seismic Action - **M Yasumura**

- 45 - 15 - 4 Seismic Response of Timber Frames with Laminated Glass Glass Infill - **V Rajčić, R Žarnić**
- 45 - 15 - 5 Modeling Wood Structural Panel Portal Frame Response - **T Skaggs, B Yeh**
- 45 - 15 - 6 Simplified Cross-laminated Timber Wall Modeling for Linear-elastic Seismic Analysis - **I Sustersic, B Dujic**
- 45 - 16 - 1 The Reduced Cross Section Method for Timber Members Subjected to Compression, Tension and Bending in Fire - **M Klippel, J Schmid, A Frangi**
- 45 - 21 - 1 Evaluation of Shear Modulus of Structural Timber Utilizing Dynamic Excitation and FE Analysis - **A Olsson, B Källsner**
- 45 - 102 - 1 Assessment of Relevant Eurocode Based Design Equations in Regard to Structural Reliability - **J Köhler, R Steiger**

**Notes:**

Block Shear - **H J Larsen**

Single Shearing Properties on Various Types of Screwed Joints Tested According to ISO16670 - **K Kobayashi, M Yasumura**

Failure Criteria for Post-tensioned Timber Beams - **W van Beerschoten, A Palermo, D Carradine, A Buchanan**

Some comments on CIB-W18 paper 45-102-1 by J. Köhler, R. Steiger, G. Fink and R. Jockwer - **T Poutanen**

The withdrawal strength of 8 threaded nails types - **J Munch-Andersen, S Svensson**

Simulation of Bottom Rail Fracture in Partially Anchored Shear Walls Using XFEM - **J Vessby, E Serrano, A Olsson, U A Girhammar, B Källsner**

Some Comments on the Sugiyama Opening Coefficient method and lower-bound solutions for shear walls - **J L Jensen, Xi'an Jiaotong, B Källsner, P Quenneville, U A Girhammar**

**19. Current List of CIB-W18(A)  
Papers**



## CURRENT LIST OF CIB-W18(A) PAPERS

Technical papers presented to CIB-W18(A) are identified by a code CIB-W18(A)/a-b-c, where:

a denotes the meeting at which the paper was presented.

- 1 Princes Risborough, England; March 1973
- 2 Copenhagen, Denmark; October 1973
- 3 Delft, Netherlands; June 1974
- 4 Paris, France; February 1975
- 5 Karlsruhe, Federal Republic of Germany; October 1975
- 6 Aalborg, Denmark; June 1976
- 7 Stockholm, Sweden; February/March 1977
- 8 Brussels, Belgium; October 1977
- 9 Perth, Scotland; June 1978
- 10 Vancouver, Canada; August 1978
- 11 Vienna, Austria; March 1979
- 12 Bordeaux, France; October 1979
- 13 Otaniemi, Finland; June 1980
- 14 Warsaw, Poland; May 1981
- 15 Karlsruhe, Federal Republic of Germany; June 1982
- 16 Lillehammer, Norway; May/June 1983
- 17 Rapperswil, Switzerland; May 1984
- 18 Beit Oren, Israel; June 1985
- 19 Florence, Italy; September 1986
- 20 Dublin, Ireland; September 1987
- 21 Parksville, Canada; September 1988
- 22 Berlin, German Democratic Republic; September 1989
- 23 Lisbon, Portugal; September 1990
- 24 Oxford, United Kingdom; September 1991
- 25 Åhus, Sweden; August 1992
- 26 Athens, USA; August 1993
- 27 Sydney, Australia; July 1994
- 28 Copenhagen, Denmark; April 1995
- 29 Bordeaux, France; August 1996
- 30 Vancouver, Canada; August 1997
- 31 Savonlinna, Finland; August 1998
- 32 Graz, Austria, August 1999
- 33 Delft, The Netherlands; August 2000
- 34 Venice, Italy; August 2001
- 35 Kyoto, Japan; September 2002
- 36 Colorado, USA; August 2003
- 37 Edinburgh, Scotland, August 2004
- 38 Karlsruhe, Germany, August 2005
- 39 Florence, Italy, August 2006
- 40 Bled, Slovenia, August 2007
- 41 St. Andrews, Canada 2008
- 42 Dübendorf, Switzerland 2009
- 43 Nelson, New Zealand 2010
- 44 Alghero, Italy 2011
- 45 Växjö, Sweden 2012

b denotes the subject:

- 1 Limit State Design
- 2 Timber Columns
- 3 Symbols
- 4 Plywood
- 5 Stress Grading
- 6 Stresses for Solid Timber
- 7 Timber Joints and Fasteners
- 8 Load Sharing
- 9 Duration of Load
- 10 Timber Beams
- 11 Environmental Conditions
- 12 Laminated Members
- 13 Particle and Fibre Building Boards
- 14 Trussed Rafters
- 15 Structural Stability
- 16 Fire
- 17 Statistics and Data Analysis
- 18 Glued Joints
- 19 Fracture Mechanics
- 20 Serviceability
- 21 Test Methods
- 100 CIB Timber Code
- 101 Loading Codes
- 102 Structural Design Codes
- 103 International Standards Organisation
- 104 Joint Committee on Structural Safety
- 105 CIB Programme, Policy and Meetings
- 106 International Union of Forestry Research Organisations

c is simply a number given to the papers in the order in which they appear:

Example: CIB-W18/4-102-5 refers to paper 5 on subject 102 presented at the fourth meeting of W18.

Listed below, by subjects, are all papers that have to date been presented to W18. When appropriate some papers are listed under more than one subject heading.

## LIMIT STATE DESIGN

- 1-1-1 Limit State Design - H J Larsen
- 1-1-2 The Use of Partial Safety Factors in the New Norwegian Design Code for Timber Structures - O Brynildsen
- 1-1-3 Swedish Code Revision Concerning Timber Structures - B Noren
- 1-1-4 Working Stresses Report to British Standards Institution Committee BLC/17/2
- 6-1-1 On the Application of the Uncertainty Theoretical Methods for the Definition of the Fundamental Concepts of Structural Safety - K Skov and O Ditlevsen
- 11-1-1 Safety Design of Timber Structures - H J Larsen
- 18-1-1 Notes on the Development of a UK Limit States Design Code for Timber - A R Fewell and C B Pierce
- 18-1-2 Eurocode 5, Timber Structures - H J Larsen
- 19-1-1 Duration of Load Effects and Reliability Based Design (Single Member) - R O Foschi and Z C Yao
- 21-102-1 Research Activities Towards a New GDR Timber Design Code Based on Limit States Design - W Rug and M Badstube
- 22-1-1 Reliability-Theoretical Investigation into Timber Components Proposal for a Supplement of the Design Concept - M Badstube, W Rug and R Plessow
- 23-1-1 Some Remarks about the Safety of Timber Structures - J Kuipers
- 23-1-2 Reliability of Wood Structural Elements: A Probabilistic Method to Eurocode 5 Calibration - F Rouger, N Lheritier, P Racher and M Fogli
- 31-1-1 A Limit States Design Approach to Timber Framed Walls - C J Mettem, R Bainbridge and J A Gordon
- 32 -1-1 Determination of Partial Coefficients and Modification Factors- H J Larsen, S Svensson and S Thelandersson
- 32 -1-2 Design by Testing of Structural Timber Components - V Enjily and L Whale
- 33-1-1 Aspects on Reliability Calibration of Safety Factors for Timber Structures – S Svensson and S Thelandersson
- 33-1-2 Sensitivity studies on the reliability of timber structures – A Ranta-Maunus, M Fonselius, J Kurkela and T Toratti
- 41-1-1 On the Role of Stiffness Properties for Ultimate Limit State Design of Slender Columns– J Köhler, A Frangi, R Steiger

## TIMBER COLUMNS

- 2-2-1 The Design of Solid Timber Columns - H J Larsen
- 3-2-1 The Design of Built-Up Timber Columns - H J Larsen
- 4-2-1 Tests with Centrally Loaded Timber Columns - H J Larsen and S S Pedersen
- 4-2-2 Lateral-Torsional Buckling of Eccentrically Loaded Timber Columns- B Johansson
- 5-9-1 Strength of a Wood Column in Combined Compression and Bending with Respect to Creep - B Källsner and B Norén
- 5-100-1 Design of Solid Timber Columns (First Draft) - H J Larsen
- 6-100-1 Comments on Document 5-100-1, Design of Solid Timber Columns - H J Larsen and E Theilgaard
- 6-2-1 Lattice Columns - H J Larsen
- 6-2-2 A Mathematical Basis for Design Aids for Timber Columns - H J Burgess

- 6-2-3 Comparison of Larsen and Perry Formulas for Solid Timber Columns-  
H J Burgess
- 7-2-1 Lateral Bracing of Timber Struts - J A Simon
- 8-15-1 Laterally Loaded Timber Columns: Tests and Theory - H J Larsen
- 17-2-1 Model for Timber Strength under Axial Load and Moment - T Poutanen
- 18-2-1 Column Design Methods for Timber Engineering - A H Buchanan, K C Johns,  
B Madsen
- 19-2-1 Creep Buckling Strength of Timber Beams and Columns - R H Leicester
- 19-12-2 Strength Model for Glulam Columns - H J Blaß
- 20-2-1 Lateral Buckling Theory for Rectangular Section Deep Beam-Columns-  
H J Burgess
- 20-2-2 Design of Timber Columns - H J Blaß
- 21-2-1 Format for Buckling Strength - R H Leicester
- 21-2-2 Beam-Column Formulae for Design Codes - R H Leicester
- 21-15-1 Rectangular Section Deep Beam - Columns with Continuous Lateral Restraint -  
H J Burgess
- 21-15-2 Buckling Modes and Permissible Axial Loads for Continuously Braced Columns - H J  
Burgess
- 21-15-3 Simple Approaches for Column Bracing Calculations - H J Burgess
- 21-15-4 Calculations for Discrete Column Restraints - H J Burgess
- 22-2-1 Buckling and Reliability Checking of Timber Columns - S Huang, P M Yu and  
J Y Hong
- 22-2-2 Proposal for the Design of Compressed Timber Members by Adopting the Second-Order  
Stress Theory - P Kaiser
- 30-2-1 Beam-Column Formula for Specific Truss Applications - W Lau, F Lam and J D Barrett
- 31-2-1 Deformation and Stability of Columns of Viscoelastic Material Wood - P Becker and K  
Rautenstrauch
- 34-2-1 Long-Term Experiments with Columns: Results and Possible Consequences on Column  
Design – W Moorkamp, W Schelling, P Becker, K Rautenstrauch
- 34-2-2 Proposal for Compressive Member Design Based on Long-Term Simulation Studies – P  
Becker, K Rautenstrauch
- 35-2-1 Computer Simulations on the Reliability of Timber Columns Regarding Hygrothermal  
Effects- R Hartnack, K-U Schober, K Rautenstrauch
- 36-2-1 The Reliability of Timber Columns Based on Stochastic Principles - K Rautenstrauch,  
R Hartnack
- 38-2-1 Long-term Load Bearing of Wooden Columns Influenced by Climate – View on Code -  
R Hartnack, K Rautenstrauch
- 45-2-1 Design of Timber Columns Based on 2nd Order Structural Analysis - M Theiler, A  
Frangi, R Steiger

## SYMBOLS

- 3-3-1 Symbols for Structural Timber Design - J Kuipers and B Norén
- 4-3-1 Symbols for Timber Structure Design - J Kuipers and B Norén
- 28-3-1 Symbols for Timber and Wood-Based Materials - J Kuipers and B Noren
- 1 Symbols for Use in Structural Timber Design

## PLYWOOD

- 2-4-1 The Presentation of Structural Design Data for Plywood - L G Booth
- 3-4-1 Standard Methods of Testing for the Determination of Mechanical Properties of Plywood - J Kuipers
- 3-4-2 Bending Strength and Stiffness of Multiple Species Plywood - C K A Stieda
- 4-4-4 Standard Methods of Testing for the Determination of Mechanical Properties of Plywood - Council of Forest Industries, B.C.
- 5-4-1 The Determination of Design Stresses for Plywood in the Revision of CP 112 - L G Booth
- 5-4-2 Veneer Plywood for Construction - Quality Specifications - ISO/TC 139. Plywood, Working Group 6
- 6-4-1 The Determination of the Mechanical Properties of Plywood Containing Defects - L G Booth
- 6-4-2 Comparison of the Size and Type of Specimen and Type of Test on Plywood Bending Strength and Stiffness - C R Wilson and P Eng
- 6-4-3 Buckling Strength of Plywood: Results of Tests and Recommendations for Calculations - J Kuipers and H Ploos van Amstel
- 7-4-1 Methods of Test for the Determination of Mechanical Properties of Plywood - L G Booth, J Kuipers, B Norén, C R Wilson
- 7-4-2 Comments Received on Paper 7-4-1
- 7-4-3 The Effect of Rate of Testing Speed on the Ultimate Tensile Stress of Plywood - C R Wilson and A V Parasin
- 7-4-4 Comparison of the Effect of Specimen Size on the Flexural Properties of Plywood Using the Pure Moment Test - C R Wilson and A V Parasin
- 8-4-1 Sampling Plywood and the Evaluation of Test Results - B Norén
- 9-4-1 Shear and Torsional Rigidity of Plywood - H J Larsen
- 9-4-2 The Evaluation of Test Data on the Strength Properties of Plywood - L G Booth
- 9-4-3 The Sampling of Plywood and the Derivation of Strength Values (Second Draft) - B Norén
- 9-4-4 On the Use of the CIB/RILEM Plywood Plate Twisting Test: a progress report - L G Booth
- 10-4-1 Buckling Strength of Plywood - J Dekker, J Kuipers and H Ploos van Amstel
- 11-4-1 Analysis of Plywood Stressed Skin Panels with Rigid or Semi-Rigid Connections- I Smith
- 11-4-2 A Comparison of Plywood Modulus of Rigidity Determined by the ASTM and RILEM CIB/3-TT Test Methods - C R Wilson and A V Parasin
- 11-4-3 Sampling of Plywood for Testing Strength - B Norén
- 12-4-1 Procedures for Analysis of Plywood Test Data and Determination of Characteristic Values Suitable for Code Presentation - C R Wilson
- 14-4-1 An Introduction to Performance Standards for Wood-base Panel Products - D H Brown
- 14-4-2 Proposal for Presenting Data on the Properties of Structural Panels - T Schmidt
- 16-4-1 Planar Shear Capacity of Plywood in Bending - C K A Stieda
- 17-4-1 Determination of Panel Shear Strength and Panel Shear Modulus of Beech-Plywood in Structural Sizes - J Ehlbeck and F Colling
- 17-4-2 Ultimate Strength of Plywood Webs - R H Leicester and L Pham

- 20-4-1 Considerations of Reliability - Based Design for Structural Composite Products - M R O'Halloran, J A Johnson, E G Elias and T P Cunningham
- 21-4-1 Modelling for Prediction of Strength of Veneer Having Knots - Y Hirashima
- 22-4-1 Scientific Research into Plywood and Plywood Building Constructions the Results and Findings of which are Incorporated into Construction Standard Specifications of the USSR - I M Guskov
- 22-4-2 Evaluation of Characteristic values for Wood-Based Sheet Materials - E G Elias
- 24-4-1 APA Structural-Use Design Values: An Update to Panel Design Capacities - A L Kuchar, E G Elias, B Yeh and M R O'Halloran

## STRESS GRADING

- 1-5-1 Quality Specifications for Sawn Timber and Precision Timber - Norwegian Standard NS 3080
- 1-5-2 Specification for Timber Grades for Structural Use - British Standard BS 4978
- 4-5-1 Draft Proposal for an International Standard for Stress Grading Coniferous Sawn Softwood - ECE Timber Committee
- 16-5-1 Grading Errors in Practice - B Thunell
- 16-5-2 On the Effect of Measurement Errors when Grading Structural Timber- L Nordberg and B Thunell
- 19-5-1 Stress-Grading by ECE Standards of Italian-Grown Douglas-Fir Dimension Lumber from Young Thinnings - L Uzielli
- 19-5-2 Structural Softwood from Afforestation Regions in Western Norway - R Lackner
- 21-5-1 Non-Destructive Test by Frequency of Full Size Timber for Grading - T Nakai
- 22-5-1 Fundamental Vibration Frequency as a Parameter for Grading Sawn Timber - T Nakai, T Tanaka and H Nagao
- 24-5-1 Influence of Stress Grading System on Length Effect Factors for Lumber Loaded in Compression - A Campos and I Smith
- 26-5-1 Structural Properties of French Grown Timber According to Various Grading Methods - F Rouger, C De Lafond and A El Quadrani
- 28-5-1 Grading Methods for Structural Timber - Principles for Approval - S Ohlsson
- 28-5-2 Relationship of Moduli of Elasticity in Tension and in Bending of Solid Timber - N Burger and P Glos
- 29-5-1 The Effect of Edge Knots on the Strength of SPF MSR Lumber - T Courchene, F Lam and J D Barrett
- 29-5-2 Determination of Moment Configuration Factors using Grading Machine Readings - T D G Canisius and T Isaksson
- 31-5-1 Influence of Varying Growth Characteristics on Stiffness Grading of Structural Timber - S Ormarsson, H Petersson, O Dahlblom and K Persson
- 31-5-2 A Comparison of In-Grade Test Procedures - R H Leicester, H Breitingner and H Fordham
- 32-5-1 Actual Possibilities of the Machine Grading of Timber - K Frühwald and A Bernasconi
- 32-5-2 Detection of Severe Timber Defects by Machine Grading - A Bernasconi, L Boström and B Schacht
- 34-5-1 Influence of Proof Loading on the Reliability of Members – F Lam, S Abayakoon, S Svensson, C Gyamfi
- 36-5-1 Settings for Strength Grading Machines – Evaluation of the Procedure according to prEN 14081, part 2 - C Bengtsson, M Fonselius

- 36-5-2 A Probabilistic Approach to Cost Optimal Timber Grading - J Köhler, M H Faber
- 36-7-11 Reliability of Timber Structures, Theory and Dowel-Type Connection Failures - A Ranta-Maunus, A Kevarinmäki
- 38-5-1 Are Wind-Induced Compression Failures Grading Relevant - M Arnold, R Steiger
- 39-5-1 A Discussion on the Control of Grading Machine Settings – Current Approach, Potential and Outlook - J Köhler, R Steiger
- 39-5-2 Tensile Proof Loading to Assure Quality of Finger-Jointed Structural timber - R Katzengruber, G Jeitler, G Schickhofer
- 40-5-1 Development of Grading Rules for Re-Cycled Timber Used in Structural Applications - K Crews
- 40-5-2 The Efficient Control of Grading Machine Settings - M Sandomeer, J Köhler, P Linsenmann
- 41-5-1 Probabilistic Output Control for Structural Timber - Fundamental Model Approach – M K Sandomeer, J Köhler, M H Faber
- 42-5-1 Machine Strength Grading – a New Method for Derivation of Settings - R Ziethén, C Bengtsson
- 43-5-1 Quality Control Methods - Application to Acceptance Criteria for a Batch of Timber - F Rouger
- 43-5-2 Influence of Origin and Grading Principles on the Engineering Properties of European Timber - P Stapel, J W v. d. Kuilen, A Rais
- 44-5-1 Assessment of Different Knot-Indicators to Predict Strength and Stiffness Properties of Timber Boards - G Fink, M Deublein, J Köhler
- 44-5-2 Adaptive Production Settings Method for Strength Grading - G Turk, A Ranta-Maunus
- 44-5-3 Initial Settings for Machine Strength Graded Structural Timber - R Ziethén, C Bengtsson
- 45-5-1 Harmonised Tensile Strength Classes - J K Denzler
- 45-5-2 Visual Strength Grading in Europe - P Stapel, J W G van de Kuilen, O Strehl

#### STRESSES FOR SOLID TIMBER

- 4-6-1 Derivation of Grade Stresses for Timber in the UK - W T Curry
- 5-6-1 Standard Methods of Test for Determining some Physical and Mechanical Properties of Timber in Structural Sizes - W T Curry
- 5-6-2 The Description of Timber Strength Data - J R Tory
- 5-6-3 Stresses for EC1 and EC2 Stress Grades - J R Tory
- 6-6-1 Standard Methods of Test for the Determination of some Physical and Mechanical Properties of Timber in Structural Sizes (third draft) - W T Curry
- 7-6-1 Strength and Long-term Behaviour of Lumber and Glued Laminated Timber under Torsion Loads - K Möhler
- 9-6-1 Classification of Structural Timber - H J Larsen
- 9-6-2 Code Rules for Tension Perpendicular to Grain - H J Larsen
- 9-6-3 Tension at an Angle to the Grain - K Möhler
- 9-6-4 Consideration of Combined Stresses for Lumber and Glued Laminated Timber - K Möhler
- 11-6-1 Evaluation of Lumber Properties in the United States - W L Galligan and J H Haskell
- 11-6-2 Stresses Perpendicular to Grain - K Möhler

- 11-6-3 Consideration of Combined Stresses for Lumber and Glued Laminated Timber (addition to Paper CIB-W18/9-6-4) - K Möhler
- 12-6-1 Strength Classifications for Timber Engineering Codes - R H Leicester and W G Keating
- 12-6-2 Strength Classes for British Standard BS 5268 - J R Tory
- 13-6-1 Strength Classes for the CIB Code - J R Tory
- 13-6-2 Consideration of Size Effects and Longitudinal Shear Strength for Uncracked Beams - R O Foschi and J D Barrett
- 13-6-3 Consideration of Shear Strength on End-Cracked Beams - J D Barrett and R O Foschi
- 15-6-1 Characteristic Strength Values for the ECE Standard for Timber - J G Sunley
- 16-6-1 Size Factors for Timber Bending and Tension Stresses - A R Fewell
- 16-6-2 Strength Classes for International Codes - A R Fewell and J G Sunley
- 17-6-1 The Determination of Grade Stresses from Characteristic Stresses for BS 5268: Part 2 - A R Fewell
- 17-6-2 The Determination of Softwood Strength Properties for Grades, Strength Classes and Laminated Timber for BS 5268: Part 2 - A R Fewell
- 18-6-1 Comment on Papers: 18-6-2 and 18-6-3 - R H Leicester
- 18-6-2 Configuration Factors for the Bending Strength of Timber - R H Leicester
- 18-6-3 Notes on Sampling Factors for Characteristic Values - R H Leicester
- 18-6-4 Size Effects in Timber Explained by a Modified Weakest Link Theory- B Madsen and A H Buchanan
- 18-6-5 Placement and Selection of Growth Defects in Test Specimens - H Riberholt
- 18-6-6 Partial Safety-Coefficients for the Load-Carrying Capacity of Timber Structures - B Norén and J-O Nylander
- 19-6-1 Effect of Age and/or Load on Timber Strength - J Kuipers
- 19-6-2 Confidence in Estimates of Characteristic Values - R H Leicester
- 19-6-3 Fracture Toughness of Wood - Mode I - K Wright and M Fonselius
- 19-6-4 Fracture Toughness of Pine - Mode II - K Wright
- 19-6-5 Drying Stresses in Round Timber - A Ranta-Maunus
- 19-6-6 A Dynamic Method for Determining Elastic Properties of Wood - R Görlacher
- 20-6-1 A Comparative Investigation of the Engineering Properties of "Whitewoods" Imported to Israel from Various Origins - U Korin
- 20-6-2 Effects of Yield Class, Tree Section, Forest and Size on Strength of Home Grown Sitka Spruce - V Picardo
- 20-6-3 Determination of Shear Strength and Strength Perpendicular to Grain - H J Larsen
- 21-6-1 Draft Australian Standard: Methods for Evaluation of Strength and Stiffness of Graded Timber - R H Leicester
- 21-6-2 The Determination of Characteristic Strength Values for Stress Grades of Structural Timber. Part 1 - A R Fewell and P Glos
- 21-6-3 Shear Strength in Bending of Timber - U Korin
- 22-6-1 Size Effects and Property Relationships for Canadian 2-inch Dimension Lumber - J D Barrett and H Griffin
- 22-6-2 Moisture Content Adjustments for In-Grade Data - J D Barrett and W Lau

- 22-6-3 A Discussion of Lumber Property Relationships in Eurocode 5 - D W Green and D E Kretschmann
- 22-6-4 Effect of Wood Preservatives on the Strength Properties of Wood - F Ronai
- 23-6-1 Timber in Compression Perpendicular to Grain - U Korin
- 24-6-1 Discussion of the Failure Criterion for Combined Bending and Compression - T A C M van der Put
- 24-6-3 Effect of Within Member Variability on Bending Strength of Structural Timber - I Czmocho, S Thelandersson and H J Larsen
- 24-6-4 Protection of Structural Timber Against Fungal Attack Requirements and Testing- K Jaworska, M Rylko and W Nozynski
- 24-6-5 Derivation of the Characteristic Bending Strength of Solid Timber According to CEN-Document prEN 384 - A J M Leijten
- 25-6-1 Moment Configuration Factors for Simple Beams- T D G Canisius
- 25-6-3 Bearing Capacity of Timber - U Korin
- 25-6-4 On Design Criteria for Tension Perpendicular to Grain - H Petersson
- 25-6-5 Size Effects in Visually Graded Softwood Structural Lumber - J D Barrett, F Lam and W Lau
- 26-6-1 Discussion and Proposal of a General Failure Criterion for Wood - T A C M van der Put
- 27-6-1 Development of the "Critical Bearing": Design Clause in CSA-086.1 - C Lum and E Karacabeyli
- 27-6-2 Size Effects in Timber: Novelty Never Ends - F Rouger and T Fewell
- 27-6-3 Comparison of Full-Size Sugi (*Cryptomeria japonica* D.Don) Structural Performance in Bending of Round Timber, Two Surfaces Sawn Timber and Square Sawn Timber - T Nakai, H Nagao and T Tanaka
- 28-6-1 Shear Strength of Canadian Softwood Structural Lumber - F Lam, H Yee and J D Barrett
- 28-6-2 Shear Strength of Douglas Fir Timbers - B Madsen
- 28-6-3 On the Influence of the Loading Head Profiles on Determined Bending Strength - L Muszyński and R Szukala
- 28-6-4 Effect of Test Standard, Length and Load Configuration on Bending Strength of Structural Timber- T Isaksson and S Thelandersson
- 28-6-5 Grading Machine Readings and their Use in the Calculation of Moment Configuration Factors - T Canisius, T Isaksson and S Thelandersson
- 28-6-6 End Conditions for Tension Testing of Solid Timber Perpendicular to Grain - T Canisius
- 29-6-1 Effect of Size on Tensile Strength of Timber - N Burger and P Glos
- 29-6-2 Equivalence of In-Grade Testing Standards - R H Leicester, H O Breitingner and H F Fordham
- 30-6-1 Strength Relationships in Structural Timber Subjected to Bending and Tension - N Burger and P Glos
- 30-6-2 Characteristic Design Stresses in Tension for Radiata Pine Grown in Canterbury - A Tsehaye, J C F Walker and A H Buchanan
- 30-6-3 Timber as a Natural Composite: Explanation of Some Peculiarities in the Mechanical Behaviour - E Gehri
- 31-6-1 Length and Moment Configuration Factors - T Isaksson

- 31-6-2 Tensile Strength Perpendicular to Grain According to EN 1193 - H J Blaß and M Schmid
- 31-6-3 Strength of Small Diameter Round Timber - A Ranta-Maunus, U Saarelainen and H Boren
- 31-6-4 Compression Strength Perpendicular to Grain of Structural Timber and Glulam - L Damkilde, P Hoffmeyer and T N Pedersen
- 31-6-5 Bearing Strength of Timber Beams - R H Leicester, H Fordham and H Breitingner
- 32-6-1 Development of High-Resistance Glued Robinia Products and an Attempt to Assign Such Products to the European System of Strength Classes - G Schickhofer and B Obermayr
- 32-6-2 Length and Load Configuration Effects in the Code Format - T Isaksson
- 32-6-3 Length Effect on the Tensile Strength of Truss Chord Members - F Lam
- 32-6-4 Tensile Strength Perpendicular to Grain of Glued Laminated Timber - H J Blaß and M Schmid
- 32-6-5 On the Reliability-based Strength Adjustment Factors for Timber Design - T D G Canisius
- 34-6-1 Material Strength Properties for Canadian Species Used in Japanese Post and Beam Construction - J D Barrett, F Lam, S Nakajima
- 35-6-1 Evaluation of Different Size Effect Models for Tension Perpendicular to Grain Design - S Aicher, G Dill-Langer
- 35-6-2 Tensile Strength of Glulam Perpendicular to Grain - Effects of Moisture Gradients - J Jönsson, S Thelandersson
- 36-6-1 Characteristic Shear Strength Values Based on Tests According to EN 1193 - P Glos, J Denzler
- 37-6-1 Tensile Strength of Nordic Birch - K H Solli
- 37-6-2 Effect of Test Piece Orientation on Characteristic Bending Strength of Structural Timber - P Glos, J K Denzler
- 37-6-3 Strength and Stiffness Behaviour of Beech Laminations for High Strength Glulam - P Glos, J K Denzler, P W Linsenmann
- 37-6-4 A Review of Existing Standards Related to Calculation of Characteristic Values of Timber - F Rouger
- 37-6-5 Influence of the Rolling-Shear Modulus on the Strength and Stiffness of Structural Bonded Timber Elements - P Fellmoser, H J Blass
- 38-6-1 Design Specifications for Notched Beams in AS:1720 - R H Leicester
- 38-6-2 Characteristic Bending Strength of Beech Glulam - H J Blaß, M Frese
- 38-6-3 Shear Strength of Glued Laminated Timber - H Klapp, H Brüninghoff
- 39-6-1 Allocation of Central European hardwoods into EN 1912 - P Glos, J K Denzler
- 39-6-2 Revisiting EN 338 and EN 384 Basics and Procedures - R Steiger, M Arnold, M Fontana
- 40-6-1 Bearing Strength Perpendicular to the Grain of Locally Loaded Timber Blocks - A J M Leijten, J C M Schoenmakers
- 40-6-2 Experimental Study of Compression and Shear Strength of Spruce Timber - M Poussa, P Tukiainen, A Ranta-Maunus
- 40-6-3 Analysis of Tension and Bending strength of Graded Spruce Timber - A Hanhijärvi, A Ranta-Maunus, H Sarkama, M Kohsaku, M Poussa, J Puttonen
- 41-6-1 Design of Inclined Glulam Members with an End Notch on the Tension Face - A Asiz, I Smith
- 41-6-2 A New Design Approach for End-notched Beams - View on Code - K Rautenstrauch, B Franke, S Franke, K U Schober

- 41-6-3 The Design Rules in Eurocode 5 for Compression Perpendicular to the Grain - Continuous Supported Beams - H J Larsen, T A C M van der Put, A J M Leijten
- 41-6-4 Size Effects in Bending – J K Denzler, P Glos
- 42-6-1 Variability of Strength of European Spruce - A Ranta-Maunus, J K Denzler
- 42-6-2 Impact Loaded Structural Timber Elements Made from Swiss Grown Norway Spruce - R Widmann, R Steiger
- 42-6-3 Modelling the Bending Strength of Timber Components –Implications to Test Standards - J Köhler, M Sandomeer, T Isaksson, B Källsner
- 43-6-1 The Bearing Strength of Timber Beams on Discrete Supports - A Jorissen, B de Leijer, A Leijten
- 44-6-1 Impact of Material Properties on the Fracture Mechanics Design Approach for Notched Beams in Eurocode 5 - R Jockwer, R Steiger, A Frangi, J Köhler
- 44-6-2 Interaction of Shear Stresses and Stresses Perpendicular to the Grain - R Steiger, E Gehri

#### TIMBER JOINTS AND FASTENERS

- 1-7-1 Mechanical Fasteners and Fastenings in Timber Structures - E G Stern
- 4-7-1 Proposal for a Basic Test Method for the Evaluation of Structural Timber Joints with Mechanical Fasteners and Connectors - RILEM 3TT Committee
- 4-7-2 Test Methods for Wood Fasteners - K Möhler
- 5-7-1 Influence of Loading Procedure on Strength and Slip-Behaviour in Testing Timber Joints - K Möhler
- 5-7-2 Recommendations for Testing Methods for Joints with Mechanical Fasteners and Connectors in Load-Bearing Timber Structures - RILEM 3 TT Committee
- 5-7-3 CIB-Recommendations for the Evaluation of Results of Tests on Joints with Mechanical Fasteners and Connectors used in Load-Bearing Timber Structures - J Kuipers
- 6-7-1 Recommendations for Testing Methods for Joints with Mechanical Fasteners and Connectors in Load-Bearing Timber Structures (seventh draft) - RILEM 3 TT Committee
- 6-7-2 Proposal for Testing Integral Nail Plates as Timber Joints - K Möhler
- 6-7-3 Rules for Evaluation of Values of Strength and Deformation from Test Results - Mechanical Timber Joints - M Johansen, J Kuipers, B Norén
- 6-7-4 Comments to Rules for Testing Timber Joints and Derivation of Characteristic Values for Rigidity and Strength - B Norén
- 7-7-1 Testing of Integral Nail Plates as Timber Joints - K Möhler
- 7-7-2 Long Duration Tests on Timber Joints - J Kuipers
- 7-7-3 Tests with Mechanically Jointed Beams with a Varying Spacing of Fasteners - K Möhler
- 7-100-1 CIB-Timber Code Chapter 5.3 Mechanical Fasteners;CIB-Timber Standard 06 and 07 - H J Larsen
- 9-7-1 Design of Truss Plate Joints - F J Keenan
- 9-7-2 Staples - K Möhler
- 11-7-1 A Draft Proposal for International Standard: ISO Document ISO/TC 165N 38E
- 12-7-1 Load-Carrying Capacity and Deformation Characteristics of Nailed Joints - J Ehlbeck
- 12-7-2 Design of Bolted Joints - H J Larsen
- 12-7-3 Design of Joints with Nail Plates - B Norén

- 13-7-1 Polish Standard BN-80/7159-04: Parts 00-01-02-03-04-05.  
"Structures from Wood and Wood-based Materials. Methods of Test and Strength Criteria for Joints with Mechanical Fasteners"
- 13-7-2 Investigation of the Effect of Number of Nails in a Joint on its Load Carrying Ability - W Nozynski
- 13-7-3 International Acceptance of Manufacture, Marking and Control of Finger-jointed Structural Timber - B Norén
- 13-7-4 Design of Joints with Nail Plates - Calculation of Slip - B Norén
- 13-7-5 Design of Joints with Nail Plates - The Heel Joint - B Källsner
- 13-7-6 Nail Deflection Data for Design - H J Burgess
- 13-7-7 Test on Bolted Joints - P Vermeyden
- 13-7-8 Comments to paper CIB-W18/12-7-3 "Design of Joints with Nail Plates"-  
B Norén
- 13-7-9 Strength of Finger Joints - H J Larsen
- 13-100-4 CIB Structural Timber Design Code. Proposal for Section 6.1.5 Nail Plates -  
N I Bovim
- 14-7-1 Design of Joints with Nail Plates (second edition) - B Norén
- 14-7-2 Method of Testing Nails in Wood (second draft, August 1980) - B Norén
- 14-7-3 Load-Slip Relationship of Nailed Joints - J Ehlbeck and H J Larsen
- 14-7-4 Wood Failure in Joints with Nail Plates - B Norén
- 14-7-5 The Effect of Support Eccentricity on the Design of W- and WW-Trussed with Nail Plate Connectors - B Källsner
- 14-7-6 Derivation of the Allowable Load in Case of Nail Plate Joints Perpendicular to Grain - K Möhler
- 14-7-7 Comments on CIB-W18/14-7-1 - T A C M van der Put
- 15-7-1 Final Recommendation TT-1A: Testing Methods for Joints with Mechanical Fasteners in Load-Bearing Timber Structures. Annex A Punched Metal Plate Fasteners - Joint Committee RILEM/CIB-3TT
- 16-7-1 Load Carrying Capacity of Dowels - E Gehri
- 16-7-2 Bolted Timber Joints: A Literature Survey - N Harding
- 16-7-3 Bolted Timber Joints: Practical Aspects of Construction and Design; a Survey -  
N Harding
- 16-7-4 Bolted Timber Joints: Draft Experimental Work Plan - Building Research Association of  
New Zealand
- 17-7-1 Mechanical Properties of Nails and their Influence on Mechanical Properties of Nailed  
Timber Joints Subjected to Lateral Loads - I Smith, L R J Whale,  
C Anderson and L Held
- 17-7-2 Notes on the Effective Number of Dowels and Nails in Timber Joints - G Steck
- 18-7-1 Model Specification for Driven Fasteners for Assembly of Pallets and Related Structures  
- E G Stern and W B Wallin
- 18-7-2 The Influence of the Orientation of Mechanical Joints on their Mechanical Properties - I  
Smith and L R J Whale
- 18-7-3 Influence of Number of Rows of Fasteners or Connectors upon the Ultimate Capacity of  
Axially Loaded Timber Joints - I Smith and G Steck
- 18-7-4 A Detailed Testing Method for Nailplate Joints - J Kangas
- 18-7-5 Principles for Design Values of Nailplates in Finland - J Kangas

- 18-7-6 The Strength of Nailplates - N I Bovim and E Aasheim
- 19-7-1 Behaviour of Nailed and Bolted Joints under Short-Term Lateral Load - Conclusions from Some Recent Research - L R J Whale, I Smith and B O Hilson
- 19-7-2 Glued Bolts in Glulam - H Riberholt
- 19-7-3 Effectiveness of Multiple Fastener Joints According to National Codes and Eurocode 5 (Draft) - G Steck
- 19-7-4 The Prediction of the Long-Term Load Carrying Capacity of Joints in Wood Structures - Y M Ivanov and Y Y Slavic
- 19-7-5 Slip in Joints under Long-Term Loading - T Feldborg and M Johansen
- 19-7-6 The Derivation of Design Clauses for Nailed and Bolted Joints in Eurocode 5 - L R J Whale and I Smith
- 19-7-7 Design of Joints with Nail Plates - Principles - B Norén
- 19-7-8 Shear Tests for Nail Plates - B Norén
- 19-7-9 Advances in Technology of Joints for Laminated Timber - Analyses of the Structural Behaviour - M Piazza and G Turrini
- 19-15-1 Connections Deformability in Timber Structures: A Theoretical Evaluation of its Influence on Seismic Effects - A Ceccotti and A Vignoli
- 20-7-1 Design of Nailed and Bolted Joints-Proposals for the Revision of Existing Formulae in Draft Eurocode 5 and the CIB Code - L R J Whale, I Smith and H J Larsen
- 20-7-2 Slip in Joints under Long Term Loading - T Feldborg and M Johansen
- 20-7-3 Ultimate Properties of Bolted Joints in Glued-Laminated Timber - M Yasumura, T Murota and H Sakai
- 20-7-4 Modelling the Load-Deformation Behaviour of Connections with Pin-Type Fasteners under Combined Moment, Thrust and Shear Forces - I Smith
- 21-7-1 Nails under Long-Term Withdrawal Loading - T Feldborg and M Johansen
- 21-7-2 Glued Bolts in Glulam-Proposals for CIB Code - H Riberholt
- 21-7-3 Nail Plate Joint Behaviour under Shear Loading - T Poutanen
- 21-7-4 Design of Joints with Laterally Loaded Dowels. Proposals for Improving the Design Rules in the CIB Code and the Draft Eurocode 5 - J Ehlbeck and H Werner
- 21-7-5 Axially Loaded Nails: Proposals for a Supplement to the CIB Code - J Ehlbeck and W Siebert
- 22-7-1 End Grain Connections with Laterally Loaded Steel Bolts A draft proposal for design rules in the CIB Code - J Ehlbeck and M Gerold
- 22-7-2 Determination of Perpendicular-to-Grain Tensile Stresses in Joints with Dowel-Type Fasteners - A draft proposal for design rules - J Ehlbeck, R Görlacher and H Werner
- 22-7-3 Design of Double-Shear Joints with Non-Metallic Dowels A proposal for a supplement of the design concept - J Ehlbeck and O Eberhart
- 22-7-4 The Effect of Load on Strength of Timber Joints at high Working Load Level - A J M Leijten
- 22-7-5 Plasticity Requirements for Portal Frame Corners - R Gunnewijk and A J M Leijten
- 22-7-6 Background Information on Design of Glulam Rivet Connections in CSA/CAN3-086.1-M89 - A proposal for a supplement of the design concept - E Karacabeyli and D P Janssens

- 22-7-7 Mechanical Properties of Joints in Glued-Laminated Beams under Reversed Cyclic Loading - M Yasumura
- 22-7-8 Strength of Glued Lap Timber Joints - P Glos and H Horstmann
- 22-7-9 Toothed Rings Type Bistyp 075 at the Joints of Fir Wood - J Kerste
- 22-7-10 Calculation of Joints and Fastenings as Compared with the International State - K Zimmer and K Lissner
- 22-7-11 Joints on Glued-in Steel Bars Present Relatively New and Progressive Solution in Terms of Timber Structure Design - G N Zubarev, F A Boitemirov and V M Golovina
- 22-7-12 The Development of Design Codes for Timber Structures made of Compositive Bars with Plate Joints based on Cylindrical Nails - Y V Piskunov
- 22-7-13 Designing of Glued Wood Structures Joints on Glued-in Bars - S B Turkovsky
- 23-7-1 Proposal for a Design Code for Nail Plates - E Aasheim and K H Solli
- 23-7-2 Load Distribution in Nailed Joints - H J Blass
- 24-7-1 Theoretical and Experimental Tension and Shear Capacity of Nail Plate Connections - B Källsner and J Kangas
- 24-7-2 Testing Method and Determination of Basic Working Loads for Timber Joints with Mechanical Fasteners - Y Hirashima and F Kamiya
- 24-7-3 Anchorage Capacity of Nail Plate - J Kangas
- 25-7-2 Softwood and Hardwood Embedding Strength for Dowel type Fasteners - J Ehlbeck and H Werner
- 25-7-4 A Guide for Application of Quality Indexes for Driven Fasteners Used in Connections in Wood Structures - E G Stern
- 25-7-5 35 Years of Experience with Certain Types of Connectors and Connector Plates Used for the Assembly of Wood Structures and their Components- E G Stern
- 25-7-6 Characteristic Strength of Split-ring and Shear-plate Connections - H J Blass, J Ehlbeck and M Schlager
- 25-7-7 Characteristic Strength of Tooth-plate Connector Joints - H J Blass, J Ehlbeck and M Schlager
- 25-7-8 Extending Yield Theory to Screw Connections - T E McLain
- 25-7-9 Determination of  $k_{def}$  for Nailed Joints - J W G van de Kuilen
- 25-7-10 Characteristic Strength of UK Timber Connectors - A V Page and C J Mettem
- 25-7-11 Multiple-fastener Dowel-type Joints, a Selected Review of Research and Codes - C J Mettem and A V Page
- 25-7-12 Load Distributions in Multiple-fastener Bolted Joints in European Whitewood Glulam, with Steel Side Plates - C J Mettem and A V Page
- 26-7-1 Proposed Test Method for Dynamic Properties of Connections Assembled with Mechanical Fasteners - J D Dolan
- 26-7-2 Validatory Tests and Proposed Design Formulae for the Load-Carrying Capacity of Toothed-Plate Connected Joints - C J Mettem, A V Page and G Davis
- 26-7-3 Definitions of Terms and Multi-Language Terminology Pertaining to Metal Connector Plates - E G Stern
- 26-7-4 Design of Joints Based on in V-Shape Glued-in Rods - J Kangas
- 26-7-5 Tests on Timber Concrete Composite Structural Elements (TCCs) - A U Meierhofer
- 27-7-1 Glulam Arch Bridge and Design of it's Moment-Resisting Joints - K Komatsu and S Usuku

- 27-7-2 Characteristic Load - Carrying Capacity of Joints with Dowel - type Fasteners in Regard to the System Properties - H Werner
- 27-7-3 Steel Failure Design in Truss Plate Joints - T Poutanen
- 28-7-1 Expanded Tube Joint in Locally DP Reinforced Timber - A J M Leijten, P Ragupathy and K S Virdi
- 28-7-2 A Strength and Stiffness Model for the Expanded Tube Joint - A J M Leijten
- 28-7-3 Load-carrying Capacity of Steel-to Timber Joints with Annular Ring Shanked Nails. A Comparison with the EC5 Design Method - R Görlacher
- 28-7-4 Dynamic Effects on Metal-Plate Connected Wood Truss Joints - S Kent, R Gupta and T Miller
- 28-7-5 Failure of the Timber Bolted Joints Subjected to Lateral Load Perpendicular to Grain - M Yasumura and L Daudeville
- 28-7-6 Design Procedure for Locally Reinforced Joints with Dowel-type Fasteners - H Werner
- 28-7-7 Variability and Effects of Moisture Content on the Withdrawal Characteristics for Lumber as Opposed to Clear Wood - J D Dolan and J W Stelmokas
- 28-7-8 Nail Plate Capacity in Joint Line - A Kevarinmäki and J Kangas
- 28-7-9 Axial Strength of Glued-In Bolts - Calculation Model Based on Non-Linear Fracture Mechanics - A Preliminary Study - C J Johansson, E Serrano, P J Gustafsson and B Enquist
- 28-7-10 Cyclic Lateral Dowel Connection Tests for seismic and Wind Evaluation - J D Dolan
- 29-7-1 A Simple Method for Lateral Load-Carrying Capacity of Dowel-Type Fasteners - J Kangas and J Kurkela
- 29-7-2 Nail Plate Joint Behaviour at Low Versus High Load Level - T Poutanen
- 29-7-3 The Moment Resistance of Tee and Butt - Joint Nail Plate Test Specimens - A Comparison with Current Design Methods - A Reffold, L R J Whale and B S Choo
- 29-7-4 A Critical Review of the Moment Rotation Test Method Proposed in prEN 1075 - M Bettison, B S Choo and L R J Whale
- 29-7-5 Explanation of the Translation and Rotation Behaviour of Prestressed Moment Timber Joints - A J M Leijten
- 29-7-6 Design of Joints and Frame Corners using Dowel-Type Fasteners - E Gehri
- 29-7-7 Quasi-Static Reversed-Cyclic Testing of Nailed Joints - E Karacabeyli and A Ceccotti
- 29-7-8 Failure of Bolted Joints Loaded Parallel to the Grain: Experiment and Simulation - L Davenne, L Daudeville and M Yasumura
- 30-7-1 Flexural Behaviour of GLT Beams End-Jointed by Glued-in Hardwood Dowels - K Komatsu, A Koizumi, J Jensen, T Sasaki and Y Iijima
- 30-7-2 Modelling of the Block Tearing Failure in Nailed Steel-to-Timber Joints - J Kangas, K Aalto and A Kevarinmäki
- 30-7-3 Cyclic Testing of Joints with Dowels and Slotted-in Steel Plates - E Aasheim
- 30-7-4 A Steel-to-Timber Dowelled Joint of High Performance in Combination with a High Strength Wood Composite (Parallam) - E Gehri
- 30-7-5 Multiple Fastener Timber Connections with Dowel Type Fasteners - A Jorissen
- 30-7-6 Influence of Ductility on Load-Carrying Capacity of Joints with Dowel-Type Fasteners - A Mischler

- 31-7-1 Mechanical Properties of Dowel Type Joints under Reversed Cyclic Lateral Loading - M Yasumura
- 31-7-2 Design of Joints with Laterally Loaded Dowels - A Mischler
- 31-7-3 Flexural Behaviour of Glulam Beams Edge-Jointed by Lagscrews with Steel Splice Plates - K Komatsu
- 31-7-4 Design on Timber Capacity in Nailed Steel-to-Timber Joints - J Kangas and J Vesa
- 31-7-5 Timber Contact in Chord Splices of Nail Plate Structures - A Kevarinmäki
- 31-7-6 The Fastener Yield Strength in Bending - A Jorissen and H J Blaß
- 31-7-7 A Proposal for Simplification of Johansen`s Formulae, Dealing With the Design of Dowelled-Type Fasteners - F Rouger
- 31-7-8 Simplified Design of Connections with Dowel-type fasteners - H J Blaß and J Ehlbeck
- 32-7-1 Behaviour of Wood-Steel-Wood Bolted Glulam Connections - M Mohammad and J H P Quenneville
- 32-7-2 A new set of experimental tests on beams loaded perpendicular-to-grain by dowel-type joints- M Ballerini
- 32-7-3 Design and Analysis of Bolted Timber Joints under Lateral Force Perpendicular to Grain - M Yasumura and L Daudeville
- 32-7-4 Predicting Capacities of Joints with Laterally Loaded Nails - I Smith and P Quenneville
- 32-7-5 Strength Reduction Rules for Multiple Fastener Joints - A Mischler and E Gehri
- 32-7-6 The Stiffness of Multiple Bolted Connections - A Jorissen
- 32-7-7 Concentric Loading Tests on Girder Truss Components - T N Reynolds, A Reffold, V Enjily and L Whale
- 32-7-8 Dowel Type Connections with Slotted-In Steel Plates - M U Pedersen, C O Clorius, L Damkilde, P Hoffmeyer and L Esklidsen
- 32-7-9 Creep of Nail Plate Reinforced Bolt Joints - J Vesa and A Kevarinmäki
- 32-7-10 The Behaviour of Timber Joints with Ring Connectors - E Gehri and A Mischler
- 32-7-11 Non-Metallic, Adhesiveless Joints for Timber Structures - R D Drake, M P Ansell, C J Mettem and R Bainbridge
- 32-7-12 Effect of Spacing and Edge Distance on the Axial Strength of Glued-in Rods - H J Blaß and B Laskewitz
- 32-7-13 Evaluation of Material Combinations for Bonded in Rods to Achieve Improved Timber Connections - C J Mettem, R J Bainbridge, K Harvey, M P Ansell, J G Broughton and A R Hutchinson
- 33-7-1 Determination of Yield Strength and Ultimate Strength of Dowel-Type Timber Joints – M Yasumura and K Sawata
- 33-7-2 Lateral Shear Capacity of Nailed Joints – U Korin
- 33-7-3 Height-Adjustable Connector for Composite Beams – Y V Piskunov and E G Stern
- 33-7-4 Engineering Ductility Assessment for a Nailed Slotted-In Steel Connection in Glulam– L Stehn and H Johansson
- 33-7-5 Effective Bending Capacity of Dowel-Type Fasteners - H J Blaß, A Bienhaus and V Krämer
- 33-7-6 Load-Carrying Capacity of Joints with Dowel-Type Fasteners and Interlayers - H J Blaß and B Laskewitz
- 33-7-7 Evaluation of Perpendicular to Grain Failure of Beams caused by Concentrated Loads of Joints – A J M Leijten and T A C M van der Put

- 33-7-8 Test Methods for Glued-In Rods for Timber Structures – C Bengtsson and C J Johansson
- 33-7-9 Stiffness Analysis of Nail Plates – P Ellegaard
- 33-7-10 Capacity, Fire Resistance and Gluing Pattern of the Rods in V-Connections – J Kangas
- 33-7-11 Bonded-In Pultrusions for Moment-Resisting Timber Connections – K Harvey, M P Ansell, C J Mettem, R J Bainbridge and N Alexandre
- 33-7-12 Fatigue Performance of Bonded-In Rods in Glulam, Using Three Adhesive Types - R J Bainbridge, K Harvey, C J Mettem and M P Ansell
- 34-7-1 Splitting Strength of Beams Loaded by Connections Perpendicular to Grain, Model Validation – A J M Leijten, A Jorissen
- 34-7-2 Numerical LEFM analyses for the evaluation of failure loads of beams loaded perpendicular-to-grain by single-dowel connections – M Ballerini, R Bezzi
- 34-7-3 Dowel joints loaded perpendicular to grain - H J Larsen, P J Gustafsson
- 34-7-4 Quality Control of Connections based on in V-shape glued-in Steel Rods – J Kangas, A Kevarinmäki
- 34-7-5 Testing Connector Types for Laminated-Timber-Concrete Composite Elements – M Grosse, S Lehmann, K Rautenstrauch
- 34-7-6 Behaviour of Axially Loaded Glued-in Rods - Requirements and Resistance, Especially for Spruce Timber Perpendicular to the Grain Direction – A Bernasconi
- 34-7-7 Embedding characteristics on fibre reinforcement and densified timber joints - P Haller, J Wehsener, T Birk
- 34-7-8 GIROD – Glued-in Rods for Timber Structures – C Bengtsson, C-J Johansson
- 34-7-9 Criteria for Damage and Failure of Dowel-Type Joints Subjected to Force Perpendicular to the Grain – M Yasumura
- 34-7-10 Interaction Between Splitting and Block Shear Failure of Joints – A J M Leijten, A Jorissen, J Kuipers
- 34-7-11 Limit states design of dowel-fastener joints – Placement of modification factors and partial factors, and calculation of variability in resistance – I Smith, G Foliente
- 34-7-12 Design and Modelling of Knee Joints - J Nielsen, P Ellegaard
- 34-7-13 Timber-Steel Shot Fired Nail Connections at Ultimate Limit States - R J Bainbridge, P Larsen, C J Mettem, P Alam, M P Ansell
- 35-7-1 New Estimating Method of Bolted Cross-lapped Joints with Timber Side Members - M Noguchi, K Komatsu
- 35-7-2 Analysis on Multiple Lag Screwed Timber Joints with Timber Side Members - K Komatsu, S Takino, M Nakatani, H Tateishi
- 35-7-3 Joints with Inclined Screws - A Kevarinmäki
- 35-7-4 Joints with Inclined Screws - I Bejtka, H J Blaß
- 35-7-5 Effect of distances, Spacing and Number of Dowels in a Row on the Load Carrying Capacity of Connections with Dowels failing by Splitting - M Schmid, R Frasson, H J Blaß
- 35-7-6 Effect of Row Spacing on the Capacity of Bolted Timber Connections Loaded Perpendicular-to-grain - P Quenneville, M Kasim
- 35-7-7 Splitting Strength of Beams Loaded by Connections, Model Comparison - A J M Leijten
- 35-7-8 Load-Carrying Capacity of Perpendicular to the Grain Loaded Timber Joints with Multiple Fasteners - O Borth, K U Schober, K Rautenstrauch
- 35-7-9 Determination of fracture parameter for dowel-type joints loaded perpendicular to wooden grain and its application - M Yasumura

- 35-7-10 Analysis and Design of Modified Attic Trusses with Punched Metal Plate Fasteners - P Ellegaard
- 35-7-11 Joint Properties of Plybamboo Sheets in Prefabricated Housing - G E Gonzalez
- 35-7-12 Fiber-Reinforced Beam-to-Column Connections for Seismic Applications - B Kasal, A Heiduschke, P Haller
- 36-7-1 Shear Tests in Timber-LWAC with Screw-Type Connections - L Jorge, H Cruz, S Lopes
- 36-7-2 Plug Shear Failure in Nailed Timber Connections: Experimental Studies - H Johnsson
- 36-7-3 Nail-Laminated Timber Elements in Natural Surface-Composite with Mineral Bound Layer - S Lehmann, K Rautenstrauch
- 36-7-4 Mechanical Properties of Timber-Concrete Joints Made With Steel Dowels - A Dias, J W G van de Kuilen, H Cruz
- 36-7-5 Comparison of Hysteresis Responses of Different Sheating to Framing Joints - B Dujič, R Zarnić
- 36-7-6 Evaluation and Estimation of the Performance of the Nail Joints and Shear Walls under Dry/Humid Cyclic Climate - S Nakajima
- 36-7-7 Beams Transversally Loaded by Dowel-Type Joints: Influence on Splitting Strength of Beam Thickness and Dowel Size - M Ballerini, A Giovanella
- 36-7-8 Splitting Strength of Beams Loaded by Connections - J L Jensen
- 36-7-9 A Tensile Fracture Model for Joints with Rods or Dowels loaded Perpendicular-to-Grain - J L Jensen, P J Gustafsson, H J Larsen
- 36-7-10 A Numerical Model to Simulate the Load-Displacement Time-History of Multiple-Bolt Connections Subjected to Various Loadings - C P Heine, J D Dolan
- 36-7-11 Reliability of Timber Structures, Theory and Dowel-Type Connection Failures - A Ranta-Maunus, A Kevarinmäki
- 37-7-1 Development of the "Displaced Volume Model" to Predict Failure for Multiple-Bolt Timber Joints - D M Carradine, J D Dolan, C P Heine
- 37-7-2 Mechanical Models of the Knee Joints with Cross-Lapped Glued Joints and Glued in Steel Rods - M Noguchi, K Komatsu
- 37-7-3 Simplification of the Neural Network Model for Predicting the Load-Carrying Capacity of Dowel-Type Connections - A Cointe, F Rouger
- 37-7-4 Bolted Wood Connections Loaded Perpendicular-to-Grain- A Proposed Design Approach - M C G Lehoux, J H P Quenneville
- 37-7-5 A New Prediction Formula for the Splitting Strength of Beams Loaded by Dowel Type Connections - M Ballerini
- 37-7-6 Plug Shear Failure: The Tensile Failure Mode and the Effect of Spacing - H Johnsson
- 37-7-7 Block Shear Failure Test with Dowel-Type Connection in Diagonal LVL Structure - M Kairi
- 37-7-8 Glued-in Steel Rods: A Design Approach for Axially Loaded Single Rods Set Parallel to the Grain - R Steiger, E Gehri, R Widmann
- 37-7-9 Glued in Rods in Load Bearing Timber Structures - Status regarding European Standards for Test Procedures - B Källander
- 37-7-10 French Data Concerning Glued-in Rods - C Faye, L Le Magorou, P Morlier, J Surleau
- 37-7-11 Enhancement of Dowel-Type Fasteners by Glued Connectors - C O Clorius, A Højman
- 37-7-12 Review of Probability Data for Timber Connections with Dowel-Type Fasteners - A J M Leijten, J Köhler, A Jorissen
- 37-7-13 Behaviour of Fasteners and Glued-in Rods Produced From Stainless Steel - A Kevarinmäki

- 37-7-14 Dowel joints in Engineered Wood Products: Assessment of Simple Fracture Mechanics Models - M Snow, I Smith, A Asiz
- 37-7-15 Numerical Modelling of Timber and Connection Elements Used in Timber-Concrete-Composite Constructions - M Grosse, K Rautenstrauch
- 38-7-1 A Numerical Investigation on the Splitting Strength of Beams Loaded Perpendicular-to-grain by Multiple-dowel Connections – M Ballerini, M Rizzi
- 38-7-2 A Probabilistic Framework for the Reliability Assessment of Connections with Dowel Type Fasteners - J Köhler
- 38-7-3 Load Carrying Capacity of Curved Glulam Beams Reinforced with self-tapping Screws - J Jönsson, S Thelandersson
- 38-7-4 Self-tapping Screws as Reinforcements in Connections with Dowel-Type Fasteners- I Bejtka, H J Blaß
- 38-7-5 The Yield Capacity of Dowel Type Fasteners - A Jorissen, A Leijten
- 38-7-6 Nails in Spruce - Splitting Sensitivity, End Grain Joints and Withdrawal Strength - A Kevarinmäki
- 38-7-7 Design of Timber Connections with Slotted-in Steel Plates and Small Diameter Steel Tube Fasteners - B Murty, I Smith, A Asiz
- 39-7-1 Effective in-row Capacity of Multiple-Fastener Connections - P Quenneville, M Bickerdike
- 39-7-2 Self-tapping Screws as Reinforcements in Beam Supports - I Bejtka, H J Blaß
- 39-7-3 Connectors for Timber-concrete Composite-Bridges - A Döhrer, K Rautenstrauch
- 39-7-4 Block Shear Failure at Dowelled Double Shear Steel-to-timber Connections - A Hanhijärvi, A Kevarinmäki, R Yli-Koski
- 39-7-5 Load Carrying Capacity of Joints with Dowel Type Fasteners in Solid Wood Panels - T Uibel, H J Blaß
- 39-7-6 Generalised Canadian Approach for Design of Connections with Dowel Fasteners - P Quenneville, I Smith, A Asiz, M Snow, Y H Chui
- 40-7-1 Predicting the Strength of Bolted Timber Connections Subjected to Fire - M Fragiaco, A Buchanan, D Carshalton, P Moss, C Austruy
- 40-7-2 Edge Joints with Dowel Type Fasteners in Cross Laminated Timber - H J Blaß, T Uibel
- 40-7-3 Design Method against Timber Failure Mechanisms of Dowelled Steel-to-Timber Connections - A Hanhijärvi, A Kevarinmäki
- 40-7-4 A EYM Based Simplified Design Formula for the Load-carrying Capacity of Dowel-type Connections - M Ballerini
- 40-7-5 Evaluation of the Slip Modulus for Ultimate Limit State Verifications of Timber-Concrete Composite Structures - E Lukaszewska, M Fragiaco, A Frangi
- 40-7-6 Models for the Predictions of the Ductile and Brittle Failure Modes (Parallel-to-Grain) of Timber Rivet Connections - M Marjerrison, P Quenneville
- 40-7-7 Creep of Timber and Timber-Concrete Joints. - J W G van de Kuilen, A M P G Dias
- 40-7-8 Lag Screwed Timber Joints with Timber Side Members- K Komatsu, S Takino, H Tateishi
- 41-7-1 Applicability of Existing Design Approaches to Mechanical Joints in Structural Composite Lumber - M Snow, I Smith, A Asiz, M Ballerini
- 41-7-2 Validation of the Canadian Bolted Connection Design Proposal - P Quenneville, J Jensen
- 41-7-3 Ductility of Moment Resisting Dowelled Joints in Heavy Timber Structures - A Polastri, R Tomasi, M Piazza, I Smith

- 41-7-4 Mechanical Behaviour of Traditional Timber Connections: Proposals for Design, Based on Experimental and Numerical Investigations. Part I: Birdsmouth - C Faye, P Garcia, L Le Magorou, F Rouger
- 41-7-5 Embedding Strength of European Hardwoods - U Hübner, T Bogensperger, G Schickhofer
- 42-7-1 Base Parameters of Self-tapping Screws - G Pirnbacher, R Brandner, G Schickhofer
- 42-7-2 Joints with Inclined Screws and Steel Plates as Outer Members - H Krenn, G Schickhofer
- 42-7-3 Models for the Calculation of the Withdrawal Capacity of Self-tapping Screws - M Frese, H J Blaß
- 42-7-4 Embedding Strength of New Zealand Timber and Recommendation for the NZ Standard - S Franke, P Quenneville
- 42-7-5 Load Carrying Capacity of Timber-Wood Fiber Insulation Board – Joints with Dowel Type Fasteners - G Gebhardt, H J Blaß
- 42-7-6 Prediction of the Fatigue Resistance of Timber-Concrete-Composite Connections - U Kuhlmann, P Aldi
- 42-7-7 Using Screws for Structural Applications in Laminated Veneer Lumber - D M Carradine, M P Newcombe, A H Buchanan
- 42-7-8 Influence of Fastener Spacings on Joint Performance - Experimental Results and Codification - E Gehri
- 42-7-9 Connections with Glued-in Hardwood Rods Subjected to Combined Bending and Shear Actions - J L Jensen, P Quenneville
- 43-7-1 Probabilistic Capacity Prediction of Timber Joints under Brittle Failure Modes - T Tannert, T Vallée, and F Lam
- 43-7-2 Ductility in Timber Structures - A Jorissen, M Fragiacomio
- 43-7-3 Design of Mechanically Jointed Concrete-Timber Beams Taking into Account the Plastic Behaviour of the Fasteners - H J Larsen, H Riberholt, A Ceccotti
- 43-7-4 Design of Timber-Concrete Composite Beams with Notched Connections - M Fragiacomio, D Yeoh
- 43-7-5 Development of Design Procedures for Timber Concrete Composite Floors in Australia and New Zealand - K Crews, C Gerber
- 43-7-6 Failure Behaviour and Resistance of Dowel-Type Connections Loaded Perpendicular to Grain - B Franke, P Quenneville
- 43-7-7 Predicting Time Dependent Effects in Unbonded Post-Tensioned Timber Beams and Frames - S Giorgini, A Neale, A Palermo, D Carradine, S Pampanin, A H Buchanan
- 43-7-8 Simplified Design of Post-tensioned Timber Frames - M Newcombe, M Cusieli, S Pampanin, A Palermo, A H Buchanan
- 44-7-1 Pull-through Capacity in Plywood and OSB - J Munch-Andersen, J D Sørensen
- 44-7-2 Design Concept for CLT - Reinforced with Self-Tapping Screws - P Mestek, H Kreuzinger, S Winter
- 44-7-3 Fatigue Behaviour of the Stud Connector Used for Timber-Concrete Composite Bridges – K Rautenstrauch, J Mueller
- 44-7-4 The Stiffness of Beam to Column Connections in Post-Tensioned Timber Frames – T Smith, W van Beerschoten, A Palermo, S Pampanin, F C Ponzo
- 44-7-5 Design Approach for the Splitting Failure of Dowel-Type Connections Loaded Perpendicular to Grain - Bettina Franke, Pierre Quenneville
- 45-7-1 A Stiffness-based Analytical Model for Wood Strength in Timber Connections loaded Parallel to Grain: Riveted Joint Capacity in Brittle and Mixed Failure - P Zarnani, P Quenneville

- 45-7-2 Beams Loaded Perpendicular to Grain by Connections – Combined Effect of Edge and End Distance - J L Jensen, P Quenneville, U A Girhammar, B Källsner
- 45-7-3 L Block Failure of Dowelled Connections Subject to Bending Reinforced with Threaded Rods - J-F Bocquet, C Barthram, A Pineur
- 45-7-4 Block Shear Failure of Wooden Dowel Connections - G Stapf, S Aicher, N Zisi
- 45-7-5 Requirements on Ductility in Timber Structures - F Brühl, U Kuhlmann

#### LOAD SHARING

- 3-8-1 Load Sharing - An Investigation on the State of Research and Development of Design Criteria - E Levin
- 4-8-1 A Review of Load-Sharing in Theory and Practice - E Levin
- 4-8-2 Load Sharing - B Norén
- 19-8-1 Predicting the Natural Frequencies of Light-Weight Wooden Floors - I Smith and Y H Chui
- 20-8-1 Proposed Code Requirements for Vibrational Serviceability of Timber Floors - Y H Chui and I Smith
- 21-8-1 An Addendum to Paper 20-8-1 - Proposed Code Requirements for Vibrational Serviceability of Timber Floors - Y H Chui and I Smith
- 21-8-2 Floor Vibrational Serviceability and the CIB Model Code - S Ohlsson
- 22-8-1 Reliability Analysis of Viscoelastic Floors - F Rouger, J D Barrett and R O Foschi
- 24-8-1 On the Possibility of Applying Neutral Vibrational Serviceability Criteria to Joisted Wood Floors - I Smith and Y H Chui
- 25-8-1 Analysis of Glulam Semi-rigid Portal Frames under Long-term Load - K Komatsu and N Kawamoto
- 34-8-1 System Effect in Sheathed Parallel Timber Beam Structures – M Hansson, T Isaksson
- 35-8-1 System Effects in Sheathed Parallel Timber Beam Structures part II. - M Hansson, T Isaksson
- 39-8-1 Overview of a new Canadian Approach to Handling System Effects in Timber Structures - I Smith, Y H Chui, P Quenneville

#### DURATION OF LOAD

- 3-9-1 Definitions of Long Term Loading for the Code of Practice - B Norén
- 4-9-1 Long Term Loading of Trussed Rafters with Different Connection Systems - T Feldborg and M Johansen
- 5-9-1 Strength of a Wood Column in Combined Compression and Bending with Respect to Creep - B Källsner and B Norén
- 6-9-1 Long Term Loading for the Code of Practice (Part 2) - B Norén
- 6-9-2 Long Term Loading - K Möhler
- 6-9-3 Deflection of Trussed Rafters under Alternating Loading during a Year - T Feldborg and M Johansen
- 7-6-1 Strength and Long Term Behaviour of Lumber and Glued-Laminated Timber under Torsion Loads - K Möhler
- 7-9-1 Code Rules Concerning Strength and Loading Time - H J Larsen and E Theilgaard
- 17-9-1 On the Long-Term Carrying Capacity of Wood Structures - Y M Ivanov and Y Y Slavic

- 18-9-1 Prediction of Creep Deformations of Joints - J Kuipers
- 19-9-1 Another Look at Three Duration of Load Models - R O Foschi and Z C Yao
- 19-9-2 Duration of Load Effects for Spruce Timber with Special Reference to Moisture Influence - A Status Report - P Hoffmeyer
- 19-9-3 A Model of Deformation and Damage Processes Based on the Reaction Kinetics of Bond Exchange - T A C M van der Put
- 19-9-4 Non-Linear Creep Superposition - U Korin
- 19-9-5 Determination of Creep Data for the Component Parts of Stressed-Skin Panels - R Kliger
- 19-9-6 Creep an Lifetime of Timber Loaded in Tension and Compression - P Glos
- 19-1-1 Duration of Load Effects and Reliability Based Design (Single Member) - R O Foschi and Z C Yao
- 19-6-1 Effect of Age and/or Load on Timber Strength - J Kuipers
- 19-7-4 The Prediction of the Long-Term Load Carrying Capacity of Joints in Wood Structures - Y M Ivanov and Y Y Slavic
- 19-7-5 Slip in Joints under Long-Term Loading - T Feldborg and M Johansen
- 20-7-2 Slip in Joints under Long-Term Loading - T Feldborg and M Johansen
- 22-9-1 Long-Term Tests with Glued Laminated Timber Girders - M Badstube, W Rug and W Schöne
- 22-9-2 Strength of One-Layer solid and Lengthways Glued Elements of Wood Structures and its Alteration from Sustained Load - L M Kovaltchuk, I N Boitemirova and G B Uspenskaya
- 24-9-1 Long Term Bending Creep of Wood - T Toratti
- 24-9-2 Collection of Creep Data of Timber - A Ranta-Maunus
- 24-9-3 Deformation Modification Factors for Calculating Built-up Wood-Based Structures - I R Kliger
- 25-9-2 DVM Analysis of Wood. Lifetime, Residual Strength and Quality - L F Nielsen
- 26-9-1 Long Term Deformations in Wood Based Panels under Natural Climate Conditions. A Comparative Study - S Thelandersson, J Nordh, T Nordh and S Sandahl
- 28-9-1 Evaluation of Creep Behavior of Structural Lumber in Natural Environment - R Gupta and R Shen
- 30-9-1 DOL Effect in Tension Perpendicular to the Grain of Glulam Depending on Service Classes and Volume - S Aicher and G Dill-Langer
- 30-9-2 Damage Modelling of Glulam in Tension Perpendicular to Grain in Variable Climate - G Dill-Langer and S Aicher
- 31-9-1 Duration of Load Effect in Tension Perpendicular to Grain in Curved Glulam - A Ranta-Maunus
- 32-9-1 Bending-Stress-Redistribution Caused by Different Creep in Tension and Compression and Resulting DOL-Effect - P Becker and K Rautenstrauch
- 32-9-2 The Long Term Performance of Ply-Web Beams - R Grantham and V Enjily
- 36-9-1 Load Duration Factors for Instantaneous Loads - A J M Leijten, B Jansson
- 39-9-1 Simplified Approach for the Long-Term Behaviour of Timber-Concrete Composite Beams According to the Eurocode 5 Provisions - M Fragiaco, A Ceccotti

## TIMBER BEAMS

- 4-10-1 The Design of Simple Beams - H J Burgess
- 4-10-2 Calculation of Timber Beams Subjected to Bending and Normal Force - H J Larsen
- 5-10-1 The Design of Timber Beams - H J Larsen
- 9-10-1 The Distribution of Shear Stresses in Timber Beams - F J Keenan
- 9-10-2 Beams Notched at the Ends - K Möhler
- 11-10-1 Tapered Timber Beams - H Riberholt
- 13-6-2 Consideration of Size Effects in Longitudinal Shear Strength for Uncracked Beams - R O Foschi and J D Barrett
- 13-6-3 Consideration of Shear Strength on End-Cracked Beams - J D Barrett and R O Foschi
- 18-10-1 Submission to the CIB-W18 Committee on the Design of Ply Web Beams by Consideration of the Type of Stress in the Flanges - J A Baird
- 18-10-2 Longitudinal Shear Design of Glued Laminated Beams - R O Foschi
- 19-10-1 Possible Code Approaches to Lateral Buckling in Beams - H J Burgess
- 19-2-1 Creep Buckling Strength of Timber Beams and Columns - R H Leicester
- 20-2-1 Lateral Buckling Theory for Rectangular Section Deep Beam-Columns - H J Burgess
- 20-10-1 Draft Clause for CIB Code for Beams with Initial Imperfections - H J Burgess
- 20-10-2 Space Joists in Irish Timber - W J Robinson
- 20-10-3 Composite Structure of Timber Joists and Concrete Slab - T Poutanen
- 21-10-1 A Study of Strength of Notched Beams - P J Gustafsson
- 22-10-1 Design of Endnotched Beams - H J Larsen and P J Gustafsson
- 22-10-2 Dimensions of Wooden Flexural Members under Constant Loads - A Pozgai
- 22-10-3 Thin-Walled Wood-Based Flanges in Composite Beams - J König
- 22-10-4 The Calculation of Wooden Bars with flexible Joints in Accordance with the Polish Standart Code and Strict Theoretical Methods - Z Mielczarek
- 23-10-1 Tension Perpendicular to the Grain at Notches and Joints - T A C M van der Put
- 23-10-2 Dimensioning of Beams with Cracks, Notches and Holes. An Application of Fracture Mechanics - K Riipola
- 23-10-3 Size Factors for the Bending and Tension Strength of Structural Timber - J D Barret and A R Fewell
- 23-12-1 Bending Strength of Glulam Beams, a Design Proposal - J Ehlbeck and F Colling
- 23-12-3 Glulam Beams, Bending Strength in Relation to the Bending Strength of the Finger Joints - H Riberholt
- 24-10-1 Shear Strength of Continuous Beams - R H Leicester and F G Young
- 25-10-1 The Strength of Norwegian Glued Laminated Beams - K Solli, E Aasheim and R H Falk
- 25-10-2 The Influence of the Elastic Modulus on the Simulated Bending Strength of Hyperstatic Timber Beams - T D G Canisius
- 27-10-1 Determination of Shear Modulus - R Görlacher and J Kürth
- 29-10-1 Time Dependent Lateral Buckling of Timber Beams - F Rouger

- 29-10-2 Determination of Modulus of Elasticity in Bending According to EN 408 - K H Solli
- 29-10-3 On Determination of Modulus of Elasticity in Bending - L Boström, S Ormarsson and O Dahlblom
- 29-10-4 Relation of Moduli of Elasticity in Flatwise and Edgewise Bending of Solid Timber - C J Johansson, A Steffen and E W Wormuth
- 30-10-1 Nondestructive Evaluation of Wood-based Members and Structures with the Help of Modal Analysis - P Kuklik
- 30-10-2 Measurement of Modulus of Elasticity in Bending - L Boström
- 30-10-3 A Weak Zone Model for Timber in Bending - B Källsner, K Salmela and O Ditlevsen
- 30-10-4 Load Carrying Capacity of Timber Beams with Narrow Moment Peaks - T Isaksson and J Freysoldt
- 37-10-1 Design of Rim Boards for Use with I-Joists Framing Systems - B Yeh, T G Williamson
- 40-10-1 Extension of EC5 Annex B Formulas for the Design of Timber-concrete Composite Structures - J Schänzlin, M Fragiaco
- 40-10-2 Simplified Design Method for Mechanically Jointed Beams - U A Girhammar
- 41-10-1 Composite Action of I-Joist Floor Systems - T G Williamson, B Yeh
- 41-10-2 Evaluation of the Prestressing Losses in Timber Members Prestressed with Unbonded Tendons - M Fragiaco, M Davies
- 41-10-3 Relationship Between Global and Local MOE – J K Denzler, P Stapel, P Glos
- 42-10-1 Relationships Between Local, Global and Dynamic Modulus of Elasticity for Soft- and Hardwoods – G J P Ravenshorst, J W G van de Kuilen

#### ENVIRONMENTAL CONDITIONS

- 5-11-1 Climate Grading for the Code of Practice - B Norén
- 6-11-1 Climate Grading (2) - B Norén
- 9-11-1 Climate Classes for Timber Design - F J Keenan
- 19-11-1 Experimental Analysis on Ancient Downgraded Timber Structures - B Leggeri and L Paolini
- 19-6-5 Drying Stresses in Round Timber - A Ranta-Maunus
- 22-11-1 Corrosion and Adaptation Factors for Chemically Aggressive Media with Timber Structures - K Erler
- 29-11-1 Load Duration Effect on Structural Beams under Varying Climate Influence of Size and Shape - P Galimard and P Morlier
- 30-11-1 Probabilistic Design Models for the Durability of Timber Constructions - R H Leicester
- 36-11-1 Structural Durability of Timber in Ground Contact – R H Leicester, C H Wang, M N Nguyen, G C Foliente, C McKenzie
- 38-11-1 Design Specifications for the Durability of Timber – R H Leicester, C-H Wang, M Nguyen, G C Foliente
- 38-11-2 Consideration of Moisture Exposure of Timber Structures as an Action - M Häglund, S Thelandersson
- 45-11-1 Building Climate – Long-term Measurements to Determine the Effect on the Moisture Gradient in Large-span Timber Structures - P Dietsch, A Gamper, M Merk, S Winter

## LAMINATED MEMBERS

- 6-12-1 Directives for the Fabrication of Load-Bearing Structures of Glued Timber - A van der Velden and J Kuipers
- 8-12-1 Testing of Big Glulam Timber Beams - H Kolb and P Frech
- 8-12-2 Instruction for the Reinforcement of Apertures in Glulam Beams - H Kolb and P Frech
- 8-12-3 Glulam Standard Part 1: Glued Timber Structures; Requirements for Timber (Second Draft)
- 9-12-1 Experiments to Provide for Elevated Forces at the Supports of Wooden Beams with Particular Regard to Shearing Stresses and Long-Term Loadings - F Wassipaul and R Lackner
- 9-12-2 Two Laminated Timber Arch Railway Bridges Built in Perth in 1849 - L G Booth
- 9-6-4 Consideration of Combined Stresses for Lumber and Glued Laminated Timber - K Möhler
- 11-6-3 Consideration of Combined Stresses for Lumber and Glued Laminated Timber (addition to Paper CIB-W18/9-6-4) - K Möhler
- 12-12-1 Glulam Standard Part 2: Glued Timber Structures; Rating (3rd draft)
- 12-12-2 Glulam Standard Part 3: Glued Timber Structures; Performance (3 rd draft)
- 13-12-1 Glulam Standard Part 3: Glued Timber Structures; Performance (4th draft)
- 14-12-1 Proposals for CEI-Bois/CIB-W18 Glulam Standards - H J Larsen
- 14-12-2 Guidelines for the Manufacturing of Glued Load-Bearing Timber Structures - Stevin Laboratory
- 14-12-3 Double Tapered Curved Glulam Beams - H Riberholt
- 14-12-4 Comment on CIB-W18/14-12-3 - E Gehri
- 18-12-1 Report on European Glulam Control and Production Standard - H Riberholt
- 18-10-2 Longitudinal Shear Design of Glued Laminated Beams - R O Foschi
- 19-12-1 Strength of Glued Laminated Timber - J Ehlbeck and F Colling
- 19-12-2 Strength Model for Glulam Columns - H J Blaß
- 19-12-3 Influence of Volume and Stress Distribution on the Shear Strength and Tensile Strength Perpendicular to Grain - F Colling
- 19-12-4 Time-Dependent Behaviour of Glued-Laminated Beams - F Zaupa
- 21-12-1 Modulus of Rupture of Glulam Beam Composed of Arbitrary Laminae - K Komatsu and N Kawamoto
- 21-12-2 An Appraisal of the Young's Modulus Values Specified for Glulam in Eurocode 5- L R J Whale, B O Hilson and P D Rodd
- 21-12-3 The Strength of Glued Laminated Timber (Glulam): Influence of Lamination Qualities and Strength of Finger Joints - J Ehlbeck and F Colling
- 21-12-4 Comparison of a Shear Strength Design Method in Eurocode 5 and a More Traditional One - H Riberholt
- 22-12-1 The Dependence of the Bending Strength on the Glued Laminated Timber Girder Depth - M Badstube, W Rug and W Schöne
- 22-12-2 Acid Deterioration of Glulam Beams in Buildings from the Early Half of the 1960s - Preliminary summary of the research project; Overhead pictures - B A Hedlund
- 22-12-3 Experimental Investigation of normal Stress Distribution in Glue Laminated Wooden Arches - Z Mielczarek and W Chanaj

- 22-12-4 Ultimate Strength of Wooden Beams with Tension Reinforcement as a Function of Random Material Properties - R Candowicz and T Dziuba
- 23-12-1 Bending Strength of Glulam Beams, a Design Proposal - J Ehlbeck and F Colling
- 23-12-2 Probability Based Design Method for Glued Laminated Timber - M F Stone
- 23-12-3 Glulam Beams, Bending Strength in Relation to the Bending Strength of the Finger Joints - H Riberholt
- 23-12-4 Glued Laminated Timber - Strength Classes and Determination of Characteristic Properties - H Riberholt, J Ehlbeck and A Fewell
- 24-12-1 Contribution to the Determination of the Bending Strength of Glulam Beams - F Colling, J Ehlbeck and R Görlacher
- 24-12-2 Influence of Perpendicular-to-Grain Stressed Volume on the Load-Carrying Capacity of Curved and Tapered Glulam Beams - J Ehlbeck and J Kürth
- 25-12-1 Determination of Characteristic Bending Values of Glued Laminated Timber. EN-Approach and Reality - E Gehri
- 26-12-1 Norwegian Bending Tests with Glued Laminated Beams-Comparative Calculations with the "Karlsruhe Calculation Model" - E Aasheim, K Solli, F Colling, R H Falk, J Ehlbeck and R Görlacher
- 26-12-2 Simulation Analysis of Norwegian Spruce Glued-Laminated Timber - R Hernandez and R H Falk
- 26-12-3 Investigation of Laminating Effects in Glued-Laminated Timber - F Colling and R H Falk
- 26-12-4 Comparing Design Results for Glulam Beams According to Eurocode 5 and to the French Working Stress Design Code (CB71) - F Rouger
- 27-12-1 State of the Art Report: Glulam Timber Bridge Design in the U.S. - M A Ritter and T G Williamson
- 27-12-2 Common Design Practice for Timber Bridges in the United Kingdom - C J Mettem, J P Marcroft and G Davis
- 27-12-3 Influence of Weak Zones on Stress Distribution in Glulam Beams - E Serrano and H J Larsen
- 28-12-1 Determination of Characteristic Bending Strength of Glued Laminated Timber - E Gehri
- 28-12-2 Size Factor of Norwegian Glued Laminated Beams - E Aasheim and K H Solli
- 28-12-3 Design of Glulam Beams with Holes - K Riipola
- 28-12-4 Compression Resistance of Glued Laminated Timber Short Columns- U Korin
- 29-12-1 Development of Efficient Glued Laminated Timber - G Schickhofer
- 30-12-1 Experimental Investigation and Analysis of Reinforced Glulam Beams - K Oiger
- 31-12-1 Depth Factor for Glued Laminated Timber-Discussion of the Eurocode 5 Approach - B Källsner, O Carling and C J Johansson
- 32-12-1 The bending stiffness of nail-laminated timber elements in transverse direction- T Wolf and O Schäfer
- 33-12-1 Internal Stresses in the Cross-Grain Direction of Wood Induced by Climate Variation – J Jönsson and S Svensson
- 34-12-1 High-Strength I-Joist Compatible Glulam Manufactured with LVL Tension Laminations – B Yeh, T G Williamson
- 34-12-2 Evaluation of Glulam Shear Strength Using A Full-Size Four-Point Test Method – B Yeh, T G Williamson
- 34-12-3 Design Model for FRP Reinforced Glulam Beams – M Romani, H J Blaß

- 34-12-4 Moisture induced stresses in glulam cross sections – J Jönsson
- 34-12-5 Load Carrying Capacity of Nail-Laminated Timber under Concentrated Loads – V Krämer, H J Blaß
- 34-12-6 Determination of Shear Strength Values for GLT Using Visual and Machine Graded Spruce Laminations – G Schickhofer
- 34-12-7 Mechanically Jointed Beams: Possibilities of Analysis and some special Problems – H Kreuzinger
- 35-12-1 Glulam Beams with Round Holes – a Comparison of Different Design Approaches vs. Test Data - S Aicher L Höfflin
- 36-12-1 Problems with Shear and Bearing Strength of LVL in Highly Loaded Structures - H Bier
- 36-12-2 Weibull Based Design of Round Holes in Glulam - L Höfflin, S Aicher
- 37-12-1 Development of Structural LVL from Tropical Wood and Evaluation of Their Performance for the Structural Components of Wooden Houses. Part-1. Application of Tropical LVL to a Roof Truss - K Komatsu, Y Idris, S Yuwasdiki, B Subiyakto, A Firmanti
- 37-12-2 Reinforcement of LVL Beams With Bonded-in Plates and Rods - Effect of Placement of Steel and FRP Reinforcements on Beam Strength and Stiffness - P Alam, M P Ansell, D Smedley
- 39-12-1 Recommended Procedures for Determination of Distribution Widths in the Design of Stress Laminated Timber Plate Decks - K Crews
- 39-12-2 In-situ Strengthening of Timber Structures with CFRP - K U Schober, S Franke, K Rautenstrauch
- 39-12-3 Effect of Checking and Non-Glued Edge Joints on the Shear Strength of Structural Glued Laminated Timber Beams - B Yeh, T G Williamson, Z A Martin
- 39-12-4 A Contribution to the Design and System Effect of Cross Laminated Timber (CLT) - R Jöbstl, T Moosbrugger, T Bogensperger, G Schickhofer
- 39-12-5 Behaviour of Glulam in Compression Perpendicular to Grain in Different Strength Grades and Load Configurations - M Augustin, A Ruli, R Brandner, G Schickhofer
- 40-12-1 Development of New Constructions of Glulam Beams in Canada - F Lam, N Mohadevan
- 40-12-2 Determination of Modulus of Shear and Elasticity of Glued Laminated Timber and Related Examination - R Brandner, E Gehri, T Bogensperger, G Schickhofer
- 40-12-3 Comparative Examination of Creep of GTL and CLT-Slabs in Bending - R A Jöbstl, G Schickhofer,
- 40-12-4 Standard Practice for the Derivation of Design Properties of Structural Glued Laminated Timber in the United States - T G Williamson, B Yeh
- 40-12-5 Creep and Creep-Rupture Behaviour of Structural Composite Lumber Evaluated in Accordance with ASTM D 6815 - B Yeh, T G Williamson.
- 40-12-6 Bending Strength of Combined Beech-Spruce Glulam - M Frese, H J Blaß
- 40-12-7 Quality Control of Glulam: Shear Tests of Glue Lines - R Steiger, E Gehri
- 41-12-1 Paper withdrawn by the author
- 41-12-2 Bending Strength of Spruce Glulam: New Models for the Characteristic Bending Strength - M Frese, H J Blass,
- 41-12-3 In-Plane Shear Strength of Cross Laminated Timber - R A Joebstl, T Bogensperger, G Schickhofer
- 41-12-4 Strength of Glulam Beams with Holes - Tests of Quadratic Holes and Literature Test Results Compilation - H Danielsson, P J Gustafsson
- 42-12-1 Glulam Beams with Holes Reinforced by Steel Bars – S Aicher, L Höfflin

- 42-12-2 Analysis of X-lam Panel-to-Panel Connections under Monotonic and Cyclic Loading - C Sandhaas, L Boukes, J W G van de Kuilen, A Ceccotti
- 42-12-3 Laminating Lumber and End Joint Properties for FRP-Reinforced Glulam Beams - T G Williamson, B Yeh
- 43-12-4 Validity of Bending Tests on Strip-Shaped Specimens to Derive Bending Strength and Stiffness Properties of Cross-Laminated Solid Timber (CLT) - R Steiger, A Gülzow
- 42-12-5 Mechanical Properties of Stress Laminated Timber Decks - Experimental Study - K Karlsson, R Crocetti, R Kliger
- 43-12-1 Fatigue Behaviour of Finger Jointed Lumber - S Aicher, G Stapf
- 43-12-2 Experimental and Numerical Investigation on the Shear Strength of Glulam - R Crocetti, P J Gustafsson, H Danielsson, A Emilsson, S Ormarsson
- 43-12-3 System Effects in Glued Laminated Timber in Tension and Bending - M Frese, H J Blaß
- 43-12-4 Experimental Investigations on Mechanical Behaviour of Glued Solid timber - C Faye, F Rouger, P Garcia
- 44-12-1 Properties of CLT-Panels Exposed to Compression Perpendicular to their Plane- T Bogensperger, M Augustin, G Schickhofer
- 44-12-2 Strength of Spruce Glulam Subjected to Longitudinal Compression – M Frese, M Enders-Comberg, H J Blaß, P Glos
- 44-12-3 Glued Laminated Timber: A proposal for New Beam Layups - F Rouger, P Garcia
- 44-12-4 Glulam Beams with Internally and Externally Reinforced Holes – Test, Detailing and Design – S Aicher
- 44-12-5 Size Effect of Bending Strength in Glulam Beam - F Lam
- 45-12-1 Asymmetrically Combined Glulam - Simplified Verification of the Bending Strength - M Frese, H J Blaß
- 45-12-2 Determination of Shear Strength of Structural and Glued Laminated Timber - R Brandner, W Gatternig, G Schickhofer
- 45-12-3 Shear Resistance of Glulam Beams with Cracks - A Pousette, M Ekevad
- 45-12-4 Experimental Investigation on in-plane Behaviour of Cross-laminated Timber Elements - M Andreolli, A Polastri, R Tomasi

#### PARTICLE AND FIBRE BUILDING BOARDS

- 7-13-1 Fibre Building Boards for CIB Timber Code (First Draft)- O Brynildsen
- 9-13-1 Determination of the Bearing Strength and the Load-Deformation Characteristics of Particleboard - K Möhler, T Budianto and J Ehlbeck
- 9-13-2 The Structural Use of Tempered Hardboard - W W L Chan
- 11-13-1 Tests on Laminated Beams from Hardboard under Short- and Longterm Load - W Nozynski
- 11-13-2 Determination of Deformation of Special Densified Hardboard under Long-term Load and Varying Temperature and Humidity Conditions - W Halfar
- 11-13-3 Determination of Deformation of Hardboard under Long-term Load in Changing Climate - W Halfar
- 14-4-1 An Introduction to Performance Standards for Wood-Base Panel Products - D H Brown
- 14-4-2 Proposal for Presenting Data on the Properties of Structural Panels - T Schmidt
- 16-13-1 Effect of Test Piece Size on Panel Bending Properties - P W Post

- 20-4-1 Considerations of Reliability - Based Design for Structural Composite Products - M R O'Halloran, J A Johnson, E G Elias and T P Cunningham
- 20-13-1 Classification Systems for Structural Wood-Based Sheet Materials - V C Kearley and A R Abbott
- 21-13-1 Design Values for Nailed Chipboard - Timber Joints - A R Abbott
- 25-13-1 Bending Strength and Stiffness of Izopanel Plates - Z Mielczarek
- 28-13-1 Background Information for "Design Rated Oriented Strand Board (OSB)" in CSA Standards - Summary of Short-term Test Results - E Karacabeyli, P Lau, C R Henderson, F V Meakes and W Deacon
- 28-13-2 Torsional Stiffness of Wood-Hardboard Composed I-Beam - P Olejniczak

#### TRUSSED RAFTERS

- 4-9-1 Long-term Loading of Trussed Rafters with Different Connection Systems - T Feldborg and M Johansen
- 6-9-3 Deflection of Trussed Rafters under Alternating Loading During a Year - T Feldborg and M Johansen
- 7-2-1 Lateral Bracing of Timber Struts - J A Simon
- 9-14-1 Timber Trusses - Code Related Problems - T F Williams
- 9-7-1 Design of Truss Plate Joints - F J Keenan
- 10-14-1 Design of Roof Bracing - The State of the Art in South Africa - P A V Bryant and J A Simon
- 11-14-1 Design of Metal Plate Connected Wood Trusses - A R Egerup
- 12-14-1 A Simple Design Method for Standard Trusses - A R Egerup
- 13-14-1 Truss Design Method for CIB Timber Code - A R Egerup
- 13-14-2 Trussed Rafters, Static Models - H Riberholt
- 13-14-3 Comparison of 3 Truss Models Designed by Different Assumptions for Slip and E-Modulus - K Möhler
- 14-14-1 Wood Trussed Rafter Design - T Feldborg and M Johansen
- 14-14-2 Truss-Plate Modelling in the Analysis of Trusses - R O Foschi
- 14-14-3 Cantilevered Timber Trusses - A R Egerup
- 14-7-5 The Effect of Support Eccentricity on the Design of W- and WW-Trusses with Nail Plate Connectors - B Källsner
- 15-14-1 Guidelines for Static Models of Trussed Rafters - H Riberholt
- 15-14-2 The Influence of Various Factors on the Accuracy of the Structural Analysis of Timber Roof Trusses - F R P Pienaar
- 15-14-3 Bracing Calculations for Trussed Rafter Roofs - H J Burgess
- 15-14-4 The Design of Continuous Members in Timber Trussed Rafters with Punched Metal Connector Plates - P O Reece
- 15-14-5 A Rafter Design Method Matching U.K. Test Results for Trussed Rafters - H J Burgess
- 16-14-1 Full-Scale Tests on Timber Fink Trusses Made from Irish Grown Sitka Spruce - V Picardo
- 17-14-1 Data from Full Scale Tests on Prefabricated Trussed Rafters - V Picardo
- 17-14-2 Simplified Static Analysis and Dimensioning of Trussed Rafters - H Riberholt
- 17-14-3 Simplified Calculation Method for W-Trusses - B Källsner

- 18-14-1 Simplified Calculation Method for W-Trusses (Part 2) - B Källsner
- 18-14-2 Model for Trussed Rafter Design - T Poutanen
- 19-14-1 Annex on Simplified Design of W-Trusses - H J Larsen
- 19-14-2 Simplified Static Analysis and Dimensioning of Trussed Rafters - Part 2 - H Riberholt
- 19-14-3 Joint Eccentricity in Trussed Rafters - T Poutanen
- 20-14-1 Some Notes about Testing Nail Plates Subjected to Moment Load - T Poutanen
- 20-14-2 Moment Distribution in Trussed Rafters - T Poutanen
- 20-14-3 Practical Design Methods for Trussed Rafters - A R Egerup
- 22-14-1 Guidelines for Design of Timber Trussed Rafters - H Riberholt
- 23-14-1 Analyses of Timber Trussed Rafters of the W-Type - H Riberholt
- 23-14-2 Proposal for Eurocode 5 Text on Timber Trussed Rafters - H Riberholt
- 24-14-1 Capacity of Support Areas Reinforced with Nail Plates in Trussed Rafters - A Kevarinmäki
- 25-14-1 Moment Anchorage Capacity of Nail Plates in Shear Tests - A Kevarinmaki and J. Kangas
- 25-14-2 Design Values of Anchorage Strength of Nail Plate Joints by 2-curve Method and Interpolation - J Kangas and A Kevarinmaki
- 26-14-1 Test of Nail Plates Subjected to Moment - E Aasheim
- 26-14-2 Moment Anchorage Capacity of Nail Plates - A Kevarinmäki and J Kangas
- 26-14-3 Rotational Stiffness of Nail Plates in Moment Anchorage - A Kevarinmäki and J Kangas
- 26-14-4 Solution of Plastic Moment Anchorage Stress in Nail Plates - A Kevarinmäki
- 26-14-5 Testing of Metal-Plate-Connected Wood-Truss Joints - R Gupta
- 26-14-6 Simulated Accidental Events on a Trussed Rafter Roofed Building - C J Mettem and J P Marcroft
- 30-14-1 The Stability Behaviour of Timber Trussed Rafter Roofs - Studies Based on Eurocode 5 and Full Scale Testing - R J Bainbridge, C J Mettern, A Reffold and T Studer
- 32-14-1 Analysis of Timber Reinforced with Punched Metal Plate Fasteners- J Nielsen
- 33-14-1 Moment Capacity of Timber Beams Loaded in Four-Point Bending and Reinforced with Punched Metal Plate Fasteners – J Nielsen
- 36-14-1 Effect of Chord Splice Joints on Force Distribution in Trusses with Punched Metal Plate Fasteners - P Ellegaard
- 36-14-2 Monte Carlo Simulation and Reliability Analysis of Roof Trusses with Punched Metal Plate Fasteners - M Hansson, P Ellegaard
- 36-14-3 Truss Trouble – R H Leicester, J Goldfinch, P Paevere, G C Foliente
- 40-14-1 Timber Trusses with Punched Metal Plate Fasteners - Design for Transport and Erection - H J Blaß
- 45-14-1 Robustness Analysis of Timber Truss Systems - D Čizmar, V Rajčić

## STRUCTURAL STABILITY

- 8-15-1 Laterally Loaded Timber Columns: Tests and Theory - H J Larsen
- 13-15-1 Timber and Wood-Based Products Structures. Panels for Roof Coverings. Methods of Testing and Strength Assessment Criteria. Polish Standard BN-78/7159-03

- 16-15-1 Determination of Bracing Structures for Compression Members and Beams - H Brüninghoff
- 17-15-1 Proposal for Chapter 7.4 Bracing - H Brüninghoff
- 17-15-2 Seismic Design of Small Wood Framed Houses - K F Hansen
- 18-15-1 Full-Scale Structures in Glued Laminated Timber, Dynamic Tests: Theoretical and Experimental Studies - A Ceccotti and A Vignoli
- 18-15-2 Stabilizing Bracings - H Brüninghoff
- 19-15-1 Connections Deformability in Timber Structures: a Theoretical Evaluation of its Influence on Seismic Effects - A Ceccotti and A Vignoli
- 19-15-2 The Bracing of Trussed Beams - M H Kessel and J Natterer
- 19-15-3 Racking Resistance of Wooden Frame Walls with Various Openings - M Yasumura
- 19-15-4 Some Experiences of Restoration of Timber Structures for Country Buildings - G Cardinale and P Spinelli
- 19-15-5 Non-Destructive Vibration Tests on Existing Wooden Dwellings - Y Hirashima
- 20-15-1 Behaviour Factor of Timber Structures in Seismic Zones. - A Ceccotti and A Vignoli
- 21-15-1 Rectangular Section Deep Beam - Columns with Continuous Lateral Restraint - H J Burgess
- 21-15-2 Buckling Modes and Permissible Axial Loads for Continuously Braced Columns- H J Burgess
- 21-15-3 Simple Approaches for Column Bracing Calculations - H J Burgess
- 21-15-4 Calculations for Discrete Column Restraints - H J Burgess
- 21-15-5 Behaviour Factor of Timber Structures in Seismic Zones (Part Two) - A Ceccotti and A Vignoli
- 22-15-1 Suggested Changes in Code Bracing Recommendations for Beams and Columns - H J Burgess
- 22-15-2 Research and Development of Timber Frame Structures for Agriculture in Poland- S Kus and J Kerste
- 22-15-3 Ensuring of Three-Dimensional Stiffness of Buildings with Wood Structures - A K Shenghelia
- 22-15-5 Seismic Behavior of Arched Frames in Timber Construction - M Yasumura
- 22-15-6 The Robustness of Timber Structures - C J Mettem and J P Marcroft
- 22-15-7 Influence of Geometrical and Structural Imperfections on the Limit Load of Wood Columns - P Dutko
- 23-15-1 Calculation of a Wind Girder Loaded also by Discretely Spaced Braces for Roof Members - H J Burgess
- 23-15-2 Stability Design and Code Rules for Straight Timber Beams - T A C M van der Put
- 23-15-3 A Brief Description of Formula of Beam-Columns in China Code - S Y Huang
- 23-15-4 Seismic Behavior of Braced Frames in Timber Construction - M Yasumara
- 23-15-5 On a Better Evaluation of the Seismic Behavior Factor of Low-Dissipative Timber Structures - A Ceccotti and A Vignoli
- 23-15-6 Disproportionate Collapse of Timber Structures - C J Mettem and J P Marcroft

- 23-15-7 Performance of Timber Frame Structures During the Loma Prieta California Earthquake - M R O'Halloran and E G Elias
- 24-15-2 Discussion About the Description of Timber Beam-Column Formula - S Y Huang
- 24-15-3 Seismic Behavior of Wood-Framed Shear Walls - M Yasumura
- 25-15-1 Structural Assessment of Timber Framed Building Systems - U Korin
- 25-15-3 Mechanical Properties of Wood-framed Shear Walls Subjected to Reversed Cyclic Lateral Loading - M Yasumura
- 26-15-1 Bracing Requirements to Prevent Lateral Buckling in Trussed Rafters - C J Mettem and P J Moss
- 26-15-2 Eurocode 8 - Part 1.3 - Chapter 5 - Specific Rules for Timber Buildings in Seismic Regions - K Becker, A Ceccotti, H Charlier, E Katsaragakis, H J Larsen and H Zeitter
- 26-15-3 Hurricane Andrew - Structural Performance of Buildings in South Florida - M R O'Halloran, E L Keith, J D Rose and T P Cunningham
- 29-15-1 Lateral Resistance of Wood Based Shear Walls with Oversized Sheathing Panels - F Lam, H G L Prion and M He
- 29-15-2 Damage of Wooden Buildings Caused by the 1995 Hyogo-Ken Nanbu Earthquake - M Yasumura, N Kawai, N Yamaguchi and S Nakajima
- 29-15-3 The Racking Resistance of Timber Frame Walls: Design by Test and Calculation - D R Griffiths, C J Mettem, V Enjily, P J Steer
- 29-15-4 Current Developments in Medium-Rise Timber Frame Buildings in the UK - C J Mettem, G C Pitts, P J Steer, V Enjily
- 29-15-5 Natural Frequency Prediction for Timber Floors - R J Bainbridge, and C J Mettem
- 30-15-1 Cyclic Performance of Perforated Wood Shear Walls with Oversize Oriented Strand Board Panels - Ming He, H Magnusson, F Lam, and H G L Prion
- 30-15-2 A Numerical Analysis of Shear Walls Structural Performances - L Davenne, L Daudeville, N Kawai and M Yasumura
- 30-15-3 Seismic Force Modification Factors for the Design of Multi-Storey Wood-Frame Platform Construction - E Karacabeyli and A Ceccotti
- 30-15-4 Evaluation of Wood Framed Shear Walls Subjected to Lateral Load - M Yasumura and N Kawai
- 31-15-1 Seismic Performance Testing On Wood-Framed Shear Wall - N Kawai
- 31-15-2 Robustness Principles in the Design of Medium-Rise Timber-Framed Buildings - C J Mettem, M W Milner, R J Bainbridge and V. Enjily
- 31-15-3 Numerical Simulation of Pseudo-Dynamic Tests Performed to Shear Walls - L Daudeville, L Davenne, N Richard, N Kawai and M Yasumura
- 31-15-4 Force Modification Factors for Braced Timber Frames - H G L Prion, M Popovski and E Karacabeyli
- 32-15-1 Three-Dimensional Interaction in Stabilisation of Multi-Storey Timber Frame Buildings - S Andreasson
- 32-15-2 Application of Capacity Spectrum Method to Timber Houses - N Kawai
- 32-15-3 Design Methods for Shear Walls with Openings - C Ni, E Karacabeyli and A Ceccotti
- 32-15-4 Static Cyclic Lateral Loading Tests on Nailed Plywood Shear Walls - K Komatsu, K H Hwang and Y Itou
- 33-15-1 Lateral Load Capacities of Horizontally Sheathed Unblocked Shear Walls – C Ni, E Karacabeyli and A Ceccotti

- 33-15-2 Prediction of Earthquake Response of Timber Houses Considering Shear Deformation of Horizontal Frames – N Kawai
- 33-15-3 Eurocode 5 Rules for Bracing – H J Larsen
- 34-15-1 A simplified plastic model for design of partially anchored wood-framed shear walls – B Källsner, U A Girhammar, Liping Wu
- 34-15-2 The Effect of the Moisture Content on the Performance of the Shear Walls – S Nakajima
- 34-15-3 Evaluation of Damping Capacity of Timber Structures for Seismic Design – M Yasumura
- 35-15-1 On test methods for determining racking strength and stiffness of wood-framed shear walls - B Källsner, U A Girhammar, L Wu
- 35-15-2 A Plastic Design Model for Partially Anchored Wood-framed Shear Walls with Openings - U A Girhammar, L Wu, B Källsner
- 35-15-3 Evaluation and Estimation of the Performance of the Shear Walls in Humid Climate - S Nakajima
- 35-15-4 Influence of Vertical Load on Lateral Resistance of Timber Frame Walls - B Dujič, R Žarnić
- 35-15-5 Cyclic and Seismic Performances of a Timber-Concrete System - Local and Full Scale Experimental Results - E Fournely, P Racher
- 35-15-6 Design of timber-concrete composite structures according to EC5 - 2002 version - A Ceccotti, M Fragiaco, R M Gutkowski
- 35-15-7 Design of timber structures in seismic zones according to EC8- 2002 version - A Ceccotti, T Toratti, B Dujič
- 35-15-8 Design Methods to Prevent Premature Failure of Joints at Shear Wall Corners - N Kawai, H Okiura
- 36-15-1 Monitoring Light-Frame Timber Buildings: Environmental Loads and Load Paths – I Smith et al.
- 36-15-2 Applicability of Design Methods to Prevent Premature Failure of Joints at Shear Wall Corners in Case of Post and Beam Construction - N Kawai, H Isoda
- 36-15-3 Effects of Screw Spacing and Edge Boards on the Cyclic Performance of Timber Frame and Structural Insulated Panel Roof Systems - D M Carradine, J D Dolan, F E Woeste
- 36-15-4 Pseudo-Dynamic Tests on Conventional Timber Structures with Shear Walls - M Yasumura
- 36-15-5 Experimental Investigation of Laminated Timber Frames with Fiber-reinforced Connections under Earthquake Loads - B Kasal, P Haller, S Pospisil, I Jirovsky, A Heiduschke, M Drdacky
- 36-15-6 Effect of Test Configurations and Protocols on the Performance of Shear Walls - F Lam, D Jossen, J Gu, N Yamaguchi, H G L Prion
- 36-15-7 Comparison of Monotonic and Cyclic Performance of Light-Frame Shear Walls - J D Dolan, A J Toothman
- 37-15-1 Estimating 3D Behavior of Conventional Timber Structures with Shear Walls by Pseudodynamic Tests - M Yasumura, M Uesugi, L Davenne
- 37-15-2 Testing of Racking Behavior of Massive Wooden Wall Panels - B Dujič, J Pucelj, R Žarnić
- 37-15-3 Influence of Framing Joints on Plastic Capacity of Partially Anchored Wood-Framed Shear Walls - B Källsner, U A Girhammar
- 37-15-4 Bracing of Timber Members in Compression - J Munch-Andersen
- 37-15-5 Acceptance Criteria for the Use of Structural Insulated Panels in High Risk Seismic Areas - B Yeh, T D Skaggs, T G Williamson Z A Martin

- 37-15-6 Predicting Load Paths in Shearwalls - Hongyong Mi, Ying-Hei Chui, I Smith, M Mohammad
- 38-15-1 Background Information on ISO STANDARD 16670 for Cyclic Testing of Connections - E Karacabeyli, M Yasumura, G C Foliente, A Ceccotti
- 38-15-2 Testing & Product Standards – a Comparison of EN to ASTM, AS/NZ and ISO Standards – A Ranta-Maunus, V Enjily
- 38-15-3 Framework for Lateral Load Design Provisions for Engineered Wood Structures in Canada - M Popovski, E Karacabeyli
- 38-15-4 Design of Shear Walls without Hold-Downs - Chun Ni, E Karacabeyli
- 38-15-5 Plastic design of partially anchored wood-framed wall diaphragms with and without openings - B Källsner, U A Girhammar
- 38-15-6 Racking of Wooden Walls Exposed to Different Boundary Conditions - B Dujič, S Aicher, R Žarnić
- 38-15-7 A Portal Frame Design for Raised Wood Floor Applications - T G Williamson, Z A Martin, B Yeh
- 38-15-8 Linear Elastic Design Method for Timber Framed Ceiling, Floor and Wall Diaphragms - Jarmo Leskelä
- 38-15-9 A Unified Design Method for the Racking Resistance of Timber Framed Walls for Inclusion in EUROCODE 5 - R Griffiths, B Källsner, H J Blass, V Enjily
- 39-15-1 Effect of Transverse Walls on Capacity of Wood-Framed Wall Diaphragms - U A Girhammar, B Källsner
- 39-15-2 Which Seismic Behaviour Factor for Multi-Storey Buildings made of Cross-Laminated Wooden Panels? - M Follesa, M P Lauriola, C Minowa, N Kawai, C Sandhaas, M Yasumura, A Ceccotti
- 39-15-3 Laminated Timber Frames under dynamic Loadings - A Heiduschke, B Kasal, P Haller
- 39-15-4 Code Provisions for Seismic Design of Multi-storey Post-tensioned Timber Buildings - S Pampanin, A Palermo, A Buchanan, M Fragiaco, B Deam
- 40-15-1 Design of Safe Timber Structures – How Can we Learn from Structural Failures? - S Thelandersson, E Frühwald
- 40-15-2 Effect of Transverse Walls on Capacity of Wood-Framed Wall Diaphragms—Part 2 - U A Girhammar, B Källsner
- 40-15-3 Midply Wood Shear Wall System: Concept, Performance and Code Implementation - Chun Ni, M Popovski, E Karacabeyli, E Varoglu, S Stiemer
- 40-15-4 Seismic Behaviour of Tall Wood-Frame Walls - M Popovski, A Peterson, E Karacabeyli
- 40-15-5 International Standard Development of Lateral Load Test Method for Shear Walls - M Yasumura, E Karacabeyli
- 40-15-6 Influence of Openings on Shear Capacity of Wooden Walls - B Dujič, S Klobcar, R Žarnić
- 41-15-1 Need for a Harmonized Approach for Calculations of Ductility of Timber Assemblies - W Muñoz, M Mohammad, A Salenikov, P Quenneville
- 41-15-2 Plastic Design of Wood Frame Wall Diaphragms in Low and Medium Rise Buildings - B Källsner, U A Girhammar
- 41 15-3 Failure Analysis of Light Wood Frame Structures under Wind Load - A Asiz, Y H Chui, I Smith
- 41-15-4 Combined Shear and Wind Uplift Resistance of Wood Structural Panel Shearwalls B Yeh, T G Williamson
- 41-15-5 Behaviour of Prefabricated Timber Wall Elements under Static and Cyclic Loading – P Schädle, H J Blass

- 42-15-1 Design Aspects on Anchoring the Bottom Rail in Partially Anchored Wood-Framed Shear Walls - U A Girhammar, B Källsner
- 42-15-2 New Seismic Design Provisions for Shearwalls and Diaphragms in the Canadian Standard for Engineering Design in Wood - M Popovski, E Karacabeyli, Chun Ni, P Lepper, G Doudak
- 42-15-3 Stability Capacity and Lateral Bracing Force of Metal Plate Connected Wood Truss Assemblies - Xiaobin Song, F Lam, Hao Huang, Minjuan He
- 42-15-4 Improved Method for Determining Braced Wall Requirements for Conventional Wood-Frame Buildings - Chun Ni, H Rainer, E Karacabeyli
- 43-15-1 Influence of the Boundary Conditions on the Racking Strength of Shear Walls with an Opening - M Yasumura
- 43-15-2 Influence of Different Standards on the Determination of Earthquake Properties of Timber Shear Wall Systems - P Schädle, H J Blaß
- 43-15-3 Full-Scale Shear Wall Tests for Force Transfer Around Openings - T Skaggs, B Yeh, F Lam
- 43-15-4 Optimized Anchor-Bolt Spacing for Structural Panel Shearwalls Subjected to Combined Shear and Wind Uplift Forces - B Yeh, E Keith, T Skaggs
- 44-15-1 A Proposal for Revision of the Current Timber Part (Section 8) of Eurocode 8 Part 1 - M Follesa, M Fragiaco, M P Lauriola
- 44-15-2 Influence of Vertical Loads on Lateral Resistance and Deflections of Light-Frame Shear Walls - M Payeur, A Salenikovich, W Muñoz
- 44-15-3 Modelling Force Transfer Around Openings of Full-Scale Shear Walls - T Skaggs, B Yeh, F Lam, Minghao Li, D Rammer, J Wacker
- 44-15-4 Design of Bottom Rails in Partially Anchored Shear Walls Using Fracture Mechanics - E Serrano, J Vessby, A Olsson, U A Girhammar, B Källsner
- 44-15-5 Notes on Deformation and Ductility Requirements in Timber Structures. - K A Malo, P Ellingsbø, C Stamatopoulos
- 44-15-6 Enhanced Model of the Nonlinear Load-bearing Behaviour of Wood Shear Walls and Diaphragms - M H Kessel, C Hall
- 44-15-7 Seismic Performance of Cross-Laminated Wood Panels - M Popovski, E Karacabeyli
- 44-15-8 Evaluation of Plywood Sheathed Shear Walls with Screwed Joints Tested According to ISO 21581 - K Kobayashi, M Yasumura
- 44-15-9 Influence of Connection Properties on the Ductility and Seismic Resistance of Multi-Storey Cross-Lam Buildings - I Sustersic, M Fragiaco, B Dujic
- 45-15-1 Performance Based Design and Force Modification Factors for CLT Structures - S Pei, M Popovski, J van de Lindt
- 45-15-2 Seismic Behaviour of Wood-Concrete Frame Shear-wall System and Comparison with Code Provisions - L Pozza, R Scotta, A Polastri, A Ceccotti
- 45-15-3 Determination of Failure Mechanism of CLT Shear Walls Subjected to Seismic Action - M Yasumura
- 45-15-4 Seismic Response of Timber Frames with Laminated Glass Glass Infill - V Rajčić, R Žarnić
- 45-15-5 Modeling Wood Structural Panel Portal Frame Response - T Skaggs, B Yeh
- 45-15-6 Simplified Cross-laminated Timber Wall Modeling for Linear-elastic Seismic Analysis - I Sustersic, B Dujic

## FIRE

- 12-16-1 British Standard BS 5268 the Structural Use of Timber: Part 4 Fire Resistance of Timber Structures
- 13-100-2 CIB Structural Timber Design Code. Chapter 9. Performance in Fire
- 19-16-1 Simulation of Fire in Tests of Axially Loaded Wood Wall Studs - J König
- 24-16-1 Modelling the Effective Cross Section of Timber Frame Members Exposed to Fire - J König
- 25-16-1 The Effect of Density on Charring and Loss of Bending Strength in Fire - J König
- 25-16-2 Tests on Glued-Laminated Beams in Bending Exposed to Natural Fires - F Bolonius Olesen and J König
- 26-16-1 Structural Fire Design According to Eurocode 5, Part 1.2 - J König
- 31-16-1 Revision of ENV 1995-1-2: Charring and Degradation of Strength and Stiffness - J König
- 33-16-1 A Design Model for Load-carrying Timber Frame Members in Walls and Floors Exposed to Fire - J König
- 33-16-2 A Review of Component Additive Methods Used for the Determination of Fire Resistance of Separating Light Timber Frame Construction - J König, T Oksanen and K Towler
- 33-16-3 Thermal and Mechanical Properties of Timber and Some Other Materials Used in Light Timber Frame Construction - B Källsner and J König
- 34-16-1 Influence of the Strength Determining Factors on the Fire Resistance Capability of Timber Structural Members – I Totev, D Dakov
- 34-16-2 Cross section properties of fire exposed rectangular timber members - J König, B Källsner
- 34-16-3 Pull-Out Tests on Glued-in Rods at High Temperatures – A Mischler, A Frangi
- 35-16-1 Basic and Notional Charring Rates - J König
- 37 - 16 - 1 Effective Values of Thermal Properties of Timber and Thermal Actions During the Decay Phase of Natural Fires - J König
- 37 - 16 - 2 Fire Tests on Timber Connections with Dowel-type Fasteners - A Frangi, A Mischler
- 38-16-1 Fire Behaviour of Multiple Shear Steel-to-Timber Connections with Dowels - C Erchinger, A Frangi, A Mischler
- 38-16-2 Fire Tests on Light Timber Frame Wall Assemblies - V Schleifer, A Frangi
- 39-16-1 Fire Performance of FRP Reinforced Glulam - T G Williamson, B Yeh
- 39-16-2 An Easy-to-use Model for the Design of Wooden I-joists in Fire - J König, B Källsner
- 39-16-3 A Design Model for Timber Slabs Made of Hollow Core Elements in Fire - A Frangi, M Fontana
- 40-16-1 Bonded Timber Deck Plates in Fire - J König, J Schmid
- 40-16-2 Design of Timber Frame Floor Assemblies in Fire - A Frangi, C Erchinger
- 41-16-1 Effect of Adhesives on Finger Joint Performance in Fire - J König, J Norén, M Sterley
- 42-16-1 Advanced Calculation Method for the Fire Resistance of Timber Framed Walls -S Winter, W Meyn
- 42-16-2 Fire Design Model for Multiple Shear Steel-to-Timber Dowelled Connections - C Erchinger, A Frangi, M Fontana
- 42-16-3 Comparison between the Conductive Model of Eurocode 5 and the Temperature Distribution Within a Timber Cross-section Exposed to Fire - M Fragiaco, A Menis, P Moss, A Buchanan, I Clemente

- 43-16-1 Light Timber Frame Construction with Solid Timber Members – Application of the Reduced Cross-section Method - J König, J Schmid
- 43-16-2 Fire Exposed Cross-Laminated Timber - Modelling and Tests - J Schmid, J König, J Köhler
- 43-16-3 Timber-Concrete Composite Floors in Fire - J O'Neill, D Carradine, R Dhakal, P J Moss, A H Buchanan, M Fragiacomio
- 44-16-1 Gypsum Plasterboards and Gypsum Fibreboards – Protective Times for Fire Safety Design of Timber Structures –A Just, J Schmid, J König
- 45-16-1 The Reduced Cross Section Method for Timber Members Subjected to Compression, Tension and Bending in Fire - M Klippel, J Schmid, A Frangi

#### STATISTICS AND DATA ANALYSIS

- 13-17-1 On Testing Whether a Prescribed Exclusion Limit is Attained - W G Warren
- 16-17-1 Notes on Sampling and Strength Prediction of Stress Graded Structural Timber - P Glos
- 16-17-2 Sampling to Predict by Testing the Capacity of Joints, Components and Structures - B Norén
- 16-17-3 Discussion of Sampling and Analysis Procedures - P W Post
- 17-17-1 Sampling of Wood for Joint Tests on the Basis of Density - I Smith, L R J Whale
- 17-17-2 Sampling Strategy for Physical and Mechanical Properties of Irish Grown Sitka Spruce - V Picardo
- 18-17-1 Sampling of Timber in Structural Sizes - P Glos
- 18-6-3 Notes on Sampling Factors for Characteristic Values - R H Leicester
- 19-17-1 Load Factors for Proof and Prototype Testing - R H Leicester
- 19-6-2 Confidence in Estimates of Characteristic Values - R H Leicester
- 21-6-1 Draft Australian Standard: Methods for Evaluation of Strength and Stiffness of Graded Timber - R H Leicester
- 21-6-2 The Determination of Characteristic Strength Values for Stress Grades of Structural Timber. Part 1 - A R Fewell and P Glos
- 22-17-1 Comment on the Strength Classes in Eurocode 5 by an Analysis of a Stochastic Model of Grading - A proposal for a supplement of the design concept - M Kiesel
- 24-17-1 Use of Small Samples for In-Service Strength Measurement - R H Leicester and F G Young
- 24-17-2 Equivalence of Characteristic Values - R H Leicester and F G Young
- 24-17-3 Effect of Sampling Size on Accuracy of Characteristic Values of Machine Grades - Y H Chui, R Turner and I Smith
- 24-17-4 Harmonisation of LSD Codes - R H Leicester
- 25-17-2 A Body for Confirming the Declaration of Characteristic Values - J Sunley
- 25-17-3 Moisture Content Adjustment Procedures for Engineering Standards - D W Green and J W Evans
- 27-17-1 Statistical Control of Timber Strength - R H Leicester and H O Breitingner
- 30-17-1 A New Statistical Method for the Establishment of Machine Settings - F Rouger
- 35-17-1 Probabilistic Modelling of Duration of Load Effects in Timber Structures - J Köhler, S Svenson
- 38-17-1 Analysis of Censored Data - Examples in Timber Engineering Research - R Steiger, J Köhler

- 39-17-1 Possible Canadian / ISO Approach to Deriving Design Values from Test Data - I Smith, A Asiz, M Snow, Y H Chui
- 44-17-1 Influence of Sample Size on Assigned Characteristic Strength Values – P Stapel, G J P Ravenshorst, J W G van de Kuilen

#### GLUED JOINTS

- 20-18-1 Wood Materials under Combined Mechanical and Hygral Loading - A Martensson and S Thelandersson
- 20-18-2 Analysis of Generalized Volkersen - Joints in Terms of Linear Fracture Mechanics - P J Gustafsson
- 20-18-3 The Complete Stress-Slip Curve of Wood-Adhesives in Pure Shear - H Wernersson and P J Gustafsson
- 22-18-1 Perspective Adhesives and Protective Coatings for Wood Structures - A S Freidin
- 34-18-1 Performance Based Classification of Adhesives for Structural Timber Applications - R J Bainbridge, C J Mettem, J G Broughton, A R Hutchinson
- 35-18-1 Creep Testing Wood Adhesives for Structural Use - C Bengtsson, B Källander
- 38-18-1 Adhesive Performance at Elevated Temperatures for Engineered Wood Products - B Yeh, B Herzog, T G Williamson
- 39-18-1 Comparison of the Pull-out Strength of Steel Bars Glued in Glulam Elements Obtained Experimentally and Numerically - V Rajčić, A Bjelanović, M Rak
- 39-18-2 The Influence of the Grading Method on the Finger Joint Bending Strength of Beech - M Frese, H J Blaß
- 43-18-1 Comparison of API, RF and MUF Adhesives Using a Draft Australian/New Zealand Standard - B Walford

#### FRACTURE MECHANICS

- 21-10-1 A Study of Strength of Notched Beams - P J Gustafsson
- 22-10-1 Design of Endnotched Beams - H J Larsen and P J Gustafsson
- 23-10-1 Tension Perpendicular to the Grain at Notches and Joints - T A C M van der Put
- 23-10-2 Dimensioning of Beams with Cracks, Notches and Holes. An Application of Fracture Mechanics - K Riipola
- 23-19-1 Determination of the Fracture Energie of Wood for Tension Perpendicular to the Grain - W Rug, M Badstube and W Schöne
- 23-19-2 The Fracture Energy of Wood in Tension Perpendicular to the Grain. Results from a Joint Testing Project - H J Larsen and P J Gustafsson
- 23-19-3 Application of Fracture Mechanics to Timber Structures - A Ranta-Maunus
- 24-19-1 The Fracture Energy of Wood in Tension Perpendicular to the Grain - H J Larsen and P J Gustafsson
- 28-19-1 Fracture of Wood in Tension Perpendicular to the Grain: Experiment and Numerical Simulation by Damage Mechanics - L Daudeville, M Yasumura and J D Lanvin
- 28-19-2 A New Method of Determining Fracture Energy in Forward Shear along the Grain - H D Mansfield-Williams
- 28-19-3 Fracture Design Analysis of Wooden Beams with Holes and Notches. Finite Element Analysis based on Energy Release Rate Approach - H Petersson
- 28-19-4 Design of Timber Beams with Holes by Means of Fracture Mechanics - S Aicher, J Schmidt and S Brunold

- 30-19-1 Failure Analysis of Single-Bolt Joints - L Daudeville, L Davenne and M Yasumura
- 37 - 19 - 1 Determination of Fracture Mechanics Parameters for Wood with the Help of Close Range Photogrammetry - S Franke, B Franke, K Rautenstrauch
- 39-19-1 First Evaluation Steps of Design Rules in the European and German codes of Transverse Tension Areas - S Franke, B Franke, K Rautenstrauch

#### SERVICEABILITY

- 27-20-1 Codification of Serviceability Criteria - R H Leicester
- 27-20-2 On the Experimental Determination of Factor  $k_{def}$  and Slip Modulus  $k_{ser}$  from Short- and Long-Term Tests on a Timber-Concrete Composite (TCC) Beam - S Capretti and A Ceccotti
- 27-20-3 Serviceability Limit States: A Proposal for Updating Eurocode 5 with Respect to Eurocode 1 - P Racher and F Rouger
- 27-20-4 Creep Behavior of Timber under External Conditions - C Le Govic, F Rouger, T Toratti and P Morlier
- 30-20-1 Design Principles for Timber in Compression Perpendicular to Grain - S Thelandersson and A Mårtensson
- 30-20-2 Serviceability Performance of Timber Floors - Eurocode 5 and Full Scale Testing - R J Bainbridge and C J Mettem
- 32-20-1 Floor Vibrations - B Mohr
- 37 - 20 - 1 A New Design Method to Control Vibrations Induced by Foot Steps in Timber Floors - Lin J Hu, Y H Chui
- 37 - 20 - 2 Serviceability Limit States of Wooden Footbridges. Vibrations Caused by Pedestrians - P Hamm
- 43-20-1 The Long Term Instrumentation of a Timber Building in Nelson NZ - the Need for Standardisation - H W Morris, S R Uma, K Gledhill, P Omenzetter, M Worth

#### TEST METHODS

- 31-21-1 Development of an Optimised Test Configuration to Determine Shear Strength of Glued Laminated Timber - G Schickhofer and B Obermayr
- 31-21-2 An Impact Strength Test Method for Structural Timber. The Theory and a Preliminary Study - T D G Canisius
- 35-21-1 Full-Scale Edgewise Shear Tests for Laminated Veneer Lumber- B Yeh, T G Williamson
- 39-21-1 Timber Density Restrictions for Timber Connection Tests According to EN28970/ISO8970 - A Leijten, J Köhler, A Jorissen
- 39-21-2 The Mechanical Inconsistence in the Evaluation of the Modulus of Elasticity According to EN384 - T Bogensperger, H Unterwieser, G Schickhofer
- 40 - 21 - 1 ASTM D198 - Interlaboratory Study for Modulus of Elasticity of Lumber in Bending - A Salenikovich
- 40 - 21 - 2 New Test Configuration for CLT-Wall-Elements under Shear Load - T Bogensperger, T Moosbrugger, G Schickhofer
- 41-21-1 Determination of Shear Modulus by Means of Standardized Four-Point Bending Tests - R Brandner, B Freytag, G Schickhofer
- 43-21-1 Estimation of Load-Bearing Capacity of Timber Connections - J Munch-Andersen, J D Sørensen, F Sørensen

- 43-21-2 A New Method to Determine Suitable Spacings and Distances for Self-tapping Screws - T Uibel, H J Blaß
- 45-21-1 Evaluation of Shear Modulus of Structural Timber Utilizing Dynamic Excitation and FE Analysis - A Olsson, B Källsner

#### CIB TIMBER CODE

- 2-100-1 A Framework for the Production of an International Code of Practice for the Structural Use of Timber - W T Curry
- 5-100-1 Design of Solid Timber Columns (First Draft) - H J Larsen
- 5-100-2 A Draft Outline of a Code for Timber Structures - L G Booth
- 6-100-1 Comments on Document 5-100-1; Design of Solid Timber Columns - H J Larsen and E Theilgaard
- 6-100-2 CIB Timber Code: CIB Timber Standards - H J Larsen and E Theilgaard
- 7-100-1 CIB Timber Code Chapter 5.3 Mechanical Fasteners; CIB Timber Standard 06 and 07 - H J Larsen
- 8-100-1 CIB Timber Code - List of Contents (Second Draft) - H J Larsen
- 9-100-1 The CIB Timber Code (Second Draft)
- 11-100-1 CIB Structural Timber Design Code (Third Draft)
- 11-100-2 Comments Received on the CIB Code - U Saarelainen; Y M Ivanov, R H Leicester, W Nozynski, W R A Meyer, P Beckmann; R Marsh
- 11-100-3 CIB Structural Timber Design Code; Chapter 3 - H J Larsen
- 12-100-1 Comment on the CIB Code - Sous-Commission Glulam
- 12-100-2 Comment on the CIB Code - R H Leicester
- 12-100-3 CIB Structural Timber Design Code (Fourth Draft)
- 13-100-1 Agreed Changes to CIB Structural Timber Design Code
- 13-100-2 CIB Structural Timber Design Code. Chapter 9: Performance in Fire
- 13-100-3a Comments on CIB Structural Timber Design Code
- 13-100-3b Comments on CIB Structural Timber Design Code - W R A Meyer
- 13-100-3c Comments on CIB Structural Timber Design Code - British Standards Institution
- 13-100-4 CIB Structural Timber Design Code. Proposal for Section 6.1.5 Nail Plates - N I Bovim
- 14-103-2 Comments on the CIB Structural Timber Design Code - R H Leicester
- 15-103-1 Resolutions of TC 165-meeting in Athens 1981-10-12/13
- 21-100-1 CIB Structural Timber Design Code. Proposed Changes of Sections on Lateral Instability, Columns and Nails - H J Larsen
- 22-100-1 Proposal for Including an Updated Design Method for Bearing Stresses in CIB W18 - Structural Timber Design Code - B Madsen
- 22-100-2 Proposal for Including Size Effects in CIB W18A Timber Design Code - B Madsen
- 22-100-3 CIB Structural Timber Design Code - Proposed Changes of Section on Thin-Flanged Beams - J König
- 22-100-4 Modification Factor for "Aggressive Media" - a Proposal for a Supplement to the CIB Model Code - K Erler and W Rug
- 22-100-5 Timber Design Code in Czechoslovakia and Comparison with CIB Model Code - P Dutko and B Kozelouh

## LOADING CODES

- 4-101-1 Loading Regulations - Nordic Committee for Building Regulations
- 4-101-2 Comments on the Loading Regulations - Nordic Committee for Building Regulations
- 37-101-1 Action Combination Processing for the Eurocodes Basis of Software to Assist the Engineer - Y Robert, A V Page, R Thépaut, C J Mettem
- 43-101-1 Dependant Versus Independent Loads in Structural Design - T Poutanen

## STRUCTURAL DESIGN CODES

- 1-102-1 Survey of Status of Building Codes, Specifications etc., in USA - E G Stern
- 1-102-2 Australian Codes for Use of Timber in Structures - R H Leicester
- 1-102-3 Contemporary Concepts for Structural Timber Codes - R H Leicester
- 1-102-4 Revision of CP 112 - First Draft, July 1972 - British Standards Institution
- 4-102-1 Comparison of Codes and Safety Requirements for Timber Structures in EEC Countries - Timber Research and Development Association
- 4-102-2 Nordic Proposals for Safety Code for Structures and Loading Code for Design of Structures - O A Brynildsen
- 4-102-3 Proposal for Safety Codes for Load-Carrying Structures - Nordic Committee for Building Regulations
- 4-102-4 Comments to Proposal for Safety Codes for Load-Carrying Structures - Nordic Committee for Building Regulations
- 4-102-5 Extract from Norwegian Standard NS 3470 "Timber Structures"
- 4-102-6 Draft for Revision of CP 112 "The Structural Use of Timber" - W T Curry
- 8-102-1 Polish Standard PN-73/B-03150: Timber Structures; Statistical Calculations and Designing
- 8-102-2 The Russian Timber Code: Summary of Contents
- 9-102-1 Svensk Byggnorm 1975 (2nd Edition); Chapter 27: Timber Construction
- 11-102-1 Eurocodes - H J Larsen
- 13-102-1 Program of Standardisation Work Involving Timber Structures and Wood-Based Products in Poland
- 17-102-1 Safety Principles - H J Larsen and H Riberholt
- 17-102-2 Partial Coefficients Limit States Design Codes for Structural Timberwork - I Smith
- 18-102-1 Antiseismic Rules for Timber Structures: an Italian Proposal - G Augusti and A Ceccotti
- 18-1-2 Eurocode 5, Timber Structures - H J Larsen
- 19-102-1 Eurocode 5 - Requirements to Timber - Drafting Panel Eurocode 5
- 19-102-2 Eurocode 5 and CIB Structural Timber Design Code - H J Larsen
- 19-102-3 Comments on the Format of Eurocode 5 - A R Fewell
- 19-102-4 New Developments of Limit States Design for the New GDR Timber Design Code - W Rug and M Badstube
- 19-7-3 Effectiveness of Multiple Fastener Joints According to National Codes and Eurocode 5 (Draft) - G Steck
- 19-7-6 The Derivation of Design Clauses for Nailed and Bolted Joints in Eurocode5 - L R J Whale and I Smith

- 19-14-1 Annex on Simplified Design of W-Trusses - H J Larsen
- 20-102-1 Development of a GDR Limit States Design Code for Timber Structures - W Rug and M Badstube
- 21-102-1 Research Activities Towards a New GDR Timber Design Code Based on Limit States Design - W Rug and M Badstube
- 22-102-1 New GDR Timber Design Code, State and Development - W Rug, M Badstube and W Kofent
- 22-102-2 Timber Strength Parameters for the New USSR Design Code and its Comparison with International Code - Y Y Slavik, N D Denesh and E B Ryumina
- 22-102-3 Norwegian Timber Design Code - Extract from a New Version - E Aasheim and K H Solli
- 23-7-1 Proposal for a Design Code for Nail Plates - E Aasheim and K H Solli
- 24-102-2 Timber Footbridges: A Comparison Between Static and Dynamic Design Criteria - A Ceccotti and N de Robertis
- 25-102-1 Latest Development of Eurocode 5 - H J Larsen
- 25-102-1A Annex to Paper CIB-W18/25-102-1. Eurocode 5 - Design of Notched Beams - H J Larsen, H Riberholt and P J Gustafsson
- 25-102-2 Control of Deflections in Timber Structures with Reference to Eurocode 5 - A Martensson and S Thelandersson
- 28-102-1 Eurocode 5 - Design of Timber Structures - Part 2: Bridges - D Bajolet, E Gehri, J König, H Kreuzinger, H J Larsen, R Mäkipuro and C Mettem
- 28-102-2 Racking Strength of Wall Diaphragms - Discussion of the Eurocode 5 Approach - B Källsner
- 29-102-1 Model Code for the Probabilistic Design of Timber Structures - H J Larsen, T Isaksson and S Thelandersson
- 30-102-1 Concepts for Drafting International Codes and Standards for Timber Constructions - R H Leicester
- 33-102-1 International Standards for Bamboo – J J A Janssen
- 35-102-1 Design Characteristics and Results According to EUROCODE 5 and SNIIP Procedures - L Ozola, T Keskküla
- 35-102-2 Model Code for the Reliability-Based Design of Timber Structures - H J Larsen
- 36-102-1 Predicted Reliability of Elements and Classification of Timber Structures - L Ozola, T Keskküla
- 36-102-2 Calibration of Reliability-Based Timber Design Codes: Choosing a Fatigue Model - I Smith
- 38-102-1 A New Generation of Timber Design Practices and Code Provisions Linking System and Connection Design - A Asiz, I Smith
- 38-102-2 Uncertainties Involved in Structural Timber Design by Different Code Formats - L Ozola, T Keskküla
- 38-102-3 Comparison of the Eurocode 5 and Actual Croatian Codes for Wood Classification and Design With the Proposal for More Objective Way of Classification - V Rajcic A Bjelanovic
- 39-102-1 Calibration of Partial Factors in the Danish Timber Code - H Riberholt
- 41-102-1 Consequences of EC 5 for Danish Best Practise - J Munch-Andersen
- 41-102-2 Development of New Swiss standards for the Assessment of Existing Load Bearing Structures – R Steiger, J Köhler
- 41–102-3 Measuring the CO2 Footprint of Timber Buildings – A Buchanan, S John

45-102-1 Assessment of Relevant Eurocode Based Design Equations in Regard to Structural Reliability - J Köhler, R Steiger

#### INTERNATIONAL STANDARDS ORGANISATION

- 3-103-1 Method for the Preparation of Standards Concerning the Safety of Structures (ISO/DIS 3250) - International Standards Organisation ISO/TC98
- 4-103-1 A Proposal for Undertaking the Preparation of an International Standard on Timber Structures - International Standards Organisation
- 5-103-1 Comments on the Report of the Consultation with Member Bodies Concerning ISO/TC/P129 - Timber Structures - Dansk Ingeniorforening
- 7-103-1 ISO Technical Committees and Membership of ISO/TC 165
- 8-103-1 Draft Resolutions of ISO/TC 165
- 12-103-1 ISO/TC 165 Ottawa, September 1979
- 13-103-1 Report from ISO/TC 165 - A Sorensen
- 14-103-1 Comments on ISO/TC 165 N52 "Timber Structures; Solid Timber in Structural Sizes; Determination of Some Physical and Mechanical Properties"
- 14-103-2 Comments on the CIB Structural Timber Design Code - R H Leicester
- 21-103-1 Concept of a Complete Set of Standards - R H Leicester

#### JOINT COMMITTEE ON STRUCTURAL SAFETY

- 3-104-1 International System on Unified Standard Codes of Practice for Structures - Comité Européen du Béton (CEB)
- 7-104-1 Volume 1: Common Unified Rules for Different Types of Construction and Material - CEB
- 37-104-1 Proposal for a Probabilistic Model Code for Design of Timber Structures - J Köhler, H Faber

#### CIB PROGRAMME, POLICY AND MEETINGS

- 1-105-1 A Note on International Organisations Active in the Field of Utilisation of Timber - P Sonnemans
- 5-105-1 The Work and Objectives of CIB-W18-Timber Structures - J G Sunley
- 10-105-1 The Work of CIB-W18 Timber Structures - J G Sunley
- 15-105-1 Terms of Reference for Timber - Framed Housing Sub-Group of CIB-W18
- 19-105-1 Tropical and Hardwood Timbers Structures - R H Leicester
- 21-105-1 First Conference of CIB-W18B, Tropical and Hardwood Timber Structures Singapore, 26 - 28 October 1987 - R H Leicester

#### INTERNATIONAL UNION OF FORESTRY RESEARCH ORGANISATIONS

- 7-106-1 Time and Moisture Effects - CIB W18/IUFRO 55.02-03 Working Party



**INTERNATIONAL COUNCIL FOR RESEARCH AND INNOVATION  
IN BUILDING AND CONSTRUCTION**

**WORKING COMMISSION W18 - TIMBER STRUCTURES**

**DESIGN OF TIMBER COLUMNS BASED ON 2<sup>ND</sup> ORDER  
STRUCTURAL ANALYSIS**

M Theiler

A Frangi

ETH Zürich, Institute of Structural Engineering IBK, Zürich

R Steiger

Empa, Structural Engineering Research Laboratory, Dübendorf

SWITZERLAND

**MEETING FORTY FIVE**

**VÄXJÖ**

**SWEDEN**

**AUGUST 2012**

---

Presented by M Theiler

G Schickhofer asked if there was any allowance for out of plane torsional buckling. M Theiler responded no. H Larsen stated that it was a déjà vu and test results should be compared to theoretical value at the mean level. M Theiler stated that they used mean values for comparison to test results and Monte Carlo simulations to obtain characteristic values. J Köhler commented about the sensitivity and importance of representing stiffness especially in the slender column. M Theiler agreed and stated that the test columns were not slender as they have a slenderness ratio of 60 to 70. J Malo received clarification that the models were based on measurements performed by H Blass. Material variability within the column is assumed to be taken by variability in the strength data. F Lam received clarification of the difference in definition of slenderness ratio between N. America and Europe. G Doudak received clarification on the grading rule issues and simulation process.



# Design of timber columns based on 2<sup>nd</sup> order structural analysis

Matthias Theiler

Andrea Frangi

ETH Zürich, Institute of Structural Engineering IBK, Zürich, Switzerland

René Steiger

Empa, Materials Science and Technology, Structural Engineering Research Laboratory,  
Dübendorf, Switzerland

## 1 Introduction

Timber is a highly complex material. The mechanical properties of timber are markedly influenced by structural inhomogeneity (knots, deviated grain), by the moisture content and by the duration of load. In addition, the material properties strongly depend on type and orientation of stresses. For example, the behaviour of timber subjected to tension and compression parallel to the grain are totally different from each other. When timber is loaded in tension parallel to the grain, the stress-strain behaviour is linear-elastic up to failure and the specimens fail in brittle manner. In compression parallel to the grain timber shows linear stress-strain behaviour up to a proportional limit smaller than the ultimate strength. Beyond this limit the stiffness declines, leading to a ductile failure with softening after reaching the ultimate strength.

The behaviour of structural members subjected to axial compression or combined axial compression and bending is primarily characterised by the non-linear increase of the deformation due to the increasing eccentricity of the axial load (P-delta effect).

When designing timber members subjected to compression or combined compression and bending such as columns, compression members of truss girders or frame structures both the non-linear material behaviour and the non-linear P-delta effect have to be taken into account. Eurocode 5 [1] provides two different approaches for the design of such kind of structural elements:

- a simplified calculation model based on the *Effective Length Method*
- 2<sup>nd</sup> order structural analysis, as an alternative.

The two approaches are not consistent and can lead to different results. Hence, it is not surprising that this situation provoked controversial discussions in the scientific community [2, 3, 4, 5].

This paper describes a numerical model to analyse the load-bearing behaviour of timber members subjected to compression or combined compression and bending. The model is validated using experimental tests performed at ETH in 1995 [6]. The paper in addition presents a stochastic model on base of which the accurateness of the design approaches given in Eurocode 5 is assessed and modifications of the design approaches are suggested.

## 2 Design of timber columns

### 2.1 Effective Length Method

The *Effective Length Method* (ELM) is a concept of reducing the buckling problem of a structural system to the one of an equivalent simply supported (pinned) column [7]. When designing timber columns, the axial forces and moments are calculated based on a simple 1<sup>st</sup> order analysis and the non-linear effects are taken into account by means of a buckling factor  $k_c$ . The buckling factor  $k_c$  depends on the slenderness ratio  $\lambda$  of the column, which is defined as:

$$\lambda = \frac{\ell_{cr}}{i} \quad (1)$$

with:  $\lambda$  = slenderness ratio  $\ell_{cr}$  = effective buckling length  
 $i$  = radius of gyration.

For the ultimate limit state analysis, Eurocode 5 recommends a linear interaction model for compression and bending, where the buckling factor is used to reduce the compression strength of the timber member.

The buckling factor  $k_c$  in Eurocode 5 is based on extensive investigations by Blaß [8]. Blaß performed Monte Carlo simulations in order to determine the buckling load of timber members subjected to compression. For this purpose, a large number of timber members were simulated. The investigation considered the P-delta effect, the variability of strength and stiffness within the timber members, the geometric imperfection of the members and the non-linear behaviour of wood subjected to compression parallel to the grain.

### 2.2 2<sup>nd</sup> order structural analysis

With a 2<sup>nd</sup> order structural analysis deformed structural systems are studied. Static equilibrium is formulated taking into account geometric non-linearity. Usually linear elastic material behaviour is assumed. By introducing an initial deflection the imperfection of the structural member is accounted for. In case of a simply supported, axially loaded column the 2<sup>nd</sup> order structural analysis can easily be performed assuming sinusoidal distributed initial deflection. The initial deflection in combination with the axial load leads to an initial bending moment  $M_I$ . The P-delta effect causes a magnified moment  $M_{II}$ . This moment  $M_{II}$  can be calculated by multiplying the initial bending moment  $M_I$  by the magnification factor  $\alpha$ :

$$\alpha = \frac{1}{1 - \frac{N}{N_{Euler}}} \quad (2) \quad \text{with:} \quad N_{Euler} = \frac{\pi^2 \cdot EI}{\ell_{cr}^2} \quad (3)$$

and with:  $\alpha$  = magnification factor  $N$  = axial load acting on the column  
 $N_{Euler}$  = Euler buckling load  $E$  = modulus of elasticity (MOE)  
 $I$  = second moment of inertia  $\ell_{cr}$  = effective buckling length.

According to Eurocode 5, the ultimate limit state analysis can be performed using a nonlinear interaction model. This model considers the nonlinear interaction behaviour of wood subjected to combined compression and bending by setting the compression part in the equation to the power of 2.

Since the 2<sup>nd</sup> order structural analysis is based on linear elastic material behaviour, the increase of the deflections caused by the plastic deformation of the material is disregarded. Hence, an adjustment of the results obtained with this method is required. This can be done by reducing the stiffness of the structural member.

According to Eurocode 5, the calculation has to be performed using the design value of MOE (mean value divided by the partial safety factor  $\gamma_M$ ). Other possibilities to account for the reduction in stiffness due to the plastic deformation are to use the 5<sup>th</sup> percentile of MOE instead of the mean value or to calculate a tangent MOE. Engesser [9, 10] suggested in 1895 the reduction of the stiffness for steel columns and hence, to use the tangent modulus ( $T \approx 0.8 \cdot E$ ) instead of the MOE. Engesser's theory was first questioned by other scientists but Shanley showed in 1947 [11], that Engesser's method was a valuable possibility to model the transition between stable and instable state of equilibrium for stocky, non-slender columns and to take into account plastic deformations of the compression zone. In the former Swiss timber design code SIA 164 [12] Engesser's method was implemented. The former German timber design code DIN 1052 [13] recommended to use the 5<sup>th</sup> percentile of MOE divided by the partial safety factor  $\gamma_M$  for a 2<sup>nd</sup> order analysis of single structural members.

Alternatively, the increase of the deflections caused by the plastic deformations could be accounted for by adequately adapting the magnification factor  $\alpha$  (Eq. (2))[14] or by enlarging the assumed initial deflection. This concept of equivalent imperfections is implemented in the current version of Eurocode 3 [15] for the design of steel structures.

### 2.3 Comparison of ELM and 2<sup>nd</sup> order structural analysis

The two calculation models described in 2.1 and 2.2 respectively differ in the way of how they account for geometric and structural imperfections as well as the effects caused by the plastic behaviour of wood subjected to compression. While in ELM these effects are implicitly considered in the calculation of the buckling factor, the effects have to be accounted for explicitly when performing a 2<sup>nd</sup> order structural analysis. Furthermore, the implementation of the two calculation methods in Eurocode 5 differs with respect to the impacts of the moisture content (MC) and the duration of load (DOL). While in recent publications [2, 3, 4] mainly the impact of the MC and the DOL (modification factor  $k_{mod}$ ) on the verification of structural stability was discussed, the present paper is focused on the influence of the plastic material behaviour.

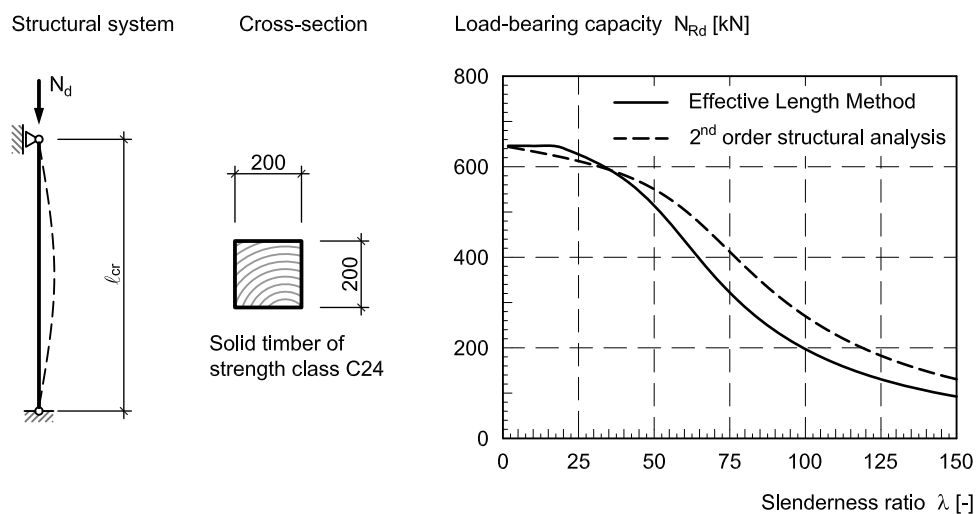


Figure 1: Comparison of ELM and 2<sup>nd</sup> order structural analysis according to Eurocode 5 for a C24 solid timber column with cross-section 200 mm x 200 mm.

Figure 1 shows an exemplary comparison between the two calculation methods for a simply supported column with a cross-section of 200 mm x 200 mm made of C24 solid timber (according to EN 338 [16]). The design value of the load-bearing capacity of the column under pure axial compression is calculated according to Eurocode 5. In this comparison, a modification factor  $k_{\text{mod}}$  equal to 1.0 is used. This is a theoretical value never used for actual design but it ensures that the influence of MC and DOL does not distort the comparison. While the two calculation methods provide similar results for stocky columns, large deviations become apparent for columns of intermediate or high slenderness. It can be seen from the graph that the values obtained with the 2<sup>nd</sup> order structural analysis are up to 40% higher than those obtained with ELM.

### 3 Strain-based model

In order to predict the global buckling behaviour of timber columns, a numerical strain-based model is implemented. Strain-based models are widely used in the design of structural members made from other construction materials than timber. For reinforced concrete (RC) columns, a strain-based model is suggested in [17]. Up to now, these models have not been common for timber columns since the failure mechanism in timber is influenced by the distinct nonlinear stress-strain relationship, which leads to a more complex calculation procedure. As a consequence, only a few applications for timber structures are reported in literature [18, 19].

Figure 2 shows the calculation procedure when applying the strain-based model. On the left hand side, the calculation of the internal force  $N_i$  and the bending moment  $M_i$  is illustrated. The calculation starts by selecting values for the strain  $\epsilon_0$  at the mass centre of the cross-section and for the curvature  $\chi_m$ . These two parameters define the strain distribution within the whole cross-section, when assuming that plane sections remain plane. Based on the strain distribution, the stress distribution is calculated using the relationship given by the stress-strain curve. Any shape of stress-strain curve can be applied in the calculation. Finally, the internal force  $N_i$  and moment  $M_i$  are estimated by integrating the stresses over the whole cross-section.

The right hand side of Figure 2 shows the calculation of the external force  $N_e$  and the bending moment  $M_e$ . The external bending moment  $M_e$  depends on the external force  $N_e$  as well as on the deformation of the column due to the initial imperfections and the P-delta effect. Since the curvature equals the 2<sup>nd</sup> derivation of the deflection curve, the maximal deflection of the column due to the P-delta effect can be calculated as follows:

$$e_{\text{II}} = \iint -\chi(x) \cdot dx^2 = \chi_m \cdot \frac{\ell_{\text{cr}}^2}{c} \quad (3)$$

with:  $e_{\text{II}}$  = maximal deflection (P-delta effect)       $\chi(x)$  = curvature along the column  
 $\chi_m$  = curvature in the middle of the column       $\ell_{\text{cr}}$  = effective buckling length  
 $c$  = integration constant.

The integration constant  $c$  depends on the shape of the deflection. For a simply supported column with sinusoidal distributed deflections the constant  $c$  is equal to  $\pi^2$ . For the further calculation, it is assumed that the initial deflection as well as the deflection caused by the P-delta effect progress in sinusoidal shape. Due to the plastic deformation of timber when subjected to compression parallel to the grain the deflections caused by the P-delta effect will deviate from the sinus curve with increasing load. However, comparative calculations reveal that this simplified assumption is a proper approximation.

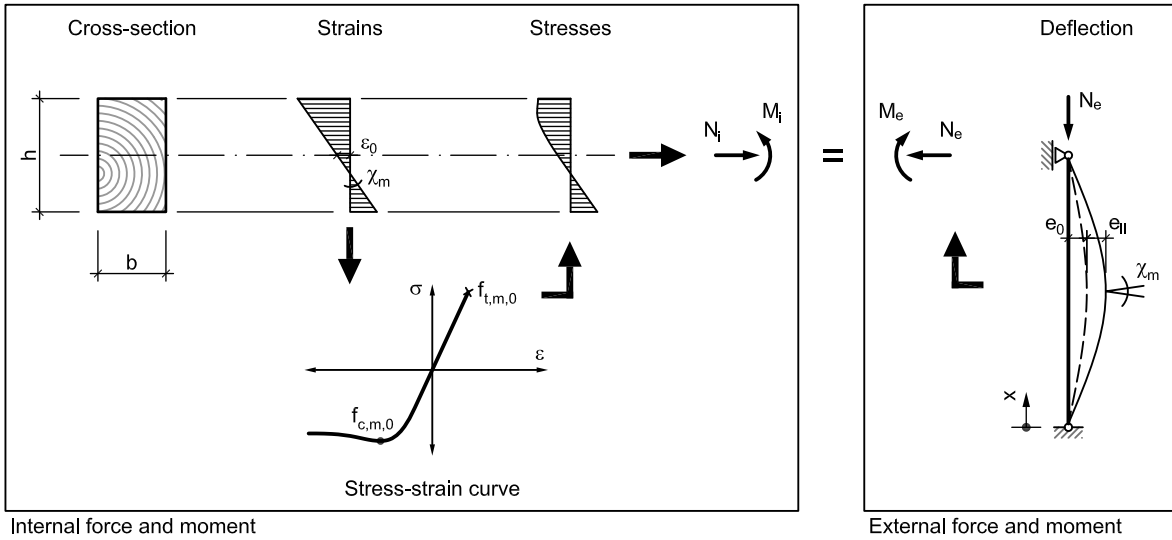


Figure 2: Calculation procedure when applying the strain-based model.

Finally, both the internal moment  $M_i$  and the external moment  $M_e$  depend on the curvature  $\chi_m$ . Hence, equilibrium between internal and external forces and moments can be obtained iteratively.

The presented strain-based model allows for studying the influence of various parameters. E.g. it can be shown that the plastic behaviour of timber when subjected to compression parallel to the grain considerably influences the buckling behaviour of columns. Therefore, the application of an adequate material model (stress-strain relation) is essential when modelling the behaviour of timber members subjected to compression. In the present study the model proposed by Glos [20] is used, since it appears to be more suitable than other material models because it is based on extensive experimental investigations on solid timber boards. In addition Glos developed the model for timber members subjected to compression and bending [21] while other models are mainly focused on timber members subjected to pure bending. Glos' model accounts for the reduction of stiffness before reaching the ultimate compression strength as well as for the subsequent softening.

Figure 3 qualitatively shows the stress-strain relationship proposed by Glos. The description of the full curve in a mathematical form asks for six parameters (Figure 3 right). The MOE in tension  $E_{t,0}$  and the tension strength describe the linear-elastic behaviour subjected to tension. When modelling bending, not the tension strength  $f_{t,0}$  of a timber member but rather the ultimate tension strength at extreme fibres position  $f_{t,m,0}$  is of interest. This strength is remarkably higher than the tension strength  $f_{t,0}$ . The four parameters  $E_{c,0}$ ,  $f_{c,m,0}$ ,  $f_{c,m,u,0}$  and  $\epsilon_{c,0}$  define the material behaviour subjected to compression. Again, not the compression strength  $f_{c,0}$  is of interest but rather the strength  $f_{c,m,0}$ , which is the compression strength of the plastic zone of a member loaded in combined compression and bending. Due to stress redistribution and since the size effects for timber subjected to compression are of minor importance, the compression strength  $f_{c,m,0}$  of the plastic zone and the compression strength  $f_{c,0}$  reaches almost the same level.

The presented strain-based model could be implemented in design codes for timber structures. For this purpose, some simplifications of the material model have to be applied since the polynomial formulation of the material model leads to a complex calculation procedure. In addition, the simplified model should be based on material properties which are listed in the corresponding product standards such as EN 338 [16].

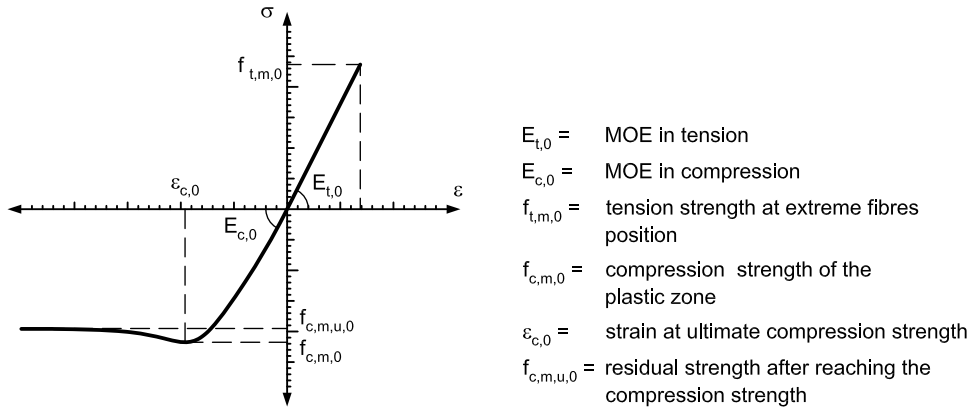


Figure 3: Qualitative representation of the stress-strain relationship for the material model proposed by Glos [20].

## 4 Comparison with experimental data

### 4.1 Experimental data and modelling

The strain-based model is validated with experimental investigations performed at ETH in 1995 [6, 22], where based on a large number of experiments, the load-bearing capacity of timber members subjected to combined axial force and bending moment was examined. The tests were performed using a four point bending test setup (Figure 4) with simultaneously acting axial force. Thereby, solid timber members were subjected to combined axial load (tension or compression) and bending moment.

The members had a length of 2.76 m and rectangular cross-sections of dimensions 80 mm x 160 mm which corresponds to a slenderness ratio  $\lambda$  of 60. The tests were carried out on two samples of different grade (C27 and C40 according to EN 338 [16]), in order to study the influence of the grade on the interaction behaviour. For each grade, eleven test series were carried out including test series with pure axial load, with pure bending moment and with different ratios of axial force and lateral forces. Each sub-sample consisted of 10 specimens. Since the tested material was strength graded by means of an ultrasonic device and by additionally assessing the density, the variation within the sub-sample could be kept low.

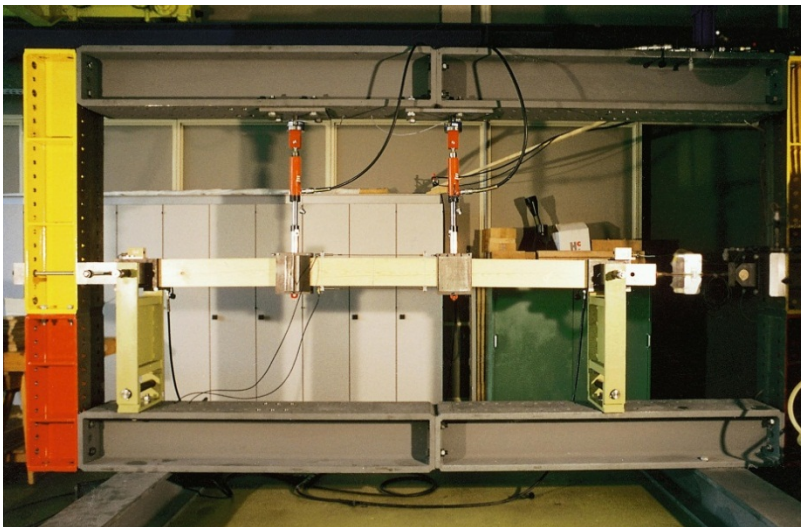


Figure 4: Setup for testing timber members subjected to combined axial force and bending moment [6, 22].

In the present study, the MOE experimentally derived in [6] is used to estimate selected mechanical properties of the single specimens such as compression strength or strain at ultimate compression strength. For this, correlations between the parameters as proposed by Steiger [23] are used. In [23] correlation estimates and regression equations were given for timber from the same growth area and for specimens of the same dimension as mentioned [6, 22]. The material properties not investigated by Steiger ( $f_{c,m,u,0}$  and  $\varepsilon_{c,0}$ ) are estimated based on the results from tests on smaller specimens performed by Glos [20].

## 4.2 Results and discussion

The load-bearing capacity of the specimens is predicted using the strain-based model based on the estimated properties. The calculation procedure described above had to be slightly modified to account for the particular test setup: The lateral load acting on the specimen influences the progression of the member's deflection. As a consequence, the integration constant  $c$  has to be adjusted iteratively for every load increment.

In Figure 5 the predicted values are compared to the experimental ones for three different ratios of axial compression and bending moment. The calculated and the experimentally determined load-bearing capacities are plotted on the Y- and X-axis, respectively. For points below the solid black line under  $45^\circ$ , the predicted values are lower than the test values, while points above the solid line represent tests, where the numerical model overestimates the load-bearing capacity of the test specimens.

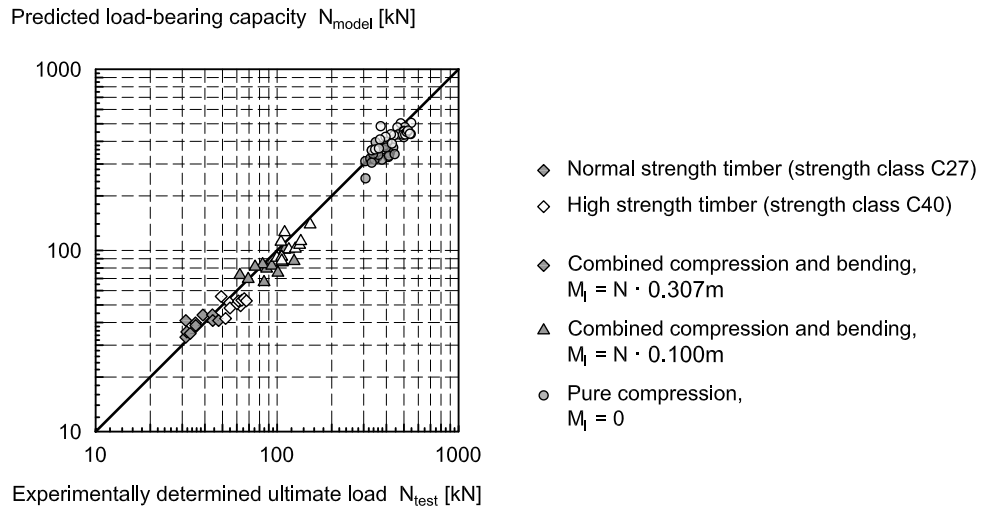


Figure 5: Comparison between the experimentally determined load-bearing capacity  $N_{test}$  and the calculated load-bearing capacity  $N_{model}$  for 80 mm x 160 mm beam-columns with a length of 2.76 m subjected to pure axial compression and to combined axial and transverse loading (4-point bending) [6, 22].

Table 1 shows a detailed comparison of the calculated and experimentally determined load-bearing capacity. For the different test series the mean value  $\mu$  of the ratio between the predicted load-bearing capacity  $N_{model}$  and the experimentally determined load-bearing capacity  $N_{test}$  is given. In addition, the coefficient of correlation  $\rho$  is listed.

The test series with pure compression or combined compression and bending exhibit a good agreement between the model and the experiments. The mean value of the ratio  $N_{model}/N_{test}$  for all test series lies in the range of 0.91 to 0.97. A high correlation is found for the modelled and the experimentally determined data.

In case of pure bending the model overestimates the load-bearing capacity. In addition, the coefficient of correlation for this test series is comparatively low. The load-bearing

capacity of members subjected to pure bending strongly depends on the tension strength at extreme fibres position  $f_{t,m,0}$ . This property is characterised by a high variability and cannot directly be determined from regression equations but rather has to be assessed based on some assumptions. In addition, only 23 experiments in pure bending were performed, whereas the test series with pure compression and combined compression and bending contained a larger database with 44 and 81 tests respectively.

Table 1: Mean value  $\mu$  and coefficient of correlation  $\rho$  of the ratio between the predicted and the experimentally determined load-bearing capacity.

Test series	Ratio	Number of tests	Axial force		Bending moment	
			$\mu$	$\rho$	$\mu$	$\rho$
	$M_I / N$	$n$	$N_{\text{model}} / N_{\text{test}}$		$M_{\text{model}} / M_{\text{test}}$	
<b>Pure bending</b>	$\infty$	23			1.22	0.61
<b>Compression and bending</b>	<b>0.307m</b>	20	0.97			
	<b>0.204m</b>	20	0.92		0.94	
	<b>0.144m</b>	20	0.93			
	<b>0.100m</b>	21	0.91			
<b>Pure compression</b>	<b>0</b>	44	0.94	0.78		
<b>Total</b>		<b>148</b>	<b>0.93</b>		<b>1.22</b>	

In general, there is a good agreement between the estimated and the experimentally derived values for timber member subjected to axial compression and combined compression and bending. The numerical model slightly underestimates the load-bearing capacity, the mean value of the ratio  $N_{\text{model}}/N_{\text{test}}$  is 0.93. For members subjected to pure bending, the numerical model is only capable of producing rough estimations since the model is not developed for this type of loading situation.

## 5 Stochastic model

### 5.1 Modelling

Monte Carlo simulations were performed in order to check the accurateness of the design approaches given in Eurocode 5. Columns of different slenderness and different strength grades were modeled with the strain-based model by assigning them randomly selected material properties. Based on a large number of 2<sup>nd</sup> order simulations, the characteristic load-bearing capacity (defined as the 5<sup>th</sup> percentile) was determined. This characteristic value was then compared to the design methods given in Eurocode 5. The model was simplified in the sense that the inhomogeneity of the material was neglected and only one set of properties was allocated to a specimen. In addition, a simple design situation with a simply supported column was chosen.

### 5.2 Material properties and stress-strain relationship

Six different material properties are needed to describe the full stress-strain relationship (Figure 3). The probability distributions of the properties as well as the correlation between the different properties have to be taken into account. The study was performed for two

different grades of solid timber (C24 and C40 according to EN 338 [16]). The characteristic values given in EN 338 were considered (see Table 2). However, the characteristic values are not sufficient for the purpose of stochastic modelling. Further information on the variability of the mechanical properties is required that can be found in the JCSS probabilistic model code (PMC) [24]. In addition, Glos [20] investigated variability and correlation of the model parameters. Using these investigations and the values given in EN 338 as a basis, a simple stochastic model could be developed.

Table 2: Characteristic values for solid timber according to EN 338.

Material property			Timber grade according to EN 338		
			C24	C40	
Modulus of elasticity	$E_{t,0} / E_{c,0}$	[N/mm <sup>2</sup> ]	Mean value	11'000	14'000
			5 <sup>th</sup> percentile	7'400	9'400
Tension strength	$f_{t,0}$	[N/mm <sup>2</sup> ]	5 <sup>th</sup> percentile	14.0	24.0
Bending strength	$f_{m,0}$	[N/mm <sup>2</sup> ]	5 <sup>th</sup> percentile	24.0	40.0
Compression strength	$f_{c,0}$	[N/mm <sup>2</sup> ]	5 <sup>th</sup> percentile	21.0	26.0

For each material property a mean value, a coefficient of variation and a probabilistic density function was estimated. For the MOE these parameters could straightforwardly be assessed. This material property was modelled according to the suggestions made by the JCSS PMC. The same mean value was chosen for both tension MOE and compression MOE. This was done with regard to a simple stochastic model as well as in order to simplify the model for its application in practice, even though various investigations (e.g. [25]) found differences in the range of several per cent between tension MOE, compression MOE and bending MOE.

The parameters for the tension strength are more demanding to evaluate. As described in section 3, not the tension strength  $f_{t,0}$  of a timber member but rather the ultimate tension strength at extreme fibres position  $f_{t,m,0}$  is of interest. As a reasonable first approach, a tension strength at extreme fibres position  $f_{t,m,0}$  slightly higher than the bending strength  $f_{m,0}$  was supposed to be appropriate. Comparative calculations revealed that this simplified assumption is accurate enough since the tension strength at extreme fibres position had only minor influence on the load-bearing capacity of the members. The compression strength  $f_{c,m,0}$  of the plastic zone was modelled according to the suggestions made for the compression strength  $f_{c,0}$  by the JCSS PMC. The stochastic parameters for the strain  $\epsilon_{c,0}$  at ultimate compression strength and the residual strength  $f_{c,m,u,0}$  after reaching the compression strength were estimated based on the data published by Glos. Table 3 summarises the input data used for the stochastic model.

Not only the probability distribution of the single parameters is of importance, but also the correlation between the parameters has to be considered. The correlation coefficient matrix used in the present study is given in Table 4. The values were mainly taken from the JCSS PMC [24]. For some parameters the correlation coefficients are well known from experimental analysis (such as the correlation between MOE and compression strength). For the parameters  $\epsilon_{c,0}$  and  $f_{c,m,u,0}$  only few information about the correlations are available. Therefore, reasonable assumptions were made based on [20].

Table 3: Mean value  $\mu$ , coefficient of variation COV, probability distribution function PDF and 5<sup>th</sup> percentile of the material parameters.

Material property			Timber grade according to EN 338		
			C24	C40	
Modulus of elasticity	$E_{t,0} / E_{c,0}$	[N/mm <sup>2</sup> ]	Mean value	11'000	14'000
			COV	22.9%	22.9%
			PDF	Lognormal	
			5 <sup>th</sup> percentile	7'390	9'400
Tension strength at extreme fibres position	$f_{t,m,0}$	[N/mm <sup>2</sup> ]	Mean value	40.7	68.0
			COV	25%	25%
			PDF	Lognormal	
			5 <sup>th</sup> percentile	26.4	44.0
Compression strength of the plastic zone	$f_{c,m,0}$	[N/mm <sup>2</sup> ]	Mean value	29.9	36.7
			COV	20%	20%
			PDF	Lognormal	
			5 <sup>th</sup> percentile	21.0	26.0
Strain at ultimate compression strength	$\epsilon_{c,0}$	[‰]	Mean value	3.8	3.8
			COV	20%	20%
			PDF	Lognormal	
			5 <sup>th</sup> percentile	2.7	2.7
Residual strength	$f_{c,m,u,0}$	[N/mm <sup>2</sup> ]	Mean value	26.2	32.2
			COV	15%	15%
			PDF	Lognormal	
			5 <sup>th</sup> percentile	20.0	24.8

Table 4: Coefficients of correlation  $\rho$  of the material parameters.

	$E_{t,0}$	$E_{c,0}$	$f_{t,m,0}$	$f_{c,m,0}$	$\epsilon_{c,0}$	$f_{c,m,u,0}$
$E_{t,0}$	1.0	0.8	0.8	0.4	-0.4	0.2
$E_{c,0}$		1.0	0.6	0.6	-0.6	0.4
$f_{t,m,0}$			1.0	0.5	-0.1	0.2
$f_{c,m,0}$				1.0	-0.2	0.8
$\epsilon_{c,0}$					1.0	-0.2
$f_{c,m,u,0}$						1.0

### 5.3 Geometric properties

In addition to the material properties, the initial deflection  $e_0$  of the column was regarded as a random variable. Ehlbeck and Blaß [26] had performed in-situ measurements of the initial deflections for 142 columns made of solid timber. The measured values were considerably smaller than the initial deflection recommended by Eurocode 5. The results of [26] were used to estimate the stochastic parameters for the relative initial deflection  $e_0 / \ell_{cr}$  (Table 5). The initial deflections were assumed to be sinusoidally distributed along the column.

Further geometric properties such as the width and the height of the cross-section or the length of the column were considered as fixed values. A quadratic cross-section with a side length of 200 mm was chosen. The length of the column was varied between 0 mm and 12'000 mm. This corresponds to a slenderness ratio  $\lambda$  in the range of 0 to 200.

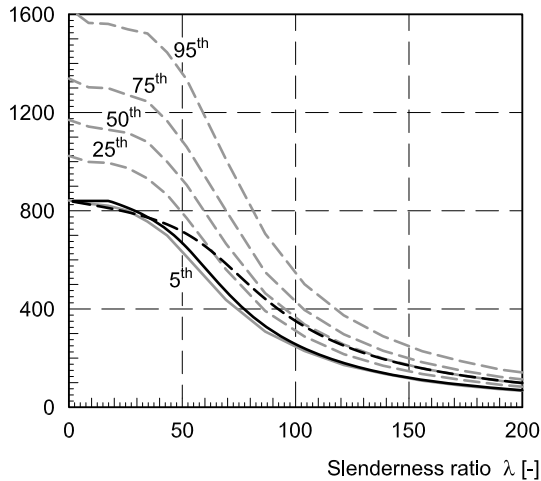
Table 5: Mean value  $\mu$ , standard deviation, probability distribution function PDF and 5<sup>th</sup> percentile of the geometric parameters.

Geometric property	Timber grade according to EN 338	
	C24	C40
Relative initial deflection $e_0 / l_{cr}$	0.0	0.0
Mean value	0.0011	0.0011
Standard dev.	Normal	
PDF	Normal	
95 <sup>th</sup> percentile	0.0017	0.0017

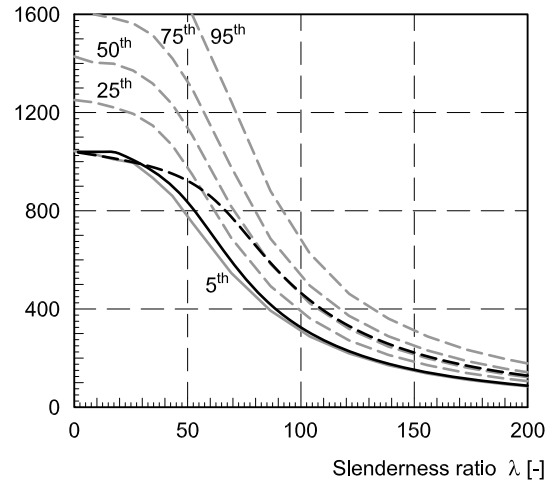
## 5.4 Results and discussion

Based on the stochastically modelled properties, 2<sup>nd</sup> order simulations were carried out with the strain-based model. For each timber grade and slenderness ratio 5'000 columns were simulated. The 5<sup>th</sup> percentile of the load-bearing capacity was determined. This characteristic value was then compared to values calculated by means of the design models given in Eurocode 5 (Figure 6).

Characteristic load-bearing capacity  $N_{Rk}$  [kN] for 200 x 200 mm<sup>2</sup> C24 column



Characteristic load-bearing capacity  $N_{Rk}$  [kN] for 200 x 200 mm<sup>2</sup> C40 column



- Effective Length Method
- - - 2<sup>nd</sup> order structural analysis
- == Percentile of the stochastic model

Figure 6: Characteristic load-bearing capacity of timber columns calculated according to Eurocode 5 and with the stochastic model for solid timber of strength classes C24 (left) and C40 (right).

It can be seen that the variation in the results is larger for stocky columns. This can be explained by the variation of the input parameter. The load-bearing capacity of stocky columns is governed by the compression strength while the load-bearing capacity of slender columns is governed by the MOE. Therefore, the variation of the results is a direct consequence of the variation of these parameters. For columns of intermediate slenderness,

various material properties as well as the initial deflection influence the load-bearing capacity.

When benchmarking to the ELM a good agreement is found. The 2<sup>nd</sup> order structural analysis may lead to an overestimation of the load-bearing capacity especially in case of columns of intermediate and high slenderness. For slender columns, the characteristic values obtained from the 2<sup>nd</sup> order structural analysis are in the range of the 50<sup>th</sup> percentile rather than the 5<sup>th</sup> percentile. This indicates that the design rules for the 2<sup>nd</sup> order structural analysis given in Eurocode 5 do not ensure an accurate design of timber members subjected to compression and therefore should be modified. However, strictly speaking this conclusion is only valid for simply supported columns made of solid timber. Other configurations and materials (glulam) have still to be evaluated. However, the problem is that there is few experimental data available in order to adapt and benchmark the strain-based model.

## 6 Assessment of the Eurocode 5 design approach

The results shown above indicate that the design rules for the 2<sup>nd</sup> order structural analysis given in Eurocode 5 should be reconsidered. As already mentioned in 2.2, other possibilities to account for the reduction in stiffness due to the plastic deformation are to use the 5<sup>th</sup> percentile of MOE instead of the mean value or to calculate a tangent MOE.

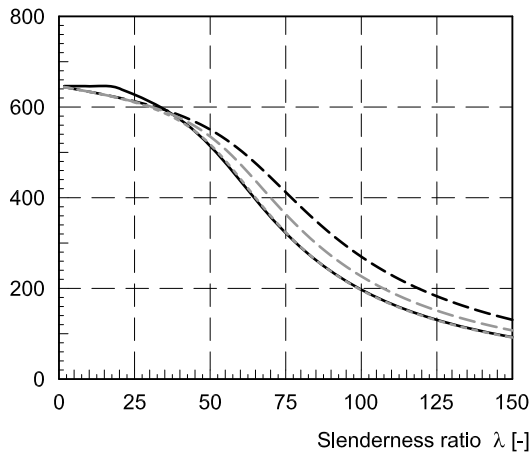
For slender columns, the MOE rather than the strength governs the load-bearing capacity of the column. Hence, it seems to be reasonable to perform the 2<sup>nd</sup> order structural analysis based on a lower-tail value of the MOE rather than a mean value. For solid timber the 5<sup>th</sup> percentile of the MOE is defined as:  $E_{0,05} = 0.67 \cdot E_{0,\text{mean}}$ .

The concept of using the tangent MOE takes into account that the plastic deformation of timber subjected to compression lead to a reduced stiffness of the timber member. This effect can be observed mainly for non-slender columns or columns of intermediate slenderness. The tangent MOE can be estimated as:  $T_{0,\text{mean}} \approx 0.8 \cdot E_{0,\text{mean}}$  [9, 10, 11].

Figure 7 shows an exemplary comparison between ELM and 2<sup>nd</sup> order structural analysis for a simply supported column with a cross-section of 200 mm x 200 mm made of solid timber (C24 and C40). The design value of the load-bearing capacity of the column under pure axial compression is calculated according to Eurocode 5. In addition, 2<sup>nd</sup> order structural analyses are performed using the 5<sup>th</sup> percentile of the MOE and the tangent MOE instead of the mean value. It can be seen from the graphs that the values obtained with reduced MOE (especially when using the 5<sup>th</sup> percentile of MOE) shows a better agreement when being benchmarked to the ELM calculation.

Alternatively, the geometrical imperfections could be replaced by equivalent imperfections. These equivalent imperfections would not only account for the geometrical deviations from the ideal state but also for the structural defects and the effects caused by the plastic material behaviour. Based on mathematical transformations, equivalent imperfections could be calculated leading to identical results compared with the ELM. However, this does not seem to be a appropriate solution. Since the initial deflection has only minor influence on the load-bearing capacity of slender columns, unrealistic large imperfections would be needed for this case. In addition, the initial deflection can depend on the required straightness of timber members which is defined in the national grading rules. As a consequence, the equivalent imperfections could be influenced by the national grading rules. Lastly, the concept of reducing the stiffness describes the physical phenomenon in a more coherent way.

Design value of the load-bearing capacity  $N_{Rd}$  [kN]  
for 200 x 200 mm<sup>2</sup> C24 column



— Effective Length Method  
 - - - 2<sup>nd</sup> order structural analysis,  $E_d = E_{0,mean} / \gamma_M$   
 . . . 2<sup>nd</sup> order structural analysis,  $E_d = E_{0,05} / \gamma_M$   
 - . - 2<sup>nd</sup> order structural analysis,  $E_d = T_{0,mean} / \gamma_M$

Design value of the load-bearing capacity  $N_{Rd}$  [kN]  
for 200 x 200 mm<sup>2</sup> C40 column

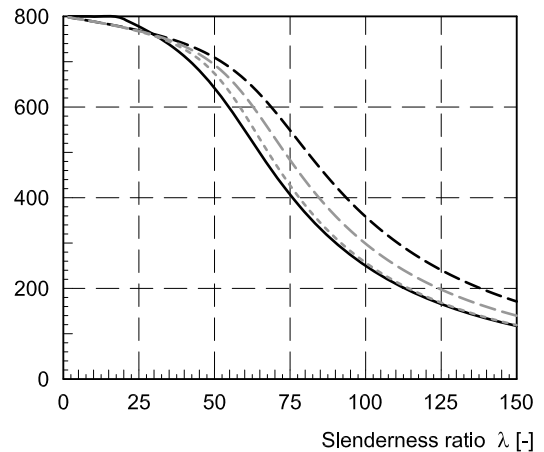


Figure 7: Comparison of ELM and 2<sup>nd</sup> order structural analysis using different design values for the MOE for a C24 (left) and C40 (right) solid timber column with cross-section 200 mm x 200 mm.

This study concentrates on the behaviour of simply supported timber columns. For structural systems such as frame structures the behaviour may be different due to the distribution of the axial load in the single members. Since the axial load influences the reduction of the stiffness due to the plastic deformations, the buckling behaviour depends on the distribution of the axial load and, as a consequence, the results obtained with the ELM or the adjusted 2<sup>nd</sup> order structural analysis can be too safe. Further investigations are required aiming at the development of design rules which ensure an economic and safe use of structural timber systems subjected to compression or combined compression and bending.

## 7 Conclusions

In this paper, a numerical strain-based model is presented which describes the behaviour of timber members subjected to compression and bending. The capability of the model in providing adequate values of load-bearing capacity of solid timber columns supported in simply beam configuration was assessed by benchmarking calculated values to experimental results from a study performed at ETH in 1995. In addition, the mechanical model was combined with a stochastic model for the material properties and according Monte Carlo simulations were performed. The results of these simulations were compared to the design rules given in Eurocode 5.

While the simplified calculation model (*Effective Length Method*) coincides with the results from the simulations, the 2<sup>nd</sup> order structural analysis may lead to an overestimation of the load-bearing capacity. This result indicates that the design rules given in Eurocode 5 should be reconsidered. In particular, modifications are suggested for the design value of the MOE which is the basis of the 2<sup>nd</sup> order structural analysis. It is suggested to use the 5<sup>th</sup> percentile of the MOE or a tangent MOE ( $T \approx 0.8 \cdot E$ ) instead of the mean value of the MOE as it is recommended in Eurocode 5.

## 7 References

- [1] CEN 2004: "EN 1995-1-1: Eurocode 5: Design of timber structures - Part 1-1: General - Common rules and rules for buildings"; European Committee for Standardization; Brussels, Belgium.
- [2] Kessel, M.H., Schönhoff, T., Hörsting, P. 2005: "Zum Nachweis von druckbeanspruchten Bauteilen nach DIN 1052:2004-08, Teil 1"; Bauen mit Holz 107 (12), 88-96.
- [3] Kessel, M.H., Schönhoff, T., Hörsting, P. 2006: "Zum Nachweis von druckbeanspruchten Bauteilen nach DIN 1052:2004-08, Teil 2"; Bauen mit Holz 108 (1), 41-44.
- [4] Möller, G. 2007: "Zur Traglastermittlung von Druckstäben im Holzbau"; Bautechnik 84 (5), 329-334.
- [5] Köhler, J., Frangi, A., Steiger, R. 2008: "On the role of stiffness properties for ultimate limit state design of slender columns"; Paper No. 41-1-1 in: Proceedings of CIB-W18 Meeting 41; St. Andrews, Canada.
- [6] Steiger, R. 1995: "Versuche an Fichten-Kanthölzern: Biegemoment-Normalkraft-Interaktion"; IBK Bericht Nr. 209, ETH Zurich; Birkhäuser; Basel, Switzerland.
- [7] Blaß, H.J. 1995: "Buckling length"; Chapter B7 in: Timber engineering, STEP 1; Centrum Hout; Almere, Netherlands.
- [8] Blaß, H.J. 1987: "Tragfähigkeit von Druckstäben aus Brettschichtholz unter Berücksichtigung streuender Einflussgrößen"; Dissertation; Universität Fridericiana Karlsruhe; Karlsruhe, Germany.
- [9] Engesser, F. 1895: "Knickfragen"; Schweizerische Bauzeitung 25 (13), 88-91.
- [10] Engesser, F. 1895: "Ueber Knickfragen"; Schweizerische Bauzeitung 26 (4), 24-26.
- [11] Shanley, F.R. 1947: "Inelastic column theory"; Journal of the Aeronautical Sciences 14 (5), 261-267.
- [12] SIA 1981: "Norm SIA 164: Holzbau"; Swiss Society of Engineers and Architects; Zurich, Switzerland.
- [13] DIN 2008: "DIN 1052: Entwurf, Berechnung und Bemessung von Holzbauwerken - Allgemeine Bemessungsregeln und Bemessungsregeln für den Hochbau"; Beuth; Berlin, Germany.
- [14] Johns, K.C., Buchanan, A.H. 1982: "Strength of timber members in combined bending and axial loading"; Paper No. 24 in: Proceedings of the IUFRO Timber Engineering Group Meeting; Sweden.
- [15] CEN 2010: "EN 1993-1-1: Eurocode 3: Design of steel structures - Part 1-1: General rules and rules for buildings"; European Committee for Standardization; Brussels, Belgium.
- [16] CEN 2009: "EN 338: Structural timber, Strength classes"; European Committee for Standardization; Brussels, Belgium.
- [17] CEB/FIP 1978: "Manual of buckling and instability"; Comité Euro-International du Béton and Fédération Internationale de la Précontrainte; The Construction Press Ltd; Lancaster, England.
- [18] Buchanan, A.H. 1984: "Strength model and design methods for bending and axial loading interaction in timber members"; Dissertation; University of British Columbia; Vancouver, Canada.
- [19] Hörsting, O.P. 2008: "Zum Tragverhalten druck- und biegebeanspruchter Holzbauteile"; Dissertation; TU Braunschweig; Braunschweig, Germany.
- [20] Glos, P. 1978: "Zur Bestimmung des Festigkeitsverhaltens von Brettschichtholz bei Druckbeanspruchung aus Werkstoff- und Einwirkungskenngrößen"; Dissertation; TU München; Munich, Germany.
- [21] Glos, P. 1981: "Zur Modellierung des Festigkeitsverhaltens von Bauholz bei Druck-, Zug- und Biegebeanspruchung"; Sonderforschungsbereich 96, TU München; München.
- [22] Steiger, R., Fontana, M. 2005: "Bending moment and axial force interacting on solid timber beams"; Materials and Structures 38 (279), 507-513.
- [23] Steiger, R. 1995: "Biege-, Zug- und Druckversuche an Schweizer Fichtenholz"; IBK Bericht Nr. 207, ETH Zürich; Birkhäuser; Basel, Switzerland.
- [24] Jonit Committee on Structural Safety 2007: "Probabilistic Model Code"; JCSS Joint Committee on Structural Safety; [www.jcss.byg.dtu.dk](http://www.jcss.byg.dtu.dk).
- [25] Steiger, R., Arnold, M. 2009: "Strength grading of Norway spruce structural timber: revisiting property relationship used in EN 338 classification system"; Wood Science and Technology 43 (3-4), 259-278.
- [26] Ehlbeck, J., Blaß, H.J. 1987: "Imperfektionsannahmen für Holzdruckstäbe"; Holz als Roh- und Werkstoff 45, 231-235.

**INTERNATIONAL COUNCIL FOR RESEARCH AND INNOVATION  
IN BUILDING AND CONSTRUCTION**

**WORKING COMMISSION W18 - TIMBER STRUCTURES**

**HARMONISED TENSILE STRENGTH CLASSES**

J K Denzler  
Holzforschung Austria, Vienna

**AUSTRIA**

**MEETING FORTY FIVE**

**VÄXJÖ**

**SWEDEN**

**AUGUST 2012**

---

Presented by J Denzler

H Blass stated that the study is proposing to lower the density which would penalize connection design. He suggested that a  $\Delta\rho$  for pine could be used to account for its higher density. J Denzler agreed. G Schickhofer stated that proof loading concept could help in terms of density. J Denzler agreed but not all companies had such equipment.



# Harmonised tensile strength classes

Dr.-Ing. Julia K. Denzler  
Holzforschung Austria, Vienna

## 1 Introduction

Safe use of timber in constructions requires that its main properties are characterised. EN 338 defines these main properties for bending members in different strength classes. Within EN 338 the main characterising properties are characteristic bending strength, mean modulus of elasticity in bending and characteristic density. All other values, e.g. tensile strength or compression strength, are defined using equations to obtain corresponding values on the safe side. EN 338 comprises so called "C" classes for softwood and poplar and so called "D" classes for hardwoods. These abbreviations are probably derived from "coniferious wood" for softwoods ("C"-classes) and from the morphogenetic term "dicotyledoneae" for hardwoods ("D"-classes), meaning that the plant seed has two embryonic leaves.

With advancing production methods the development in timber construction also was pushed forward. Today, a big amount of timber is used in glulam, where the design is based on the members predominantly loaded in tension. The growing popularity of timber products mainly loaded in tension made it necessary to create tensile strength classes comparable to bending strength classes in EN 338.

Within machine strength grading, this necessity was identified more than 10 years ago. Therefore, several tensile strength classes have been introduced in EN 14081-4, defining the basic properties:

- characteristic tensile strength ( $f_{t,0,k}$ ),
- mean modulus of elasticity in tension ( $E_{t,0,mean}$ ),
- characteristic density ( $\rho_k$ ).

This paper deals with these tensile strength classes for softwood, compares them with each other and additionally develops a proposal for harmonised classes based on test data. The aim of this paper is to propose tensile strength classes reflecting the relationships for tensile members in reality in the best way. This will lead to the best grading output available and will increase the utilization of timber. Aspects like appropriate strength class combinations for glulam are not considered.

## 2 Existing strength profiles

Up to now, several tensile strength classes are defined in EN 14081-4 or in succeeding ITT-reports, e.g. "L" classes, "LS" classes or "LD" classes. The latest version of prEN 14080 for glulam introduces "T"-classes for tension members. Tab. 1 summarizes the different strength classes with respect to characteristic tensile strength value and compares them with the corresponding values given in EN 338. For modulus of elasticity (E), EN 338 only offers a bending E. As this is comparable to the E used in tensile strength classes so far, it is also given in Tab. 1 as tensile E.

Since there is no normative document like EN 338 to define a global set of tensile strength classes, actual classes are representing the various needs in different countries: E.g. in LS classes originating from Scandinavia the density values are indicative only and are not taken into account when calculating machine settings.

Fig. 1 summarizes these classes and their relationships of characteristic tensile strength ( $f_{t,0,k}$ ) and E in tension ( $E_{t,0,mean}$ ) as well as characteristic tensile strength ( $f_{t,0,k}$ ) and density ( $\rho_k$ ).

Tab. 1 and Fig. 1 clearly identify the need to harmonise these classes in order to reduce the number of strength classes and help the user to identify the class needed.

Tab. 1: Summary of existing tensile strength profiles.

name origin		T FprEN 14080	L EN 14081-4 or ITT	LD EN 14081-4 or ITT	LS EN 14081-4 or ITT	C EN 338
$f_{t,0,k}$	N/mm <sup>2</sup>	T8 8				C14 8
$E_{t,0,mean}$	N/mm <sup>2</sup>	7000				7000
$\rho_k$	kg/m <sup>3</sup>	290				290
$f_{t,0,k}$	N/mm <sup>2</sup>	T9 9				
$E_{t,0,mean}$	N/mm <sup>2</sup>	7500				
$\rho_k$	kg/m <sup>3</sup>	300				
$f_{t,0,k}$	N/mm <sup>2</sup>	T10 10	L16 10			C16 10
$E_{t,0,mean}$	N/mm <sup>2</sup>	8000	8000			8000
$\rho_k$	kg/m <sup>3</sup>	310	310			310
$f_{t,0,k}$	N/mm <sup>2</sup>	T11 11	L17 11	LD11 11	LS11 11	C18 11
$E_{t,0,mean}$	N/mm <sup>2</sup>	9000	9000	9000	9000	9000
$\rho_k$	kg/m <sup>3</sup>	320	320	320	--*	320
$f_{t,0,k}$	N/mm <sup>2</sup>	T12 12				C20 12
$E_{t,0,mean}$	N/mm <sup>2</sup>	9500				9500
$\rho_k$	kg/m <sup>3</sup>	330				330
$f_{t,0,k}$	N/mm <sup>2</sup>	T13 13	L22 13			C22 13
$E_{t,0,mean}$	N/mm <sup>2</sup>	10000	10000			10000
$\rho_k$	kg/m <sup>3</sup>	340	340			340
$f_{t,0,k}$	N/mm <sup>2</sup>	T14 14	L24 14			C24 14
$E_{t,0,mean}$	N/mm <sup>2</sup>	11000	11000			11000
$\rho_k$	kg/m <sup>3</sup>	350	350			350
$f_{t,0,k}$	N/mm <sup>2</sup>	T14,5 14,5	L25 14,5	LD15 14,5	LS15 14,5	
$E_{t,0,mean}$	N/mm <sup>2</sup>	11000	11000	11000	11000	
$\rho_k$	kg/m <sup>3</sup>	350	350	350	--*	
$f_{t,0,k}$	N/mm <sup>2</sup>	T15 15				
$E_{t,0,mean}$	N/mm <sup>2</sup>	11500				
$\rho_k$	kg/m <sup>3</sup>	360				
$f_{t,0,k}$	N/mm <sup>2</sup>	T16 16	L27 16			C27 16
$E_{t,0,mean}$	N/mm <sup>2</sup>	11500	11500			11500
$\rho_k$	kg/m <sup>3</sup>	370	370			370

Tab. 1: Summary of existing tensile strength profiles (continued).

name origin		T FprEN 14080	L EN 14081-4 or ITT	LD EN 14081-4 or ITT	LS EN 14081-4 or ITT	C EN 338
f <sub>t,0,k</sub>	N/mm <sup>2</sup>	T18 18	L30 18	LD18 18	LS18 18	C30 18
E <sub>t,0,mean</sub>	N/mm <sup>2</sup>	12000	12000	12000	12000	12000
ρ <sub>k</sub>	kg/m <sup>3</sup>	380	380	370	--*	380
f <sub>t,0,k</sub>	N/mm <sup>2</sup>	T21 21	L35 21			C35 21
E <sub>t,0,mean</sub>	N/mm <sup>2</sup>	13000	13000			13000
ρ <sub>k</sub>	kg/m <sup>3</sup>	390	400			400
f <sub>t,0,k</sub>	N/mm <sup>2</sup>	T22 22	L36 22	LD22 22	LS22 22	
E <sub>t,0,mean</sub>	N/mm <sup>2</sup>	13000	13000	13000	13000	
ρ <sub>k</sub>	kg/m <sup>3</sup>	390	400	390	--*	
f <sub>t,0,k</sub>	N/mm <sup>2</sup>	T24 24				C40 24
E <sub>t,0,mean</sub>	N/mm <sup>2</sup>	13500				14000
ρ <sub>k</sub>	kg/m <sup>3</sup>	400				420
f <sub>t,0,k</sub>	N/mm <sup>2</sup>	T26 26	L40 26	LD26 26	LS26 26	
E <sub>t,0,mean</sub>	N/mm <sup>2</sup>	14000	14000	14000	14000	
ρ <sub>k</sub>	kg/m <sup>3</sup>	410	420	410	--*	
f <sub>t,0,k</sub>	N/mm <sup>2</sup>	T27 27	L45 27			C45 27
E <sub>t,0,mean</sub>	N/mm <sup>2</sup>	15000	15000			15000
ρ <sub>k</sub>	kg/m <sup>3</sup>	410	440			440
f <sub>t,0,k</sub>	N/mm <sup>2</sup>	T28 28				
E <sub>t,0,mean</sub>	N/mm <sup>2</sup>	15000				
ρ <sub>k</sub>	kg/m <sup>3</sup>	420				
f <sub>t,0,k</sub>	N/mm <sup>2</sup>	T30 30				C50 30
E <sub>t,0,mean</sub>	N/mm <sup>2</sup>	15500				16000
ρ <sub>k</sub>	kg/m <sup>3</sup>	430				460

\*) The density values are indicative only and are not taken into account when calculating settings.

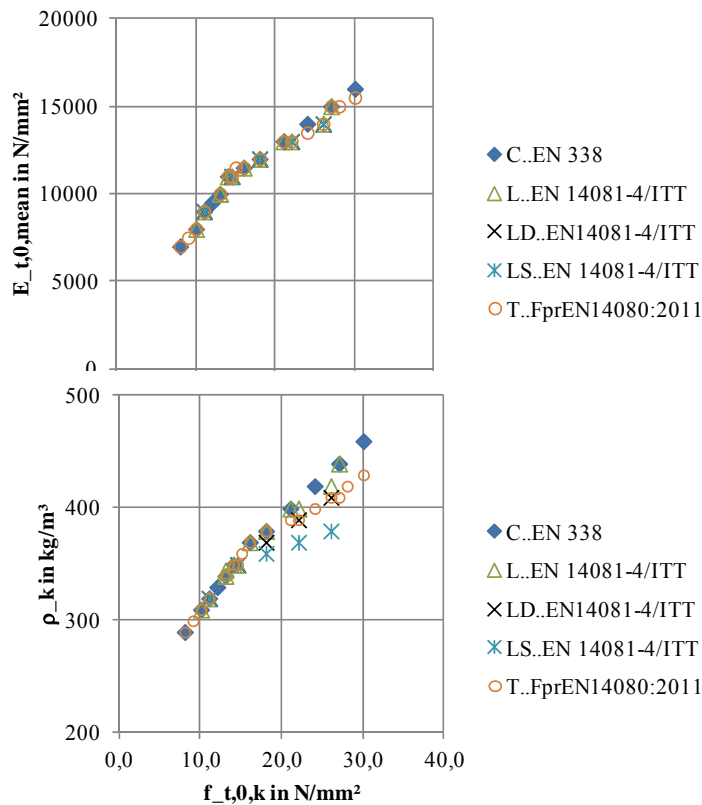


Fig. 1: Characteristic values for different tensile strength profiles.

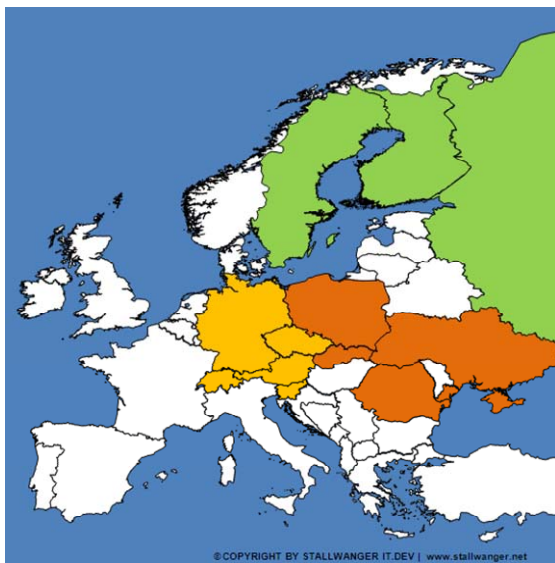
### 3 Material and Methods

#### 3.1 Material

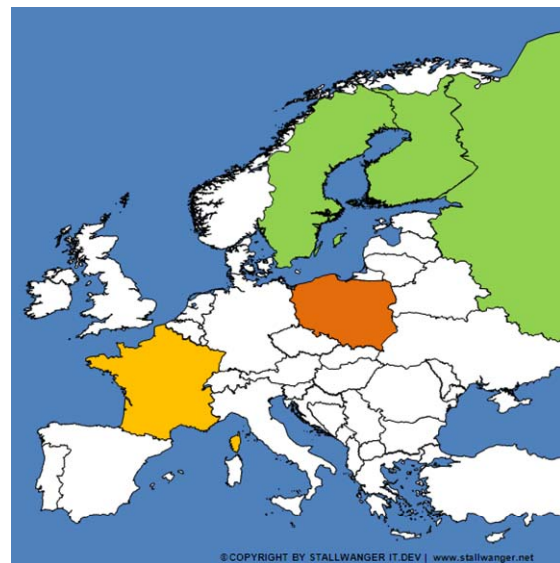
6699 specimens tested in tension were evaluated to develop an adequate proposal. The species comprised only Norway spruce (*Picea abies*), European Silver fir (*Abies alba*) and Scots pine (*Pinus sylvestris*). Other softwoods have not been considered. Norway spruce and European Silver fir are analysed together in the following as European Silver fir only comprises a small amount of pieces. Tab. 2 summarises the species and the source of the data with respect to area and country. Fig. 2 shows the chosen areas named Northern, Central and Eastern Europe and the source countries within each area divided into species, whereas the combination of Northern, Central and Eastern Europe is called Combined Europe.

Tab. 2: Overview of specimens used for the evaluation.

area	spruce / fir		total	pine		total	total
	country	no.		country	no.		
Northern Europe	FI	270	667	FI	257	634	
	RU	186		RU	171		
	SE	211		SE	206		
Central Europe	AT	1156	3879	FR	239	239	
	CH	768					
	CZ	374					
	DE	1477					
	SI	104					
Eastern Europe	PL	219	1063	PL	217	217	
	RO	313					
	SK	211					
	UA	320					
Combined Europe			5609			1090	6699



spruce/fir, n = 5609 specimens



pine, n = 1090 specimens

Fig. 2: Areas Northern, Central and Eastern Europe and source countries within each area divided into species.

All specimens have been tested in destructive tension tests according to EN 408 and EN 384. The characteristic properties of each piece were determined according to EN 384. The tensile strength values were adjusted to a width of 150 mm ( $k_h$ -factor). Most of the specimens are tested over a length of  $9 \cdot h$  following EN 408. For one country the test span differed from  $9 \cdot h$ . The tensile strength was adapted to a length of  $9 \cdot h$  following the proposal of LAM & VAROGLU 1990.

## 3.2 Methods

In machine strength grading the grading process is usually focused on strength. One main grading principle in use up to now is measuring the so called “dynamic E” based on longitudinal frequency measurement or longitudinal running time measurement, both in combination with length. Additionally, density information can improve the prediction. Also parameters like knots can improve the grading result. This principle aims at predicting E or strength. This paper makes use of this grading principle in a perfect manner: The E measured during destructive testing is used as indicating property to grade the material in a first step. In a second step, the strength measured during destructive testing is used as indicating property.

From Fig. 1 follows that "L" classes represent the relationship of most of the already existing tensile strength classes. Therefore, these "L" classes are used for comparison. To get a first impression of the relationships in tension, sliding characteristic values are calculated out of 200 specimens ordered with respect to E and divided into species. For these 200 specimens, the sliding 5<sup>th</sup>-percentile for strength, the sliding mean E and the sliding 5<sup>th</sup>-percentile for density are directly calculated using the ranking method.

Additionally, 8 different strength class combinations are examined based on strength class combinations in use according to EN 14081-4. E is considered as indicating property for this simulation. Due to the dependency of characteristic values on the number of specimens in a grade, different strength class combinations are evaluated. It is also taken into account that the sequence of strength classes within a strength class combination can influence the result. Tab. 3 summarizes the bandwidths of E and the combinations of the different bandwidths divided into species. The bandwidths are based on fulfilling at least the required characteristic strength within the class. For each bandwidth the corresponding characteristic tensile strength, the corresponding mean E in tension and the corresponding characteristic density are calculated out of the test data using the ranking method as well as the method proposed in EN 14358. If less than 20 pieces are included in a grade, the results are neglected as the ranking method is not robust in this case.

To complete the knowledge of relationships, the whole data is graded with strength as indicating property for the same strength class combinations separately for spruce/fir and pine. This simulates a grading machine predicting strength in a perfect manner not existing so far. As bandwidth, the corresponding strength requirements of each strength class are taken (Tab. 4).

Tab. 3: Bandwidths for E as indicating property and corresponding "L" class combinations for spruce/fir and pine.

bandwidth	I	II	III	IV	corresp. "L" class
spruce/fir	$\geq 12900$	$\geq 9500 \ \& \ < 12900$	$\geq 6300 \ \& \ < 9500$	$< 6300$	L40 & L30 & L17 & Reject
E_t	$\geq 11000$	$\geq 8300 \ \& \ < 11000$	$\geq 7300 \ \& \ < 8300$	$< 7300$	L36 & L25 & L17 & Reject
in	$\geq 12900$	$\geq 7600 \ \& \ < 12900$	$< 7600$		L40 & L25 & Reject
N/mm <sup>2</sup>	$\geq 11000$	$\geq 3000 \ \& \ < 11000$	$< 3000$		L36 & L17 & Reject
	$\geq 9200$	$\geq 6600 \ \& \ < 9200$	$< 6600$		L30 & L17 & Reject
	$\geq 8100$	$\geq 7400 \ \& \ < 8100$	$< 7400$		L27 & L17 & Reject
	$\geq 7100$	$< 7100$			L25 & Reject
	$\geq 5000$	$< 5000$			L22 & Reject
pine	$\geq 12900$	$\geq 10500 \ \& \ < 12900$	$\geq 6700 \ \& \ < 10500$	$< 6700$	L40 & L30 & L17 & Reject
E_t	$\geq 10800$	$\geq 9300 \ \& \ < 10800$	$\geq 8000 \ \& \ < 9300$	$< 8000$	L36 & L25 & L17 & Reject
in	$\geq 12900$	$\geq 8600 \ \& \ < 12900$	$< 8600$		L40 & L25 & Reject
N/mm <sup>2</sup>	$\geq 10800$	$\geq 6600 \ \& \ < 10800$	$< 6600$		L36 & L17 & Reject
	$\geq 9900$	$\geq 7400 \ \& \ < 9900$	$< 7400$		L30 & L17 & Reject
	$\geq 8900$	$\geq 8000 \ \& \ < 8900$	$< 8000$		L27 & L17 & Reject
	$\geq 8300$	$< 8300$			L25 & Reject
	$\geq 7100$	$< 7100$			L22 & Reject

Tab. 4: Bandwidths for tensile strength as indicating property and corresponding "L" class combinations for spruce and pine.

bandwidth	I	II	III	IV	corresp. "L" class
<b>spruce/fir</b>	$\geq 26,0$	$\geq 18,0 \ \& \ < 26,0$	$\geq 11,0 \ \& \ < 18,0$	$< 11,0$	L40 & L30 & L17 & Reject
<b>&amp; pine</b>	$\geq 22,0$	$\geq 14,5 \ \& \ < 22,0$	$\geq 11,0 \ \& \ < 14,5$	$< 11,0$	L36 & L25 & L17 & Reject
f_t	$\geq 26,0$	$\geq 14,5 \ \& \ < 26,0$	$< 14,5$		L40 & L25 & Reject
in	$\geq 22,0$	$\geq 11,0 \ \& \ < 22,0$	$< 11,0$		L36 & L17 & Reject
N/mm <sup>2</sup>	$\geq 18,0$	$\geq 11,0 \ \& \ < 18,0$	$< 11,0$		L30 & L17 & Reject
	$\geq 16,0$	$\geq 11,0 \ \& \ < 16,0$	$< 11,0$		L27 & L17 & Reject
	$\geq 14,5$	$< 14,5$			L25 & L17 & Reject
	$\geq 13,0$	$< 13,0$			L22 & Reject

## 4 Results

Fig. 3 shows the relationship between characteristic tensile strength, mean E in tension and characteristic density divided into species based on the sliding percentiles of 200 specimens with respect to E. For pine the comparison of the characteristic values and the "L" classes shows that the relationship between E and characteristic tensile strength is fitting quite well and the relationship between characteristic density and characteristic tensile strength is not problematic at all. For spruce/fir the relationship between E and characteristic tensile strength has the same tendency on a slightly lower level compared to the "L" classes. For the relationship between characteristic density and characteristic tensile strength the tendency seems to be different. The data shows a lower increase as presumed in the "L" classes.

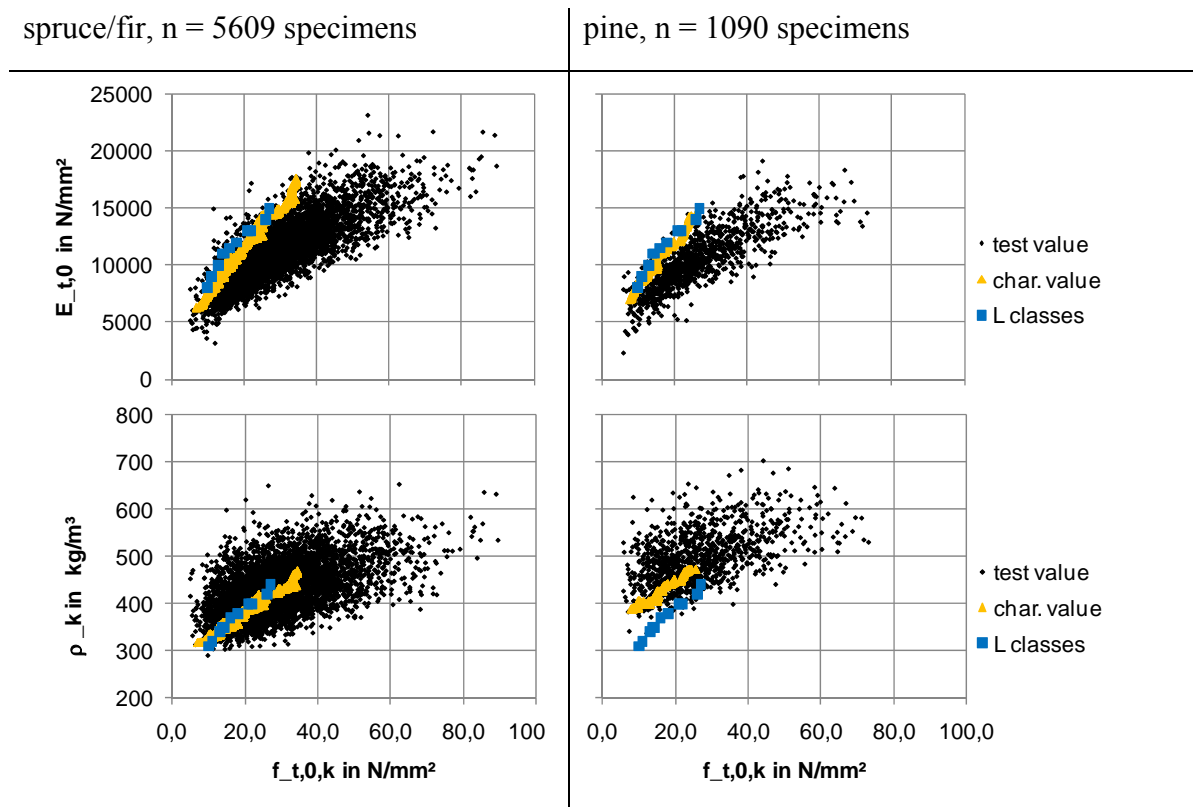


Fig. 3: Relationships for spruce/fir and pine in tension divided into species.

Fig. 4 and Fig. 5 show the results of the simulated grading with E as indicating property for spruce/fir, Fig. 6 and Fig. 7 for pine. The grading is based on all data available for each species. Nevertheless, the results are presented for Combined Europe as well as Northern, Central and Eastern Europe using the same bandwidth to show possible differences.

For Combined Europe the relationship between E and tensile strength seems to fit to the given "L" classes especially around  $f_{t,k} = 18 \text{ N/mm}^2$ . For lower strength values, the data shows lower E-values than assumed in the "L" classes whereas the relationship for higher strength values seems to be reversed. This relationship is mainly based on Central European data as more than 3/5 of the data for spruce comes from Central Europe. Based on this dataset, the relationship between E and tensile strength seems to be on a slightly lower level for Northern and Eastern Europe compared to Central Europe.

The relationship between density and strength seems to be slightly overestimated by the "L" classes on a combined level. Especially for Northern and Eastern Europe the density is on a lower level as assumed by the "L" classes for the same strength.

The results for pine do not seem to be critical: The data confirms the "L" class relationship between E and characteristic tensile strength with a slightly lower level for Northern Europe and slightly higher level for Eastern Europe. The relationship of density and strength is uncritical as density of pine is far above the requirement.

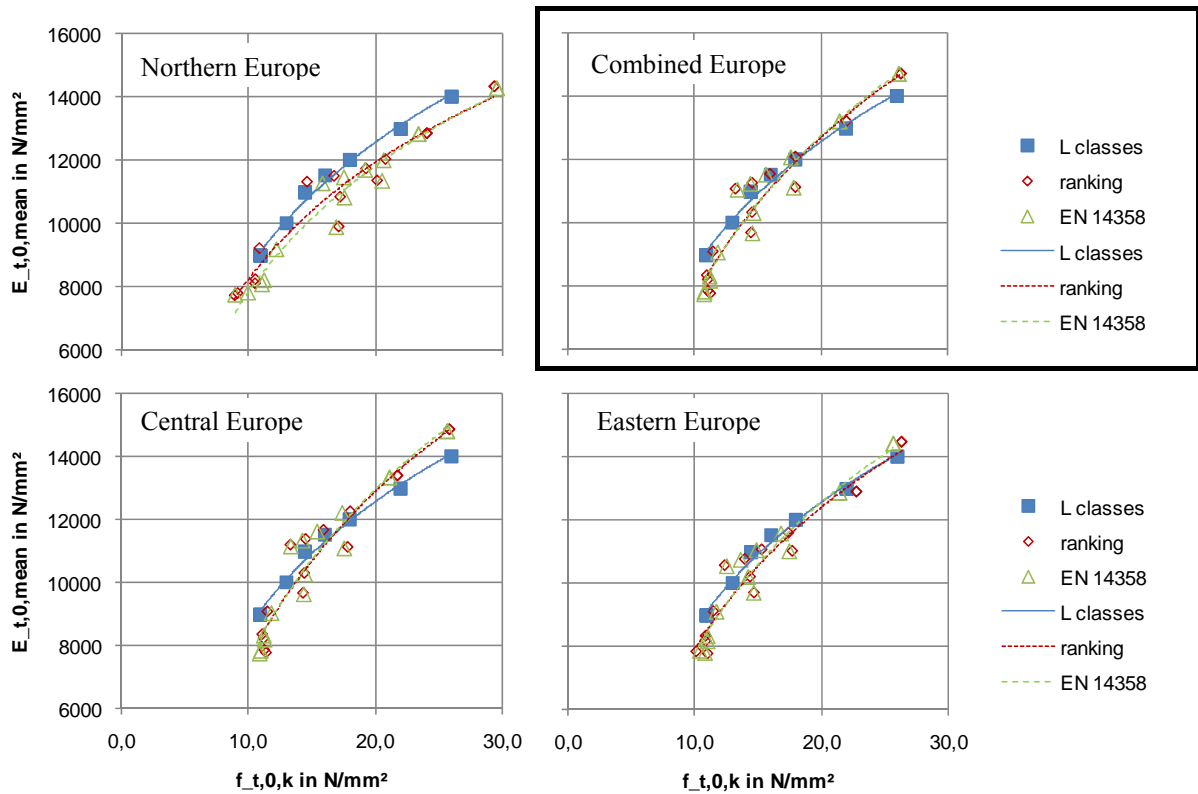


Fig. 4: E versus tensile strength for spruce/fir, n = 5609 specimens.

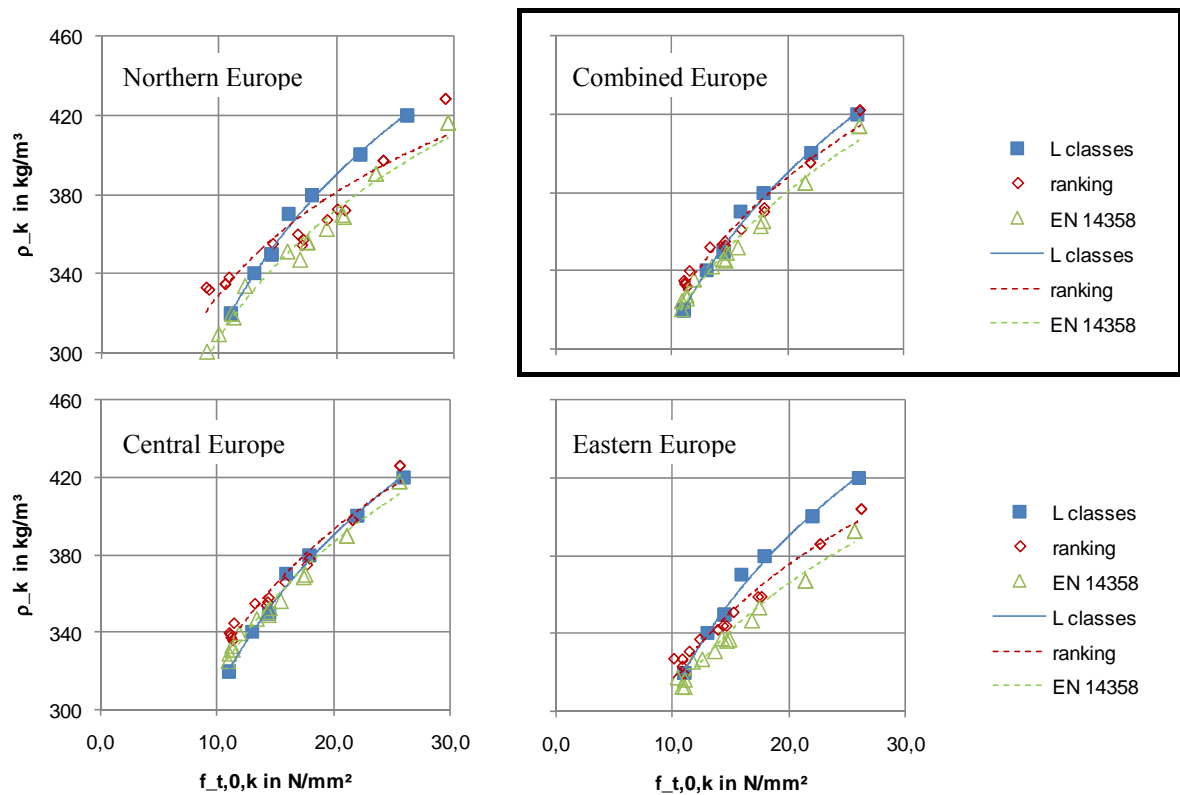


Fig. 5: Density versus tensile strength for spruce/fir, n = 5609 specimens.

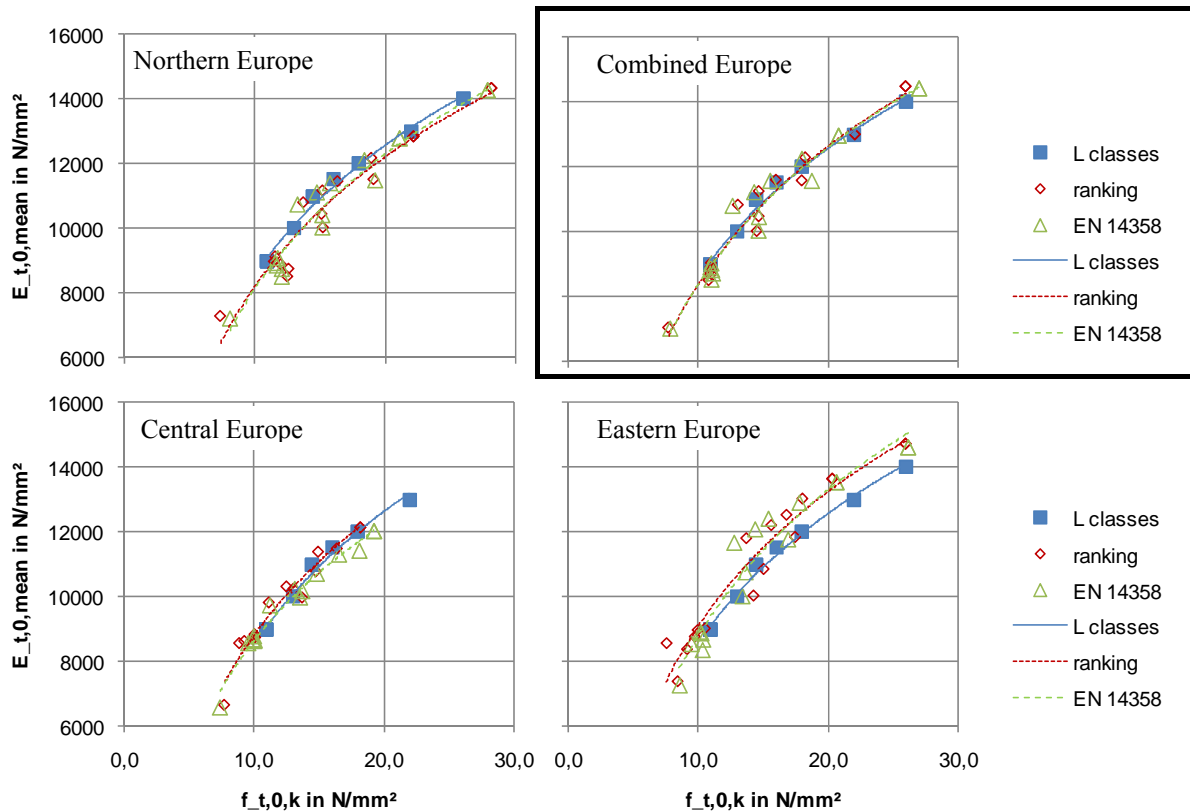


Fig. 6: E versus tensile strength for pine, n = 1060 specimens.

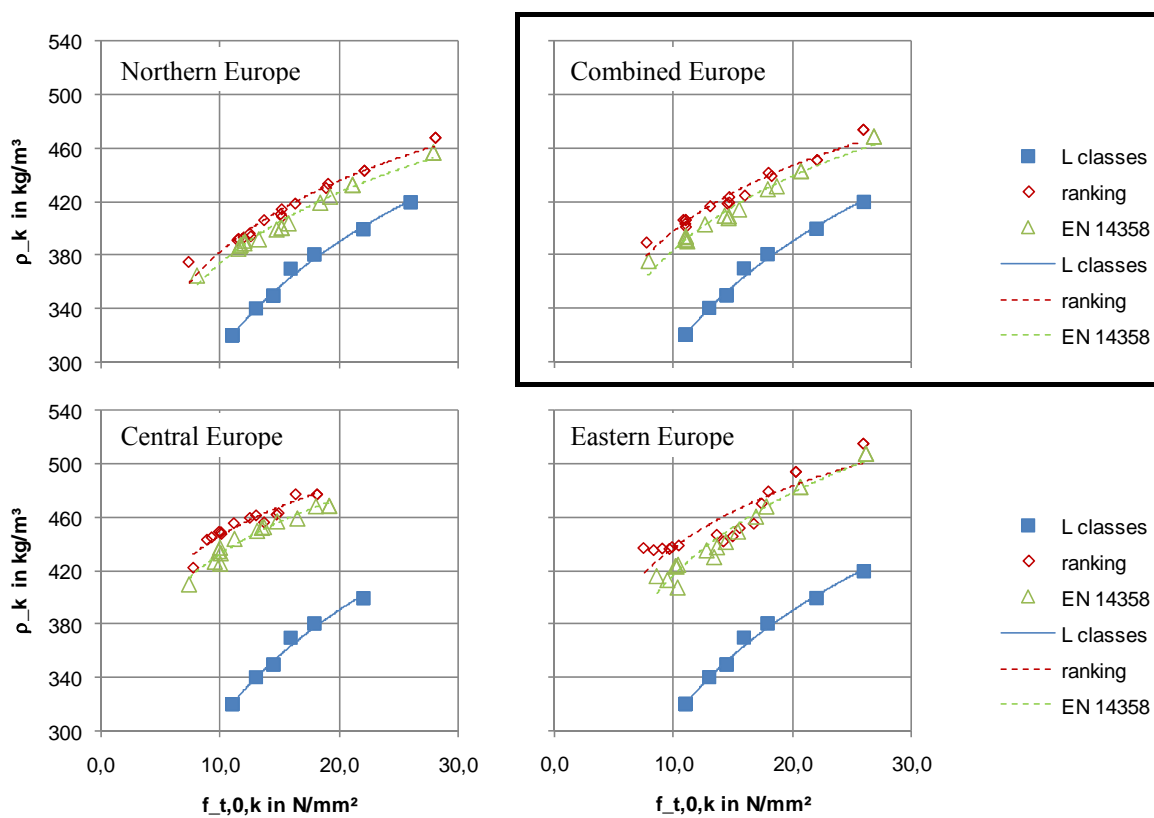


Fig. 7: Density versus tensile strength for pine, n = 1060 specimens.

Grading with respect to strength gives another picture of coherency. Fig. 8 shows the relationships divided into species for Combined Europe. For both species the relationship between E in tension and characteristic tensile strength is clearly lower than assumed by the "L" classes. This discrepancy is approximately in line with the finding of BURGER & GLOS 1998 who found a relationship of  $E_{\text{bending}} / E_{\text{tension}} = 1,09$ . For both species, there is a distinct difference between values higher than  $E = 11.000 \text{ N/mm}^2$  and values below  $E = 11.000 \text{ N/mm}^2$ . All values higher than  $E = 11.000 \text{ N/mm}^2$  belong to the highest bandwidth graded (bandwidth I in Tab. 4). All values below  $E = 11.000 \text{ N/mm}^2$  belong to the second or third bandwidth graded (bandwidths II and III in Tab. 4). This is an effect of the grading procedure which is not as clearly pronounced if graded according to E.

Grading based on strength as indicating property leads to much lower characteristic density values for spruce for the same strength as assumed in the "L" classes. This is only the case for spruce. For pine, the density values clearly exceed the ones given in the "L" classes.

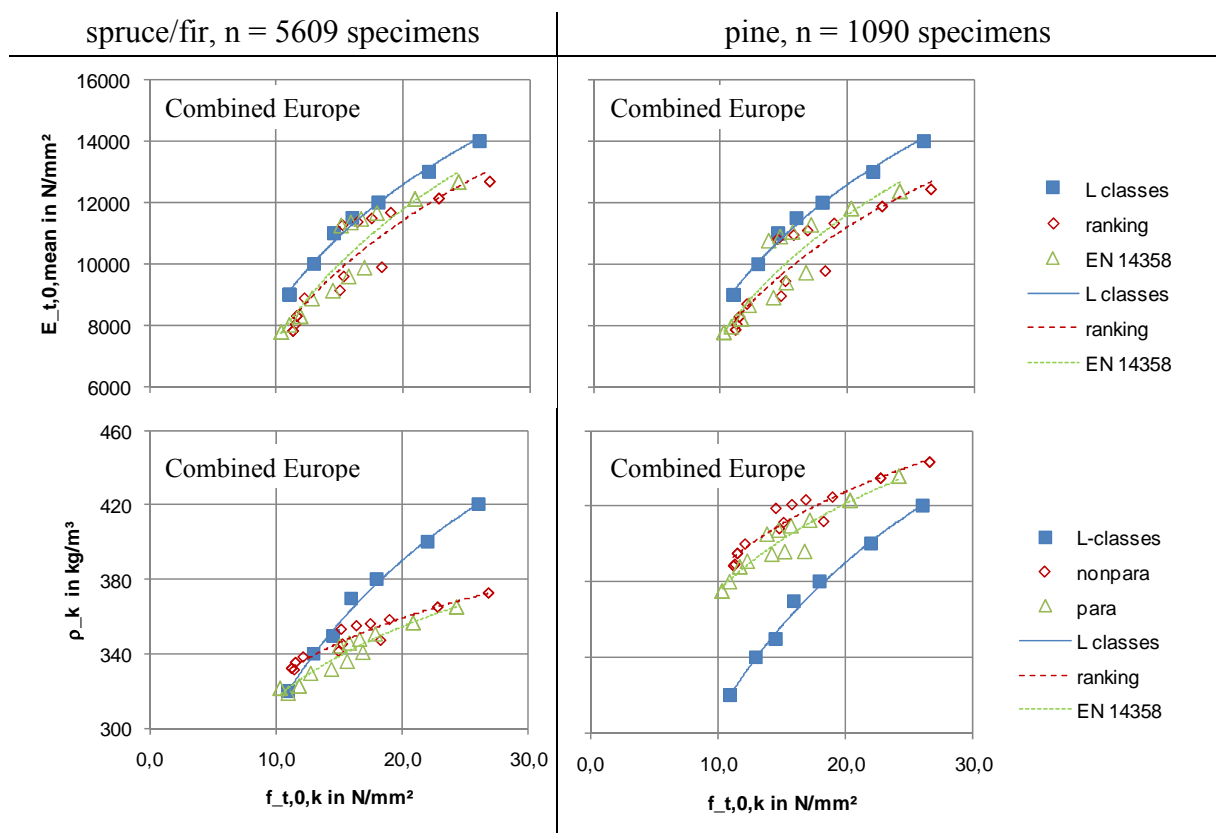


Fig. 8: E and density versus tensile strength for combined Europe divided into species, n = 6699 specimens.

## 5 Discussion

The already existing tensile strength classes like "L", "LS", "LD" or "T" exhibit slight differences within the relationships of characteristic tensile strength, mean E in tension and characteristic density (Fig. 1). Strength classes like "LS", where density is indicative only, indicate that there might be problems in fulfilling the density requirement within a grade for some parts of Europe. The analysis of more than 6600 specimens clearly shows that the relationships are dependent on the grading procedure.

The relationship between mean E in tension and characteristic tensile strength based on sliding characteristic values follows the relationship given in EN 338 (Fig. 3). This procedure assumes that one grade is graded in one pass without access to high or low class specimens. For spruce/fir the deviation between the data and the "L" classes for the relationship of E and strength is approximately 10%. This is also true if grading is based on strength as indicating property for 8 different grade combinations (Fig. 8) and was already stated by BURGER & GLOS 1998. In case of grading based on E as indicating property the level is comparable. For spruce, the slope is slightly increased leading to slightly higher E values for strength classes L36 and L40.

The relationship between characteristic density and characteristic strength gives another picture: For pine, this relationship is not critical at all. For spruce/fir, the density values especially in the high strength classes are not fulfilled for all three methods (sliding percentile, grading based on E, grading based on strength). A major deviation is found for grading with respect to strength. For grading based on E the relationship between tensile strength and density given in the "L" classes seem to fit for Central Europe, but is too demanding for Northern or Eastern Europe. This is already indicated by the "T" classes in FprEN 14080, which include a slightly lower density especially for strength classes higher than C35.

Tab. 5 proposes adopted strength classes for tension members based on the given test results. These profiles are tailored on spruce data, knowing that other softwood species may have other relationships. The name is a combination out of "C" for coniferous and combined with a "T" for tension.

The proposal links the tensile strength classes to the bending strength classes in EN 338 based on E. For the same E, the tensile strength of the proposal is slightly higher than given in the C classes. This finding is supported by EN 338 itself: The relationship of characteristic tensile strength to characteristic bending strength is fixed with 0.6 on the safe side. Therefore, this equation is only valid if tensile strength is calculated out of given bending strength values, and not vice versa. In reality, this relationship is assumed to be higher. In the proposal the relationship developed with the data is approximately 0.64.

The relationship between mean E in tension and characteristic density is not too different from EN 338. For the high strength classes, the proposal slightly reduces the density values. This is based on the test data especially from Northern and Eastern Europe. Beside climatic influences, this effect may be based on different sawing pattern for boards and scantlings. Alternatively, one can argue that changing the relationship of characteristic strength and mean E is necessarily accompanied by a change in the relationship of mean E and characteristic density.

Due to the high amount of strength classes in EN 338, also the amount of strength classes in Tab. 5 is very high. It is advisable to reduce the amount of strength classes in both cases for reasons of practicability. Within this proposal, main relevant grades are highlighted. Last but not least the proposed tensile strength profiles should be harmonised with possible combinations in glulam production. This is not done yet. So far the proposal is focused in getting the best grading results out of the material available.

Fig. 14 compares the proposal with the existing tensile strength.

Tab. 5: Proposal for tensile strength profiles based on spruce test data (main relevant grades highlighted).

Proposal name	$f_{t,0,k}$ in N/mm <sup>2</sup>	$E_{t,0,mean}$ in N/mm <sup>2</sup>	$\rho_k$ in kg/m <sup>3</sup>	existing	$f_{t,0,k}$ in N/mm <sup>2</sup>	$E_{m,0,mean}$ in N/mm <sup>2</sup>	$\rho_k$ in kg/m <sup>3</sup>
				EN 338			
CT 9*)	9	7.000	290	C14	8	7.000	290
CT 11*)	11	8.000	310	C16	10	8.000	310
CT 12*)	12	9.000	320	C18	11	9.000	320
CT 13*)	13	9.500	330	C20	12	9.500	330
CT 14*)	14	10.000	340	C22	13	10.000	340
CT 15*)	15	11.000	350	C24	14	11.000	350
CT 17*)	17	11.500	360	C27	16	11.500	370
CT 19*)	19	12.500	380	C30	18	12.000	380
CT 22*)	22	13.000	390	C35	21	13.000	400
CT 25*)	25	14.000	400	C40	24	14.000	420
CT 28*)	28	14.500	410	C45	27	15.000	440

\*) named with respect to tensile strength

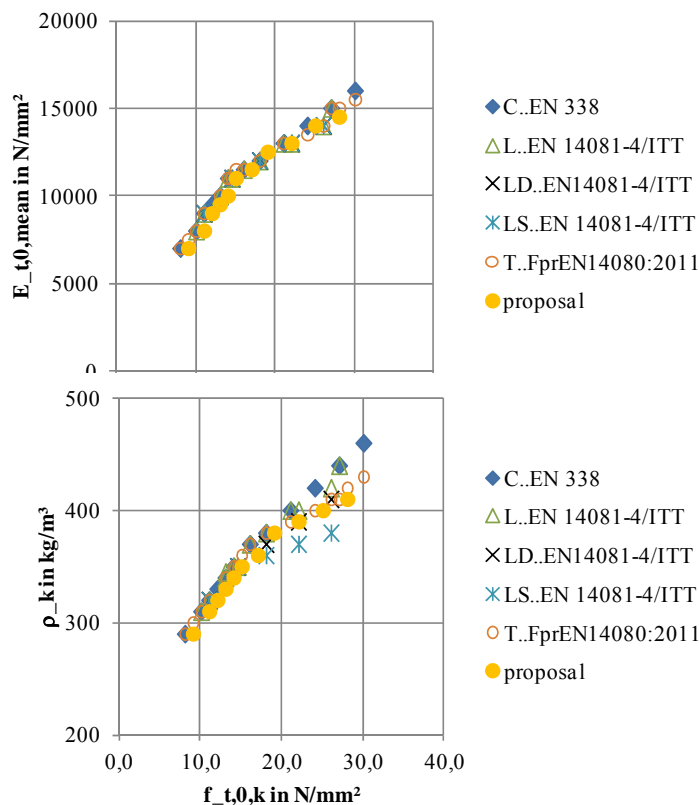


Fig. 14: Characteristic values for different tensile strength profiles including proposal.

## 6 Conclusion

The actual situation with a lot of different tensile strength classes in EN 14081-4, ITT and prEN 14080 is not satisfying and causes questions and misunderstandings due to their sheer number. To use timber as best as possible, the relationship of characteristic tensile strength, mean E in tension and characteristic density should follow reality as good as possible. If inadequate relationships are used for the derivation of strength classes, the grading is mainly based on the most critical property, whereas the other two can be easily fulfilled. This would lead to inefficient use of timber.

This paper aimed to harmonise these profiles. Based on more than 6600 test data, the relationship between tensile strength, E in tension and density was determined for spruce and pine based on three different methods: sliding percentiles, grading based on E as indicating property and grading based on strength as indicating property. The results show that firstly, the tensile strength classes in use represent reality with a slightly overestimated relationship between E and density in high strength classes and secondly, the tensile strength values seem to be too conservative compared to the mean E in tension.

Harmonised tensile strength classes with slightly adopted relationships between characteristic tensile strength and mean E in tension as well as characteristic tensile strength and characteristic density are proposed mainly following the results of spruce. The possible difference between modulus of elasticity in tension and modulus of elasticity in bending is superposed by grading inaccuracies and therefore, not directly assigned to the proposal. The relationship between tensile strength and density is modified, because the increase in density with increasing strength for tension members is not as pronounced as assumed in EN 338, especially for Northern and Eastern Europe.

## **7 Acknowledgment**

The first part of the data used in this paper originates from the "Gradewood" project which was part of the ERA-NET Wood Wisdom Net. The project was funded by national technology development bodies, e.g. Federal Ministry of Education and Research, the association of the European wood industry CEI-Bois as well as national funding bodies, e.g. the Austrian Research Promotion agency FFG. The contributions from all funding organisations and other support are gratefully acknowledged. The second part of the data originates from the "Combigrade" project and was placed at disposal from VTT. The third part of the data was placed at disposal from MiCROTEC. Both valuable contributions are also gratefully acknowledged.

## **8 Literature**

EN 338. Structural timber – Strength classes. European Committee for Standardization, Brussels, 2009.

EN 384. Structural timber - Determination of characteristic values of mechanical properties and density". European Committee for Standardization, Brussels, 2010.

EN 408 Timber structures - Structural timber and glued laminated timber - Determination of some physical and mechanical properties. European Committee for Standardization, Brussels, 2010.

FprEN 14080 Timber structures – Glued laminated timber and glued solid timber. Working document of CEN TC 124 / WG 3. 12-2011.

EN 14081-4. Timber structures — Strength graded structural timber with rectangular cross section — Part 4: Machine grading — Grading machine settings for machine controlled systems. European Committee for Standardization, Brussels, 2009.

EN 14358. Timber structure – Calculation of characteristic 5-percentile values and acceptance criteria for a sample. European Committee for Standardization, Brussels, 2006.

BURGER, N.; GLOS, P. (1995): Verhältnis zwischen Zug- und Biegeelastizitätsmoduln von Vollholz. Holz Roh- Werkst. 53 (1995) 73-74.

LAM, F.; VAROGLU, E. (1990): Effect of length on the tensile strength of lumber. For. Prod. J. 40(5): 37-4



**INTERNATIONAL COUNCIL FOR RESEARCH AND INNOVATION  
IN BUILDING AND CONSTRUCTION**

**WORKING COMMISSION W18 - TIMBER STRUCTURES**

**VISUAL STRENGTH GRADING IN EUROPE**

P Stapel

J W G van de Kuilen

O Strehl

Holzforschung München, Technische Universität München

**GERMANY**

J W G van de Kuilen

Faculty of Civil Engineering and Geosciences, Delft University of Technology

**THE NETHERLANDS**

**MEETING FORTY FIVE**

**VÄXJÖ**

**SWEDEN**

**AUGUST 2012**

---

Presented by P Stapel

S Winter commented that one of the reasons for the observed difference could be related to the type of harvesting. P Stapel responded that they did not observe any clear sawn damage and do not believe problems with machine parts. F Lam asked did you observe compression wood. P Stapel responded no. J Denzler asked whether bending values were corrected. P Stapel responded yes kh was used and the possible influence of thickness was discussed. A Jorissen asked for clarification of slide 17 regarding C18 and C16 grades. Total KAR for DIN C18 was 0.43 and BS C16 was 0.36. R Steiger commented on Swiss visual grading standard and reasons to change to DIN standard. There is one for grading of laminates and one for grading of solid timber. There are additional grading rules for laminates which can be tried and one might get better results. P Stapel stated that they did not use laminates for this analysis. J Köhler stated that deviation from nominal value was a concern. The occurrence of structural failure did not seem to agree with the observed results. J Denzler stated in central Europe C30 was not produced. Without the high grades C24 might get a better fit. J Munch Andersen commented about the small difference from different strength classes. R Steiger commented on the amount of rejects experienced with the Swiss AS standard.



# Visual strength grading in Europe

P. Stapel<sup>1</sup>, J.W.G. van de Kuilen<sup>1,2</sup>, O. Strehl<sup>1</sup>

<sup>1</sup>Holzforschung München, Technische Universität München  
Winzererstr. 45, 80797 München, Germany

<sup>2</sup>Faculty of Civil Engineering and Geosciences, Delft University of Technology  
2600 GA Delft, The Netherlands

## 1 Introduction

The major part of structural timber on the European market is graded visually. While for machine graded timber European standards exist and are commonly used (EN 14081 - 2 & EN 14081 - 3), visual grading is done mainly based on national standards. These national standards are usually customized to optimise the grading results for the timber resources of the country publishing the standard, taking into account growth conditions, local preferences for certain cross-sections and silvicultural differences. Hence national grading rules are assessing knot size, growth ring width or local slope of grain differently. Depending on the standard, the raw material can be graded into up to four grades. Some pieces of sawn timber do not fulfil the requirements for the lowest grade and get rejected.

EN 1912 lists how for many standards and species, the national grades are assigned to strength classes as given in EN 338. Assignments are restricted not only for certain species, but also for geographical areas or certain cross-sections. For additional entries in EN 1912 reports according to EN 384 are required today. The second option for adding a species is to have a long experience of use. This option did not lead to any additions in the last few years.

EN 384 includes some sections which can be interpreted in different ways. E.g.: “The test material shall be representative of the population. It shall represent the timber source, sizes, and quality that will be graded in production.” For European softwoods the term representative usually requires a considerable amount of test pieces.

The substantial testing efforts of today are in contrast to the assignments which have been introduced 15 years ago. For some grading standards, large growth areas are specified. The extreme example is CNE Europe (stands for Central, North and Eastern Europe). Verification of these claims is part of this paper.

There are only a few publications focusing on the comparison of national grading rules. Johansson et al (1992) compared INSTA, DIN and ECE rules. Spruce timber from Germany and Sweden was graded and tested in bending (255 pcs) and tension (245 pcs). When compared to published strength values for the highest grade of INSTA and DIN, the reached bending strength values seemed to be extraordinary high. INSTA 142 - T3 Class reached a 5%-characteristic bending strength of 38.5 MPa, while DIN 4074 S13 Class reached 36.9 MPa in bending. Also, all lower classes showed significant higher values than what is to

be expected from the current strength class assignments in EN 1912. Similar effects were found for MoE and density. The results were not analysed separately for the different origins. Small scale comparisons for a limited number of specimens were carried out by Almazán et al (2008) for German pine graded by DIN 4074 and UNE 56544 or by Riberholt (2008) for European spruce graded according to Chinese visual rules. Visual grading is addressed in several available CIB-articles (Uzielli (1986), Fewell (1984), Barrett et al (1992), Stapel et al (2010)). None of these focused on the comparison of different grading rules and the assignment according to EN 1912.

About 12000 pieces of softwood were graded and tested in tension or bending. We used the following grading standards for the classification of the pieces: DIN 4074-1:2012-06, BS 4978:2007+A1:2011, DS/INSTA 142:2009 (E), NF B 52-001-1:2011 and SIA 265/1:2009. Timber was available from Central, Northern and Eastern Europe. Spruce, pine, larch, Douglas fir and Sitka spruce were tested in edgewise bending or tension. We analyse three main factors influencing the grading. The analysis in this article is done with particular emphasis on:

1. available cross-sections,
2. the source of the timber,
3. the used grading standards.

## 2 Material

The dataset which was analysed can be roughly separated into four sections. A total of more than 12000 pieces can be separated for two different loading modes, bending and tension. Furthermore the dataset is divided by the available knot data. In 60 % of all cases every single knot of the piece was measured (**single knots available, SKA**). For the remaining 40 % no single knot data is available. Only the largest knot area ratio was measured for these pieces (**KAR only available, KOA**). Table 1 summarizes this data.

Table 1: Summary of the available data.

Data	Bending	Tension	Total
KOA data available	5773	7064	12837
Additional SKA data available	3054	4587	7641

Before we further subdivide the data a short description of the source of the data and the testing procedure is given: Only sawfalling material was used. All data for which single knot values (SKA) are available were tested at Holzforschung München between 1995 and 2012. The major part of the remaining data was recorded during the Gradewood project finished in 2011.

All destructive tests were performed according to EN 408:2010. The factors given in EN 384:2010 ( $k_h$ -factor,  $k_l$ -factor) were applied. A symmetrical two point loading was used for the determination of bending strength, usually over a span of 18 times the depth. The orientation of the board in edgewise bending tests was chosen randomly. For tension tests usually a span of 9 times the depth was used. Whenever possible the weakest section along the beam axis was tested.

For the SKA data the most important visual grading parameters were measured. These are mainly knots, but also growth ring width and slope of grain, even though the latter is hardly ever determined in visual grading. Slope of grain is visually hardly detectable and no effective grading supporting measurement system is available. For the analysis the slope of grain is left out. For the knots the position over the length of the board as well as the size on each of the

four sides has been recorded with an accuracy of a millimeter. Knots smaller than 5 millimeters were not recorded. For bending tests knots were only recorded in the section between or close to the loading points, for tension tests between the grips. Visual grading for KOA data needs to be based on the total KAR value only, as no other data is available. The available data is restricted to the maximum knot area ratio. The tKAR is defined as the knot area within 150 mm projected on the end grain divided by the area of the cross section. Overlapping areas are only counted once.

Table 2 summarizes the available data and gives mean values and coefficients of variation for strength, modulus of elasticity, density and total KAR. (CE=Central Europe, EE=Eastern Europe).

Table 2: Summary of the available data. MoR, MoE, density and t KAR given for the total data.

testing mode	species	source	N total	SKA	MoR in MPa		MoE in MPa		Density in kg/m <sup>3</sup>	t KAR	
					mean	cov	mean	cov	mean	mean	cov
bending	pine	PL	219	0	39.0	0.42	12500	0.28	515	0.26	
		SE	209	0	45.1	0.34	11300	0.24	481	0.21	
	Sitka spruce	UK	607	607	29.6	0.31	7900	0.29	404	0.37	
		CE	1880	1880	39.1	0.33	11500	0.26	438	0.27	
	spruce	EE	840	0	35.7	0.31	10000	0.24	396	0.30	
		FR	115	0	42.8	0.26	11800	0.20	440	0.22	
		PL	433	432	38.5	0.31	11400	0.25	434	0.32	
		SE	345	135	42.5	0.36	11800	0.26	450	0.26	
		SI	1125	0	43.7	0.30	12000	0.24	445	0.25	
		CE	324	324	24.8	0.50	10900	0.25	493	0.36	
		Douglas fir	CE	326	326	26.8	0.47	10400	0.27	540	0.31
			CE	264	264	25.3	0.42	10400	0.25	525	0.31
	tension	pine	FI	257	0	31.7	0.39	11400	0.20	492	0.25
			FR	239	0	20.3	0.41	9000	0.25	512	0.32
PL		456	455	28.6	0.44	11300	0.26	529	0.26		
RU		171	0	20.4	0.43	9600	0.22	442	0.33		
SE		206	0	29.7	0.39	10400	0.22	485	0.24		
spruce		CE	2895	2895	30.4	0.40	11500	0.23	448	0.28	
		CH	442	0	25.1	0.45	10900	0.24	439	0.28	
		EE	844	0	26.2	0.42	10300	0.21	395	0.30	
		LV	106	106	30.4	0.38	11700	0.24	466	0.33	
		PL	219	217	28.5	0.37	11600	0.23	446	0.30	
	SE	211	0	27.4	0.38	10100	0.23	415	0.24		
	CE	2895	2895	30.4	0.40	11500	0.23	448	0.28		
	CH	442	0	25.1	0.45	10900	0.24	439	0.28		

testing mode	species	source	N total	SKA	MoR in MPa mean cov	MoE in MPa mean cov	Density in kg/m <sup>3</sup> mean cov	t KAR mean cov
tension	spruce	SI	104	0	34.0 0.44	12300 0.22	442 0.09	0.25 0.43

For visual grading the size of the pieces might have an influence on the grading results. For DIN (grading of joists), the size of the smallest cross-sections is of importance. The frequency of the thickness is shown in Figure 1 for pieces tested in bending and in tension.

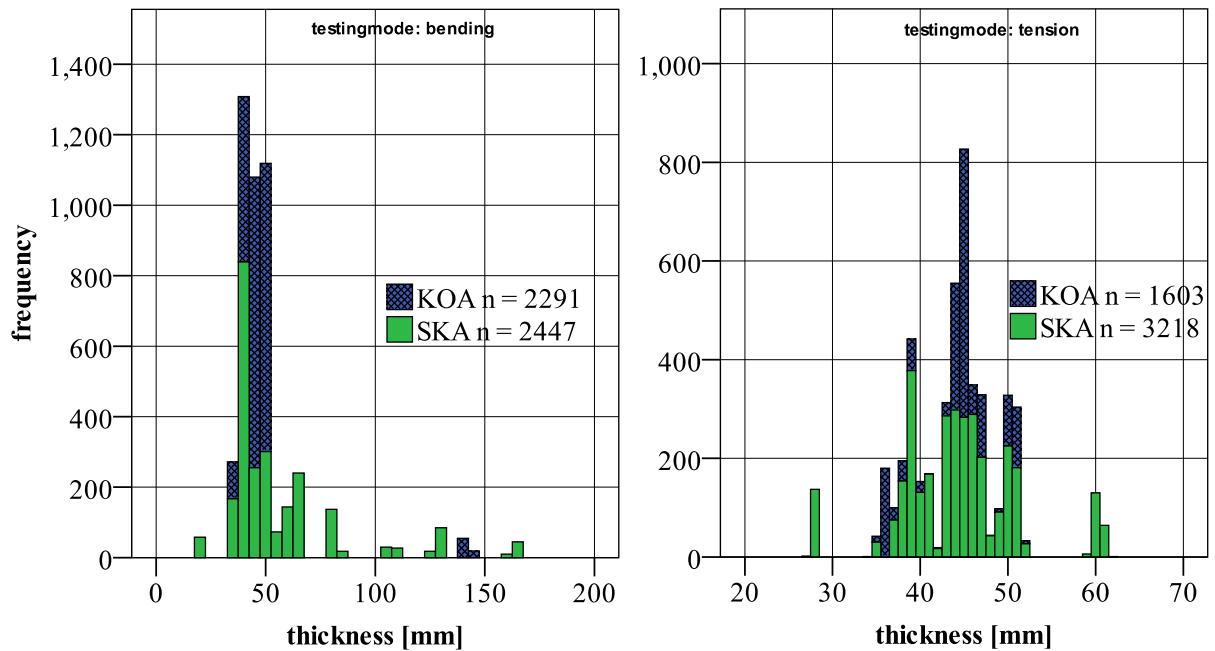


Figure 1: Frequency distribution for thickness divided by bending and tension, showing the available knot data.

### 3 Methods

The heterogeneous availability of knot data makes it necessary to differentiate between SKA and KOA datasets. For SKA data more grading rules have been considered. For the KOA dataset thresholds have been defined for different grades based on the visual grading standards DIN 4074-1 and BS 4978. For these standards many sources are listed in EN 1912 5<sup>th</sup>-percentile values of the characteristic strength and density are determined non-parametric, for MoE, the mean is determined. Grading is carried out for pieces tested in bending as well as for pieces tested in tension, although assignments in EN 1912 are based on bending strength. Tension test results are compared to the strength values given in EN 338 based on the bending strength multiplied by the factor 0.6, which is expected to be on the safe side.

## SKA

Grading for SKA data was done according to DIN 4074-1, BS 4978, INSTA 142, NF B 52-001-1 and SIA 265. DIN 4074-1 includes different sets of grading rules for “Kantholz” (joists), “Brett/ Bohle” (boards) and “Latten” (battens). The joist-grading is used for all pieces loaded in edgewise bending. Grading rules for joists and boards were applied. For joists the optional criteria called “Schmalseitenast” was applied.

Knots are the most important grading parameter in all rules. Differences can be found in the way the knot parameters are measured. Depending on the standard the minimum knot diameter, the knot projected on the end grain of the board or the knot size measured parallel to the edge of the board needs to be determined. Not only single knots, but also knot clusters are considered in all of the used standards. The length of the board over which the single knots are added up to a knot cluster is for some standards equal to the width of the board, other standards use a standard length of 150 mm. Additional parameters which we used for the classification were growth ring width, the proportion of compression wood and the appearance of a pith when such parameters were given in the respective standards.

The SIA rules allow for different measuring principles depending on whether boards or joists are graded. Our analysis is limited to the grading of joists. The INSTA rules are depending on the cross-section. Timber with thicknesses between 25 mm and 45 mm and a width between 50 mm and 75 mm was not considered. This results in fewer available pieces for the INSTA analysis. The French standard refers to EN 1310 for the measurement of features. The NF itself considers different thresholds depending on the species. Only spruce and pine were analysed. For both standards the wording is not explicit for all types of knots, which leaves some room for interpretation. The standards were discussed with grading experts and used to the best of our knowledge.

The difference between grading standards is not only caused by different ways of determining knot sizes. The number of visual strength classes differs from standard to standard. While BS has two classes, INSTA has four, both without considering reject. This fact influences the assignment of visual grades to strength classes in EN 338 as given in EN 1912. Table 3 lists the strength classes which correspond to the visual grades for the main softwood species – spruce, fir and pine. For expository purpose we did not consider minor differences for single species in this table. The SIA classes are not included in EN 1912, but according strength classes are given directly in the SIA.

Table 3: Strength class requirements according to EN 338 and corresponding visual grades as given in EN 1912 for main softwood species.

EN 338	$f_{m,k}$ MPa	$E_{0,mean}$ MPa	$P_k$ kg/m <sup>3</sup>	DIN	BS	INSTA	NF	SIA
C 35	35.0	13000	400	-	-	-	-	-
C 30	30.0	12000	380	S13	-	T3	ST1	-
C 27	27.0	11500	370	-	-	-	-	-
C 24	24.0	11000	350	S10	SS	T2	ST2	FKI&FKII
C 20	20.0	9500	330	-	-	-	-	FKIII
C 18	18.0	9000	320	S7	-	T1	ST3	-
C 16	16.0	8000	310	-	GS	-	-	-
C 14	14.0	7000	290	-	-	T0	ST4	-

The allocation given in Table 3 is only valid for a limited source area. DIN and BS are valid for timber from Central, North and Eastern Europe, INSTA for Northern and North Eastern Europe and NF for France only. SIA does not restrict its grading rules to timber from a certain area.

In the following we try to stick to C-classes as much as possible. Species not listed in this table will also be linked to a referring C-class as given in EN 1912. The SKA data is not analysed separately for different sources. All pieces for which single knot data were available were considered in this analysis.

## **KOA**

More datasets can be used for visual grading if only the KAR values are used. These requires the derivation of fixed threshold values, as – other than for national grading rules – there are no such values for grades based on KAR. Values are derived based on the visual grading results for DIN and BS grading. We try to do this by matching the yield for both grading strategies using the SKA dataset. Example: SKA and KOA data is available for 2447 pieces graded according to DIN (joists). For the DIN grading into S13 a maximum knot value of 0.2 is allowed. In addition other parameters were also considered during grading. Let us assume that this results in yield of 18 %. Now a KAR value for this dataset is chosen, which gives us approximately the same yield.

The grading results from the KOA dataset are analysed with special respect to the source of the timber, as timber from different regions is available. Even if the grading results might be influenced by the varying cross-sections, this seems reasonable as the available cross-sections are not restricted by DIN or BS. Test results for timber loaded in tension are not considered in detail. Only single aspects are highlighted.

## **Cross-section**

The SKA dataset is separated for thickness of pieces, to check the influence of the dimensions on the grading results for the different measuring principles. As a first step six different category groups were formed giving an equal number of pieces in each group. This was done for spruce independent of the loading mode. In a second step the results for spruce tested in bending were analysed more precisely, forming four different groups formed on the basis of the thickness. For these pieces the resulting strength in the different classes was additionally analysed.

## **4 Results**

Before focusing on the results for different grading rules and sources, the influence of the cross-section depending on the grading procedure is shown. Figure 2 shows the influence of the cross-section for the most important grading parameters of DIN and BS. While for large thicknesses the values are closer together, larger differences are found for smaller ones. Very large knot values are not found for both standards, if the thickness gets bigger.

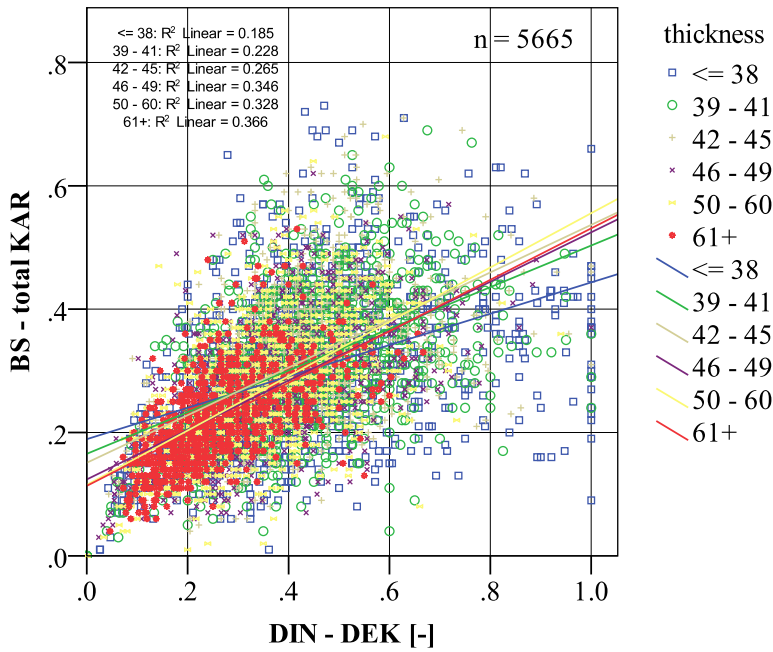


Figure 2: Important grading parameters total KAR (BS) and DEK (DIN) influenced by the thickness.

To check whether there is an influence of the cross-sections on the strength values for the two standards, the thicknesses are grouped again and are plotted against the strength. Figure 3 compares the main DIN to the BS grading parameter. The quality of the strength prediction is higher for the BS. Both parameters promise higher strength prediction accuracy for small thicknesses.

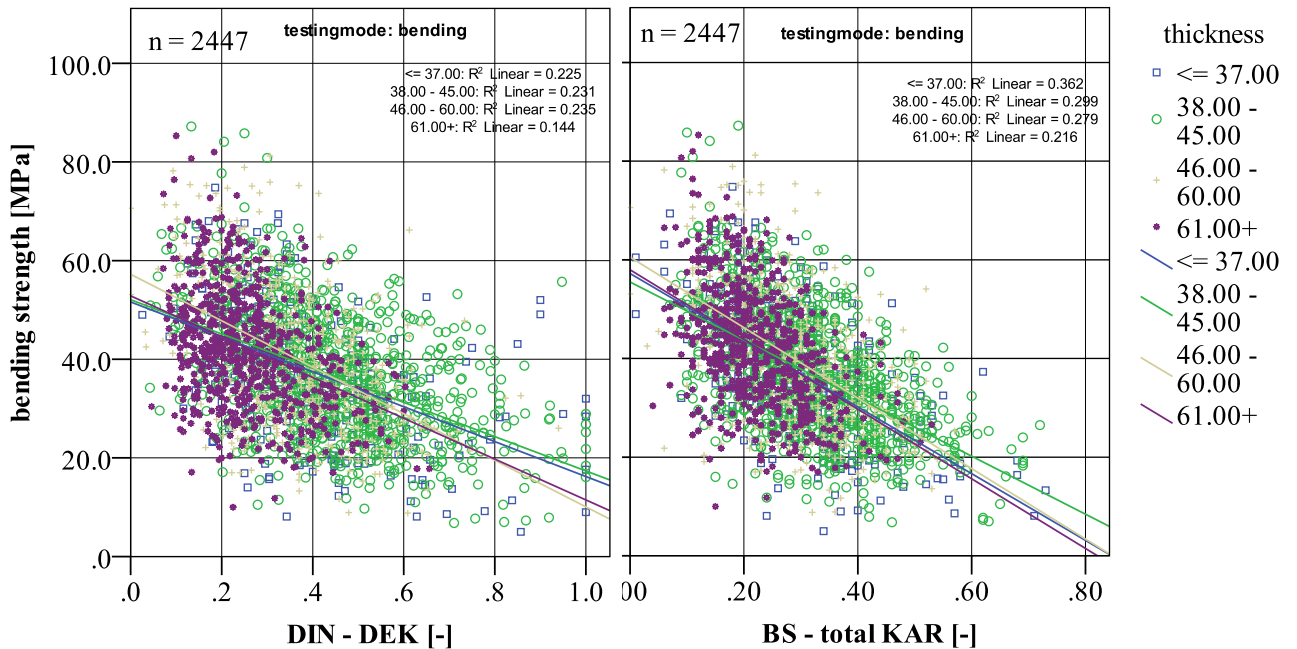


Figure 3: Quality of strength prediction for DIN and KAR separated for thickness – for spruce tested in bending.

Grading output based on the knot values shown in Figure 3, together with the other grade determining properties leads to the results given in Table 4.

Table 4: Grading results for different cross-sections.

Thickness mm	str. class	grading rule	N	$f_{m,k}$ MPa	$E_{0,mean}$ MPa	$P_k$ kg/m <sup>3</sup>
<= 37	C30	DIN	28	26.3	15200	387
	C24	BS	111	28.4	14300	387
	C24	DIN	94	17.1	13200	364
	C18	DIN	65	17.0	10700	347
	C16	BS	49	14.7	11100	350
38 – 45	C30	DIN	57	31.8	14200	397
	C24	BS	454	24.7	12600	371
	C24	DIN	369	21.7	12000	366
	C18	DIN	386	19.2	10700	368
	C16	BS	232	19.5	11000	372
46 – 60	C30	DIN	67	36.4	15000	402
	C24	BS	341	24.6	12900	357
	C24	DIN	296	23.0	12100	357
	C18	DIN	178	19.4	10500	354
	C16	BS	120	18.9	10500	352
61+	C30	DIN	220	26.8	12200	383
	C24	BS	597	26.1	12000	377
	C24	DIN	381	24.2	11700	366
	C18	DIN	68	21.3	10700	356
	C16	BS	56	18.2	9700	338

All MoE and density values in Table 4 reach the requirements. For thickness-classes of 38-45 mm 46-60 mm strength values are slightly below or above the required strength values. The worst value within these two groups results from 369 pieces graded into C24. The characteristic strength reaches a value of only 21.7 MPa. Strength values for the remaining classes are too low for several grades.

Grading results are given separately for SKA and KOA data. For the SKA data the analysis with respect the grading rule is of special importance, while for the KOA data the analysis is focused on the source of the timber.

## SKA

Single knot data was available for six different groups. There is bending data available for spruce and Sitka spruce and tension test data for spruce, pine, Douglas fir and larch.

Table 5 gives the grading results sorted by grading rules, as this is the important factor for the SKA analysis. Not all strength classes given in this table are listed in EN 1912 for the respective species. Some assignments are taken from national standards.

Table 5. Grading results for different grading rules.

rule	load mode	species	str.class	n	$f_{m/k}$ MPa	$E_{0,mean}$ MPa	$P_k$ kg/m <sup>3</sup>	yield
BS	bending	spruce	C24	1503	25.6	12600	373	61%
			C16	457	18.9	10700	361	19%
		sitka	C18	179	22.4	9400	347	30%
			C14	178	17.5	7900	340	29%
	tension	spruce	C24	1848	18.5	12500	376	57%
			C16	662	13.8	10700	365	21%
		pine	C24	397	16.9	12300	453	55%
			C18	155	10.2	9800	422	22%
		douglas	C18	92	16.3	12700	434	28%
			C14	68	11.0	11100	425	21%
		larch	C24	147	15.6	11500	451	45%
			C16	68	11.8	10500	439	21%
DIN-B	bending	spruce	C30	297	28.2	14200	395	12%
			C24	1012	20.7	11900	364	41%

rule	load mode	species	str.class	n	$f_{m/t,k}$ MPa	$E_{0,mean}$ MPa	$P_k$ kg/m <sup>3</sup>	yield		
DIN-B	bending	spruce	C18	986	20.0	11000	363	40%		
			sitka	C30	18	27.1	10900	361	3%	
			C24	160	21.4	9200	355	26%		
		C16	188	16.6	8300	350	31%			
	tension	spruce	C30	484	22.6	13600	393	15%		
			C24	1326	15.4	11700	368	41%		
			C18	1152	13.6	10900	368	36%		
		pine	C30	113	28.2	14100	503	16%		
			C24	271	13.8	11200	434	38%		
			C18	252	11.0	10200	435	35%		
		douglas	C35	43	17.7	13700	444	13%		
			C24	151	11.7	11000	427	47%		
			C16	113	8.5	10000	419	35%		
		larch	C30	42	22.7	12400	478	13%		
			C24	145	12.3	10800	457	45%		
			C16	123	8.0	9500	449	38%		
		DIN-K	bending	spruce	C30	372	29.1	13300	386	15%
					C24	1140	22.7	12000	363	47%
C18	697				19.1	10700	361	29%		
sitka	C30			7	37.3	11200	392	1%		
	C24		218	20.0	8800	349	36%			
	C16		169	17.8	8400	354	28%			
	tension		spruce	C30	335	20.7	13800	390	10%	
C24				1473	17.0	11900	369	46%		
C18				1082	13.4	10700	369	34%		
pine			C30	108	25.6	13600	480	15%		
			C24	286	14.7	11800	448	40%		
			C18	225	10.4	9600	417	31%		
douglas	C35		36	16.1	13100	433	11%			
	C24		60	13.6	12100	436	19%			
	C16		117	12.9	10700	424	36%			
larch	C30		32	20.3	13300	492	10%			
	C24		128	12.9	11000	449	39%			
	C16		87	8.2	9800	446	27%			
INSTA	bending	spruce	C30	396	28.5	13500	389	18%		
			C24	619	25.6	12500	366	27%		
			C18	928	20.0	10900	359	41%		
			C14	210	12.8	9700	360	9%		
	sitka	C24	52	16.1	8500	351	9%			
		C24	127	19.7	8900	345	21%			
		C18	239	15.1	7900	337	39%			
		C14	95	15.3	6800	345	16%			
	tension	spruce	C30	371	21.8	13600	382	13%		
			C24	760	19.2	12400	369	27%		
			C18	1197	15.1	11100	366	43%		
			C14	327	11.3	9900	365	12%		
		pine	C30	98	25.7	13800	499	16%		
			C24	129	18.2	12400	450	22%		
			C18	231	11.9	10500	415	39%		
			C14	89	8.8	9200	429	15%		
		douglas	C30	17	17.6	13900	467	5%		
			C24	35	10.6	13000	435	11%		
C18			132	13.4	11000	426	41%			
C14			88	9.5	9900	416	27%			
larch		C30	36	16.8	12700	471	11%			
		C24	62	16.6	11600	452	19%			
	C18	126	8.6	9900	442	39%				
	C14	59	11.9	9700	461	18%				
NF	bending	spruce	C30	52	28.1	14300	373	2%		
			C24	763	20.5	12400	371	31%		
			C18	897	21.1	11500	359	37%		
	tension	spruce	C30	178	24.4	14000	406	6%		
			C24	1167	17.0	12000	371	36%		
			C18	1065	14.7	11300	364	33%		

rule	load mode	species	str.class	n	$f_{m/k}$ MPa	$E_{0,mean}$ MPa	$P_k$ kg/m <sup>3</sup>	yield	
NF	tension	pine	C30	16	12.0	13200	499	2%	
			C24	158	20.0	13100	471	22%	
			C18	200	12.7	10800	434	28%	
			C14	257	10.2	10100	431	36%	
SIA	bending	spruce	C24	100	30.5	14300	409	4%	
			C24	369	23.8	12800	377	15%	
			C20	390	22.8	12100	366	16%	
		sitka	C24	5	39.1	10700	409	1%	
			C24	39	22.1	9400	331	6%	
			C20	62	17.9	9000	332	10%	
		tension	spruce	C24	180	23.1	14300	412	6%
				C24	272	17.7	12800	371	9%
				C20	379	18.0	12300	372	12%
	pine		C24	67	25.5	14000	487	9%	
			C24	62	19.4	12600	480	9%	
			C20	91	14.5	11500	450	13%	
	larch		C24	14	27.4	13700	498	4%	
			C24	40	15.8	12000	472	12%	
			C20	39	8.0	10600	431	12%	
	douglas		C24	15	17.6	15000	465	5%	
			C24	34	16.0	12900	436	11%	
		C20	18	11.5	11700	441	6%		

In the following the single grading rules are pointed out:

BS: Grading according to BS results in characteristic values above the requirements for all species, loading modes and grades. The highest possible grade is C24. Reject rates vary between 20 % for spruce up to 51 % for Douglas fir.

DIN-B: For grading according to the DIN rules for boards no assignment is given in EN 1912. Visual classes listed there are based on the rules for joists. The strength classes listed in Table 5 are taken from the referring joist grading. The results are above the requirements for spruce and pine tested in tension. For other possible combinations the strength requirements are not fulfilled in several cases. The target value for spruce tested in bending is clearly missed for C24.

DIN-K: Strength values for Sitka spruce, larch and Douglas fir do not meet the requirements for the listed strength classes. Also for spruce tested in bending the strength requirements are shortly missed. Tension tests for spruce and pine show safe results.

INSTA: For spruce and pine, the reached strength values are above or close to the requirements. Douglas and larch show strength values below the requirements in single classes. For Sitka spruce most strength requirements are not fulfilled. Depending on the combination of loading mode and species the reject rates vary between 5 and 16 percent.

NF: Characteristic values are reached except for the strength values of C30 and C24 for spruce tested in bending and for C30 of pine (n=16 only). The yield in C30 is low, while yields in C24 and C18 are close together.

SIA: For SIA no strength classes higher than C24 are listed in the national standard. The two national classes FK1 and FK2 are both assigned to strength class C24. Characteristic values are usually kept. Reject values are extremely high.

## KOA

If no single knot data was available the grading was based on total KAR values only. The chosen thresholds for the KOA grading are illustrated in Figure 4. For the DIN grading the single knot value is plotted over the total KAR. For the KOA grading this means, that those pieces with total KAR values equal or below 0.16 are assigned to strength class C30. Of course the pieces in this grade differ from the pieces which were assigned to C30 (S13) using

the real DIN grading. For the BS the difference is smaller, as the main grading parameter is the KAR value, which is used in the BS anyway. Yet a difference exists, as margin KAR values are a second important grading parameter based on knot measurements close to the edges of the pieces. Differences between the assignments according to BS and to the new assignment for the KOA grading can be estimated by looking at Figure 4.

The exact values which would lead to approximately the same yield are given in Table 6. The threshold values between the different test modes or species are small. For C24 the total KAR value to be used is always 0.29 except for DIN grading where this value is slightly higher – 0.30. The differences reach a maximum for grading into C30 according to DIN yields. Values vary between 0.13 and 0.16 in this case. As these values are close together, the following grading procedure is only based on the total KAR values for spruce tested in bending.

Table 6: Total KAR values which give a comparable yield to the grading standards DIN or BS respectively.

	spruce bending		spruce tension		pine tension	
	DIN	BS	DIN	BS	DIN	BS
C30	0.16		0.14		0.13	
C24	0.30	0.29	0.29	0.29	0.29	0.29
C18	0.43		0.42		0.41	
C16		0.36		0.36		0.37

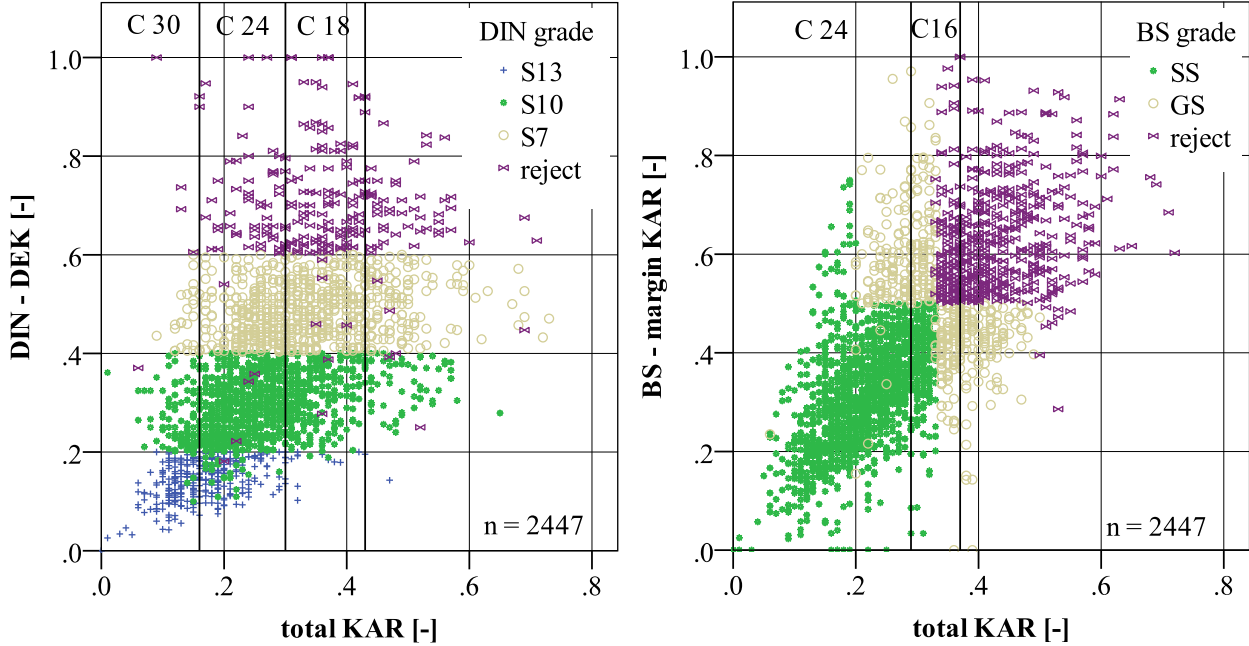


Figure 4: Threshold values for the KOA grading for spruce tested in edgewise bending.

Table 7 shows the according grading results for bending. As shown at the top of Table 7 the characteristic values for data from CE are lower, compared to the SKA grading which includes timber from Poland and Sweden (Table 5). The calculated total KAR threshold value of 0.16 for C30 leads to a characteristic bending strength of 28.0 MPa instead of 29.1 MPa. The relative yield is slightly higher for KOA grading. Throughout all grades the characteristic values for BS are closer to the required values. This might be due to the fact that there is no grade for grading timber into C30 and the better material is not creamed of. On the contrary

one might also argue that if a higher grade would have existed, the grade boundaries for C24 (SS-Grade) would need some adjustment.

Table 7: Grading results for KOA data –bending only.

source	species	str. class	vis .stand.	N	$f_{m,k}$ MPa	$E_{0,mean}$ MPa	$P_k$ kg/m <sup>3</sup>	yield
CE	spruce	C30	DIN	315	28.0	13400	390	17%
		C24	BS	1186	24.8	12500	374	63%
		C24	DIN	931	23.8	12100	367	50%
		C18	DIN	471	17.2	10300	358	25%
		C16	BS	337	18.9	10700	359	18%
EE	spruce	C30	DIN	73	28.5	11500	336	9%
		C24	BS	424	23.6	11000	340	51%
		C24	DIN	384	23.2	10800	342	46%
		C18	DIN	289	18.0	9200	336	34%
		C16	BS	200	20.0	9600	336	24%
FR	spruce	C30	DIN	31	25.1	12200	379	27%
		C24	BS	94	26.5	12000	381	82%
		C24	DIN	68	25.4	11800	375	59%
		C18	DIN	14	16.5	11200	376	12%
		C16	BS	15	23.3	11300	375	13%
PL	pine	C30	DIN	69	19.9	14400	452	32%
		C24	BS	134	21.2	13900	441	61%
		C24	DIN	70	21.5	13200	434	32%
		C18	DIN	49	13.1	11000	435	22%
		C16	BS	39	13.4	11200	434	18%
	spruce	C30	DIN	25	19.1	14600	411	6%
		C24	BS	194	24.7	12800	373	45%
		C24	DIN	188	24.4	12500	372	43%
		C18	DIN	169	19.9	10500	356	39%
		C16	BS	106	19.9	11100	356	25%
SE	pine	C30	DIN	73	30.1	13000	439	35%
		C24	BS	165	26.5	11700	420	79%
		C24	DIN	99	24.9	10700	412	47%
		C18	DIN	34	15.3	9500	403	16%
		C16	BS	31	15.1	9800	407	15%
	spruce	C30	DIN	63	24.5	12700	370	18%
		C24	BS	231	23.7	12200	360	67%
		C24	DIN	177	23.2	12000	355	51%
		C18	DIN	74	15.2	11400	346	21%
		C16	BS	58	13.8	11800	345	17%
SI	spruce	C30	DIN	231	34.8	13800	388	21%
		C24	BS	798	27.4	12600	383	71%
		C24	DIN	602	25.2	12000	379	54%
		C18	DIN	246	20.4	10600	363	22%
		C16	BS	194	21.1	10800	367	17%

Going through the table and focusing on the source of the timber we want to highlight the following issues:

Eastern Europe: Independent of the followed grading procedure, the strength values obtained are close to the required values. This goes together with a considerable reduction in yield compared to Central Europe. However, the resulting density values are well below the requirements. The requirement for C30 is 380 kg/m<sup>3</sup>, only 336 kg/m<sup>3</sup> are reached.

France: The dataset from France is too small to get reliable answers.

Poland (pine): Strength values are far below the requirements for all grades. MoE and density values are met.

Poland (spruce): Except for the bending strength, which is only based on the minimum value of 25 pieces, the characteristic values are met.

Sweden: For Swedish pine, yields are at least as high as for pine from Poland. Contrary to pine from Poland, the characteristic values are met. For spruce the characteristic value for

C30 is too low.

Slovenia: Timber from Slovenia shows extraordinary good strength values and consequently good grading results with low reject rates. Graded using the threshold values based on DIN, the reject rate is as low as 3%.

Grading output for tension is presented without precise listing of the results and only for those groups for which no SKA data is available.

PINE: Pine tension data with missing SKA data is available from FI, FR, RU and SE. Table 2 shows that there are already big differences in strength properties for the ungraded timber. These differences are reflected in the grading results. For timber from FI and SE the required values are reached. While the yields are close together, Finnish timber shows tensile strength values far above the requirements (26.8 MPa for C30, n=54/ 17.9 MPa for C24-DIN, n=123). Timber from FR and RU shows clearly lower values for the ungraded samples. The grading leads to low yields for timber from RU and to high yields for FR. This results in an almost safe output for RU, while timber from FR fails the strength requirements by far. Grading into C24-BS leads to a characteristic strength of 8.9 MPa (n=105), where 14 MPa is required.

SPRUCE: For spruce tested in tension the differences for the ungraded material are small for different sources. The values for timber from CH, EE and SE are close together, while the timber from SI shows higher values again (Table 2). For the small dataset from SI all requirements are fulfilled. Also, the grading results for the other sources are closer to the required values compared to the results for pine. The required strength values for C18-DIN and C16 for timber from SE are not reached. Eastern European timber keeps the strength values - except for C30 (16.6 MPa) - but fails the density requirements again. Timber from CH does not reach the strength requirements for C24-DIN and C18 (13.1 MPa, 9.3 MPa).

## 5 Discussion

Table 4 clearly shows that visual grading can strongly be influenced by the cross-section. Although the results are not totally out of range, grading results for large and small thicknesses often do not fulfill the requirements. Especially for large thicknesses a lot of material is available. 220 pieces graded into C30 reach a characteristic bending strength of just 26.8 MPa. This is related to the knots, usually not reaching values of above 0.5 (DEK and tKAR) as can be seen in Figure 3. Downgrading of boards into C24 is not accurate enough. However, strength values for C24-BS are high compared to the smaller cross-sections, as the larger cross-sections lead to a homogenization of the material. Trying to assign higher classes than C24 according to BS rules would also cause problems. Considering absolute knot sizes like in EN 1310 could help to obtain higher strength values for larger timber dimensions. Actually, the NF which uses EN 1310, reaches the required values for larger thicknesses. Unfortunately in this case the yields are very poor.

For strength classes above C24 there should be limitations on the size of the specimens. Disregarding the cross-section for the allocation of national grades to C-Classes is not justified according to these results.

### SKA

BS: The assignments based on the BS standard are safe. The main reason for this is that C 24 is the highest possible grade. However, if the grading is done correctly, the reject rates are also high. Due to the sophisticated and rather complicated measuring method it is questionable, if these high reject rates are actually reached in practice. If the rules are applied correctly, around 20 % of the timber needs to be rejected, if not more.

DIN-B: Lately, there has been a discussion about the effect of using elements graded as

boards, but applied as joists (edgewise bending). Neglecting the influence of the cross-section (which has an influence) the grading results for pieces tested in edgewise bending are not generally bad. For C30 from spruce a characteristic strength of 28.2 MPa is reached, for C18 20.0 MPa. However with 20.7 MPa the strength for C24 is too low. Allocating spruce and pine tested in tension to the given classes seems reasonable. However, this is not true for Douglas fir and larch. Characteristic strength values in these cases are not reached, except for a small sample of larch graded into C30. The suggested strength classes for Sitka spruce are simply too high. Lower classes similar to those used in BS can easily be reached.

DIN-K: The discussion about Douglas fir, larch and Sitka spruce is close to the discussion for DIN-B grading. Looking more closely at the grading of Sitka spruce, this seems possible if the strength classes used in the BS are adopted. For Sitka spruce we need to focus on MoE as this is usually the grade restricting property. Having 225 pieces in one grade would result in a MoE value of 8900 MPa. The yields resulting from DIN are higher compared to yields from BS. This is not only true for Sitka spruce, where the reject is lower by 5%, but also for spruce tested in bending, where reject is only half of that of BS. The yields for C24 and higher are comparable.

INSTA: Generally speaking the INSTA seems to work well for pine and spruce from Central Europe. The problems that exist for Douglas fir and larch are equally serious as for other standards. Using an additional strength class with C14 leads to a lower total reject rate. No other standard gives less reject. This does not mean that the yields in higher classes are especially high. Unlike the BS, the INSTA assigns Sitka spruce to the strength classes C24, C18 and C14. As the source given in EN 1912 for the INSTA is not the UK, but Norway and Denmark, the possible higher quality of Sitka spruce from these countries could lead to different results. Classes above C20 can definitely not be reached for Sitka spruce from the UK.

NF: Using absolute knot values as grading criteria is unique within the analysed standards. This is also one reason why the yields in C30 are low compared to the other standards. The effectiveness of this method can certainly not be shown by the resulting characteristic values. The resulting bending strength for C24 is 20.5 MPa, while 21.1 MPa is reached for C18. Hence this standard does not seem applicable for grading Central European timber.

SIA: Knots in the SIA are measured at right angles to the length of the pieces, which is comparable to other grading standards. Extreme threshold values lead to extremely high reject rates. A ratio of 1/3 for the single knot is the value which leads to a rejection of the piece. Single knots of that size are still allowed according to the INSTA where, as edge knots they are graded into C30. The practical use of a standard with reject rates between 65 % and 83 % does not seem logical.

## **KOA**

For Central European timber the required strength values are not completely met for DIN KOA grading. This is okay, as the KOA grading was only based on the yield in the different grades. This shows that the KOA grading results have to be judged carefully, especially for the DIN based results. Figure 4 makes the difference between DIN and BS rules obvious. Let us consider the highest visual grades in both cases. For DIN the new C30 grade (KOA grading) consists of pieces originally graded into all possible DIN grades. S13 accounts for a maximum of 50% in the KOA C30 grade. The BS pieces which are now assigned to C24 originate mainly from the SS grade. Only a small number of pieces originally graded into GS grade is added (where a margin KAR above 0.5 is combined with a total KAR between 0.2 and 0.29).

Eastern Europe: Using visual grading for predicting the bending strength of Eastern European timber works. Due to the low quality material this leads to low yields in the strength classes. 45 % of the pieces do not reach strength class C24 or higher for DIN grading, but the assignment seems to be correct. As for the KOA grading, no parameter predicting the density (growth ring width) is available. For this low density material (Table 2) the required density values are not met. Looking at the characteristic values independent of the grade, it is highly questionable whether the growth ring width is good enough to predict density and reach the density requirements for C24 or higher.

France: The dataset from France is too small for reliable statements with regard to the applicability of either DIN or BS standard.

Poland (pine): Visual grading of pine from Poland does not work when applying DIN or BS standards. For all classes and grading standards the strength values are much too low. This cannot be motivated by low strength values for the ungraded material, as the mean value is in the range of ungraded spruce data.

Poland (spruce): Only 25 out of 433 pieces are graded into C30. This does not indicate a high quality raw material. For C24 required values are met, both for DIN and BS.

Sweden: Grading Swedish timber visually leads to reasonable grading results, except for C30 where 63 pieces out of 345 in this grade have a characteristic strength value of only 24.5 MPa.

Slovenia: Table 2 already shows very high mean values for the timber properties in the ungraded dataset. This general trend is also reflected in the grading results with high yields and extremely good characteristic values. If the ungraded spruce material shows values which are moving in the upper range of possible strength, MoE and density distributions, the choice of the grading standard should be done focussing on the yield only, as the grading results will always be safe. However, the question may be raised if the sample is representative for the timber growing in the country.

Comparing bending and tension, it seems more likely that required characteristic values for pieces tested in tension are met. Many deviations from the required strength values are small or can be explained. For instance, the timber from Switzerland was tested over a longer span than 9x the height, leading to lower strength values (length effect).

When comparing results for French and Russian pine, the following observations can be made: Raw data is almost equal for both countries (see Table 2). However, the yields for French timber are much higher, but the characteristic tension strength values are much lower than those required (8.9 MPa instead of 14 MPa for C24). As also the mean knot values of the ungraded material are close together for both sources, we checked the correlation between total KAR and tension strength. For the whole dataset of pine loaded in tension a value of  $R^2=0.47$  is found. For Russian pine  $R^2= 0.46$  while for French pine it is only  $R^2=0.18$ . Hence a reliable prediction of the strength of French pine using total KAR seems to be impossible.

## **6 Conclusions**

We have tested three parameters (cross-sections, source of the timber, grading standard) for their influence on visual grading results. The biggest influence is caused by the used grading standards. Not only different rules of measuring knots, but also an unequal number of grades have an influence on the results.

Independent of the standard an effect of the cross-section and the source of the graded timber can be stated. The results show that it is not possible to grade C30 using large cross-sections, because for visual grading usually ratios based on knot size and dimension of the timber are used.

Grading results in terms of reached characteristic values are similar for DIN, BS and INSTA. For sources for which SKA data was available they are usually met or nearly met. Having only two grades in a standard (such as BS) makes it easier to reach the required values for all possible combinations of species and type of loading. All three standards could be used for Central European timber.

Reject rates are lowest for INSTA as only here a grade for C 14 exists. This trend is not transferable to high grades. Yields for C24 and higher vary from 62% for grading according to DIN to 45% for grading according to INSTA (spruce, bending). For all three standards characteristic values are close to the required values with a maximum below of around 10%, considering European spruce. Absolute reject rates for visual grading vary depending on several factors, such as cross-section, grading standard or knot definitions. In practice these rates even will be higher as here the central section has been graded while in practice the full board length will be graded.

The results for NF show low yields for C30. The distinction between C24 and C18 is not really sharp. This leads to equal yields and similar characteristic values for these two grades. Hence characteristic values for C18 are met while for C24 they are not, considering CE spruce. The SIA 265/1:2009 standard leads to extreme reject rates. A practical use is not possible.

Visual grading results are influenced by the source of the timber. Especially grading into C30 seems to be problematic in a number of cases. Depending on species, source and grading rules declared growth areas need clarification for a number of standards and growth areas cannot be extended without additional testing.

Allocations in EN 1912 for softwoods are not correct in a number of cases, and a review seems necessary. New limits for source areas and cross-sections are required. This can only be done based on a review of reports, where the respective grading standards have proven their applicability for the listed source and cross-section.

## 7 References

Almazán AFJ, Prieto HE, Martitegui AF, Richter C (2008): Comparison of the Spanish visual strength grading standard for structural sawn timber (UNE 56544) with the German one (DIN4074) for Scots pine (*Pinus sylvestris* L.) from Germany. *Holz Roh Werkst* (2008) 66: 253–258.

Barrett JD, Lam F, Lau W (1992): Size Effects in Visually Graded Softwood Structural Lumber. CIB W 18 paper 25-6-5, Åhus, Sweden.

BS 4978: 2007+A1:2011: Visual strength grading of softwood. BSI. London.

DIN 4074-1:2012-06: Sortierung von Holz nach der Tragfähigkeit, Nadelschnittholz. DIN. Berlin.

DS/INSTA 142:2009 (E): Nordic visual strength grading rules for timber. Dansk Standard. Charlottenlund.

EN 1310:1997 Round and sawn timber – Method of measurement of features. CEN European Committee for Standardization, Brussels.

EN 338:2010 Structural timber - Strength classes. CEN European Committee for Standardization, Brussels.

EN 384:2010 Structural Timber – Determination of characteristic values of mechanical properties and density. CEN European Committee for Standardization, Brussels.

EN 408:2010 Timber structures – Structural timber and glued laminated timber- Determination of some physical and mechanical properties. CEN European Committee for Standardization, Brussels.

EN 1912:2012 Structural timber - Strength classes - Assignment of visual grades and species. CEN European Committee for Standardization, Brussels.

Fewell A (1984): The Determination of Softwood Strength Properties for Grades, Strength Classes and Laminated Timber for BS 5268: Part 2. CIB W 18 paper 17-6-2, Rapperswill, Switzerland.

Johansson CJ, Brundin J, Gruber R (1992): Stress grading of Swedish and German Timber. A comparison of machine stress grading and three visual grading systems. Swedish National Testing and Research Institute. Building Technology. SP Report 23:94

NF B 52-001:2011 Règles d'utilisation du bois dans les constructions; Classement visuel pour employ en structure pour les principales essences résineuses et feuillues. AFNOR. Saint-Denis.

Riberholt H (2008): European spruce - *Picea abies* - graded by Chinese visual rules. Technical University of Denmark, Department of Civil Engineering. BYG Rapport (ISBN: 978-8-77877-25-72).

Stapel P, v.d. Kuilen JW, Rais A (2010): Influence of Origin and Grading Principles on the Engineering Properties of European Timber. CIB W 18 paper 43-5-2, Nelson, New Zealand.

SIA 265/1:2009 Holzbau – Ergänzende Festlegungen. SIA. Zürich.

Uzielli L (1986): Stress-Grading by ECE Standards of Italian-Grown Douglas-Fir Dimension Lumber from Young Thinnings. CIB W 18 paper 19-5-1, Florence, Italy.



**INTERNATIONAL COUNCIL FOR RESEARCH AND INNOVATION  
IN BUILDING AND CONSTRUCTION**

**WORKING COMMISSION W18 - TIMBER STRUCTURES**

**A STIFFNESS-BASED ANALYTICAL MODEL FOR WOOD STRENGTH IN  
TIMBER CONNECTIONS LOADED PARALLEL TO GRAIN:  
RIVETED JOINT CAPACITY IN BRITTLE AND MIXED FAILURE MODES**

P Zarnani

P Quenneville

The University of Auckland

NEW ZEALAND

**MEETING FORTY FIVE**

**VÄXJÖ**

**SWEDEN**

**AUGUST 2012**

---

Presented by P Zarnani

C Sigrist asked about the purpose to study these failure modes as we had to avoid them. P Zarnani responded that the model provided a means to predict in order to avoid the brittle failure mode. I Smith asked whether the EC approach was more conservative than the Canadian approach. P Zarnani responded yes because effective thickness rather than entire thickness was used therefore more conservative. R Steiger asked about the specimens whether the analysis considered one side versus two side failures and whether the study accounts for series systems. P Zarnani responded that this was not considered. F Lam stated that you could use MLE procedure to account for this. S Aicher and P Quenneville discussed strain in the front plane is within the limit of the shearing strain in the side block. S Aicher stated that these should be compatible. P Quenneville stated that the block moved as a solid block. A Jorissen asked what happened when the bottom and side blocks were thin. P Zarnani stated that the model considered this. H Blass stated that net tension failure could happen. I Smith asked how many additional pages in the code were needed. P Zarnani stated three pages.



# A stiffness-based analytical model for wood strength in timber connections loaded parallel to grain: Riveted joint capacity in brittle and mixed failure modes

Pouyan Zarnani, Pierre Quenneville  
University of Auckland, New Zealand

## 1 Introduction

### 1.1 Motivation

In existing wood strength prediction models for parallel to grain failure in timber connections using dowel-type fasteners, the minimum, maximum or the summation of the tensile and shear capacities of the failed wood block planes are considered. This results in disagreements between the experimental values and the predictions. It is postulated that these methods are not appropriate since the stiffness in tensile and shear planes differs and this leads to uneven load distribution amongst the resisting planes [1,2]. For instance, in a plug shear failure (Fig. 1a), the contribution of the bottom or lateral shear planes to the wood resistance cannot simply be considered as a function of their respective area as the connection load is not shared uniformly among the resisting planes due to the unequal stiffness of the adjacent wood volumes loading the fasteners. In the proposed analysis, the shortcoming of the existing predictive models is taken into account.

The present study focuses on the timber rivet connections. Timber rivets are tight-fit fasteners made of hardened steel from 40 to 90 mm long and 3.2 by 6.4 mm in rectangular cross section used in high capacity steel-timber-steel connections. They are used in Canada and the U.S. In the Canadian and American standards, there is no closed form solution for the wood strength prediction of this type of connection [3]. Also, the standards restrict the use of rivets to specific configurations and for glulam and sawn timber of some limited species. A close-form analytical method to determine the load-carrying capacity of wood under parallel-to-grain loading in rivet connection in timber products is thus proposed. For the wood strength, the stiffness of the adjacent loading volumes and strength of the failure planes subjected to non-uniform shear and tension stresses are considered. The effective wood thickness for the brittle failure mode is derived and related to the elastic deformation of the rivets. A mixed failure mode is also defined (a mixture of brittle and ductile) and depends on the governing ductile failure mode of the rivets. To help the designer, an algorithm is presented which allows the designer to calculate the resistances associated with the predictions of the different possible brittle, ductile and mixed failure modes.

Results of tests on New Zealand Radiata Pine LVL and glulam and test data available from literature confirm the validity of this new method and show that it can be used as a design provision for timber riveted connections. The proposed method can be extended to other small dowel type fastener such as nails and screws.

### 1.2 Available predictive models

The most significant work on timber rivets is that of Foschi and Longworth [4] which is the basis for the timber rivet design procedures in the Canadian O86-09 [5] and the U.S. NDS [6] codes. The authors proposed a prediction model (Eq. 1) based on finite element analysis for calculating the wood strength,  $P_w$ , of a rivet connection loaded parallel-to-grain which brittle failure involves the tensile,  $P_t$ , and shear,  $P_v$ , capacities of the failure surfaces of the wood. The authors provided tables of values for numerically derived factors ( $K$ ,  $\beta$ ,  $\alpha$  and  $\gamma$ ) which are related to the

connection geometry. Using their approach, good predictions of the resistance of their Douglas fir-Larch glulam samples were obtained.

$$P_w = \min \begin{cases} P_t = \frac{f_{t,k} A_t}{K_t \beta_t \alpha_t \gamma_h} \\ P_v = \frac{f_{v,k} A_v}{K_s \beta_s \gamma_h} \end{cases} \quad (1)$$

In Eurocode 5 [7], Annex A, the wood resistance of dowel-type timber connections in plug shear failure is determined using Equation 2. The European equation is based on the maximum of the tensile resistance of the end face or the sum of the shear resistances of the side and bottom faces correspondent to the effective wood depth,  $t_{ef}$ , which depends on the governing ductile failure mode.

$$P_w = \max \begin{cases} 1.5 A_{t,ef} f_{t,k} \\ 0.7 A_{v,ef} f_{v,k} \end{cases} \quad (2)$$

In another study of rivet connections, Stahl et al. [3] presented a simplified analysis for the wood strength. They assumed that the tensile and the shear capacities are additive. Their proposed equation (Eq. 3) is based on three possible wood failure modes shown in Figure 1. Their proposed model for wood strength in brittle failure mode had slightly better predictions in comparison to the ones from the Canadian code.

$$P_w = \min (P_a, P_b, P_c), P_i = 0.2 f_{t,m} A_{t_i} + 0.2 f_{v,m} A_{v_i} \quad (3)$$

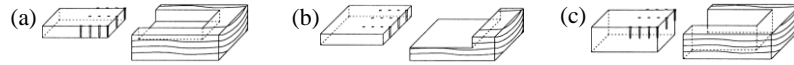


**Figure 1:** Proposed wood failure modes by Stahl [3]

## 2 Proposed analysis for wood strength

The proposed analysis for wood strength is best explained using the analogy of a linear elastic spring system in which the applied load transfers from the wood member to the failure planes in conformity with the relative stiffness ratio of each resisting adjacent volume to the individual failure plane (Fig. 2). By predicting these volumes stiffness, one can derive the portion of the connection load that is channelled to each resisting plane and from the resistance of each failure planes, one can determine which failure plane triggers the connection failure.

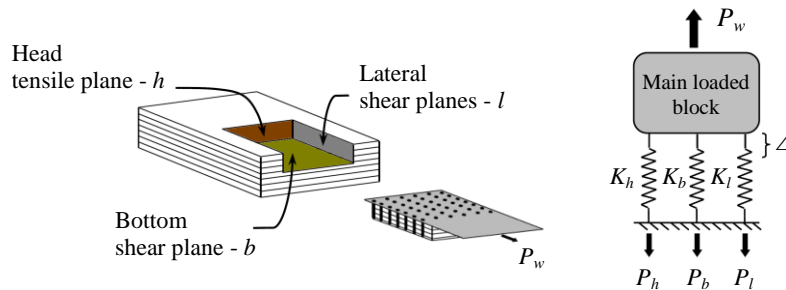


**Figure 2:** Proposed elastic spring model

The difference in the loads channelled to the tensile and shear planes is a function of the modulus of elasticity and modulus of rigidity, the volume of wood surrounding each of the failure planes (bottom, end and edge distances- $d_z$ ,  $d_a$  and  $d_e$ ) and also the connection geometry.

## 2.1 Head tensile plane stiffness

In a rivet connection, the load is transferred from the steel plate to the wood block through the rivets. The load which is applied to the wood increases as it reaches the head of the joint (Fig. 3). The load distribution in the row of rivets is assumed to be linear. Johnsson and Stehn [2], using a load distribution model based on a spring system, showed that the maximum variation from the linear assumption was approximately 12%. The head tensile plane stiffness can then be derived by considering the tensile deformation of the loaded block,  $\Delta$ , which is given by

$$\Delta = \frac{L}{EA_{th}(N_C - 1)} \sum_{i=1}^{N_C-1} \frac{P_h i}{N_C} = \frac{P_h L}{2EA_{th}} \quad (4)$$

where  $E$  is the modulus of elasticity,  $L$  is the length subjected to the tensile stress and  $A_{th}$  the area subjected to the tensile stress at the head of the block. Thus, the average tensile stiffness for the head plane would be

$$K_h = \frac{2EA_{th}}{L} \quad (5)$$

These equations use the connection geometry variables shown in Figure 4 and all dimensions are in mm.

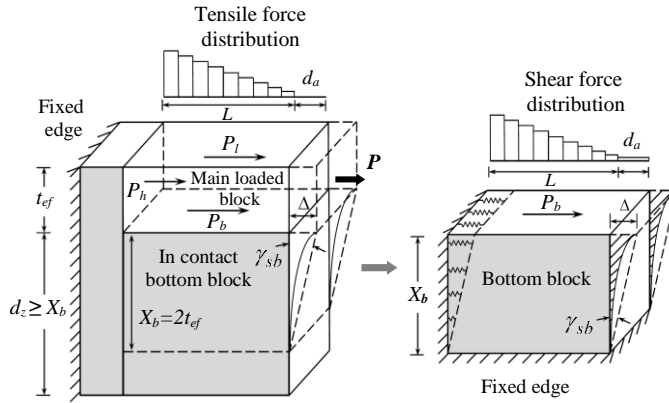


Figure 3: Simplified analytical model

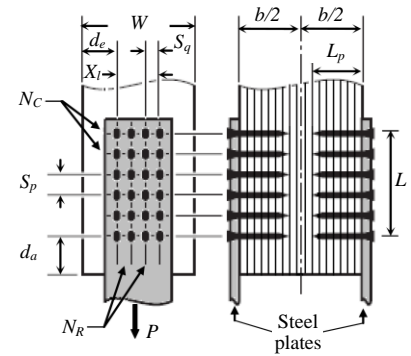


Figure 4: Definition of connection geometry variables

## 2.2 Bottom shear plane stiffness

By developing their FE model, Foschi and Longworth [4] studied the effect of the bottom distance  $d_z$  on the bottom plane shear stress. They observed that the shear stresses vary when  $d_z$  is less than 2 times the rivet penetration,  $L_p$ . They also considered that the thickness of the failed block  $t_{ef}$  is equal to  $L_p$ . Their observation is applied when considering the effective depth of the wood bottom block in contact with the main loaded block (Fig. 3). To simplify the model, and estimate the distortion of the bottom block, it is considered fixed at the bottom edge and subjected to shear stresses on the top surface. Dividing the sum of the bottom shear forces  $P_b$  by the total area over which they act  $A_{sb}$  defines the average shear stress  $\tau_{sb}$ :

$$\tau_{sb} = \frac{P_b}{A_{sb}} = \gamma_{sb} G = \frac{\Delta}{X_b} G \quad (6)$$

in which  $G$  is the modulus of rigidity,  $\gamma_{sb}$  the shear strain and  $X_b$  the maximum effective depth of the bottom block defined as  $X_b = 2t_{ef}$ . Thus, the average pure shear stiffness would be  $K_{sb} = GA_{sb}/X_b$ . However, as it is shown in Figure 3, the bottom block has a fixed edge at its head on its entire cross section which increases the stiffness and prevents deformation under the applied shear force. Setting the deformation at the top of the bottom block equal to  $\Delta$ , it is assumed that this deformation decreases in a nonlinear form as it reaches the bottom and

approaches zero at the fixed bottom edge. It is assumed that the average deflection resulting from the tension load on the bottom block cross section can be theoretically considered as equal to  $\Delta/10$ . Thus, the additional average tensile stiffness for the bottom block cross section,  $K_{tb}$ , can be estimated as  $K_{tb} = EA_{tb}/(10L)$  where  $A_{tb}$  is the effective tensile area of the bottom block given as  $A_{tb}=S_qX_b(N_R-1)$ . Summing the two components (tension and shear), the average bottom shear plane stiffness can be defined by

$$K_b = K_{sb} + K_{tb} \quad (7)$$

Foschi and Longworth [4] observed that when the bottom distance  $d_z$  becomes less than  $X_b$ , the bottom shear stress decreases and the load thus released is transferred almost in its entirety to the tensile plane. To take this effect into account, a factor  $H$  is proposed [8]. This factor can be considered as the reduction rate of the bottom shear plane stiffness,  $H$  (Eq. 8), as a result of decreasing the bottom distance  $d_z$  less than  $X_b$ .

$$\begin{cases} H=0 & , \text{ If } d_z \geq X_b \\ H=0.25 (2 - d_z / t_{ef})^2 & , \text{ If } d_z < X_b \end{cases} \quad (8)$$

$$\text{Thus, } K_b = (1 - H)(K_{sb} + K_{tb}) \quad (9)$$

This relationship was obtained through observation of the resistance contribution of the bottom block shear plane in the experimental study where the depth of the member was varied.

### 2.3 Lateral shear planes stiffness

Assuming that the mechanical properties of the wood for lateral and bottom shear planes are the same, the correspondent equations for the two side lateral shear planes can be developed similarly. The average pure shear stiffness for the lateral planes would become  $K_{sl} = A_{sl}G/X_l$  where  $A_{sl}$  is the summation of the areas subjected to the lateral shear stress and  $X_l$  the maximum effective edge distance (equal to 2 times the half of the distance between the first and the last rows, which is comparable to  $X_b=2t_{ef}$  for the bottom shear plane). The additional average tensile stiffness can be given as  $K_{tl} = EA_{tl}/(10L)$  in which  $A_{tl}$  is the effective tensile area of the lateral blocks and is  $A_{tl} = 2t_{ef}X_l$ . Consequently, the average lateral shear planes stiffness can be defined by

$$K_l = (1 - F)(K_{sl} + K_{tl}) \quad (10)$$

This time, the reduction factor for lateral shear planes stiffness [8],  $F$  is determined using:

$$\begin{cases} F=0 & , \text{ If } d_e \geq 1.25X_l \\ F=0.16 (2.5 - d_e / (X_l/2))^2 & , \text{ If } d_e < 1.25X_l \end{cases} \quad (11)$$

The relationship for  $F$  has also been obtained through observation of the resistance contribution of the side block shear planes in the experimental study where the width of the member was varied.

### 2.4 Closed-form approach

By predicting the stiffness of the wood surrounding each of the failure planes ( $K_h$ ,  $K_b$  and  $K_l$ ), one can predict the proportion of the total connection load applied to each plane,  $R_i = K_i / \sum K$ . By further establishing the resistance of each of the failure planes as a function of a strength criterion, one can verify which of the failure planes governs the resistance of the entire connection. Thus, the wood load carrying capacity of the connection (Eq. 12) is the load which results in the earlier failure of one of the resisting planes due to being overloaded and equals to the minimum of  $P_{wh}$ ,  $P_{wb}$  and  $P_{wl}$ . In other words, the wood strength of the connection is the total capacity of the one plane which fails first plus a portion of strength capacity of the other planes.

Moreover, while one plane fails, then the load transfers to the rest of the planes in accordance with their relative stiffness ratios. It could be possible that the occurrence of the first failure of one plane does not correspond with the maximum load of the connection.

$$P_w = N_p \cdot \min \begin{cases} P_{wh} = f_{t,m} A_{th} \left(1 + \frac{K_b}{K_h} + \frac{K_l}{K_h}\right) \\ P_{wb} = f_{v,m} C_{ab} A_{sb} \left(1 + \frac{K_h}{K_b} + \frac{K_l}{K_b}\right) \\ P_{wl} = \frac{C_{al} A_{sl} K_b}{C_{ab} A_{sb} K_l} P_{wb} \end{cases} \quad (12)$$

In equation 12,  $f_{t,m}$  is the wood mean strength in tension parallel to the grain (MPa) and  $f_{v,m}$  is the wood mean strength in shear along the grain (MPa). Also,  $C_{ab}$  and  $C_{al}$  are the ratios of the average to maximum stresses on the bottom and lateral shear planes respectively given by Equations 13 and 14. These coefficients are derived based on the increasing load distribution on the shear planes (Fig. 3). The factor  $k_e$  is applied to  $C_{al}$  to account for the reduction of the resisting area due to the cracks formation on the lateral planes, estimated at 20% of the failed block thickness while  $d_e$  is less than  $1.25X_l$ .

$$C_{ab} = \frac{S_p (N_c (N_c + 1) / 2 - 1) + d_a}{N_c (L + d_a)} \quad (13)$$

$$C_{al} = k_e C_{ab} \begin{cases} k_e = 1 & , \text{ If } d_e \geq 1.25X_l \\ k_e = 0.8 & , \text{ If } d_e < 1.25X_l \end{cases} \quad (14)$$

It should be noted that for a connection having only one plate,  $N_p=1$ , the member thickness value,  $b$ , to be used to determine  $d_z = b/2 - t_{ef}$  is twice the thickness of the wood.

## 2.5 Effective wood thickness

### 2.5.1 Brittle failure

In current tests on LVL and glulam, the average thickness of the failed block,  $t_{block}$ , in the majority of the brittle failures was observed at approximately  $0.85L_p$ . This thickness corresponds to the elastic deformation of the rivets since there were no observed plastic deflections. For brittle failure modes, the effective wood thickness (Eq. 15) is determined from the elastic deformation of the rivet modelled as a beam on an elasto-plastic foundation (Fig. 5). The rivet is supported by springs with bilinear response that simulate the local nonlinear embedment behaviour of the timber surrounding it. For more details regarding the model, refer to Zarnani and Quenneville [9].

### 2.5.2 Mixed failure

For some connection groups, considerable decrease of  $t_{block}$  combined to a distortion of rivets was visible. This failure mode is defined as the mixed mode since the wood fails with some deflection of the rivets before they reach complete yielding. In these groups,  $t_{block}$  corresponded to the effective wood thickness,  $t_{ef}$ , depending on the governing failure mode of the rivets. Since rivets are always used in single shear and the rivet head can be considered to be rotationally fixed where it is wedged into the steel plate's hole, only three yield modes need to be considered [3] (Fig. 6).  $t_{ef}$  can be derived using Equation 16 based on Johansen's yield theory [10] which is the foundation for the EYM prediction formulas in Eurocode 5 [7]. The proposed prediction for the wood strength showed good agreement with observed values of  $t_{block}$  for these groups. In Equation 16,  $d_l$  is the rivet cross-section dimension bearing on the wood parallel-to-grain, (equal to 3.2 mm);  $f_{h,0}$  is the embedment strength of the wood which can be determined as a function of

$d_l$  and the density of the wood [11]; and  $M_{y,l}$  is the parallel-to-grain moment capacity of the rivet, equal to 30000 Nmm [3].

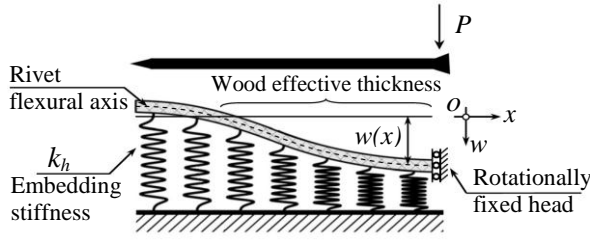


**Figure 5:** Spring model of elastic deformation of rivet as a beam on an elasto-plastic foundation

$$t_{ef,e} \sim \begin{cases} 0.95L_p & , \text{ for } L_p \text{ equals to } 28.5 \text{ mm} \\ 0.85L_p & , \text{ for } L_p \text{ equals to } 53.5 \text{ mm} \\ 0.75L_p & , \text{ for } L_p \text{ equals to } 78.5 \text{ mm} \end{cases} \quad (15)$$

## 2.6 Proposed procedure

Based on the observation that the effective wood thickness differs in brittle and mixed failure modes which affect the wood strength, the following procedure, shown in Figure 7 is suggested to determine the load carrying capacity of the riveted connection for the possible brittle, ductile and mixed failure modes. In this paper, the rivet strength and its yielding mode are based on experimental results which also can be predicted by a consistent yield model proposed by Zarnani and Quenneville [11].

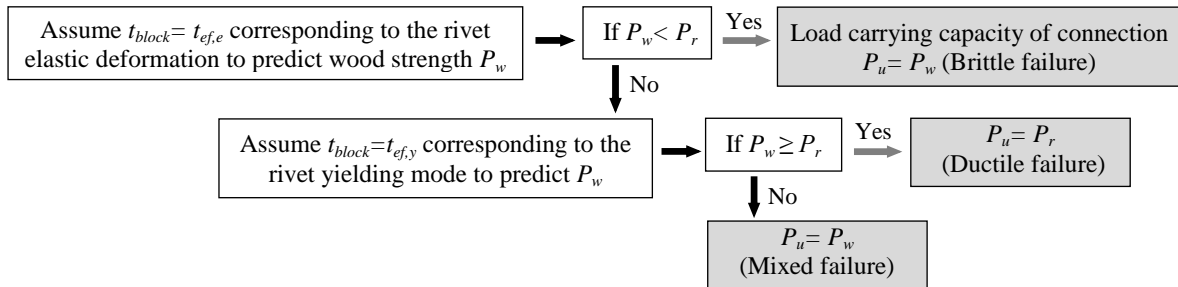


**Figure 7:** Proposed algorithm for different possible brittle, ductile and mixed failure modes

## 3 Experimental program

Laboratory tests were set up to evaluate the effect of bottom, edge and end distances on the connection strength and to prompt wood failures and maximize the amount of observations on the brittle mechanism. Specimens were manufactured from New Zealand Radiata Pine LVL grade 10 and glulam with grade of GL8. The tests series were divided into 26 groups for LVL and 6 groups for glulam. 3 replicates were tested for each group of specimens for LVL and 4 replicates for glulam. The parameters for connection geometries (Fig. 4) used varied from 4 to 8 for  $N_R$  and  $N_C$ ; from 15 to 25 mm for  $S_q$  and 25 to 50 mm for  $S_p$ ;  $L_p$  from 28.5 to 78.5 mm (with rivet lengths  $L_r$  of 40, 65 and 90 mm);  $d_z$  from  $0.1X_b$  to  $1.1X_b$ ;  $d_e$  from  $0.2X_l$  to  $1.9X_l$  and  $d_a$  from 50 to 125 mm. For more details regarding the connections configuration refer to Zarnani and Quenneville [1]. A typical specimen in the testing frame is shown in Figure 8. All specimens were conditioned to 20°C and 65% relative humidity to attain a target 12% equilibrium moisture condition (EMC). The wood had an average density of 590 and 480 kg/m<sup>3</sup> with a coefficient of variation of 4% and 9% and at the time of the tests, an average moisture content of 11.5% and 11% for LVL and glulam respectively. Material characteristics were also evaluated [1] but for brevity, are not reported in this paper.

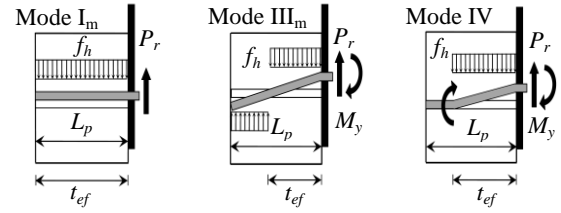


**Figure 6:** Effective thickness based on rivet embedment length in different yielding modes

$$t_{ef,y} = \begin{cases} L_p & \text{Mode I}_m \\ \sqrt{\frac{M_{y,l}}{f_{h,0}d_l} + \frac{L_p^2}{2}} & \text{Mode III}_m \\ 2\sqrt{\frac{M_{y,l}}{f_{h,0}d_l}} & \text{Mode IV} \end{cases} \quad (16)$$

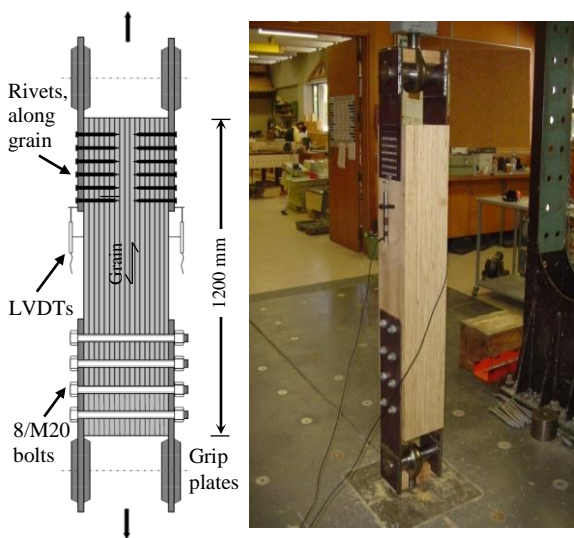
## 4 Results and discussion

### 4.1 Connection tensile tests

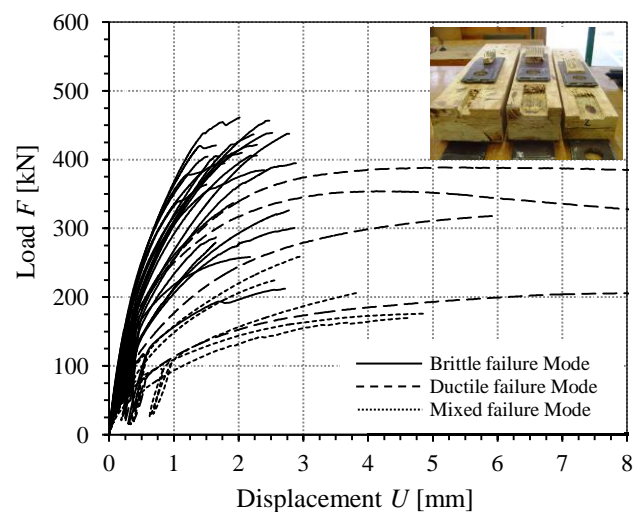
The load-slip curve of each group was plotted (Fig. 9) and the ultimate load and the types of failure were recorded. The peak loads ranged from 159 kN to 468 kN. The effect of failure modes on the load-displacement plots is shown in Figure 9. The displacements observed in ductile failures with complete yielding of the rivets are far beyond the usual range of serviceability, but they indicate that the connections would be suitable for use in seismic design if rivet yielding failure mode controls [12]. In case of brittle failures, the maximum connection deformation was 2 to 3 mm and the wood rupture occurred suddenly. Beyond the connection deformation of 0.5 mm, it can be observed that the load-slip curves for brittle failures show some inelastic behaviour. This can be explained by the plastic response of the wood embedment behaviour next to the rivet head during the elastic deformation of the rivets [11]. For mixed mode failures in which wood failed before final yielding of the rivets, more deflection can be seen compared to brittle failures due to some rivet deformation.

Results for the LVL and glulam groups tested are listed in Tables 1 and 2 respectively. After observing the test results, the groups were matched and identified based on the modes of failure. In Tables 1 and 2, BRG, MIG and DUG stand for tests series with brittle, mixed and ductile modes of failure correspondingly, additionally, L stands for LVL and G for glulam. The thickness of the failed blocks and predominant modes of failure observed are also listed in the tables. Along with the results, connection capacities have been calculated using the proposed analysis.

Test groups with tightly spaced rivet pattern exhibited a brittle failure (Fig. 10). A sudden failure happened where a block of wood bounded by the rivet group perimeter was pulled away from either one side or both sides of the specimens. As shown in Tables 1 and 2, in the BRG test series, the failed block thickness  $t_{block}$  were observed at approximately  $0.85L_p$  which corresponds to the elastic deformation of the rivets since no plastic deflection was observed as in Figure 10a. However, in the MIG test series, the  $t_{block}$  value is significantly lower with visible distortion of the rivets (Fig. 10b). In these mixed failure mode cases, the load-carrying capacity of the wood is based on the stiffness and strength of the tensile and shear planes corresponding to the effective depth of the wood,  $t_{ef,y}$ .

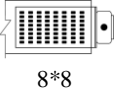
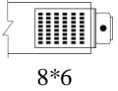
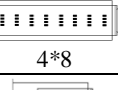
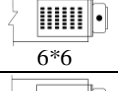
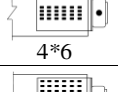
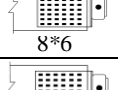
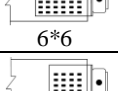
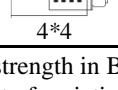
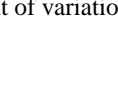


**Figure 8:** Typical specimen in testing apparatus



**Figure 9:** Typical load-slip plots for joint tensile tests in brittle, mixed and ductile failure modes

**Table 1: Strength and failure mode predictions using the proposed method compared to experimental results on LVL**

LVL groups	No. of rows by columns ( $N_R * N_C$ )	Rivet penetration $L_p$ (mm)	Proposed wood strength $P_w$ (kN) $t_{block}=t_{ef,e}$	Rivet strength $P_r$ * (kN)	$t_{block}$ (mm)	Proposed wood strength $P_w$ (kN) $t_{block}=t_{ef,y}$	Connection strength (prediction/test result)	
					Proposed/Observed		Mean ultimate load <sup>†</sup> $P_u$ (kN)	Failure mode
BRG1-L		28.5	314	461	27.1( $t_{ef,e}$ ) / 23	-	314/358	Brittle/Brittle
BRG2-L		28.5	362	461	27.1( $t_{ef,e}$ ) / 27	-	362/370	Brittle/Brittle
BRG3-L		28.5	380	461	27.1( $t_{ef,e}$ ) / 24	-	380/375	Brittle/Brittle
BRG4-L		28.5	376	461	27.1( $t_{ef,e}$ ) / 21	-	376/391	Brittle/Brittle
BRG5-L		28.5	381	461	27.1( $t_{ef,e}$ ) / 28	-	381/402	Brittle/Brittle
BRG6-L		28.5	378	461	27.1( $t_{ef,e}$ ) / 26	-	378/410	Brittle/Brittle
BRG7-L		28.5	391	461	27.1( $t_{ef,e}$ ) / 26	-	391/435	Brittle/Brittle
BRG8-L		53.5	419	692	45.5( $t_{ef,e}$ ) / 48	-	419/463	Brittle/Brittle
BRG9-L		53.5	392	519	45.5( $t_{ef,e}$ ) / 43	-	392/384	Brittle/Brittle
BRG10-L		53.5	440	519	45.5( $t_{ef,e}$ ) / 42	-	440/419	Brittle/Brittle
BRG11-L			53.5	432	519	45.5( $t_{ef,e}$ ) / 44	-	432/427
BRG12-L	53.5		432	519	45.5( $t_{ef,e}$ ) / 41	-	432/398	Brittle/Brittle
BRG13-L	53.5		436	519	45.5( $t_{ef,e}$ ) / 41	-	436/456	Brittle/Brittle
BRG14-L	53.5		440	519	45.5( $t_{ef,e}$ ) / 46	-	440/468	Brittle/Brittle
BRG15-L	53.5		427	519	45.5( $t_{ef,e}$ ) / 47	-	427/437	Brittle/Brittle
BRG16-L	53.5		434	519	45.5( $t_{ef,e}$ ) / 42	-	434/445	Brittle/Brittle
BRG17-L		53.5	441	345	40.1( $t_{ef,y}$ ) / 50	362	345/290	Ductile/Brittle
BRG18-L		28.5	237	259	27.1( $t_{ef,e}$ ) / 24	-	237/247	Brittle/Brittle
BRG19-L		53.5	334	388	45.5( $t_{ef,e}$ ) / 46	-	334/315	Brittle/Brittle
MIG20-L		78.5	436	417	26.7( $t_{ef,y}$ ) / 29	233	233/245	Mixed IV/Mixed IV
MIG21-L		78.5	338	278	26.7( $t_{ef,y}$ ) / 27	176	176/207	Mixed IV/Mixed IV
MIG22-L		53.5	255	259	45.5( $t_{ef,e}$ ) / 35	-	255/214	Brittle/Mixed III <sub>m</sub>
MIG23-L		28.5	178	172	24.2( $t_{ef,y}$ ) / 19	166	166/159	Mixed III <sub>m</sub> /Mixed III <sub>m</sub>
DUG24-L		28.5	505	345	24.2( $t_{ef,y}$ ) / -	498	- /345	Ductile III <sub>m</sub> / Ductile III <sub>m</sub>
DUG25-L		53.5	515	388	40.1( $t_{ef,y}$ ) / -	479	- /388	Ductile III <sub>m</sub> / Ductile III <sub>m</sub>
DUG26-L		78.5	419	185	26.7( $t_{ef,y}$ ) / -	213	- /185	Ductile IV/ Ductile IV

\* The rivet strength in BRG and MIG groups are based on the rivet capacity derived from DUG tests.

† Coefficient of variation (COV%) for brittle/mixed failure modes 4-9 % and for ductile failure modes 2-4%.

**Table 2: Strength and failure mode predictions using the proposed method compared to experimental results on glulam**

Glulam groups	No. of rows by columns ( $N_R * N_C$ )	Rivet penetration $L_p$ (mm)	Proposed wood strength $P_w$ (kN) $t_{block}=t_{ef,e}$	Rivet strength $P_r$ (kN)	$t_{block}$ (mm)	Proposed wood strength $P_w$ (kN) $t_{block}=t_{ef,y}$	Connection strength (prediction/test result)	
					Proposed/Observed		Mean ultimate load <sup>†</sup> $P_u$ (kN)	Failure mode
BRG1-G	8*8	53.5	340	531	45.5( $t_{ef,e}$ ) / 46	-	340/335	Brittle/Brittle
BRG2-G	8*6	53.5	328	398	45.5( $t_{ef,e}$ ) / 45	-	328/301	Brittle/Brittle
BRG3-G	6*8	28.5	188	272*	27.1( $t_{ef,e}$ ) / 25	-	188/224	Brittle/Brittle
BRG4-G	4*8	53.5	226	266	45.5( $t_{ef,e}$ ) / 50	-	226/315	Brittle/Brittle
MIG5-G	4*6	78.5	222	217*	29.7( $t_{ef,y}$ ) / 28	127	127/160	Mixed IV/Mixed IV
MIG5-G	6*6	53.5	397	298	40.6( $t_{ef,y}$ ) / -	379	- /298	Ductile III <sub>m</sub> / Ductile III <sub>m</sub>

† Coefficient of variation (COV%) for brittle/mixed failure modes 11-17 % and for ductile failure modes 8%.

\* Values are based on the tests conducted by Buchanan and Lai [16] on Radiata Pine glulam with the same density.

## 4.2 Validation of new analysis and comparison with other models

Strength predictions of the current tests and tests available in the literature were made using the new method to compare it with codes equations and other analytical models. The CSA O86-09 [5], Eurocode 5 [7] and the prediction model proposed by Stahl et al. [3] were used in the comparison. Using the U.S. (NDS) equations [6], result in similar predictions as the O86 code ones after correcting for limit state definition.

### 4.2.1 Current test data

Based on the proposed analysis, in the BRG test groups (Table 1 and 2), the wood strength for  $t_{block}=t_{ef,e}$  was lower than the rivets yielding strength  $P_r$  and consequently the failure mode was brittle. However, in the MIG test groups, the wood strength for  $t_{block}=t_{ef,e}$  was more than the rivets strength. The strength of the connection was thus checked for the possible mixed or ductile modes of failure. Since in these test series the wood strength for  $t_{block}=t_{ef,y}$  was weaker than the rivets strength, therefore a mixed mode failure occurred for the connection with a load carrying capacity less than the rivets resistance. As shown in Table 1 and 2, there is very good agreement between the predictions and observations for the thickness of the failed block, the governing failure mode, and the strength of the connection. Figure 11 shows the strength predictions of the experimental groups using the proposed analysis and the predictions from O86-09, EC5 and Stahl's method. The proposed analysis results in more precise predictions with a correlation coefficient ( $r^2$ ) of 0.91 and a mean absolute error (MAE) of -3.4% and a standard deviation (STDEV) of 10.3%.

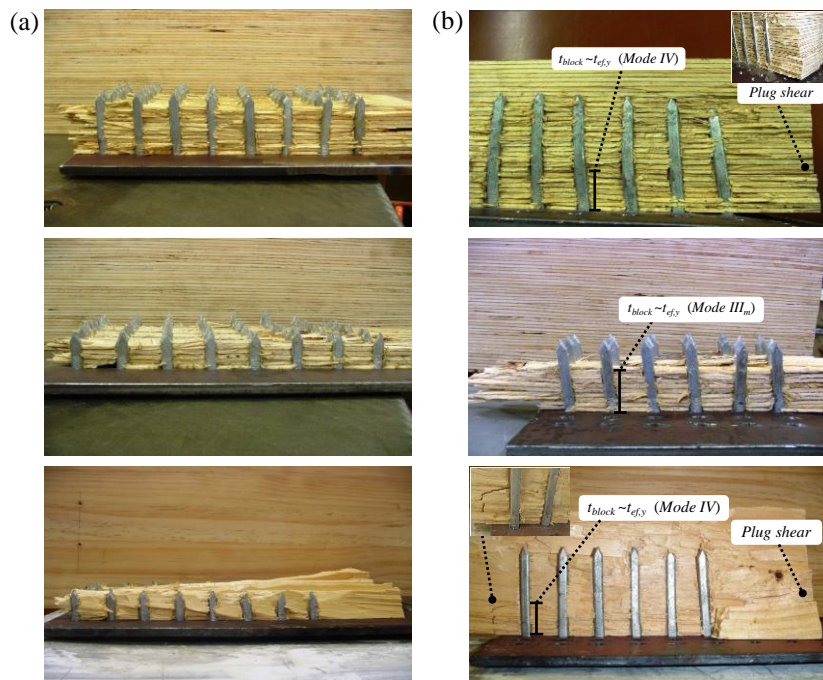


**Figure 10:** Effective thickness in LVL and glulam; (a) Brittle failure mode, (b) Mixed failure mode

One can note that the predictions using the other models are mostly constant for the tests with approximate capacities of 350 kN to 450 kN (Fig. 11b). These are the tests series conducted to observe the effects of bottom, edge and end distances. For instance, as the bottom distance  $d_z$  gets larger due to increase in timber thickness, the capacity of the connection gets higher as asserted by Stahl et al. [3] as well. The predictions based on the proposed analysis are shown in Figure 12 for test groups BRG1-L to BRG3-L which are identical in every parameter except the bottom distance. Thicker specimen with larger  $d_z$  induces more stiffness for the resisting bottom shear plane. Therefore, the stiffness ratio of the resisting bottom plane increases and reduces for

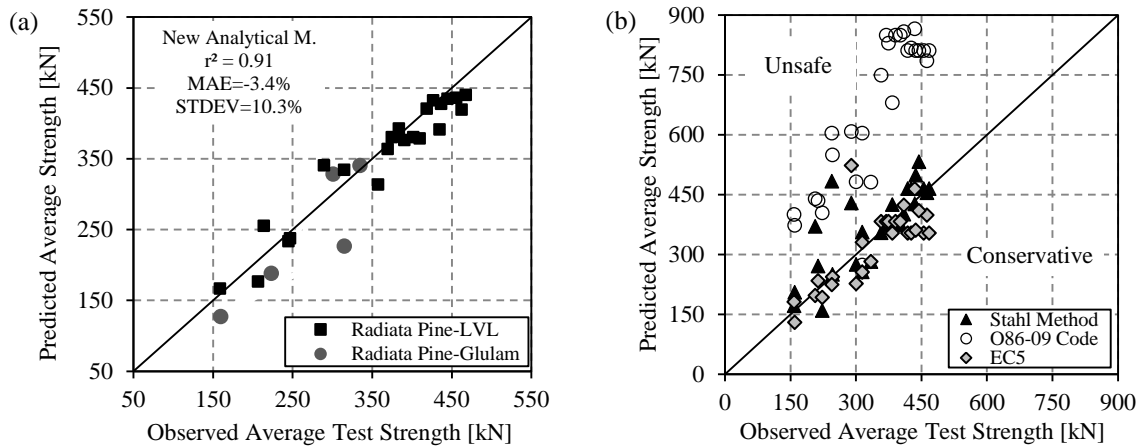


**Figure 11:** Comparison of analyses and the current test data in brittle/mixed failure modes; (a) New analysis, (b) Stahl’s method, O86 code and EC5

the other resisting planes (Fig. 12a). Subsequently, a higher proportion of the applied load transfers to the bottom resisting plane and the maximum stress lowers on the lateral shear and head tensile planes in comparison to the stresses for a thinner specimen. In these test series, as the triggering failure is at the head tensile plane, the connection capacity increases as the bottom shear plane takes a greater proportion of the connection load (Fig. 12b). The same behavior is observed when the edge distance  $d_e$  is increased. However, the predictions by the O86 code show an opposite behavior with a decreasing trend in thicker specimens. This is explained by the fact that the Canadian code includes a volume effect on the shear strength which negatively affects the connection capacity. The results from current tests and those from Stahl et al. [3] disprove the size effect based on the Weibull weakest link theory of brittle failure adopted in the Canadian and also U.S. codes. In fact, the size of the wood surrounding the main loaded block affects the proportion of the load channelled to the resisting shear planes rather than the shear strength of the wood. For instance, the strength of a connection with minimal edge and bottom distances can be simply predicted as the tensile capacity of the head plane since there is very little proportion of the connection load channelled to the bottom and lateral shear planes. Also, as shown in Figure 11, the O86 predictions are overestimated. Moreover, for mixed failures, the predictions using Stahl’s method are non-conservative. These overestimated values are due to the fact that Stahl’s equation considers the full length of the rivet penetration as the effective wood thickness and do not consider the possibility of mixed mode failure. Thus, the necessity for predicting the connection strength under a mixed mode of failure is required.

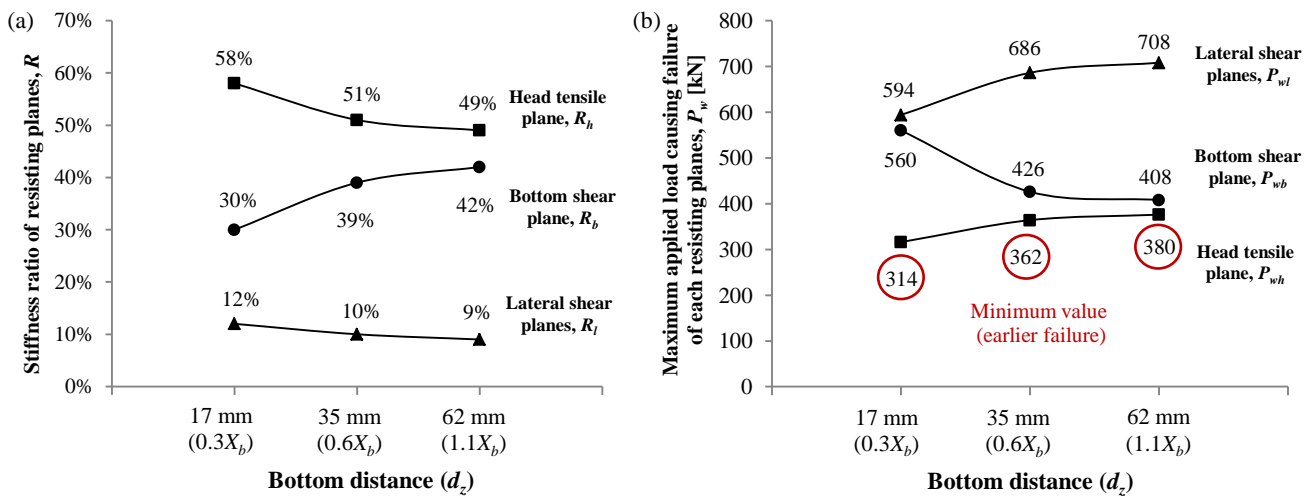


**Figure 12:** The effect of increasing the bottom distance; (a) Stiffness ratio of resisting planes, (b) Maximum applied load causing failure of each resisting planes

## 4.2.2 Data available in the literature

A similar comparison was made using data available in the literature and current test data (Fig. 13). Five sets of data were considered from the literature: tests performed by Foschi and Longworth [4] on Douglas Fir-Larch glulam, Buchanan and Lai [14] on Radiata Pine glulam, Karacabeyli et al. [15] on Hem-Fir solid timber, Stahl et al. [3] on Southern Pine glulam, and Marjerrison [16] on Douglas Fir-Larch and Spruce Pine glulam. For comparison purposes, all available data and design code predictions were transferred to mean short term values.

By comparing the prediction models (Fig. 13), it can be deduced that there is more conformity between the predictions using the proposed analysis and the available test data. The predictions from the proposed method results in a higher correlation coefficient (0.87) and a lower STDEV (20.3%) (Table 3). The predictions using Stahl's method are better than the ones using the O86 code and EC5 model. There is considerable strength over prediction for a connection with a large end distance using Stahl's method and the EC5. This supports the theory developed here which states that by adding to the end distance, the load carrying capacity of the connection doesn't increase correspondingly to the additional shear resistance surface due to larger end distance. The values obtained using O86 code results in overestimated values with the highest STDEV of 44.5% and MAE of 75.9% (final factored resistance has the required reliability and safety).

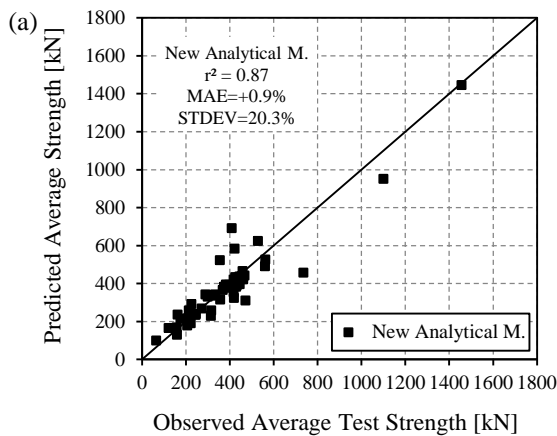


**Table 3:** Comparison of fit for the prediction models of wood strength

Design model	Correlation coefficient ( $r^2$ ) all data/ literature	Standard deviation (STDEV)	Mean absolute error (MAE)
New Analysis	0.87/0.86	20.3%	+0.9%
Stahl's Method	0.78/0.82	29.4%	+2.1%
O86-09 Code	0.77/0.81	44.5%	+75.9%
Eurocode 5:2004	0.70/0.68	28.7%	+0.2%

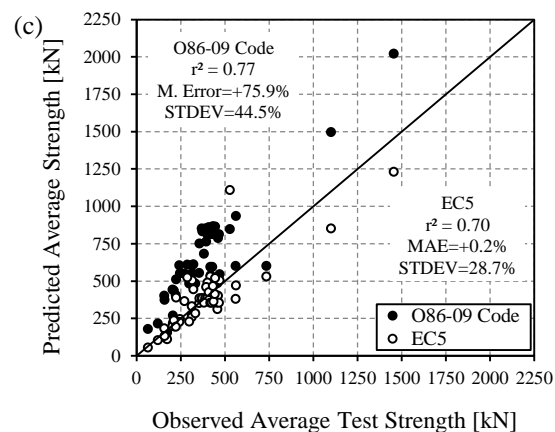
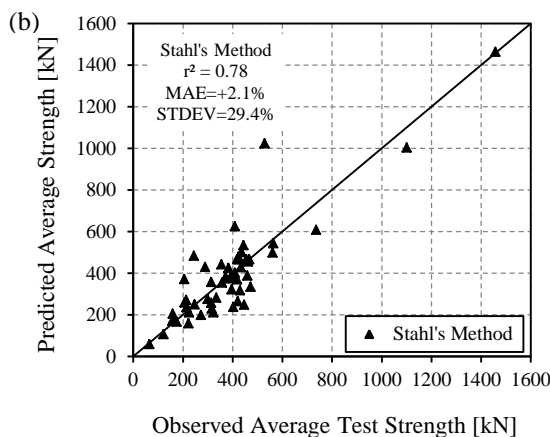


**Figure 13:** Comparison of analyses and test data (current and literature data) in brittle/mixed failure modes; (a) new analytical method, (b) Stahl's method, (c) O86 code and EC5

## 5 Conclusions

A close form stiffness-based analytical model to determine the wood block tear-out resistance of riveted connections in timber products is proposed. The method takes into account the strength of the failure planes and the stiffness of the adjacent wood channelling the member load to these planes. Results of current tests and from tests available from literature confirm that this closed

form analytical method can be used as design method resulting in more precise predictions for timber riveted connections. Based on the proposed design model, an efficient connection design can be made by decreasing the difference between the capacity of the wood and the rivets. The proposed method can be extended to other small dowel type fastener; e.g. nails and screws for connection design improvement and failure modes prediction.

## 6 Acknowledgements

The authors wish to thank the New Zealand Structural Timber Innovation Company (STIC) for funding this research work.

## 7 References

- [1] Zarnani P., Quenneville P.: Predictive analytical model for wood capacity of rivet connections in glulam and LVL. In proceedings of 12<sup>th</sup> WCTE, Auckland, New Zealand, 2012.
- [2] Johnsson H., Stehn L.: Plug shear failure in nailed timber connections: Load distribution and failure initiation. *Holz-als Roh und Werkstoff*, 62:455-464, 2004.
- [3] Stahl D. C. , Wolfe R. W. , and Begel M.: Improved analysis of timber rivet connections. *J Struct Eng ASCE*, 130(8):1272-1279, 2004.
- [4] Foschi R. O., Longworth J.: Analysis and design of griplam nailed connections. *J Struct Div ASCE*, 101(12):2537-2555, 1975.
- [5] Canadian Standards Association (CSA). CAN/CSA-O86.09: Engineering design in wood (limit states design). Mississauga, Ontario, 2009.
- [6] American Forest and Paper Association (AF&PA). NDS-2001: National design specification (NDS) for wood construction. Washington, DC, 2001.
- [7] European Committee for Standardization (CEN). EN 1995-1-1:2004: Eurocode 5-Design of timber structures. Brussels, Belgium, 2004.
- [8] Zarnani P., Quenneville P.: New analytical method and experimental verification of timber rivet connections loaded parallel-to-grain. In proceedings of the CSCE Annual Conference, Struct Div, Ottawa, Canada, 2011.
- [9] Zarnani P., Quenneville P.: Wood effective thickness in brittle and mixed failure modes of timber rivet connections. In proceedings of 12<sup>th</sup> WCTE, Auckland, New Zealand, 2012.
- [10] Johansen K. W.: Theory of timber connections. *Publications of International Association for Bridge and Structural Engineering*, 9:249-262, 1949.
- [11] Zarnani P., Quenneville P.: Reliable yield model for strength prediction of timber rivet connection under ductile failure. In proceedings of 12<sup>th</sup> WCTE, Auckland, New Zealand, 2012.
- [12] Begel M., Wolfe R. W., and Stahl D. C.: Timber rivet connections in US domestic species. Res Pap FPL-RP-619. Madison, WI: US Department of Agriculture, Forest Service, Forest Products Laboratory, 2004.
- [13] European Committee for Standardization (CEN). N 408:2003: Structural timber and glued laminated timber-Determination of some physical and mechanical properties. Brussels, Belgium, 2003.
- [14] Buchanan A. H., Lai J. C.: Glulam rivets in Radiata Pine. *Can J Civ Eng*, 21(2):340-350, 1994.
- [15] Karacabeyli E., Fraser H., and Deacon W.: Lateral and withdrawal load resistance of glulam rivet connections made with sawn timber. *CJCE*, 25(1):128-138, 1998.
- [16] Marjerrison M. R.: Analysis of timber rivet connections loaded parallel to grain. MSc dissertation, Dept of Civil Eng, The Royal Military College of Canada, Ontario, Canada, 2007.

**INTERNATIONAL COUNCIL FOR RESEARCH AND INNOVATION  
IN BUILDING AND CONSTRUCTION**

**WORKING COMMISSION W18 - TIMBER STRUCTURES**

**BEAMS LOADED PERPENDICULAR TO GRAIN BY CONNECTIONS  
– COMBINED EFFECT OF EDGE AND END DISTANCE**

J L Jensen

P Quenneville

The University of Auckland

**NEW ZEALAND**

U A Girhammar

Luleå University of Technology

B Källsner

Linnæus University and SP Technical Research Institute of Sweden

**SWEDEN**

**MEETING FORTY FIVE**

**VÄXJÖ**

**SWEDEN**

**AUGUST 2012**

---

Presented by P Quenneville

A Frangi asked whether cross banded LVL could be made to address this issue. P Quenneville responded that yes we had done this but there was a limit. I Smith asked how this work compared to other species and tests. P Quenneville said that other tests were done mostly at midpoint and could not be compared. Also extrapolation to multi bolt cases was quite a step away. A Jorissen asked and received clarification about the definition of parameters in slide 27.



# **Beams loaded perpendicular to grain by connections**

## **– Combined effect of edge and end distance**

Jørgen L. Jensen, Pierre Quenneville  
The University of Auckland, New Zealand

Ulf Arne Girhammar  
Luleå University of Technology, Sweden

Bo Källsner  
Linnæus University and SP Technical Research Institute of Sweden

### **Abstract**

The paper proposes a new generalized model for determination of the splitting capacity of beams loaded perpendicular to the grain by connections. The generalized model is based on a previously presented quasi-nonlinear fracture mechanics model, and includes as a special case the linear elastic fracture mechanics model, on which the current European and Canadian timber design codes are based. The model further includes the effect of the end distance on the splitting capacity, which currently is not considered in timber design codes or other analytical models. Test results are presented for validation of the model. Some points to be considered in some major timber design codes are pointed out.

### **1 Introduction**

The European [1] and Canadian [2] timber design codes have in recent years decided to introduce equations for design against splitting of beams loaded perpendicular to the grain by connections. The equations applied in [1] and [2] are based on the linear elastic fracture mechanics (LEFM) model first presented in [3]. For further references on the derivation of the model presented in [3], see for instance also [4] and [5]. For further reading on issues related to the model first presented in [3], see for instance also [6]-[9]. Alternative simple analytical fracture mechanics models for the purpose considered here may be found in [10]-[14], and a comprehensive review may be found in [15].

Among the models mentioned above, only the model presented in [14] takes into account the influence of the end distance on the splitting capacity. The model is a quasi-nonlinear fracture mechanics (QNLFM) model based on a model for a Timoshenko-beam on a Winkler-foundation, and considers in principle a single fastener located close to the edge and close to the end of a beam. This paper presents new results of splitting tests on single

bolts located close to the edge and the end of beams of Radiata pine laminated veneer lumber (LVL) for the purpose of validation of the proposed QNLFM model.

Further, a semi-empirical generalization of the model is proposed, which facilitates the use of the model for connections located far from or close to the end of a beam, and which contains the model first presented in [3] and now used as the basis for [1] and [2] as a special case.

## 2 Theory

The LEFM model presented in [3] reads:

$$P_u = 2bC_1 \sqrt{\frac{h_e}{1 - \frac{h_e}{h}}} \quad , \quad C_1 = \sqrt{\frac{5}{3}GG_f} \quad (1)$$

where  $P_u$  is the load acting on the connection,  $b$  is the width of the beam,  $h$  is the depth of the beam,  $h_e$  is the loaded edge distance (i.e. the distance from the loaded edge to the fastener farthest from the edge),  $G$  is the shear modulus, and  $G_f$  is the fracture energy. The problem is in general a mixed mode fracture problem, and the edge distance, location of the connection, support conditions etc. determine the mixed mode ratio. However, the fracture energy for pure mode I fracture may be used as a conservative estimate, and it will usually be a good estimate.

It can be shown that Eq. (1) appears as a special case of a more general derivation of the model than originally given in [3], namely if the deformations from the bending are ignored and only the shear deformations are considered, see [4] or [5].

The model presented in [10] is likewise based on an assumption of a displacement field that only takes into account shear deformations. The very nature of this model means that the beam depth does not come into play, only the loaded edge distance. The solution given in [10] reads in a slightly generalized form:

$$P_u = 2b\sqrt{2GG_f h_e / \beta_s} \quad (2)$$

where  $\beta_s$  is a shear correction factor, which in [10] is assumed to be  $\beta_s = 1.0$ , but which in ordinary beam theory is assumed to be  $\beta_s = 6/5$  for rectangular cross sections. Using  $\beta_s = 6/5$ , Eq. (2) becomes

$$P_u = 2bC_1\sqrt{h_e} \quad , \quad C_1 = \sqrt{\frac{5}{3}GG_f} \quad (3)$$

It is noticed that Eq. (3) results from Eq. (1) for  $h_e/h \rightarrow 0$ . This is of course no coincidence, and the physics behind this fact can easily be understood.

In [11] and [12], a QNLFM solution is given for a connection loading a beam far from the beam end. Notice that also here, like in the model presented in [10], the very nature of the beam on elastic foundation model on which the QNLFM is built, does not involve the beam depth, but only the loaded edge distance. The solution reads:

$$\begin{aligned}
P_u &= \gamma P_{u,\text{LEFM}} \\
P_{u,\text{LEFM}} &= 2bC_1\sqrt{h_e} \quad , \quad C_1 = \sqrt{\frac{5}{3}GG_f} \\
\gamma &= \frac{\sqrt{2\zeta+1}}{\zeta+1} \quad , \quad \zeta = \frac{C_1}{f_t} \sqrt{10\frac{G}{E} \frac{1}{h_e}}
\end{aligned} \tag{4}$$

where  $E$  is the parallel-to-grain modulus of elasticity (MOE) of the beam and  $f_t$  is the perpendicular-to-grain tensile strength of the beam.

It is noticed that  $P_{u,\text{LEFM}}$  in Eq. (4) is exactly the solution given by Eq. (3). Since Eq. (3) is a special case of Eq. (1), it is also reasonable to imagine that Eq. (4) in the same way is a special case of a more general model, which at present just has not yet been derived. Alternatively, the generalization of Eq. (4) as given by Eq. (5) may be considered empirical.

$$\begin{aligned}
P_u &= \gamma P_{u,\text{LEFM}} \\
P_{u,\text{LEFM}} &= 2bC_1 \sqrt{\frac{h_e}{1-\frac{h_e}{h}}} \quad , \quad C_1 = \sqrt{\frac{5}{3}GG_f} \\
\gamma &= \frac{\sqrt{2\zeta+1}}{\zeta+1} \quad , \quad \zeta = \frac{C_1}{f_t} \sqrt{10\frac{G}{E} \frac{1}{h_e}}
\end{aligned} \tag{5}$$

Eq. (5) thus contains Eq. (1), which forms the basis of the European [1] and Canadian [2] timber design codes, as a special case, namely for  $f_t \rightarrow \infty$ .

While the models given by Eqs. (3)-(5) only require that the connections are located sufficiently far from the beam end or supports, the model given by Eq. (1) theoretically requires that the connection is located at mid-span of a simply supported beam. EC5 [1], however, applies Eq. (1) to all locations of the connection and all support conditions. For a simply supported beam with a connection very close to one of the supports (and thus very close to the beam end), EC5 [1] predicts half the splitting failure load as compared with the connection located at mid-span. Usually, no splitting will occur in reality if the connection is located very close to the support. EC5 [1] also predicts half the splitting capacity if the connection is located in a cantilever beam as compared with the simply supported beam loaded at mid-span. In case of a cantilever beam, EC5 [1] predicts the same splitting capacity irrespective of the location of the connection; A connection located at the free end of a cantilever beam of length  $L$  leads to the same splitting capacity as a connection located at  $L/2$ .

In [14], a QNLFM solution was derived for a single force acting perpendicular to the grain close to the edge and close to the end of a beam following the same principles as those leading to Eq. (4). The solution reads:

$$P_u = P_{u,LEFM} \cdot \min \left\{ \begin{array}{l} \frac{1}{2\sqrt{2\zeta+1}} + \frac{bf_t l_e}{P_{u,LEFM}} \\ \frac{\sqrt{2\zeta+1}}{\zeta+1} \end{array} \right. \quad (6)$$

$$P_{u,LEFM} = 2bC_1 \sqrt{h_e} \quad , \quad C_1 = \sqrt{\frac{5}{3}} G G_f \quad , \quad \zeta = \frac{C_1}{f_t} \sqrt{10 \frac{G}{E} \frac{1}{h_e}}$$

where  $l_e$  is the end distance. Eq. (6) is in fact an approximate, linearized solution. The failure load,  $P_u$ , is a nonlinear function of the ratio  $l_e/h_e$ , and the solution given in Eq. (6) is the minimum of the tangent to  $P_u$  taken at  $l_e/h_e = 0$  and the asymptote for  $l_e/h_e \rightarrow \infty$  (i.e. the solution given by Eq. (4)).

With exactly the same argument as for Eq. (4), Eq. (6) may be generalized to:

$$P_u = P_{u,LEFM} \cdot \min \left\{ \begin{array}{l} \frac{1}{2\sqrt{2\zeta+1}} + \frac{bf_t l_e}{P_{u,LEFM}} \\ \frac{\sqrt{2\zeta+1}}{\zeta+1} \end{array} \right. \quad (7)$$

$$P_{u,LEFM} = 2bC_1 \sqrt{\frac{h_e}{1 - \frac{h_e}{h}}} \quad , \quad C_1 = \sqrt{\frac{5}{3}} G G_f \quad , \quad \zeta = \frac{C_1}{f_t} \sqrt{10 \frac{G}{E} \frac{1}{h_e}}$$

Eq. (7) gives the solution for connections loaded close to the end or far from the end of a beam, and contains Eq. (1) as a special case.

It should be noticed that all the models and equations presented here were derived considering a single force acting on the beam. Real connections usually consist of multiple fasteners, and the use of models considering a single force has been subject to debate. Empirical models taking into account multiple fasteners have been presented [16], [17], and the German timber design code [18] presently includes such a model. No analytical model currently exists, which takes into account multiple fasteners. For e.g. simply supported beams, it seems that modelling a multiple fastener connection as a single force works sufficiently well in many situations, but the circumstances under which this simplifying assumption is reasonable are still not clear. While it may be sufficient to model a multiple fastener connection as a single force for connections in simply supported beams, the concept leads to problems for multiple fastener connections located very close to the end of a beam. Here the distance from the outermost fastener to the end grain may be much less than the distance from the centroid of the fastener group to the outermost fastener. Further work is therefore needed to clarify whether or how Eq. (6) or Eq. (7) can be used for multiple fastener connections. At present, the model is primarily intended for use with moment-resisting connections, where a single fastener located close to the edge and close to the end grain is the primary cause of splitting.

### 3 Experiments

Tests were conducted on LVL made from New Zealand grown Radiata pine (*Pinus radiata*). Two series of splitting tests, Series A and Series B were conducted on LVL beams. In addition to the splitting tests, material property tests were conducted for determination of the perpendicular-to-grain tensile strength and the mode I fracture energy of the LVL. Further, so-called plate specimen tests [8] were conducted.

#### 3.1 Materials and methods

All tests reported here were conducted on LVL made from New Zealand grown Radiata pine (*Pinus radiata*) (HySpan from Carter-Holt-Harvey). All specimens were taken from the same batch.

##### Material property tests

The perpendicular-to-grain tensile strength of the LVL was tested using specimens as shown in Fig. 1 in accordance with [19]. The mode I fracture energy was tested using a setup as shown in Fig. 2 and in accordance with [20] (apart from the fact that the supports and loading point consisted of simple smooth steel rollers). Tests for direct determination of the so-called fracture parameter,  $C_1$ , were conducted on plate specimens as shown in Fig. 3 and in accordance with [8]. 15 replicates were tested for all set-ups.

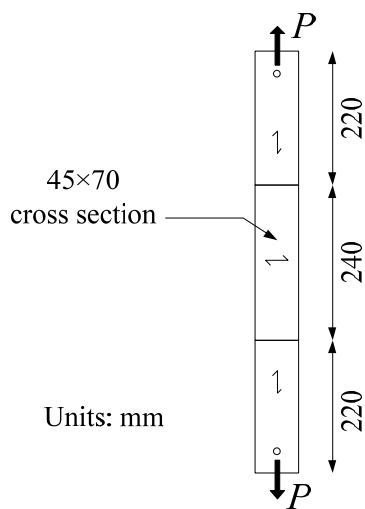


**Fig. 1** Specimen for perpendicular-to-grain tensile strength

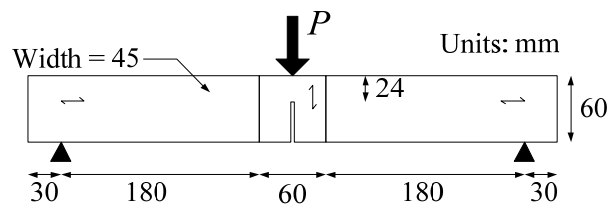


**Fig. 2** Specimen for mode I fracture energy

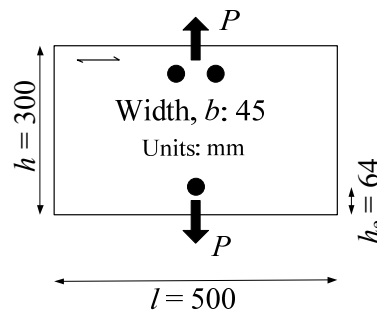


**Fig. 3** Plate specimen for direct determination of the fracture parameter

## Splitting tests

### Series A

Fig. 4 shows the geometry and setup used for the simply supported beams in test Series A. All beams had a  $45 \times 300 \text{ mm}^2$  cross section. Bolts were 16 mm hot-dip galvanized, bolt holes in the steel plates were 16 mm and in the timber 17 mm. Two very closely spaced bolts were used consistently for all specimens in order to avoid embedment failures especially for the specimens with  $h_e = 8d$  ( $d$  being the diameter of the bolt). Beams loaded at mid-span and quarter-span were tested. Two different edge distances,  $h_e = 4d$  and  $h_e = 8d$ , were tested. 10 replicates were tested, i.e. a total of 40 beams.

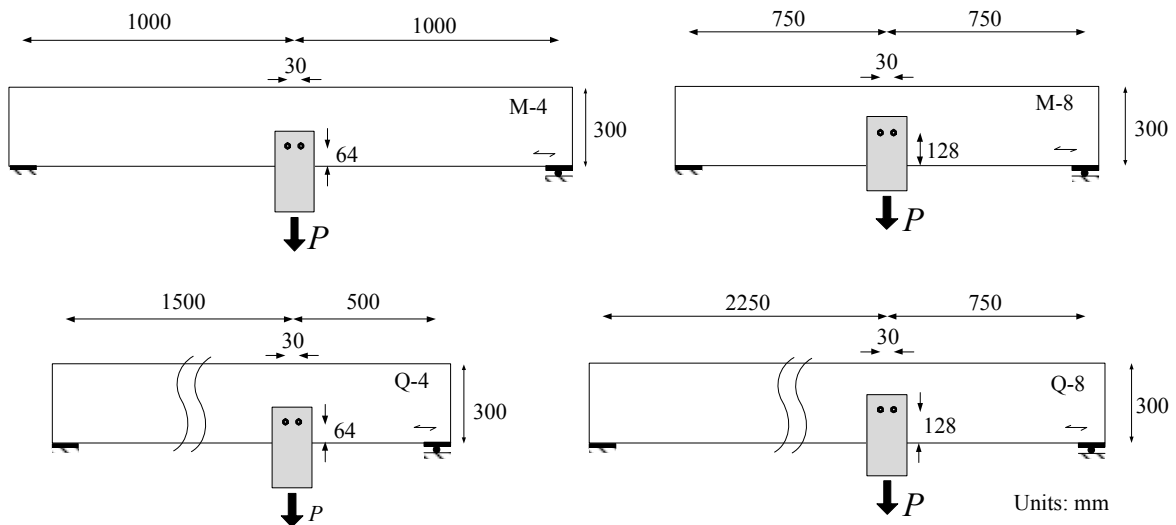


Fig. 4 Setup and geometry for Series A

### Series B

Fig. 5 shows the geometry and setup used for the simply supported beams in test Series B. All beams had a  $45 \times 300 \text{ mm}^2$  cross section. Bolts were 16 mm warm galvanized, bolt holes in the steel plates were 16 mm and in the timber 17 mm.

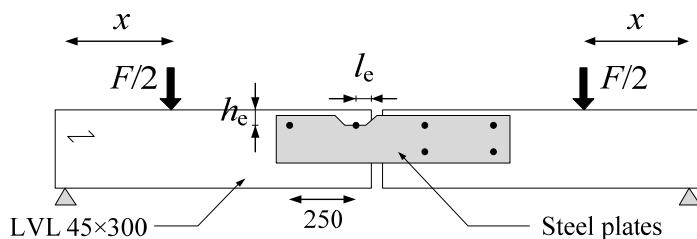


Fig. 5 Setup and geometry for Series B

The tested beams (left half in Fig. 5) all had a length of approximately 1100 mm. Two different edge distances were tested,  $h_e = 2d = 32 \text{ mm}$  and  $h_e = 4d = 64 \text{ mm}$ .

For  $h_e = 2d$ , end distances of  $l_e = 3d, 5d$ , and  $8d$  were tested.

For  $h_e = 4d$ , end distances of  $l_e = 3d, 5d, 8d, 12d$ , and  $16d$  were tested.

For each combination of edge and end distances 10 replicates were tested, i.e. in total 80 specimens.

The load,  $P_u$ , acting perpendicular to the grain direction on the critical bolt closest to the end of the test specimen is given by  $P_u = Fx/(500 \text{ mm})$ , where  $F$  is the total load applied by the testing machine and  $x$  is given in Fig. 5.  $x = 290 \text{ mm}$  was used for  $h_e = 2d$ , and  $x = 435 \text{ mm}$  was used for  $h_e = 4d$ .

## 3.2 Test results

### Material properties

The results of the material property tests are summarized in Table 1.

**Table 1** Material properties of tested LVL

	Mean	COV [%]
$\omega$ [%]	9	-
$\rho$ [kg/m <sup>3</sup> ]	599	2
$E$ [MPa]	15750	3
$G$ [MPa]	787	(3)
$f_t$ [MPa]	1.50	12
$G_f$ [N/mm]	0.95	15
$C_1$ [N/mm <sup>1.5</sup> ]	22.7	8

In Table 1,  $\omega$  is the moisture content,  $\rho$  is the density at the given moisture content,  $E$  is the parallel-to-grain modulus of elasticity,  $G$  is the shear modulus,  $f_t$  is the perpendicular-to-grain tensile strength,  $G_f$  is the mode I fracture energy, and  $C_1$  is the fracture parameter. The shear modulus was not measured but estimated using  $G = E/20$ . The modulus of elasticity is the dynamic modulus of elasticity, which was determined using a log-grader for measuring the acoustic wave speed.

### Splitting tests

Series A

The mean failure loads and coefficient of variation (COV) for the specimens tested in Series A are given in Table 2. For the geometry of the specimens, see Fig. 4.

**Table 2** Experimental splitting failure loads, Series A

Specimen	Mean failure load [kN]	COV [%]
M-4	20.3	13
M-8	36.6	9
Q-4	19.3	8
Q-8	37.0	10

## Series B

The mean failure loads and coefficient of variation (COV) for the specimens tested in Series B are given in Table 3. For geometry of the specimens, see Fig. 5.

**Table 3** Experimental splitting failure loads, Series B

$d$ [mm]	16							
$h_e/d$	2			4				
$l_e/h_e$	1.5	2.5	4	0.75	1.25	2	3	4
Mean failure load [kN]	7.3	9.9	10.9	8.6	12.9	16.0	19.5	21.3
COV [%]	16	11	16	9	14	8	6	6

## 4 Discussion

It is noticed from Table 2 that there is no statistically significant difference in splitting capacity between beams loaded at mid-span and beams loaded at quarter-span. The mid-span to quarter-span failure load ratios for  $h_e = 4d$  and  $h_e = 8d$  are 1.06 and 0.99, respectively. EC5 [1] predicts a ratio of 1.5. The Canadian code [2] does not consider any difference in splitting resistance as a result of the location of the connection.

Table 4 shows the theoretical to experimental failure load ratios for the beams tested in Series A for Eqs. (1) and (5). In case of Eq. (1), the mean value of the  $C_1$ -factor as determined directly by the plate specimen tests and given in Table 1 has been used for calculation of the theoretical failure load. Use of the measured value of the fracture energy in Eq. (1) leads to significantly less good agreement with the test results. The results given for Eq. (5) are based on the measured values of the fracture energy and the perpendicular-to-grain tensile strength.

**Table 4** Theoretical to experimental failure load ratios for Series A

Specimen	$h_e$ [mm]	Eq. (1)	Eq. (5)
M-4	64	0.91	1.04
M-8	128	0.83	1.05
Q-4	64	0.95	1.10
Q-8	128	0.83	1.03

Eq. (5) is in very good agreement with test results. More tests should be conducted to confirm the extraordinary good agreement. It should be noticed that the theoretical failure loads are based on all measured material properties, except for the shear modulus, which has been estimated as  $G = E/20$ . No sort of fitting is involved. The perpendicular-to-grain tensile strength is known to be volume dependent, but here standard tests in accordance with [19] lead to excellent results. It should be verified that this is also the case for other wood products and species.

Fig. 6 shows a comparison of the experimental failure loads obtained in Series B and the theoretical failure loads calculated by means of Eq. (7). Also, the theoretical failure loads have been obtained using the experimentally determined values of the fracture energy and the perpendicular-to-grain tensile strength as given in Table 1. The agreement between experiments and theory is striking. Also in [14], very good agreement was obtained

between experiments and Eq. (6), but here the perpendicular-to-grain tensile strength was determined in a way, which cannot be said to be truly independent from Eq. (6). More tests should be conducted to confirm that the extraordinary good agreement between theory and experiments also hold for other wood species and product if using Eq. (7) with material properties determined in accordance with [19] and [20].

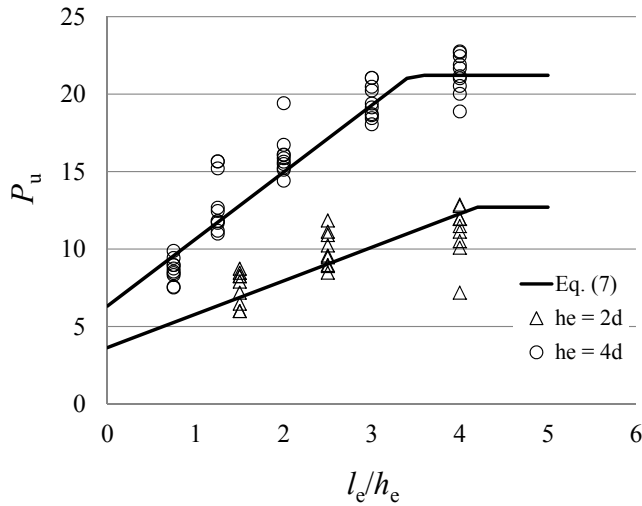


**Fig. 6** Comparison of theoretical and experimental results of Series B

It should be noticed that Eqs. (4)-(7), which are all based on the quasi-nonlinear fracture mechanics models, require the fracture energy as well as the perpendicular-to-grain tensile strength as input. This is in opposition to the linear elastic fracture mechanics model given by Eq. (1), which relies solely on the fracture energy. Eq. (1) produces fairly good estimates of the splitting capacity if the fracture parameter,  $C_1$ , is determined directly by means of plate specimens, but sometimes produces less good estimates if the  $C_1$ -factor is determined from the measured fracture energy. Also in [21] was Eq. (4) found to lead to better results than Eq. (1) if the calculations were based on the measured fracture energy. While Eq. (1) solely relies on the fracture energy, the German timber design code [18] solely relies on the perpendicular-to-grain tensile strength.

In [22], tests on connections loading Douglas fir glulam beams perpendicular to the grain are reported. The dimensions, edge distances and test setups for the Douglas fir glulam beams were the same as reported here for the Radiata pine LVL beams. The beam tests as well as plate specimen tests show that the mean splitting failure load for the Radiata pine LVL is rather precisely twice the value for Douglas fir glulam. Perpendicular-to-grain tensile strength tests using the same testing method [19] and size of specimens as used for the LVL specimens resulted in a mean tensile strength of 2.3 MPa with a COV of 30%. These results indicate that the splitting capacity is not determined by the perpendicular-to-grain tensile strength alone as assumed in the German timber design code [18].

The available results may indicate that both the perpendicular-to-grain tensile strength and the fracture energy influence the splitting capacity as predicted by the quasi-nonlinear fracture mechanics models. This point should be investigated further.

## 5 Conclusions

An analytical model based on quasi-nonlinear fracture mechanics was presented for calculation of the splitting capacity of beams loaded perpendicular to the grain by connections. The model is capable of predicting the splitting capacity under consideration of not only the loaded edge distance, but also the end distance. Tests were presented showing excellent agreement with the theoretical predictions both for connections located in the span of a simply supported beam and for connections placed close to the end of a beam. The connections used in the tests in principle all consisted of single bolts.

Apart from giving a contribution to the validation of the proposed quasi-nonlinear fracture mechanics model for calculation of the splitting capacity, the tests also suggest that: (1) EC5 is wrong in predicting a major influence of the location of a connection in the span of a simply supported beam. (2) The splitting capacity is influenced by the perpendicular-to-grain tensile strength as well as by the fracture energy. EC5 assumes that the capacity depends only on the fracture energy, while the German timber design code assumes that the capacity depends only on the perpendicular-to-grain tensile strength.

## Acknowledgements

The research presented in this paper was generously funded by the New Zealand Structural Timber Innovation Company (STIC) and by the European Union's Structural Funds – The Regional Fund.

The experimental work reported is to a large extent due to Rayan Hoshino, Harith Barakat, Aaron Arnold and Kyle Rolland as partial fulfilment of the requirements for a bachelor degree in civil engineering at The University of Auckland. Their contributions are much appreciated.

## References

1. European Committee for Standardization (CEN)(2004) EN 1995-1-1:2004 Design of Timber Structures. Brussels, Belgium.
2. Canadian Standards Association (2009) CSA O86-09 Engineering Design in Wood. Toronto, Canada.
3. van der Put TACM, Leijten AJM (2000) Evaluation of perpendicular to grain failure of beams caused by concentrated loads of joints. In: Proceeding of the International Council for Research and Innovation in Building and Construction, CIB-W18, Meeting Thirty-Three, Delft, The Netherlands, paper 33-7-7.
4. Jensen JL (2003) Splitting strength of beams loaded by connections. In: Proceeding of the International Council for Research and Innovation in Building and Construction, CIB-W18, Meeting Thirty-Six, Colorado, USA, paper 36-7-8.
5. Jensen JL (2005) Splitting strength of beams loaded perpendicular to grain by dowel joints. *J Wood Sci* 51:480-485.
6. Leijten AJM, Jorissen A (2001) Splitting strength of beams loaded by connections perpendicular to grain – Model verification. In: Proceeding of the International Council for Research and Innovation in Building and Construction, CIB-W18, Meeting Thirty-Four, Venice, Italy, paper 34-7-1.

7. Leijten AJM (2002) Splitting strength of beams loaded by connections – Model comparison. In: Proceeding of the International Council for Research and Innovation in Building and Construction, CIB-W18, Meeting Thirty-Five, Kyoto, Japan, paper 35-7-7.
8. Yasumura M (2002) Determination of fracture parameter for dowel-type joints loaded perpendicular to wooden grain and its application. In: Proceeding of the International Council for Research and Innovation in Building and Construction, CIB-W18, Meeting Thirty-Five, Kyoto, Japan, paper 35-7-9.
9. Ballerini M, Giovanella A (2003) Beams transversally loaded by dowel-type joints: Influence on splitting strength of beam thickness and dowel size. In: Proceeding of the International Council for Research and Innovation in Building and Construction, CIB-W18, Meeting Thirty-Six, Colorado, USA, paper 36-7-7.
10. Larsen HJ, Gustafsson PJ (2001) Dowel joints loaded perpendicular to grain. In: Proceedings of the International Council for Research and Innovation in Building and Construction, CIB-W18, Meeting Thirty-Four, Venice, Italy, paper 34-7-3.
11. Jensen JL, Gustafsson PJ, Larsen HJ (2003) A tension fracture model for joints with rods or dowels loaded perpendicular to grain. In: Proceedings of the International Council for Research and Innovation in Building and Construction, CIB-W18, Meeting Thirty-Six, Colorado, USA, paper 36-7-9.
12. Jensen JL (2005) Quasi-non-linear fracture mechanics analysis of the splitting failure of single dowel joints loaded perpendicular to grain. *J Wood Sci* 51:559-565.
13. Jensen JL (2005) Quasi-non-linear fracture mechanics analysis of splitting failure in simply supported beams loaded perpendicular to grain by dowel joints. *J Wood Sci* 51:577-582.
14. Jensen JL (2005) Quasi-non-linear fracture mechanics analysis of splitting failure in moment-resisting dowel joints. *J Wood Sci* 51:583-588.
15. Schoenmakers JCM (2010) Fracture and failure mechanisms in timber loaded perpendicular to grain by mechanical connections. Ph.D.-thesis, University of Technology Eindhoven, The Netherlands.
16. Ballerini M, Rizzi M (2007) Numerical analysis for the prediction of the splitting strength of beams loaded perpendicular-to-grain by dowel-type connections. *Materials and Structures* 40:139-149.
17. Franke B, Quenneville P (2011): Design approach for the splitting failure of doweltype connections loaded perpendicular to grain. In: Proceeding of the International Council for Research and Innovation in Building and Construction, CIB-W18, Meeting Forty-Four, Alghero, Italy, paper 44-7-5.
18. Deutsches Institut für Normung e. V. (2008) DIN 1052:2008 Entwurf, Berechnung und Bemessung von Holzbauwerken – Allgemeiner Berechnungsregeln und Bemessungsregeln für den Hochbau, Berlin, Germany.
19. Comite Europeen de Normalisation (CEN) (2003) EN 408 Timber structures - Structural timber and glue laminated timber - Determination of some physical and mechanical properties. Brussels, Belgium.
20. NT Build 422 Wood (1993) Fracture energy in tension perpendicular to the grain. Nordtest, Espo, Finland.

21. Hindman DP, Finkenbinder DE, Loferski JR, Line P (2010) Strength of sawn lumber and wood composite connections loaded perpendicular to grain: Fracture mechanics equations. *J. Mater. Civ. Eng.* 22:1226-1234.
22. Jensen JL, Quenneville P (2011): Splitting of beams loaded perpendicular to the grain by connections – some issues with EC5. In: *Proceeding of the International Council for Research and Innovation in Building and Construction, CIB-W18, Meeting Forty-Four, Alghero, Italy, Note.*

**INTERNATIONAL COUNCIL FOR RESEARCH AND INNOVATION  
IN BUILDING AND CONSTRUCTION**

**WORKING COMMISSION W18 - TIMBER STRUCTURES**

**L BLOCK FAILURE OF DOWELLED CONNECTIONS SUBJECT TO BENDING  
REINFORCED WITH THREADED RODS**

J-F Bocquet

C Barthram

LERMAB Laboratory, Henri Poincaré University, Nancy,

FRANCE

A Pineur

Bureau d'Etudes Greisch

BELGIUM

**MEETING FORTY FIVE**

**VÄXJÖ**

**SWEDEN**

**AUGUST 2012**

---

Presented by J-F Bocquet

H Blass asked why there was not a kbending. J-F Bocquet stated that data did not support kbending >1 as values were near bending capacity of beam. P Zarnani received confirmation that the distribution of stresses inside the joint was not discussed even though different detailed analyses were made where it was important to take into account the elastic properties of the material. They also discussed the contribution of shear from the screw reinforcements. K Malo asked whether the normal stresses were caused by applied axial forces. J-F Bocquet stated that external normal forces were not used in the tests.



# **L block failure of dowelled connections subject to bending reinforced with threaded rods**

Jean-François BOCQUET\*

*Associate Professor,*

Charles BARTHAM\*

*Ing Ph.D Student*

\* *LERMAB Laboratory, ENSTIB,*

*Henri Poincaré University, Nancy, France*

Arnaud PINEUR

*Engineer*

*Bureau d'Etudes Greisch LIEGE science park Allée des Noisetiers 25*

*4031 LIEGE Belgium*

## **1 Summary**

The paper presents the analyses of potential block shear failures of dowelled joints in bending: failure criteria based on block shear failure principle are then proposed. The paper reports the results of two experimental studies. Joints of important size were submitted to monotonic bending. These joints were transversally reinforced with treaded rods to avoid tensile failure perpendicular to the grain. An “L” shaped block failure as the design criteria was experimentally confirmed by the tests for the two kinds of joints. In the case of circular patterned joints, the estimation was 20,7 % lower than the test results due to the important yielding of the dowels and crushing of the timber. For the grid patterned joints with two slotted in steel metal plates, the “L” shape block failure never occurred at the same time in the three timber member parts: the estimation was 17,8 % lower.

## **2 Introduction**

Brittle failures of dowelled connections are only partly discussed in current design standards. The described brittle failure modes are either row splitting, block shear or plug shear and are only valid for connections subjected to axial forces. In these types of connections, the contact between the dowel and the wood induces tensile forces perpendicular to the grain, even though the load applied is parallel to the grain.

In the case of bending loads, the failure modes are not easy to define. Moreover, the stress tension field perpendicular to the grain and the shear stress field are more difficult to establish: this is due to the variable transverse forces induced directly by the distribution of the moment on the dowels. The complex interaction between transverse and shear stresses make the shear behaviour less predictable and often leads to early failures.

Different studies show that the ductility of dowelled timber connections submitted to axial forces can be increased by preventing perpendicular to the grain tensile failure by screws.

In a recent study [1], joints in bending are reinforced and tested with self-tapping screws. When failure appears, these connections show particular failure modes. One of those is an “L” shaped block failure. Based on the principle of the block shear failure criterion, a design method is first proposed. In order to verify this criterion, two different types of dowelled connections were transversally reinforced with threaded rods and tested in bending: a transport joint with a circular pattern and a timber to steel connection having multiple shear planes with a grid pattern. Since only few connections were tested, the results are then discussed.

### 3 Context analysis

#### 3.1 Block shear principle

Since Johansen's work [2], a set of researches have converged to advance the design of timber joints. This approach is now integrated to the Eurocode 5 [3] leaving the least possible to empiricism. The design of timber joints is based on the ductile embedment behaviour of wood, on the plastic behaviour of the steel fasteners and on the spacing and edge-end distances which should ensure that the plastic threshold is reached. Many authors like Falbusch [4], Jorissen [5] and Quenneville and Mohammad [6] state that when dowel connections are subject to tension, three principal brittle failure modes can appear: net tension failure, row splitting or row shearing failure and block shear failure (*this last mode will be called a "C" mode failure because of its shape in the rest of the paper*).

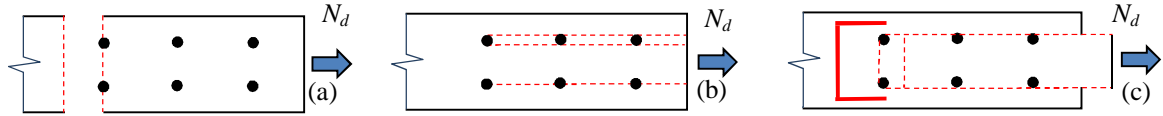


Figure 1 : Observed failure modes for timber bolted connections (a) net tension failure (b) splitting or row shearing failure (c) block shear failure.

Block shear takes into account the brittle properties of wood in longitudinal tension and shear. It estimates the load bearing capacity of tearing out a solid block from a joint. The failure is governed by the strongest of the tensile and shear resistance of the connected area. A first design criterion was proposed in EC5 (A). Hanhijärvi et al. [7] and Kairi [8] have consolidated and optimised this approach. However, they state that it is difficult to predict the failure mode (splitting or block shear) due to the variability of the strength of wood in transverse tension. When the connection is only subject to axial tensile forces, the elastic and plastic load distributions are very similar. This means that the shape of the block failure does not evolve as a function of the load. When the load includes a bending moment, for example, the load distribution depends on the degree of plasticity of the dowels in the connection. Since shear and tensile resistance show a fragile behaviour, their contribution to ultimate resistance against block shear cannot be cumulated. In this case, the strongest link will thus specify the resistance of the joint, it is therefore when the strongest strength estimated in the criterion is reached that the overall failure occurs, hence the failure criterion proposed in the Annexe A of the EC5 (A) [3] (equation (1)).

$$F_{bs,Rk} = \max \begin{cases} 1,5 A_{net,t} f_{t,o,k} \\ 0,7 A_{net,v} f_{v,k} \end{cases} \quad (\text{see EC5 (A) [3] for subscript description}) \quad (1)$$

This formulation can be rewritten to an equivalent one stating that it is the failure mode which has the lowest ratio which is the strongest (equation (2)).

$$\eta_{bs,Rd} \leq \min \begin{cases} \frac{\sigma_{t,0,d}}{k_{tens} \times f_{t,0,d}} \\ \frac{\tau_d}{k_{shear} \times f_{v,d}} \end{cases} \leq 1 \quad (2)$$

$$\text{with } \sigma_{t,0,d} = \frac{N_d}{A_{net,t}}, \tau_d = \frac{N_d}{A_{net,v}}, k_{tens} = 1,5 \text{ and } k_{shear} = 0,7$$

Writing the criterion in this format allows accounting for more complex force torsors than simple axial tensile forces.

### 3.2 Un-reinforced connections failure in bending

When subject to bending moments, timber dowelled connections (timber to timber or timber to steel) are prone to splitting even before the ultimate load is reached (Figure 2). These failures are caused by an interaction of transverse tension and shear induced by the load, shrinkage, and the evolution of the mechanical properties over time. Splitting is hard to predict: this makes the final failure mode difficult to define and therefore the load bearing capacity of the connection cannot be predicted with accuracy.

In order to prevent these cracks from appearing before the failure of the connection, different reinforcements can be considered. One of them consists in only reinforcing the transverse tension strength by using self-tapping screws [9],[10] for connections of small dimensions. The screws are usually inserted across the grain and do not reinforce the longitudinal shearing strength. To reinforce the transverse tension and the shear, there are few other options than to glue plywood on the sides of the different elements composing the connection [11]. This makes the manufacturing process complicated and therefore limits its usage in the industry. However, it also reinforces the embedment when the plywood is placed in the shear planes.

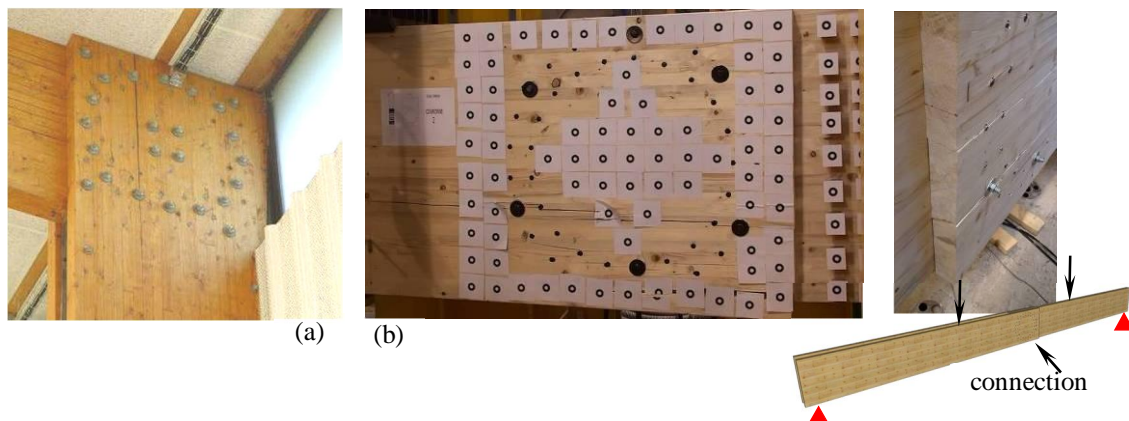


Figure 2 : Shear and tensile failure propagated in the connection area for circular patterns: (a) frame corner (b) transport joint.

### 3.3 Four bolts beam to column timber joint reinforced with screws

More recently, Lam et al. [1] have studied connections composed of 4 bolts reinforced by self-tapping screws subject to a bending moment and shearing forces. They showed that the reinforcement increases the ductility of the connections (Figure 3(a)) and avoids splitting, row shear and block shear. Before these experiments, un-reinforced joints had been tested and showed row splitting (Figure 3(b)). Those joints were then retrofitted with self-tapping screws and tested again.

The failures of the retrofitted specimen show either a net section bending failure (Figure 3(c)) or an “L” shaped bloc failure (Figure 3 (d)). This failure shape was however particular because the length of the column was very short. It can be observed that a tear-out bloc with a classical “C” shape was also almost declared. This last type of failure is potentially weaker than the net failure mode and should therefore be chosen as a design shape mode when dowelled connections are subject to bending moments. It can then be said that if the design of the joint is up to prevent this brittle failure mode, full plasticity of the joint can be reached.

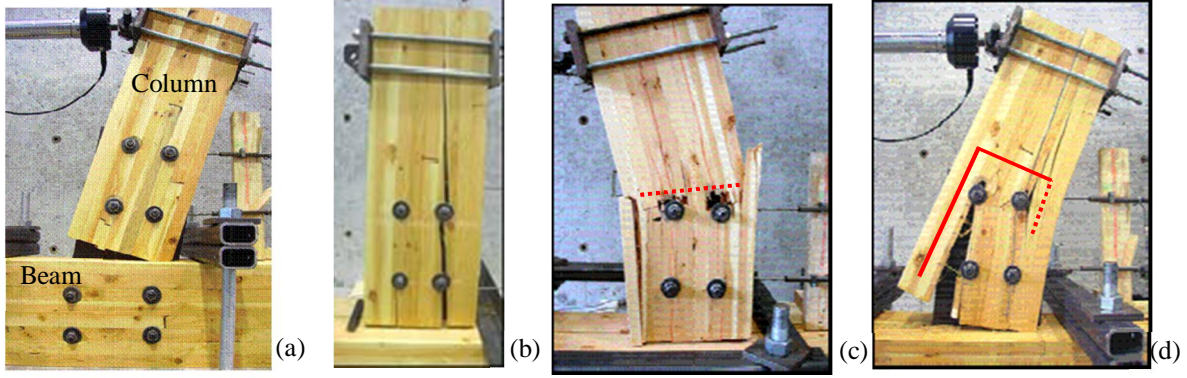


Figure 3 : Connection specimens: (a) reinforced with monotonic loading (b) unreinforced with monotonic loading, (c) retrofitted with cyclic loading, (d) retrofitted with monotonic loading, [1]

## 4 Block shear failure criteria proposal for reinforced dowelled timber joint

Based on the previous observations, it is noticed that if a suitable transverse reinforcement is adopted the effect of transverse tension is limited. Therefore a “C”-shaped failure mode or an “L” shaped one are favoured. Considering the block shear principle, the “C” and “L” modes are subsequently formulated. In order to introduce the bending stresses in the design criteria, the formulation proposed in paragraph 3 is considered (equation (2)). The smallest ratio from “C”- or “L”-block failure analysis indicates the strongest mode, and therefore the one to consider in the design.

$$\eta_{block\ failure} \leq \min \{ \eta_{block\ C} ; \eta_{block\ L} \} \leq 1 \quad (3)$$

where  $\eta_{block\ C}$  and  $\eta_{block\ L}$  are respectively the ratio of “C”- and “L”-block failure developed here after. The set of coefficients  $k_{tens}$ ,  $k_{comp}$ ,  $k_{shear, comp}$  and  $k_{shear}$  has been defined referring to available values and principle of the EC5.

- $k_{tens} = f_{m,k} / f_{t,0,k} \approx 1,5$  (EC5(A) [3]): *being localised in the joint area, characteristic tensile strength statistically increases,*
- $k_{comp} = f_{m,k} / f_{c,0,k} \approx 1$ : *these strengths are quite similar,*
- $k_{shear, comp} = 1,25$  [12] : *in the compressed area of the joint, row shear strength is increased because the induced transverse tensile stress field is more favourable,*
- $k_{shear} = 0,7$  (EC5 (A) [3]): *all along a row of dowels, the shear stress field is not uniform.*

### 4.1 “C” block shear failure

“C” block shear failure is similar to block shear failure where the central part of the connection tears away from the beam. Figure 4 presents the “C”-block shear failure equilibrium of the central block. The central block is held by the strongest resistance provided by:

- the normal stresses in the transverse net section A-A,
- the shear stresses on the upper and lower net section (B-B and C-C) parallel to the beam axis.

Furthermore, the shear block resistance is also limited by the normal stress capacity of the so called block-up and block-down parts. The “C” block shear design criterion is hence formulated as:

$$\eta_{block\ C} = \min \{ \eta_{block\ Ci} ; \eta_{block\ Cud} \} \quad (4)$$

In order to estimate the normal stresses, it is considered with regards to EC5 (5.2) [3] that in the compressed area, the reduction of the cross section has not to be considered when the drilled holes are filled with dowels.

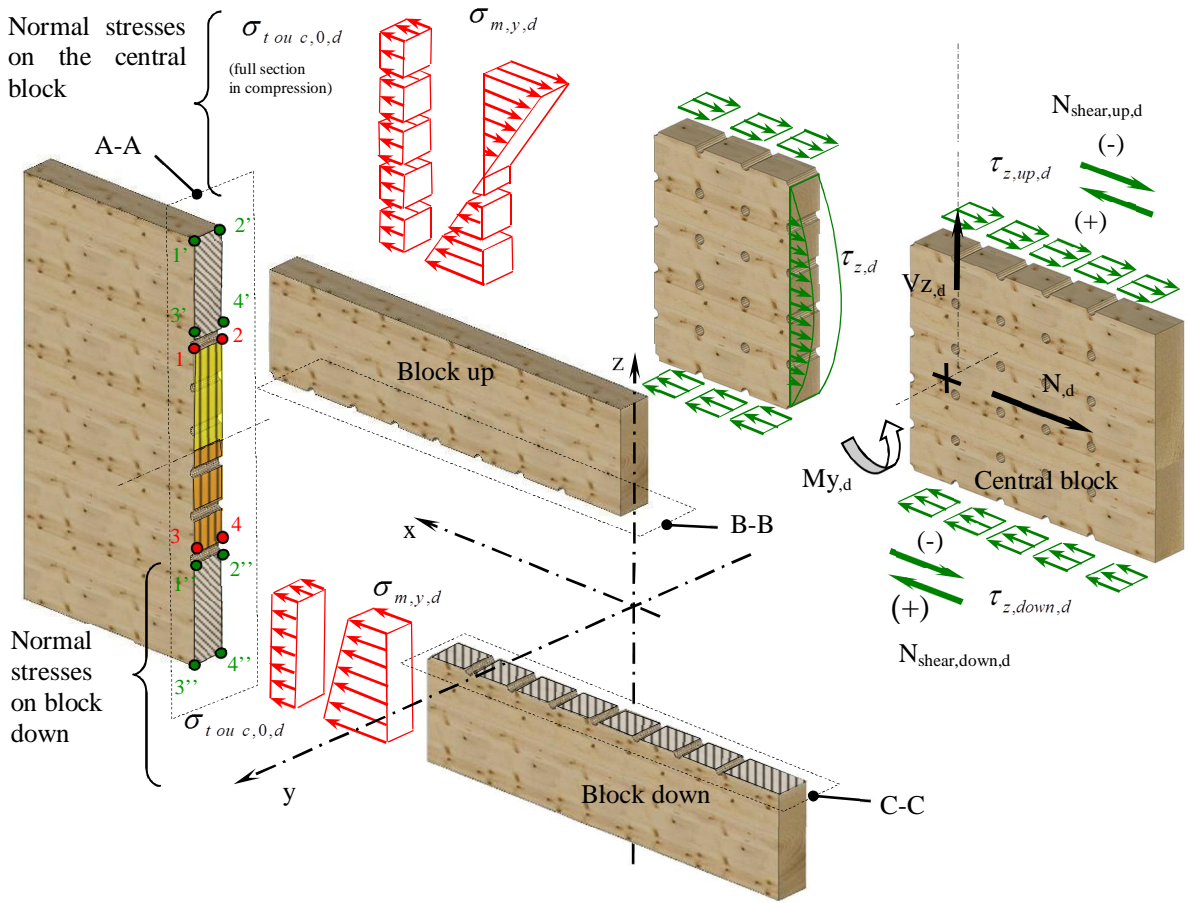


Figure 4 : C block shear principle: efforts, stresses and geometry.

The block resistance due to normal stresses  $\eta_{block Ci}$  is expressed below. This block resistance is also limited to the shear capacity of the block itself:

$$\eta_{block Ci} = \max \left\{ \begin{array}{l} \text{at points 1,2,3,4} \left\{ \begin{array}{l} \frac{\sigma_{t,0,d}}{k_{tens} f_{t,0,d}} + \frac{\sigma_{m,y,d}}{f_{m,y,d}} \\ \left( \frac{\sigma_{c,0,d}}{k_{comp} f_{c,0,d}} \right)^2 + \frac{\sigma_{m,y,d}}{f_{m,y,d}} \end{array} \right. \\ \frac{\tau_{z,d}}{f_{v,d}} \text{ at its maximum all along the joint} \end{array} \right. \quad (5)$$

The central block resistance due to shear stresses  $\eta_{block Cud}$  is presented below.

$$\eta_{block Cud} = \max \left\{ \max \left\{ \eta_{block sh up} ; \eta_{block up} \right\} ; \max \left\{ \eta_{block sh down} ; \eta_{block down} \right\} \right\} \leq 1 \quad (6)$$

When the shear plane belongs to an area compressed parallel to the grain, a favourable  $k_{shear,comp}$  coefficient is introduced.

$$\eta_{block sh up} = \left\{ \left( N_{shear,up,d} \geq 0 \right) \frac{\tau_{z,up,d}}{k_{shear,comp} \times k_{shear} f_{v,d}} ; \left( N_{shear,up,d} < 0 \right) \frac{\tau_{z,up,d}}{k_{shear} f_{v,d}} \right\} \quad (7)$$

$$\eta_{block\ sh\ down} = \left\{ \left( N_{shear,down,d} \geq 0 \right) \frac{\tau_{z,down,d}}{k_{shear,comp} \times k_{shear} f_{v,d}} ; \left( N_{shear,down,d} < 0 \right) \frac{\tau_{z,down,d}}{k_{shear} f_{v,d}} \right\} \quad (8)$$

In order to limit the shear capacity of the upper and lower shear plane, the normal stress capacity of the so called block up and block down parts are expressed below:

$$\eta_{block\ up} = \max \text{ at points } 1', 2', 3', 4' \text{ block up} \left\{ \begin{array}{l} \frac{\sigma_{t,0,d}}{k_{tens} f_{t,0,d}} + \frac{\sigma_{m,y,d}}{f_{m,y,d}} \\ \left( \frac{\sigma_{c,0,d}}{k_{comp} f_{c,0,d}} \right)^2 + \frac{\sigma_{m,y,d}}{f_{m,y,d}} \end{array} \right. \quad (9)$$

$$\eta_{block\ down} = \max \text{ at points } 1'', 2'', 3'', 4'' \text{ block down} \left\{ \begin{array}{l} \frac{\sigma_{t,0,d}}{k_{tens} f_{t,0,d}} + \frac{\sigma_{m,y,d}}{f_{m,y,d}} \\ \left( \frac{\sigma_{c,0,d}}{k_{comp} f_{c,0,d}} \right)^2 + \frac{\sigma_{m,y,d}}{f_{m,y,d}} \end{array} \right. \quad (10)$$

## 4.2 L block shear failure

L block shear failure is a mode where the central part and the top part of the connection tear away from the beam. Figure 5 presents the “L” block shear failure equilibrium of the “L” block part. This block is held by the strongest resistance provided by:

- the normal stresses in the transverse net section A-A,
- the shear and transverse stresses combined with the reinforcement on the lower net longitudinal section B-B.

For symmetrically dowelled joints with dowels distributed over the whole connected area, it is evidence that the resistance of this last mode will be much lower than the previous one. Moreover, the normal strength of the  $h-h_L$  part will be very small. The L block shear design criterion is then formulated as written below and could be further completed for non-symmetrically reinforced joint:

$$\eta_{block\ L} = \min \left\{ \eta_{block\ Li}; \eta_{block\ Shear\ L} \right\} \quad (11)$$

The block resistance due to normal stresses  $\eta_{block\ Li}$  is expressed below. This block resistance is also limited to the shear capacity of the block itself:

$$\eta_{block\ Li} = \max \left\{ \begin{array}{l} \text{at points } 1, 2, 3, 4 \left\{ \begin{array}{l} \frac{\sigma_{t,0,d}}{k_{tens} f_{t,0,d}} + \frac{\sigma_{m,y,d}}{f_{m,y,d}} \\ \left( \frac{\sigma_{c,0,d}}{k_{comp} f_{c,0,d}} \right)^2 + \frac{\sigma_{m,y,d}}{f_{m,y,d}} \end{array} \right. \\ \frac{\tau_{z,d}}{f_{v,d}} \text{ at its maximum all along the joint} \end{array} \right. \quad (12)$$

The block resistance due to shear stresses  $\eta_{block\ shear\ L}$  is considered to be much smaller than the previous one.

$$block\ shear\ L\ strenght \approx 0 \Rightarrow \eta_{block\ shear\ L} \gg \gg \eta_{block\ Li} \quad (13)$$

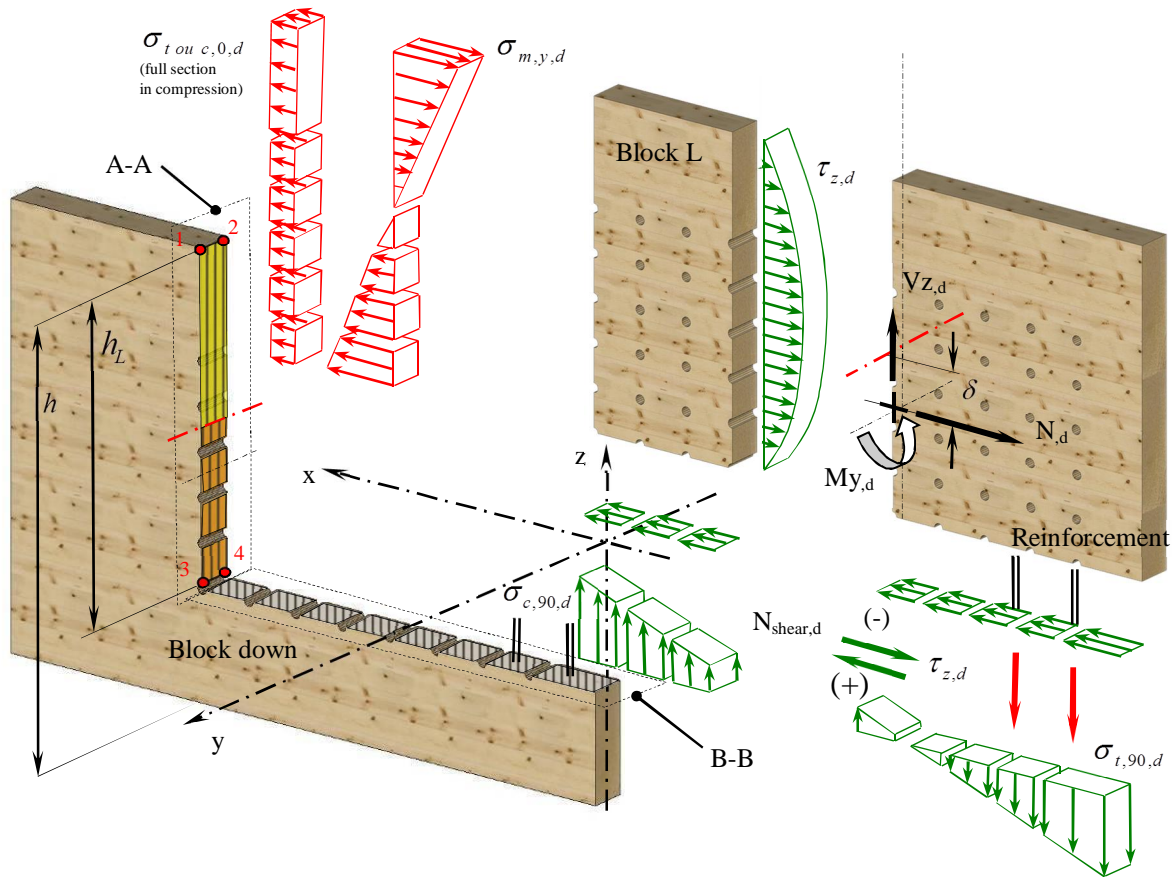


Figure 5 : L block shear principle, efforts, stresses and geometry.

## 5 Experimental joint tests

### 5.1 Reinforced doweled connections with a circular pattern

In order to confirm the criteria developed above, a first series of dowelled connections was tested [13]. 4 dowelled connections were tested comprising 46 dowels of 16 mm diameter distributed on two concentric circular patterns. The specimens were composed of 2 glulam beams of section 80x1000 mm connected to a third having a section of 160x1000 mm (Figure 6). All but the first specimen were empirically reinforced across the grain by SFS WB 16 mm rods inserted in pre-drilled holes (Figure 8).

- The first specimen (case 0) was not reinforced.
- The second specimen (case 1) was reinforced by three rods at both ends of the connection. This reinforcement is called non-homogeneous reinforcement because the density of rods is different in the central member and in the outer members. It is the minimal reinforcement tested in this study.
- The third specimen (case 2) was reinforced by four rods at both ends of the connection. This reinforcement is called homogeneous because the density of rods is the same in the central and outer members.
- The last specimen (case 3) was the most reinforced and comprises 8 rods at both ends of the connection.

These connections were subject to pure bending in order to emphasize the effect of shearing forces (Figure 6). These experiments showed that the reinforcement was able to prevent

splitting due to transverse tension which appeared for a lower load with the un-reinforced specimen (Figure 7).

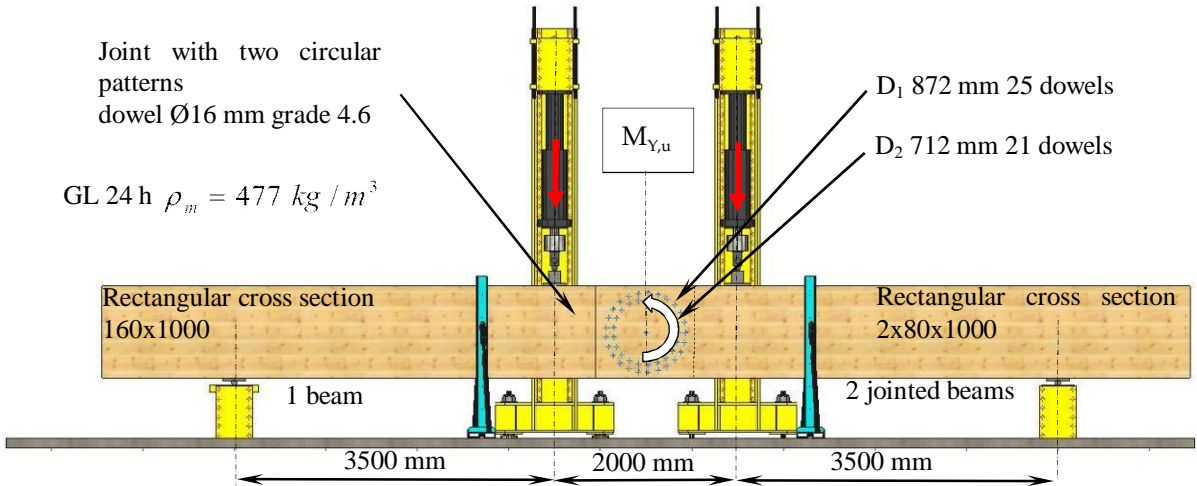


Figure 6 : Four point-bending test set up to apply pure bending moment inside the connection.

Case 0

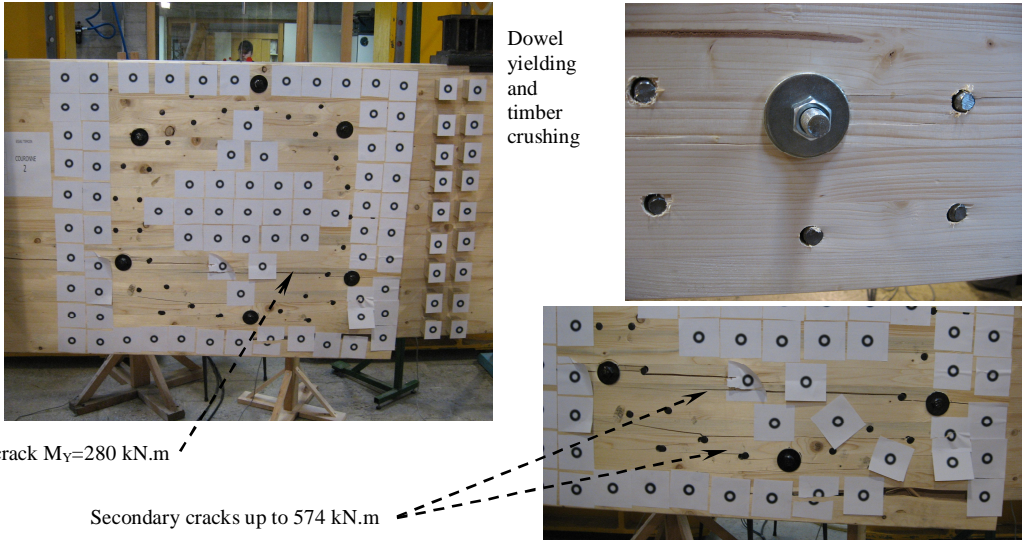


Figure 7 : Shear and tensile perpendicular to the grain failures for the unreinforced circular patterns dowelled joints.

“L” shear bloc failure was observed for the three reinforced specimens with moments close to 500 kN.m. This load was near the complete yielding of the joint which was estimated at 580 kN.m . The failure modes of every reinforced specimen are described in (Figure 8). On the one hand we can notice that in order to prevent transverse splitting a minimum amount of reinforcement is necessary. It can also be said that this minimal reinforcement must be homogenous over the connected beams. On the other hand it can be said that too much reinforcement can affect the mechanical behaviour of the connection by weakening the timber beams. This is especially true if the reinforcement is located where the stresses in timber are the highest.

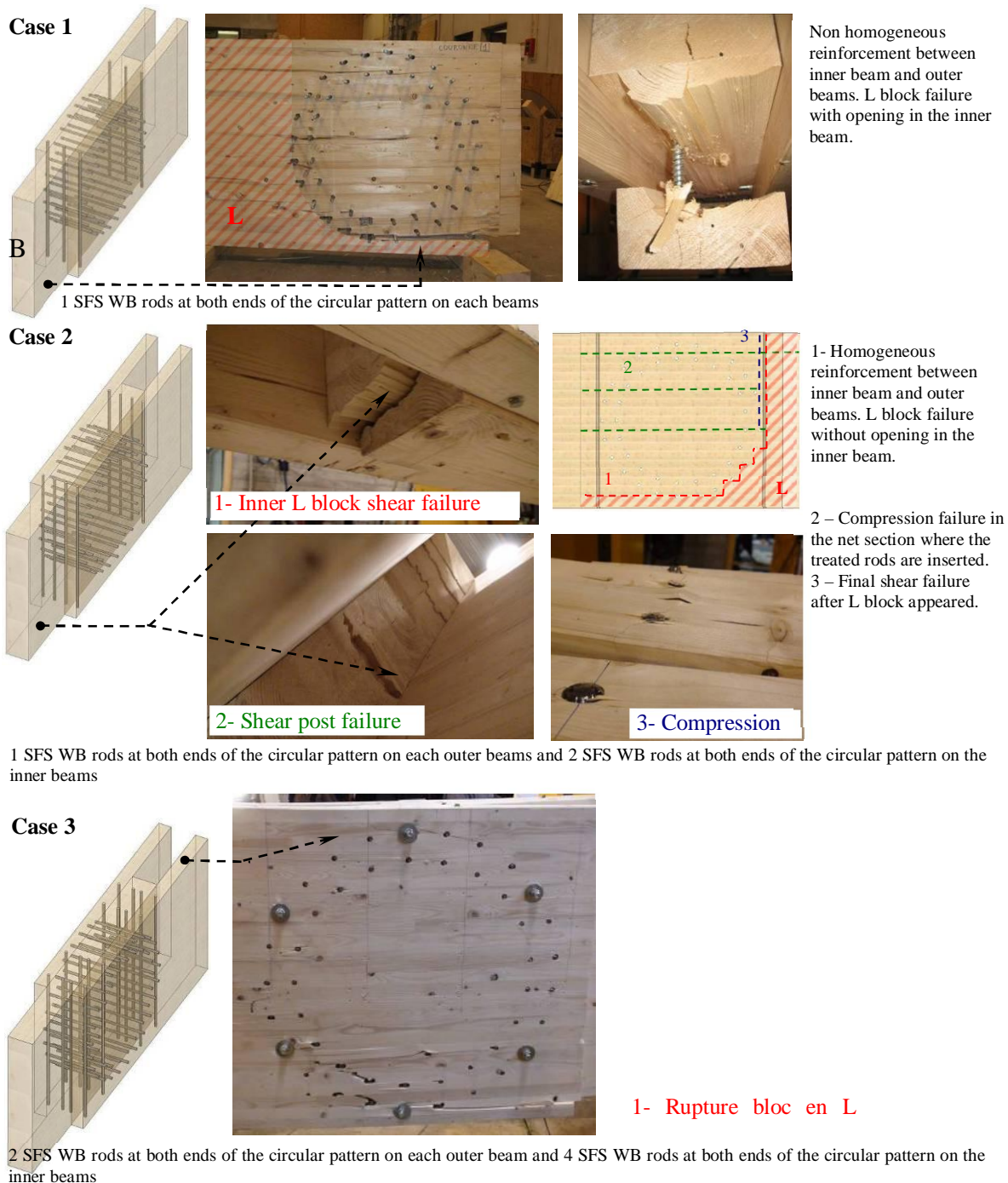


Figure 8 : L block failures for different reinforced circular patterns dowelled joints.

## 5.2 Reinforced doweled connections with a grid pattern

Extra tests were performed to validate the design of the connections of the roof structure of the “Fondation Louis Vuitton pour la Création” currently being erected in Paris [14]. These connections are jointing the timber beams to steel elements. Six reinforced connections were tested. These specimens were constituted of 400x1200 mm larch glulam beams reinforced by 8 SFS WB 16 mm rods inserted empirically only at the end of the joint (Figure 9). The connection was composed of 220 stainless steel dowels ( $f_{u,k} = 988 \text{ Mpa}$ ) of 16 mm (clearance 0,5 mm) diameter distributed on a rectangular grid connecting the beams to the slotted in steel plates. The three first tests (test 1, test 2 and test 3) were performed with a specific reinforced

steel joint in order to avoid failure of steel as a consequence of its lower dispersion. The three others received the normal designed stainless steel joint. They were previously subjected to non-destructive tests to measure the transverse rigidity of the joint.

In order to emphasize shear bloc failure in the connection, the first three tests were performed in three-points bending. Two beams (test 4 and 5) were sawn over a third of their width on the outer parts to artificially take into account the  $k_{cr}$  coefficient proposed in the amendment A1 [15]. They were tested in four-point bending to favour shear in the connection. The last specimen (test 6) was also tested in four-point bending with a moisture content above the fibre saturation point. “L” shear bloc failure was observed for moments close to 3000 kN.m. This is due to the fact that no transverse tension failures and no row failures occurred thanks to transverse reinforcement.

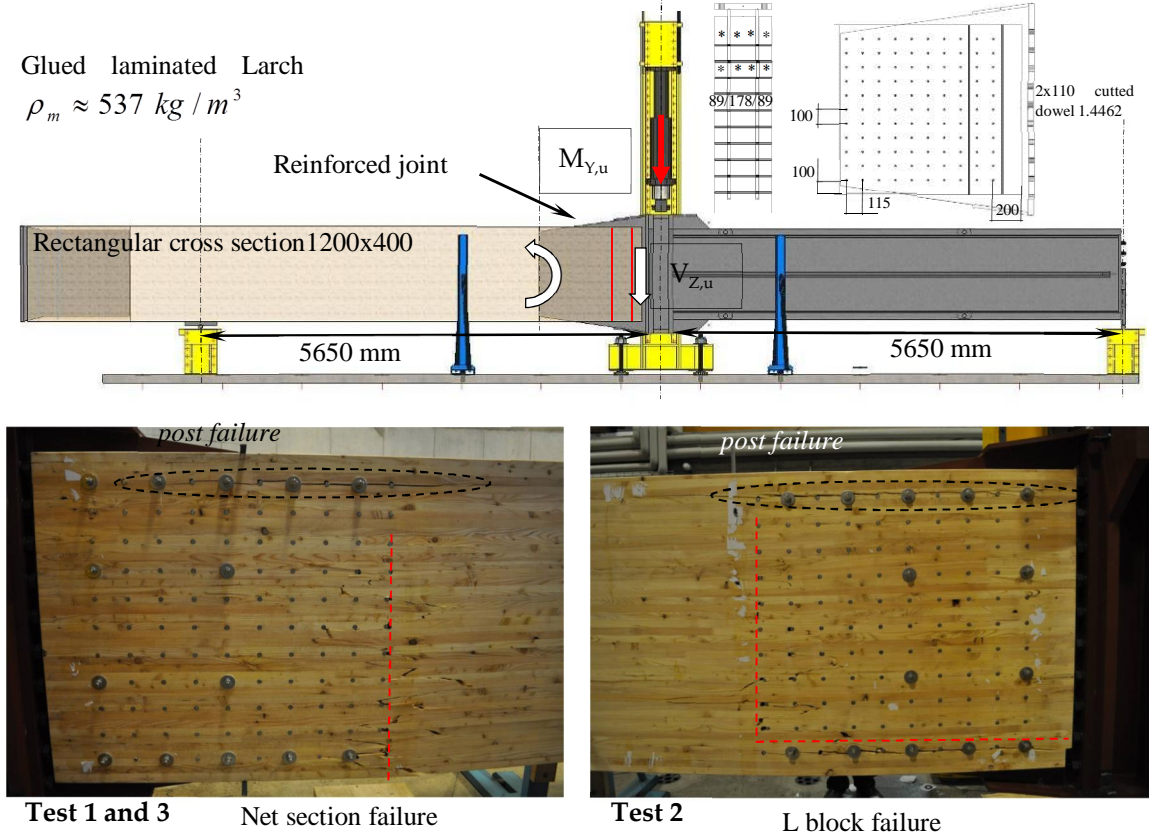
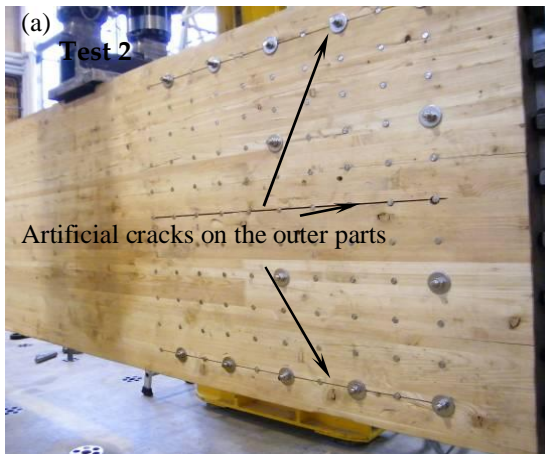
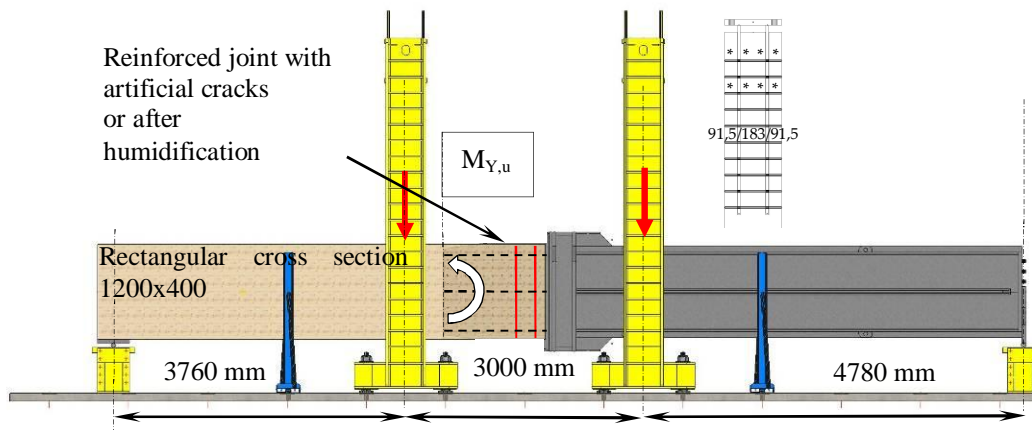
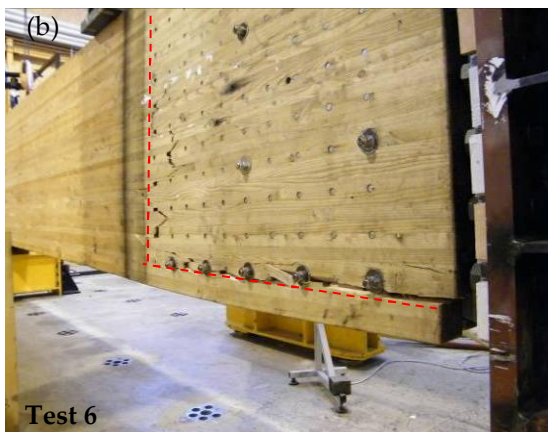


Figure 9 : Bending test apparatus in three-point bending loading and net failure and L block failure of rectangular grid patterns (“Fondation Louis Vuitton pour la Création” connections).

It has been noticed that after the net failure or the “L” block failure occurred, a post failure split appeared on the compression side of the beam due to post-failure rotation of the beam. It has also been observed that the timber was perfectly held by the reinforcement rods.



Cracks over 1/3 of the thickness



L block failure in the inner part and one in the outer parts



Figure 10: L block failure of rectangular grid pattern “Fondation Louis Vuitton pour la Création” connection in four-point bending loading (a) with artificial cracks on the outer parts (b) after humidification.

In test 4, the “L” block failure didn’t fully develop due to the presence of knots. “L” block failures were observed on the outer parts of test 5 and for the first time it was also observed in the central part for test 6 (Figure 10). In spite of favouring shear by the artificial cracks and the pure bending load, no shear cracks appeared on the faces of the beams. Increasing the humidity creates swelling in the joints. This did not have any noticeable effect on the failure mode observed.

## 6 Results and discussion

During the tests, the load and displacement at mid span were recorded (Figure 11). The moment applied was then calculated. For the specimens tested in three-point bending, the moment is calculated at the junction of the stainless steel fitting and the steel beam. Figure 10 presents the evolution of the bending moment as a function of the deflexion at mid span for the two different types of connections. A brittle failure can be noticed for all the grid patterned joints. This is due to the fact that the plastic moment of the dowels was very high. The dowels in the connections that have a circular pattern were almost all yielded. Even the unreinforced joint reached the plastic moment without an important decrease in rigidity although a shear failure occurred prematurely.

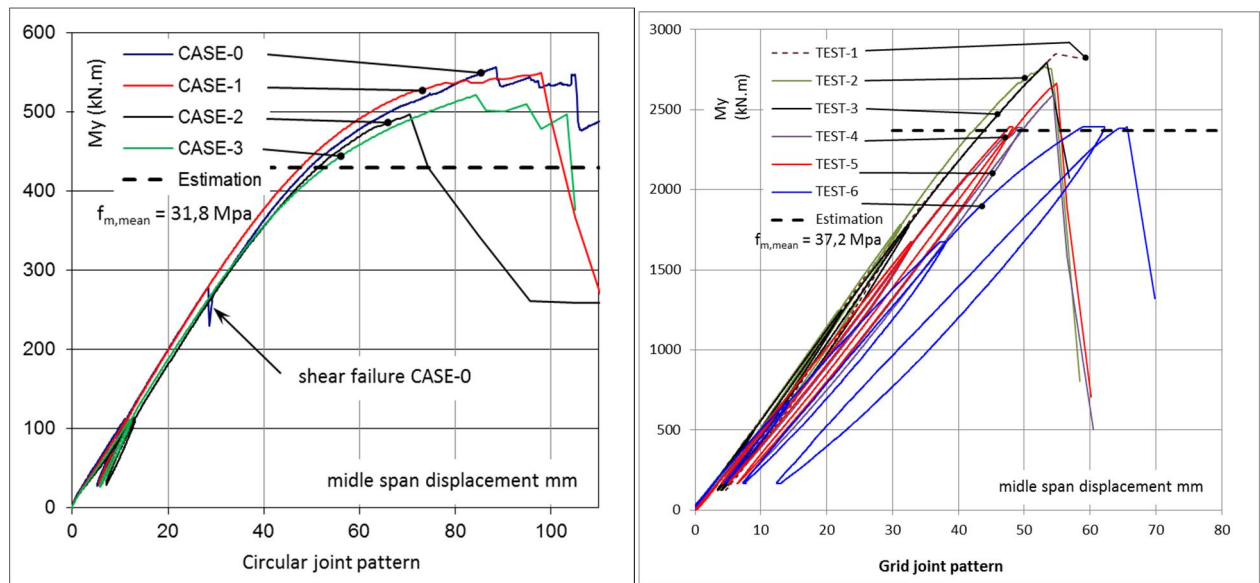


Figure 11 : Moment versus mid span deflection of the circular pattern joint tests and of the grid joint tests.

### 6.1 Circular pattern joints analysis:

Although the glulam used in these tests was certified GL24h, the measured density was of  $477 \text{ kg/m}^3$  for a humidity of 12 %. This value is slightly higher than an ordinary value close to  $440 \text{ kg/m}^3$ . If a coefficient of variation of 15% is considered, the mean flexural strength is calculated to be 32 Mpa.

In order to use the above criteria, the net section must be more clearly defined for circular patterns. On the compression side of the beam it is supposed that the dowels do not decrease the resistant section. On the contrary, on the tension side of the beam it is considered necessary to take into account the decrease in section caused by the holes. A representation of this hypothesis is shown in figure 12.

The experimental results are shown in table 1. Except for the un-reinforced specimen, the estimated failure mode was always an “L” shear block failure. The observed failure modes correspond well to those predicted. Indeed, only “L” shear block failures were observed. They were either located in the central member or in the outer members. The ultimate load was estimated with a maximum error of 26 %. For the un-reinforced specimen, although the predicted failure mode is in accordance with the observed failure, the ultimate load was estimated by 51 %. This last estimation was based on the calculation of the shear force induced by the pure bending moment in the joint as described by Racher [16]. A coefficient of variation of 0,15 was also taken into account for shear strength.

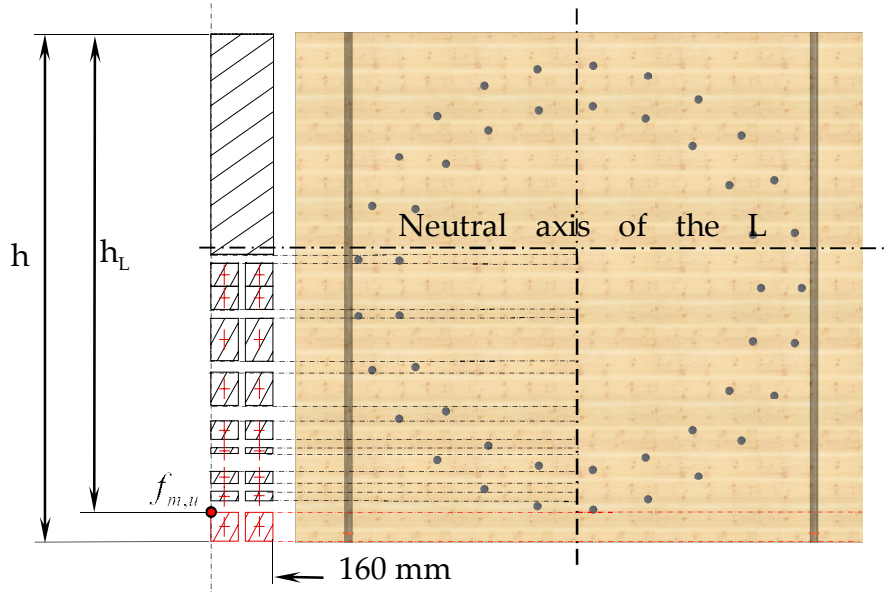


Figure 12 : Net “L” section considered for the estimation  $f_{m,u}$  for circular patterns.

Taking into account the observed failures, it is possible to estimate the ultimate flexural strength for the reinforced specimens and the ultimate shear strength for the un-reinforced specimen. It can be seen that the flexural strength is about 38 MPa (Table 1). This value is higher than the expected value of 32 MPa. On top of this, the stresses were estimated by considering an elastic distribution of the load on the dowels and therefore a linear distribution of the stress in the timber members. Figure 11 clearly shows that when failure occurred the connections were already in a plastic phase. Both these reasons can explain the discrepancies between the estimated and observed failure values. Nonetheless the “L” block shear failure underestimates the strength which makes it a conservative criterion.

Table 1 : Efforts at failure, predicted failure modes, test failure modes and stress at failure

Type	Test	$M_{Y,u}$ (kN.m)	$M_{Y,est}$ (kN.m)	Estimation error	Predicted failure modes			Test failure modes			$f_{m,u}$ or $f_{v,u}$ (MPa)
					Outer	Inner	Outer	Outer	Inner	Outer	
Circular pattern	Case 0	280/539	574	<b>-51%</b>	$f_v$	$f_v$	$f_v$	$f_v$	0	$f_v$	2,02
	Case 1	546	430	<b>+27%</b>	<b>L</b>	<b>L</b>	<b>L</b>	<b>0</b>	<b>L</b>	<b>0</b>	38,82
	Case 2	493,5	430	<b>+14,7%</b>	<b>L</b>	<b>L</b>	<b>L</b>	<b>0</b>	<b>L</b>	<b>0</b>	36,64
	Case 3	518	430	<b>+20,4%</b>	<b>L</b>	<b>L</b>	<b>L</b>	<b>L</b>	<b>0</b>	<b>L</b>	38,45

**L** : L block failure , **I** : net section failure, **0** : no failure,  $f_v$  : shear failure

## 6.2 Grid pattern joints analysis:

For the grid patterned connections, whatever the loading, the previous formulations always predicted an “L” shaped block failure. However, two connections tested in three-point bending and having the reinforced steel fitting, showed a net section failure. This leads to a reliable estimation of the strength when failure occurred (Table 2). Figure 13 presents the inertia and the location where the bending stresses is calculated at failure. It is considered that the failure happens when this fibre reaches its maximum strength.

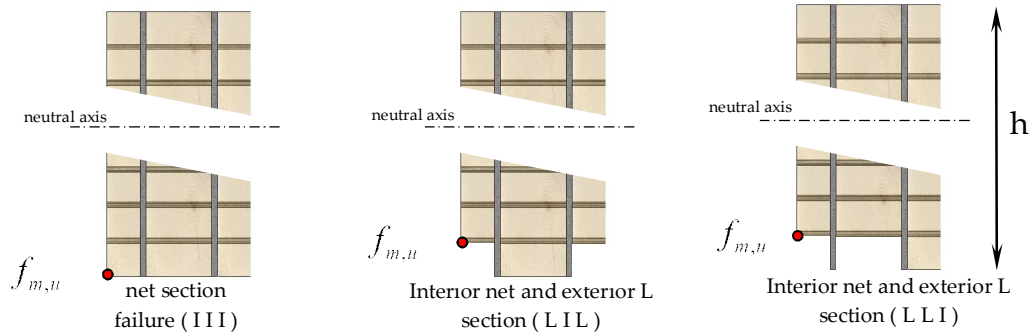


Figure 13 : Net section considered for the estimation  $f_{m,u}$  for grid patterns.

The Larch glulam was considered to be a GL 28 h with a coefficient of variation of 0.15. Given the low variability of the results, it seems that the glulam had a mean strength higher than supposed with a low coefficient of variation. The connections tested in four-point bending with a stainless steel fitting showed slightly lower strengths than with the reinforced steel fitting. The strength of the humid connection was unaffected although the failure mode was different. Its rigidity was nonetheless lower. The failure mode for these three connections was an “L” shaped block failure. However, since these connections were subject to high bending loads to test the transverse rigidity, it may be possible that their strength was affected. Because no pure “L” block mode happened, all the bending moment where over the estimation: 2437,5 kN.m for stainless steel metal joint and 2370,9 kN.m for reinforced steel metal joint.

Table 2 : Efforts at failure, predicted failure modes, test failure modes and stress at failure (the moments indicated are situated at the end of the metal joint for grid patterns)

Type	Test	$M_{Y,u}$ (kN.m)	$V_{Z,u}$ (kN)	$M_{Y,est}$ (kN.m)	Estimation error	Predicted failure modes			Test failure modes			$f_{m,u}$ (Mpa)
						Outer	Inner	Outer	Outer	Inner	Outer	
Grid pattern (reinforced fitting)	Test 1	2936,1	-658,4	2370	+23,8%	L	L	L	I	I	I	35,4
	Test 2	2859,2	-640,6	2370	+20,6%	L	L	L	L	I	L	36,4
	Test 3	2884,2	-646,4	2370	+21,7	L	L	L	I	I	I	34,8
Grid pattern with cracks (stainless steel fitting)	Test 4	2683,3	0	2437,5	+10%	L	L	L	L	I	L	33,3
	Test 5	2752,7	0	2437,5	+12,9%	L	L	L	L	I	L	34,2
Grid pattern (high moisture content)	Test 6	2481,3	0	Dry 2437,5	+2%	L	L	L	L	L	I	34

L : L block failure , I : net section failure.

## 7 Conclusions

The tests conducted showed that a transverse reinforcement could maintain and avoid splitting in the connected area of important size joints when subjected to bending. A further work is needed to define a rational and optimum reinforcement. The consequences of swelling and shrinkage in the reinforced area were partially tackled but need further investigations. A typical failure mode with an “L” shape was confirmed several times under monotonic loading: as predicted the “C” failure never occurred. A high stress at failure was observed in the

connected area which confirms that  $f_{t,0,k} \approx f_{m,k}$  and therefore  $k_{tens} \approx 1,5$ . An elastic limit was proposed for the block shear failure. In the case of a high yielding of the joint, a plastic analysis of the joint has to be conducted to evaluate the distribution of the normal stresses, the failure criteria appeared then more difficult to define.

*Acknowledgements:*

*This research was partially supported by the “Fondation Louis Vuitton pour la Création” and SFS intec. The authors would like to thank “EIFFAGE Construction Métallique” for their appreciation of the benefits to be gained from research.*

## 8 References

- [1] Lam F., Wrede M. C., Yao C.C., Gu J. J. (2010) - Moment resistance of bolted timber connections with perpendicular to grain reinforcements. The University of British Columbia Vancouver, BC, Canada.
- [2] Johansen K.W. (1949) - Theory of timber connections. International association of bridge and structural engineering, vol 9, pp. 249–62.
- [3] NF EN 1995-1 (2005) - Conception et calcul des structures en bois – Partie 1.1 : Généralités – Règles communes et règles pour le bâtiment.
- [4] Fahlbusch, H., 1949 Ein Beitrag zur Frage der Tragfähigkeit von bolzen in Holz bei statischer Belastung. Braunschweig : Institut für Maschinenkonstruktion und Leichtbau, technische Hochschule Braunschweig. Bericht Nr. 49-9.
- [5] Jorissen A.J.M. (1996) - State of the art : symmetrical timber connections with dowel type fasteners in double shear. Delft University of technology 4-96-5/MFJ-3.
- [6] Quenneville J.H.P., Mohammad M. (2000) - On the failure modes and strength of steel-to-timber bolted connections loaded parallel-to-the grain. Can.J.Eng., vol. 27, pp. 761-763.
- [7] Antti Hanhijärvi, Ari Kevarinmäki (2008) - Timber failure mechanisms in high-capacity dowelled connections of timber to steel. Experimental results and design-ESPOO 2008 VTT Publications 677- ISBN 978-951-38-7090-4 (URL:<http://www.vtt.fi/publications/index.jsp>).
- [8] Matti Kairi (2004) Block shear failure test with dowel –type connection in diagonal LVL structure. CIB W18 Meeting thirty-seven Edinburgh scotland August 2004.
- [9] Bejtka I. (2005) - Verstärkungen von Bauteilen aus Holz mit Vollgewindeschrauben. Dissertation, Lehrstuhl für Ingenieurholzbau und Baukonstruktionen, Universität Karlsruhe, Germany.
- [10] Blass H.J., Bejtka I., Uibel T. (2006) - Tragfähigkeit von Verbindungen mit selbstbohrenden Holzschrauben mit Vollgewinde. Karlsruher Berichte zum Ingenieurholzbau 4, Universität Karlsruhe, Germany. als Holzverbindungsmittel. Deutsches Institut für Bautechnik, Berlin.
- [11] Bouchair A, Racher P., Bocquet JF., “Analysis of dowelled timber to timber moment-resisting joints” published online 23 January 2007 RILEM 2007 Materials and Structures (2007) 40 : 1127-1141.
- [12] Biger J.P, Bocquet J-F, Racher P – (August 2000) - Testing and designing the joints for the pavillon of Utopia. World Conférence Timber Engineering, paper 4.3.3, Whistler, Canada.
- [13] Chambon N., Charnot N (2009) - Vérification d’assemblages en cisaillement. PFE ENSTIB / SFS INTEC, ENSTIB, France.
- [14] Bocquet J.F. (2011) - Rapport d’essais des assemblages sur blocs des verrières de la Fondation Louis Vuitton. 122p, ENSTIB, France.
- [15] NF EN 1995-1-1/A1 (2008) - Conception et calcul des structures en bois – Partie 1.1 : Généralités – Règles communes et règles pour le bâtiment.
- [16] Racher . P, “Moment resisting connection” STEP 1 Lecture C16 – 1995 \_ ISBN 90-5645-011-8



**INTERNATIONAL COUNCIL FOR RESEARCH AND INNOVATION  
IN BUILDING AND CONSTRUCTION**

**WORKING COMMISSION W18 - TIMBER STRUCTURES**

**BLOCK SHEAR FAILURE OF WOODEN  
DOWEL CONNECTIONS**

G Stapf

S Aicher

N Zisi

Materials Testing Institute (MPA) University of Stuttgart

GERMANY

**MEETING FORTY FIVE**

**VÄXJÖ**

**SWEDEN**

**AUGUST 2012**

---

Presented by G Stapf

I Smith commented that in Canada we did not believe the simple model could explain the complicated stress state. It was a fitting exercise. F Lam commented that the real stress state is complicated with the non-homogeneous and orthogonal elastic properties of wood as well as the possible occurrence of tensile stresses perpendicular to grain even from slight misalignment of the connectors. W Seim stated the FE model used was plane stress and isotropic. He questioned how 3 D model could affect the results. G Stapf stated that a non-isotropic 3 D model would show bending of the dowel was important. P Quenneville commented that what we had was not perfect but added to our understanding. P Zarnani commented on the cases of large dowels and more dowels in a row. F Stapf agreed that the load distribution between the dowels was important and wider connections were being considered. A Jorissen asked and received clarification on the comparison to code that there could be unsafe cases. M Yasumura received clarification of the observed failure mode was due to the oak glulam with high density. H Blass suggested also the quality of steel in dowels were usually higher than specification which could help to explain the failure mode.



# BLOCK SHEAR FAILURE OF WOODEN DOWEL CONNECTIONS

Gordian Stapf, Simon Aicher, Nikola Zisi  
Materials Testing Institute (MPA) University of Stuttgart

## 1. Introduction

In timber or steel-timber connections with dowel-type fasteners with more than one row of dowels counted perpendicular to grain, block shear failure has to be taken into account according to Eurocode 5 (EC 5) [4]. An explicit structural design method is given in the informative Annex A of EC 5. The North American timber design codes incorporate block shear verifications of dowelled joints, too. Since 2005, the German timber design code also requires the mandatory proof of block shear integrity. This is stipulated in the informative Annex J of DIN 1052 [2] which is identical to Annex A of EC 5.

On the one hand, experiences over the last seven years have shown that it is often difficult to demonstrate the block shear resistance of a timber connection with dowel-type fasteners with the code's specified equations. On the other hand, recorded cases of damage are very rare where the damage is related to block shear failures of timber connections designed without paying regard to this issue and not passing the block shear design verification according to recent standards.

Looking at block shear failure from a scientific point of view, it is evident that one faces a rather complex load transfer mechanism. Several questions addressing the interaction of different failure mechanisms and the activation of load transferring areas arise. The fact that North American standards and EC 5 answer these questions in a fundamentally different way shows that there is still great potential for optimizing the calculation approaches used in timber design. In any case, unified design rules should reflect the field experience of no/little structural failures.

The paper gives a detailed review of the differences between EC 5 and the North American timber design standards as well as of the relevant literature. The experimental part deals with the interaction between tension and shear during a block shear failure.

## 2. Block Shear Failure in Eurocode 5 in Comparison with North American Standards

### 2.1. Shear Strength

In the National Design Code for wood constructions of the USA (NDS 2005) [5], shear strength  $f_v$  has to be reduced in case of block shear failure by the factor  $k_{red,bs,v} = 0.5$ . This significant reduction has been ascribed to the uneven load distribution by the dowels, i. e. an uneven/triangular load distribution between two dowels along the grain. The reduction factors in the Canadian timber design code CSA 086 [1] and in EC 5 were derived from test results and are  $k_{red,bs,v} = 0.6$  and  $k_{red,bs,v} = 0.7$ , respectively.

It should be noted that the factor for taking into account the distribution of stresses,  $k_{dis}$ , for a triangular load distribution can be calculated according to [7] as

$$k_{dis,triangle} = \left(\frac{1}{m+1}\right)^{1/m} = 0.7 \quad (1)$$

where  $m = 5$  represents the Weibull exponent for shear [7]. Thus the factor  $k_{red,bs,v}$  could be raised to

$$k_{red,bs,v} = \frac{k_{red,triangle}}{k_{dis,triangle}} = \frac{0.5}{0.7} = 0.7 \quad (2)$$

Another explanation for the reduced shear capacity  $f_{v,bs} = k_{red,bs,v} \cdot f_v$  consists in the superimposed load perpendicular to the grain that causes splitting along different dowel rows.

## 2.2. Net Tension Strength

In Eurocode 5 net tension strength  $f_{t,0}$  in cases of block shear failure can be raised by a factor of  $k_{bs,t} = 1.5$ . In contrast, CSA 086 provides a whole set of net tension strengths  $f_{t,0,net}$  which are 1.28 to 1.34 times larger than the gross section strength  $f_{t,0}$ , whereas NDS 2005 does not allow for any enlargement of the tension strength parallel to grain.

The larger tension strength of net cross-sections between dowel holes in comparison to gross cross-sections can be justified by the length effect. The length effect can be estimated by means of EN 1194 [3], where reference length  $l_{ref} = 2000$  mm and size factor  $k_{size} = 1/m = 0.1$  are provided. The size factor  $k_{size} = 0.1$  is also in agreement with the current literature [11]. The length of the net section to be considered regarding weakenings caused by drill holes for fasteners can be taken as  $l_{net} = 150$  mm from DIN 1052 and is a good approximation for failure patterns observed during the actual tests. This dataset leads to

$$k_{bs,t} = \left(\frac{l_{ref}}{l_{net}}\right)^{k_{size}} = \left(\frac{2000}{150}\right)^{0.1} = 1.30 \quad (3)$$

and is therefore rather similar to the values stated in CSA-086.

## 2.3. Coaction of Shear and Tension

Both of the aforementioned North American Design Codes allow for adding the shear resistance  $R_{bs,v}$  and the resistance against net tension failure  $R_{bs,t}$ , i. e.:

$$R_{bs} = R_{bs,v} + R_{bs,t} \quad (4a)$$

In EC 5 the block shear capacity  $R_{bs}$  is defined as the maximum value of the two capacities  $R_{bs,v}$  and  $R_{bs,t}$  (see Fig. 1), i. e.:

$$R_{bs} = \max(R_{bs,v}, R_{bs,t}). \quad (4b)$$

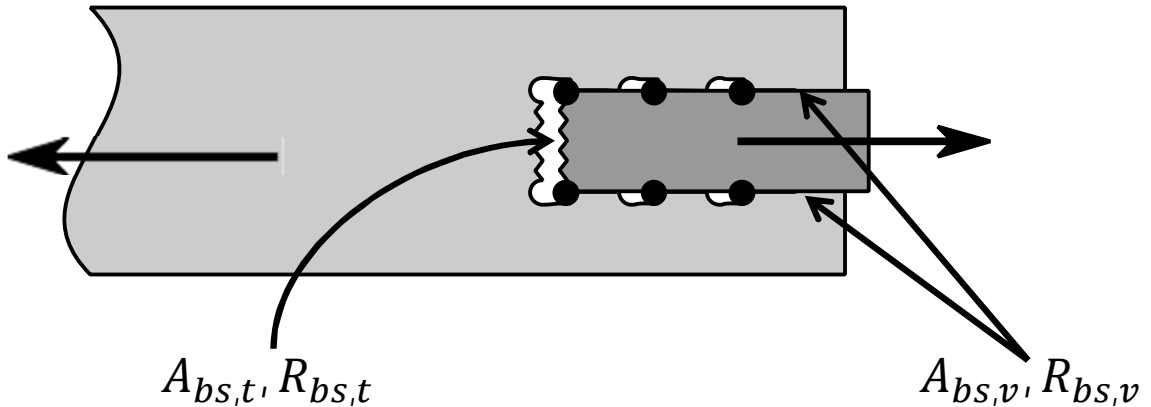


**Figure 1:** Doweled connection with block shear failure. The illustration indicates the resistance against tension failure  $R_{bs,t}$  in the net cross-sectional area perpendicular to the grain  $A_{bs,t}$  at the end of the shear block and the resistance against shear failure  $R_{bs,v}$  in the net shear area  $A_{bs,v}$  at both sides of the shear block parallel to load axis.

## 2.4. Row Shear Resistance

In both North American codes, the possibility of row shear failure (Figure 2) has to be taken into account as well, whereas EC 5 does not list this failure mode. The shear strength reduction in case of row shear is  $f_{v,rs} = k_{red,rs,v} \cdot f_v$  with ( $k_{red,rs,v} = k_{red,bs,v}$ ) and thus similar to the shear strength reduction in the case of block shear (Section 2.1).

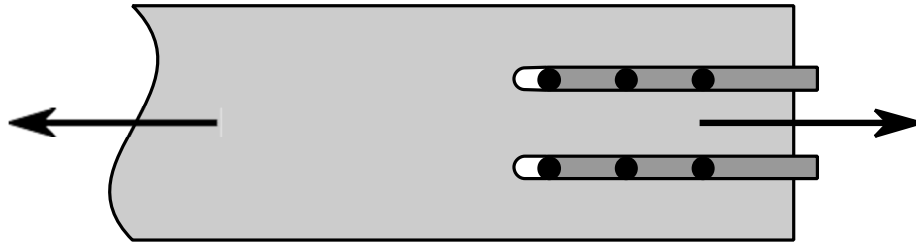


**Figure 2:** Doweled connection with row shear failure.

## 2.5. Influence of Bending of the Dowels

In NDS 2005 and CSA 086, the shear area  $A_{bs,v}$  always consists exclusively of the two lateral areas  $A_{bs,v,par}$  that are parallel to the axes of the dowels, i. e.  $A_{bs,v} = A_{bs,v,par}$  (see Figure 3). In EC 5, in all cases of failure modes that involve the bending of the dowels (failure modes a, b, d, e, g and h), a third area  $A_{bs,v,perp}$  emerges which is perpendicular to the axes of the dowels, i. e.

$$A_{bs,v} = A_{bs,v,par} + A_{bs,v,perp}. \quad (5)$$

The absence of the shear area perpendicular to the dowels  $A_{bs,v,perp}$  in the North American design codes could rely on the assumptions i) that the dowels give additional shear resistance and thus prevent splitting or ii) that the bending of the dowels is crucial for failure and hence the development of  $A_{bs,v,perp}$  is a secondary failure mechanism.

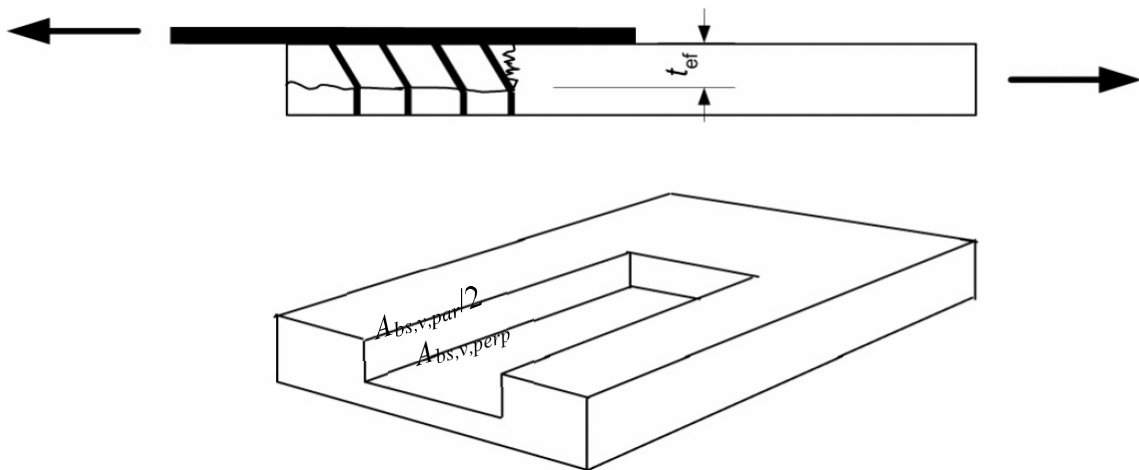


**Figure 3:** In the case of a bending failure mode of the dowels according to EC 5, a third shear area perpendicular to the axes of the dowels  $A_{bs,v,perp}$  can occur additional to the lateral shear areas  $A_{bs,v,par}$ .

The relevance of a third shear plane perpendicular to the dowels,  $A_{bs,v,perp}$ , for a primary failure mode was considered in several investigations related to small diameter fasteners like nails and rivets [8-10,14]. For dowel type connections,  $A_{bs,v,perp}$  usually does not appear in tests [13]. This is due to the considerably larger diameters of the connectors and the typically smaller thickness of the timber members. However, drawing a line between “small



Each test series contained four test groups A to D while an additional test group E was only tested in test series II. The test groups were designed in such a manner to enable a quantification of the load carrying effect of shear and/or tension on the total capacity of the connection as well as of the effect of the reinforcement with screws. In the following, details of the different test groups are specified. Side views of the specimens of the five test groups are shown in Figure 6.

Test group A: Reference specimens with neither saw cuts nor screws.

Test group B: Specimens with two saw cuts per side member perpendicular to joint axis in order to suppress load transfer via shear ( $R_{bs,v}$ ) and thus allow exclusively load transfer via net tension ( $R_{bs,t}$ ). (Note: Screw reinforcement prevented unintended failure modes but did not contribute to the tension resistance.)

Test group C: Specimens with a centre cut per side member perpendicular to joint axis between the innermost dowel holes to suppress load transfer via tension ( $R_{bs,t}$ ) and thus allow load transfer exclusively via shear ( $R_{bs,v}$ ).

Test group D: Specimens with screw reinforcement (without cuts).

Test group E: Similar to test group C, however with screw reinforcement to check the effect of the screws on the shear capacity.



**Figure 5:** View of specimen No. 5 of test group C of test series I in the testing machine.

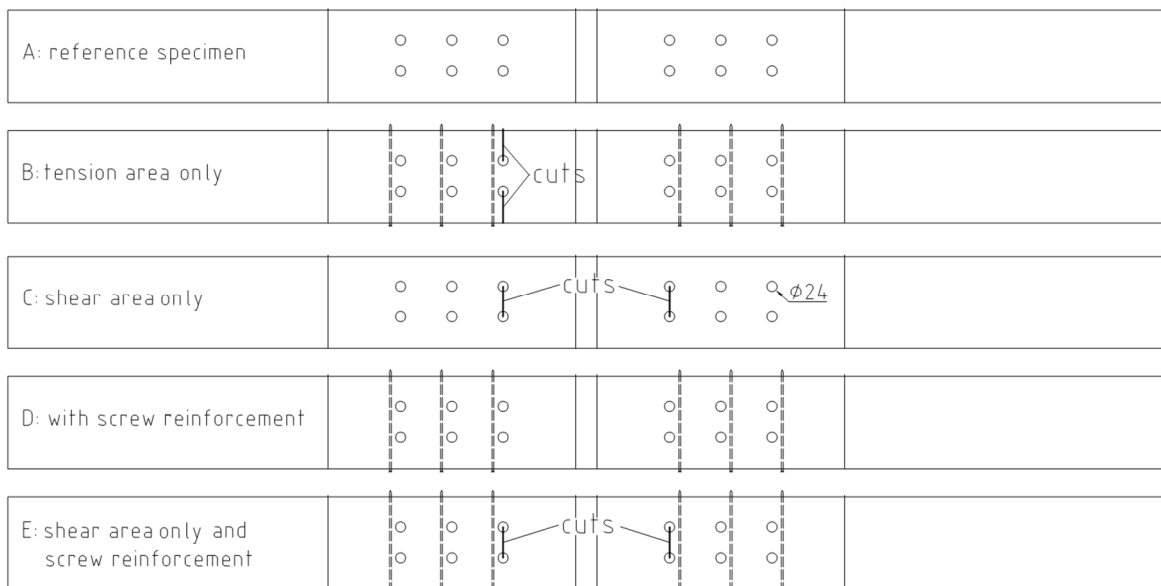


**Figure 6:** Views of the test groups A to E, within test series I and II, respectively (Note: test group E not in series I).

## 4. Finite Element Calculations

Finite element models of wooden dowel joint connections with different hole arrangements were generated and analyzed by means of the ANSYS software package. In all cases the plate was modeled with 2D 8-node structural solid elements. Plane stress conditions were assumed and appropriate wood material properties were used to simulate orthotropic linear elastic behavior. A unit tension load was applied as a pressure at the far edge of the model. Initially two different approaches as specified in [12] were considered for modeling the bolt-loaded hole. The first approach consisted of applying radial displacement boundary conditions at the hole in the semicircular contact face opposite to the loading direction. The affected nodes while restrained in the radial direction were free to move in the tangential direction. The second approach consisted of inclusion of the bolts to the existing model and simulating the contact between the bolts and the plate. The same element type was used to model the bolts and isotropic linear elastic material properties for steel were used. In order to avoid stress concentrations several central nodes in the bolt region were restrained in both orthogonal directions. The only nonlinearity considered in this model was the contact itself. Both models implied either explicitly or implicitly that the bolts will not bend and yield at the applied stresses. Having in mind the above stated crude modeling assumptions, both models produced comparable stress distributions along the plate. Since the ‘costs’ of the former, simple model were lower with regard to parametric studies it was adopted for modeling all subsequent bolt arrangements.

## 5. Test Results

The ultimate loads and the failure modes of both test series are compiled in Table 1. Mean values are given in the table as no other statistical evaluation makes sense with regard to the small sample size of two specimens per test group.

**Table 1:** Results of test series I and II.

test group	test layout	reinforcement with screws	shear area	tension area	test series I (side member thickness: 31 mm)			test series II (side member thickness: 60 mm)		
					F <sub>ult</sub>	F <sub>ult,mean</sub>	failure mode*	F <sub>ult</sub>	F <sub>ult,mean</sub>	failure mode*
					kN	kN		kN	kN	
A	reference specimen	no	active	active	121.4	125.5	BS/Sp	356.0	348.1	BS/RS
							Sp	340.2		BS
B	tension area only	not active	cut	active	73.0	77.6	BS/Sp	135.0	146.1	BS
					82.3		Sp	157.3		BS
C	shear area only	no	active	cut	101.5	88.2	BS	200.2	205.9	BS
					74.9		BS/Sp	211.6		BS
D	with screw reinforcement	yes	active	active	143.4	150.0	BS/Emb/RS	322.0	353.1	BS
					156.6		Sp/RS	384.1		BS
E	like C + screw reinforcement	yes	active	cut	-	-	-	220.0	213.1	BS
					-		-	206.2		BS

\* BS = Block shear, Sp = Splitting, Emb = Embedment, RS = Row Shear

The two ultimate load values of every test differed maximally by 15 % with two exceptions (test series I, test group C (denoted I.C): 30 %; test group II.D: 18 %). The difference between the two results of each reference specimen test group A was exceptionally small (7 % and 5 % for test series I and II, respectively).

Even though test series II was designed to forward yielding with one yield hinge per shear plane as its dominant dowel failure mode (failure mode j in EC 5), a third shear plane  $A_{bs,v,perp}$  did not arise in any of the specimens.

It can be seen that the entire test results from series I (thickness of side members: 31 mm) incorporate splitting along the dowel rows. The observation of the surfaces of the side members during the tests also revealed that a lot of cracks appeared before reaching the ultimate load in test series I. By contrast, the side members of test series II were virtually uncracked before the very brittle failures occurred.

The stated observations of the failure modes serve as an explanation for the fact that the average ultimate loads of test series I in test groups A, C and D are significantly lower than 50 % of the average ultimate loads of test series II.

Screw reinforcement had significant effect on ultimate load in test series I ( $F_{ult,I,D} = 1.20 \cdot F_{ult,I,A}$ ). But it also impacted on the failure mode, as for instance revealed in test group A where failure was related to splitting to a considerably larger extent than in test group D.

Conversely, in test series II screw reinforcement only had a very minor effect on ultimate load ( $F_{ult,II,D} = 1.01 \cdot F_{ult,I,A}$ ;  $F_{ult,II,E} = 1.03 \cdot F_{ult,I,C}$ ) and no visible effect on failure mode as splitting did not occur in any test group.

The ultimate load values of the reference specimens (test group A) are consistently larger than the single values of test groups B and C where either shear area  $A_{bs,v}$  or tension area  $A_{bs,t}$  were suppressed. In the case of test series II, the values of test groups B ( $F_{ult,II,B}$ ) and C ( $F_{ult,II,C}$ ) added up nicely to a combined load capacity that was almost exactly as large as the ultimate load of the reference specimens ( $F_{ult,II,A}$ ):

$$F_{ult,II,B} + F_{ult,II,C} = 146.1 + 205.9 = 352.0 \text{ kN} = 1.01 \cdot F_{ult,II,A}$$

In test series I, the results of the summed-up ultimate loads of test group B ( $F_{ult,I,B}$ ) and C ( $F_{ult,I,C}$ ) were considerably larger than the load capacity of the reference specimens ( $F_{ult,I,A}$ ) and even somewhat larger than the capacity of the screw reinforced specimens of test group D ( $F_{ult,I,D}$ ):

$$F_{ult,I,B} + F_{ult,I,C} = 77.6 + 88.2 = 165.8 \text{ kN} = 1.32 \cdot F_{ult,I,A} = 1.11 \cdot F_{ult,I,D}$$

## 6. Simple Design Model

The test results clearly show that the design approach of EC 5 is too conservative, because it completely neglects the coaction of shear and tension. (Note: The EC 5-factor  $k_{bs,t} = 1.5$  seems to account partly for the coaction without paying regard to the actual joint geometry). Even though the results yielded an almost complete coaction of the two load transferring components shear and net tension, the existing literature shows [6] that the shear and tension capacities do not always contribute completely to the overall capacity of the connection.

The basic idea for the model stems from a simple assumption of force flow as shown in Figure 7 and explained below.

- I. The load is transferred into a wood member via the embedment directly under the dowels ( $F_d$ ).
- II. From the compression zone under the dowel, the load  $F_D$  has to commute to a tension strain at both sides of the dowels via shear ( $F_D/2$ ), regardless of whether this is inside or outside the joint block. If this load transfer is not possible, the connection should break in row shear failure mode, which has to be checked in advance.
- III. After accumulating over all dowels along the fibre, the tension load has to pass through the cross-section that surrounds the dowels which are furthest away from the end grain, being the crucial net tension section. According to the model, as long as the net tension area of the joint block does not fail, there must be a certain interaction between the joint block and the remaining timber sections on both sides of the block.

IV. In addition to the mentioned interaction of shear capacity, there could be a contribution from shear, depending on the relative displacement between the joint block and the lateral areas, which is not captured by the model.

V. As can be seen in Figure 7, the fraction of the load which is transmitted laterally to both sides of the joint block ( $F/2$  in Figure 7a and  $F/3$  in Figure 7b) depends on the amount of dowel rows (counted perpendicular to fibre)  $n_{\perp}$ .

VI. In other words, the net tension capacity can be raised by a factor

$$k_{BS} = \frac{n_{\perp} \cdot 2}{n_{\perp} \cdot 2 - 2} \quad (6)$$

which results in  $k_{BS} = 2$  for  $n_{\perp} = 2$  (Figure 7a) and  $k_{BS} = 1.5$  for  $n_{\perp} = 3$  (Figure 7b). (Note:  $k_{BS}$  is a geometrical factor and is the total load divided by the load shares transferred via  $A_{bs,t}$  according to the simplified assumptions as shown in Figure 7.)

VII. After the crucial net tension area of the joint block has failed, there is still the possibility of the shear area to hold the whole joint block; this is possible if the shear capacity is sufficient.

VIII. The proposed model is essentially a modification of the EC 5 model

$$R_{bs} = \max(R_{bs,v}, k_{bs} \cdot R_{bs,t}) \quad (7)$$

where

$$R_{bs,v} = k_{bs,v} \cdot f_{v,k} \cdot A_{bs,v}$$

and

$$R_{bs,t} = k_{bs,t} \cdot f_{t,0,k} \cdot A_{bs,t}$$

plus the introduction of a row shear proof.

(Note:  $k_{bs,t} \neq k_{BS}$  accounts for strength effects and is regarded in section 7.)

IX. The model is only valid under the assumption that a third shear plane perpendicular to the dowels  $A_{bs,v,perp}$  does not occur.

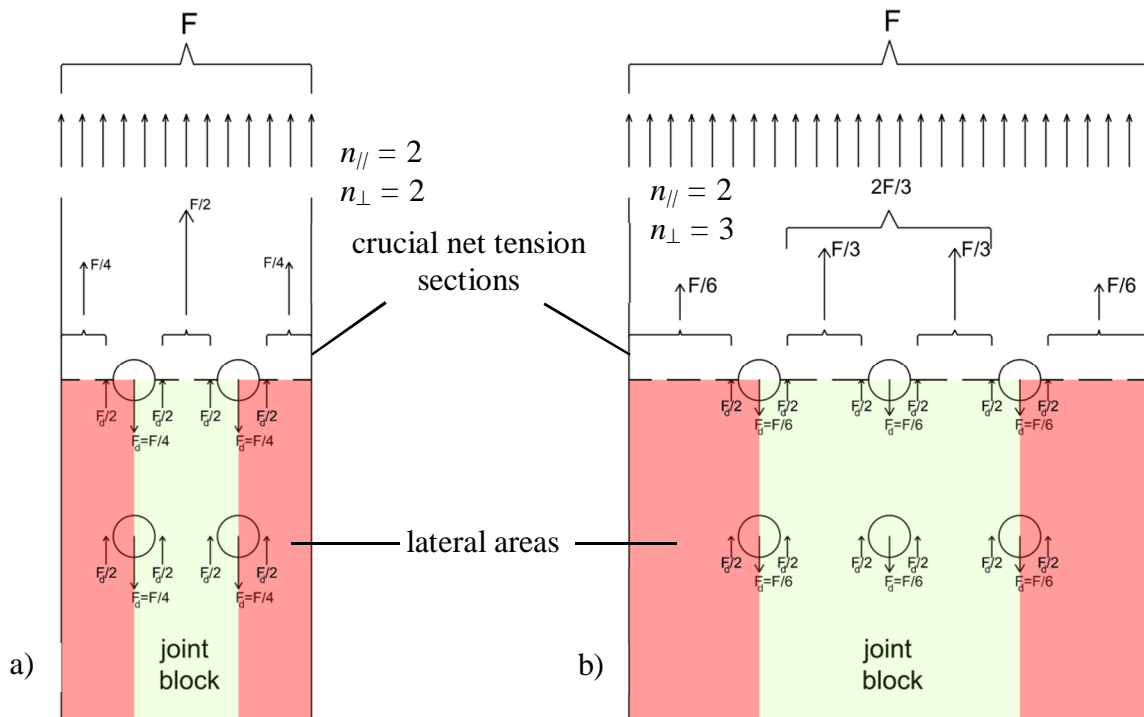


**Figure 7:** Assumptions for the force flow in case of a) two ( $n_{\perp} = 2$ ) and b) three ( $n_{\perp} = 3$ ) rows of dowels (counted perpendicular to grain) as basis for the simple design model.

## 7. Calibration and Verification of the Model with Test Results and Finite Element Calculations

Due to the low very small specimen numbers in every test group, the calculation of characteristic values of every test group would have led to “undue” conservative results. Alternatively, the results obtained in the tests were plotted over the calculated characteristic values in order to calibrate the strength parameters  $k_{bs,v}$  and  $k_{bs,t}$ . First, the strength parameters were assumed to be  $k_{bs,v} = 0.7$  and  $k_{bs,t} = 1.3$  as theoretically derived in Sections 2.1 and 2.2, respectively. Hence, in case the calculated characteristic values were larger than the ultimate load in test, i. e. data points were left to the diagonal line, the model was considered unsafe and the strength parameters were decreased by steps of 0.1 until the plot appeared as can be seen in Figure 8. (Note: The sole experimental result left to the diagonal line is related to a specimen subjected to splitting.) This reported adaptive process was mainly governed by the results of test groups B and C, where the load was transferred exclusively either via shear or tension.

The following parameters were obtained:

$$k_{bs,v} = 0.6 \quad \text{and} \quad k_{bs,t} = 1.1.$$

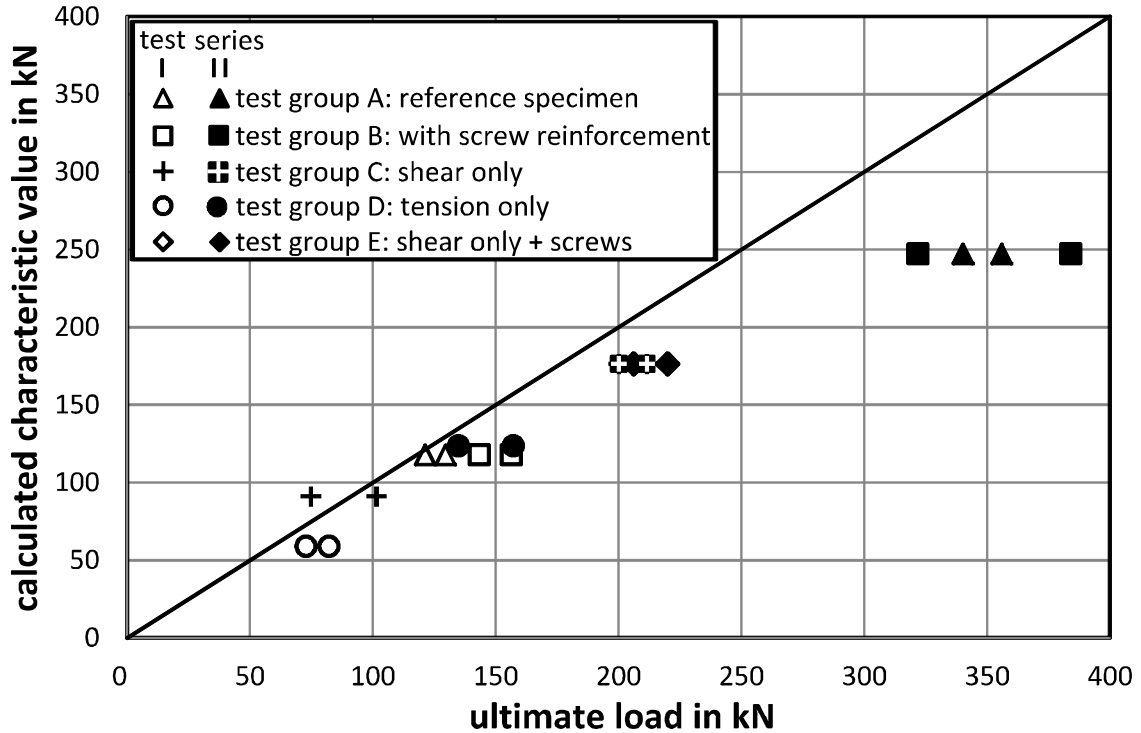


**Figure 8:** Comparison of calculated characteristic values with ultimate loads obtained from the tests.

The relatively conservative estimate of the reference specimens (test group A) of test series II (see Figure 8) can be explained by a contribution of the lateral areas of the connection that stems from strain differences between the joint block and the lateral areas. This phenomenon could be shown by the finite element calculations which allocated 63 % of the load to the lateral areas whereas only 50 % are captured by the proposed simple design model. However, when raising the spacing of the dowel perpendicular to the fibre from three times ( $a_2 = 3 \cdot d = 72 \text{ mm}$ ) to five times ( $a_2 = 5 \cdot d = 120 \text{ mm}$ ) the diameter of the dowel, the contribution of the lateral areas drops from 63 % to 54 % which is rather close to the analytical value according to Eq. (6). In another calculation, the edge distance per-

pendicular to fibre was raised from 74 mm to 120 mm, which changed the load fraction of the lateral areas to 70 %.

The FE model was also applied to connections with four dowels in each row counted parallel to grain ( $n_{\parallel} = 4$ ). The numerical results revealed that the load ratio between the joint block and the lateral areas is not dependent on the number of dowels per row.

When adapting to  $n_{\perp} = 3$  rows of dowels (counted perpendicular to grain), the load share of the lateral members dropped from 63 % to 47 % with spacing  $a_2 = 3 \cdot d$  and to 38 % with spacing  $a_2 = 5 \cdot d$  (model prediction: 33 %). For a similar joint with  $n_{\perp} = 4$  rows of dowels the load share of the lateral members was 38 % with spacing  $a_2 = 3 \cdot d$  and 28 % with spacing  $a_2 = 5 \cdot d$  (model prediction: 25 %), respectively.

## 8. Summary and Conclusions

The comparison of the block shear proof of dowel connections in North American Codes and EC 5 revealed significant differences.

In order to calibrate the stated differences an ongoing experimental and computational study was performed. A major focus of the experimental study was to clearly separate the block shear resistances related to tension and shear strength. A further aim addressed the possible interaction of both controversially discussed load transferring mechanisms.

In the cases of block shear failure and row shear failure, the shear strength  $f_v$  has to be reduced because of non-uniform load application by the dowels. The value of  $k_{red,bs,v} = 0.6$  of CSA-086 could be confirmed by the test results. The difference to the theoretically derived value of  $k_{red,bs,v} = 0.7$  can be explained by a non-uniform load distribution over the length of the joint.

Based on the present results, a simplified provisional design model was derived based on the EC 5 provisions was derived. Contrary to the EC 5 model, a clear separation between geometrically bound load shares and strength effects is captured.

Theoretical considerations justify raising the tension strength parallel to fibre  $f_{t,0}$  in cases of block shear failure by a factor  $k_{bs,t} = 1.3$ . This would be in line with CSA-086, which provides an entire set of strength values  $f_{t,0,net}$  in all cases of a possible net tension failure. However, the obtained limited test results led to a considerably smaller strength increase of only  $k_{bs,t} = 1.1$ . This might be due to the inhomogeneous stress distribution in the net tension area what will be addressed by Weibull integration in on-going investigations.

Since row shear failure could be observed during the tests and is in line with the basic ideas of the proposed model, it should be included in EC 5.

The tests revealed that screw reinforcement does not improve the block shear joint capacity in general.

## 9. Acknowledgment

The authors thank the graduate student Mr. Hsuan-Hsiung Fang who produced all the specimens and performed all the tests in the context of his diploma thesis.

## References

- [1] CSA-O86-09. Engineering Design in Wood.
- [2] DIN 1052:2008. Design of Timber Structures – General Rules and Rules for Buildings.
- [3] DIN EN 1194:1999. Timber Structures – Glued Laminated Timber – Strength Classes and Determination of Characteristic Values; German Version EN 1194:1999.

- [4] DIN EN 1995-1-1:2010. Eurocode 5: Design of Timber Structures – Part 1-1: General – Common Rules and Rules for Buildings; German Version EN 1995-1-1:2004 + AC:2006 + A1:2008.
- [5] ANSI /AF&PA NDS-2005. National Design Specification (NDS) for Wood Construction with Commentary and Supplement: Design Values for Wood Construction.
- [6] Biger J, Bocquet J, Racher P (2000), Testing and Designing the Joints for the Pavilion of Utopia. Proceedings of the 6th World Conference on Timber Engineering WCTE, Whistler Resort, British Columbia, Canada.
- [7] Colling F (1986), Influence of the Volume and the Stress Distribution on the Strength of a Beam with Rectangular Cross Section – Determination of the Fullness-Parameters, Examples. *European Journal of Wood and Wood Products* 44(5), 179–183.
- [8] Foschi R, Longworth J (1975), Analysis and Design of Griplam Nailed Connections. *Journal of the Structural Division* 101 (12), 2537–2555.
- [9] Johnsson H (2004), Plug Shear Failure in Nailed Timber Connections – Avoiding Brittle and Promoting Ductile Failures. PhD thesis, Lulea University of Technology.
- [10] Kangas J (1999), Walford GB, Gaunt DJ (Ed.), Block Tearing Failure in Nailed Steel-to-Timber Joints. Proceedings of Pacific Timber Engineering Conference, Rotorua, New Zealand.
- [11] Lam F, Varoglu E (1990), Effect of Length on the Tensile Strength of Lumber. *Forest Products Journal* 40(5), 37–42.
- [12] Okutan B (2001), Stress and Failure Analysis of Laminated Composite Pinned Joints. Ph.D. Dissertation, Dokuz Eylul University, Izmir, Turkey.
- [13] Sjödin J, Johansson C (2007), Influence of Initial Moisture Induced Stresses in Multiple Steel-to-Timber Dowel Joints. *European Journal of Wood and Wood Products* 65(1), 71–77.
- [14] Zarnani P, Quenneville P (2012), Predictive Analytical Model for Wood Capacity of Rivet Connections in Glulam and LVL. Quenneville P, (Ed.), Proceedings of the 12th World Conference on Timber Engineering WCTE, Auckland, New Zealand.



**INTERNATIONAL COUNCIL FOR RESEARCH AND INNOVATION  
IN BUILDING AND CONSTRUCTION**

**WORKING COMMISSION W18 - TIMBER STRUCTURES**

**REQUIREMENTS ON DUCTILITY IN TIMBER STRUCTURES**

F Brühl

U Kuhlmann

Institute of Structural Design, Universität Stuttgart

GERMANY

**MEETING FORTY FIVE**

**VÄXJÖ**

**SWEDEN**

**AUGUST 2012**

---

Presented by F Brühl

W van Beerschoten commented about the assumed shape of the stress distribution that triangular stress distribution might be more appropriate. He also commented on the over strength factor. F Brühl agreed that the over strength factor was a driving factor. K Malo asked and received clarification on the characteristic strength of the connection. T Poutanen asked about the benefit in terms of numerical value. F Brühl stated that they did not have a number. P Quenneville questioned whether this connection was the most effective as plates with inclined wood screw underneath was also an option. W van Beerschoten questioned about damage after a big earthquake as large deformation might lead to non-repairable problems. F Brühl stated that in case of Europe this should be okay. I Smith commented and discussed the analog of links in a chain versus link in a double chain and practical achievement of ductility was difficult. K Malo discussed alternative of using the steel bracket. J Munch Andersen stated if you followed P Quenneville's suggestion of the alternative connection it would not be good for fire performance. M Frese asked why put a gap between screws and dowel. F Brühl stated that this was a practical approach and contact was not doable on site.



# Requirements on ductility in timber structures

Frank Brühl & Ulrike Kuhlmann

Institute of Structural Design

Universität Stuttgart, Germany

## 1 Introduction

Ductility has become a demand especially on timber joints that is motivated by several aspects: In the view of robustness, see EN 1991-1-7 [24], the possibility of redistribution of loading in indeterminate structures is of high interest. A considerable advantage may also be achieved in common design due to the redistribution of internal forces in indeterminate structures (see 5.1(3) in EN 1995-1-1 [26]).

*For structures able to redistribute the internal forces via connections of adequate ductility, elastic-plastic methods may be used for the calculation of the internal forces in the members.*

In both cases redistribution can only be achieved if the first formed “plastic hinge” allows for sufficient rotational capacity. This is possible if the plastic hinge is formed in a joint with sufficient ductility. The demand of ductile joints may be derived from the verification of the available rotation of the joint in comparison to the required rotation in the structural system. However, information about the ductile behavior of different types of connections and joints are not yet implemented in the standard [26]. There is an additional aspect where information on joint ductility may be useful: for seismic design [27]. Although the behavior of doweled connections under a cyclic loading is not the same as under a monotonic loading, the design concepts may be transferred to each other.

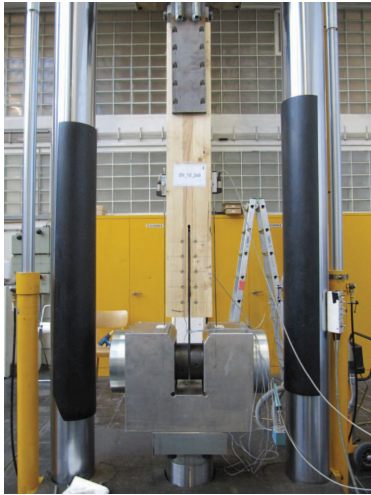
The aim of this paper is to give a first approach of a mechanical model, to predict the behavior of semi-rigid joints in timber structures with the focus on the bearing capacity and the rotation capacity. Experiments have been conducted to identify the load-deflection behavior of selected dowel arrangements and to verify the mechanical model. In a second step the model has been simplified to give an approach for the practical application.

In addition the attention is given to the material scattering of timber. A computer model has been developed to determine the variation of the beam end rotations caused by the scattering of the modulus of elasticity. To ensure that a ductile behavior of the joint takes place before a brittle member fails, an overstrength factor is defined based on the proposal of [10, 9].

## 2 Mechanical model

### 2.1 General

In the frame of two research programs [13, 12] a mechanical model has been developed based on experiments realized in two test series. First pure tension tests were conducted on dowel connections



(a) Experiments on connections



(b) Experiments on joints

**Figure 1:** Conducted experiments

(comp. Fig.1(a)) and second four point bending tests were realized on joints composed of dowel connections and a compression zone (comp. Fig. 1(b)). The tension tests were conducted to obtain the load-displacement behavior of pure connections with reinforced dowel type fasteners [1]. The same connections were implemented in the second test setup within the tension zone of moment resistant joints in order prove the rotational capacity.

## 2.2 Experiments

### 2.2.1 Materials and test method

Prior to testing materials used for the test specimens were evaluated carefully. The presented experiments were realized with dowels with a diameter of 12 mm and a steel grade of S235. Stress-strain tests on a set of dowels taken from the same lot showed a mean value of ultimate tensile strength of 581 N/mm<sup>2</sup>. The ultimate tensile strength of S235 according to [21] should range between 360 N/mm<sup>2</sup> and 510 N/mm<sup>2</sup>. Therefore it is supposed, that the basic material of the dowels belong to a higher steel grade. Previous investigations on dowel type connections had also shown a higher tensile strength [18, 16].

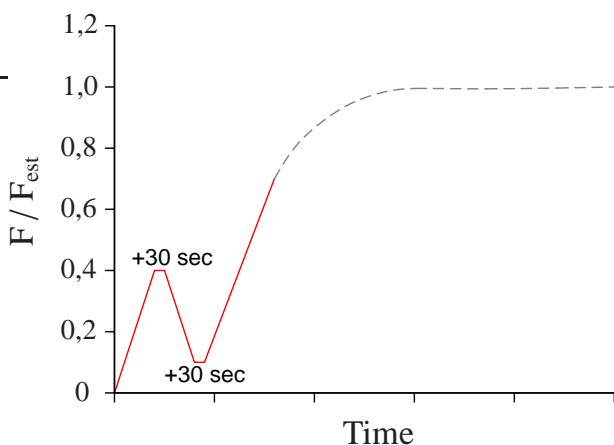


**Figure 2:** Modified test performance according to EN 26891

The timber grade for both setups was chosen to grade GL24h. The aim was to ensure that the dowels for both test setups were embedded in the same timber grade. MiCROTEC<sup>®</sup> GmbH scanned all of the processed lamellae with its Golden Eye 706 quality scanner to detect the material properties. The mean density for all lamellae within the connection tests was 443,5 kg/m<sup>3</sup> and for the joint tests 444,4 kg/m<sup>3</sup>. Hence the results of the pure

connection tests can be transferred to the joint tests.

Both test series were carried out displacement controlled following [28], with a certain modification (comp. Fig. 2): The experiments were continued until a failure of the test specimens occurred, or a decrease of the load to 80% of the maximum load was reached [22], unlike the proposed experiment termination at a displacement of 15 mm. Thus the maximum possible deflection respectively the maximum feasible rotation could be determined.

### 2.2.2 Connection tests

Tests with three different dowel arrangements were conducted with dowels of a diameter of 12 mm. A steel cover was adjusted on the top of the specimens with self drilling screws to ensure that only one connection was tested (comp. Fig. 1(a)). The dowel arrangements varied from a rather stretched configuration of 5x2 dowels, to a compact arrangement of 3x3 dowels and a wide alignment of 2x4 dowels, where the first number indicates the number of dowels parallel to the grain, and the second the number of dowels perpendicular to the grain. Each test series consists of four single tests. Figure 3 shows the mean test results of the different dowel arrangements with a diameter of 12 mm.

Based on the ductility definition  $D_f = u_f / u_y$  [14, 3] a ductility ratio of 9 to 9.5 could be achieved. Thus these types of connections can be classified as highly ductile [17]. Within this consideration the displacement at yielding ( $u_y$ ) was determined based on the regulations [22, 29], and  $u_f$  describes the displacement at failure.

The results are normalized to the bearing resistance calculated based on the initial measured material properties [19] (comp. Fig. 3). The connections show a good accordance of the initial stiffness and the bearing resistance. Furthermore it can be confirmed, that the load carrying capacity of reinforced doweled connections is almost identical, independent of the dowel arrangement [2].

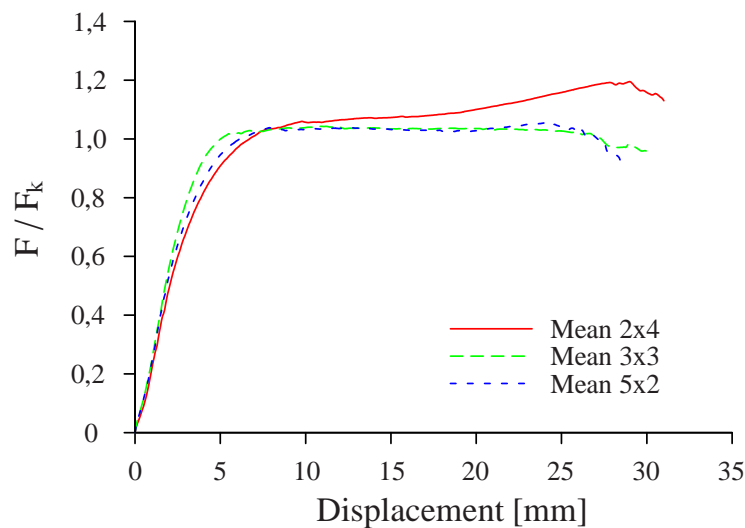


**Figure 3:** Mean values of the load-displacement behavior of the conducted experiments (Ø 12mm)

### 2.2.3 Joint tests

A four-point bending moment test setup was chosen to conduct the experiments on the moment-rotation capacity of joints (comp. Fig. 1(b)). The bending moment was transferred by a defined com-

pression zone (steel block 65mm x 180mm) on the top, and the previous tested dowel connections in the tension zone.

Figure 4 shows the mean value of the experiments with a dowel diameter of 12 mm. The displayed rotation refers to the angle of either one side of the joint (comp. Fig. 4). The comparison shows that the inner lever arm is directly linked to the bending moment capacity. The stretched dowel arrangement of 5x2 dowels had a larger lever arm and therefore a higher bending moment resistance compared to an extended connection of 2x4 dowels with a smaller lever arm. Furthermore the stiffness is decreasing with a decrease of the inner lever arm.

The arrangement of the dowels has a further influence on the moment-rotation behavior. For a stretched arrangement the decrease of the plastic level is more pronounced as for a wide alignment. The loss of moment capacity leads to a geometrical characteristic, which is explained in the next paragraph.

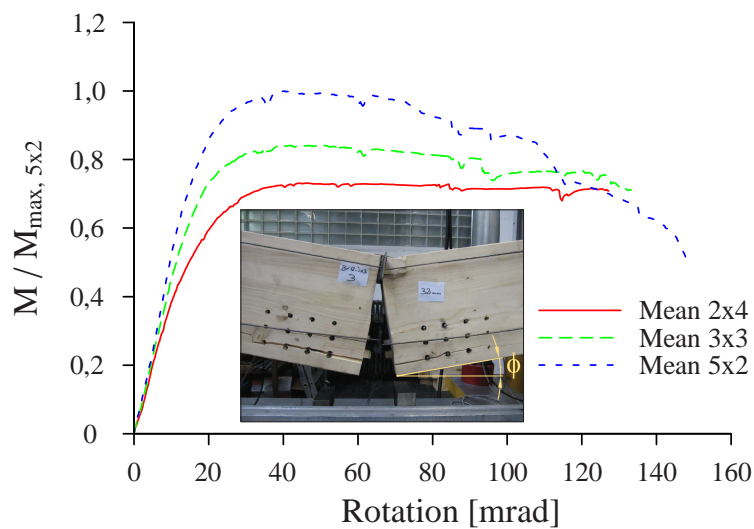


**Figure 4:** Mean values of the moment-rotation behavior of the conducted experiments ( $\varnothing$  12mm) (normalized to the maximum moment of dowel arrangement (5x2))

## 2.3 Development of a mechanical model

### 2.3.1 General

To describe the moment-rotation behavior of semi-rigid joints, it is desirable to develop a model which describes the behavior in a reliable manner, reliable not only on the calculation of the moment carrying capacity of the joint, but also on the prediction of the rotational capacity.

### 2.3.2 Introduction of the single components

Following the design philosophy of the so called component model [25], the single load carrying elements, the components, are characterized within the overall joint. Figure 5 shows the joint with these single elaborated components. The mechanical properties of the single components, will be presented in the following.

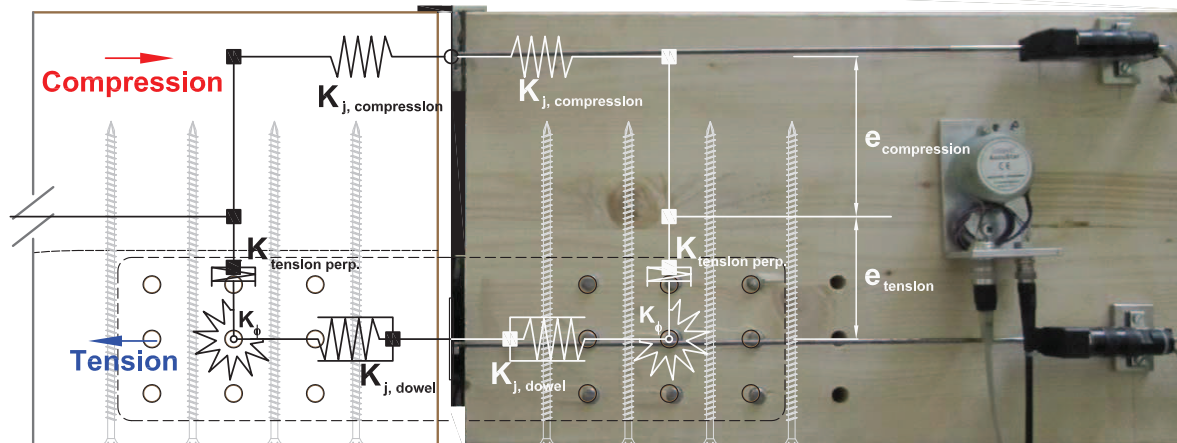


**Figure 5:** Joint with its single components

### Component acting in compression

The load-displacement behavior of the compression zone within the conducted experiments forms the basis of the component acting in compression. The compression zone forms a steel block with a height of 65 mm and a width, which is equal to the beam width, of 180 mm.

The displacement was measured on the front- and the back-side and on the left- and right-hand side within the center of the compression zone. To determine the initial stiffness of the compression zone, the mean value of the load deflection behavior within the compression zone from the 9 bending tests conducted on dowels with a diameter of 12 mm from the front- and back-side was defined. Based on EN 26891 [28] a mean value of  $K_{\text{compression}} = 303 \text{ kN/mm}$  was determined with a variation coefficient of 15,7 %.

To classify the results of the evaluation, the value is compared with the stiffness of the notch within TCC structures. Conducted experiments on notched connections with a timber grade of GL32h and a depth of 40 mm showed [11] a stiffness of 387 kN/mm on a 22 cm wide beam. Therefore the determined stiffness of 303 kN/mm on a 18 cm wide beam (GL24h) is within the range of the identified value in TCC structures.

### Component acting in tension

The load-slip behavior of the pure dowel connection has been specified in the first test series (comp. section 2.2.2). Hence the nonlinear behavior of the different dowel configurations is known.

### Component acting perpendicular to the grain

Stresses perpendicular to the grain occur on the top of the dowel arrangement due to the rotation of the dowel alignment. The stresses increase with stretched arrangements. Since all of the connections were reinforced with fully threaded self tapping screws, the screws were extended to reinforce the connection in addition for stresses perpendicular to the grain (comp. Fig. 5). Therefore a brittle failure due to stresses perpendicular was avoided.

## Rotational component due to the dowel arrangement

The dowel arrangement causes a moment within the connection due to the rotation of the joint. The created bending moment within the dowel connection of the joint can be determined by:

$$M_\phi = K_\phi \cdot \phi \quad (1) \quad \text{with:} \quad K_\phi = K_{dowel} \cdot I_P \quad (2)$$

The moment-rotation behavior of the dowel arrangement follows thereby the load-displacement behavior of a dowel, depending on the polar moment of inertia ( $I_P$ ) of the arrangement.

### 2.3.3 Geometrical influence

The decrease of the bearing resistance within the plastic level (comp. section 2.2.3) is a geometrical effect of the decrease of the inner lever arm with an increase of the rotation (comp. Eq. (3)). Within this paper it is suggested, that the center of the dowel arrangement rotates with a distance “ $r$ ” from the top of the joint (comp. Fig. 6).

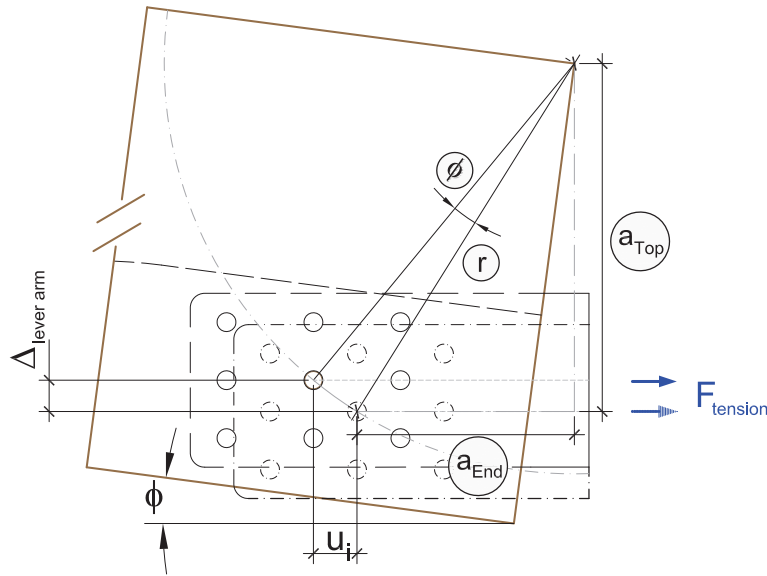


**Figure 6:** Geometrical influence on the inner lever arm

The factor  $k_\phi$  is introduced to consider the reduction of the bending moment.

$$k_\phi = \frac{\text{inner lever arm} - \Delta_{\text{lever arm}}}{\text{inner lever arm}} \quad (3)$$

The decrease of the lever arm ( $\Delta_{\text{lever arm}}$ ) is calculated by:

$$\Delta_{\text{lever arm}} = \sqrt{u_i^2 - b^2} \quad (4)$$

$$b = 2 \cdot r \cdot \sin\left(\frac{\phi}{2}\right) \quad (5)$$

$$\text{with:} \quad r = \sqrt{a_{\text{end}}^2 + a_{\text{top}}^2} \quad (\text{comp. Fig. 6})$$

$$u_i = \text{Displacement}$$

$$\phi = \text{Rotation on each side}$$

### 2.3.4 Assembly of the mechanical model

In the final step the single components are assembled to the joint model. The moment capacity of the joint is found as the sum of the contributions of the single components.

$$\begin{aligned} M_{joint} &= M_{\phi} + F_{tension} \cdot e_{tension} + F_{compression} \cdot e_{compression} \\ &= M_{\phi} + F_{tension/compression} \cdot e \end{aligned} \quad (6)$$

with

$M_{\phi}$	: Comp. Eq. (1)	$e_{tension}$	: Lever arm from the beam center line to the center of the dowel arrangement (comp. Fig. 5)
$F_{tension/compression}$	: Force within the tension or the compression zone	$e_{compression}$	: Lever arm from the beam center line to the center of gravity within the compression zone (comp. Fig. 5)
$e$	: Inner lever arm		

However, due to the moment caused by the rotation ( $M_{\phi}$ ) the tension force respectively the compression force decreases. Furthermore, the rotation of the dowel arrangement results in additional

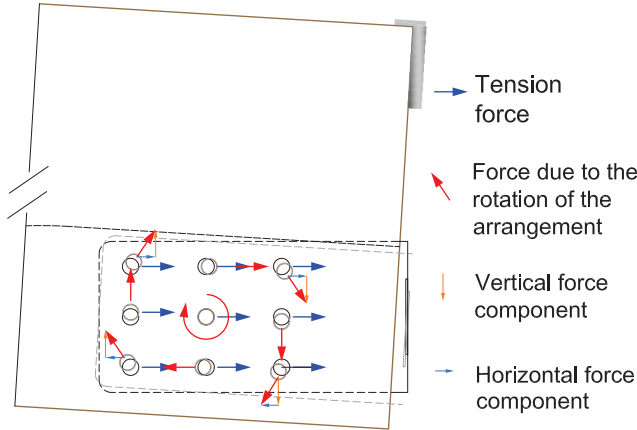


**Figure 7:** Forces acting on the dowel arrangement due to the rotation

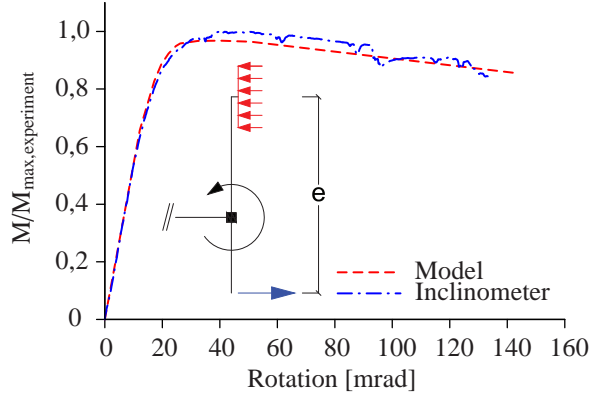
forces acting perpendicular to the center of the dowel arrangement (comp. Fig. 7). The additional forces are divided to horizontal and vertical components. In sum these components are in equilibrium and do not form an resultant effect. Due to the equilibrium of the inner forces and the bending moment the various components are depending on each other. The bearing resistance is found for every rotation step by using iteration. The factor  $k_{\phi}$  is calculated within every step to consider the decrease of the inner lever arm. Figure 8 shows the comparison of the different appraisals of the inner lever arm. The component model gives a good accordance of the initial stiffness and the bearing resistance for

an infinite stiffness of the compression zone and a lever arm from the center of the dowel group to the center of the compression zone (comp. Fig. 8(a)).

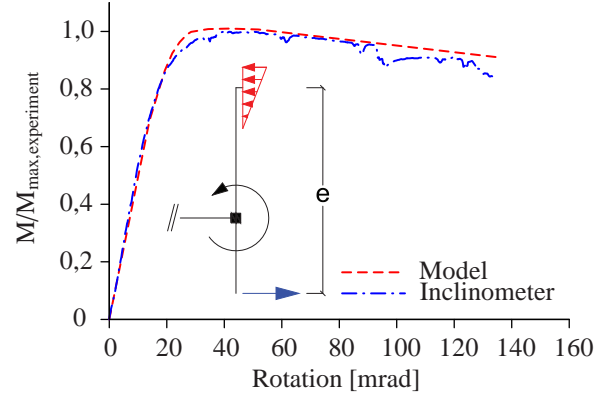
The second approach is characterized by a stiffness of the compression zone of 303 kN/mm (comp. paragraph 2.3.2) and a triangular stress distribution within the compression zone (comp. Fig. 8(b)). This approach shows a slightly higher bearing resistance.

## 2.4 Simplified mechanical model

A simplified model has been developed to give an approach for the practical application. The approach is consistent with known methods and is based on the bearing resistance and the stiffness values of EN 1995-1-1 [26].



(a) Infinite stiffness in compression, center of gravity in the middle of the compression zone



(b)  $K_{\text{compression}} = 303 \text{ kN/mm}$ , triangular stress distribution within the compression zone

**Figure 8:** Comparison of the mechanical model with the experiments depending on the inner lever arm ( $\text{Ø}12, 3 \times 3$ )

The method follows the procedure of the component model [25], which describes the moment-rotation behavior of a joint as a trilinear approach.

The first part of the trilinear graph is found with the initial stiffness. Hence the first point is given by:

$$F_1 = \frac{2}{3} \cdot F_{v,Rk} \quad (7) \quad u_1 = \frac{F_1}{K_1} = \frac{\frac{2}{3} \cdot F_{v,Rk}}{\frac{\rho_k^{1,5}}{23} \cdot d} \quad (8)$$

The bearing resistance ( $F_{v,Rk}$ ) of the connection was calculated as the minimum value obtained from the formulas (f, g, h) based on EN 1995-1-1 [26, Chap. 8.2.3] with a characteristic value of the density [19, 20] ( $\rho_k=380 \text{ kg/m}^3$ ) and a steel grade of S355 ( $f_{u,k}=510 \text{ N/mm}^2$ ). The initial stiffness ( $K_{\text{ser}}=K_1$ ) was also calculated based on EN 1995-1-1 [26, Chap. 7.1] with the characteristic density ( $\rho_k$ ). A steel grade of S355 was chosen since the ultimate tensile strength of the dowels in the conducted experiments indicated a higher steel grade than S235 (comp. paragraph 2.2.1).

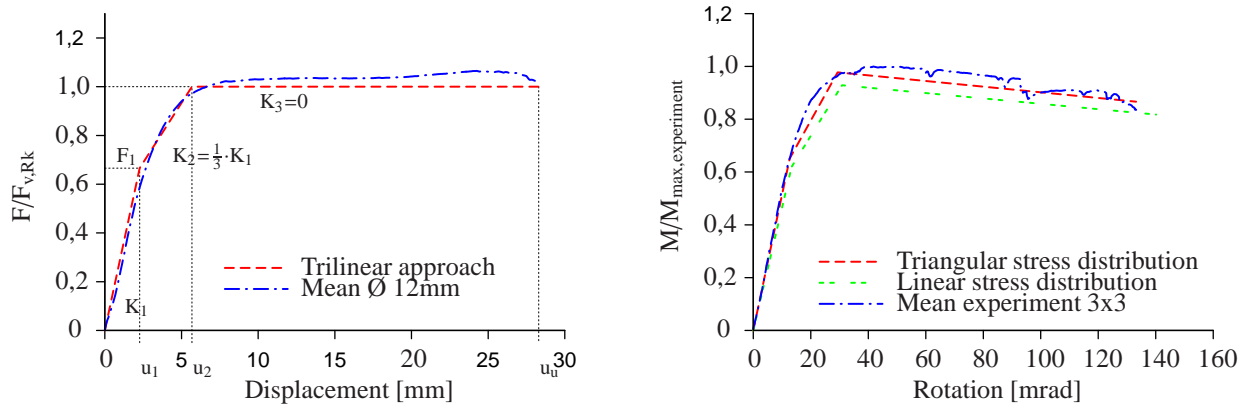
The stiffness of the second part is characterized by a stiffness of one third of the initial stiffness, thus the second point is given by:

$$F_2 = F_{v,Rk} \quad (9) \quad u_2 = u_1 + \frac{\Delta F}{\frac{1}{3} \cdot F_1} = u_1 + \frac{F_{v,Rk}}{K_1} = \frac{\frac{2}{3} \cdot F_{v,Rk}}{K_1} + \frac{F_{v,Rk}}{K_1} = \frac{\frac{5}{3} \cdot F_{v,Rk}}{K_1} \quad (10)$$

The ultimate displacement ( $u_u$ ) is found as the 2% fractile value of the conducted tension tests with a dowel diameter of 12 mm. The ultimate displacement has been determined to 28.3 mm with a variation coefficient of 11,6 %.

Figure 9(a) shows the comparison of the load-displacement curve following the trilinear approach with the mean value of the conducted component tests in tension. The trilinear approach shows a good accordance with the mean value of the experiments on dowels with a diameter of 12 mm. The stiffness and the bearing resistance show a good correlation (comp. Fig. 9(a)).

The trilinear approach of the moment-rotation behavior of the joint only considers the previous determined trilinear approach of the tension zone (comp. Fig. 9(b)). The center of gravity within the compression zone is set to one third of the height of the compression zone or to the middle of the



(a) Comparison of the load-displacement curve of the trilinear approach with the mean value of the experiments of the tension component ( $\text{\O}12$ )

(b) Comparison of the moment-rotation curve of the trilinear approach with a dowel arrangement of 3x3 dowels ( $\text{\O}12$ ), calculated with different assumptions of the inner lever arm with test results

**Figure 9:** Comparison of a trilinear approach with the conducted experiments

compression zone. The bending moment at the ultimate rotation is multiplied by the factor  $k_\phi$  to consider the decrease of the lever arm. The approach shows a good correlation of the initial stiffness with measured values, whereas the approximation based on a lever arm to the middle of the compression zone slightly underestimates the bearing resistance.

### 3 Requirements due to the material scattering

#### 3.1 General

The natural material scattering of timber has a direct influence on the bearing resistance of joints and the deformation of load-bearing elements within a structure. In order to apply the elastic-plastic design method within timber structures, it is indispensable to observe these influences on a structure.

#### 3.2 Overstrength factor for reinforced doweled connections

In order to activate the ductility in a structure, it is essential to ensure that the ductile deformation takes place before a brittle collapse of a structural member occurs. An overstrength factor is introduced within the capacity based design method [15], which ensures that the ductile element behaves

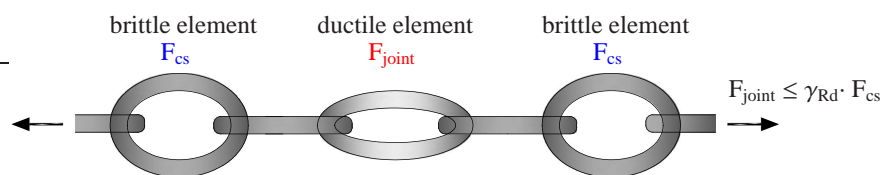


**Figure 10:** Series of different load-bearing elements [15]

ductile before a brittle member fails (comp. Fig. 10).

The overstrength factor ( $\gamma_{Rd}$ ) is defined as the ratio between the 95<sup>th</sup> percentile of the connection ( $F_{0.95}$ ) and the design value of the connection ( $F_{v,d}$ ) [9].

$$\gamma_{Rd} = \frac{F_{0.95}}{F_{v,d}} = \frac{F_{0.95}}{F_{0.05}} \cdot \frac{F_{0.05}}{F_{v,k}} \cdot \frac{F_{v,k}}{F_{v,d}} = \gamma_{sc} \cdot \gamma_{an} \cdot \gamma_M \quad (11)$$

thereby the different  $\gamma$ -values represent

- $\gamma_{sc}$  = The scattering within the experiments
- $\gamma_{an}$  = The accordance of the formulas to determine the characteristic value
- $\gamma_M$  = The material safety factor

The partial material factor ( $\gamma_M$ ) of the connection should be assumed as 1,0 in the ductile design [9] as recommended in [27]. The 5<sup>th</sup> percentile and the 95<sup>th</sup> percentile of the bearing resistance are found by using the formulas according to EN 14358 [23].

$$\bar{y} = \frac{1}{n} \cdot \sum_{i=1}^n \ln(x_i) \quad (12) \quad f_{0.05} = e^{\bar{y} - k_s \cdot s_y} \quad (14)$$

$$s_y = \sqrt{\frac{1}{n-1} \cdot \sum_{i=1}^n (\ln(x_i) + \bar{y})^2} \quad (13) \quad f_{0.95} = e^{\bar{y} + k_s \cdot s_y} \quad (15)$$

All of the test specimens with a diameter of 12 mm had the same dimensions and were reinforced. Hence the bearing resistance of one single dowel was calculated per test series. Therefore 11 tests were available for the statistical calculation. The fractile factor  $k_s$  is given as 2.08 according to [23]. The evaluation shows that within this consideration the European Yielding Model [8] [26] slightly

**Table 1:** Statistical data to evaluate the overstrength factor  $\gamma_{Rd}$

Experiment	n	$k_s$	$F_{v,k}$ [26] [kN]	$F_{0.05}$ [kN]	$F_{0.95}$ [kN]	$\gamma_{an}$	$\gamma_{sc}$	$\gamma_{Rd}$
dowel Ø 12mm	11	2.08	26.36	24.71	33.64	0.94	1.36	<b>1.28</b>

underestimates the 5<sup>th</sup> percentage of the conducted experiments ( $\gamma_{an} < 1.0$ ). The experimental results show a large scattering of the experimental results ( $\gamma_{cs} > 1.0$ ). Therefore the scattering within the bearing resistance of the connection gives a large contribution to the overstrength factor. The overstrength factor found by [9] ranges between 1.2 and 1.85. The determined factor of 1.28 is due to the reinforcement on the lower border of the range found by [9] on unreinforced timber to timber connections. Therefore the determined factor is lower as the recommended factor of 1.6 by [9].

### 3.3 Requirements on the beam end-rotation

Within the elastic-plastic design method it is necessary to compare the required rotation capacity with the existing capacity of the joint. Since the modulus of elasticity scatters within a timber element the influence of the material scattering on the beam end rotation is analyzed [4]. A factor  $k_{mat}$  is



**Figure 11:** Beam model to investigate the influence of the modulus of elasticity

introduced to the verification of the rotation to consider the material scattering.

$$k_{\text{mat}} \cdot \phi_{\text{req}} \leq \phi_{\text{exist}} \quad (16)$$

The differential equation of the bending line is solved with the numerical integration for certain bending moment distributions. A computer model has been developed based on [6] to quantify the influence of the scattering modulus of elasticity. The single lamella of a glulam beam has been divided into 150 mm long cells. Each cell allocates a statistically assigned modulus of elasticity. Figure 11 shows the different magnitudes of the modulus of elasticity in different colours. Table 2 displays the

**Table 2:** Input data of statistical evaluation

Input data	Magnitude
$E_{0,mean}$	$11600 \frac{N}{mm^2}$ [19]
COV of each board	0.13 [7]
COV within each board	0.069 [5]
Number of each calculation	100000

input data of the developed computer program. Within every step in length 100000 calculations were performed with a changing modulus of elasticity based on [7, 5]. The statistical distribution of the modulus of elasticity within the single lamella is assumed as lognormal distributed [5], and among the lamellae as normal distributed [7].

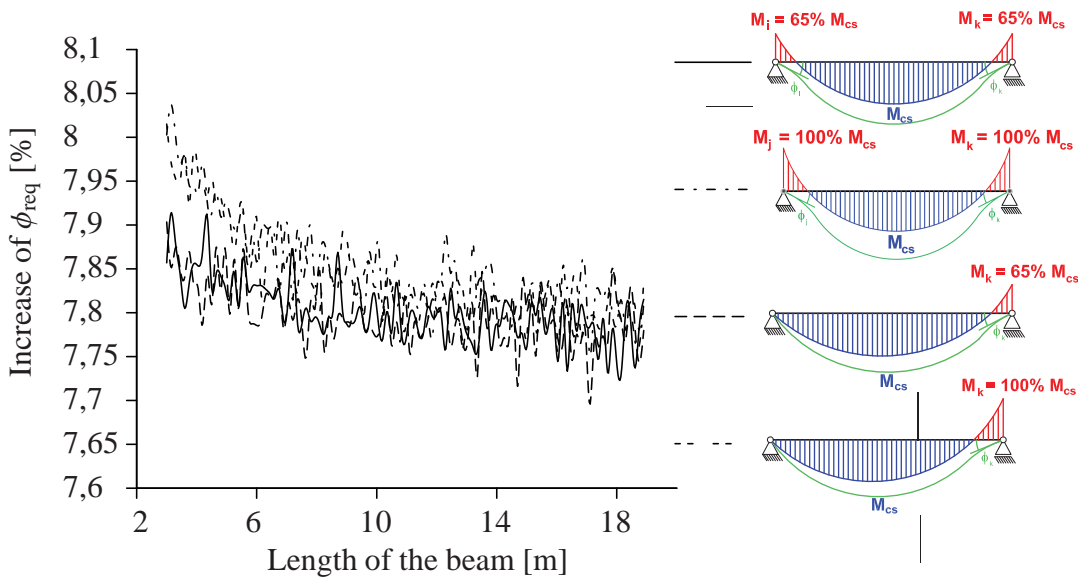


**Figure 12:** Increase of the required rotation for different bending moment distributions

Figure 12 shows the increase of the required rotation depending on various bending moment distributions of a beam element. The scattering of the modulus of elasticity has a direct influence on the beam end rotations. Considering a scattering of the modulus of elasticity within a beam element the required beam end rotation increases of about 8% depending on the length of the beam element. Therefore a factor  $k_{\text{mat}}$  of 1.10 is proposed to prove the required rotation (comp. Eq. (16)).

## 4 Conclusions

Based on the experiments it has been shown, that a ductile behavior cannot only be achieved under an axial load but also under a bending moment. A mechanical model, based on the component method, has been introduced to describe the moment rotation behavior of a joint. This model was simplified to give an approach for the practical application.

To consider the scattering of the material properties an overstrength factor was determined to ensure, that a ductile behavior occurs before a brittle element fails. The influence of the material scattering on the beam end rotations has been determined based on the bending line. It was found that the required beam end rotations should be increased of about 10% compared to a homogenous calculation.

The opportunity to calculate the available rotational capacity of joints based on the component model and the possibility to consider the material scattering open up the elastic-plastic design method in timber structures.

## Acknowledgement

This research work (16184N) within the International Association for Technical Issues related to Wood (iVTH e.V.), is supported in the program of “Industriellen Gemeinschaftsforschung (IGF)” and financed by the German Federation of Industrial Research Association (AiF) [13]. Furthermore we would like to thank “Deutschen Institut für Bautechnik (DIBt)” for their support [12].

## References

- [1] BEJTKA, I.: *Verstärkungen von Bauteilen aus Holz mit Vollgewindeschrauben*, Universität Karlsruhe, Lehrstuhl für Ingenieurholzbau und Baukonstruktionen, Diss., 2005
- [2] BLAß, H.-J. ; BEJTKA, I. ; UIBEL, T.: *Tragfähigkeit von Verbindungen mit selbstbohrenden Holzschrauben / Lehrstuhl für Ingenieurholzbau und Baukonstruktionen, Universität Karlsruhe (TH). Universitätsverlag Karlsruhe, 2006. – Karlsruher Berichte zum Ingenieurholzbau, Issue 4*
- [3] BRUEHL, F. ; KUHLMANN, U.: *Connection ductility in timber structures considering the moment-rotation behavior. In: World Conference on Timber engineering. Auckland, New Zealand, July 2012*
- [4] BRUEHL, F. ; KUHLMANN, U. ; JORISSEN, A.: *Consideration of plasticity within the design of timber structures due to connection ductility. In: Structural Engineer 33 (2011), p. 3007–3017*
- [5] COLLING, F. ; SCHERBERGER, M.: *Die Streuung des Elastizitätsmoduls in Brettschichtholz. In: Holz als Roh- und Werkstoff 45 (1987), p. 95–99*

- [6] EHLBECK, J. ; COLLING, F. ; GÖRLACHER, R.: Einfluss keilgezinkter Lamellen auf die Biegefestigkeit von Brettschichtholzträgern Teil 1: Entwicklung eines Rechenmodells. In: *Holz als Rohstoff* 43 (1985), p. 333–337
- [7] JCSS - JOINT COMMITTEE ON STRUCTURAL SAFETY: Probabilistic Model Code. Part 3: Resistance Models. 2006 (3.5 Properties of timber). – research report
- [8] JOHANSEN, K. W.: Theory of timber connections. In: *IABSE-International Association for Bridge and Structural Engineering* 9 (1949), p. 249–262
- [9] JORISSEN, A. ; FRAGIACOMO, M.: General notes on timber ductility. In: *Structural Engineer* 33 (2011), p. 2987–2997
- [10] JORISSEN, A. ; FRAGIACOMO, M.: Ductility in timber structures. In: *Proceedings of the meeting No. 43 of Working Commission W18 - Timber Structures, CIB*, Nelson, New Zealand, 2010
- [11] KUHLMANN, U. ; ALDI, P.: Ermüdungsfestigkeit von Holz-Beton-Verbundträgern im Staßenbrückenbau / Institut für Konstruktion und Entwurf. 2010. – final report, research program on behalf of DGfH/iVTH, supported by AiF, research report AiF 15052 N
- [12] KUHLMANN, U. ; BRÜHL, F.: Robuste Holztragwerke durch duktile Anschlüsse mit stiftförmigen Verbindungsmitteln / Deutsches Institut für Bautechnik DIBt. 2011. – research report
- [13] KUHLMANN, U. ; BRÜHL, F.: Vorteilhaftes Bemessung von Holztragwerken durch duktile, plastische Anschlüsse / Institut für Konstruktion und Entwurf. 2012. – final report, research program on behalf of iVTH, supported by AiF, research report AiF 16184 N
- [14] MUÑOZ, W. ; MOHAMMAD, M. ; SALENIKOVICH, A. ; QUENNEVILLE, P.: Need for a harmonized approach for calculations of ductility of timber assemblies. In: *Proceedings of the meeting No. 41 of Working Commission W18 - Timber Structures, CIB*, St. Andrews, Canada, August 2008
- [15] PAULAY, T. ; PRIESTLEY, M.J.N.: *Seismic design of reinforced concrete and masonry buildings*. John Wiley & Sons, Inc., 1992
- [16] SCHICKHOFER, G. ; AUGUSTIN, M. ; JEITLER, G.: Einführung in die Verbindungstechnik mit Stabdübeln, Schrauben und eingeklebten Stahlstangen. In: *6. Grazer Holzbau-Fachtagung*, 2007
- [17] SMITH, I. ; ASIZ, A. ; SNOW, M. ; CHUI, I.H.: Possible Canadian / ISO approach to deriving design values from test data. In: *Proceedings of the meeting No. 39 of Working Commission W18 - Timber Structures, CIB*, Florence, Italy, August 2006
- [18] WERNER, H.: *Tragfähigkeit von Holz-Verbindungen mit stiftförmigen Verbindungsmitteln unter Berücksichtigung streuender Einflussgrößen*, Universität Fridericiana zu Karlsruhe, Diss., December 1993

## Standards

- [19] DIN 1052: *Entwurf, Berechnung und Bemessung von Holzbauwerken - Allgemeine Bemessungsregeln für den Hochbau*. DIN-Deutsches Institut für Normung e.V., 2008
- [20] E DIN EN 14080: *Holzbauwerke - Brettschichtholz und Balkenschichtholz - Anforderungen; deutsche Fassung prEN 14080:2011*. DIN-Deutsches Institut für Normung e.V., 2011

- [21] EN 10025-2: *Hot rolled products of structural steels. Technical delivery conditions for - non-alloy structural steels*. European Committee for Standardization (CEN), Brussels
- [22] EN 12512: *Timber structures - Test methods - Cyclic testing of joints made with mechanical fasteners*. European Committee for Standardization (CEN), Brussels
- [23] EN 14358: *Timber structures - Calculation of characteristic 5-percentile values and acceptance criteria for a sample*. European Committee for Standardization (CEN), Brussels, 2006
- [24] EN 1991-1-7: *Eurocode 7: Actions on structures; Part 1-7: General actions - Accidental actions*. European Committee for Standardization (CEN), Brussels
- [25] EN 1993-1-8: *Eurocode 3: Design of steel structures - Part 1-8: Design of joints*. European Committee for Standardization (CEN), Brussels
- [26] EN 1995-1-1: *Eurocode 5: Design of timber structures; Part 1-1: General - Common rules and rules for buildings*. European Committee for Standardization (CEN), Brussels
- [27] EN 1998: *Eurocode 8: Design of structures for earthquake resistance*. European Committee for Standardization (CEN), Brussels
- [28] EN 26891: *Timber structures - Joints made with mechanical fasteners - General principles for the determination of strength and deformation characteristics*. European Committee for Standardization (CEN), Brussels
- [29] SIA 265: *Holzbau*. Schweizerischer Ingenieur- und Architektenverein, 2003

**INTERNATIONAL COUNCIL FOR RESEARCH AND INNOVATION  
IN BUILDING AND CONSTRUCTION**

**WORKING COMMISSION W18 - TIMBER STRUCTURES**

**BUILDING CLIMATE – LONG-TERM MEASUREMENTS TO  
DETERMINE THE EFFECT ON THE MOISTURE GRADIENT IN  
LARGE-SPAN TIMBER STRUCTURES**

P Dietsch

A Gamper

M Merk

S Winter

Lehrstuhl für Holzbau und Baukonstruktion  
Technische Universität München

GERMANY

**MEETING FORTY FIVE**

**VÄXJÖ**

**SWEDEN**

**AUGUST 2012**

---

Presented by P Dietsch

J Köhler commented that the work was useful and had agreement with his own results. G Schickhofer commented that the work was important and asked about using different  $k_{mod}$  factors for different cases. He also asked for comments on the use of reinforcement. P Dietsch responded that this was a balance between scientific knowledge. This was important for large span glulam structures with beams of large widths. The type of reinforcement must consider its suitability in high moisture conditions. S Aicher questioned the conclusion that the timber should be produced to the moisture condition of use. This point is already in the code but never followed in practice. F Lam asked why correction to low moisture contents were not done as the study had such information. P Dietsch replied that the data was not suitable for this consideration because different types of wood were involved. S Winter stated that in combination with precipitation the erection time of the building was also important.



# Building Climate – long-term measurements to determine the effect on the moisture gradient in large-span timber structures

P. Dietsch, A. Gamper, M. Merk, S. Winter  
Lehrstuhl für Holzbau und Baukonstruktion  
Technische Universität München, Germany

## 1 Introduction and Objective

The reaction of wood to moisture forms an integral part of any task in connection with this natural and renewable building material. This also applies to the planning, execution and maintenance of buildings built with wood or wood-based products. From logging the tree to the anticipated use, e.g. as a structural element, wood will go through various phases of processing and shape in which it is subjected to varying environmental conditions. Their influence on the wood moisture content can be illustrated by the “moisture chain”, sketched in Figure 1.

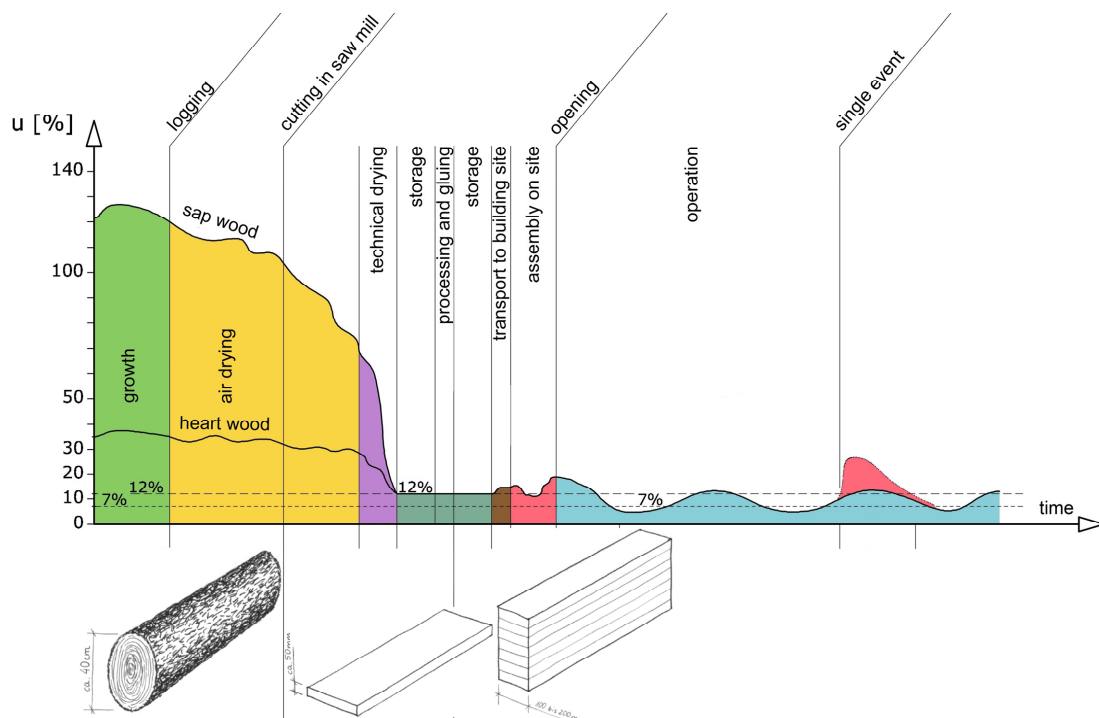


Figure 1: Sketch of a possible „moisture chain“, i.e. exposure to moisture from the tree to glued-laminated timber elements in the building

Changes in wood moisture content lead to changes of virtually all physical and mechanical properties (e.g. strength and stiffness properties) of wood. In EN 1995-1-1 [1], this is accounted for by classifying the timber elements into one of three possible service classes according to the climatic conditions during the design service life. An additional effect of changes of the wood moisture content is the associated shrinkage or swelling of the material. Since the outermost sections of the wood cross-sections will adapt to the climatic conditions at first, the resulting moisture gradient and the associated shrinkage or swelling will lead to internal stresses in the cross-section. If these stresses locally exceed the very low tension perpendicular to grain strength of wood, the result will be a stress relief in form of cracks which can reduce the load-carrying capacity of structural timber elements in e.g. shear or tension perpendicular to the grain. The evaluation of damages in large-span timber structures ([2] - [4]) shows that a prevalent type of damage is pronounced cracking in the glue lines and lamellas of glulam timber elements. Figures 2 and 3 show the types of damage and causes of damage deduced from the dataset of 245 assessments of large-span timber structures, which were evaluated at the Chair for Timber Structures and Building Construction. Almost half of the damages can be attributed to low or high moisture content or severe changes of the same. The total number of damages and causes of damage exceed the total number of structures since a structure can contain more than one type of damage.

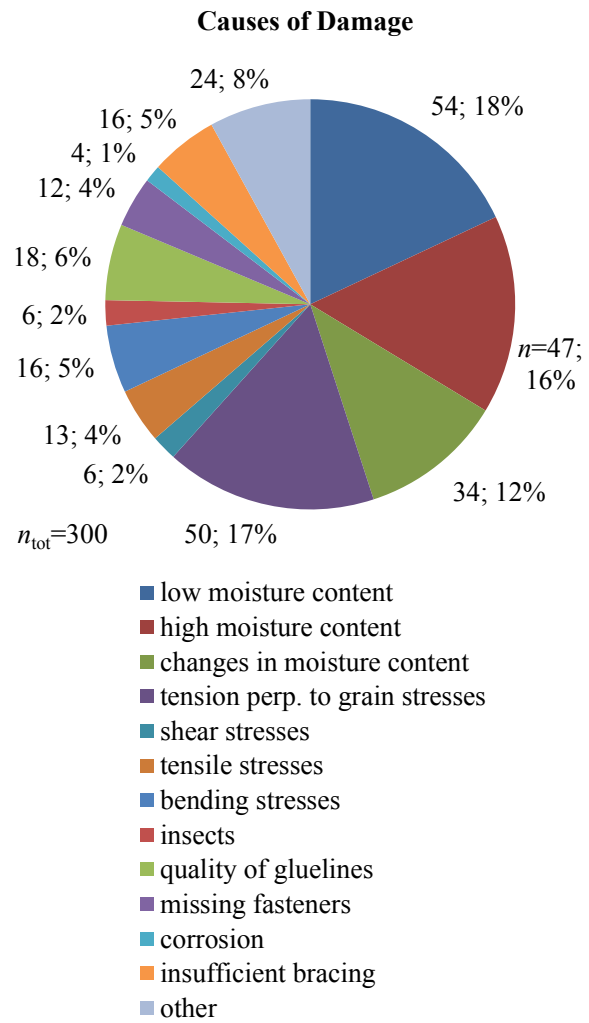
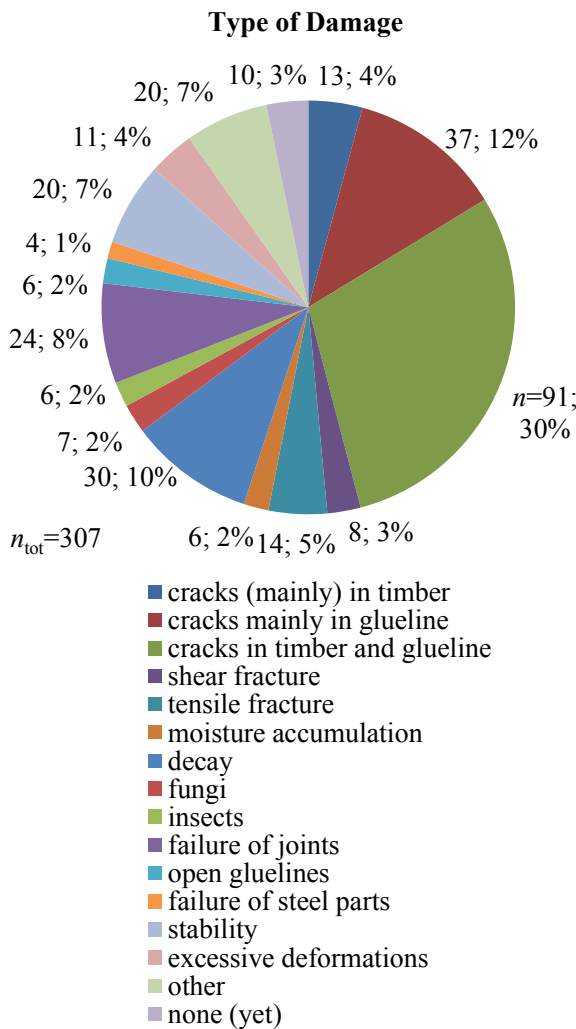


Figure 2: Type of damage from an evaluation of 245 assessments of large-span timber structures [5]

Figure 3: Causes of damage from an evaluation of 245 assessments of large-span timber structures [5]

Low or high moisture contents or severe changes of the same could sometimes be attributed to local conditions (e.g. roof leakage) but in the majority of cases, they could be explained by the climatic conditions, depending on the construction type and use of the building, and seasonal variations of the building climate. Figure 4 contains timber moisture content and climatic conditions for all structures for which such information was obtained during the assessment of the building. If multiple measurements of moisture content were taken, the given value represents the mean of these measurements. If measurements were taken at different depths, the mean of the near-surface measurements (mostly at 15 mm depth) is given. All evaluated measurements represent snap-shots of the situation at the date of assessment. They do neither give indications on the timber moisture content at the opening of the building (beginning of operation) nor on seasonal variations of the same. The measured timber moisture contents for buildings in Service Class 1 [1] show pronounced variations around a mean value of  $u = 10.7\%$ . The corresponding measurements of temperature and relative humidity feature a pronounced variation as well. Structural elements in Service Class 2 show smaller variations ( $u_{\text{mean}} = 14.9\%$ ). Structural elements in Service Class 3 unsurprisingly feature large variations of timber moisture content ( $u_{\text{mean}} = 22.4\%$ ) and building climate. The mean values of timber moisture content in dependence of the Service Class correspond well with the values compiled in [2].

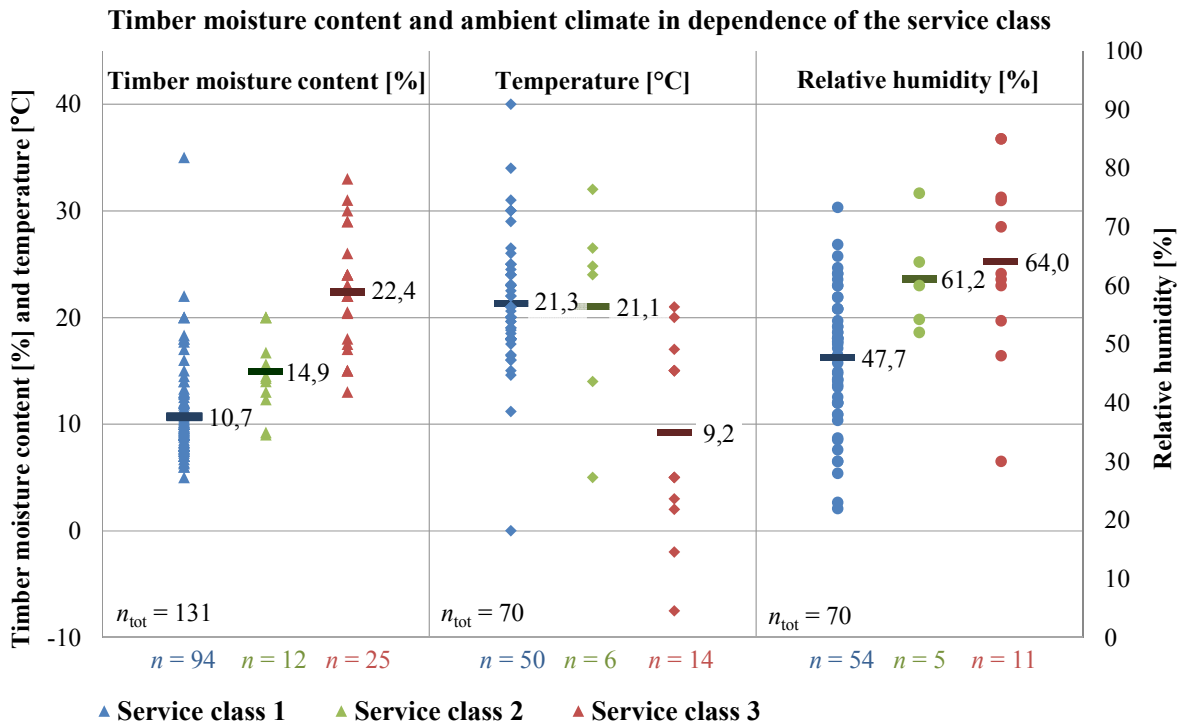


Figure 4: Timber moisture content and ambient climate in dependence of the service class, from the evaluation of 245 assessments of large-span timber structures [5]

The large variations in timber moisture content, temperature and relative humidity for buildings in Service Class 1 can partly be traced back to the diversity of types of use of these buildings. A differentiation of timber moisture content in dependence of the building use is given in Figure 5. This comparison only contains types of use for which a minimum of three buildings could be evaluated. The timber moisture contents in closed and heated buildings are oftentimes noticeably low. If structural elements, featuring high timber moisture contents due to deficient roof structures were excluded, the mean values of timber moisture content in closed and heated buildings would all fall below  $u = 10\%$ . 47% of the evaluated structures featured timber elements with moisture contents below 10%. The

mean values determined for riding rinks ( $u_{\text{mean}} = 18.2\%$ ) and ice-skating rinks ( $u_{\text{mean}} = 21.6\%$ ) support their categorization in Service Class 2 respectively Service Class 3 [6].

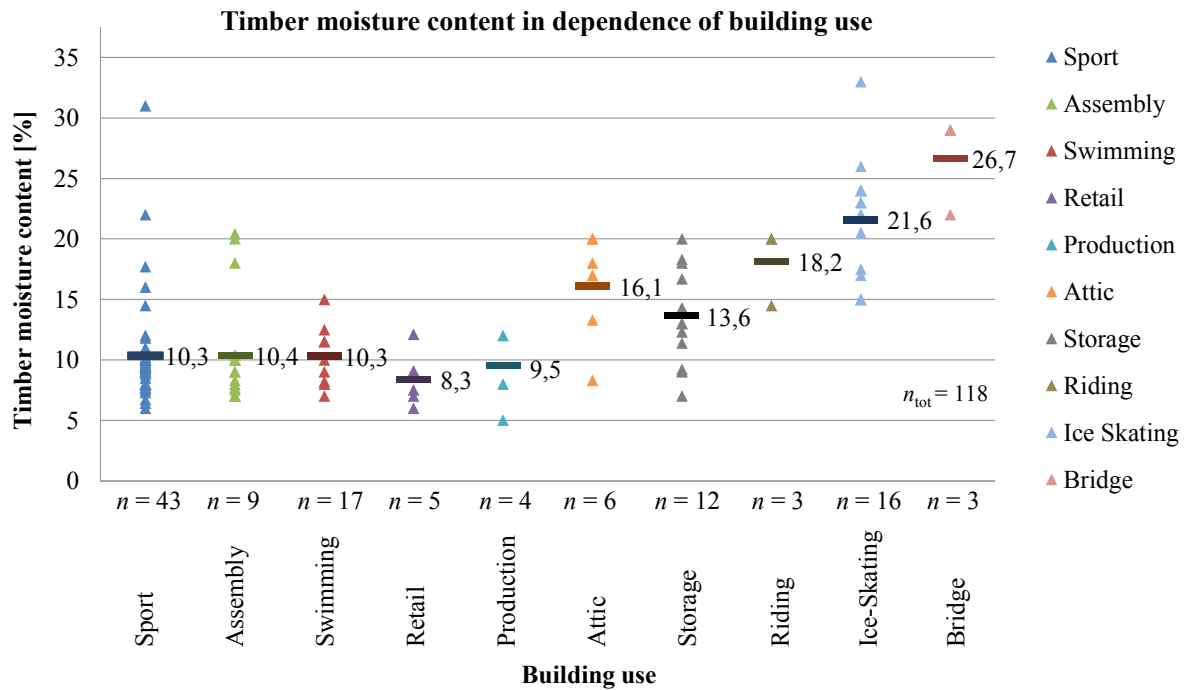


Figure 5: Timber moisture content in dependence of the type of building use, from an evaluation of 245 assessments of large-span timber structures [5]

Information on the sequence and magnitude of seasonal variations can only be obtained through long-term measurements of climate data (temperature, relative humidity) and timber moisture content. In the case of (large-span) timber structures, the measurement of moisture in different depths of the cross-section is of particular interest to draw conclusions on the magnitude and velocity of adjustment of the moisture distribution to changing climatic conditions. Although past research projects covered the long-term measurement of timber moisture content and/or temperature and relative humidity [7] – [14], none of them was carried out under the objective to enable a comparison between timber structures in large buildings of different types of use. The same is valid for the long-term measurement of moisture content at different depths on structural timber elements in-situ (phase “operation” in Figure 1). Both objectives should be covered within the research project presented.

## 2 Realisation of the research project

### 2.1 Chosen types of use and choice of objects

Within the research project, long-term measurements of timber moisture content, temperature and relative humidity in a total of 21 objects (halls with large-span timber roof structures) with seven different types of use (see Table 1) were realized. While all objects in uses “indoor swimming pool”, “gymnasium” and “production and sales” were heated and featured closed building envelopes, all objects in uses “riding rink”, “agriculture” and “warehouse” were unheated and featured partly open building envelopes. In the case of ice-skating rinks, only closed objects (climatized and non-climatized) were chosen since results for open or partly open ice-rinks are already available [11], [13]. When selecting the

objects, attention was given to cover the typical types structural systems for large-span timber roof structures. Only structures featuring softwood glulam with at least 140 mm width were included. In each object, the data was collected at two different points of measurement in order to capture possibly varying climatic conditions, e.g. due to solar radiation or the influence of heating systems. All necessary information for each object (e.g. building envelope, environmental conditions, climatization, structural system, element dimensions, surface treatment and position of the points of measurement) was prepared in separate building information sheets, including ground view, sectional view and photo documentation.

Table 1: Chosen types of use and number of objects in each use

Use	Number	Use	Number
Indoor swimming pool	3	Production and Sales	2
Ice rink	4	Agriculture (livestock)	3
Riding rink	3	Warehouse	3
Gymnasium	3	Total	21

## 2.2 Chosen method of measurement and verification of measured data

The electrical resistance measurement method was chosen for the measurements of the timber moisture content since this method constitutes a reliable and widely applied method, allowing for the non-destructive measurement of moisture gradients across the cross-section at one specific location (see e.g. [15]).

On this basis, a measuring system was developed in cooperation with the project partner. The system had to be able to cover moisture contents in the low range which implies the measurement of high electrical resistances (e.g. 6 % MC in spruce  $\approx 10^{12} \Omega$ ). Subsequently, the chosen system, was installed on test specimens of glued-laminated timber from spruce and exposed to very dry, very humid and varying climate in the climate chambers of the materials testing laboratory at the Technische Universität München. The moisture contents were continuously measured with the measurement equipment and compared to the results of cyclic measurements with a calibrated reference moisture meter (GANN Hydromette RTU 600). There was neither a significant difference in the results of the two measurement systems, nor when using different types of electrodes. For further verification, two independent series of 4 x 6 test specimens from spruce ( $L \times B \times H = 85 \times 60 \times 30$  mm) were produced and stored under four different controlled climatic conditions (20° C / 33 % RH; 20° C / 65 % RH; 20° C / 85% RH and 20° C / 100 % RH) which were realized by saturated saline solutions. For the very dry climate, only a relative humidity of about 45 % could be reached. This is explained by the industrial quality of the saline solution in combination with the fact that complete air-tightness of the container could not be achieved.

After the specimen had reached constant weight, their moisture content was measured with the chosen moisture meter (Scantronik Gigamodule) and two reference meters (GANN Hydromette RTU 600 and Greisinger GMH 3850). By subsequent kiln-drying, the actual moisture content was determined. Within the range of timber moisture content measured during this research project ( $u_{\max} = 19$  %), good agreement was obtained for moisture contents between 12 % and 18 %, see Figure 6. Maximum absolute deviations in moisture content of 1.3 % were measured for the dry specimen, whereby the chosen moisture meter as well as the reference moisture meter tend to underestimate the actual moisture content at low ranges.

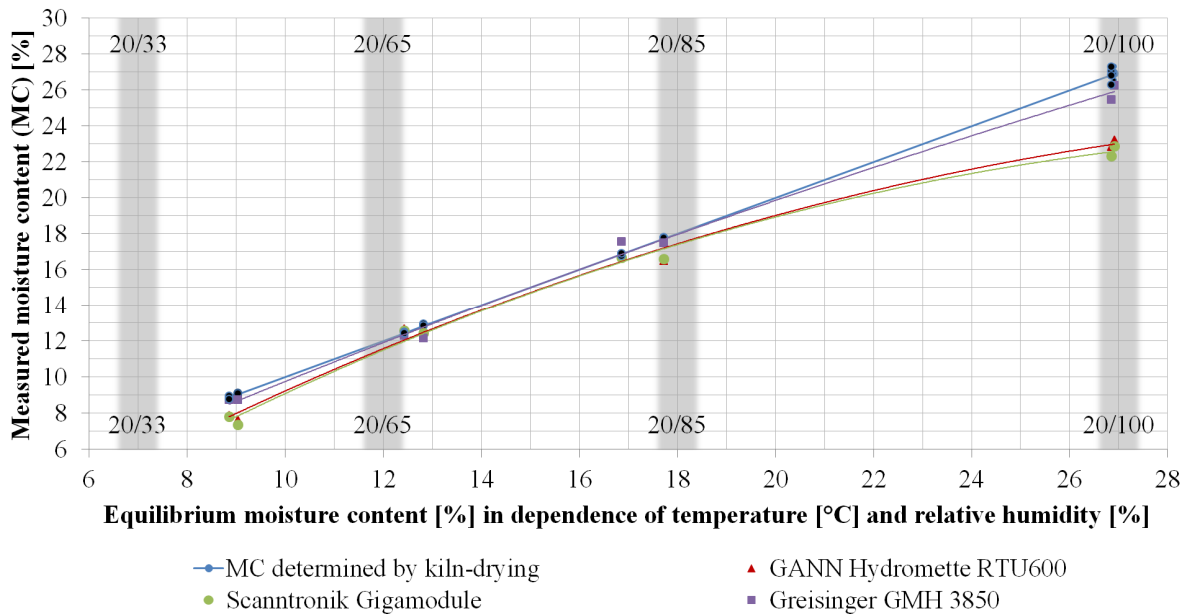


Figure 6: Results of the laboratory tests to verify the results obtained by chosen method for long-term measurements (resistance method – Scantronik Gigamodule)

## 2.2 Installation of measuring equipment, readout and processing of data

At each point of measurement, four pairs of teflon-isolated electrodes (GANN) with varying length were installed to enable the measurement of moisture content in clearly defined depths of the cross-section. To prevent erroneous measurements in case of surface condensate, the heads of the electrodes were also partly teflon-isolated, see Figure 7. For exact positioning of the electrodes in one lamella, ideally perpendicular to the grain, a drill guide featuring two diameters for each depth was used in connection with a drilling template. The ram-in electrodes were connected to the moisture meter by custom-built, shielded coaxial cables. The moisture meter developed in cooperation with the project partner enables the determination of moisture content at up to eight channels. The measurements which were generated every hour at both points of measurement were subsequently transmitted to a data logger. The climate data was recorded via a second data logger in combination with a sensor unit for relative humidity and air temperature. In addition, the surface temperatures at the two points of measurement were recorded to allow for the temperature compensation of the moisture content, see Figure 7.

After installation of the measuring equipment at two locations of the roof structure in each of the 21 objects, the data stored in the data loggers was read out three times over the measurement period. A manual readout was preferred to remote transmission since it could be combined with a reference measurement with another moisture meter, a function control as well as a control of the point of measurement itself. During these controls and the subsequent data analysis, a few notable issues were observed. In the indoor swimming pools, the chlorous climate resulted in accelerated corrosion and temporary malfunction of the climate sensors, necessitating their exchange. In ice-skating rink “B2”, a power line, although attached to the opposite side of the beam, led to an occasional shifting of the measurements for the duration of a few hours. Condensation around the point of measurement in objects “C3” and “G1” caused a short-circuit between the non-isolated plug-connections of the electrodes, resulting in a temporary deviation of the measurements for the duration of a few days. In all cases, the respective data was ignored and linear

interpolation was applied between the last and first set of correct measurements.

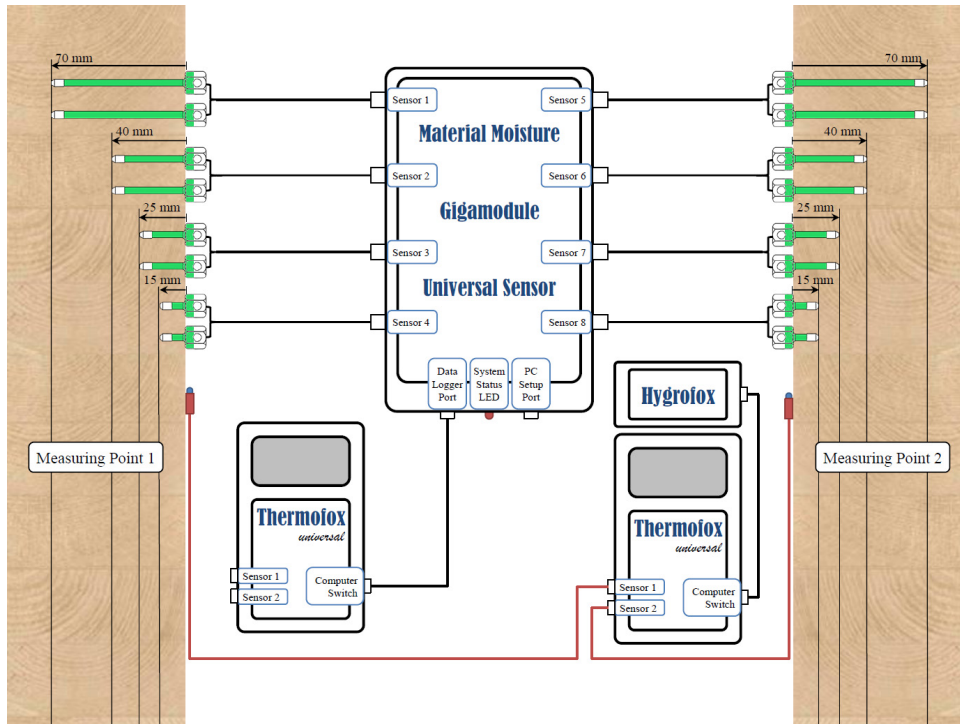


Figure 7: Systematic presentation of the measuring equipment

To analyze the data, a program on the basis of Excel was developed which made it possible to read the large amounts of data at the end of the planned duration of measurement and to further process and graphically illustrate the data in different charts. When converting the raw data, i.e. measurements of electrical resistance into timber moisture contents, a compensation of the effect of temperature was undertaken. For this, the actual material temperatures in the different depths were calculated from the measured surface temperatures, using the explicit Euler method [16] in combination with values for thermal conductivity given in e.g. [17] (see also [18], [19]). A modification of the measured timber moisture content with respect to the differences to the values determined by kiln-drying, observed during the laboratory tests, was not undertaken.

For comparative reasons, the measurements of relative humidity and temperature were used to determine the equilibrium moisture content prevailing in the cross-section near the surface as a moving average over ten days. This was done by applying the theoretical model of Hailwood & Horrobin [20] in combination with the coefficients determined by [21] (see also [18]). The influence of surface treatments which were present on the timber roof structure of ice-skating rinks “B1” and “B4” was not considered since the type of treatment could not be determined unambiguously.

### 3 Results

#### 3.1 Processing and representation of results

Within the evaluation period from 1 October 2010 to 30 September 2011, a total of over 2.2 million readings were collected and analyzed by means of a specially developed program. The data read from the data loggers was prepared as curves (time series) of relative and absolute humidity and temperature at the location of measurement over time,

see Figure 8. The same type of representation was chosen for the measurements of timber moisture content in the four depths of the cross-section, see Figure 9. This figure also contains the calculated equilibrium moisture content.

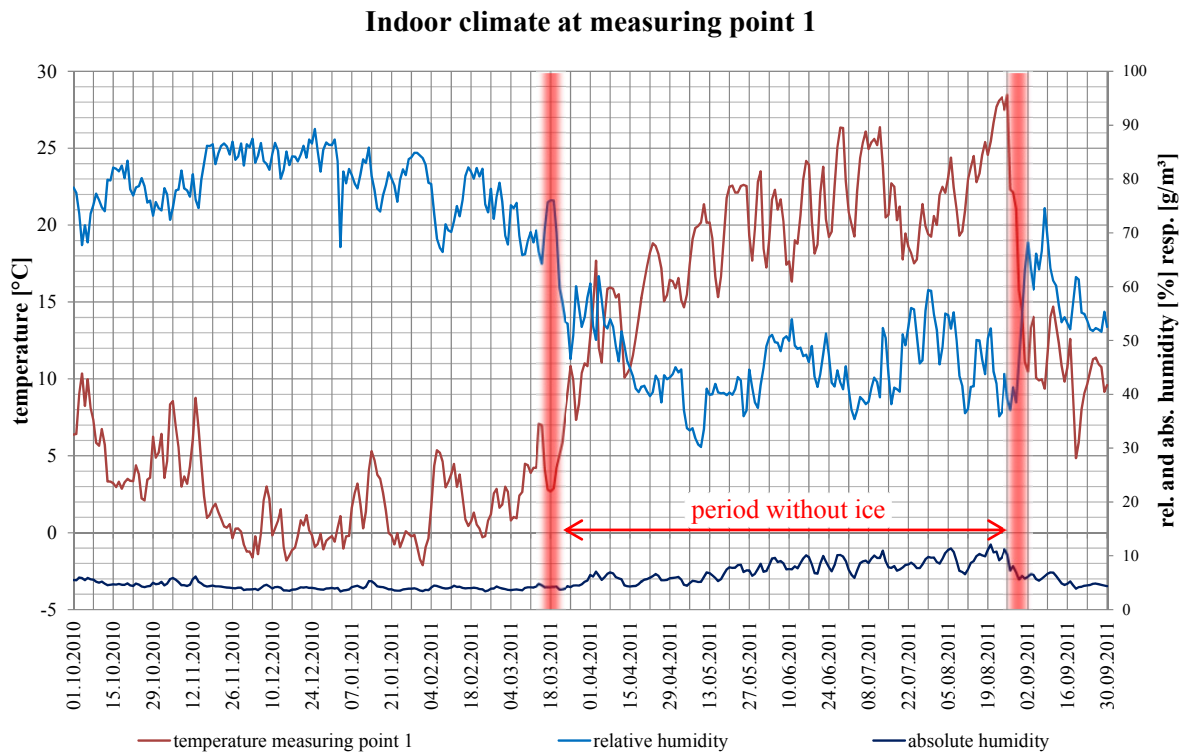


Figure 8: Variation of the relative and absolute humidity and the reference temperature over the measurement period, exemplary given for the ice rink in Buchloe

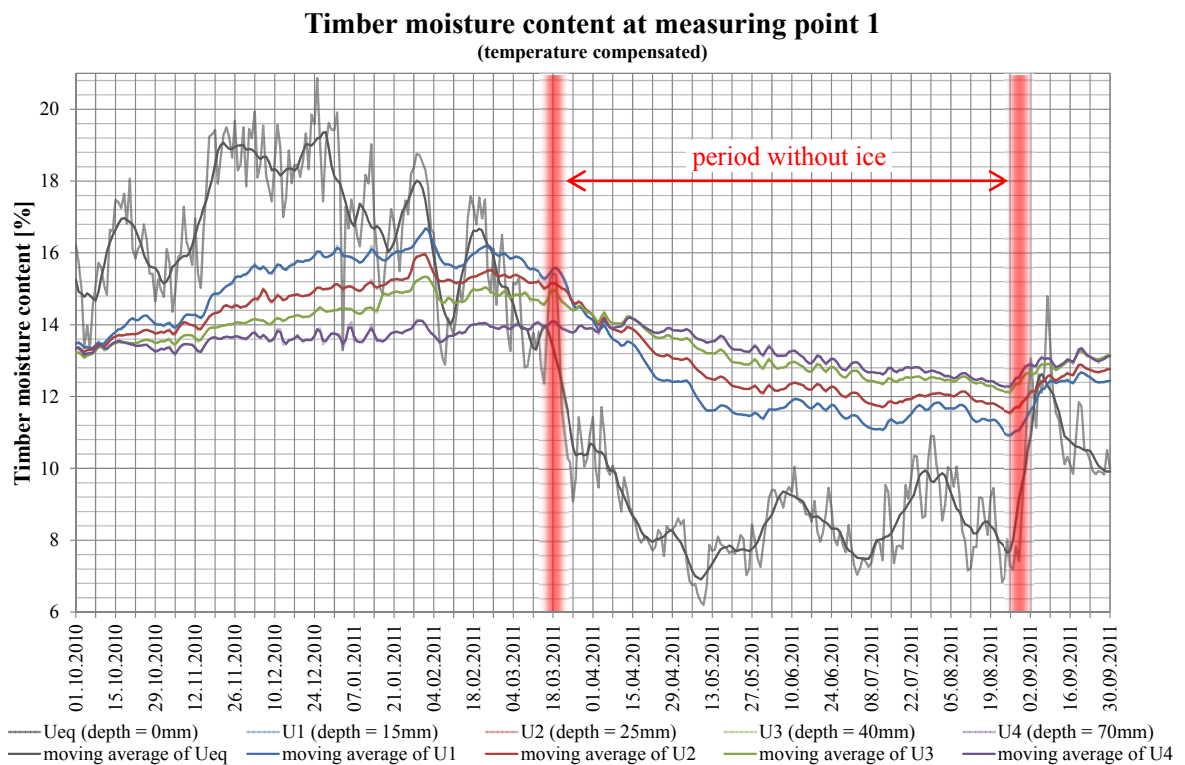


Figure 9: Variation of timber moisture content at different depths of the cross-section over the measurement period, exemplary given for the ice rink in Buchloe

In addition, graphical representations over the cross section were derived for the timber moisture content. This type of representation allows to create envelope curves of minimum and maximum timber moisture contents, see Figure 10, as well as envelope curves of minimum and maximum timber moisture gradient  $\text{grad}(u) = du / dx$ , see Figure 11. The graphical representations confirm the damped and delayed adaptation of timber moisture content with increasing depth.

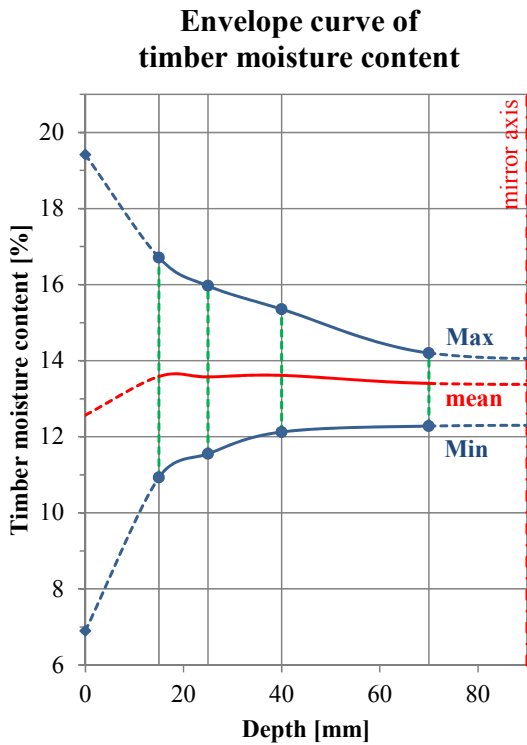


Figure 10: Envelope curve of the timber moisture content at different depths of the cross section, exemplary given for the ice rink in Buchloe

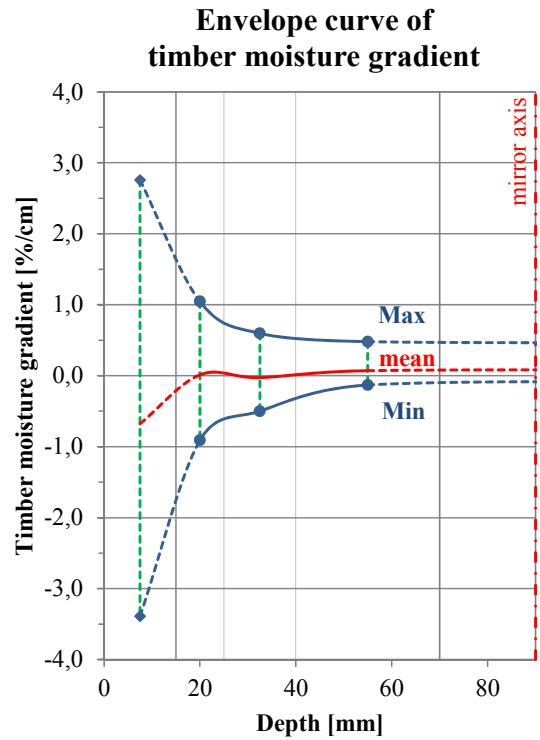


Figure 11: Envelope curve of the timber moisture gradient at different depths of the cross section, exemplary given for the ice rink in Buchloe

### 3.2. Results and remarks with regard to the different types of use

In the following, a summary of the results of all objects will be given in tabular format, see Table 2. This type of representation was chosen since a graphical representation is directly comprehensible but does not allow for a quick and concise overview of the results of all objects. For the graphical representations, the interested reader is kindly referred to the final report [22] of the research project. The table contains the mean values of relative humidity and temperature (both based on daily mean values) as well as the mean value of timber moisture content, averaged across all depths. In addition, the maximum amplitude, i.e. the difference between maximum and minimum value measured during the evaluation period, is given for all parameters. For the timber moisture content, the maximum gradient between two depths as well as the maximum difference in timber moisture content between the outermost (15 mm) and the innermost point of measurement (70 mm) is given. Figure 12 contains a graphical explanation of all data given in Table 2.

A comparison of the results of the individual types of building use confirms the expected large range of possible climatic conditions in buildings with timber structures. Evaluated for all types of use, the average timber moisture contents were between 4.4 % and 17.1 %.

As expected, the moisture gradients are lower in insulated and heated buildings than in non-insulated, partly open buildings with stronger influence of the naturally varying outdoor climate. If not explicitly stated, the numerical values of timber moisture content, temperature and relative humidity given in the following, represent mean values.

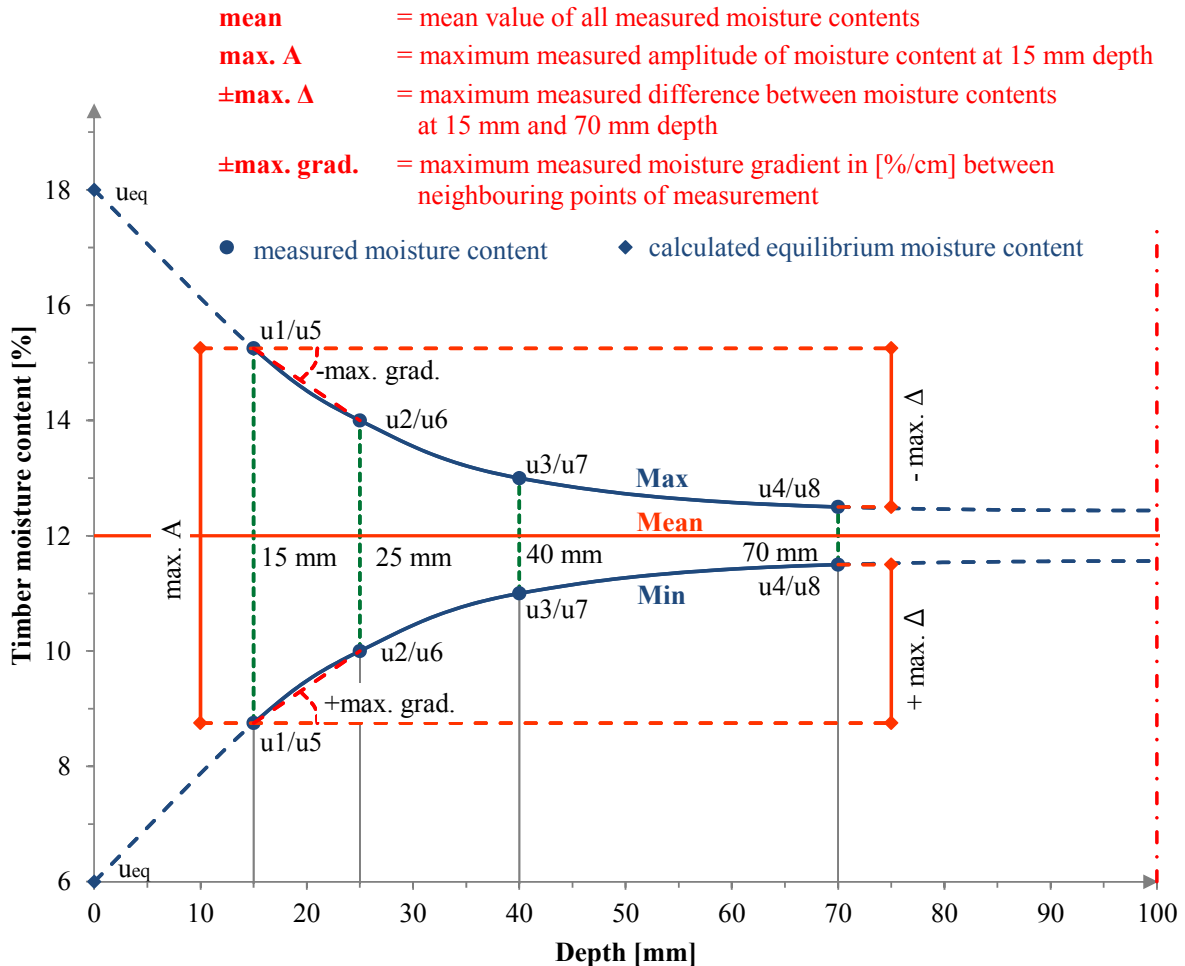


Figure 12: Sketch of envelope curve of moisture contents in the timber cross-section including notation of analyzed parameters

Very constant climatic conditions ( $T \approx 30^{\circ}\text{C}$ , 50 % RH) were found for indoor swimming pools (objects “A1” and “A3”) during standard operation. The timber moisture content featured small variations and small gradients. Transition zones to the outside air (object “A2”) represent an exception due to the lowering of the temperature which results in higher and more fluctuating relative humidity and timber moisture content.

In gymnasiums (objects “D”), constant climate was observed as well. The relative humidity was between 40 % and 50 % and since all objects were heated, the temperatures mostly remained constant at about  $20^{\circ}\text{C}$ . This resulted in constant timber moisture contents between 8 % and 10 % and very small moisture gradients. Object “D1” represents an exception since the roof structure is situated in a shed roof with skylights. This resulted in high temperatures and low relative humidities (RH = 28 %). The respective structural elements were very dry (MC of 4 % - 6 %). It should be noted that the measuring equipment tends to slightly underestimate the moisture contents at the low range, see section 2.2.

The climate in both objects “E - production and sales facilities” is only partially comparable due to their different type of use. Both halls are non-insulated and partly open

but due to the heating system, the influence of the outside climate on temperature and relative humidity are damped. Therefore the timber moisture gradient was relatively constant. In object “E2”, the metal processing and ironwork resulted in high temperatures below the roof (temporarily above 30°), combined with very low relative humidities (temporarily below 20 %). The resulting timber moisture content was about 5 %.

Table 2: Numerical summary of results of measurements

Object	Moisture content at measuring point 1						Moisture content at measuring point 2						Temperature		rel. Humidity	
	mean	max. A	±max. Δ	±max. grad.	mean	max. A	±max. Δ	±max. grad.	mean	max. A	±max. Δ	±max. grad.	mean	max. A	mean	max. A
	[% MC]			[%/cm]			[% MC]			[%/cm]			[°C]		[% rh]	
A1	8,75	1,44	+0,05	-1,01	+0,18	-0,11	9,26	1,23	+0,22	-0,36	-0,03	-0,49	29,68	6,67	48,26*	6,75*
A2	16,09	1,68	+0,52	-1,39	+0,36	-0,55	14,96	2,62	+0,66	-1,60	+0,27	-1,31	28,72	6,04	88,60*	19,40*
A3	8,67	1,83	-2,32	-4,73	-0,66	-1,41	7,70	1,89	-0,21	-1,70	-0,30	-1,04	30,48	19,50	45,55*	28,95*

\* In these objects, a temporary malfunction of the climate sensors was encountered. The values given represent the periods of regular measurement.

Object	Moisture content at measuring point 1				Moisture content at measuring point 2				Temperature		rel. Humidity					
	mean	max. A	±max. Δ	±max. grad.	mean	max. A	±max. Δ	±max. grad.	mean	max. A	mean	max. A				
	[% MC]			[%/cm]	[% MC]			[%/cm]	[°C]		[% rh]					
B1	15,08	6,44	+1,69	-1,74	0,54	-0,89	13,91	4,23	+3,25	-0,45	0,27	-0,68	9,42	26,15	68,98	43,96
B2	13,54	5,80	+2,84	-1,95	1,0	-0,9	15,25	6,56	+3,87	-1,86	0,8	-1,2	9,86	29,90	62,20	59,06
B3	10,82	5,06	+1,64	-3,77	1,05	-1,54	9,58	4,00	+1,67	-2,14	0,40	-1,28	19,91	14,13	40,21	57,00
B4	13,32	1,93	+0,60	-0,93	-0,16	-0,73	14,91	2,83	+2,08	+0,35	+0,69	+0,05	9,16	18,82	68,31	44,67

Object	Moisture content at measuring point 1						Moisture content at measuring point 2						Temperature		rel. Humidity	
	mean	max. A	±max. Δ	±max. grad.	mean	max. A	±max. Δ	±max. grad.	mean	max. A	±max. Δ	±max. grad.	mean	max. A	mean	max. A
	[% MC]			[%/cm]			[% MC]			[%/cm]			[°C]		[% rh]	
C1	17,12	3,31	+1,03	-1,29	0,54	-0,65	16,39	3,43	+2,84	-0,03	1,25	0,23	13,28	22,51	79,71	52,63
C2	15,50	5,14	+3,01	-0,10	+2,77	+0,14	15,84	3,91	+1,51	-1,15	+0,70	-0,78	10,53	28,63	77,79	48,57
C3	14,43	5,84	+1,47	-2,69	+1,13	-0,71	15,48	4,52	+1,59	-1,77	+0,49	-0,78	9,76	30,48	77,85	52,29

Object	Moisture content at measuring point 1						Moisture content at measuring point 2						Temperature		rel. Humidity	
	mean	max. A	±max. Δ	±max. grad.	mean	max. A	±max. Δ	±max. grad.	mean	max. A	±max. Δ	±max. grad.	mean	max. A	mean	max. A
	[% MC]			[%/cm]			[% MC]			[%/cm]			[°C]		[% rh]	
D1	4,37	2,15	+0,28	-0,59	+0,16	-0,26	5,95	1,22	-0,02	-1,05	-0,16	-0,73	27,38	26,68	27,66	29,65
D2	7,98	2,02	+0,94	-0,71	+0,26	-0,18	8,10	2,06	+0,64	-1,13	+0,18	-0,65	20,58	16,72	42,77	42,01
D3	10,20	3,02	+0,52	-1,33	0,10	-0,76	10,01	2,66	+0,16	-1,67	0,12	-0,67	20,84	7,90	51,21	33,95

Object	Moisture content at measuring point 1						Moisture content at measuring point 2						Temperature		rel. Humidity	
	mean	max. A	±max. Δ	±max. grad.	mean	max. A	±max. Δ	±max. grad.	mean	max. A	±max. Δ	±max. grad.	mean	max. A	mean	max. A
	[% MC]			[%/cm]			[% MC]			[%/cm]			[°C]		[% rh]	
E1	7,70	1,85	+1,17	-0,65	0,11	-0,51	7,77	1,55	+1,28	-0,28	0,13	-0,51	18,35	17,50	40,86	38,59
E2	4,80	1,86	+0,74	-0,54	+0,31	-0,66	4,69	2,19	+1,10	-0,93	+0,85	-0,54	27,09	21,32	25,78	49,93

Object	Moisture content at measuring point 1						Moisture content at measuring point 2						Temperature		rel. Humidity	
	mean	max. A	±max. Δ	±max. grad.	mean	max. A	±max. Δ	±max. grad.	mean	max. A	±max. Δ	±max. grad.	mean	max. A	mean	max. A
	[% MC]			[%/cm]			[% MC]			[%/cm]			[°C]		[% rh]	
F1	16,52	3,69	+2,51	-0,48	+1,16	+0,33	15,77	3,07	+2,59	-1,82	+1,86	+0,54	11,59	21,58	74,67	45,60
F2	14,88	5,72	+2,86	+0,06	2,05	0,70	15,12	3,70	+2,05	-0,19	1,41	0,10	14,24	22,39	68,35	48,05
F3	14,48	4,83	+5,38	+1,35	+2,77	+0,91	15,25	4,52	+5,09	+1,18	+2,58	+0,73	12,60	28,17	69,22	54,08

Object	Moisture content at measuring point 1						Moisture content at measuring point 2						Temperature		rel. Humidity	
	mean	max. A	±max. Δ	±max. grad.	mean	max. A	±max. Δ	±max. grad.	mean	max. A	±max. Δ	±max. grad.	mean	max. A	mean	max. A
	[% MC]			[%/cm]			[% MC]			[%/cm]			[°C]		[% rh]	
G1	10,53	8,68	+3,59	-3,01	+3,22	-1,19	13,94	6,30	+2,78	-1,40	+2,15	-0,72	10,12	32,64	74,32	62,49
G2	13,27	6,12	+4,63	-1,25	+1,38	-1,16	12,69	3,61	+2,49	-0,67	+1,00	-0,48	9,67	32,46	67,13	54,01
G3	11,55	3,57	+1,44	-1,72	+0,29	-1,12	12,07	2,87	+1,75	-0,71	+0,67	-0,65	13,36	25,60	61,35	44,04

The ambient climate in closed, non-air conditioned ice rinks (objects “B1” and “B2”) was marked by a distinct change between winter (T = 4° C; 75 % RH) and summer months (i.e.

ice-free period with  $T = 15^{\circ}\text{C}$ ; 60 % RH). The timber moisture content in ice-skating rinks was high and varied noticeably. In air-conditioned buildings (objects “B3” and “B4”), this effect was significantly damped. In objects “B1” and “B4”, the film-forming surface treatment showed a damping effect on the moisture gradient. During operation (ice season), the timber moisture content in structural timber elements above the ice was on average 1.5 % higher than in elements above other areas. It should be noted that the measurements were taken at the side faces of the beams and not at the bottom side facing the ice. Surfaces facing the ice cool down due to radiation exchange. This can lead to condensation, partly resulting in the formation of an ice-layer, and in the case of timber elements to increased moisture content, see e.g. [11].

The climate in riding rinks (objects “C”) was marked by seasonal variations leading to high amplitudes of temperature and relative humidity, the latter at high level (RH = 78 %). During the winter months, the combination of cold air in the non-insulated and unheated buildings and the humidity introduced by the sprinklers (to capture the dust), frequently resulted in condensation. As in other types of buildings which are influenced by the outside climate, the timber moisture contents were higher (MC  $\approx$  16 %) and featured stronger seasonal variability. Due to the seasonal nature of the variations, these result in noticeable but not in exceptionally high timber moisture gradients.

Similarly strong seasonal variations of climatic condition were found for agricultural buildings with livestock (objects “F”), the relative humidity being slightly lower (RH = 70 %). In the winter months, the interaction of the cold outside air and increased humidity in the non-insulated, unheated and partly open buildings resulted in high timber moisture contents and partly in condensation.

Since warehouses (objects “G”) are oftentimes realized as partly open buildings, the climate is highly influenced by the outside climate. The mean timber moisture contents were between 10 % and 14 %, their variation was amongst the highest of all evaluated types of use. Object “G1” is used to store plants during winter. The additional humidity introduced by the plants resulted in high relative humidity and occasionally in extensive condensation. The structural elements below skylights (i.e. exposed to direct sunlight) featured the highest amplitude and moisture gradient of all objects evaluated.

In addition to the previously described, construction and use-dependent climatic conditions, do the results of the research project highlight one more important aspect. Temporary interventions, such as renovations or changes of use (temporary or permanent) can lead to major changes in climatic conditions, which are reflected by distinct changes in timber moisture content. Within this research project, strong drying of timber elements (renovation of indoor swimming pool “A3” and temporary conversion of ice-skating rink “B3”) as well as strong moistening of dry timber elements (conversion of former metal-processing production facility “E2”) was measured. Although the evaluation period could sometimes not cover the full effect of the intervention, a noticeable increase of the moisture gradient was observed. Accordingly, care should be taken during such interventions to realize a decelerated change of climatic conditions.

## 4 Conclusions

Historically the subject of moisture content of structural timber elements tended to be treated from the viewpoint of how to prevent high moisture contents to inhibit decay or growth of fungi. The evaluation of damages in large-span timber structures shows that cracking parallel to the grain due to low or severe changes of moisture content is amongst the prevalent types of damage in such structures. These cracks reduce the residual cross-

section to transfer tension perpendicular to grain or shear stresses. Shrinkage related cracking might be less pronounced in structural elements from solid timber if the correct sawing patterns are applied. Structural elements from glued-laminated timber with large cross-sections are more vulnerable in that aspect due to their decelerated adaptability to changing ambient climate. Fast and/or significant changes of ambient climate can be due to the type of construction and use of the building. Locally, these changes can be intensified, e.g. around skylights or in the vicinity of heating systems. In buildings with constant but dry climate, the most severe change of the same will mostly occur during the first winter of operation, after assembly and closure of the building.

A decelerated change of internal climate can be realized by adjusting heating systems to not reduce the relative humidity too fast and too strong. An artificial air humidification, e.g. in the form of evaporation basins is another possibility to damp the speed of drying of the structural timber elements. An alternative is a surface treatment, e.g. in the form of products which damp the moisture absorption and release in the first years of operation of the building (to counter fast drying of newly installed elements in constant but dry climates). In areas with strong but periodic changes of moisture content, protective covering in the form of panel materials could be another feasible measure. The last-mentioned possibility is momentarily being investigated and measured in a separate research project carried out by the authors in collaboration with the Studiengemeinschaft Holzleimbau e.V. In addition, it is intended to continue the measurements presented in ten objects with seasonally varying climate. Hereby the measurement equipment shall be upgraded in order to take additional measurements of the temperature within the cross-section. These measurements shall be used to verify the approach to calculate the material temperature in the different depths on the basis of the measured surface temperatures.

A potential implementation of the conclusions presented would be to include such information in textbooks or commented versions of codes, highlighting the benefits of using timber elements which feature a moisture content mirroring the expected average moisture content. Although the expected average moisture content is to be determined individually for each building, examples of classification of buildings of specific use into Service Classes (e.g. riding rinks, ice-skating halls) could be given. To increase the awareness towards dry climates it could be worthwhile to consider including a note in the code stating that the average moisture content of softwoods in heated and insulated buildings (Service Class 1) will in most cases be below 10 %.

The objective of this research project was to provide data, enabling an overview over climatic conditions and resulting timber moisture contents which can occur in large buildings of different use. To establish realistic reference values with regard to damage potential (cracking), further research in form of modeling and sensitivity studies, in combination with laboratory tests is necessary.

## **Acknowledgement**

The research project was kindly supported by the following industry partners: Scantronik Mugrauer, DE-Zorneding; Studiengemeinschaft Holzleimbau e.V., DE-Wuppertal, bauart Konstruktions GmbH + Co. KG, DE-Lauterbach, Konstruktionsgruppe Bauen AG, DE-Kempten. Special gratitude is extended to the Research Initiative "Future Building" for funding the project with financial means of the Federal Office for Building and Regional Planning. In addition, the authors wish to acknowledge the help of students Michael Kraus, Manuel Waidelich, Stephanie Riedler und Astrid Indefrey during the readout and charting of data.

## Literature

- [1] EN 1995-1-1:2004, Eurocode 5: Design of Timber Structures – Part 1-1: General – Common rules and rules for buildings, European Committee for Standardization CEN, Brussels, Belgium, 2004.
- [2] Blaß, H.-J., Frese, M., Schadensanalyse von Hallentragwerken aus Holz, Band 16 der Reihe Karlsruher Berichte zum Ingenieurholzbau, KIT Scientific Publishing, Karlsruhe, 2010
- [3] Frühwald, E., Serrano, E., Toratti, T., Emilsson, A., Thelandersson, S., Design of safe timber structures – How can we learn from structural failures in concrete, steel and timber?, Report TVBK-3053, Div. of Struct. Eng, Lund University, 2007
- [4] Dietsch, P., Winter, S., Assessment of the Structural Reliability of all wide span Timber Structures under the Responsibility of the City of Munich, Proceedings 33<sup>rd</sup> IABSE Symposium, Bangkok, Thailand, September 9-11 2009
- [5] Dietsch, P., Einsatz und Berechnung von Schubverstärkungen für Brettschichtholzbauteile, Dissertation, Technische Universität München, submitted in 07/2012.
- [6] Blaß, H., J., Ehlbeck, J., Kreuzinger, H., Steck, G., Erläuterungen zu DIN 1052:2004-08, Bruderverlag, Karlsruhe, 2004
- [7] Meierhofer, U., & Sell, J. Physikalische Vorgänge in wetterbeanspruchten Holzbauteilen – 2. und 3. Mitteilung, Holz als Roh- und Werkstoff, 37 (6+12), 1979, pp. 227-234 and 447-454
- [8] Krabbe, E., Neuhaus, H., Über Konstruktion, Klima und Holzfeuchtigkeit eines Hallenbades, Bauen mit Holz, 91 (4), 1989, pp. 214-217
- [9] Koponen, S., Puurakenteiden kosteudenhallinta rakentamisessa, TKK-TRT Report 1-0502, Helsinki, 2002
- [10] Evans, F., Kleppe, O., Dyken, T., Monitoring of Timber Bridges in Norway - Results, Report Norsk Treteknisk Institutt, Oslo, 2007
- [11] Feldmeier, F., Ergebnisse und Schlussfolgerungen aus den Felduntersuchung einer Eissporthalle, Tagungsband Ingenieurholzbau - Karlsruher Tage, 2007, pp. 98-104
- [12] Brischke, C., Rapp, A. O., Untersuchung des langfristigen Holzfeuchteverlaufs an ausgewählten Bauteilen der Fußgängerbrücke in Essing, Arbeitsbericht der Bundesforschungsanstalt für Forst- und Holzwirtschaft, Hamburg, 2007
- [13] Marquardt, H., Mainka, G.-W., Tauwasserausfall in Eissporthallen, Bauphysik, 30 (2), 2008, pp. 91-101
- [14] Niemz, P., Gereke, T., Auswirkungen kurz- und langzeitiger Luftfeuchteschwankungen auf die Holzfeuchte und die Eigenschaften von Holz, Bauphysik, 31 (6), 2009, pp. 380-385
- [15] Ressel, J., B., Fundamentals of wood moisture content measurement, Course notes, COST E53 Training School “Methods for measuring of moisture content and assessment of timber quality”, BFH, Hamburg, October 17 – 19 2006
- [16] Euler, L., Institutiones Calculi differentialis, Berlin, 1755
- [17] Kollmann, F., Coté, W., A., Principles of Wood Science and Technology I: Solid Wood, Springer, Berlin, 1968
- [18] Fortuin, G., Anwendung mathematischer Modelle zur Beschreibung der technischen Konvektionstrocknung von Schnittholz, Dissertation, Universität Hamburg, 2003
- [19] Keylwerth, R., Noack, D., Über den Einfluß höherer Temperaturen auf die elektrische Holzfeuchtigkeitsmessung nach dem Widerstandsprinzip, Holz als Roh- und Werkstoff, 14 (5), 1956, pp. 162-172.
- [20] Hailwood, A. J., Horrobin, S., Absorption of water by polymers: analysis in terms of a simple model, Transactions of the Faraday Society, Vol. 42b, 1946, pp. 84-92
- [21] Simpson, W. T., (1973), Predicting equilibrium moisture content of wood by mathematical models, Wood and Fiber Science, 5 (1), 1973, pp. 41-48
- [22] Gamper, A., Dietsch, P., Merk, M., Winter, S., Gebäudeklima - Langzeitmessung zur Bestimmung der Auswirkungen auf Feuchtegradienten in Holzbauteilen, Final Report, Lehrstuhl für Holzbau und Baukonstruktion, Technische Universität München, 2012

\* This list only includes references in direct connection to this paper. A complete list of references with regard to the project is given in the final report.

**INTERNATIONAL COUNCIL FOR RESEARCH AND INNOVATION  
IN BUILDING AND CONSTRUCTION**

**WORKING COMMISSION W18 - TIMBER STRUCTURES**

**ASYMMETRICALLY COMBINED GLULAM –  
SIMPLIFIED VERIFICATION OF THE BENDING STRENGTH**

M Frese

H J Blaß

Karlsruhe Institute of Technology (KIT)  
Holzbau und Baukonstruktionen

GERMANY

**MEETING FORTY FIVE**

**VÄXJÖ**

**SWEDEN**

**AUGUST 2012**

---

Presented by M Frese

J Köhler commented that not enough samples were considered in the simulation as the results seem to be unstable. M Frese stated that 1000 replicates were considered in the simulation and one could smooth the results with regression. He clarified also that E1 and E2 ratio was the ratio of the E of the outer and intermediate zone. Higher ratios imply more loads and stresses are attached to the higher grade lumber. S Aicher commented that as the results were based on 600 mm deep beam, would the same results apply to 2 m deep beams. M Frese responded that yes they had to take into account of the percentage of the different grades. G Stapf asked what assumptions were made for the laminates. M. Frese would look into the details and discuss with G Stapf. G Stapf asked why only considered MOE in compression and not the MOE in tension for moisture content adjustment. M Frese stated that there was no moisture adjustment method for MOE in tension and engineers in general did not consider this. T Poutanen stated that one option was to consider proof loading of the bottom chord. M Frese will discuss with T Poutanen directly. A Jorissen asked and received clarification of the glulam grades and moisture content adjustment procedures where moisture content was considered in the regression equations with E and compression strength. I Smith commented that the use of different seeds in the random number generator might solve the sample size stability issue. T Poutanen received clarification that 100% failure was in the bottom chord as this was the failure criterion chosen and plastic deformation zone did not stop the calculations. A Olsson stated that experience with solid boards failure initiate in compression and then tension fracture. He asked whether there was a coupling effect. M Frese and H Blass responded that there were differences between the failure modes of high grade timber and glulam.



# Asymmetrically combined glulam – simplified verification of the bending strength

Matthias Frese, Hans Joachim Blaß  
Karlsruher Institut für Technologie, Holzbau und Baukonstruktionen

Asymmetrically combined glulam (ACG) with superior grade boards in the outer tension zone only, could be an economic glulam product for beams. However, the problem is the low nominal strength due to the minor strength class related to the compression zone. Using a computer model the bending capacity of ACG is simulated. In doing so, the compressive stress is not limited by a nominal strength. Thus plastic strains are allowed to a certain extent. The influences of different cross section lay-ups and different moisture contents on the bending capacity are examined as well. Based on the results, the effective bending MOE and the effective characteristic bending strength are calculated. Depending on the strength classes used in ACG, few laminations of superior grade boards enhance the glulam strength significantly. On the basis of MOEs reflecting the stiffness relations in ACG accurately, a simplified verification of the bending strength restricted to the tension zone is possible.

## 1 Introduction

Glued laminated timber is used for a large portion of structural members in long-span primary structural systems. Usually, the cross sections are deep and require a considerable quantity of strength graded boards. As an example, Figure 1 shows a roof structure with almost 3 m deep glulam girders stressed in bending. The volume of the girders shown makes it necessary to use boards of superior grade economically. Thus only the outermost tension zone of girders like these consists of boards of superior grade.

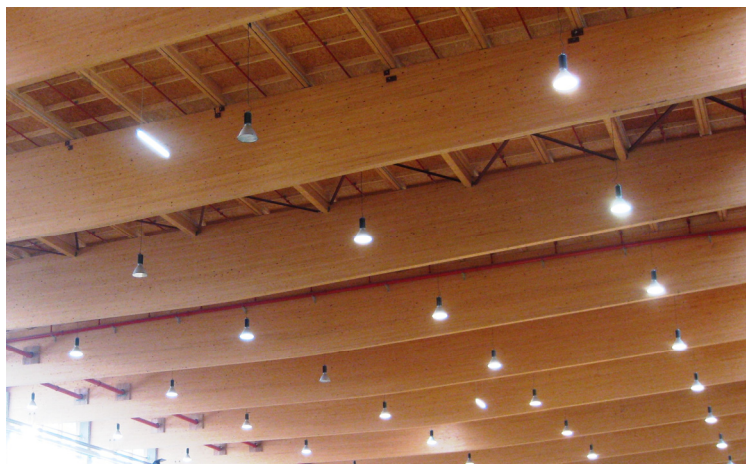


Figure 1: Long-span roof structure

Homogeneous glulam (HG) consists of boards of one single grade. Symmetrically combined glulam (SCG) possesses a cross section lay-up with boards of superior grade in the outer portions and boards of lower grade in the inner one. For economic reasons, it is used particularly for bending members. Above all, asymmetrically combined glulam (ACG), with boards of

superior grade in the outer tension zone only, could be a more economic alternative compared to HG and SCG.

ACG is used to a certain extent for bending members already since decades. Explicit standard specifications were given for example in [1,2]. Related to the European standard specification, [3] implicitly contains the possibility to determine the characteristic bending strength of – within certain restrictions – arbitrary assembled cross section lay-ups. Against the background of [3], the problem of ACG stressed in bending is the comparatively low nominal value of the bending strength due to a minor strength class in the compression zone. Furthermore a procedure is still missing how to estimate the MOEs of the laminations to reflect the stiffness conditions in ACG realistically. An efficient mechanical reflection was recently included in [4]: Based on a numerical study on ACG (on behalf of the association of German and foreign glulam manufacturers) it is suggested that the verification of the bending strength in the outer compression zone may be disregarded; by doing so certain conditions have to be met. The present paper is a further development of this mechanical reflection. The paper aims at examining and defining the relevant boundary conditions concerning a simplified verification of the bending strength in ACG.

A schematic stress distribution in the cross section of ACG due to a bending moment is shown in Figure 2. The distribution reflects a realistic  $E_1/E_2$ -ratio of 1.24, in which  $E_1$  and  $E_2$  represent the zone-dependent MOEs. The sketch exemplifies that the compressive stress exceeds the local nominal strength ( $f_{m,g,k,2}$ ) in the compression zone (= zone 2), when the maximum tensile stress reaches the local nominal strength ( $f_{m,g,k,1}$ ) in the tension zone (= zone 1).

An existing computer model for glulam (CM), already used for different strength simulations [5,6,7], was modified to determine the bending capacity of ACG. The CM considers the stochastic character of the mechanical properties of boards by representing the natural variation of the strength and the MOE empirically. Both values refer to the grain direction. The strength and the MOE values are simulated by corresponding regression equations. They are assigned as material properties to the elements of a finite element model which constitutes the glulam structure to be analysed. Based on the simulation results obtained, it is shown that the theory of composite beams (TCB) is a suitable method to determine the load carrying capacity of ACG by manual calculations.

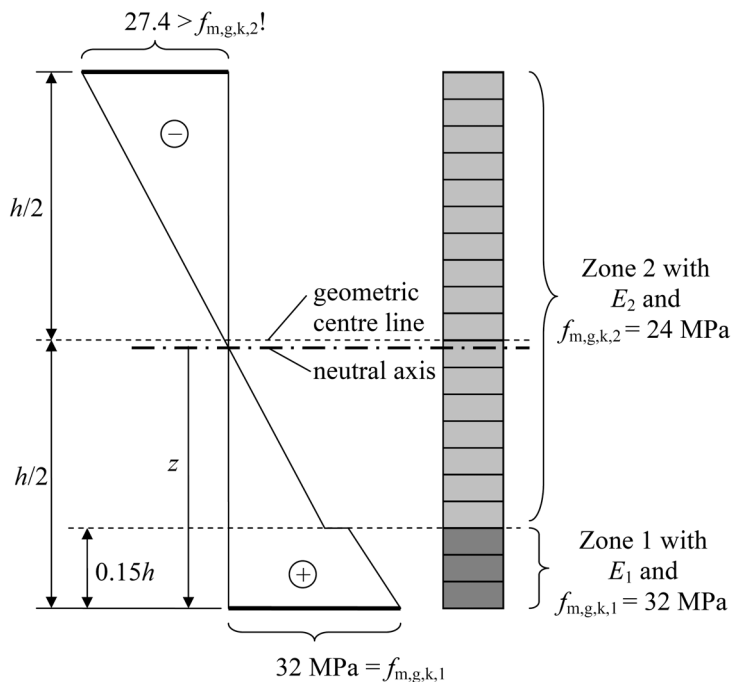


Figure 2: Example of a stress distribution in ACG

## 2 Numerical Analysis

### 1.1 Test programme

Three beam types (I, II and III) were examined numerically. According to Table 1 each beam type comprises two different glulam strength classes. These strength classes have the meaning of target strength classes of which the characteristic bending strength has to be approximately fulfilled by the empirically represented boards and finger joints. The specific test configuration simulated by the CM is shown in Figure 3. The variable  $n = \{0, 1, 2, \dots, 20\}$  enables a stepwise conversion of the cross section lay-up: for  $n = 0$  the simulated boards belong exclusively to the strength class present in zone 2; for  $n$  greater than 0 and less than 20 the beam contains boards of both strength classes; for  $n = 20$  the boards belong exclusively to the strength class in zone 1. This stepwise conversion is the basis to estimate the influence of a gradual improvement of the type-dependent cross section lay-ups on the mechanical properties. The influence of the wood moisture content ( $u$ ) on the bending capacity was also examined. The CM considers the influence of the moisture content in the compression zone. From an engineering point of view the impact of changing moisture content on the mechanical properties for tension is negligible. Thus the CM does not consider the moisture content in the tension zone. The moisture contents 12 %, 16 % and 20 % were simulated. These moisture contents are representative for the equilibrium moisture contents of timber exposed to indoor climate and for timber, which is exposed to outdoor climate protected by a roof. Each beam type was analysed with one thousand simulations per  $n$ , with  $n = \{0, 1, 2, \dots, 20\}$ , and per moisture content. This results in 63 thousand simulations per beam type.

Table 1: Glulam strength classes used for the beam types

Type	Zone 1	Zone 2
I	GL24h	GL20h
II	GL28h	GL24h
III	GL32h	GL24h

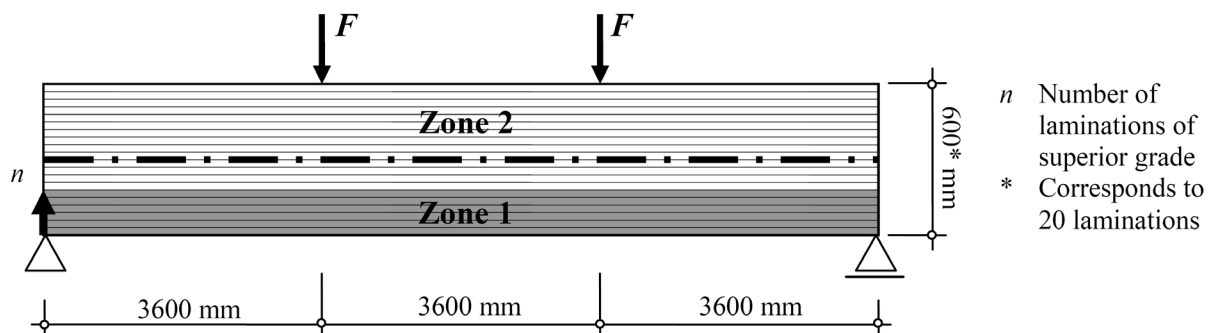


Figure 3: Test configuration following [8]

### 1.2 Methods

Simulating the bending tests, the compressive stress is not limited by any nominal strength of the given target strength classes. Compared to HG or SCG, plastic strains may therefore occur to a higher extent in the compression zone. For each single simulation the CM identifies the minimal plastic strain (without elastic strain) in the compression zone and stores the corresponding value. The minimal plastic strain refers to the single element of the compression

zone which shows the highest absolute value of plastic deformation. Thus the influence, which results from compressive stress beyond the linear material performance, can be described and any harmful effects of “crushing parallel to the grain” can be estimated. Based on the simulated load displacement relations and the simulated load carrying capacities ( $F$ ) using the second moment of area ( $I$ ) and the section modulus ( $W$ ), respectively, the effective bending modulus of elasticity ( $MOE_{mean,sim}$ ) and the effective characteristic bending strength ( $f_{m,g,k,sim}$ ) are calculated. Additional simulations were conducted to determine the compressive and tensile MOEs which are locally present in the numerically examined cross section lay-ups of all beam types. These MOEs were estimated by particular simulations of bending, tensile and compression tests on glulam, cf. [5,6,7]. The compressive and tensile MOEs such obtained are of importance for the interpretation of the simulated bending strength values and for the further evaluation on the basis of the theory of composite beams. Figure 4, top shows the position of the tensile MOEs ( $E_{1,t}$  and  $E_{2,t}$ ) present in zone 1 and 2; Figure 4, bottom shows the corresponding positions of the compressive MOEs ( $E_{1,c}$  and  $E_{2,c}$ ). The simulated compression tests include also the variation of the wood moisture content with 12 %, 16 % and 20 %.

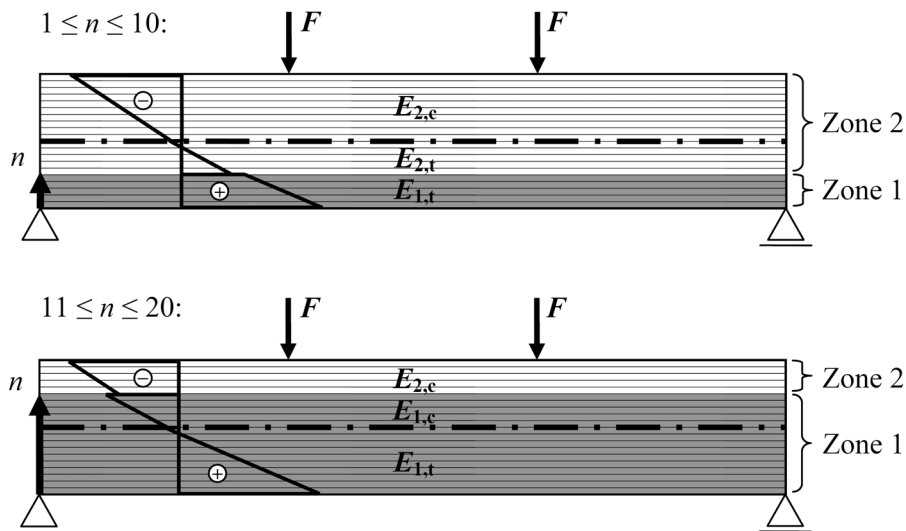


Figure 4: Local MOEs in dependence on the depth of the zone 1 and the position of the geometric centre line; the inserted stress distributions are related to an exemplary MOE relation

### 3 Results

The left diagrams in Figure 5 show the mean simulated bending MOE in dependence on the converted cross section lay-up. The s-shaped course of the given values is as expected: for  $n = 0$  the MOE is minimal and for  $n = 20$  it is maximal; for small and high  $n$ -values the gradient becomes maximal; for  $n$ -values between 7 and 13 the MOE does not change due to the conversion of the cross section lay-up near the geometric centre line. The higher the moisture content the lower is the MOE. This is caused by the decreasing MOE in the compression zone as consequence of the increasing moisture content. These connections prove the plausibility between the input data and the output data of the CM. The right diagrams in Figure 5 show the plastic strain in dependence on the converted cross section lay-up. Each symbol represents the minimal plastic strain out of one thousand extreme values. These extreme values were identified in one thousand single simulations per  $n$ . Under common consideration of the three beam types and of the three moisture contents none of the values is lower than -1.7 %. On closer examination plastic strains do not occur in simulations with strengths below the level of the characteristic bending strength. Under design loads the compressive stresses in ACG

therefore lie far below the elastic limit. Table 2 contains the tensile and compressive MOEs which are locally present in the simulated beams. As agreed the tensile MOEs are independent of the moisture content and the compressive MOEs depend on it. The ratio  $\alpha$  represents the difference in stiffness between the tensile MOEs and the ratio  $\beta$  between the tensile and compressive MOE of the outermost laminations in the tension and compression zone, respectively.

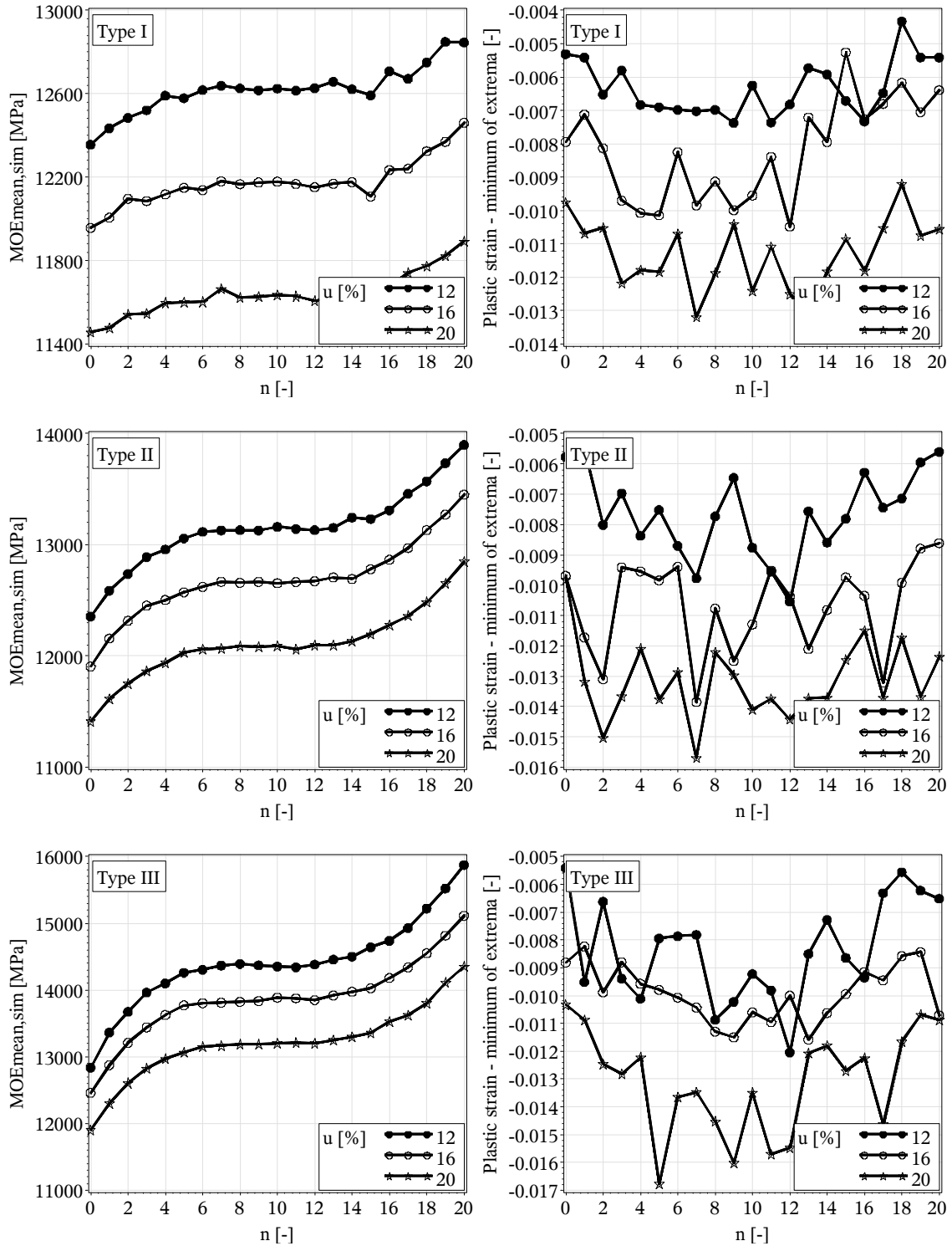


Figure 5: *left* Bending MOE and *right* plastic strain over converted cross section lay-up

Table 2: Local MOEs [MPa] and difference in stiffness relations

Type	u [%]	$E_{1,t}$	$E_{2,t}$	$E_{1,c}$	$E_{2,c}$	$\alpha = E_{1,t}/E_{2,t}$	$\beta = E_{1,t}/E_{2,c}$
I	12			12600	12200		~1.07
	16	13000	12500	11600 <sup>a</sup>	11200 <sup>a</sup>	~1.04	~1.16
	20			10600 <sup>b</sup>	10300 <sup>b</sup>		~1.26
II	12			13800	12200		~1.16
	16	14100	12500	12700 <sup>a</sup>	11200 <sup>a</sup>	~1.13	~1.26
	20			11600 <sup>b</sup>	10300 <sup>b</sup>		~1.37
III	12			15500	12600		~1.29
	16	16300	13000	14200 <sup>a</sup>	11600 <sup>a</sup>	~1.25	~1.41
	20			13000 <sup>b</sup>	10600 <sup>b</sup>		~1.54

<sup>a</sup>92 % and <sup>b</sup>84 % of the reference value for 12 % moisture content, both percentages are found in the study of the moisture influence on glulam stressed in compression [7]

Figure 6 shows the simulated effective bending strength values. The left diagrams refer to the characteristic bending strength ( $f_{m,g,k,sim}$ ) and the right ones to the mean bending strength ( $f_{m,g,mean,sim}$ ). The lower the ratio  $\alpha$ , the more pronounced the initial strength increase; this applies for the small  $n$ -values only. While one lamination of superior grade enhances the entire cross section of the type I, at least three of superior grade are necessary to enhance type III significantly, cf. [9]. The greater the ratio  $\beta$ , the more pronounced the strength difference between the local maximum ( $n \approx 10$ ) and the local minimum ( $n \approx 13$ ). This difference is in particular evident in the development of the mean strength for type III and  $u = 20$  % (s. Figure 6, last diagram). Considering economically advantageous lay-ups with small  $n$ -values only, 16 % moisture content hardly affects the characteristic bending strength compared to 12 %. The influence of 20 % is moderate as the characteristic bending strength decreases about 1 to 2 MPa.

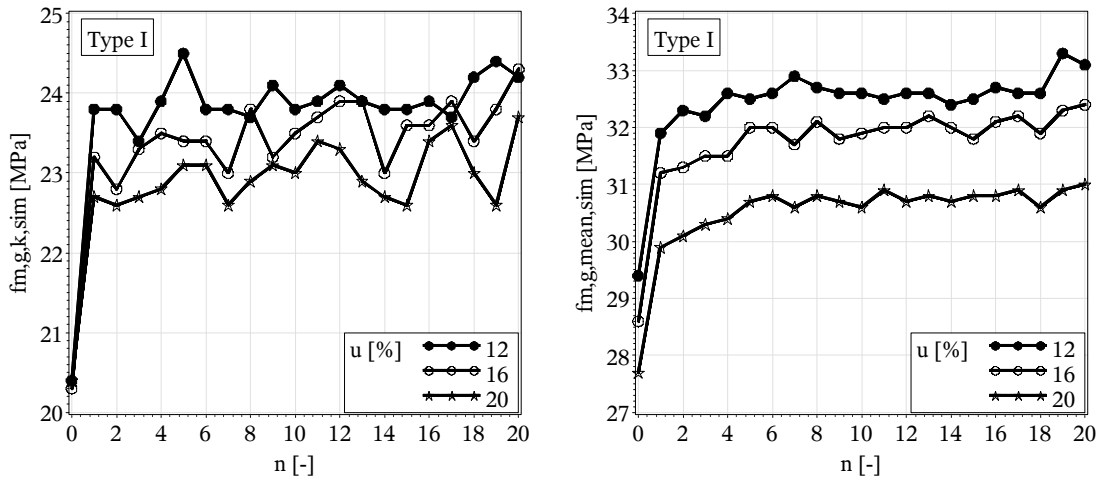


Figure 6: Bending strength over converted cross section lay-up, *left* characteristic and *right* mean value

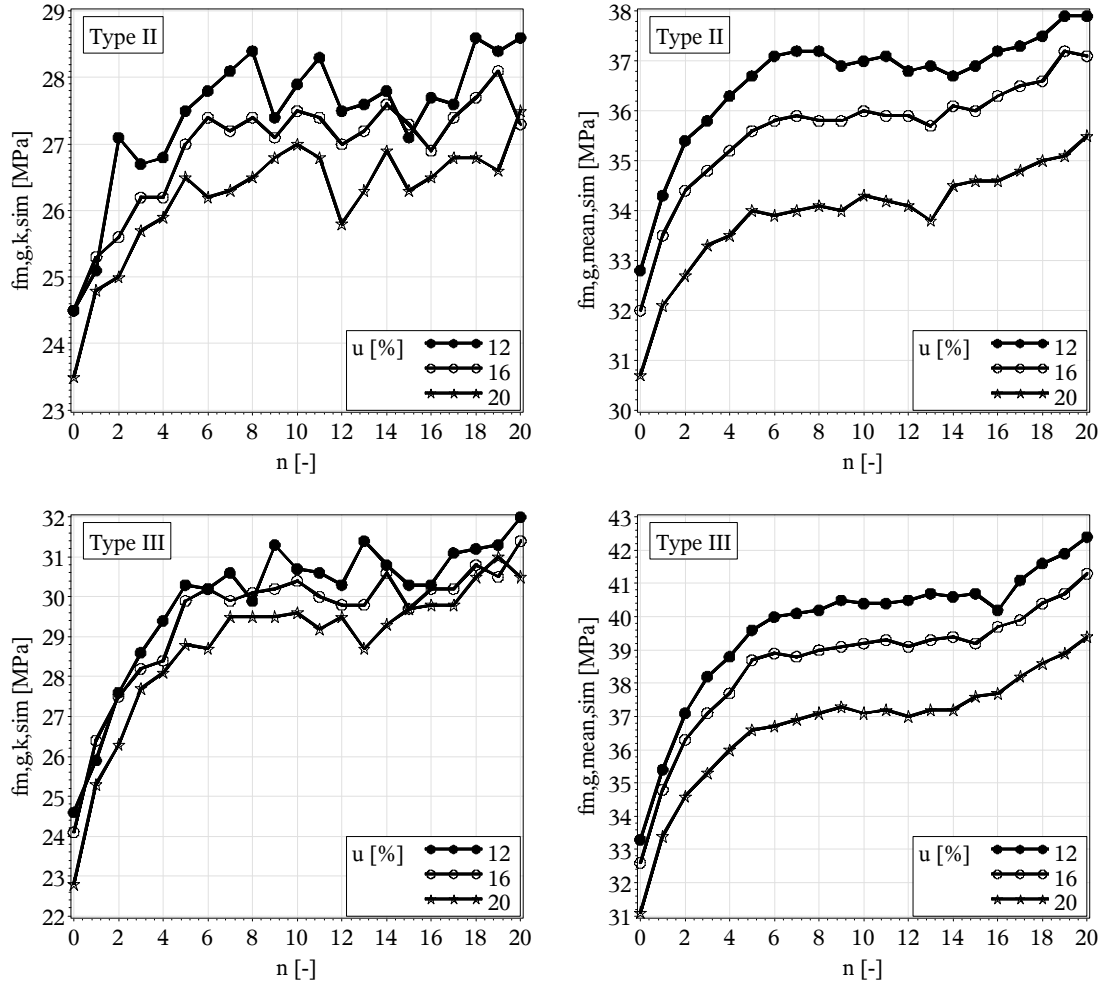


Figure 6: (cont.) Bending strength over converted cross section lay-up, *left* characteristic and *right* mean value

Due to the stochastic character of the strength simulation, marginal deviations between the simulated characteristic bending strengths and the corresponding nominal strengths of the target strength classes occur to a certain extent. Taking this into account the simulation was calibrated so that the simulated characteristic bending strengths slightly exceed the nominal values of 20, 24, 28 and 32 MPa. Table 3 contains the simulated characteristic bending strengths of the three types for  $n = 0$  and  $n = 20$  and for the moisture content of 12 %. The given values represent the characteristic bending strength for the case that the beams only consist of material either for zone 1 or for zone 2.

Table 3: Simulated bending strength [MPa]

Type	$n = 0$ (only zone 2)		$n = 20$ (only zone 1)	
	Target	$f_{m,g,k,sim,2}$	Target	$f_{m,g,k,sim,1}$
I	GL20h	20.4	GL24h	24.3
II	GL24h	24.5	GL28h	28.5
III	GL24h	24.6	GL32h	32.0

## 4 Model for practical application

The simulated characteristic bending strengths are twice compared to analytically calculated strength values. The corresponding analytical calculations are based on the theory of composite beams.

- The first calculation by equation (1), the corresponding function (2) and term (3) considers the stiffness relations as exactly as possible. The effective strength depends on the characteristic bending strength ( $f_{m,g,k,1}$ ), which is simulated for the types I to III as quoted in term (3) and given in Table 3, the effective bending stiffness ( $EI_{\text{eff}}$ ) according to the function (2) considering the zone-dependent MOEs (Table 2), the distance  $z$  between the neutral axis and the lower edge, the tensile MOE present in zone 1 ( $E_{1,t}$ ) and the section modulus ( $W$ ).

$$f_{m,g,k,\text{TCB}} = \frac{f_{m,g,k,1} \cdot EI_{\text{eff}}}{\frac{z \cdot E_{1,t}}{W}} \quad (1)$$

$$EI_{\text{eff}} = f(n, t, b, E_{1,t}, E_{2,t}, E_{1,c}, E_{2,c}) \quad (2)$$

$$f_{m,g,k,1} = \{ 24.3 \text{ MPa}, 28.5 \text{ MPa}, 32.0 \text{ MPa} \} \quad (3)$$

- The second calculation by equation (4) with the function (5) considers the stiffness relations when the simulated beams are simply modelled as a combination of two strength classes (Table 1). The effective strength depends on the same characteristic bending strength quoted in term (3). The strength-class-dependent MOEs in function (5), taken from prEN 14080, are compiled in Table 4.

$$f_{m,g,k,\text{TCB}} = \frac{f_{m,g,k,1} \cdot EI_{\text{eff}}}{\frac{z \cdot E_1}{W}} \quad (4)$$

$$EI_{\text{eff}} = f(n, t, b, E_1, E_2) \quad (5)$$

Table 4: prEN-14080-MOEs [MPa] and difference in stiffness relations

Type	classified as	$E_1$ $E_{0,g,\text{mean}}$ in zone 1	$E_2$ $E_{0,g,\text{mean}}$ in zone 2	$\alpha = E_1/E_2$
I	GL24h/GL20h	11500	8000	~1.44
II	GL28h/GL24h	12500	11500	~1.09
III	GL32h/GL24h	14000	11500	~1.22

The results of both calculations are effective characteristic bending strengths denoted by  $f_{m,g,k,\text{TCB}}$ . In agreement with the simulation results, equations (1) and (4) do not consider any nominal strength in the compression zone; both equations are valid for  $n = \{1, 2, \dots, 20\}$ . The functions (2) and (5) of the effective bending stiffness are given in general terms only. In it, the lamination depth is  $t$  and the beam width is  $b$ . The comparison between the simulated and the calculated characteristic bending strengths is shown in Figure 7.

- First calculation based on up to four zone-dependent MOEs: Considering the stochastic character of the simulation results and inaccuracies concerning the MOEs in the function

(2) each of the nine diagrams shows a good agreement between the simulation and equation (1). The analytically calculated courses correctly reflect the simulated relations between the stepwise converted cross section lay-ups and the characteristic bending strengths. This agreement is proven between  $n = 1$  and  $n = 20$ . Also the relations between the moisture contents and the strength levels are reflected correctly. The theory of composite beams is therefore a suitable means to calculate the effective bending strength even disregarding the bending strength in the compression zone.

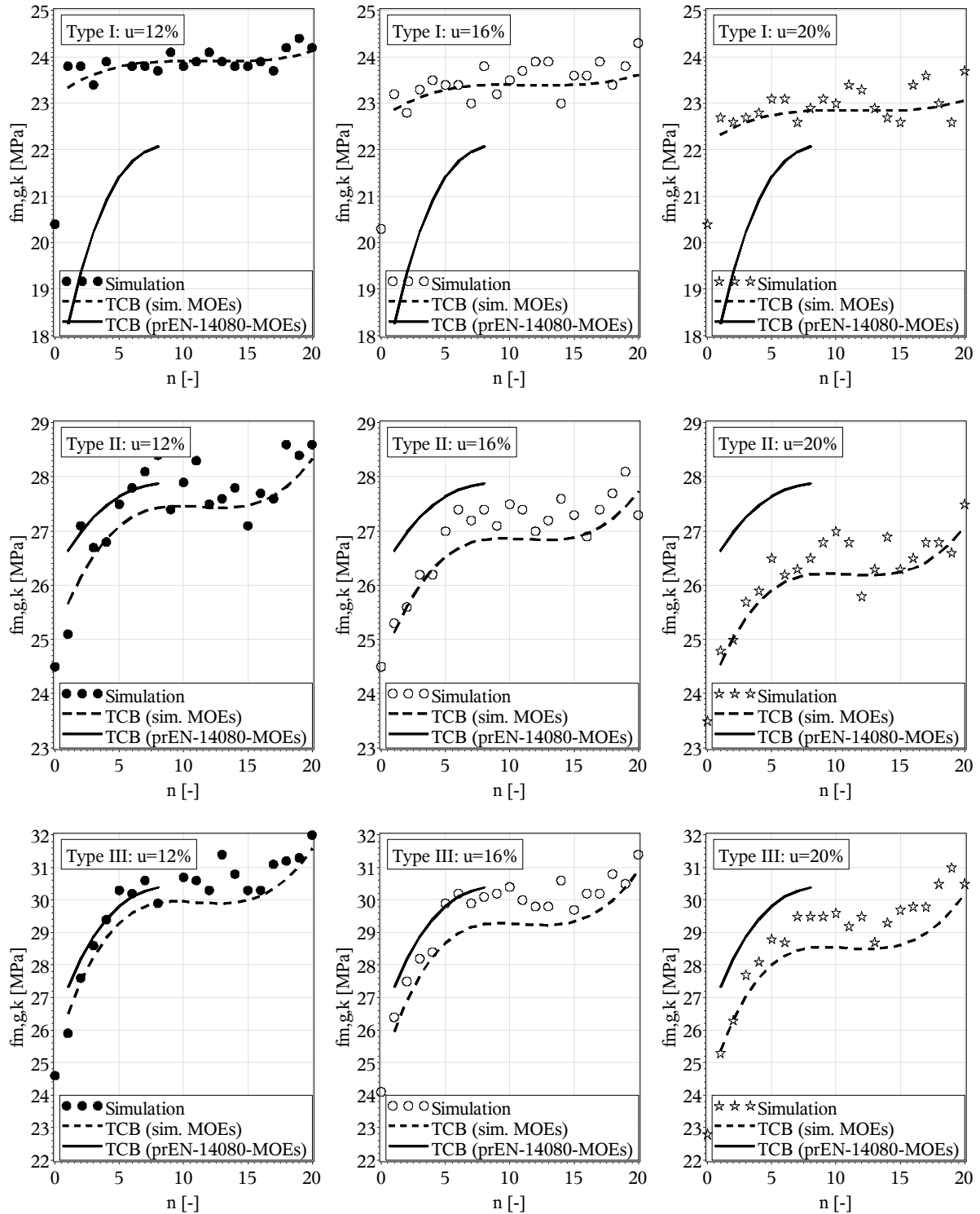


Figure 7: Simulation and models

- Second calculation based on prEN-14080-MOEs: Obviously there is no systematic agreement between the sections of the courses (evaluated between  $n = 1$  and  $n = 7$ , economical cross section lay-ups) according to equation (4) and the simulation results. Except for type I equation (4) leads to “unsafe” strength values since the prEN-14080-MOEs are not in line with the simulated stiffness relations. prEN 14080 does not provide any possibility to consider the moisture influence on the MOE systematically; compared to the equation (1) the courses stay therefore on the same strength level and do not move downwards when the moisture content increases.

## 5 Conclusions

- In asymmetrically combined glulam (ACG) the fraction of laminations in the outermost tension zone comprising superior grade boards should cover 10 % to 20 % of the cross section; at least two laminations of superior grade boards have to be arranged.
- Based on the agreement with simulation results obtained from this study, the theory of composite beams is a reliable method to calculate the load carrying capacity of ACG manually. However, further research is needed in regard to the estimation of accurate zone-dependent MOEs in ACG. These MOEs have to reflect the real material- and moisture-dependent stiffness. The bending MOEs in [4] are partly unsuitable to represent the material- and moisture-dependent stiffness reliably.
- In the verification of the bending strength of ACG, using the theory of composite beams, the local verification of the bending strength in the compression zone may be disregarded. However, the following conditions have to be met: The difference between the nominal strengths of the boards used for the laminations in ACG must not exceed 8 MPa. The ratio between the tensile MOEs of the laminations used must not exceed 1.25. In doing so, plastic effects in the compression zone do not occur under design loads.
- Compared to 12 % moisture content, 20 % causes a reduction in characteristic bending strength of round 1.5 MPa. This applies to homogeneous and asymmetrically combined glulam.
- It is conceivable to use stiffness data which are available from mechanical strength grading to estimate the zone-dependent stiffness. In particular results from measurements of longitudinal vibrations might be used.

## 6 References

- [1] DIN 1052:1969 Holzbauwerke – Berechnung und Ausführung (Design of timber structures)
- [2] AITC 117-71 (1971) Standard specifications for structural glued laminated timber of Douglas Fir, Western Larch, Southern Pine and California Redwood. American Institute of Timber Construction
- [3] EN 1194:1999 Timber structures – Glued laminated timber – Strength classes and determination of characteristic values
- [4] prEN 14080:2011 Timber structures – Glued laminated timber and glued solid timber – Requirements
- [5] M Frese, HJ Blaß (2008) Bending strength of spruce glulam – new models for the characteristic bending strength. CIB-W18/41-12-2, St. Andrews by the Sea, Canada
- [6] M Frese, HJ Blaß (2010) System effects in glued laminated timber in tension and bending. CIB-W18/43-12-3, Nelson, New Zealand
- [7] M Frese, M Enders-Comberg, HJ Blaß, P Glos (2011) Strength of spruce glulam subjected to longitudinal compression. CIB-W18/44-12-2, Alghero, Italy
- [8] EN 408:2010 Timber structures – Structural timber and glued laminated timber – Determination of some physical and mechanical properties
- [9] RF Pellerin, MD Strickler (1972) Proof loading of tension laminations for large glued-laminated beams. Forest Products Journal 22:24-30

**INTERNATIONAL COUNCIL FOR RESEARCH AND INNOVATION  
IN BUILDING AND CONSTRUCTION**

**WORKING COMMISSION W18 - TIMBER STRUCTURES**

**DETERMINATION OF SHEAR STRENGTH OF STRUCTURAL AND  
GLUED LAMINATED TIMBER**

R Brandner  
W Gatternig  
G Schickhofer

Graz University of Technology, Institute of Timber Engineering and Wood  
Technology  
Competence Center holz.bau forschungs gmbh

AUSTRIA

**MEETING FORTY FIVE**

**VÄXJÖ**

**SWEDEN**

**AUGUST 2012**

---

Presented by R Brandner

F Lam stated that it was good to see data from Europe indicating size effect in shear strength of wood that agreed with Canadian results. F Lam questioned the influence of overhang on shear strength of beams and whether the reinforcing self-tapping screws against bearing failure might influence the shear strength. R Brandner stated that past results from Graz indicated that there was no overhang effect and explained that the self-tapping screws did not influence shear failure. F Lam received confirmation that shear failures initiated in the zone between the support and the loading head. BJ Yeh stated that overhang could serve as reinforcement and there were limits specified in ASTM test method. BJ Yeh felt that difference from Canadian approach the results seemed to indicate that it was only a depth effect on shear and not a volume effect as there wasn't any influence of specimen width. J Denzler commented that couldn't explain why small specimens had these low strength values especially for the low strength class. S Aicher commented that length of the constant shear stress and not only depth should have an influence on shear strength. He further stated that ASTM 4 point bending test procedures for estimating shear strength might be better since in the 3 point bending tests used in this study where the influence of decreasing shear length as the beam deflects was an issue. P Dietsch received confirmation that shear failure near the top of the screws were not observed. He questioned whether the self-tapping screws needed to be that long. R Brandner stated based on test experience, the length of the screws could be reduced but not based on calculations. K Malo received confirmation that the shear area was defined as the product between specimen depth and length of constant stress zone. He asked whether one would use this data directly in FEM simulation. R Brandner stated that it should not be used in FEM analysis directly.



# Determination of Shear Strength of Structural and Glued Laminated Timber

R BRANDNER <sup>1)2)</sup>; W GATTERNIG <sup>2)</sup>; G SCHICKHOFER <sup>1)2)</sup>

Graz University of Technology, Institute of Timber Engineering and Wood Technology <sup>1)</sup>  
Competence Center holz.bau forschungs gmbh <sup>2)</sup>

## 1 Abstract

The shear strength of structural and glued laminated timber (GLT) is comprehensively discussed. This is done in respect to quantification of characteristic shear strengths, the influence of stressed volume, the crack coefficient  $k_{cr}$  according EN 1995-1-1 [1] as well as the influence and specification of an adequate test method for the investigation of reliable and reproducible standardised properties relevant for standards (e.g. EN 338 [2], prEN 14080 [3] and EN 1995-1-1 [1]).

The shown research project involves a comprehensive literature survey and testing of structural timber in shear. State-of-the-art includes structural timber and GLT, the examination of various test methods as well as physical and mechanical influences on shear strength, in particular the influence of size. Furthermore, a test configuration was developed which enables coherent determination of shear strength of structural timber and GLT. The examination of shear strength performed on structural timber of Norway spruce involved series of various dimensions and grades. Therefore, I-beams were tested in three-point bending. The specimens of interest (webs) were chosen randomly from a specific nominal grading class. Preparation of flanges included stiffness grading and proof loading. Evaluation of shear strength was done by application of simple beam theory assuming composite action between web and flanges. Afterwards the values of more plate-like specimen were corrected based on comparative computations by means of FEM. By testing, the influence of stressed volume, the size effect, and the relationship between bending and shear strength as given in EN 384 [4] and EN 338 [2] were investigated. Additionally, shear deformation was measured in the largest test specimens by means of shear fields placed in zones of constant shear force.

The aim of the research work is to support a comprehensive study and a basis for decision finding regarding the standardisation of characteristic shear strengths of structural timber and GLT of softwoods, in particular Norway spruce, providing a coherent system of testing, material, evaluation and design standards. In conclusion, it can be noted that there is a significant dependency between the shear strength and the shear-stressed zones. According to this, an adjustment of current standards, in which the geometrical dimensions are taken into account by means of a correction factor, is proposed.

## 2 Introduction

The main structural elements in timber engineering are beams or girders stressed in bending. Thus, bending characteristics normally govern the design process. Although all these elements are also stressed in shear, shear resistance seldom limits ULS design. Nevertheless, in some cases, in particular in (i) elements with a low span to depth ratio, (ii) tapered elements, or (iii) elements with notches, shear strength may also become a decisive characteristic, determining ultimate design.

Beside these facts, relevant for practical timber engineering, in general characteristics shall be regulated reliable, accurate and reproducible. Therefore agreement and balancing between the methods applied for determination (test method & configuration), the evaluation and analysis of test results (mechanics and stochastics), the regulation of material and product characteristics and the design procedure is required, regardless its importance.

To enable demanded consistency and the transfer of test data to reference conditions it is required to have quantitative information about the main influences on shear strength, at least accurate enough for engineering purposes. Thereby the main influences on shear strength can be categorised into (i) climatic conditions (moisture content & temperature), (ii) characteristics of test material including size & scale effects, (iii) test method & configuration, (iv) effects of duration of load & cyclic or dynamical loading, a.o. Aspects (i) to (iii) are treated further in this paper.

Concerning (i) literature data are presented in Tab. 1. It can be concluded that moisture content has a significant and practical relevant influence on shear strength of about 3% reduction of  $f_v$  with each percentage increase in  $u$ . Nevertheless, with increasing moisture content also a change in failure behaviour can be expected, meaning that brittleness may be somehow reduced.

Tab. 1 Shear strength: overview of influencing parameters moisture content and temperature

Literature source	Moisture Content ( $u$ )	Temperature ( $T$ )
Kollmann [5] (Pine)	~2.4% / 1% $\Delta$ MC	--
Kretschmann & Green [6] (Southern Pine)	~2.7% / 1% $\Delta$ MC	--
Rammer & McLean [7] (Douglas Fir & Southern Pine)	~5.3% / 1% $\Delta$ MC	--
Gerhards [8]	~2.6% / 1% $\Delta$ MC	0.4% / $\Delta$ 1°C
<b>Correction proposed</b>	<b>3% / 1% <math>\Delta</math> MC</b> <b>for 8% <math>\leq u \leq 20\%</math></b> $u_{\text{ref}} = 12\%$ acc. EN 384 [4]	<b>none for</b> <b>15°C <math>\leq T \leq 25^\circ\text{C}</math></b>

Concerning category (ii) a controversy discussion of the relationships between shear strength and other physical properties like density and stiffness characteristics is given. For example, results of Müller et al. [9] and Dahl & Malo [10] reflect no significant correlation between  $f_v$  and  $\rho$  for clear wood. Poussa et al. [11] found the same for GLT. Glos & Denzler [12] report a positive correlation between shear strength in RL-plane ( $f_{v,RL}$ ) and  $\rho_{12}$ . This can be argued by increasing latewood and thus increasing quantity of annual growth rings that have to be sheared. In contrast,  $f_{v,TL}$  (TL plane) and  $f_{v,45^\circ}$  (in-between RL & TL) are solely determined by the resistance of earlywood which density behaves nearly constant within a timber species. A certain correlation between  $f_v$  and  $\rho$  was also reported by Riyanto [13] (torsion tests) and by Rammer et al. [14] (structural timber, bending). Concerning stiffness e.g. Lam et al. [15] found no correlation between  $f_v$  and  $E_{m,0}$ . Shear tests of Dahl & Malo [10] reflect some correlation between shear modulus and strength in all plane directions, but only significant in RT. Comparable results concerning RL and TL are reported in Müller et al. [9]. Some papers discuss also the relationship between shear and bending (tension) strength, in particular on the 5%-level as for example explicitly and implicitly anchored in EN 338 [16], EN 338 [2] or EN 1194 [17], respectively, see

$$f_{v,k} = \min \left\{ 0.20 \cdot f_{m,k}^{0.8}; 3.8 \right\}, \quad f_{v,k} = \min \left\{ 1.6 + 0.1 \cdot f_{m,k}; 4.0 \right\} \quad (1)$$

according EN 338 [16] for C14 ÷ C50 and according EN 338 [2] for C14 ÷ C50, respectively, and

$$f_{v,g,k} = 0.32 \cdot f_{t,0,l,k}^{0.80} \quad (2)$$

according EN 1194 [17], for GL24c/h ÷ GL36c/h. Just for a general consideration: Solely theoretically, implementation of the relationship  $f_{t,0,k} = 0.60 \cdot f_{m,k}$  as anchored in EN 338 [16], [2] in equ. (1) leads to a formulation comparable with that anchored for GLT, see equ. (2). Beside this, Rammer & Soltis [18], Glos & Denzler [12] and Denzler & Glos [19] found no significant relationship between  $f_v$  and  $f_m$  and overall no significant influence of timber quality on shear strength. Although the relationship  $f_v$  and  $f_m$  can be questioned generally, because of deviating failure zones and different influencing parameters, nevertheless and in view of current European regulations, this aspect was also analysed within the herein reported research project. In this context, it appears meaningful to discuss the failure behaviour of wood in shear in RL- and TL-plane. By means of microscopic fracture surface analysis Keenan [20], [21] and Müller et al. [9] (besides mixing of RL and TL) conclude that shear failure in RL-plane is a combination of transwall failure in early- and latewood without rays and intrawall failure in latewood with rays. In TL-plane, failure is reported to occur solely as interaction of

intra- and transwall fracture in earlywood cells. Thereby rays may act as reinforcement in TL but as drawback in RL, introducing some rolling shear. As consequence  $f_{v,RL}$  is normally higher than  $f_{v,TL}$ . E.g. Keenan et al. [22] found about 6%, Denzler & Glos [19] about 20% and Dahl & Malo [10] about 40% higher mean values of  $f_{v,RL}$  in comparison to  $f_{v,TL}$ , whereas no significant difference was reported in Müller et al. [9]. A significant difference between  $f_{v,RL}$  and  $f_{v,TL}$  is also stated by Quaile & Keenan [23] and Bendsten & Porter [24].

The orientation of shear planes is also of relevance if shear interacts with stresses perpendicular to grain. By testing clear wood Keenan [20], [21] observed a significant influence on  $f_{v,RL}$  whereas  $f_{v,TL}$  was widely not affected. In case of interaction of  $\tau_{090}$  with  $\sigma_{c,90} \rightarrow f_{c,90}$  nearly a doubling of  $f_{v,RL,mean}$  was considered whereas  $f_{v,TL,mean}$  increased only about 20%. In case of  $\sigma_{t,90} \rightarrow f_{t,90}$  the mean shear strength  $f_{v,RL,mean}$  dropped down to about 50% and less,  $f_{v,TL,mean}$  to about 90% and less. It is argued that  $f_v$  in RL is influenced by some kind of friction whereas  $f_v$  in TL is not. Irrespective of shear plane orientation comparable results were found by Spengler [25] who observed an increase in  $f_{v,mean}$  up to about 50% and a decrease of 60% and more.

Tab. 2 Overview of crack coefficients  $k_{cr}$  according National Annexes of EN 1995-1-1 [1]

EN 1995-1-1 (Annex)	Country	$k_{cr,ST}$	$k_{cr,GLT}$	Comments
EN 1995-1-1:2009 [1]	EU	0.67	0.67	[-]
ON B 1995-1-1/NA:2010 [26]	Austria	0.67	0.83	$f_{v,k}$ independent of strength class: solid timber $f_{v,k} = 3.1$ N/mm <sup>2</sup> ; GLT $f_{v,k} = 3.0$ N/mm <sup>2</sup>
DK EN 1995-1-1/NA:2010 [27]	Denmark	1.0	1.0	[-]
DIN EN 1995-1-1/NA:2010 [28]	Germany	$2.0 / f_{v,k}$	$2.5 / f_{v,k}$	$f_{v,k}$ acc. EN 338 [2] & EN 1194 [17] $k_{cr}$ includes long-time effects; $k_{cr} \neq f$ {accepted crack depth}
SFS-EN 1995-1-1/A1:2008 [29]	Finland	0.67 1.0	0.67 1.0	in heated rooms or in corresponding moist. cond. (MC) permanently high MC; service class 2 & 3
prNF EN 1995-1-1/NA:2008 [30]	France	0.67 1.0 0.67	0.67 1.0 0.67	service class 1 & 2 with $d > 150$ mm, service class 1 & 2 for all other cases service class 3 – for all cases
DNA EN 1995-1-1/NA:2010 [31]	Netherlands	1.0 0.8	1.0 0.8	for beams with I- or T-section and a web of ST or GLT: $k_{cr} = 1.0$ , if $b_{web} / b_{flange} \geq 1.0$ , $k_{cr} = 0.8$ if $b_{web} / b_{flange} \leq 0.5$ , otherwise $k_{cr}$ acc. linear interpolation
UNI EN 1995-1-1/NA:2008 [32]	Italy			
NS-EN 1995-1-1/NA:2010 [33]	Norway			
PN-EN 1995-1-1/NA:2010 [34]	Poland			
SR EN 1995-1-1/NB:2008 [35]	Romania			
SS-EN 1995-1-1/A1:2008 [36]	Sweden			
STN EN 1995-1-1/NA:2008 [37]	Slovakia	0.67	0.67	[-]
SIST EN 1995-1-1/A1:2001 [38]	Slovenia			
ČSN EN 1995-1-1/NA:2007 [39]	Czech Republic			
BS EN 1995-1-1/A1:2008 [40]	Great Britain			
CYS EN 1995-1-1/A1:2011 [41]	Cyprus			

More related to structural timber and the aspect of knottiness Wilson & Cottingham [42] found no significant effect on  $f_v$  in case of higher or lower share of knots (lower or higher timber quality). Schickhofer [43] arguments higher shear strengths in glulam of lower timber quality due to a higher share of knots and a higher curvature of annual rings together with a higher amount of latewood in shear plane as reinforcement in contrast to GLT built up of high-grade lamellas. Denzler & Glos [19] argue that the activation of knots as reinforcement depends on the stressed shear plane. Following them, this activation can be expected in TL but not in RL. Concerning checks Yeh & Williamson [44] noticed that these typically occur in RL-plane, weakening shear resistance by reduction of shear area. This circumstance is perhaps not relevant for GLT but for edgewise loaded structural timber, see also Rammer [45] and his comments to ASTM D 3737-93 [46]. Rammer & McLean [7] analysed the influence of splits and checks on structural timber of Douglas Fir, Southern Pine and Engelmann Spruce. Test results revealed a decrease in  $f_v$  with increasing depth of checks. Predictions of  $f_v$  by means of fracture mechanics (mode II) delivered too conservative values, which indicate an influence of counteracting effects, e.g. positive size effects. Current European design standard for timber structures, EC 5 [1], considers the influence of cracks by the crack coefficient  $k_{cr}$ . Explicitly this

coefficient reduces the effective width of components stressed in shear and thus implicitly the characteristic shear strength, see

$$w_{eff} = w \cdot k_{cr} \quad (3)$$

Of course the quantification of this coefficient can be done individually by each member of the European Union. Tab. 2 lists current regulations in national annexes. Thereby diverse national regulations are found, e.g. linkage to national shear strengths (Germany), regulations in dependency to service classes (Finland & France) or in dependency of the geometry of cross sections (Netherlands). Following Tab. 2 most of European Union members agree with the regulations in the basic document EN 1995-1-1 [1], which assumes equal vulnerability of structural timber and GLT concerning cracking during exposure & life-time of structures. Austria accounts for expectable reduced cracking in GLT due to restricted dimensions of GLT-lamellas and balancing of stresses in the homogenised product GLT. France also considers the linkage between dimension and tendency to cracks. Nevertheless, in some nations timber and engineered timber products seem to behave differently, irrespective of their original provenience of raw material and production site. Germany regulates  $k_{cr}$  explicitly as factor, which calibrates European shear strengths to national values. Considering current values of  $f_{v,k}$  for structural timber and GLT according EN 338 [2] and EN 1194 [17], respectively, it consequences that higher quality timber is associated with lower  $k_{cr}$ -values. This is contrary to practical observations and expectations, e.g. for C14 and  $\geq$  C24 acc. EN 338 [2]:  $k_{cr} = 2.0 / 3.0 = 0.67$  and  $2.0 / 4.0 = 0.50$ , respectively, for GL24h and GL36h acc. EN 1194 [17]:  $k_{cr} = 2.5 / 2.7 = 0.93$  and  $2.5 / 4.3 = 0.58$ , respectively. Generally, it appears that there is definitive need for detailed clarification and harmonisation of European regulations.

Another important and perhaps one of the main parameters influencing shear strength is defined by its relation to the size of components and the volume exposed to shear. Again, controversial discussions in literature and consequently contradicting or insufficient regulations in standards are present. Thereby, as beams stressed in shear fail rather brittle the applicability and more often the validity of Weibull's weakest link theory (WLT; Weibull [47]) is presumed in discussions of size effects. This is in particular of interest as many of the assumptions underlying this theory are violated by the material timber. Nevertheless, e.g. Foschi & Barrett [48], [49] and Colling [50] applied WLT based on  $f_v \sim 2pWD$  for the explanation of size effects and the influence of stress distribution on shear strength. Thereby WD-shape parameters of  $\beta = 5.53$  and  $5.00$ , respectively, were applied, corresponding to  $CoV[f_v] = 20.9\%$  and  $22.9\%$ . Huggins et al. [51], Rammer et al. [14] and Rammer & Soltis [18] used the power model of WLT for the relationship between  $f_v$  and size. Thereby power parameters in the range of  $-0.20$  to  $-0.24$  for  $A_s$  (Rammer & Soltis [18], ST & GLT; Asselin [52], ST) and  $-0.15$  for  $V_s$  (Asselin [52], ST), which are far in line with previously mentioned  $\beta$ , were found by means of power regression analysis. In contrast, Longworth [53] and Keenan [20], [21] used logarithmic regression models to account for size effects on  $f_v$ , in particular in dependency of  $A_s$ . According 2pWD and extreme value theory a constant  $CoV[f_v]$ , independent of the volume under shear stress, depth or shear area is given. Thus size effects on  $f_{v,mean}$  and  $f_{v,05}$  are predicted to be equal. Observations made by Keenan et al. [22] contradict this circumstance. In contrast to  $f_{v,mean}$  practically no influence of  $V_s$  on  $f_{v,05}$  was observed. Based on simulations Klapp & Brüningshoff [54] concluded that WLT clearly overestimates depth and length effects on  $f_v$  of GLT. Of course, results of these simulations have to be treated with caution because the input data on basis of test results of Denzler & Glos [19] is censored. The applied test configuration failed in securing representative data of structural timber because tests on e.g. specimen with knots failed due to other reasons. In addition, the assumption of ND as representative statistical distribution model (RSDM) and deterministic treatment of  $f_v$  within each board in GLT-lamellas are additionally questionable aspects. Although shear failures in timber appear brittle, in modelling the characterisation as quasi-brittle is recommended. This is argued by the observation that some specimens show the ability to a further load increase even after partial failures. Mistler [55] and much earlier Daniels [56] developed models to account for parallel system action and the ability to redistribute stresses after partial failures. Such a parallel system in timber stressed in shear can e.g. be associated with increasing width, in timber bridge decks or flatwise-loaded GLT, see also Rammer [45]. Consequently, a reduction in  $f_v$  with increasing width in magnitude comparable with the influence of depth or length is not expected. For example, Yeh & Williamson [44] and Keenan [20], [21] found no influence on or even an increase of  $f_{v,mean}$  with increasing width of

structural timber and GLT. In contrast, shear area  $A_s$ , which is by definition a function of width and test length, is often confirmed and proposed as main geometric parameter for prediction of size effects on  $f_v$ , see e.g. Keenan [20], [21], Longworth [53], Keenan et al. [22], Rammer & Soltis [18], Asselin [52], Rammer et al. [14] and Gehri [57].

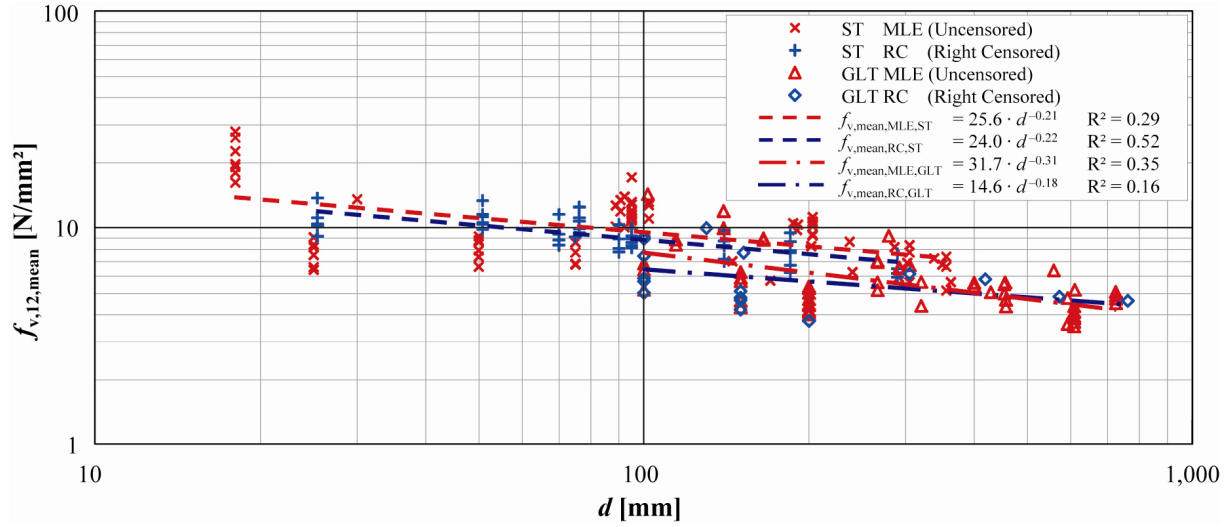


Fig. 1 Mean shear strength  $f_{v,12,mean}$  vs. depth  $d$  for GLT and ST: right-censored data and MLE-estimates

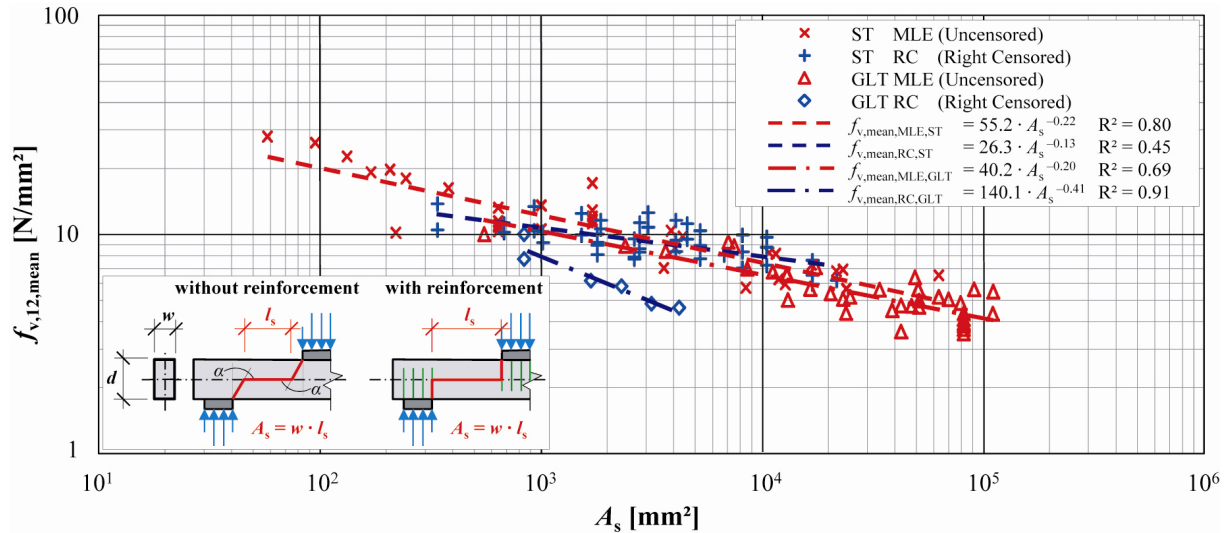


Fig. 2 Mean shear strength  $f_{v,12,mean}$  vs. shear area  $A_s$  for GLT and ST: right-censored data and MLE-estimates

On basis of a comprehensive literature survey of Lackner [58] the existence and magnitude of size effects on shear strength of structural timber (ST) and glued laminated timber (GLT, glulam) are discussed. For comparability of test data, solely results of shear strength gained from (three-, four- and five-point) bending tests performed on I-beams as well as prismatic cross sections but of various softwood species were considered. In the analysis,  $f_v$  following a two-parameter lognormal distribution (2pLND) as RSDM was assumed. All data was corrected to  $u_{ref} = 12\%$  according the proposal in Tab. 1. Parameters of shear ( $f_{v,mean}$ ,  $CoV[f_v]$ , etc.) and geometry were related to each other by means of regression and correlation analysis. In addition to Lackner [58] further data sets were included. The maximum-likelihood estimation technique (MLE) for right censored data was applied on data sets where early failures e.g. in bending or compression occurred, so far all required information was available. The parameters of 2pLND were estimated by maximising the log-likelihood function

$$\ln[L(\hat{\theta}|x_i)] = \max_{\theta} \left[ \ln[L(\theta|x_i)] \right], \text{ with } L(\hat{\theta}|x_i) = \prod_{i=1}^n f_{X_i}(x_i|\theta)^{d_i} \cdot [1 - F_{X_i}(x_i|\theta)]^{1-d_i} \quad (4)$$

with indicator variable  $d_i = 1$  if the event equals the target and  $d_i = 0$  otherwise.

Overall, 198 test-series of 23 literature sources were considered as shown in Tab. 9 (annex). Fig. 1 and Fig. 2 contain right-censored (RC) data and statistics from MLE of GLT and ST separately. Fig. 1 shows the dependency between  $f_{v,\text{mean}}$  and the depth  $d$ . This plot is based on 77# GLT samples (60# adopted by MLE) and 120# ST samples (70# adopted by MLE). Fig. 2 shows the dependency between  $f_{v,\text{mean}}$  and the shear area  $A_s$  of the tested samples. This plot is based on 45# GLT samples (39# adopted by MLE) and 80# ST samples (34# adopted by MLE). Hereby  $A_s$  was defined as the product of width and the length under constant maximum shear stress between support and loading minus an assumed length influenced by compression stresses considering a load distribution angle of  $\alpha = 30^\circ$  in standard tests and  $\alpha = 0^\circ$  in case of reinforcement against compression perpendicular to grain, see Fig. 2.

Although the quantity of tests included in Fig. 1 is much higher than in Fig. 2, the degree of determination of  $f_v$  vs.  $d$  is much lower than of  $f_v$  vs.  $A_s$ , for  $f_v$  of both, ST and GLT. Beside of  $f_{v,\text{MLE,GLT}}$  vs.  $d$  all power parameters of regression models are comparable and about 0.20, which is in-line with previously given literature data. In both plots, shear strength of GLT is on average below that of ST. This was already earlier observed by Soltis & Rammer [59] who remarked also a comparable size effect on GLT and ST and the fact that  $f_{v,\text{ST}} > f_{v,\text{GLT}}$ . Some explanations regarding this last circumstance are discussed later. All regression models applied on MLE-estimates reflect clearly the influence of censored data analysis giving overall higher estimates for  $f_{v,\text{mean}}$  by more or less comparable power parameters.

Overall, these two plots should clarify the answer of ongoing discussions and the question if size effects on shear strength of structural timber or GLT exist or not. This aspect is in particular of interest as current European standards do not include any size effect for structural timber and GLT whereas in a previous version (prEC 5 [60]) the influence of  $V_s$  on  $f_{v,05}$  was considered based on a 2pWD with  $\beta = 5$ , also for beams of continuous prismatic cross section! Nevertheless, beside the analysis of size effects on arithmetic means, based on data in Tab. 9, also the relationship between  $\text{CoV}[f_{v,\text{MLE}}]$  of ST and GLT vs. depth and shear area were analysed briefly. It was found that in both graphs of ST the  $\text{CoV}[f_{v,\text{MLE}}]$  increases with increasing dimensions, whereas vice versa was found for GLT. It can be concluded that the independency of shear resistances between GLT-lamellas in case of increasing depth (often in-line with an increase in length and thus in  $A_s$ ) provokes a decrease in variation due to serial system action. In contrast, an increase in depth of edgewise stressed structural timber seems to enlarge the possibilities how shear failures can develop and thus provokes raising of variability. Overall, these are only tendencies and fitted power models deliver insignificant slope parameters. Thus the assumption of a constant behaving  $\text{CoV}[f_v] = 15\%$  for both, ST and GLT, appears reasonable.

Based on the discussions in regard to influences on shear strength, e.g. of shear plane (RL, TL), knottiness, checks & splits and size, it can be concluded that differences between structural timber (primary stressed edgewise) and GLT (lamellas primary stressed flatwise) can be expected! For example, the gain in shear strength in RL, e.g. by stressing timber elements edgewise, is counteracted by the influence of checks and knots which are in particular common in timber from the centre of logs. Nevertheless, if the width of such specimen is increased it can be assumed that shear strength remains constant or becomes even slightly higher due to parallel system action. An increase in depth causes an enlargement of the zone under nearly maximum shear stress. Consequently, the probability that a weaker section arises within this zone increases. In particular in timber which origins near the pith, also the probability that the slope of annual rings exceeds nearly  $45^\circ$  increases. Thus, a failure in TL can be expected. In standard test procedures, test span is normally a function of depth. Thus an increase of depth coincides directly with an increase in length and thus also with an enlargement of  $A_s$ . Consequently, a distinctive reduction of shear strength due to size effects is expected. In contrast, edgewise stressed GLT suffers from shear failures in TL. In high quality timber, which lacks of reinforcing knots together with TL-failure plane, lower shear strength than in edgewise stressed structural timber is expected. An increase in width of GLT in case of lamellas of low strength, which is normally cut near the centre of logs, increases the probability that the curvature of annual rings becomes steeper, at least at the outer regions of lamellas. This aspect, together with a higher share of knots as reinforcement, raises shear strength. Nevertheless, in deeper GLT-beams again the zone of maximum shear stress increases. In contrast to structural timber, an increasing amount of lamellas is involved suffering from serial system action. Hereby even a higher size effect than in structural timber can be presumed as the lamellas and thus their individual shear resistances are iid (identical and

independent distributed). To conclude, there are two main reasons why shear resistance in GLT can be expected to be lower than in structural timber of the same quality: the first aspect is that failure primary occurs in the weaker TL-plane, although and in particular in lower strength timber a positive effect from reinforcing knots can be expected. Secondly, the iid shear resistance of GLT-lamellas, which raises the magnitude of size effects.

The third category (iii) deals with influences on shear strength caused by test method & configuration. Starting with configurations for testing small clear specimen, the shear block test according ASTM D 2555-98 [61] & ASTM D 143-94 [62], the shear test of EN 408 [63] (former EN 1193 [64]), the torsion test, Iosipescu & Arcan test and the three-, four- or five-point bending tests (3pB, 4pB, 5pB) can be mentioned. Hereby specimen with I- or prismatic cross section are used. The general aim is to initiate nearly constant and pure shear stresses, but this aim is practically only (nearly) reached by Iosipescu, Arcan or torsion tests (see e.g. Dahl & Malo [65] and Gupta & Siller [66]). All other configurations suffer from interaction of shear with compression or tension stresses perpendicular to grain or local stress peaks which lead to unrealistic shear strengths, if explicit consideration in analysis, in particular the later use in engineering practice, is taken into account (see e.g. Gupta & Siller [66] and Riyanto [13]). Furthermore, due to the orthotropic material shear resistances of in total three different shear planes, RL, TL and RT are required.

In structural and glued laminated timber, the aims on an adequate test configuration are comparable. In Europe EN 408 anchors a shear test configuration for a specimen of length  $300 \pm 2$  mm, a width of  $32 \pm 1$  mm and a depth of  $55 \pm 1$  mm. The specimen shall be glued to steel plates, mounted in a test machine and loaded in an angle between the load direction and the longitudinal axis of the test sample of  $14^\circ$ . Based on the results of e.g. Denzler & Glos [19] it was concluded that this shear test configuration is not adequate to derive shear strength values representative for structural timber. Characteristics of ST like knots or knot clusters cannot be tested in shear because of early failures in the glue-line between the metal plates and the specimen and / or due to exceedance of resistances perpendicular to grain. Hereby it is not only a censoring of data but due to scaling effects in particular a censoring of the material itself. This makes a reliable derivation of  $f_v$  by means of MLE for right censored data even impossible. Comparable remarks are reported for the shear block test configuration of ASTM. Hereby shear resistances of clear wood are derived whereby local stress peaks and the interaction of shear stresses with moments additionally occur. Riyanto [13] provides a valuable overview of pros and cons of various test configurations. Although he confirmed that shear strength of clear wood correlates with that of structural timber, irrespective of the applied test method, he proposed to apply 3pB configuration for derivation of practical relevant shear strengths. Nevertheless, for determination of shear strength of the material rather than of a structural component he suggests to use torsion tests. Based on own experiences made and in review of literature (e.g. Quaille & Keenan [23], Schickhofer & Obermayr [67], Schickhofer [43], Korin [68], [69], Riyanto [13] and Gehri [57]), the following aspects are seen as worthwhile to consider:

- 1) shear stress distribution during testing should be of practical relevance: It is recommended to perform bending tests. Hereby 3pB instead of 5pB is preferred, not only because of the advantage of a statically determined system;
- 2) it is recommended to test I-beams: Hereby flanges are characterised by high resistance in bending and compression perpendicular to grain. The web, representing the test specimen, has comparably low resistance in shear. For a failure rate in shear of  $\geq 90\%$  shear forces should be calculated equivalent to  $f_{v,95}$ . At this load level edge bending resistance of flanges should be  $\geq f_{m,05}$ . The test span follows from optimisation of shear and bending resistance. If the bending resistance of the associated strength class is below the requirements it is advised to proof load bottom flanges in tension parallel to grain by applying a proof stress  $\sigma_{t,0,pl} = \sigma_{m,05} \mid \tau_{95} = f_{v,95}$ . The use of slotted I-beams, e.g. according Korin [69], is not advised. Hereby the test section (web) is judged as being not representative. In I-beams, the shear stress distribution within the web leads to higher fullness parameters. This means that the probability of failure is higher if compared to prismatic cross sections of same geometry and size. Consequently, minor conservative shear strengths are derived. In this respect, shear failure is initiated in one of two possible shear zones. Thus a serial system of two is given;

- 3) equality of  $E_{0,flange} \approx E_{0,web}$  per specimen is recommended: This is to prevent jumps in the normal bending stresses;
- 4) a maximum difference of shear stresses at contact zone between web and flange of  $\leq 5 \text{ N/mm}^2$  is proposed: Hereby shear failures in the transition zone between web and flange and in particular in the glue-line have to be prevented;
- 5) the application of reinforcements in compression perpendicular to grain is advised: Full-threaded self-tapping screws or glued-in rods as reinforcements at supports and centre loading area are recommended. This was already outlined by Gehri [57] who focused in particular on the application of glued-in rods, to minimise the volume of specimen by maximising the volume stressed in shear and to assure nearly uniform shear stress distributions in longitudinal direction of the beam between the nearest corners of loading and support plates;
- 6) evaluation of  $f_v$  by means of simple beam theory, rigid compound action and MLE should be applied: Hereby the failure made by applying simple beam theory for a plate-like specimen should be corrected, e.g. by performing FE-analysis as shown e.g. in Keenan [20] and Aicher & Ohnesorge [70]. For example, Quaile & Keenan [23] state that at least a distance of two times the depth between support and loading should be kept; otherwise  $f_v$  evaluated according simple beam theory is overestimated. Early failures in bending or compression shall be considered in the application of MLE for right-censored data. After careful judgement, the same procedure shall be also applied for specimen (e.g. with checks) already before testing;
- 7) the bending stiffness of the load-distribution plates at supports and loading zone should be equivalent with that of the I-beam: This is recommended to prevent local stress concentrations and local failure in compression perpendicular to grain;

Overall, a comprehensive overview of relevant aspects, concerning the definition of a shear test configuration for testing structural timber and GLT, was given. As next above statements are clarified for the herein tested samples and the experiences are discussed.

### 3 Materials and Methods

#### 3.1 Material

The accomplished test program involves seven series analysing shear strength by means of I-beams tested in 3pB and one series for determination of bending characteristics on prismatic specimens by means of standard 4pB tests. The material used was Norway spruce (*Picea abies* (L.) Karst.) of provenience Styria (Austria, Central Europe). It was kiln dried and visually graded to S10+ (DIN 4074-1 [71]), representing strength class C24+ according EN 338 [2]. To reduce influences by the radial position within the log (wood zones, share of knots, affinity to checking, etc.) a constant normal distance between pith and right side of the web specimen of 60 mm was chosen. Before final testing, several pre-examinations were made, e.g. determination of moisture content, density and modulus of elasticity  $E_{dyn,0,12}$  based on eigenfrequency measurement device of Eiser & Kastner [72]. The static modulus of elasticity  $E_{t,0,12,est}$  was estimated based on results of Eiser & Unterwieser [73], see

$$E_{t,0,12,est} = \frac{E_{dyn,0}}{1,04} \cdot [1 + (u - 12\%) \cdot 2] \quad (5)$$

Results of  $E_{t,0,est,12}$  were used for stiffness grading and fitting of web and flanges with a maximum difference of  $E_{t,0,est,12,flange}$  and  $E_{t,0,est,12,web}$  of  $1,000 \text{ N/mm}^2$ . The estimation of the relationship  $f_{m,05}$  vs.  $f_{v,95}$ , done by Lackner [58], based on a regression function gained from GLT shear tests of Schickhofer [43]. After availability of improved estimates from literature, an adaptation of the tests was necessary. As the material was already ordered and most of the specimens fabricated, adaptation was only possible in the span / depth ratio. That is why this ratio varies finally as shown in Tab. 3. After updating of information, the proof loading performed on bottom flanges was not sufficient in all series causing a higher share of bending failures than initially presumed. The estimation of forces was done by applying simple beam theory and rigid composite action. To account for the bias made by

applying simple beam theory on a more plate-like specimen, an FE-analysis was additionally performed. FE-modelling and results will be presented later (see section 3.2). A rigid connection between web and flanges was assured by means of polyurethane adhesive. Overall, more detailed information about the material, preparation and testing can be found in Lackner [58] and Gattermig [74].

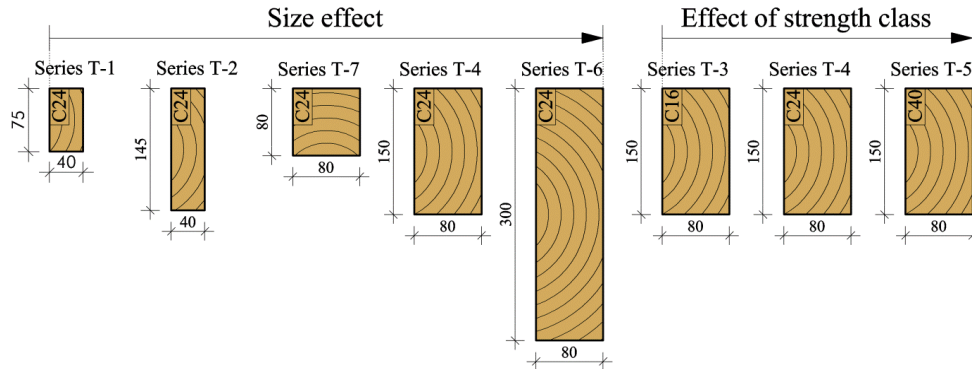


Fig. 3 Nominal cross sections and quality of test specimen (web) for analysing size effects (left) and the effect of timber quality (right)

The influence of size on shear strength was analysed by means of five series of varying depth and / or width (see Fig. 3, left). For falsification of the relationship  $f_{m,05}$  vs.  $f_{v,05}$  as anchored in EN 338 [16], [2] three series (T-3 to T-5; see Fig. 3, right), were tested in addition. The allocation of specimen to T-3 to T-5 was done according their stiffness, with  $E_{t,0,12,est,mean} \approx E_{0,mean,EN\ 338}$ , to C16 (T-3), C24 (T-4) and C40 (T-5).

The suitability of allocation of stiffness graded specimen to the strength class system of EN 338 [2] was controlled by an additional series T-8 tested in standard 4pB according EN 408 [63]. An overview of main specifications and results of mean density and stiffness of all series is provided in Tab. 3.

Tab. 3 Specifications of series T-1 to T-8 and mean values of  $E_{t,0,12,est}$  and  $\rho_{12}$

	Series	Material	Quantity	Dimensions				Characteristics	
				Global		Web	Flange	Web	Web
				$l$	$l_{ef}$	$w_w / d_w$	$w_f / d_f$	$E_{t,0,12,est,mean}$	$\rho_{12,mean}$
	[--]	[--]	[--]	[mm]	[mm]	[mm]	[mm]	[N/mm <sup>2</sup> ]	[kg/mm <sup>3</sup> ]
Shear Tests (3pB)	T-1	spruce C24+	* 40 #	985	$3.7 \cdot d_w$	40/75	110/40	11,307	447
	T-2	spruce C24+	* 34 #	1,970	$3.1 \cdot d_w$	40/145	110/80	12,191	449
	T-3	spruce C16	** 11 #	1,970	$2.2 \cdot d_w$	80/150	220/80	8,505	389
	T-4	spruce C24	* 40 #	1,970	$3.2 \cdot d_w$	80/150	220/80	11,420	414
	T-5	spruce C40	** 40 #	1,970	$3.7 \cdot d_w$	80/150	220/80	14,247	467
	T-6	spruce C24+	* 20 #	3,940	$3.7 \cdot d_w$	80/300	220/160	11,708	417
	T-7	spruce C24+	* 36 #	1,200	$3.3 \cdot d_w$	80/80	220/80	10,747	430
4pB	Series	Material	Quantity	$l$	$w$	$d$	$E_{t,0,12,est,mean}$	$\rho_{12,mean}$	
	T-8	spruce C24+	* 50 #	2,850	80	150	12,125	441	

\* ... strength class according EN 338 [2]

\*\* ... allocation to strength class system according EN 338 [2] solely by stiffness grading

## 3.2 Methods

### 3.2.1 Test configuration for determination of shear strength and modulus

Based on the discussions in chapter 2 a 3pB-test configuration together with an I-beam of optimised geometry was developed to meet widely all before defined requirements (see Lackner [58] and Gattermig [74]). The proposed configuration, which in principle enables coherent determination of shear strength and shear modulus of structural timber, GLT and other linear engineered timber products, is presented in Fig. 4. Further requirements on test procedure, e.g. climate, moisture content

and time to failure were taken equivalent to the standard 4pB-test according EN 408 [63]. There are some benefits of the test configuration additional to the listing (chapter 2) above:

- the configuration enables testing of practical relevant shear characteristics on a wide range of timber species and quality including all their growth characteristics and by means of a representative shear area;
- loading in bending corresponds to the common load condition of beams in real timber structures;
- testing is possible on common bending test devices with just a few minor adaptations.

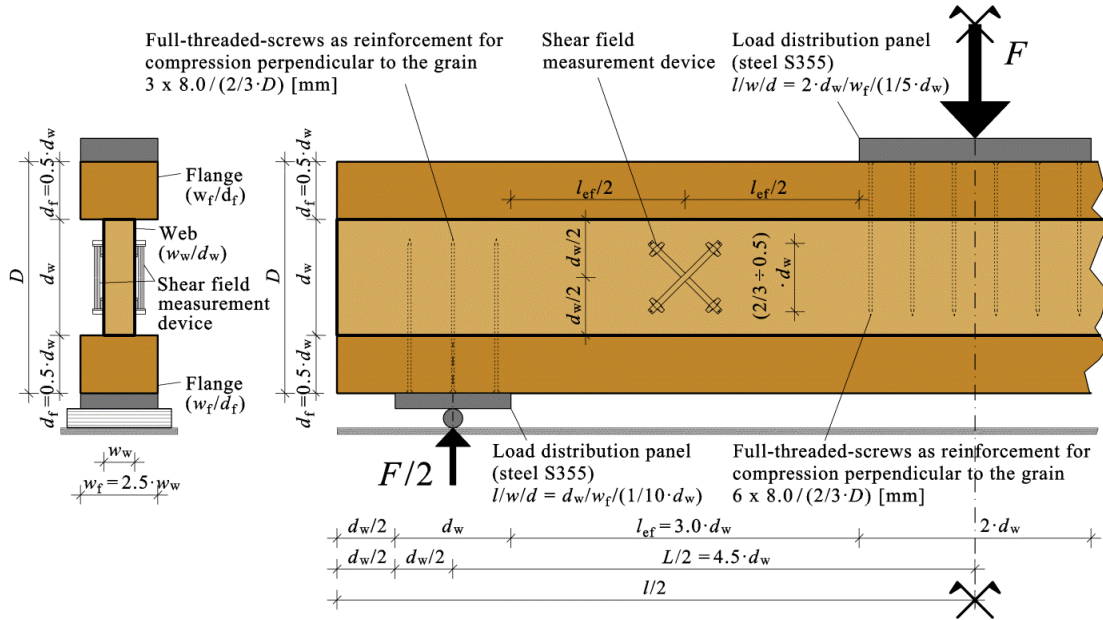


Fig. 4 3pB-test configuration for the determination of shear characteristics of structural timber, GLT and other suitable linear engineered timber products

### 3.2.2 FE-analysis for comparison of shear stresses according simple beam- and plate-theory

The proposed 3pB shear test configuration has a span to depth ratio of  $L/D = 4.5$  (tested series:  $3.4 \div 5.0$ ), which represents more a plate than a linear member. Thus calculation of shear stress by means of linear elastic beam theory is somehow biased. To enable a suitable correction, a FE-analysis was implemented for modelling prismatic and I-beam cross sections with and without reinforcement (see Fig. 5). Based on 2D modelling in FE-program RFEM (version 4.xx) mirroring the test configuration as shown in Fig. 4, the influence of varying  $L/D$  ratios on shear stress in the centre between support and loading and in neutral axis was analysed. Therefore the reference cross-section of the web of an I-beam with  $w_w/d_w = 80/150$  mm and in addition a beam with rectangular cross section of  $w/d = 80/150$  mm was used.

The FE-model itself is based on an orthotropic material representing C24 according EN 338 [2], with  $E_{0,mean} = 11,000$  N/mm<sup>2</sup>,  $G_{090,mean} = 690$  N/mm<sup>2</sup> and  $E_{90,mean} = 370$  N/mm<sup>2</sup>. A mesh-size of  $15 \times 15$  mm<sup>2</sup> was applied. The web and flanges were modelled as rectangular surfaces assuming a rigid composite action in-between. The width of the web and flanges was implemented by means of a “theoretical orthotropic width” due to the limitations of RFEM in respect to 3D modelling of orthotropic materials.

In specimens without reinforcement, the load was applied as uniformly distributed line-load placed on a load distribution panel. The support was modelled with the aid of the support distribution panel and a point-support instead of a roller bearing. In specimens with reinforcement against early failures in compression perpendicular to grain the load was initiated by line-loads along the length of the full-threaded screws. The supports were modelled as line-spring-supports along the bedding-screws.

The results of FE-analysis as ratio between shear stress according FEM ( $\tau_{xy,FE}$ ) and shear stress calculated by means of simple beam theory ( $\tau_{xy,BT}$ ) are shown in Fig. 5. Thereby and as expected a clear and increasing bias in  $\tau_{xy,BT}$  with decreasing  $L/D$ -ratio can be quantified. For the proposed shear

test configuration and up to  $L/D \geq 6$  the differences between specimen with and without reinforcement are negligible. Following Quaile & Keenan [23] who recommended a distance between support and loading of  $\geq 2 \cdot D$  a bias in  $\tau_{xy,BT}$  of about 10% and 20% in testing prismatic or I-beam cross sections, respectively, can be expected. Following the results in Fig. 5 application of simple beam theory for calculation of shear strength clearly overestimates real shear resistance with decreasing  $L/D$ -ratio. As the use of this theory is common and accurate enough in engineering practice and structural components with a common  $L/D$ -ratio of  $15 \div 20$  it is required to correct  $f_{v,12,BT}$  derived from tests to “real” shear strengths relevant for practice. This is done later in chapter 5.

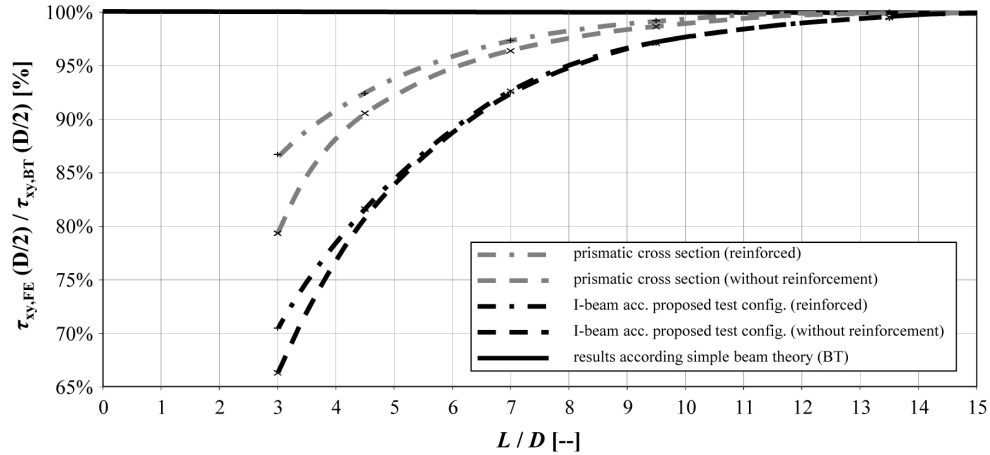


Fig. 5 Relationship between the shear stress according FE-analysis  $\tau_{xy,FE}$  and according simple beam theory  $\tau_{xy,BT}$  in dependency of the  $L/D$ -ratio: prismatic cross sections and I-beams, with or without reinforcement

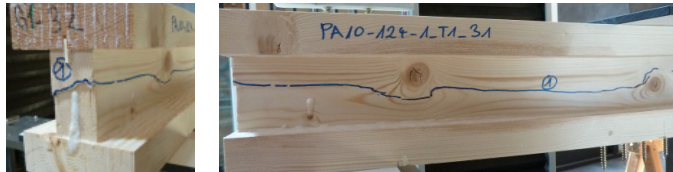
## 4 Results

### 4.1 Results of 3pB shear tests

Tab. 4 gives a failure classification schema of all main causes observed during testing, together with a brief description and the total realised quantities (see also Tab. 5). A summary of main statistics of all test results is provided in Tab. 5. Based on the moisture content  $u$ , determined for every specimen at the time of testing (according ON EN 13183-1 [75], except series T-6: determined by means of Gann Hydromette M4050), density and E-modulus were transferred to  $u_{ref} = 12\%$  according EN 384 [76]. Adaptation of shear strength was done according the proposal in Tab. 1. Statistics of  $f_{v,12}$  involve only specimens which failed in shear within the web (S\_WEB).

As shown in Fig. 4, in series T-6 also shear modulus  $G_{090,12,SF}$  was determined according Brandner et al. [77] but with adaptation to account for the I-beam. Values were transferred to  $u_{ref} = 12\%$  equal to E-modulus according EN 384 [76]. In total 8 of 10 tests of series T-6 with shear measurement devices and without checks in measurement domain could be accepted. The main statistics are:  $G_{090,12,mean} = 599 \text{ N/mm}^2$  ( $G_{090,12,50} = 586 \text{ N/mm}^2$ ) and  $CoV[G_{090,12}] = 12.0\%$ . Furthermore, simple linear regression analysis of  $G_{090,12}$  vs. density  $\rho_{12} [\text{kg/m}^3]$ ,  $E_{t,0,12,est} [\text{N/mm}^2]$  and  $f_{v,12} [\text{N/mm}^2]$  gave adjusted squared correlation coefficients ( $R^2_{adj}$ ) of +0.33, -0.16 and +0.33, respectively.

Tab. 4 Overview of the classified causes of failure of 3pB shear tests; series T-1 to T-7

Cause of failure	Quantity	Visualisation
<b>S_WEB</b> shear failure of web (test section)	101 #	

Cause of failure	Quantity	Visualisation	
<b>S_TRA</b> shear failure at the transition zone between web and flange (failure of glue line was not noticed)	63 #		
<b>S_PEC</b> shear failure caused by growth and production characteristics within the web (e.g. cracks or bark inclusions)	14 #		
<b>B_BFL</b> bending-tension failure of the bottom flange	25 #		
<b>OTHER</b> involving miscellaneous causes, e.g. shear failure in the upper or lower flange, bending failure in the web, etc.	18 #		

Tab. 5 Statistics of three-point bending tests carried out on I-beams of series T-1 to T-7

Series		T-1	T-2	T-3 "C16"	T-4 C24	T-5 "C40"	T-6	T-7
$u$ [%]	Mean	12.9%	11.1%	10.3%	10.0%	10.7%	11.1%	11.1%
	R (range)	1.1%	0.7%	0.8%	1.5%	1.5%	1.3%	1.6%
$\rho_{12}$ [kg/m <sup>3</sup> ]	mean	447	449	389	414	467	417	432
	median	445	448	390	413	463	421	430
	CoV	7.1%	6.0%	3.7%	5.8%	6.5%	6.5%	10.6%
$E_{t,0,12,est}$ [N/mm <sup>2</sup> ]	mean	11,307	12,191	8,505	11,420	14,247	11,708	10,747
	median	11,102	11,846	8,513	11,373	14,100	11,345	10,269
	CoV	13.2%	11.9%	8.7%	3.9%	7.1%	11.8%	9.6%
realised numbers of failure categories [-]	S_WEB	10 #	21 #	7 #	21 #	19 #	10 #	13 #
	S_TRA	11 #	7 #	--	9 #	14 #	4 #	18 #
	S_PEC	1 #	3 #	1 #	--	2 #	6 #	1 #
	B_BFL	16 #	1 #	1 #	2 #	3 #	--	2 #
	OTHER	2 #	2 #	2 #	8 #	2 #	--	2 #
	quantity	40 #	34 #	11 #	40 #	40 #	20 #	36 #
$\tau_{1,12}$ [N/mm <sup>2</sup> ]	min	5.4	2.8	3.2	5.1	3.4	1.0	4.9
	mean	7.6	6.8	6.4	6.4	6.1	4.3	7.8
	median	7.7	7.0	6.6	6.3	6.4	4.6	7.7
	max	9.5	9.9	7.7	8.3	8.0	6.5	9.0
	CoV	12.2%	22.3%	18.9%	11.9%	18.5%	34.2%	10.0%
	quantity	10 #	21 #	7 #	21 #	19 #	10 #	13 #
$f_{v,12}$ [N/mm <sup>2</sup> ]	min	6.6	3.9	5.9	5.1	3.4	2.7	7.1
	mean	7.9	6.7	6.4	6.6	6.0	4.8	8.1
	median	7.9	7.0	6.3	6.5	6.5	4.8	8.0
	max	8.9	9.5	7.2	8.3	8.0	6.5	8.9
	CoV	9.1%	19.2%	7.0%	12.9%	22.6%	22.9%	6.2%

## Results of 4p-bending tests

The main statistics of standard 4pB-tests according EN 408 [63] of series T-8 are given in Tab. 6. One of in total 50 specimens had to be rejected because of not fulfilment of the requirements on S10 / C24. Computation of global bending E-modulus  $E_{m,0,g,12}$  was done by assuming  $G_{090,mean} = 500$  N/mm<sup>2</sup>. The empirical 5%-quantile of bending strength based on rank statistics is given by  $f_{m,05} = 22.7$  N/mm<sup>2</sup>, the

characteristic value following EN 14358 [78] by  $f_{m,k} = 22.6 \text{ N/mm}^2$ . The characteristic density according EN 384 [4] reveals  $\rho_k = 404 \text{ kg/m}^3$ . Overall, the requirements of C24 according EN 338 [2] are fulfilled for E-modulus and density, the realised characteristic bending strength is a bit lower.

Tab. 6 Main statistics of 4pB-tests of series T-8

Series T-8	$u$ [%]	$\rho_{12}$ [kg/m <sup>3</sup> ]	$E_{\text{dyn},0,12}$ [N/mm <sup>2</sup> ]	$E_{m,0,1,12}$ [N/mm <sup>2</sup> ]	$E_{m,0,g,12}$ [N/mm <sup>2</sup> ]	$f_{m,u}$ [N/mm <sup>2</sup> ]
Quantity	49 #	49 #	49 #	49 #	49 #	49 #
min	9.1 %	398	7,148	6,414	6,937	21.3
mean	<b>9.7 %</b>	<b>441</b>	<b>12,611</b>	<b>11,673</b>	<b>11,873</b>	<b>44.1</b>
median	9.6 %	449	12,726	11,619	12,162	43.3
max	10.9 %	475	16,191	15,202	15,507	68.2
CoV	<b>4.2 %</b>	<b>5.1 %</b>	<b>18.5 %</b>	<b>21.0 %</b>	<b>19.9 %</b>	<b>31.4 %</b>

## 5 Discussion

Since the aim of this testing program was to determine shear strength of visually judged unchecked test specimens representative for the analysed strength classes of timber, specimens with pre-existing strength-reducing characteristics like distinctive drying-cracks or bark pockets, categorised as S\_PEC (see Tab. 4), were excluded from further statistical processing, irrespective their realised resistance in shear. Hereby it has to be outlined that experiences made during testing underline the necessity for further detailed analysis about the influence of checks and splits on shear strength, as this aspect has a decisive impact on strength but was not explicitly analysed here.

In total only 101 of 221 of in shear tested specimens failed in shear within the web. As for all other beams the information of maximum shear stress at first failure due to other reasons ( $\tau_{1,12}$ ) has been available, statistical parameters of  $f_v$  assuming 2pLND as RSDM (in line with e.g. JCSS [79]) and other statistics were estimated by applying MLE for right censored data, see equ. (4). Fig. 6 shows box-plots of shear stresses and shear strengths as well as estimates from MLE.

The MLE estimates for mean and coefficient of variation were further adjusted according the results of FE-analysis. The results and adjustment parameters are given in Tab. 7.

Tab. 7 Statistics of  $f_{v,12}$  based on estimates from MLE for right censored data, adapted in regard to FE-analysis

Series		T-1	T-2	T-3	T-4	T-5	T-6	T-7
Quantity [--]		39 #	31 #	10 #	40 #	38 #	14 #	35 #
$f_{v,MLE,12}$ [N/mm <sup>2</sup> ]	mean	8.9	7.5	6.9	6.9	7.2	5.3	8.5
	CoV	12.5%	24.4%	11.9%	12.5%	28.6%	27.1%	7.5%
	adjustment	84%	80%	74%	81%	84%	84%	75%
$f_{v,MLE,adj,12}$ [N/mm <sup>2</sup> ]	mean	<b>7.4</b>	<b>6.0</b>	<b>5.1</b>	<b>5.6</b>	<b>6.0</b>	<b>4.5</b>	<b>6.3</b>
	CoV	<b>15.0%</b>	<b>30.4%</b>	<b>16.1%</b>	<b>15.4%</b>	<b>34.3%</b>	<b>32.1%</b>	<b>10.1%</b>

Following the results, doubling of depth and thus also the tested length (nearly constant  $L/D$ -ratio) leads to a distinctive reduction in average shear strength. Results of pairwise t-test accomplished on logarithmised data comparing  $f_{v,12,MLE,adj}$  of T-1 to T-2 and T-4 to T-6 gives a rejection of the hypotheses of equal mean values at  $\alpha \leq 1\%$  significance level. In contrast, the rejection of the same hypotheses by comparing means of series T-2 and T-4, which corresponds to a doubling of width, is not possible. Pairwise t-tests performed on T-3 to T-4, T-4 to T-5 and T-3 to T-5 allow no rejection of assumed equal mean-values. Thus, a significant influence of strength class on average shear strength cannot be confirmed. Interestingly, doubling of depth (which coincides with doubling of length and  $A_s$ ; T-1 to T-2, T-4 to T-6) doubles also the  $\text{CoV}[f_{v,12,MLE,adj}]$ , whereas doubling of width (T-2 to T-4) halves the  $\text{CoV}[f_{v,12,MLE,adj}]$ . These observations are not judged as hazard results because ratios of  $L/D$  as well as mostly also the share of shear failures (aside from T-1 with only 26% share of S\_WEB) between compared test series are not that different. Although analysis of literature data (see chapter 2) indicates an increase of  $\text{CoV}[f_v]$  with increasing depth and length in structural timber the herein observed change in variability was not expected. Of course, there are no explanations for the magnitude of changing variability but some for the tendency in general.

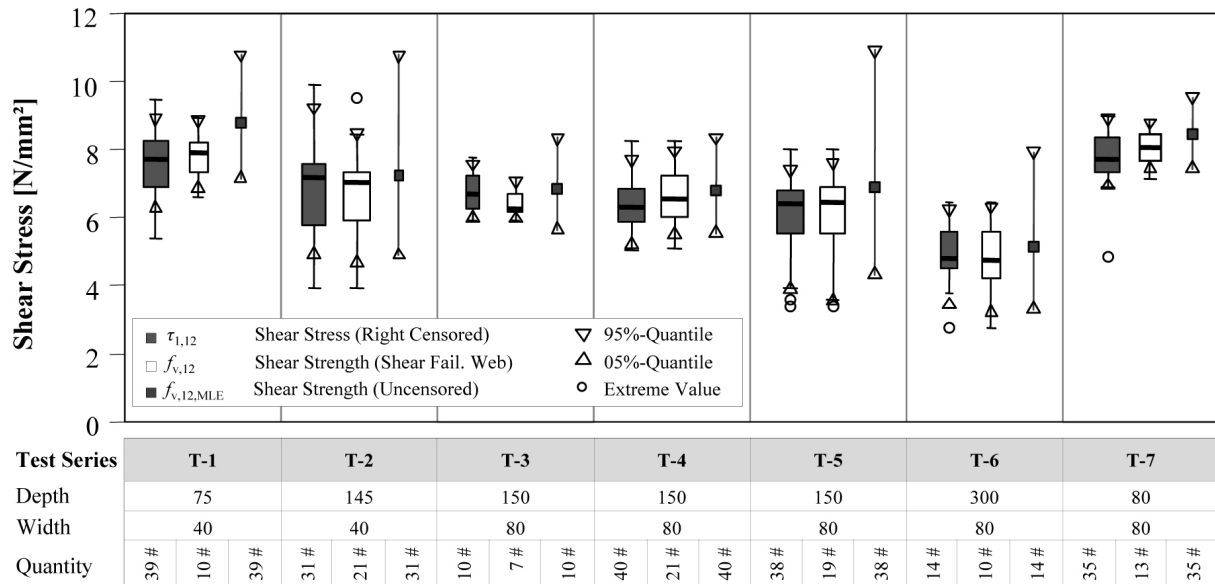


Fig. 6 Box-plots of shear stress at first failure ( $\tau_{1,12}$ ), shear strength at first failure ( $f_{v,12}$ ) and of estimates for shear strength  $f_{v,MLE,12}$  based on MLE for right-censored data: width of boxes adjusted to the number of realisations

As already outlined for edgewise stressed structural timber in chapter 2 an increase in depth reduces the gradient of the parabolic shear stress distribution in z-direction. Absolutely, this implies that a larger zone of the specimen is nearly under maximum shear stress. In case of I-beams, in proportion of web and flanges used in herein reported project, this effect is lower. The difference between maximum shear stress in centre line and that at the transition zone between web and flange is only about 10%. Thus nearly the whole cross section is under constant shear stress. Nevertheless, an increase in depth reduces also the gradient of annual rings on the outer zones of the web. Tests of Denzler & Glos [19] showed that an average gradient of  $45^\circ$  lead already to a reduction of  $f_v$ , equal to that in TL-plane. Thus it can be assumed, that shear failures in deeper beams occur more often eccentrically. Herein presented tests show increasing mean values of eccentricity, starting at about 15 mm (T-1) to about 30 mm (T-2, T-3, T-4, T-5) and to about 55 mm in T-6. In contrast, doubling of width reflected no effect on eccentricity.

The energy required for TL-shearing is lower than for RL-plane, so far clear wood is concerned, but in structural timber knots act as reinforcement in TL-plane. Occurrence of single knots and knot clusters varies not only in longitudinal direction but also in width (here depth) and also, but of lower importance, in thickness. Hereby a reduction in share of knots with increasing width (depth) can be expected. In contrast, the probability of occurrence of (visually hard or even not detectable) drying checks, which also weaken shear resistance in RL, can be also expected to increase with increasing width (depth). Consequently, with increasing depth an increase of failure causes and possible failure planes can be expected which coincides with a higher variability in realised shear strength. Due to the direct relationship of length and depth via the regulation of a constant  $L / D$ -ratio in tested specimens, even a further increase in variability can be expected. For example, the probability that knot clusters along the test length may occur and the diversity in their formation increases with increasing length.

The reduction in  $\text{CoV}[f_{v,12,MLE,adj}]$  with increasing width can be traced back to the effect of parallel system action and thus to a higher amount of varying latewood which has to be sheared. Hereby a principle change in failure plane does not occur within the practical range, thus the variability in failure causes does not increase.

Concerning the falsification of the relationship  $f_m$  vs.  $f_v$  and as already mentioned above, statistically a significant difference in  $f_{v,mean}$  between herein analysed series (T-3, T-4 & T-5) of different nominal strength (stiffness) classes could not be found, although a minor positive trend is given (see e.g. Tab. 7, Tab. 8 and Fig. 6). Due to variation in  $\text{CoV}[f_{v,12,MLE,adj}]$  this trend is not so clear on 5%-level. In Tab. 8 also 5%-quantiles calculated based on realised means but fixed  $\text{CoV}[f_v]$  are shown. Hereby two different variations are analysed; first a  $\text{CoV}[f_v] = 25\%$  as anchored in JCSS [79] and secondly a  $\text{CoV}[f_v] = 15\%$  as found on average from literature survey presented in chapter 2. In comparison to

current regulations of  $f_{v,k}$  according EN 338 [2] it can be concluded that under the conservative assumption of a  $\text{CoV}[f_v]$  of 25% congruent results based on test data and with  $f_v \sim 2\text{pLND}$  can be found. In respect to findings so far and in-line with current attempts to regulate shear strength of GLT independent of strength class in prEN 14080 [3], the same is also proposed for structural timber (see also e.g. Glos & Denzler [12] and Poussa et al. [11]). Hereby a value of  $f_{v,k} = 4.0$  at reference geometries of  $d_{\text{ref}} = 150$  mm and  $w_{\text{ref}} = 80$  mm and for visually unchecked structural components is suggested.

Tab. 8 Comparison of past and current characteristic shear strengths of EN 338 [16], [2] with test results, in dependency of (nominal) strength (stiffness) class

strength class acc. EN 338 [2]	„C16“	C24	„C40“
$f_{v,12,\text{mean},\text{MLE},\text{adj}}$	<b>5.1</b>	<b>5.6</b>	<b>6.0</b>
$f_{v,12,05\ 2\text{pLND},\text{MLE},\text{adj}}$	3.9	4.3	3.3
$f_{v,12,05\ \text{CoV}=25\%,\text{MLE},\text{adj}}$ (CoV acc. JCSS [79])	3.3	3.6	3.9
$f_{v,12,05\ \text{CoV}=15\%,\text{MLE},\text{adj}}$ (CoV acc. literature)	3.9	4.3	4.6
$f_{v,k}$ acc. EN 338 [16]	1.8	2.5	3.8
$f_{v,k}$ acc. EN 338 [2]	3.2	4.0	4.0

Furthermore, the influence of size on shear strength of edgewise stressed structural timber was examined. As the power model according WLT of Weibull [47] is very common, power regression and correlation analyses were accomplished to study the influence of width, depth, span, shear volume  $V_s$  and shear area  $A_s$ . The analysis revealed that a width effect on  $f_v$  cannot be confirmed, neither between T-1 & T-7 nor between T-2 and T-4. Nevertheless, statistical high significant power models were found for  $f_v$  vs. depth, shear stressed volume and shear area. Best predictions were found in  $f_v$  vs. depth (see also Keenan et al. [22]), with a power model of  $f_{v,12,\text{MLE},\text{adj},\text{mean}} = 35.1 \cdot d^{-0.36}$  and  $R^2 = 0.88$ . Comparable results were also achieved with  $V_s$  and  $A_s$ . Nevertheless, a standard rule to account for size effects on shear requires to be also practicable. For example,  $A_s$  can be very well determined in case of concentrated loads but not in case of uniformly distributed loads (see also Soltis & Rammer [80]). Thus, a power model for  $f_v$  vs.  $d$  is preferred. Although herein presented test data reflects a significant higher depth effect than found on average in literature, in regard to a more general regulation of size effects it is proposed to consider a power coefficient of 0.20, which is also in line with the general assumed WD-shape parameter. Thus, for  $d \neq d_{\text{ref}}$  it is recommended to regulate the depth effect on shear strength of structural timber as

$$f_{v,k} = f_{v,k,\text{ref}} \cdot k_d = \min \left\{ 4.0 \cdot \left( \frac{150}{d} \right)^{0.2} ; 4.5 \right\} \quad (6)$$

## 6 Conclusions

Within this paper, results based on a comprehensive literature survey were presented. Focus was on clarification of main influences on shear strength of structural timber and GLT, in particular on influences by (i) climatic conditions, (ii) size and scale effects and (iii) influences beside from test method and configuration. Based on gained information the relevance of the direction how shear stresses are applied (edgewise or flatwise) and the expectable differences between structural timber and GLT were figured out. Furthermore, data collection and harmonisation of international studies enabled a statistical analysis and modelling of size effects on shear strength. Hereby the relevance of size effect consideration was visualised. As common, a power regression and correlation analysis was performed revealing an average power parameter of 0.20. Analysis of  $\text{CoV}[f_v]$  in relation to size effects reflected a positive and a negative tendency, respectively, for structural timber and GLT. A review of data and publications concerning test methods turned out a preference for shear tests by means of a bending test configuration with short span-to-depth ratios. Current test configuration of EN 408 [63] is not adequate for determination of representative shear strengths; neither for structural timber nor for GLT (see e.g. Denzler & Glos [19]). Furthermore and based on some test series published in Lackner [58] a 3pB-test configuration by means of against compression failures perpendicular to grain reinforced I-beams was defined, see Fig. 4.

A comprehensive test program was accomplished to examine size effects on structural timber of Norway spruce and to falsify the relationship  $f_{m,k}$  vs.  $f_{v,k}$  or more generally between strength class and shear strength, e.g. as anchored in EN 338 [16], [2]. In total 101 of 221 specimens tested failed in shear within the web. This low proportion of shear failures can be traced back to too late information updating of shear strengths higher than initially expected. Consequently, an updated test configuration including all experiences is proposed in Fig. 4. This configuration is judged to allow also a coherent determination of shear strength (and shear modulus) of structural timber and GLT as well as of other linear engineered timber products. As early failures due to other reasons than shear cannot be precluded, it is recommended to implement MLE for right-censored data (see equ. (4)) in standards for testing and evaluation. Furthermore, a FE-analysis was performed for quantifying the bias induced in calculation of shear stresses by means of simple beam theory in case of short span-to-depth ratios. The presented correction diagram (Fig. 5) derived for the proposed test configuration enables a fast and comfortable estimation of bias and correction. It is also recommended to include this or a similar graph in the testing and evaluation standard as part of data analysis.

Following the analysis of test data, it was concluded that a width effect on shear in edgewise loaded structural timber can be neglected, whereas a depth effect with a power of 0.20 should be implemented in product and design standards. Furthermore, an increase in  $\text{CoV}[f_v]$  with increasing depth and length, but a decrease of  $\text{CoV}[f_v]$  with increasing width was observed. Several possibilities to explain this circumstance were presented qualitatively. Additionally, a dependency of shear strength on strength class could not be confirmed. Thus it is proposed to regulate shear strength constant and irrespective of the strength class.

Overall a coherent determination of shear strength should be assured. The proposed test configuration enables this circumstance. Analysis of influences on shear strength clearly outlines the necessity to regulate this characteristic in dependency of the product and stressed shear plane. It was also outlined that size effects have a significant influence on shear strength. This aspect is currently not taken into account in European standards. Need for implementation is given, a proposal made.

## 7 Acknowledgement

The research work within the project 1.2.4-1 reinforce\_connections|shear is financed by the competence centre holz.bau forschungs gmbh and performed in collaboration with the Institute of Timber Engineering and Wood Technology of the Graz University of Technology and the partners from industry involved. The project is fostered through the funds of the Federal Ministry of Economics, Family and Youth, the Federal Ministry of Transport, Innovation and Technology, the Styrian Business Promotion Agency Association and the province of Styria (A14).

The support of E. Gehri, his worthwhile and encouraging discussions and recommendations have to be gratefully acknowledged. Great thanks also to H. Lackner who performed a very good job in analysing influences on shear strength and in developing an adequate test configuration as topic of his diploma thesis.

## 8 References

Please note that the list of references is available from the authors.

## 9 Annex

Please note that the Tab. 9 is available from the authors.

**INTERNATIONAL COUNCIL FOR RESEARCH AND INNOVATION  
IN BUILDING AND CONSTRUCTION**

**WORKING COMMISSION W18 - TIMBER STRUCTURES**

**SHEAR RESISTANCE OF GLULAM BEAMS WITH CRACKS**

A Pousette

SP Technical Research Institute of Sweden

M Ekevad

Luleå University of Technology

SWEDEN

**MEETING FORTY FIVE**

**VÄXJÖ**

**SWEDEN**

**AUGUST 2012**

---

Presented by A Pousette

There was discussion that natural cracks, artificial cracks and artificial grooves were different. Natural crack could be a release of strain. In terms of shear area and shear strength issue, cracks occur due to tension perpendicular to grain stress and not by shear; therefore, the remaining area should not have higher shear strength! Consideration of varying indoor climate conditions in real buildings is important. S Winter asked for information on the international standard for the reference beam grade. Also moisture measurements in the beams and on the surface during wetting and drying should be done to quantify these as the moisture treatment. A Pousette responded that this was done and the beam grades were GL28 to GL32. She stated that the results were not too bad and seemed to be sensible. For example Type II has approximately 2/3 of the strength. Irrespective of how you make the cracks, the results make engineering sense. S. Winter stated that the question was when you had natural cracks they didn't have the same behaviour as artificial cracks. Also the natural cracks induced in this study were not representative of the extreme cases that he saw in practice. Here, the width effect was important. A Jorissen stated that it seemed problematic to get shear failure unless the span to depth ratio is  $\sim 7:1$ . For real roof structures, the span to depth ratio is larger; therefore he questioned the application of the findings. A Pousette stated that there were situations such as curved cambered beams where this could be important and also in short deep beams. J Köhler stated that the issue of production of natural cracks and the issue of internal stresses from moisture loads during conditioning are important. I Smith commented on stable crack and unstable crack development in relationship with volume effect.



# Shear Resistance of Glulam Beams with Cracks

Anna Pousette

SP Technical Research Institute of Sweden, Sweden

Mats Ekevad

Luleå University of Technology, Sweden

## Abstract

A reduction of the shear resistance was introduced with the crack factor  $k_{cr}$  in Eurocode 5. The factor 0.67 corresponds to cracks that have a depth of 1/3 of the beam width. The aim of this project was to learn more about different types of cracks and their importance for the shear strength of glulam beams. The project started with tests of five types of glulam beams, with or without cracks. The cracks had different depths and locations, three beam types had cracks made by sawing and one type had cracks from moisturing and drying. The beam dimensions were 115 mm x 315 mm x 2600 mm. Five beams of each type with cracks were tested and ten beams without cracks. The beams were Swedish standard beams made of Spruce and taken from the normal production. Three-point bending method was used for the shear tests. The beams of type 1 without cracks got mostly bending failures; the characteristic shear strength was at least 3.5 MPa. Beams with sawn grooves got lower characteristic shear values and this means a reduced cross section should be used for beams with cut grooves along the beams. Beams with drying cracks got more shear failures, but the characteristic shear strength of the beams was about the same as for beams without cracks.

## 1 Introduction

### 1.1 Background

A reduction of the shear resistance was introduced with the crack factor  $k_{cr}$  in Eurocode 5 (EN 1995:1-1). The factor 0.67 corresponds to cracks that have a depth of 1/3 of the beam width, which rarely occurs under normal conditions. The glulam industry in Sweden has not observed any problems or shear failures due to cracks with previously used shear values. The values have been proven adequate through many years of experience. Hence the design requirements do not seem reasonable at the same time as they reduce the competitiveness of glulam. It is therefore of interest with more knowledge about cracks in glulam beams, and if there is any reason for different  $k_{cr}$ -factors in Europe.

Cracks in glulam beams can reduce the strength depending on the crack depth, crack length, crack location, etc. The cracks can have impact on the shear strength as they preferably run along the beams in the direction of grain and glue lines. One important question is therefore the probability of cracks to occur in glulam beams and how different crack parameters (location, size, type, etc.) influence the development of cracks and the shear strength. This project includes tests of a number of glulam beams with cracks to determine the shear strength and the influence of different types of cracks. The aim of the project is to learn more about different types of cracks and their importance for the shear strength of glulam beams. This could also provide a basis for the choice of value of the crack factor depending on various conditions. The issue is important because the effect of cracks on the shear strength is not clear.

## **1.2 Previous research**

There are relatively few reports about the influence of cracks on the shear resistance of glulam beams. The number of cracks is normally smaller in glulam than in structural timber. Tests have been performed with different test methods to determine the shear resistance of glulam. Both the method in the standard EN 408 and methods with beams with different cross-sections and loads have been used. According to the harmonized standard EN 14080 the test method in the standard EN 408 should be used for determination of the shear resistance. Structural timber is though more appropriate for this test method than glulam with larger sizes.

Soltis and Gerhardt (1988) reviewed the state of the art in shear design of wood beams, and mentioned that strength is dependent on check depth when the depth is greater than 30 % of beam width. Theories exist but pure shear is difficult to measure and the dependence on beam size should be investigated. There can be a so called size effect for glulam; the phenomenon that the strength is reduced when the volume is increased. This is often explained as the increased probability of weak parts to occur when the volume is increased.

Schickhofer and Obermayr (1998) presented results from tests with beams with I-sections. The beams were loaded with a point load at mid span. Schickhofer (2001) reported results from tests of a total of 96 beams. The shear strength appears to be independent of the quality of glulam. The work has been reflected in the standardization work of EC5 and EN 14080. Equations in EN 1194 for calculating mechanical properties of glulam based on tested properties of the lamellas in tension were also questioned. Klapp and Brüninghoff (2005) have developed a simulation model and it has demonstrated that there is a volume effect on the shear resistance. Steiger and Gehri (2011) have studied the interaction between shear stress and tension perpendicular to the fibers and conducted beam tests using glued bars at supports. Andersson and Odén (2009) determined the shear strength in different ways with both the method in EN 408 and with beam tests. Rectangular cross sections and I-sections were studied. Gustavsson et al (2009) investigated the shear strength using a variant of EN 408 with different designs. Sundström et al (2010) studied the effects of moisture gradients on the shear strength of beams with rectangular cross sections. Their tests showed that there is no effect on the shear strength from moisture gradients and the cracks they give. Barrett and Foschi (1980) have studied the shear strength of end-cracked beams. They pointed out that end-cracks can often be positioned over the support and for that reason not constitute a risk when loaded. The glue lines are of course important for the behaviour of glulam beams, and delamination tests are regularly made during production quality control. Steiger and Gehri (2010) have proposed new test methods to ensure consistent and good testing of the glue lines.

## 2 Shear tests

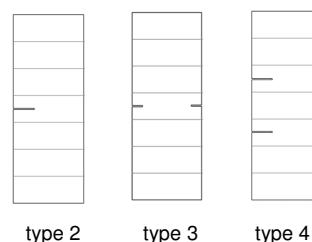
### 2.1 Tested beams

The project started with tests of four types (no. 2-5) of glulam beams prepared with different crack depths and locations and one type (no.1) without any made cracks. The beam dimensions were 115 mm x 315 mm x 2600 mm. The beams were standard beams taken from the normal production. The Swedish glulam quality CE L40c was used. Five beams of each type 2-5 were tested, and ten beams of type 1.

The cracks in beam type (2-4) were created artificially in new glulam beams by sawing grooves with a hand-held circular saw at specific depths and locations along the beams. Type 2 had one groove with the depth 30 % of the beam width, type 3 had one groove with the depth 15 % of the beam width on each side of the beam, and type 4 had two grooves with the depth 30 % of the beam width on one side, see Table 1.

Table 1. Test set up for glulam beams.

Beam type	No. of beams	Crack depth
1	10	No cracks
2	5	34,5 mm, 30 % of width, one side
3	5	17,2 mm, 15 % of width, both sides
4	5	34,5 mm, 30 % of width, two cracks one side
5	5	"Natural" cracks, CT-scanned



Beam type 5 was treated on one side with humidification with "rain" (5 hours) and drying with heating lamps (19 hours) in the SP Wood Technology laboratory in Skellefteå to generate "natural" cracks in the wood. During the treatment the moisture content and temperature was measured inside the beams near the treated surface. After humidification, the temperature was about 13.4°C and after heating, the temperature was about 24°C. The beam surface temperature on the warm side was about 48°C to 50-55°C. Measured moisture content was about 10.8 % - 12.9 %. After 28 days of varying climate the beams were CT-scanned at LTU (Luleå University of Technology) to document the cracks. Dimensions and moisture contents (about 12 %) of all beams were also documented before the shear tests.

### 2.2 Test method

Three-point bending method was used for the shear tests. The test method for determining shear strength of wood and glued laminated timber in EN 408 is difficult to use for glulam, and beam tests were furthermore chosen because bending is the most realistic load case. The stress distribution around a crack in bending can be different than in the shear test of EN 408. Different effects such as compression of the fibers from bending will influence the shear strength. A risk with bending tests is however that bending failure can occur rather than shear failure.

The three-point bending is shown in Figure 1. Roller bearings were used at both ends to prevent horizontal forces that can influence the shear test results. 300 mm long steel plates

were placed under load and at supports, but a small indentation in the top of the beams was obtained under the load. Loading was rather slow, it was chosen to about 4-6 mm/min.

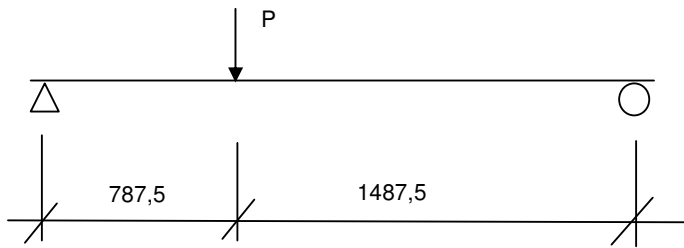


Figure 1. Point load on beam

### 3 Shear resistance

A summary of the results from the tests is shown in Table 2.

Table 2. Results of testing

Beam type	Failure type	Mean shear strength (MPa)	Char. shear strength (MPa)	Relation to beam type 1	Char. shear strength (MPa) (b= 80,5 mm)
1	2 Shear, 8 Bending*	4.44	3.50	1	-
2	5 Shear	3.41	2.24	0.64	3.20
3	4 Shear, 1 Bending*	3.86	3.18	0.90	4.54
4	5 Shear	3.52	2.81	0.80	4.01
5	4 Shear, 1 Bending*	4.78	3.80	1.08	-

\* Bending failure means that the shear strength is at least the calculated value; all values are included in the mean and the characteristic values.

#### 3.1 Shear resistance of beams with no cracks (type 1)

The beams of type 1 with no cracks got mostly bending failures or combinations of bending and shear failures, and only two beams got a real shear failure. The characteristic shear strength of all beams was estimated to be at least 3.5 MPa, but was probably higher because of the bending failures. Bending failures started at knots or finger joints in the lower lamella.

#### 3.2 Shear resistance of beams with sawn grooves (type 2-4)

For beam types with sawn grooves the characteristic values were estimated 2.24-3.18 MPa when the shear resistance was calculated from the entire cross section 115 mm x 315 mm. If instead a reduced cross section 80.5 mm x 315 mm was used, the shear strength was 3.20-4.54 MPa. This implies that a reduced cross section should be used for beams with cut grooves along the beams. For beam type 2 there was one beam that failed at much lower load than the others and an explanation for this could be that the width of the annual rings in the cracked lamella was very large and differed from the other lamellas. In one of the type 3 beams the shear failure occurred in the lamella below the lamella with the groove. The shear failures followed most often the annual ring where the groove was, only at some points they continued to an adjacent lamella or the failure occurred entirely in an adjacent lamella. Shear failure occurred at the interface between earlywood and latewood.

Narrow growth rings gave higher shear strength. Lamella orientations in the beam together with the curvature of annual rings determined the size of shear area. The sawn grooves went through the annual rings and cut the wood fibers, which is unrealistic for real cracks in wood.

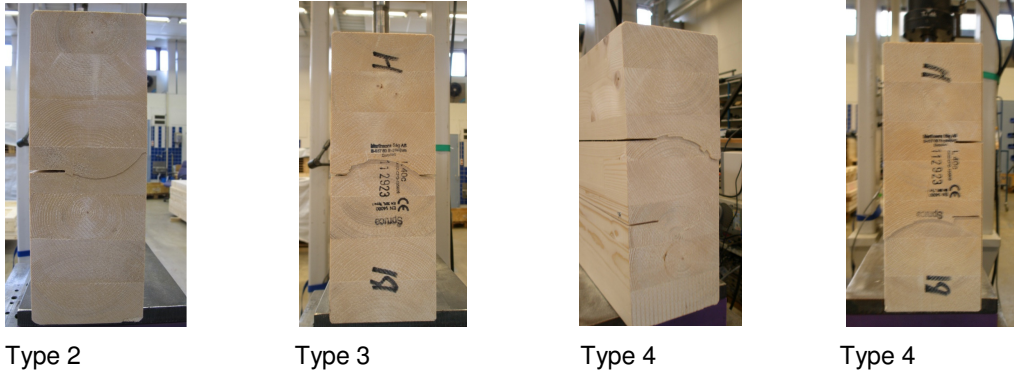


Figure 2. Typical shear failures in beam types 2-4

### 3.3 Shear resistance of beams with “natural” cracks (type 5)

For the beam type with the "natural" cracks, four out of five beams got shear failures. This was more compared to the beams without cracks and could mean that the cracks had some impact on the shear resistance. The characteristic shear strength of the beams was estimated to be at least 3.8 MPa.

The largest crack depths were approximately 20-30 mm, with a length of a few decimetres, located at various positions in height and lengthwise. The largest natural cracks occurred mainly on tangential surfaces of lamellas with pith in the middle but these cracks did not cause shear failure. The fracture takes the shortest (most direct) way across the width. A number of cracks were also formed in the wood close to a glue line, especially if there were no lamellas in the cross-section with tangential surfaces. The location depended on the orientation of the lamellas. These cracks caused sometimes failure. End-cracking occurred, and stretched at most about 70 mm from the end.

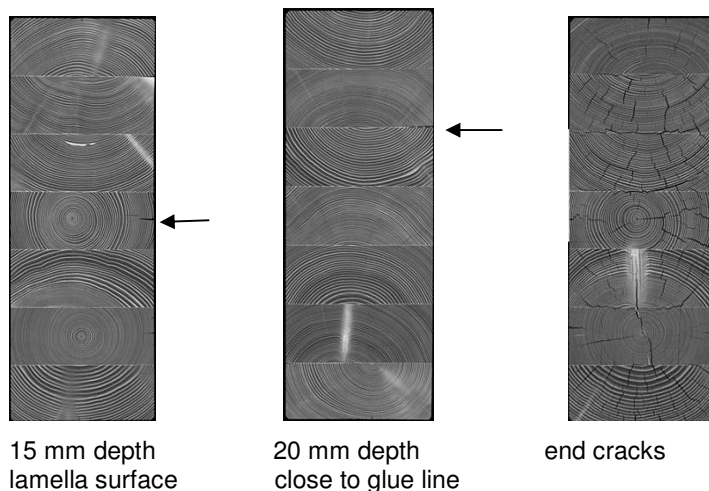


Figure 3. CT-images of beams of type 5 with typical cracks, before test

## 4 FEM simulations

Tested beam types 2-4 were moreover simulated in the commercial finite-element analysis program ABAQUS CAE version 6.10 (Saracoglu, 2011). In the simulation, the crack propagation was based on theoretical fracture criteria. Assumptions in the simulations were: local cylindrical coordinate system of each lamella, the pith location of each lamella is in the middle of the bottom edge; all lamellas has the same properties; density of all beams is the same; moisture content and temperature is constant and do not influence the beam strength; glue lines between the lamellas were not modeled; failure criterion of the wood material is based on energy considerations as derived by Griffith (1920) and linear elastic fracture mechanics; mode III (tearing) critical energy release rate is chosen very high in order to avoid crack propagation in that mode and only have mode I (opening) and mode II (sliding), maximum stress was set to a constant material property of 4 MPa.

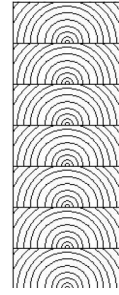


Figure 4.  
Simulated  
beam

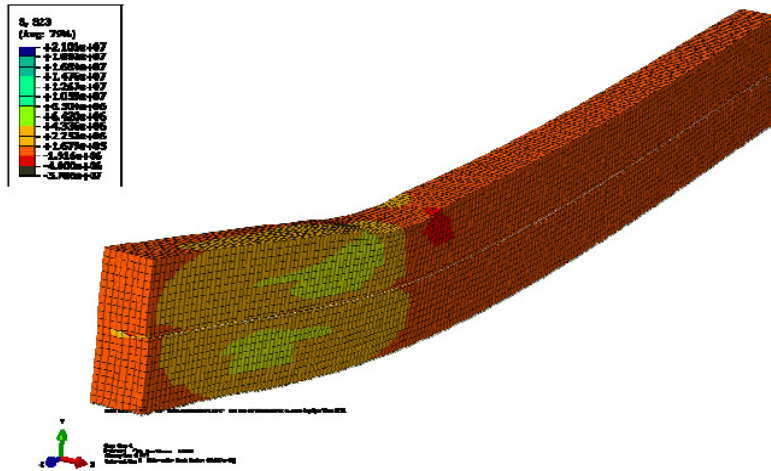


Figure 5. Beam type 2 with the shear stress at critical load.

The simulation model was modified and improved based on the experimental feedback. Beam type 1 was not modelled because it did not include any cracks. In the simulation of beam type 3, no crack propagation was obtained. The comparison between the simulations and experiments was mean shear strength 2.98 MPa from simulation and 3.32 MPa from experiment for type 2 and 3.63 MPa from simulation and 3.43 MPa from experiment for type 4. The results of the simulations are in accordance with tests, and show that sawn grooves results in a reduced shear strength, but that the shallow grooves in the type 3 have less effect. Beam type 5 with several natural cracks in different locations, different directions, with different crack lengths and depths are of course more complicated to simulate, but this is now in progress.

## 5 Discussion and conclusions

If we compare all test specimens, it can be seen that the beam type 1 with no cracks had an expected shear stress capacity. However, for more reliable results more tests are needed in order to avoid bending failures of the beams. For the beam type 2 the shear capacity

decreased compared to beam type 1. Furthermore, the number of the annual rings at the crack location influenced the shear strength. The beam type 3 had better shear capacity than beam type 2 and beam type 4. The main reason behind this was according to the FEM simulations that the shear stresses were symmetrically distributed in the beam, and in consequence not enough stress concentration occurred that initiated propagation around the crack location, compared to the beam types 2 and 4. Beam type 4 showed similar mechanical properties to beam type 2, but the shear resistance was slightly higher due to the cracks were located at a distance from the beam center.

It was difficult to create “natural” cracks in the glulam beams to get test specimens with cracks that were large enough to have influence on the shear strength, and of course this is because glulam is manufactured to not crack. From studies of drying of boards (Söderström, 1985) we know that the density has the greatest effect on the cracking and of course the drying process. The parameters that can influence are also moisture content, proportion of heartwood, pith location, annual ring width and knots. The probability for cracks to develop is physically explained that some surface energy is released. The cracks in the glulam beams usually appeared in the vicinity of the glue lines mainly due to anisotropy and lay-up of the lamellas.

Glulam beams can get many small cracks, but large cracks are the most dangerous. Production control, and especially of the glue lines is important for high-quality material. But also the wood quality and the orientation of lamellas can affect the shear strength. Lamellas with pith usually got more cracks on the surface, but these are less dangerous for the shear resistance because the fracture surface gets a long way around the pith. But of course these surface cracks should be avoided both from an aesthetic point of view and for durability reasons in outdoor use because they can bring water into the beam.

In an ongoing outdoor experiment about weathering and cracks in wooden structures (Pousette and Ö-Sandberg, 2010) about hundred glulam beams and columns with different materials and treatments are studied to see how cracks in the wooden structures develop over time and how moisture affect the cracking and the risk of rot. Cracks in the glulam beams have been measured manually every summer during 4 years. Some of the beams have cracks all along the beams. The maximum crack depth of the beams with dimensions 140 mm x 450 mm x 9000 mm varied between 15 mm and 45 mm. There have been some practical difficulties in measuring crack depths and especially widths in the beams, but it is obvious that the cracks grow over time due to shrinkage and swelling. Crack widths on the surface vary with the weather during the day. The depth is different along the cracks, and the maximum depths can be difficult to find.

It is not easy to do calculations of the behaviour of glulam beams with different crack patterns and crack sizes. It is quite easy with a well-defined crack, groove or hole. With many small cracks that occur naturally in the material, FEM simulations are the most suitable if the material properties are well known. The question is how much cracks that generally occur in glulam beams, and where and how they arise. It is natural with some cracks in wood materials, and this should preferably be part of the material properties. If the material is handled improperly so that it gets large cracks this should not be included in the general design requirements. Cut outs and holes of various shapes should of course be considered according to design rules.

The shear tests showed that the influence of natural cracks on the shear strength was not great. If glulam beams are manufactured in a good way it has proved very difficult to develop cracks, and this means the material does not normally get cracks that may affect

the strength. Cracking can occur in glulam beams because of several reasons. If the material is exposed to severe weathering or highly variable moisture conditions this should be considered. Free outdoor exposure so that free water can moisten the surface and solar heating then giving severe drying out will give cracks over time. Dry indoor climate can lead to rapid drying and shrinkage of the outer parts of glulam cross sections. Humidification during the construction so that the wood surfaces swell will give cracks during the drying process. Inappropriate design of notches, holes and mechanical joints can also result in cracking.

Shear stresses for beams are greatest near the supports, where at the same time compressive forces perpendicular to the grain have a positive impact. Load positions and locations of cracks should be investigated further.

A controlled production is important. The amount of cracks that should be allowed in glulam beams can be compared to delamination tests. For glue line integrity according to EN 386 the total delamination percentage of each cross-sectional specimen shall be less than 8-10 % depending on test methods. For a beam width of 115 mm this means that all glue lines can delaminate about 9-11 mm. For strength results from block shear tests of cross-sectional specimens the requirements are that the shear strength of each glue line shall be at least  $6.0 \text{ N/mm}^2$ , or for Coniferous wood shear strength of  $4.0 \text{ N/mm}^2$  is acceptable if the wood failure is 100%.

Although there is a possibility for a national choice in Eurocode 5, the large reduction in shear for glulam has given problems for the glulam industry in Sweden. The project about how glulam beams crack and how this affects the properties will continue so that the full capacity of the material can be used. In a preliminary statement, as not all tests are finished, it can be said that the recommended crack factor seems very low. Further testing will provide more data and include more parameters. Interesting parameters are crack size, beam dimensions, lamella type and location in the beam (center pieces with pith or not), load position.

The next series of tests will include beams with cracks produced by humidification and drying to low moisture contents corresponding to very dry indoor climate, to meet the actual conditions that may occur during construction. The new glulam beams have the same dimensions 115 mm x 315 mm x 2600 mm, and will also be complemented with beams with surface treatment, and also a group of wider beams 165 mm x 315 mm x 2600 mm. Surface treatment will affect the crack development and maybe the type of cracks. The beams will be measured and documented, moisture contents will be measured, and CT-scanning of the beams will be performed before shear tests. The new tests are delayed because it has been difficult to obtain sufficiently large cracks. To induce cracks in the beams has proven to be difficult and it takes quite a tough treatment to produce any major cracks. The CT images will be used to relate the sizes, amounts and locations of the cracks to the shear strength.

## **6 Acknowledgements**

The research presented in this paper was funded by TCN TräCentrum Norr (WoodCenter North).

The glulam beams were delivered from Martinsons Byggsystem.

## 7 References

- EN 386 Glued laminated timber – Performance requirements and minimum production requirements, 2003
- EN 14080:2005 Timber structures – Glued laminated timber - Requirements
- EN 1194:1999 Timber structures – Glued laminated timber – Strength classes and determination of characteristic values
- EN 408:2010 Timber structures – Structural timber and glued laminated timber – Determination of some physical and mechanical properties
- EN 1995-1-1:2004, Eurocode 5, Design of timber structures, Part 1-1: General – Common rules and rules for buildings
- Andersson, D., Odén, J., Träs skjuvhållfasthet och limträbalkars skjuvkapacitet – provningar och beräkningar. Examensarbete, Lunds tekniska högskola, avdelning Bärande konstruktioner, Lund, 2009.
- Barrett, J.D., Foschi, R.D., Considerations of shear strength on end-cracked beams, CIB-W18, 1980
- Gustavsson, P.-J., Emilsson, A., Crocetti, R., Ormarsson, S., Provningar av limträskjuvhållfasthet. Lunds tekniska högskola, Avdelning för Bärande konstruktioner, Lund, 2009.
- Klapp, H., Brüninghoff, H., Shear strength of glued laminated timber. CIB –W18 – Timber structures, Paper W18/38-6-3, Meeting 38 in Karlsruhe, Germany, 2005.
- Pousette, A., Ö-Sandberg, K., Outdoor tests of timber beams and columns, Proceedings of the International Conference Timber Bridges: ICTB2010, Trondheim, Norway, 2010.
- Saracoglu, E., Finite-Element Simulations of the Influence of Cracks on the Strength of Glulam Beams, Department of Mechanical Engineering, Blekinge Institute of Technology, Karlskrona, Sweden, 2011.
- Schickhofer, G., Obermayr, B., Development of an optimized test configuration to determine shear strength of glued laminated timber, CIB – W18, Paper W18/31-21-1, Meeting 31, Savonlinna, Finland, 1998.
- Schickhofer, G., Determination of shear strength values for GLT using visual and machine graded spruce laminations, CIB – W18, Paper W18/34-12-6, Meeting 34, Venice, Italy, 2001.
- Soltis, L. A., Gerhardt, T. D., Shear design of wood beams: State of the art. Forest Products Laboratory, Department of Agriculture, Forest Service, Madison, WI: U.S., 1988.
- Steiger, R., Gehri, E., Interaction of shear stresses and stresses perpendicular to the grain, CIB – W18, Paper W18/44-6-2, Meeting 44, Alghero, Italy, 2011.
- Steiger, R., Gehri, E., Quality control of glulam: Improved method for shear testing of glue lines, The Future of Quality Control for Wood & Wood Products, 4-7th May 2010, Edinburgh, The Final Conference of COST Action E53, 2010.
- Sundström, T., Kevarinmäki, A., Fortina, S., Toratti, T., Shear resistance of glulam beams under varying humidity conditions, VTT Working Paper 157, VTT, Espo, 2010.
- Söderström, O., Drying checks and end moisture contents, Rapport – TräteknikCentrum, No. I 9011062, 1990.



**INTERNATIONAL COUNCIL FOR RESEARCH AND INNOVATION  
IN BUILDING AND CONSTRUCTION**

**WORKING COMMISSION W18 - TIMBER STRUCTURES**

**EXPERIMENTAL INVESTIGATION ON IN-PLANE BEHAVIOUR OF  
CROSS-LAMINATED TIMBER ELEMENTS**

M Andreoli

R Tomasi

Department of Structural and Mechanical Engineering, University of Trento

A Polastri

CNR – IVALSA San Michele all'Adige

ITALY

**MEETING FORTY FIVE**

**VÄXJÖ**

**SWEDEN**

**AUGUST 2012**

---

Presented by R Tomasi

G Schickhofer stated that the test configuration should be compliant to the loading condition of the building and the model should be consistent. He stated that satisfying equilibrium condition only was not enough as kinematic conditions needed to be considered also. Also the diagonal shear test configuration could have compression failure; therefore, there could be an interaction effect. Diagonal shear test configuration which puts the panel in tension needs to be used. R Tomasi agreed that the model only considered equilibrium and these were their assumptions. He also agreed that the diagonal test configuration did not yield a pure shear case. The TU Graz diagonal shear device is the only tension shear apparatus that gives stiffness measurement. I Sustersic asked if there was any observed difference in results between panels produced with hydraulic and vacuum presses. R Tomasi stated that conclusion could not be drawn on this issue. F Lam asked for clarification on how many specimens were studied. R Tomasi agreed that the number of specimens were limited and would consider more next time.



# **Experimental investigation on in-plane behaviour of cross-laminated timber elements**

Mauro Andreolli, Roberto Tomasi

Department of Structural and Mechanical Engineering, University of Trento, Italy

Andrea Polastri

CNR – IVALSÀ San Michele all’Adige, Italy

## **1 Introduction**

The use of Cross Laminated Timber (CLT) as structural element for shear walls and floors in multi-storey buildings has become very popular in the recent years. Many research works have been produced, coming mostly from German or Austrian researchers, aiming to investigate the out of plane and in-plane behaviour of CLT-elements; however an harmonized standard for the product is still under discussion, and a certain variability in geometrical and technological parameters can be observed among the CLT producers.

In many situations it is necessary to characterize the mechanical properties for CLT-elements subjected to in-plane loads, such as in the case of walls elements under lateral loads, deep beams or lintel beams realized in CLT. Unfortunately so far there are not indications in the current version of EN 1995 (Eurocode 5 [1]) for ULS verification of CLT panels. Owing to the particular structure made of orthogonal layered boards, the transmission of the in-plane load in CLT panels is guaranteed by the glued surfaces between board intersections, whose mechanical properties are strictly related to their geometry configuration. Another characteristic to be taken into account, especially for the in-plane stiffness properties of the panel, is the presence of lateral glued interface at the narrow faces of the board.

In this paper an experimental campaign aimed to investigate the in-plane behaviour of cross-laminated timber elements is presented. Several deep beams made of three and five layer cross laminated panels have been tested under a four points configuration set-up.

## **2 Experimental program**

### **2.1 Material and geometry**

The experimental campaign has foreseen the test of 25 wall elements, that were dimensioned in such way as to ensure the conditions for the 4 point bending test: the tested specimens can be considered as edgewise loaded beams. The specimens were obtained from panels of various manufacturers that are characterized by variable layouts, as such, the tested specimens present variable dimensions (Table 1). The specimens were sized as

to reach shear failure, presenting thus the following dimensions: a height of 0.6 meters and a length of 3 meters.

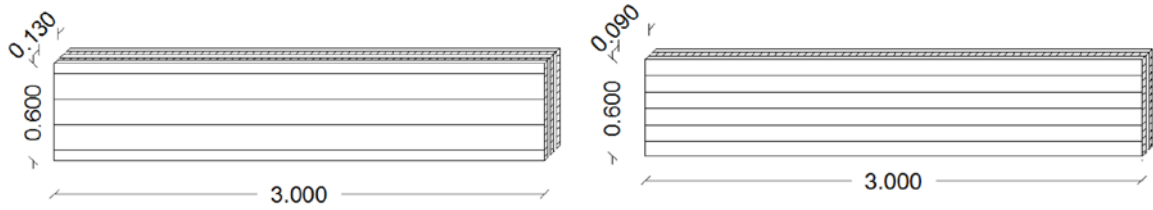


**Figure 1.** CLT deep beam geometry for three (A-3) and five layer (A-5) specimen

The experimental campaign's goal is to compare the failure mode and shear resistance of XLAM panels of different manufacturers, in particular four different typologies were used from three different producers. Four types of specimens have been considered in the analysis, changing different parameters such as number of layers, presence of lateral glued interface, board width, presence of cuts in timber boards to avoid shrinkage cracks (Table 1 and 2).

**Table 1.** Tested CLT elements: detail of the layout

A-3	A-5	B-5	C-5
			
Glued narrow surface	Glued narrow surface and cracks	Not glued narrow surface and cuts	Not glued narrow surface

**Table 2.** Tested CLT elements

producer	a* (mm)	thick. (mm)	layers	board narrow surface	n. of spec.
A-3	100	90	30-30-30	glued	4
A-5	100	130	29-21-29-21-29	glued	2
B-5	80	135	27-27-27-27-27	not glued	2
C-5	150	144	34-21-34-21-34	not glued	2
* average lateral width of the boards in CLT panels					

The panels were produced using boards rated by each manufacturer, thus, using the technical certificates provided by the manufacturers, it was possible to establish the strength classes of the panel boards. For all the panels, at least 90% of the boards were C24 strength class, each layer of the panels containing up to 10% of C16 strength class boards.

## 2.2 Experimental set-up and procedure

CUAP 03.04/06 [2] protocol and the European Standard EN 408 [3] served as the basis for the tests, this latter giving in particular a method for the determination of modulus of elasticity. The test consists of applying a load in a four point bending set-up at constant rate equal to 0.03 mm/s to a maximum load that does not exceed 40% of the estimated maximum load,  $F_{\max, \text{est}}$ . During the test, the deformation,  $w$ , is measured on both the side faces at the neutral axis. The data extracted from the test gives the load/deformation graph. Using the section of the slope between  $0.1 F_{\max, \text{est}}$  and  $0.4 F_{\max, \text{est}}$  it is possible to determine the Elasticity Modulus (MoE). After the non-destructive tests, performed to measure the Elasticity Modulus, the specimens, on the same set-up, are loaded up to failure in order to determine the ultimate strength.



**Figure 2.** Experimental set-up

As defined in the European Standard EN 408 [3], the total mid-span deformation was measured with an LVDT (Linear Voltage Displacement Transducer) fixed at the ground. The relative deflection was measured using an aluminum yoke device fixed within the area defined by the loading points and a second LVDT (see Figure 3).

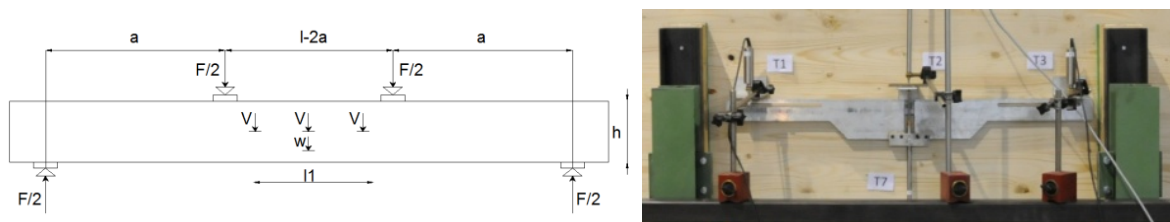


**Figure 3.** Measurement set-up and applied loads and details of the displacement transducers

In addition to the measures provided by European Standard EN 408 [3], the relative deflections at third-span were measured using two additional transducers (LVDT). All measurements were made on both faces of the specimens, using a total of 8 transducers.

**Table 3.** Geometrical characteristics of the measurement setup

	<b>l1</b>	<b>l-2a</b>	<b>a</b>
<b>definition</b>	Distance between the external LVDT	Distance between the applied loads	Distance between the load and the support
<b>(mm)</b>	800	1100	700

The tests conducted under displacement control were performed using a hydraulic MTS actuator, able to apply a maximum load of 1000 kN, equipped with a load cell. The data relating to the vertical deflection and the applied load were registered with a data acquisition control unit. In the second phase of the tests, to the failure of the specimens, the applied loads and the vertical deflections were acquired by the load cell and the displacement transducer of the hydraulic actuator.

Because of the flexural slenderness, the specimen was stabilized by the use of two lateral support positioned at the loading points.

### 3. Experimental results

The results are reported in term of MoE (Modulus of Elasticity) and MoR (Modulus of Rupture), carried out according to the formula reported in EN 408 [3][2], taking into account the net moment of inertia of the multilayer section.

#### 3.1 Modulus of elasticity and values of rupture

The MoE has been calculated according to the EN 408 [3]: starting from the experimental load displacement curve, through a regression analysis, taking into account the longest line between  $0,1 F_{max}$  and  $0,4 F_{max}$ , whose coefficient of correlation is higher than 0,99 (line included at least between  $0,2 F_{max}$  e  $0,3 F_{max}$ ), it is possible to calculate the value of the local E modulus according to the following equation:

$$E_{m,l} = \frac{al_1^2(F_2 - F_1)}{16I_{net}(w_2 - w_1)}$$

where:

$(F_2 - F_1)$ : load increase [N];

$(w_2 - w_1)$ : displacement increase corresponding to  $(F_2 - F_1)$  [mm];

a : distance between the load point and the support [mm];

$l_1$  : reference length for the E modulus determination [mm];

$I_{net}$  : net moment of inertia [mm<sup>4</sup>];

In Table 4 are indicated mean values calculated from the repetition of elastic tests performed on the same specimen; Table 4 also reports the mean values of these series of tests.

**Table 4.** MoE values according to EN 408 [3]

producer	MoE (MPa)				
	Spec. 1	Spec. 2	Spec. 3	Spec. 4	Mean
A-3	-	10898	12298	10997	11398
A-5	15845	14758	-	-	15302
B-5	14445	16661	-	-	15553
C-5	12493	10775	-	-	11634

The values of the maximum loads recorded at failure for the different specimens and the mean values of the maximum loads referred to panels from the same producer are hereafter reported, Table 5.

**Table 5.** Results of the destructive tests

producer	$F_{max}$ (kN)				
	Spec. 1	Spec. 2	Spec. 3	Spec. 4	Mean
A-3	313	324	372	310	330
A-5	506	515	-	-	511
B-5	417	405	-	-	411
C-5	565	495	-	-	530

The tested specimens reached the collapse showing different failure modes (Figure 4): the C-5 panel breaks because of bending due to a board presenting a group of knots at midpoint whereas the panels A-3; A-5 and B-5 presented the torsional shear failure mode described at paragraph 4.

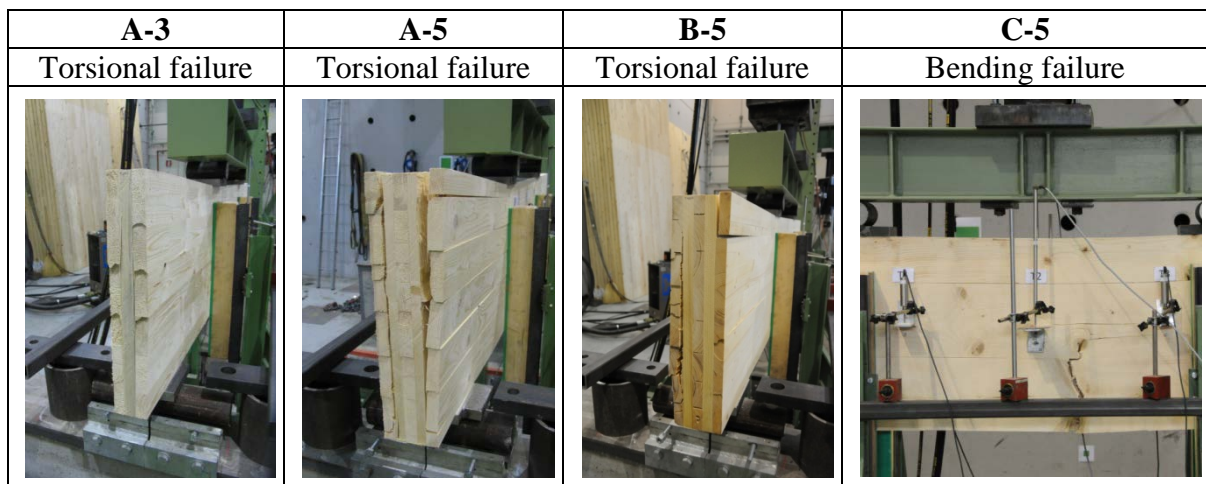


**Figure 4.** Failure mode observed for the different type of specimens

## 4. Discussion results

### 4.1 Modelling the internal in-plane stress

An efficient mechanical model for the internal stress pattern in CLT elements has been presented and discussed in different papers by University of Graz research team ([4] and [5]).

An elementary representative volume element (RVE) has been introduced, which represents the intersection between orthogonal boards, the smallest unit cell whose internal state could describe the global stress pattern of the CLT element. This element can be even further reduced to a representative volume sub-element (RVSE) resulting as an intersection of two orthogonal boards with equivalent thickness.

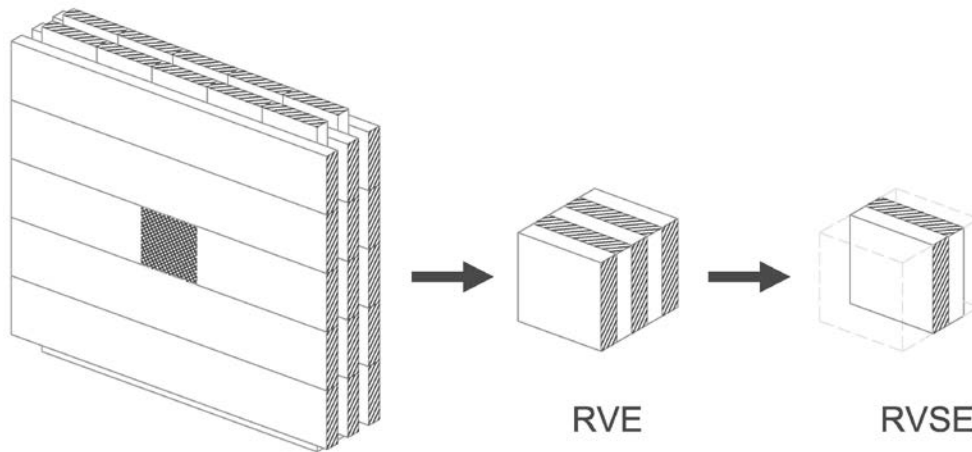


**Figure 5.** Description of the representative volume element (RVE) and sub element (RVSE) extracted from a CLT panel subjected to in-plane shear stress, according to Moosbrugger et al. [4].

This simplification allows to express the two fundamental internal stress patterns of shear and torsion arising in the RVSE with a constant board thickness of  $t/2$ .

	=		+	
$\tau_0 = \frac{V}{t \cdot a}$		$V = \tau_0 \cdot t \cdot a$		$M_T = \tau_0 \cdot t \cdot a^2$
		$\tau_v = \frac{V}{\frac{t}{2} \cdot a} = 2 \cdot \tau_0$		$\tau_T = \frac{M_t}{W_p} = 3 \cdot \tau_0 \cdot \frac{t}{a}$

**Figure 6.** Internal stress pattern in the RVSE element as result of two fundamental mechanism.

In [5] has been demonstrated that these expressions could be extended to RVE element with a symmetric multilayer stratigraphy introducing an ideal thickness  $t_i^*$  and the fictitious term  $\tau_{0^*} = \frac{V}{(\sum t_i^*) \cdot a}$  in the formula of shear and torsional stresses.

A method based on equilibrium equations can be also adopted in order to characterize the internal stress pattern in a three or five layer RVE element.

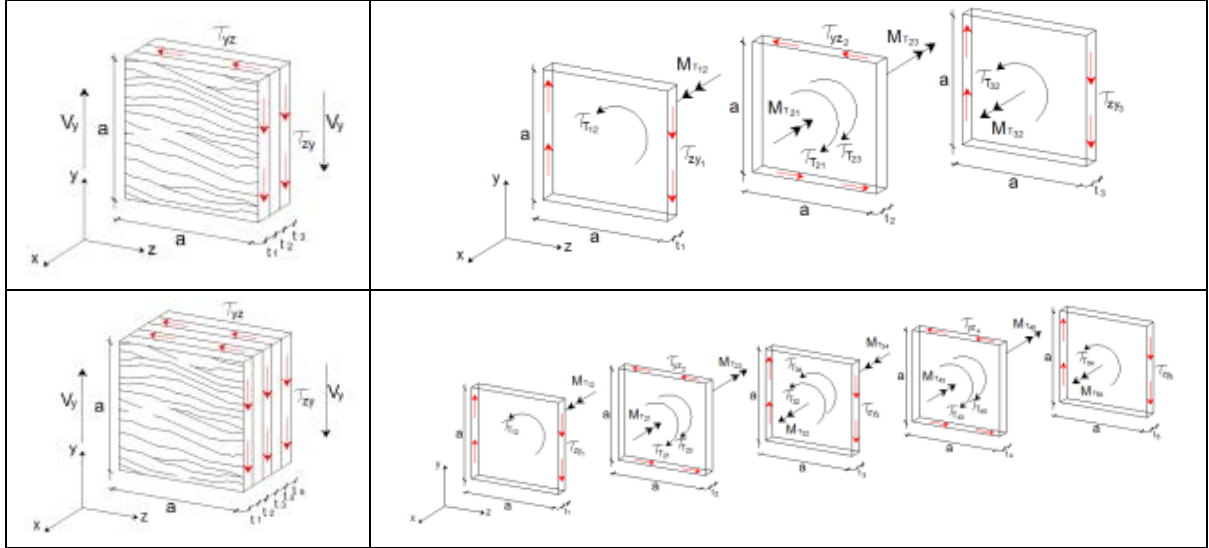


**Figure 7.** Internal stress pattern in a three and five layer RVE element.

In the case of a three layer symmetric RVE element ( $t_1 = t_3$ ) from translational equilibrium consideration could be carried out the following expressions:

$$\tau_{zy} = \tau_{zy1} = \tau_{zy3} = \frac{V_y}{a \cdot (t_1 + t_3)} = \frac{V_y}{a \cdot 2 \cdot t_1} \quad \text{shear stress in the external layers}$$

$$\tau_{yz} = \tau_{yz2} = \frac{V_y}{a \cdot t_2} \quad \text{shear stress in the middle layer}$$

The ratio between the  $\tau_{yz}$  and  $\tau_{zy}$  is:

$$\tau_{yz} = \frac{\tau_{zy} \cdot (t_1 + t_3)}{t_2} = \frac{2 \cdot \tau_{zy} \cdot t_1}{t_2}$$

The internal moment is determined in function of the internal shear stress imposing rotational equilibrium:

$$M_{T12} = M_{T21} = \tau_{zy} \cdot a^2 \cdot t_1$$

$$M_{T23} = M_{T32} = \tau_{zy} \cdot a^2 \cdot t_3 = \tau_{zy} \cdot a^2 \cdot t_1$$

Being the internal moment  $M_T$  the same for symmetry, the internal torsional stress could be expressed as:

$$\tau_T = \tau_{T21} = \tau_{T12} = \tau_{T32} = \tau_{T23} = \frac{M_T}{W} = \frac{\tau_{zy} \cdot a^2 \cdot t_1}{\frac{a^3}{3}} = 3 \cdot \frac{\tau_{zy} \cdot t_1}{a}$$

In the case of a five layer symmetric RVE element ( $t_1 = t_5$  and  $t_2 = t_4$ )

$$\tau_{zy} = \frac{V_y}{a \cdot (t_1 + t_3 + t_5)} = \frac{V_y}{a \cdot (2 \cdot t_1 + t_3)} \quad \text{shear stress in the external and middle layer}$$

$$\tau_{yz} = \frac{V_y}{2 \cdot a \cdot (t_2 + t_4)} = \frac{V_y}{2 \cdot a \cdot t_2} \quad \text{shear stress in the second and fourth layers}$$

$$\tau_{Te} = \frac{M_{Te}}{W} = \frac{\tau_{zy} \cdot a^2 \cdot t_1}{\frac{a^3}{3}} = 3 \cdot \frac{\tau_{zy} \cdot t_1}{a} \quad \text{torsional stress in the external layers}$$

$$\tau_{Ti} = \frac{M_{Ti}}{W} = \frac{\tau_{yz} \cdot a^2 \cdot t_3}{\frac{a^3}{3}} = \frac{3}{2} \cdot \frac{\tau_{yz} \cdot t_3}{a} \quad \text{torsional stress in the internal layer}$$

In the case of in-plane bending action  $M$  applied to the CLT panel, the bending stress should be calculated taking into account only the boards parallel to the stress direction. The bending stress according to CUAP document [2] is therefore defined in relation to the net cross-section modulus  $W_{net}$ :

$$W_{net} = \frac{B \cdot H^2}{6}; B = \sum b_i$$

$$\sigma = \frac{M}{W_{net}}$$

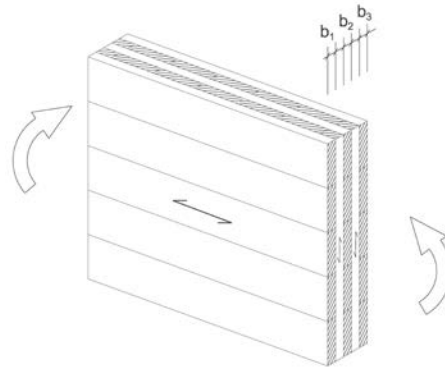


**Figure 8.** In-plane bending in CLT element.

## 4.2 Strength values of different failure modes

The strength values associated to the different failure modes encountered in the experimental campaign (bending failure of the deep beam, shear failures of boards, torsion failure of the intersection between boards) are determined according to different experimental procedures described in related literature and in product certificates. The following table illustrates the mean and characteristic values carried out by some authors for the three failure modes and the respective experimental set-up adopted.

**Table 6.** Experimental strength values of the different failure modes

Test set-up				
Failure modes	Bending	Shear perpendicular to the grain	Torsion	
References	[6]	[6]	[8]	[7][1]
n° specimens	90	20	240	-
$f_{mean}$ (MPa)	39,90	12,80	-	3,60
$f_k$ (MPa)	-	10,6	3,07	-
COV	12,1%	11,3%	-	-

The correct value to assign to the shear strength  $f_{v,k}$  is at the present under discussion [8]. Adopting the values ranging from 3,0 to 3,5 N/mm<sup>2</sup> for shear parallel to the grain as in EN 338 [9] for solid wood and glulam could be not realistic, since in CLT panel shear stresses are actually directed perpendicular to the grain. A value of 5,2 N/mm<sup>2</sup> can be found in an ETA document, but tests in laboratory with a specific set-up for shear perpendicular to the grain according to [8] have demonstrated that a significantly higher value for CLT shear strength can be expected (see Table 6).

### 4.3 Analysis of the results

From the experimental values of ruptures reported in section 3.2 the following bending and shear stress values have been carried out according to the model described in section 4.1.

**Table 7.** Experimental stress values for the different specimen at failure

	$\sigma$	$\tau_{zy}$	$\tau_{yz}$	$\tau_{T,ext}$	$\tau_{T,int}$
<b>Producer</b>	(MPa)	(MPa)	(MPa)	(MPa)	(MPa)
<b>A-3</b>	35,42	4,58	9,17	4,13	///
<b>A-5</b>	34,20	4,89	10,12	4,25	2,13
<b>B-5</b>	29,59	4,23	6,34	4,28	2,14
<b>C-5</b>	30,31	4,33	10,52	2,94	1,47

These figures can be directly compared with the experimental strength values reported in sections 4.2 carried out for the single mechanical parameter through an ad hoc set-up.

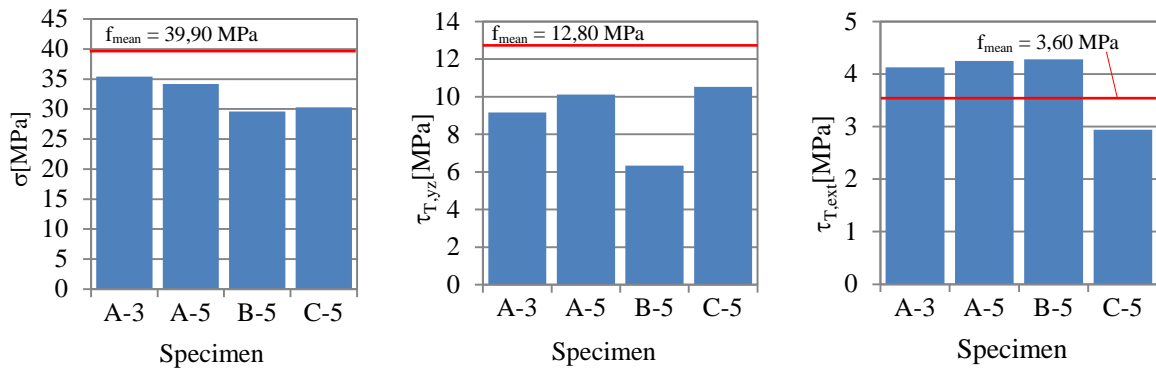


**Figure 9.** Experimental strength values for the different type of specimen tested (histograms A-3, A-5, B-5, C-5) for bending stress ( $\sigma$ ), shear stress ( $\tau_{yz}$ ), and torsional stress ( $\tau_{T,ext}$ ), compared to the strength values according to table 6 (red line).

The experimental results confirmed the capability of the proposed mechanical method to estimate the strength and the type of failure for CLT panels.

According to the experimental campaign (Figure 4), specimen A-3, A-5 and B-5 present failure modes associated to torsional effect between the orthogonal boards at the end of the beam and, as a matter of fact, for these specimen only the torsional stresses presented in Table 7 exceed the corresponding mean strength values. On other hand, this type of failure mode is prevented in specimen C-5, which representative volume element presents a higher polar section modulus due to larger size of the board width: it is worth noting that in this specimen bending failures was activated by local defects, with a bending stress value lower than the one proposed in Table 7.

Regarding the presence of lateral glued surface between boards in specimens A-3 and A-5, this seems not to influence the value of torsional stresses at failure as can be observed in column  $\tau_{T,ext}$  of Table 7. As observed in [6][2] and in Table 1, cracks due to shrinkage in some elements could have produced a similar structure to the CLT elements without adhesive between the board narrow sides.

In all specimens the shear stress values are always lower than the mean values for shear perpendicular to the grain reported in Table 7.

## 6 Conclusions and future works

The determination of the shear strength for CLT in plane is not always possible with a standard procedure similar to the one presented in the CUAP [2] or in EN 408[3], because it has been demonstrated that often bending failure is prevailing, and that the type of failure is strongly related to the “internal” geometry of the CLT panel (e.g. the width of the boards), which can also vary even between different stock of the same producers.

The estimation of strength of CLT panels subjected to in-plane load is therefore more complex compared to the case of standard glulam elements, because involves different failure modes (bending failure of the deep beam, shear failures of boards, torsion failure of the intersection between boards); correct strength estimation is so far possible only with specific ad hoc experimental set-up specifically designed for each type of failure, as described in Table 6.

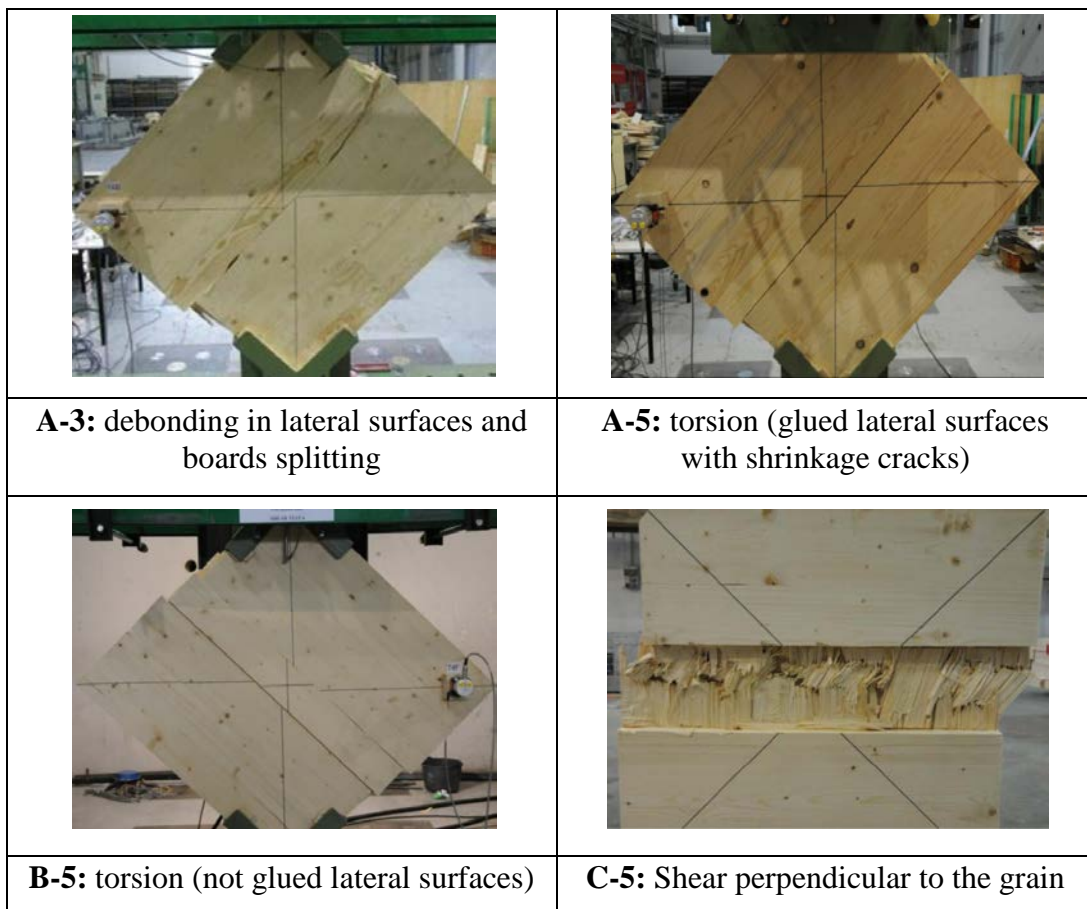


**Figure 10.** Type of failure in CLT element loaded in diagonal compression test set-up.

Diagonal compression test on CLT panel could represent a remarkable alternative set-up to carry out strength characteristics of CLT element under in-plane loads. The first results of an on-going research (see Figure 10) have demonstrated that this test configuration is able to single out the actual type of shear failure (torsional or perpendicular to the grain), and in the same time to avoid the arising of unwanted failure modes as happen in “shear” bending tests according to CUAP [2] or EN 408 [3]. It is worth noting that the types of failure reported in Figure 10 match the experimental results illustrated in Figure 4, beside the case of C-5 specimen: the diagonal test set up allowed to show that only in this latter specimen failure mode due to shear perpendicular to the grain anticipates torsional failure mode.

## 7 Acknowledgements

The Authors wish to thank the under-graduate students Nicola Berti and Francesca Mattei for their precious work done during the research.

## 8 References

- [1] EN 1995. Eurocode 5: Design of timber structures
- [2] CUAP Common Understanding of Assessment Procedure: Solid wood slab element to be used as a structural element in buildings, ETA request No 03.04/06, prepared by ”OIB Österreichisches Institut für Bautechnik”, Schenkenstraße 4, 1010 Wien, Austria, June 2005.
- [3] EN 408:2005 “Timber structures – Structural timber and glued laminated timber; Determination of some physical and mechanical properties”
- [4] Moosbrugger T., Guggenberger W., Boegensperger T., “Cross- Laminated Timber Wall Segments under homogeneous Shear- with and without Openings”, Word Conference on Timber Engineering, Portland (USA), 2006.
- [5] Technische Universität Graz, “Holz-Massivbauweise in Brettspertholz. Nachweise auf der Basis des neuen europäischen Normkonzepts”, BSPHandbuch, Graz 2009.
- [6] Joebstl R.A., Bogensperger Th., Schickhofer G., “In-plane shear strength of cross laminated timber ”, Presentation at International Council for research and innovation in building and construction, St. Andrews, Canada, 2008.
- [7] Blaß H.J., Görlacher R., Zum Trag- und Verformungsverhalten von Lignotrend-Elementen bei Beanspruchung in Plattenebene. Veröffentlichung von Karlsruher Institut für Technologie, 2001. KIT Scientific Publishing.
- [8] Boegensperger T., Moosbrugger T., Silly G., “Verification of CLT-plates under loads in plane”, Word Conference on Timber Engineering, Riva del Garda (Italy), 2010.
- [9] EN 338: 2009 Structural timber. Strength classes



**INTERNATIONAL COUNCIL FOR RESEARCH AND INNOVATION  
IN BUILDING AND CONSTRUCTION**

**WORKING COMMISSION W18 - TIMBER STRUCTURES**

**ROBUSTNESS ANALYSIS OF TIMBER TRUSS SYSTEMS**

D Čizmar

V Rajčić

Faculty of Civil Engineering, University of Zagreb

CROATIA

**MEETING FORTY FIVE**

**VÄXJÖ**

**SWEDEN**

**AUGUST 2012**

---

Presented by V Rajčić

H Larsen commented that the only thing done correctly in the Ballerup Super Arena building was robustness in that the secondary beams were designed such that if one truss failed it did not cause damage to its neighbours. In this case only two trusses failed in the structure. J Munch Andersen stated that the building had basic design errors where members were undersized. V Rajčić stated that with gross design error robustness could not be calculated. U Kuhlmann stated that concerning robustness there were two approaches. The approach of redundancy and ductility is more suitable to steel structures. Here separation of damage of members is a good means perhaps for this type of timber structure where robustness can be improved. U Kuhlmann commented that some of the tables in the presentation were interesting but missing in the paper. H Blass suggested that the presentation could be put on the CIB W18 home page. I Smith asked about wind loading where damage was also a response to the system properties. V Rajčić stated that they were waiting for information on wind loading.



# Robustness Analysis of Timber Truss Systems

Dean Čizmar, Vlatka Rajčić

Faculty of Civil Engineering, University of Zagreb, Croatia

## ABSTRACT

The robustness analysis in this paper is based on the probabilistic level and modelling of the timber material proposed in the Probabilistic Model Code of the Joint Committee on Structural Safety (JCSS). An overview of different probabilistic robustness measures and robustness investigations of timber structures is given. In total, six different timber truss structural systems are considered for this investigation. These different structural systems are analysed and compared using defined robustness measures.

## 1 INTRODUCTION

Progressive collapse is characterized by disproportion between the magnitude of a triggering event and resulting in collapse of large part or the entire structure. Robustness of structures has been recognized as a desirable property because of a several large structural system failures, such as the Ronan Point Apartment Building in 1968, where the consequences were deemed unacceptable relative to the initiating damage. After the collapse of the World Trade Center, robustness has obtained a renewed interest, primarily because of the serious consequences related to failure of advanced types of structures. In order to minimize the likelihood of such disproportional structural failures many modern building codes require robustness of the structures and provide strategies and methods to obtain robustness.

Robustness requirements are provided in two European documents: Eurocode EN 1990: Basis of Structural Design [1] and EN 1991-1-7 Eurocode 1: Part 1-7 Accidental Actions [2]. The first document provides the basic principles, e.g. it is stated that a structure shall be “designed in such a way that it will not be damaged by events like fire, explosions, impact or consequences of human errors, to an extent disproportionate to the original cause”. The EN 1991-1-7 document provides strategies and methods to obtain robustness, actions that should be considered and different design situations: 1) designing against identified accidental actions, and 2) designing unidentified actions (where designing against disproportionate collapse, or for robustness, is important).

In the JCSS Probabilistic Model Code [5] a robustness requirement is formulated as: “A structure shall not be damaged by events like fire, explosions or consequences of human errors, deterioration effects, etc. to an extent disproportionate to the severeness of the triggering event”. In order to attain adequate safety in relation with accidental loads, two basic strategies are proposed: non-structural measures (prevention, protection and mitigation) and structural measures (making the structure strong enough to withstand the loads limiting the amount of structural damage or limiting the amount of structural

damage). According to Danish design rules robustness shall be documented for all structures where consequences of failure are serious. A structure is defined as robust when those parts of the structure essential for the safety have little sensitivity with respect to unintentional loads and defects, or that an extensive failure of the structure will not occur if a limited part of the structure fails. In the last few decades many definitions of robustness have been proposed. In this paper only a brief description of probabilistic measures relevant for robustness assessment is given.

Frangopol and Curley [4] proposed a probabilistic structural redundancy index (RI):

$$RI = \frac{P_{f(dm)} - P_{f(sys)}}{P_{f(sys)}} \quad (1)$$

where  $P_{f(dm)}$  is the probability of failure of a damaged system and  $P_{f(sys)}$  is the system failure probability (no damage). The redundancy index as defined above provides a measure of the residual strength of a damaged system. They also considered the following redundancy factor:

$$\beta_R = \frac{\beta_{intact}}{\beta_{intact} - \beta_{damaged}} \quad (2)$$

where  $\beta_{intact}$  is the reliability index of the intact system and  $\beta_{damaged}$  is the reliability index of the damaged system.

Lind [4] proposed a generic measure of system damage tolerance, based on the increase in failure probability resulting from the occurrence of damage. The vulnerability ( $V$ ) of a system is defined as:

$$V = \frac{P(r_d, S)}{P(r_0, S)} \quad (3)$$

where  $r_d$  is the resistance of the damaged system,  $r_0$  is the resistance of the undamaged system, and  $S$  is the prospective loading on the system  $P(\cdot)$  is the probability of failure of the system, as a function of the load and resistance of the system. The vulnerability parameter indicates the loss of system reliability due to damage

In this paper an index of robustness is defined as a ratio between the reliability index of a damaged structure ( $\beta_{dm}$ ) and the reliability of the intact structure ( $\beta_{int}$ ) [13]:

$$I_{rob} = \frac{\beta_{dm}}{\beta_{int}} \quad (4)$$

Also a robustness factor  $F_{rob}$  can be defined as a ratio of probability of failure of damaged system ( $p_{f,dmg}$ ) and probability of failure of intact system ( $p_f$ ):

$$F_{rob} = \frac{p_{f,dmg}}{p_f} \quad (5)$$

It can be noted that beside the definitions given in equations (4) and (5) a normed index could also be introduced:

$$\overline{I}_{rob} = \frac{\beta_{dmg}}{\beta_{inorm}} \quad (6)$$

where  $\beta_{inorm}$  represents acceptable reliability index of a damaged structure. In this way different structures can be compared.

Similar to this, a normed robustness factor can be defined:

$$\overline{F}_{rob} = -\log\left(\frac{p_{f,dmg}}{p_{f,norm}}\right) \quad (7)$$

where  $p_{f,dmg}$  refers to probability of failure of the damaged system and  $p_{f,norm}$  is acceptable probability of failure of the damaged system.

Recently a new definition [12] of both the progressive collapse and the robustness is given. The probability of disproportionate collapse is calculated as a product of probabilities: the probability of an abnormal event that threatens the structure, the probability of initial damage as a result of event and the conditional probability of a disproportionate spreading of structural failure due to the initial damage. Based on this, there are the three main strategies to limit the probability of a disproportional collapse, first is to prevent the occurrence of abnormal events, the second is to prevent the occurrence of an initial damage in consequence of the occurrence of abnormal events. A third strategy is to prevent disproportionate spreading of failure of the initial damage. This part relates to the internal properties of the structure though its robustness. As such the robustness is a property that depends on the structure itself and the amount of initial damage

## 2 ROBUSTNESS OF TIMBER STRUCTURES

In the last few decades there has been intensely research concerning reliability of timber structures but robustness of timber structures has not been shown much attention. For the purpose of the project „Timber Frame 2000” [11] a six-storey experimental timber frame building was erected, in order to investigate the performance and economic prospects of medium-rise timber frame buildings in the UK. As a part of a testing programme the investigation of disproportionate collapse (robustness) was conducted. Result obtained show that this kind of timber frame system is very robust. Since timber is a complex building material, assessment of robustness is difficult to conduct. As there is obvious correlation between redundancy and robustness, redundant structures will, in principle, be a more robust than statically determinate. However, in respect to timber structures, there are not many highly redundant systems, and the obvious way to asses a robustness of such structures is to demonstrate that the part(s) of the structure essential for the reliability have little sensitivity with respect to unintentional loads and defects.

At the Faculty of Civil Engineering in Zagreb extensive experimental programme was made. First part relates to investigation of two span beams and their material characteristics in order to asses possible material ductility in bending. Next step was to asses characteristics of the metal fasteners (punched plates and screws). Final step of the project was to investigate full scale timber truss systems.

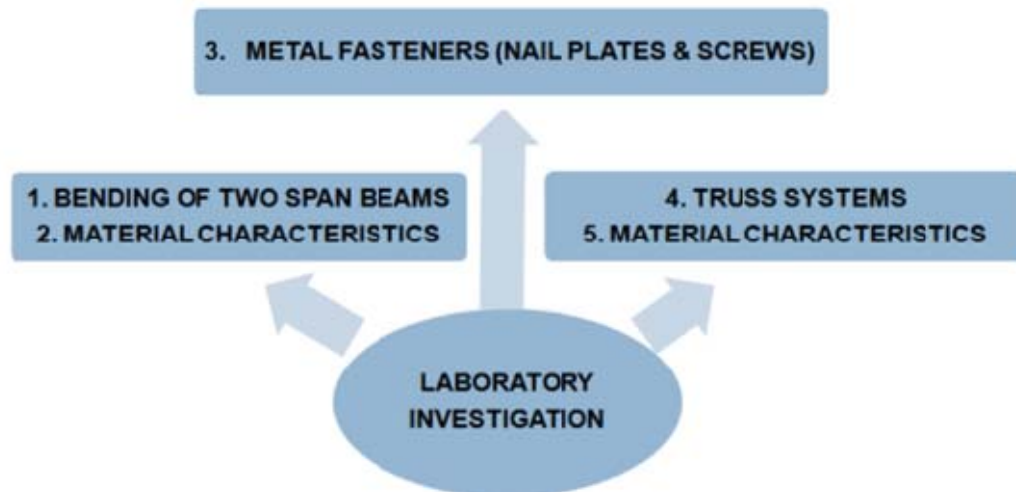


Figure 1. Overview of experimental investigations.

### 3 PROBABILISTIC MODEL

Probabilistic calculations were done by First-Order Reliability Methods (FORM) where a reliability index is estimated based on limit state functions for each of the considered failure modes. The probabilistic analysis is performed with a stochastic model for the strength parameters for whole structural elements, and not to the strength for the single laminates and the glue. Second order effects are neglected for beams subjected to compression and combined compression and bending, respectively. Buckling problems and lateral buckling is taken into account as in Eurocode 5 with deterministic coefficients. For the structural analysis a linear Finite Element analysis has been performed where the glulam truss has been modelled by beam and truss elements. Furthermore, only permanent and snow loads are considered in probabilistic analysis. Identification of the significant failure modes of this structure is difficult to perform since there are many possible failure elements. Based on the deterministic structural analysis four different failure modes are considered: 1) combination of bending and compression (M+N) in the upper chord, 2) combination of bending and tension (M+N) in the lower chord, 3) compression (N) and 4) tension in diagonal elements (N). The ultimate limit state failures are assumed to be brittle (i.e. when an element fails there is no bearing capacity left). The following failure elements are considered for these failure modes:

1. Failure in bottom cord (N+M)
2. Failure due to tension in diagonal element (N)
3. Failure due to compression in diagonal element (N)
4. Failure in top chord (N+M)

For the calculations permanent load  $G$  due to self weight and a variable snow load are taken into account. The permanent load of the roof structure, is assumed Normal distributed with an expected value  $\mu_G = 0.5 \text{ kN/m}^2$  and a coefficient of variation  $\text{COV} = 0.1$ . For the region in Croatia where the structure is located the annual maximum snow load at the ground is Gumbel distributed with a characteristic value  $S_{gk} = 1.5 \text{ kN/m}^2$  and a

coefficient of variation  $COV=0.58$ . The strength variables  $f_c$ ,  $f_m$  and  $f_t$  (compression strength parallel to grain, bending strength and tensile strength, respectively) are calculated based on the reference properties given in table 1 [7]. Table 2 shows all probabilistic variables taken into account (designation, distribution, mean value and coefficient of variation). Correlations between the stochastic variables are taken as in [5] and [7].

Table 1: Stochastic variables (dimensions in mm, strengths in  $N/mm^2$  and loads in  $N/mm$ ). N: Normal; LN: LogNormal; G: Gumbel.

Label	Variable	Distribution	Mean value	COV
$E_s$	Bending MOE	LN	11700	13%
$X_s$	Model uncertain.	LN	0.87	7%
A	Joint distance	N	3041	1%
$b_d$	Width of diagonals	N	200	4%
$h_d$	Height of diagonals	N	240	4%
$b_{dp}$	Width bottom chord	N	200	4%
$h_{dp}$	Height bottom chord	N	690	4%
$b_{gp}$	Width top chord	N	200	4%
$h_{gp}$	Height top chord	N	520	4%
$f_c$	Compression strength	LN	26.6	12%
$f_m$	Bending strength	LN	41.4	15%
$f_t$	Tension strength	LN	24.8	18%
G	Permanent load	N	6.38	10%
S	Snow load	G	3.00	58%
$X_m$	Resistance factor for bending	LN	1.55	18.6%
$X_t$	Resistance factor for tension	LN	1.59	16%
$X_c$	Resistance factor for compression	LN	1.35	8.8%

Six different truss systems (figure 2) which are used in practise are chosen and designed according to EC5 for 100% utilization of members (chords and truss members). A serviceability limit state is also considered.

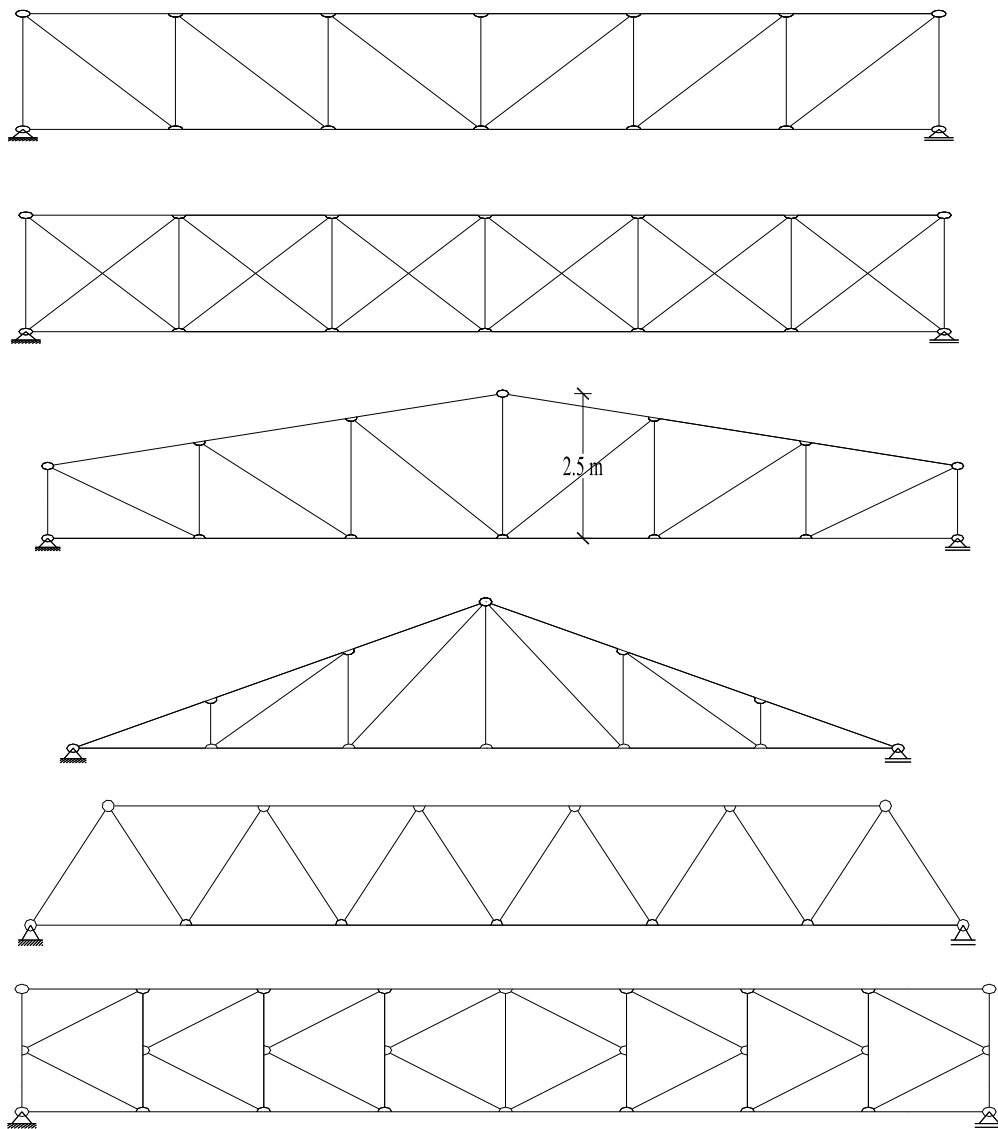


Figure 2. Overview of analysed timber trusses

## 4 METHODOLOGY AND RESULTS

After the design of truss members, for each truss the system reliability of the intact structure is calculated (an estimate of the failure probability is obtained as the arithmetic mean of the upper and lower probability bounds). For each of the previously defined failure modes a failure is assumed (figure 3) and a robustness index is calculated based on the different definitions (4), (5), (6), (7). It can be seen that for most systems (RN1, RN3, RN4, RN5, RN5 and RN6), for at least one failure scenario robustness is 0, so it can be concluded that these systems, in respect to robustness, can be considered as non robust. Truss system RN2 has much higher robustness indices (minimal robustness index  $I_{rob}=0.24$  and corresponding failure probability  $p_f=3.29 \times 10^{-2}$ ) so this system could be considered as much more robust than others. This can be explained because in this system failure of a chord or a truss element won't result in a collapse of the whole structure

(parallel system). As it can be seen, robustness factor is also a relative measure of robustness with bounds in range  $[1, 1/p_f]$ , where 1 is highest robustness possible ( $p_f = p_{f,dmg}$ ) and no robustness where  $p_{f,dmg} = 1$ . Figure 4 represents calculated robustness factors, where for truss RN2 these factors have the highest value, which means that comparing different types of trusses cannot be done. Figure 6 represents normed robustness factors where  $\beta_{norm} = 2$ . Observing the minimal value, truss type RN2 is much more robust than all the others. With this index, different truss types can be compared which is the main objective in the robustness assessment. Figure 7 (normed robustness factors) represents the similar results – considering the minimal values of assumed failures truss RN2 is much more robust.

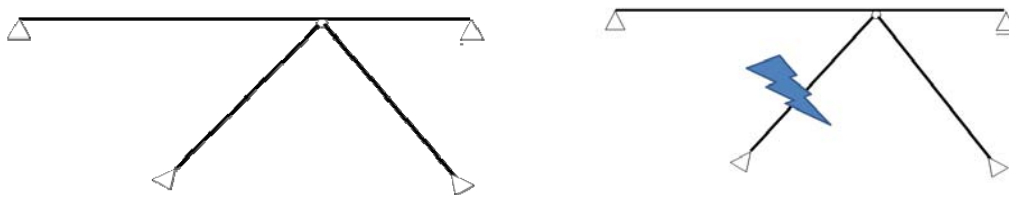


Figure 3. Example of intact (left) and damaged structure (right).

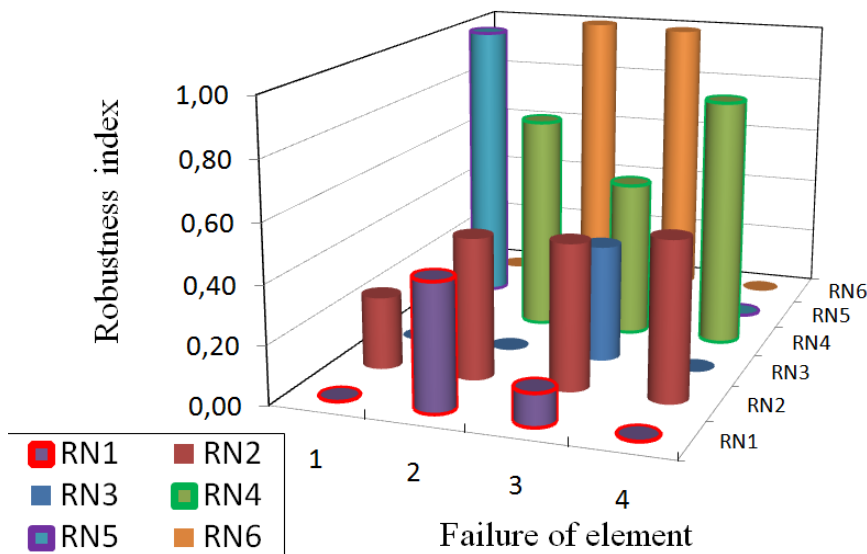


Figure 4. Robustness indices for different truss systems.

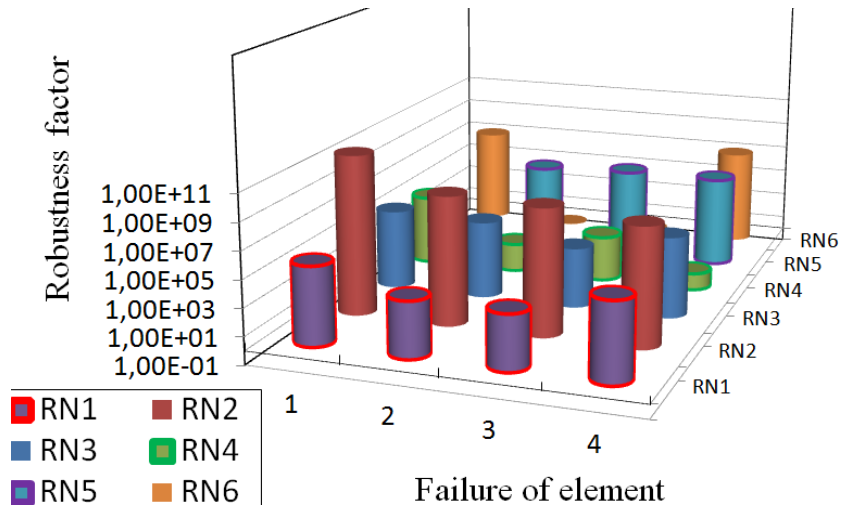


Figure 5. Robustness factors for different truss systems.

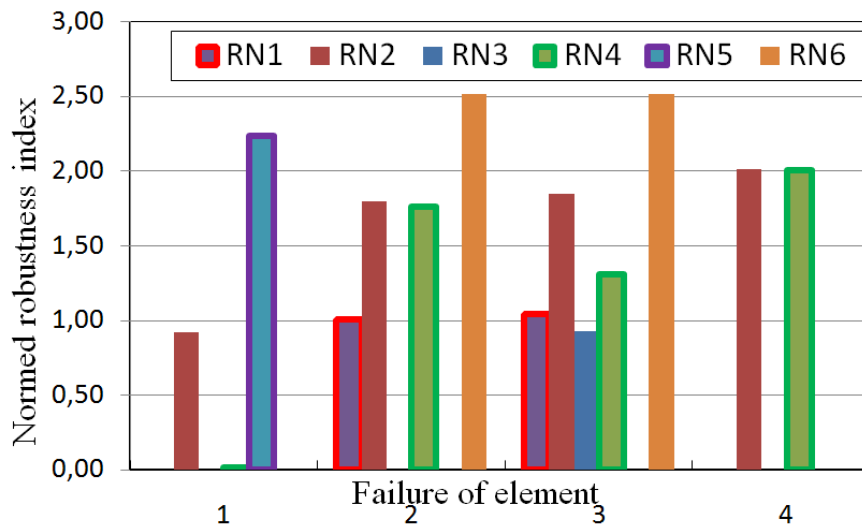


Figure 6. Normed robustness indices for different truss systems.

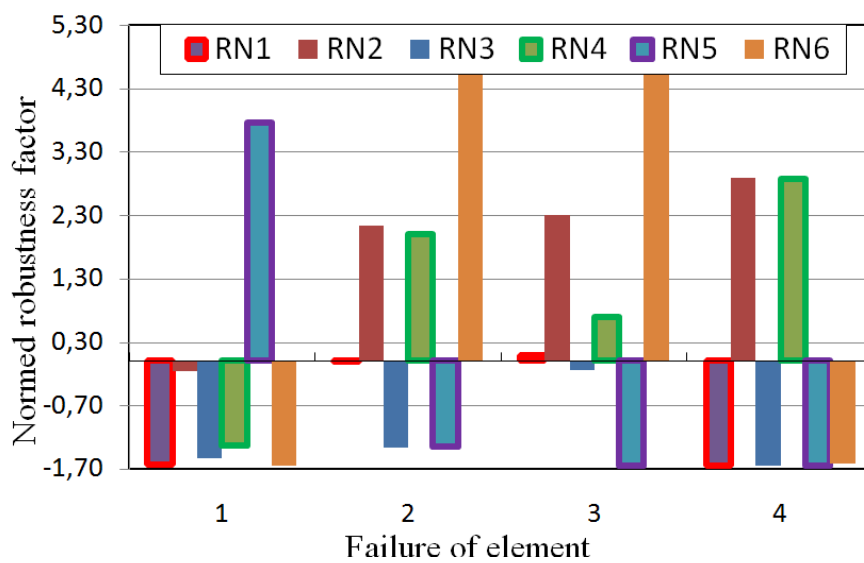


Figure 7. Normed robustness factors for different truss systems.

## 5 CONCLUSIONS

This paper presented results of robustness investigations regarding the usual timber truss systems. Different robustness measures are presented and based on them robustness indices and factors are calculated. It can be seen that proposed robustness index and robustness factors provide a relative measure of robustness which cannot be easily used for comparison of different structures. On the other hand, normed robustness index and normed robustness factor can be used in comparing different structural systems.

Results of different timber structural systems (6 different) with respect to robustness index are given. For most of the systems robustness can be considered as very low (if minimal values are chosen). It is shown that system with parallel elements (RN2) has a much higher robustness. This is because these systems have the possibility to redistribute the forces in structure. It must be noted that other systems which are not considered robust are not “bad” and should not be avoided in engineering practice, but if used, special attention should be made upon minimizing the probability of failure of elements or joints. It can be concluded that if robustness is desired (high consequence class structures) these systems should be used. If the robustness is specially desired, systems RN1, RN3 and RN4 can be easily made more robust with additional diagonal elements.

Results presented here are made on brittle models and possible influence of both material and fastener ductility is not taken into account.

## REFERENCES

- [1] CEN, *Eurocode 0 – Basis of structural design*. Brussels. 2002.
- [2] CEN, *Eurocode 1 - Actions on structures part 1–3: General actions – General actions – snow loads*. Brussels, 2003.
- [3] CEN, *Eurocode 1 - Actions on structures part 1–7: General actions – Accidental actions*. Brussels, 2006
- [4] Čizmar, D., Kirkegaard, P. H., Sørensen, J. D., Reliability and robustness evaluation of timber structures. Short Term Scientific Mission. COST E55 Action. University of Aalborg. Aalborg, 2009.
- [5] Joint Committee on Structural Safety (JCSS), *Probabilistic Model Code*, JCSS Publication, 2001.
- [6] Kirkegaard, P.H., Sørensen, J.D., Collapse Analysis of Timber Structures. in B.H.V. Topping, M. Papadrakakis, (Editors). "Proceedings of the Ninth International Conference on Computational Structures Technology". Civil-Comp Press. Stirlingshire, UK , Paper 247, 2008.
- [7] Koehler, J., Sørensen, J. D., Faber, H.M, Probabilistic modelling of timber structures, *Journal of Structural Safety*, vol. 29, issue 4: 255-267, 2007.
- [8] Rajcic, V. Čizmar, D., Poul Henning Kirkegaard, John Dalsgaard Sørensen, Robustness analysis of big spam glulam truss structure, ISCA Conference, 2010.
- [9] Wolfram Research, Inc. Mathematica, Version 7.0. Champaign. 2008.
- [10] Andrić, Boris, Čizmar, Dean, Rajčić, Vlatka. Reliability analysis for laminated timber girders. *Gradevinar* 60, pp. 513-518, 2008.
- [11] Enjily, V., The TF2000 project and its effect on medium-rise timber frame buildings in UK, BRE, URL: <http://projects.bre.co.uk/tf2000/>, 2000.
- [12] Starossek, U. & Haberland, M. (2010). Disproportionate Collapse: Terminology and Procedures. *Journal of Performance of Constructed Facilities*, 24, 519-528.

- [13] Sørensen, J. D., Framework for robustness assessment of timber structures, *Engineering Structures*, vol 33, 2011, pp.3087-3092.
- [14] Čizmar, D., Kirkegaard, P. H., Sørensen, J.D., Rajčić, V., Reliability-based robustness analysis for a Croatian sports hall, *Engineering Structures*, vol 33, 2011, pp.3118-3124.

**INTERNATIONAL COUNCIL FOR RESEARCH AND INNOVATION  
IN BUILDING AND CONSTRUCTION**

**WORKING COMMISSION W18 - TIMBER STRUCTURES**

**PERFORMANCE BASED DESIGN AND FORCE MODIFICATION FACTORS  
FOR CLT STRUCTURES**

Shiling Pei

South Dakota State University, Brookings, SD

M Popovski

FPInnovations, Advanced Building Systems, Vancouver, BC, Canada

J van de Lindt

Colorado State University, Fort Collins, CO

**MEETING FORTY FIVE**

**VÄXJÖ**

**SWEDEN**

**AUGUST 2012**

---

Presented by M Popovski

M Yasumura asked about the failure criteria for hold-down. M Popovski responded that the hold-downs took vertical uplift forces while shear connectors took shear forces. In CLT hold-downs contribute to shear response. B Dujic commented about openings in the assembly and asked how the step joints affected the results. M Popovski stated that the building was designed with step joints in openings and there was no special consideration of the influence of openings. B Dujic commented that in performance based design you did not need the R or Q factor. M Popovski stated that they did performance based design to show that it worked for CLT and R factors were chosen based on drift limits. I Smith asked what was the status of discussion on performance based design in US. M Popovski stated that the performance objectives in FEMA were used and they were considered to be conservative. I Smith commented that he wondered whether steel and concrete people were in agreement with performance based design principles. T Skaggs commented that the results show CLT without hold-down had higher R factors than cases with hold-down. M Popovski responded that hold-downs were desirable but there were trade-offs. BJ Yeh received confirmations that R factors were only applicable to the connectors. R Tomasi asked about the contribution of the corners. M Popovski stated that it was not studied but would consider it in the future. W Seim stated that forced based design was used by engineers and they would stay with this approach for a long while yet. He received confirmation that the study considered symmetrical conditions only. M Yasumura received confirmation about the rocking of the shear wall where vertical loading was included in the analysis. G Schickhofer commented that CLT element concept was originally based on the use of large panels as full elements and asked why so many small elements were used. M Popovski stated that small panels were used in building and this was a trade off between resistance and ductility. F Lam asked whether acceleration in the floors were checked. M Popovski responded that ~ 1.6 g was observed in the model. P Quenneville commented about one full panel versus many smaller panels that in US 1.2 m wide panels were produced. B Dujic stated that this was a production capacity and transportation issue.



# Performance Based Design and Force Modification Factors for CLT Structures

Shiling Pei<sup>1</sup>, Marjan Popovski<sup>2</sup>, John van de Lindt<sup>3</sup>

<sup>1</sup> Assistant Professor, South Dakota State University, Brookings, SD

<sup>2</sup> Principal Scientist, FPInnovations, Advanced Building Systems, Vancouver, BC, Canada

<sup>3</sup> George T. Abell Professor in Infrastructure, Colorado State University, Fort Collins, CO

## Abstract

In this paper, a performance-based seismic design (PBSD) of a CLT building was conducted and the seismic response of the CLT building was compared to that of a wood-frame structure tested during the NEESWood project. The results from the quasi-static tests on CLT walls performed at FPInnovations were used as input information for modelling of the CLT walls, the main lateral load resisting elements of the structure. Once the satisfactory design of the CLT mid-rise structure was established through PBSD, a force-based design was developed with varying R-factors and that design was compared to the PBSD result. In this way, suitable R-factors were calibrated so that they can yield equivalent seismic performance of the CLT building when designed using the traditional force-based design methods.

Based on the results of this study it is recommended that a value of  $R_d=2.5$  and  $R_o=1.5$  can be assigned for structures with symmetrical floor plans in the National Building Code of Canada (NBCC). In the US an  $R=4.3$  can be used for symmetrical CLT structures designed according to ASCE 7. These values can be assigned provided that the design values for CLT walls considered (and implemented in the material design standards) are similar to the values determined in this study using the kinematics model developed that includes the influence of the hold-downs in the CLT wall resistance. Design of the CLT building with those R-factors using the equivalent static procedures in the US and Canada will result in the CLT building having similar seismic performance to that of the tested wood-frame NEESWood building, which had only minor non-structural damage during a rare earthquake event.

## 1. Introduction and Previous Research

With three producers already in operation in Canada and one in planning stage in the US, the use of cross-laminated timber (CLT) is gaining popularity in North America. Since CLT is not introduced as a structural system in the building codes and material standards, one of the most important issues for designers of CLT structures in earthquake prone regions are the values for the force modification factors (R-factors) for the system. The R-factors in building codes in North America account for the capability of the structure to undergo ductile nonlinear response, which dissipates energy and increases the building period. In the 2010 edition of the NBCC [1], the elastic seismic load is reduced by two types of R-factors,  $R_o$ -factor which is related to the over-strength of the system and  $R_d$ -factor that is related to the ductility of the structure. In the major model codes in the United States, the International Building Code and the ASCE 7-10 [2], there is only one R-factor, called the response modification coefficient to reduce the seismic design force. Eurocode 8 [3], the European seismic model code, also uses only one factor ( $q$ -factor) for reduction of the seismic design force.

Efforts have already been made to quantify the  $q$ -factor for CLT structures in Eurocode 8 using incremental non-linear dynamic analyses on analytical models of three-storey structures verified by testing of components. The  $q$ -factor for any earthquake was determined using either the acceleration-based approach or the base shear approach. In the acceleration-based approach the  $q$ -factor was calculated as a ratio of the peak acceleration of an earthquake record that causes ‘near collapse’ condition in the structure and the design acceleration in the code for the location for which the building was designed [4], [5], [6]. In the base shear approach the  $q$ -factor was calculated as the ratio of the base

shear force obtained from linear elastic analysis and the base shear force at “near collapse” state of the non-linear analysis for every input ground motion [7]. This method also takes into consideration the influence of the input ground motion on the elastic response of the structure. Using the acceleration-based approach the average q-factor was found to be  $q=3.4$  and  $q=3.8$  in [5] and [7] respectively, while according to the base shear approach the average q-factor was found to be  $q=3.15$  [7].

An initial estimate for the R-factors in North America was conducted using the AC130 equivalency criteria [8]. According to the criteria, assigning an R-factor for a new wood shearwall assembly can be made by showing equivalency of its seismic performance in terms of maximum load, ductility, and storey drift (all obtained from quasi-static cyclic tests), with respect to corresponding properties of wood-frame nailed shearwalls that are already in the code. Based on the experimental tests conducted at FPInnovations [9], it was found that although not every single CLT wall configuration satisfied the response parameters as defined in AC130, the average values for the set of CLT walls did satisfy the AC130 criteria. Consequently, one may conclude that the CLT walls tested can share the same seismic modification factors with regular wood-frame shearwalls in the US, which means using an R-factor of 6.5. This corresponds to having the product of  $R_d R_o$  equal to 5.1 in Canada ( $R_d = 3.0$ ;  $R_o = 1.7$ ) which are the factors used in NBCC for nailed wood-frame shearwalls. However, at this early stage of acceptance in the design practice, the authors of [8] recommended at the time that a more conservative set of factors ( $R_d=2.0$ ;  $R_o=1.5$ ) be used for CLT structures with ductile nails or screws and hold-downs. It was also recommended that further studies such as the analyses presented in this paper and analyses according to the FEMA P-695 procedure be considered.

## 2. Objectives and Approach

The research presented in this paper contributes further to determining the R-factors for seismic design of CLT structures. The objective of the research presented in this paper is to: (a) conduct a performance-based seismic design (PBSD) for a 6-story CLT residential building by using verified CLT wall models; (b) use the PBSD building to obtain more accurate preliminary values for the response modification coefficients in ASCE 7 in the US; and (c) recommend more appropriate R-factors for seismic design CLT mid-rise buildings in NBCC. For the purposes of this study, the well-known NEESWood Capstone wood-frame building was redesigned as a CLT structure and was used as a typical mid-rise CLT structure in all analyses. The results from the quasi-static tests on CLT walls performed at FPInnovations [9] were used as input information for modelling of the CLT walls, the main lateral load resisting elements of the structure. Once the satisfactory design of the CLT mid-rise structure was established through PBSD, a force-based design was developed with varying R-factors and that design was compared to the PBSD results. In this way, suitable R-factors were calibrated for both ASCE 7 and NBCC so that they can yield equivalent seismic performance of the CLT building.

The NEESWood multi-university research project in the US developed a PBSD philosophy [10], and provided the necessary design and analysis procedures to safely increase the height of wood-frame structures in high seismic zones. The PBSD methodology developed (primarily Direct Displacement Design) focused on limiting the damage by specifying key performance requirements such as limiting the inter-story drifts. For verification purposes, the PBSD procedure was used for the seismic design of a six-story multi-family residential wood-frame apartment building [11]. This 1294 m<sup>2</sup> mid-rise structure (called the Capstone building), was tested on the E-Defense shaking table facility in Miki, Japan. During the tests, the Capstone building satisfied all performance targets imposed during the design, with only non-structural damage present even at Maximum Credible Earthquake (MCE) level shaking with probability of exceedance of 2% in 50 years [12]. The Capstone tests validated the effectiveness of the PBSD procedure developed. This procedure was employed in this study for the CLT structure to achieve similar seismic performance and generate target building design to calibrate the R-factors.

## 3. CLT Wall Modeling and Database of CLT Wall Resistances

Modeling of the CLT walls as main lateral load resisting elements of the structure was done using a kinematics model developed in Matlab (Figure 1a). The model was calibrated for various input

parameters such as size of the walls, gravity load level, number and type of brackets and location, number of hold-downs, number of step-joints (if present), number of fasteners per-bracket, etc., based on the CLT wall test data [9], and using the basic kinematics formula shown in equation (1). The fastener behavior in the model was represented using the well-known ten parameter CUREE model, which is widely used for wood based shear wall and connection modeling (Figure 1b). Example of the responses of the tested and the calibrated response of a 2.3 m long CLT wall, which uses brackets with eighteen 16d spiral nails per bracket and has step-joint with 8 4x70 mm (SFS1) screws in the middle, is shown in Figure 2. A total of 19 different models were developed for CLT walls (assemblies) with 2 different bracket types and hold-downs, with each of the 10 parameters calibrated for every model.

$$F(D) = \sum_{i=1}^n \frac{l_i}{H} f_i(d_i) + \frac{L}{2H} G = \sum_{i=1}^n \frac{l_i}{H} f_i\left(\frac{l_i}{H} D\right) + \frac{L}{2H} G \tag{1}$$

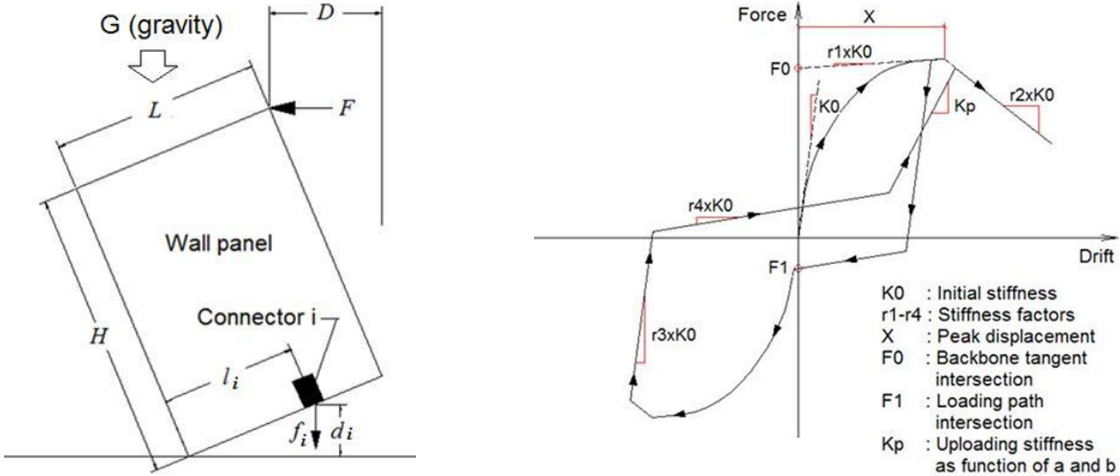


Figure 1 (a) Basic kinematics used for developing of the simplified CLT wall models; (b) Ten-parameter hysteretic model used for modeling of the CLT connections (brackets and hold-downs)

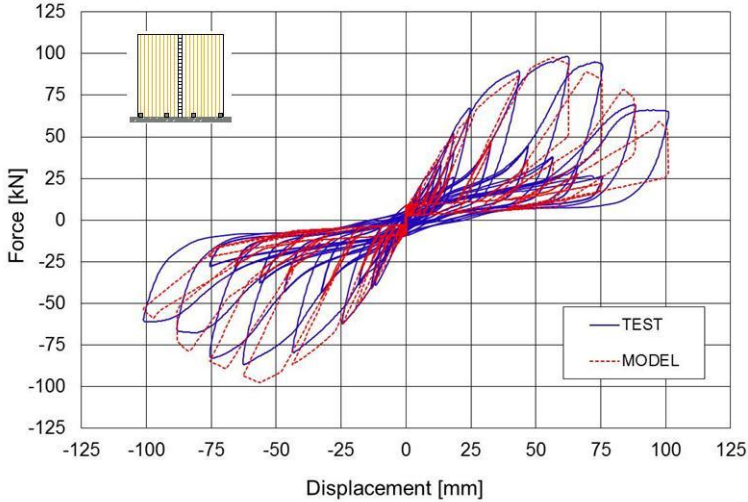


Figure 2. An example of tested and modeled (calibrated) response of a 2.3 m long CLT wall with 16d spiral nails in the brackets and a step-joint in the middle

With the numerical model and connector parameters calibrated, the hysteresis curve for any given CLT wall configuration with different connectors can be estimated numerically using the kinematics (Matlab) model. Consequently, backbone curves and lateral load design values for various CLT walls using three different fasteners in the brackets were developed. As at this point no design loads exist for CLT walls in Canada and in the US, the design levels were developed by dividing the ultimate load obtained from the hysteresis loop (by the Matlab model) by a factor of 2.8, thus obtaining the same or slightly better, level of safety as with regular wood-frame walls.

In North America a typical design practice for CLT walls at this point is to assume that entire shear force along the wall is taken by the bracket connections, while the hold-downs are placed for vertical continuity and to take the wall uplift. In other words, the contribution of the hold-downs is ignored when determining the shear capacities for the wall panels. It was recognized from experimental tests, however, that due to rocking response of CLT walls, hold-downs also contribute to the shear wall strength. Consequently, the lateral resistances for CLT walls were derived with the two options considered with and without the hold-down contribution taken into account. The capacities derived without hold-down contribution are therefore conservative compared to the walls actually installed in practice that contain hold-downs. Some of the configurations for which design values were derived are shown in Figure 3a. The notation “S” stands for **S**ingle sided brackets for each location, “DE” stands for **D**ouble sided brackets at the **E**nd of the panel only, and “DA” stands for **D**ouble **A**ll, meaning all brackets are double sided. For a case of a CLT wall with 2 brackets only, configurations DE and DA are identical.

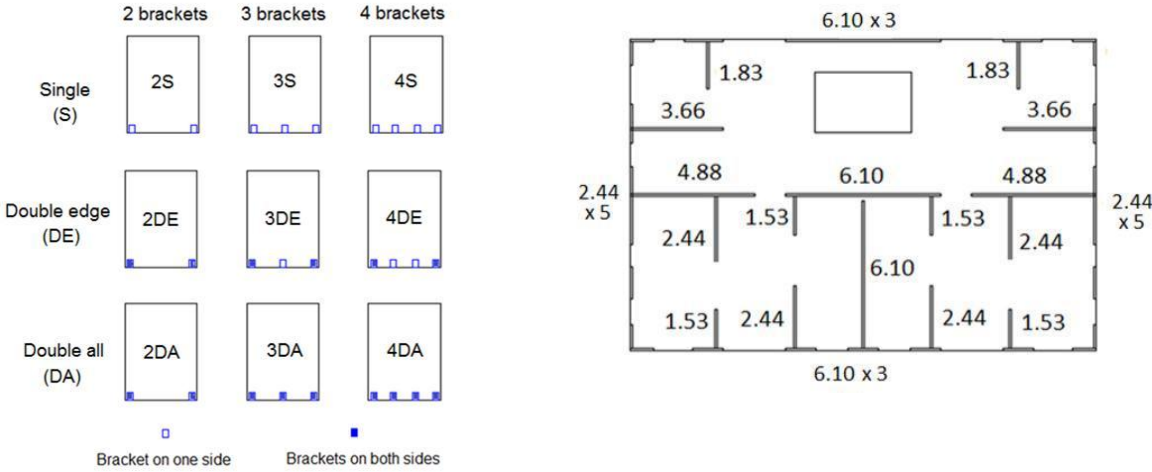


Figure 3 (a) Panel configurations for deriving design values (b) Maximum amount of CLT wall segments (lengths in m) allowed for CLT Capstone building floor plan for storeys 1 through 5

#### 4. Performance Based Seismic Design of the CLT Building

The Performance Based Seismic Design procedure developed during the NEESWood project that was used for design of the Capstone wood-frame building [10] was also here for design of the CLT structure. This procedure, also referred to as Direct Displacement Design (DDD), uses prescribed drift limit targets for the seismic design under different levels of seismic intensity. By controlling the inter-storey drift, the damage to the structural and non-structural components can be minimal even at Maximum Credible Earthquake (MCE) levels. The three DDD performance objectives considered for the NEESWood Capstone building were also used for the CLT structure (Table 1).

Table 1. Performance expectations for the CLT structure for three different levels

Performance Level	Seismic Hazard	Performance Expectations	
		Inter-storey Drift Limit [%]	Probability of Non-exceedance [%]
Level 1	50% / 50yr	1.0	50
Level 2	10% / 50yr	2.0	50
Level 3	2% / 50yr	4.0	80

Each performance requirement is specified by a probability of non-exceedance (NE) of an inter-story drift limit at specified level of seismic hazard. For instance, at level 3 (MCE level), the DDD building has a performance objective of not exceeding 4% inter-story drift 80% of the time, i.e. an 80% of NE probability. Based on the test results of single CLT walls, the implication of the inter-storey drift limits on the physical damage of the building during strong earthquakes was considered to be similar to that of a wood-frame structure. As the NEESWood wood-frame Capstone building showed that it can withstand

an MCE level earthquake with only non-structural damage using these drift targets, using the same storey drift targets for the CLT building should also lead to satisfactory building performance during severe earthquakes.

Key results from the DDD analysis were groups of target points for each story and each direction of the building. These points describe a combination of desired story shear capacity at each particular displacement or drift level for each performance expectation level (Figure 4a). The building was then designed using an iterative process so that the resistance envelope (backbone curve) of each storey and in each direction of the building was satisfying the DDD target points. Example of the backbone curves and the DDD target points for 2%/50 years hazard level for the X (longer) direction of the CLT building designed with 16D spiral nails in the brackets and the hold-downs, is given in Figure 4b.

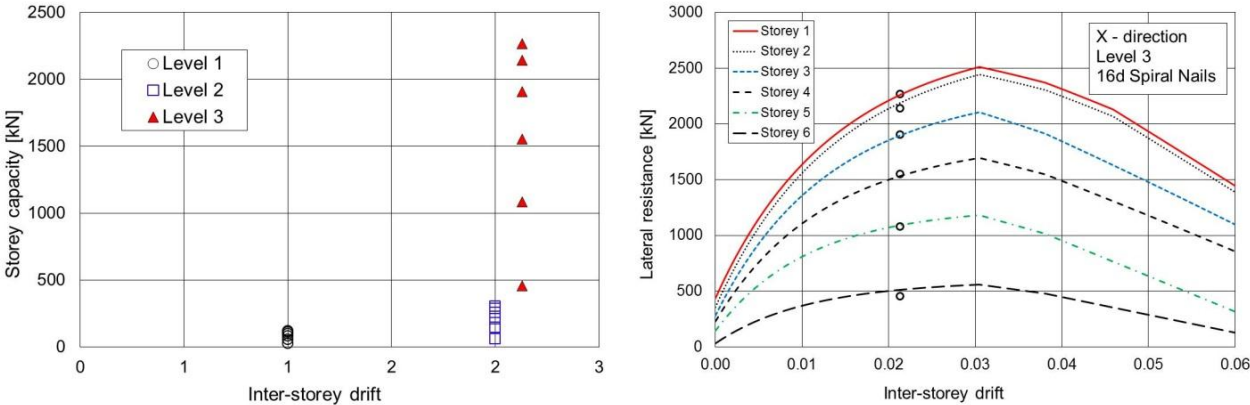


Figure 4 (a) Target points (demands) from the DDD for the 3 performance levels; (b) Backbone curves and DDD target points X-direction of the building with 16D spiral nails, level 3 hazard

Verification of the seismic response of the DDD CLT building was done by a series of nonlinear dynamic analyses using the SAPWood program. The hysteresis behavior of all CLT walls was represented in the SAPWood program using the ten parameter hysteretic model shown in Figure 1b. The parameters for each wall component were adjusted to closely match the hysteretic behavior predicted by the kinematics model. Accuracy in the time history simulation was ensured by the similarity in the backbone curves and the pinching behavior. Figure 5a shows an example comparison between the hysteresis loops for a CLT wall developed by the SAPWood computer program and the calibrated kinematics prediction in Matlab.

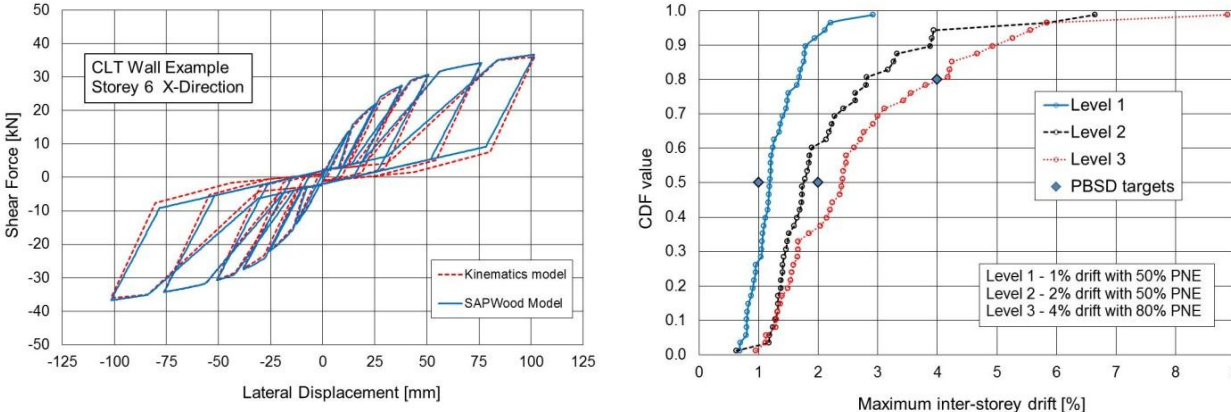


Figure 5 (a) Comparison between the hysteresis loops for a CLT wall in SAPWood and Matlab; (b) CDF curves for the CLT building designed with 16d nails, for the 3 levels of seismic hazard

The ground motion suite used included 22 bi-axial far-field ground motions used in FEMA P-695[13], scaled to three target hazard levels. The bi-axial ground motions were also rotated by 90-degrees so that the building was actually subjected to 44 different biaxial ground motions at each of the 3 intensity (hazard) levels for a total of 132 analyses for each of the 3 connectors considered. For each analysis, the

maximum inter-story drift value experienced by the structure (at any story and in either direction) was recorded and that value is represented as one data point (Figure 5b). With 44 maximum drift values for each performance/intensity level, these maximum drift values were rank-ordered and plotted as Cumulative Distribution Function (CDF) curves (Figure 5b). As shown in Figure 5b, for a CLT building with 16d spiral nails in the brackets, the PBSB targets for Levels 2 and 3 are below or on the CDF curves. This means that the building satisfied the performance requirements for these levels of seismic hazard. The level 1 performance is only partially satisfied but this should not affect the overall building performance as only insignificant damage can occur at 1% storey drift. The performance of the building designs using screws in the brackets was similar since all these designs are indeed reflection of the same set of storey backbone requirements imposed by DDD, realized using different physical connections.

## 5 Approximate R-factors for the CLT Building using ASCE 7-10 Equivalent Lateral Force Procedure Design

The Equivalent Lateral Force Procedure (ELFP) is one of the most commonly used design procedures for seismic design of multi-storey buildings in many building codes. In this section the ELFP procedure according to 2010 ASCE7 was used to determine the storey shear demand for the designed CLT Capstone building. Since the seismic demand depends on the seismic response modification coefficient (R-factor) chosen for the design, a calibration procedure was carried out to identify the most suitable R-factor for the ELFP procedure according to ASCE7. As the seismic performance of the PBSB building was verified by the nonlinear time history analyses (Figure 5b), the ELFP design using the calibrated R-factor is expected to have similar satisfactory building performance. In another words, under a MCE event for the location chosen the CLT building will have 80% chance to experience only non-structural damage, as observed during the shaking table tests of the NEESWood Capstone Wood-frame Building.

With the wall selection for the CLT building already known from the PBSB, the target (minimum) storey shear design resistance was obtained by adding the resistances of all the walls at each storey in both X and Y directions. Two cases were examined, with the hold-down resistance considered or not considered in determining the design resistance for individual CLT walls. With the target storey shear values obtained, the purpose of the R-factor calibration was to choose an R factor that will provide the same or higher resistance than the target resistance at each storey. The ELFP seismic demand was carried out according to section 12.8 of ASCE7-10 for site located in Los Angeles, California with a design spectral acceleration  $S_{DS} = 1.62g$ . The importance factor was taken as 1.0 ( $I=1.0$ ), while the calculated building period was 0.4 s.

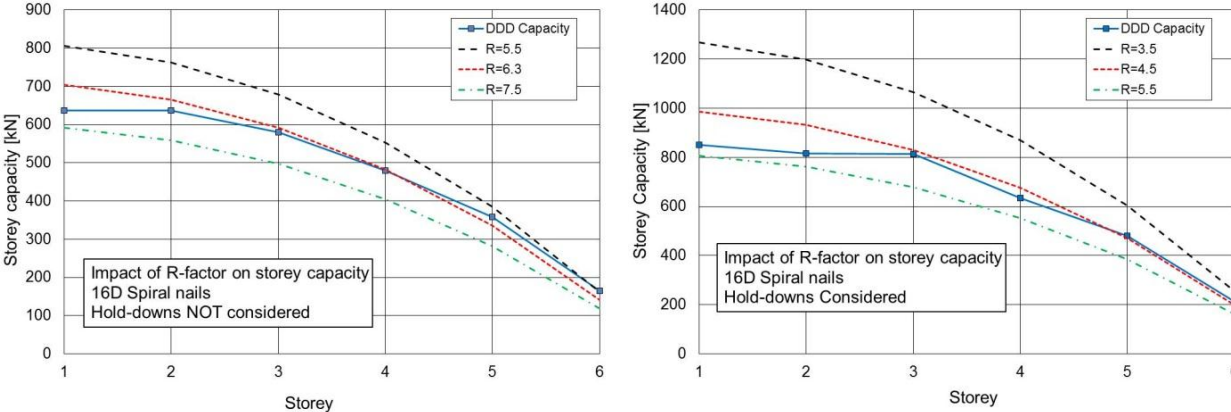


Figure 6 Effect of the variation of the R-factor on the storey shear distribution with respect to the target shear values with (a) hold-downs not considered and (b) considered in the design wall resistance

Figure 6 shows the impact of the variation of the R-factor on the storey shear distribution with respect to the target shear values for the CLT building designed with 16d spiral nails in the brackets and with hold-downs not considered (Figure 6a), or considered (Figure 6b), in the design wall resistance. The R-factor calibration showed that an R factor of 6.5 can be used for the design of the CLT building following ASCE 7-10 in case when the CLT shear wall capacity excludes the hold-down contribution (conservative

CLT design approach). If the contribution of hold-downs is included in the CLT wall capacity, the calibrated R factor has to be reduced to about 4.5 to achieve the same building performance.

Table 2. Calibrated R-factors for the CLT building according to ASCE 7 design approach

Fasteners in the brackets	Calibrated R-factors according to ASCE 7	
	Hold-down Included	Hold-down not Included
16D Nails	4.5	6.3
4x70 mm screws (SFS1)	4.3	7.0
5x90 mm screws (SFS2)	4.8	6.5

Calibrated (adequate) factors for the CLT building with the three different fasteners in the brackets are given in Table 2. As can be seen, the lowest (most conservative) R-factor that can be used in case any connector when the hold-down influence was taken into account in the CLT wall design is  $R=4.3$ . An R-factor of 6.3 can be used when the hold-down influence is not taken into account. It should be noted that any changes of the performance expectations (targets), building configuration and height, and the hazard characteristics of the location, will have an influence on the calibrated R factors shown here. However, the authors are of the opinion that such influence will not make a significant change in the range of the R-factors presented here. In other words, the ranges for the R-factors presented here are good preliminary estimates for such factors for symmetrical CLT buildings located in high seismic region in the US.

## 6 Proposed R-factors for CLT Buildings in NBCC

A slightly different approach was used for obtaining the appropriate ductility related force modification factors ( $R_d$ -factors) for the National Building Code of Canada (NBCC). The value for the over-strength related modification factor  $R_O$  that is mostly related to the over-strength in the connectors, was chosen to be constant ( $R_O=1.5$ ) throughout this process. This value is the same as for the other heavy timber systems in NBCC. The same 6-storey Capstone CLT building was used as a reference structure for developing the different building models used in the analyses. The seismic demand for the CLT structures was determined according to the Equivalent Static Force Procedure (ESFP) given in 2010 NBCC for 8 different values of the  $R_d$  factor ( $R_d=1.5, 2.0, 2.5, 3.0, 3.5, 4.0, 5.0,$  and  $6.0$ ). It was assumed that the buildings were located in Vancouver, BC (maximum spectral acceleration of  $0.96g$  at  $T=0.2s$ ) with a design spectral acceleration  $S_a=0.743g$  at the building fundamental period of  $0.4s$ . According to NBCC requirements, buildings located on firm soil with  $R_d \geq 1.5$  shall not be designed for a seismic force that is greater than the  $2/3$  of the force at  $T=0.2s$ . This force cut-off value for the design base shear was found to govern all designs, meaning that the buildings were actually designed for force equivalent to  $S_a=0.64g$ .

With the seismic demand determined for each storey, CLT walls were selected for each storey to satisfy the demands. Since design values for CLT walls with 3 types of connectors were developed (16d spiral nails, 4x70 mm SFS1 screws, and 5x90mm SFS2 screws), for each of the two hold-down design considerations (with and without hold-downs considered), a total of 6 building designs were developed for each chosen  $R_d$ -factor. Since 8 different  $R_d$  factors were considered, a total of 48 CLT Capstone building designs were generated. SAPWood models for every building design configuration were developed. The building models were developed to reflect the realistic as-built system, which includes the impact of gravity load and presence of the hold-downs. As a result, the designs generated with CLT design resistance tables without hold-downs considered in the design will lead to conservative results.

FEMA P-695 [13] suggested earthquake records were used as input ground motions in the non-linear dynamic analyses. Because all FEMA P-695 ground motions are biaxial, first the stronger ground motion component of each pair was scaled at the building natural period ( $T_a=0.4s$ ) to match the  $S_a=0.743g$  from the Vancouver design spectrum. The other component was then scaled with the same scale factor so that the PGA ratio between two components was not altered. Figure 7 shows the response spectra for the un-scaled and scaled ground motions.

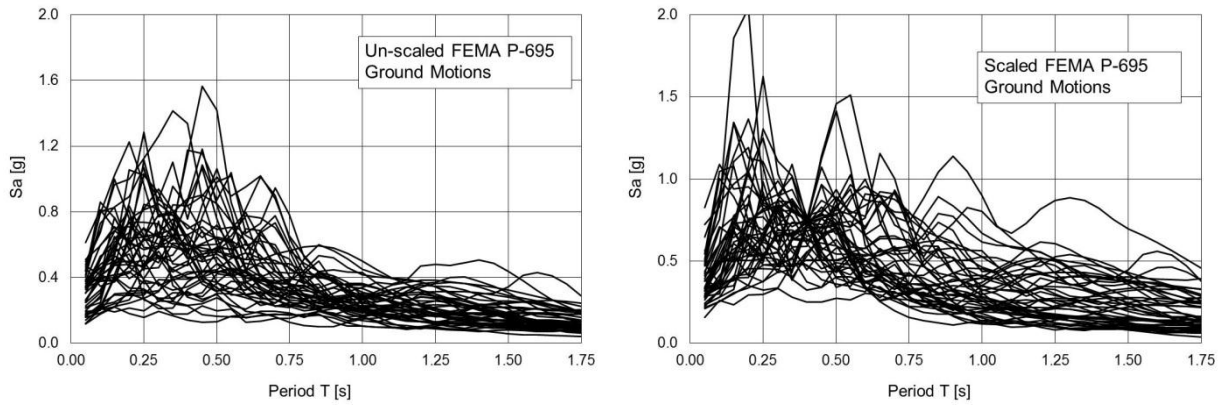


Figure 7 FEMA P-695 response spectra for the (a) un-scaled and (b) scaled ground motions

A series of 44 bi-axial nonlinear time history analyses for each of the 48 building designs (models) developed. For each analysis, the absolute maximum inter-storey drift from the building non-linear dynamic response at any storey and in any direction was recorded and rank-ordered. The distribution of these maximum drift values represents the performance of each particular design under the chosen Vancouver hazard. Examples of the cumulative distribution functions (CDFs) for the maximum inter-storey drifts for building configurations with 16d nails in the brackets and different  $R_d$ -factors are shown in Figures 8 and 9.

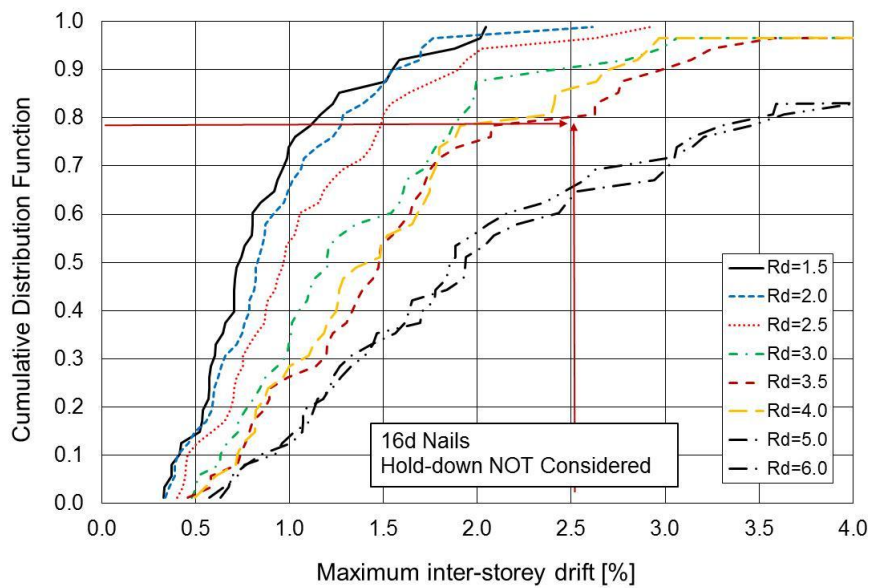


Figure 8 CDF curves for the CLT building for various  $R_d$ -factors. Building model has 16d spiral nails in the brackets and hold-down influence NOT included in the resistance values of the walls

Based on the performance of different building designs (different connectors in the brackets and  $R_d$  factors), a comprehensive evaluation of the appropriate  $R_d$  factors for achieving a prescribed performance target can be made. For example, if the acceptable performance level for the buildings is assumed as not to exceed 2.5% inter-storey drift in 80% of the cases (80% probability of non-exceedance), one just need to find the performance point corresponding to 2.5% drift on the X-axis and 0.8 CDF value on the Y-axis of the plots. All the curves above that performance point will be able to satisfy the criteria. The  $R_d$  factor that corresponds to the curve that just satisfies the performance will be the most appropriate value for that performance objective. Based on this procedure, the  $R_d$  factors that satisfy several different performance objectives are shown in Table 3. The minimum values for  $R_d$  factors for each performance target are given in red. It should be noted that not all of the performance objectives need to be satisfied at the same time. It will be up to the design engineer, the jurisdiction of interest or the code committees to decide which performance level should dictate the  $R_d$  value used for the seismic design.

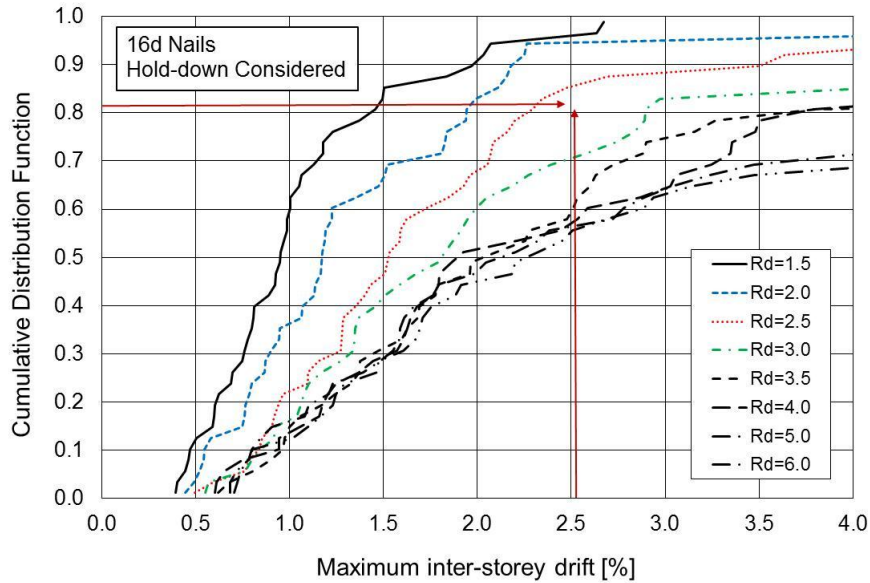


Figure 9 CDF curves for the CLT building for various  $R_d$ -factors. Building model has 16d spiral nails in the brackets and hold-down influence included in the resistance values of the walls

It can be seen from Table 3 that for each performance level the calibrated  $R_d$  values are smaller in cases where the hold-down capacity was included in the CLT wall resistance than in the cases where it was neglected. This is very logical since neglecting hold-down contribution automatically builds in extra safety level in the design. At this point when the methods for deriving design values for CLT walls are getting developed and are not agreed upon, it is prudent to take the more conservative approach for determining the calibrated  $R_d$  factor for CLT structures. If the objective of the design is to effectively control the damage and prevent collapse (2.5% storey drift) during a 2% in 50 years event, it is recommended that an  $R_d$  factor of 2.5 is used for all connectors considered for the buildings analysed. Based on the test results on the single wall components as well on the tests on 3-D CLT structures conducted so far [5], the 2.5% inter-storey drift is achievable in CLT structures without inducing excessive building damage.

Table 3. Calibrated  $R_d$  factors for the CLT building models according to 2010 NBCC design procedure

Performance targets Storey drifts and probabilities of non-exceedance (PNE)	Hold-downs NOT accounted in resistance values for CLT walls			Hold-downs accounted in resistance values for CLT walls		
	16d nails 3.9x89mm	4x70mm Screws	5x90mm Screws	16d nails 3.9x89mm	4x70mm Screws	5x90mm Screws
1.5% drift & 50% PNE	4.0	4.0	4.0	2.5	3.0	2.5
2.0% & 80% PNE	3.5	3.5	3.0	2.0	2.25	2.0
2.5% & 80% PNE	3.5	4.5	4.0	2.75	2.75	2.5
4.0% & 80% PNE	6.0	5.0	4.0	4.0	3.0	2.5

It should be noted that changes in the building configuration (unsymmetrical floor plans), building height (fundamental period), the hazard characteristics of the location, and the influence of the boundary conditions (effects of the perpendicular walls and floor slabs), will have an influence on the calibrated  $R_d$  factors shown here. However, the authors are of the opinion that such influences will either not make significant changes to the values of the  $R_d$  factors suggested or will add additional conservatism to the values (in case of the boundary conditions). Therefore the  $R_d$  values presented here are good estimates for symmetrical CLT buildings located in high seismic region in Canada. The values of  $R_d = 2.5$  and  $R_O = 1.5$  will be proposed to the NBCC Standing Committee on Earthquake Design for acceptance for symmetrical CLT structures in the 2015 NBCC.

## 7 Concluding Remarks

Based on the analyses conducted in this study, CLT as a structural system is a viable option for mid-rise buildings in moderate and high seismic regions. When adequately designed, CLT structures with symmetrical plans can sustain only limited damage under MCE earthquakes. By selecting appropriate R-factors, the Equivalent Static Design Procedures can meet the PBSO objectives selected. The results showed that although the type of fasteners used in the brackets connecting the CLT walls has effects on the R-factors, the impact was not significant. The design lateral resistance values for CLT walls were found to have more significant impact on the R-factors. For that reason, both cases, when CLT wall design resistances include and exclude the influence of the hold-downs, were used in this study. At this time when methods for deriving design values for CLT shearwalls are in the development stage and not agreed upon, it is prudent to take a more conservative approach by taking into account the influence of the hold-downs in deriving CLT wall design values. In such case the recommended values for R-factors in Canada would be  $R_d=2.5$  and  $R_o=1.5$ , while  $R=4.5$  would be the adequate value for ASCE 7. Design of such CLT buildings using these R-factors will result in buildings having similar seismic performance to that of the tested wood-frame NEESWood building.

Variation in the R-factor values as a function of the floor plan and the building height is likely to exist. However, having in mind the spectra of the records used and the responses of taller buildings of other structural systems subjected to the same records [13], it is not expected that the proposed values for the R-factors will change significantly for taller buildings, provided that the building floor plans remain symmetrical in both directions. It is recommended that further studies with a wider scope look into issues related to structures with different archetypes and non-symmetrical floor plans according to the FEMA P-695 procedure. Such procedure is planned to be undertaken soon in the US.

## 8 References

- [1] NBCC. 2005. National Building Code of Canada. Institute for Research in Construction, National Research Council of Canada, Ottawa, Ontario.
- [2] ASCE7-05 (ASCE/SEI 41-06). 2007. American Society of Civil Engineers, Minimum Design Loads for Buildings and Other Structures. ASCE, Reston, Virginia.
- [3] EN 1998-1:2004 (E). Eurocode 8: Design of structures for earthquake resistance – Part 1: General rules seismic actions and rules for buildings. European Committee for Standardization. Brussels, Belgium.
- [4] Ceccotti A., Follesa M., Kawai N., Lauriola M.P., Minowa C., Sandhaas C., Yasumura M. 2006. Which Seismic Behaviour Factor for Multi-Storey Buildings made of Cross-Laminated Wooden Panels? Proceedings of the 39th CIB W18 Meeting, paper 39-15-4, Firenze, Italy.
- [5] Ceccotti A. 2008. New Technologies for Construction of Medium-Rise Buildings in Seismic regions: The XLAM Case. Structural Engineering International SEI, 18 (2):156-165.
- [6] Schädle, P., Blaß, H.J. 2010. Earthquake behaviour of modern timber construction systems. Proceedings of the 11<sup>th</sup> World Conference on Timber Engineering, Riva del Garda, Italy.
- [7] Pozza, L., Scotta, R., Vitaliani, R. 2009. A non linear numerical model for the assessment of the seismic behaviour and ductility factor of X-lam timber structures. Proceeding of international Symposium on Timber Structures, Istanbul, Turkey, 25-27 June 2009, 151-162.
- [8] Popovski, M., Karacabeyli, E. 2011. Seismic Performance of Cross-Laminated Wood Panels. Proceedings of the 44th CIB W18 Meeting, Alghero, Italy.
- [9] Popovski, M., Karacabeyli, E., Ceccotti, A. 2011. Seismic Performance of Cross-Laminated Timber Buildings. Chapter 4 of the FPIInnovations' CLT Design Handbook, Canadian Edition.
- [10] Pang, W., Rosowsky, D.V., Pei, S., and van de Lindt, J.W. 2010. Simplified Direct Displacement Design of Six-storey Woodframe Building and Pretest Seismic Performance Assessment. ASCE Journal of Structural Engineering. 136(7): 813-825
- [11] van de Lindt, J.W., Pei, S., Pryor, S.E., Shimizu, H., and Isoda, H. 2010. Experimental seismic response of a full-scale six-story light-frame wood building. ASCE Journal of Structural Engineering, 136(10): 1262-1272.
- [12] Pei, S., van de Lindt, J.W., Pryor, S.E., Shimizu, H., and Isoda, H. 2010. Seismic testing of a full-scale six-story light-frame wood building: NEESWood Capstone test. NEESWood Report NW-04.
- [13] FEMA 2009. FEMA P695 Quantification of Building Seismic Performance Factors. Federal Emergency Management Agency, Washington, D.C.

**INTERNATIONAL COUNCIL FOR RESEARCH AND INNOVATION  
IN BUILDING AND CONSTRUCTION**

**WORKING COMMISSION W18 - TIMBER STRUCTURES**

**SEISMIC BEHAVIOUR OF WOOD-CONCRETE FRAME SHEARWALL  
SYSTEM AND COMPARISON WITH CODE PROVISIONS**

L Pozza

R Scotta

University of Padova

A Polastri

A Ceccotti

CNR – IVALSA San Michele all'Adige

ITALY

**MEETING FORTY FIVE**

**VÄXJÖ**

**SWEDEN**

**AUGUST 2012**

---

Presented by L Pozza

F Lam commented that 50% non exceedance at 4% drift corresponded to a beta of zero. In FEMA 80% non exceedance at 4% drift was recommended. B Dujic commented that the infill was connected to the timber frame and a rigid diaphragm but connected to the frame with ductile screws. He asked if there was any restriction to wood design of hybrid system as in this case there was lower q factor. He asked whether these procedures for these buildings should be used in the scope of EC5. L Pozza stated that these buildings were specific to Italy as a solution to the hot climate and the external concrete skin could also provide stiffness required to resist earthquakes. They agreed that such procedures were suitable for EC5. However the durability of the connection must be considered carefully. W Seim asked for the clarification of the definition of code related design and asked whether the same q factor could be used for taller structures such as a 4 story building. L Pozza responded that q factor might depend on the number stories and if we considered 3 d response. More work will need to be done. Code related design was referenced to  $q=1$ . Two different masses were considered so that one building was on the plateau while the second one exceeded the plateau. S Winter asked why the ventilation area was needed and asked whether the concrete was needed for weather protection. L Pozza explained that the plastic bushing reduced the clearance between the wood and the concrete and the concrete slab was the final facade. S Winter stated that the durability performance against weather was doubtful.



# Seismic behaviour of wood-concrete frame shear-wall system and comparison with code provisions

Luca Pozza, Roberto Scotta  
University of Padova, Italy

Andrea Polastri, Ario Ceccotti  
CNR – IVALSA San Michele all'Adige, Italy

**Abstract:** constructive systems adopting mixed shear walls made of a wood frame and fibrous or cementitious sheets are largely spread nowadays, particularly for prefabricated buildings. The use of gypsum boards as bracing panels is already widespread, but also fiber cement or reinforced concrete slabs can be used. The choice of such different materials allows to reach excellent thermal and acoustic insulation performance. Perhaps the demonstration of their sound structural behavior, especially towards the earthquake resistance is still to be given, and their ductility and dissipative capacities still need to be fully assessed even if some experimental tests have already been conducted. Moreover these particular constructive systems are yet not accounted in the building codes (Eurocode 5, EN 1995 [1] and Eurocode 8, EN 1998 [2]) and no guidelines are given for their seismic design in order to assure an adequate overstrength of the bracing panels and the adequacy of the fixing system of the panels to the wooden frames.

## 1 Introduction

The investigated mixed constructive system combines a typical platform frame building system with an thin external reinforced concrete board acting as a diaphragm against the horizontal forces and having also thermal and acoustic functions. A building made by the use of this mixed wood-reinforced concrete walls is a precast modular system where the wall panels are preassembled in the factory; on the construction site the single precast modular panel is then assembled connecting the adjacent panel with screws and to the foundation with mechanical fasteners (nailed holdown and bolts). The structural layout is similar to that of platform framing system. The walls are made of modular panels having a typical aspect ratio of 3:1 (3.24m high and 1.08m long). A sketch of a single panel is presented in Figure 1. The particular arrangement of the OSB panels and concrete slabs provides a continuous ventilation cavity from foundation to the roof. The presence of this continuous air layer between the two diaphragms guarantees an optimal thermo-hygrometric performance and keeps dry the wood-concrete interface avoiding the deterioration of wood. Two resistant systems with different structural functions can be identified within a modular panel: elements that carry the vertical actions and elements which react to the horizontal actions (wind and earthquake).

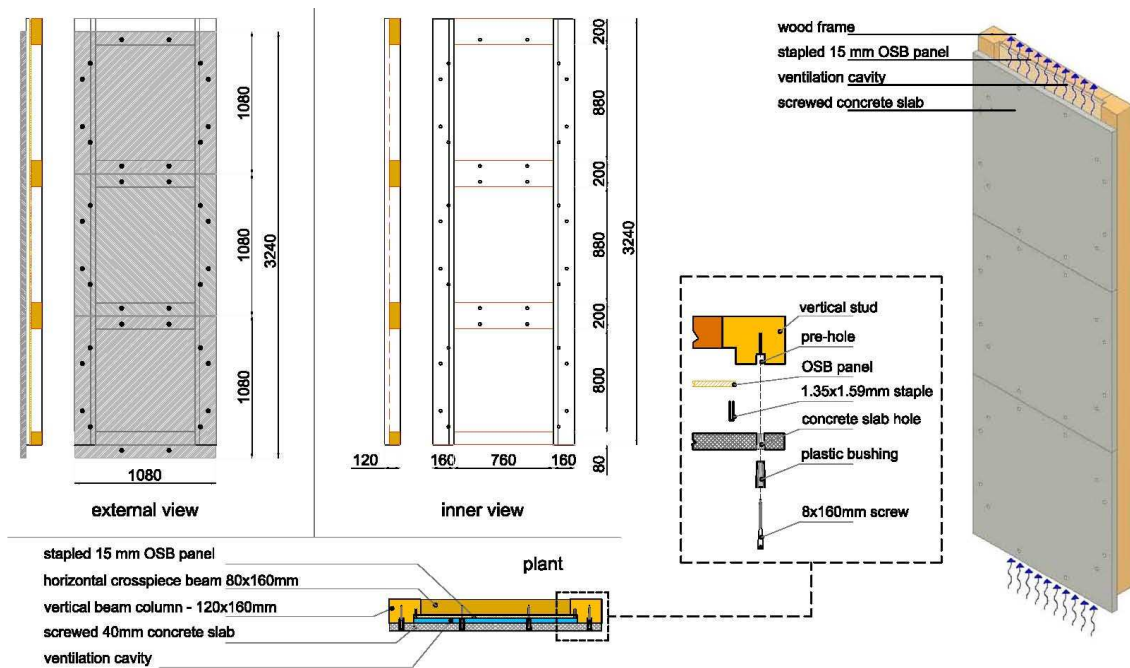


Fig. 1 View of the precast modular panel

The system loaded by the vertical loads is a wood frame structure which transfers to the foundation the vertical load (structural weight). Two adjacent modular wall panels are jointed together by the use of a vertical joint cover screwed to the vertical studs. This joint cover achieves the vertical support for the floor and roof beams.

Bracing system reacting to horizontal actions consists of two different diaphragms connected to wood frame. The first is made of three OSB panels (1080 mm x 1080 mm x 15 mm) connected with staples to the wood frame. The second consists of three square reinforced concrete board (1080 mm x 1080 mm x 40 mm). The reinforcement of the slabs is made of wire mesh knitted 60mm x 60 mm. The concrete slab is fixed to the wood frame using 8 mm diameter screws coupled with a plastic bushing. The plastic bushing serves several important functions: reduces the clearance between the concrete slab and the screw without using sealant products; acts as spacer between the horizontal transverse beams of the wood frame and the concrete board ensuring the ventilation cavity; increases bearing resistance of the screws.

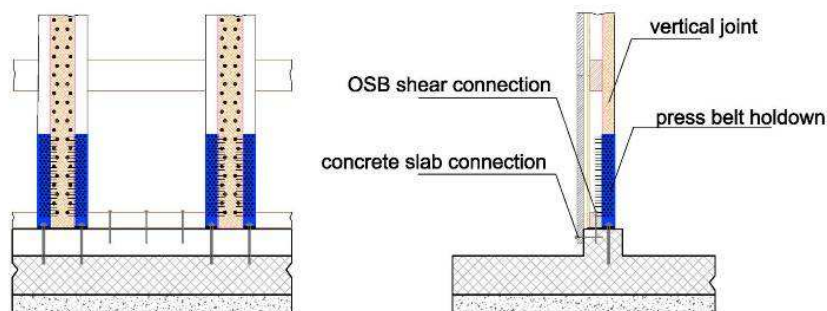


Fig. 2 View of the foundation anchor system

The modular wall panel is anchored to the foundations using special holdowns and bolts in order to avoid the raking and the slip effect respectively. The holdown is made by press bent L-profile 3 mm thick nailed at the corner formed by the vertical columns and the joint cover element. This holdown is connected to the concrete foundation with mechanical or chemical fixings as standard. The wall panel slip is prevented by fixing the bottom plate

and the concrete slab to the foundation by bolts. The shear action of OSB bracing is transferred to the foundation by anchors between the bottom horizontal beam to the concrete slab, Figure 2.

## **2 Quasi static cyclic and monotonic test**

In order to verify the effective resistant characteristics and the hysteretic behaviour of the investigated constructive system a series of experimental tests were performed. This paragraph describes the structural layout and the main characteristics of the tested walls with details about the connectors and bracing system. Test layout, instrumentation, load condition and protocol use during the cyclic test are also given. The outcomes from quasi static reversed cyclic tests are reported. Finally a comparison between this experimental results and the code provisions are given and critically discussed.

### **2.1 Test wall configuration**

Three different configuration of walls were tested: “Wall A” with a ratio of 3:1 (3.24m high and 1.08m long, one modular panel); “Wall B” aspect ratio of 3:2 (3.24m high and 2.16m long made with two adjacent modular panel) and “Wall C”, with a ratio of 1:1 which presents an window opening in the central panel, (3.24m high and 3.24 m long made of three adjacent modular panel). In sake of brevity only the outcomes from the test of "Wall B" and "Wall C" are hereafter given.

### **2.2 Test setup and instrumentation**

“Wall B” and “Wall C” were tested using different setups due to their different geometrical characteristics and load conditions. In order to faithfully reproduce the actual base connection system a base concrete foundation was provided.

The test setup used for “Wall B” is presented in Figure 3. Vertical load equal to 20 kN/m was applied using three hydraulic actuators placed on the vertical wood columns. To allow the wall uplift without variance in the vertical load the hydraulic actuators were placed in series with a spring. The “Wall C” test was carried out loading two walls arranged specular respect to load axis with the aim of balancing the torsional effects and to keep the unidirectional movement of the wall. The setup used for “Wall C” is presented in Figure 3. Lateral guides with rollers in contact to the top horizontal plate were also used to ensure unidirectional movement of the walls. Uniform vertical load equal to 20 kN/m was applied at the top of the wall through actuators and a distribution steel beam. The displacements of the wall panel were measured with transducers placed as shown in Figure 3.

### **2.3 Test procedure**

The cyclic tests were performed according to EN 12512 [3] in displacement control at rate of 0.04 mm/s. The yielding displacement,  $v_y$ , was estimated referring to preliminary test made on single modular panel "Wall A". The collapse of the wall has not been reached during the cyclic tests stopped at 80 mm displacement cycles. To verify the actual lateral load capacity and ductility of the investigated constructive system, a ramp monotonic test on the “Wall C” was performed according to EN 26891 [4] in displacement control at a rate of 0.04mm/s.

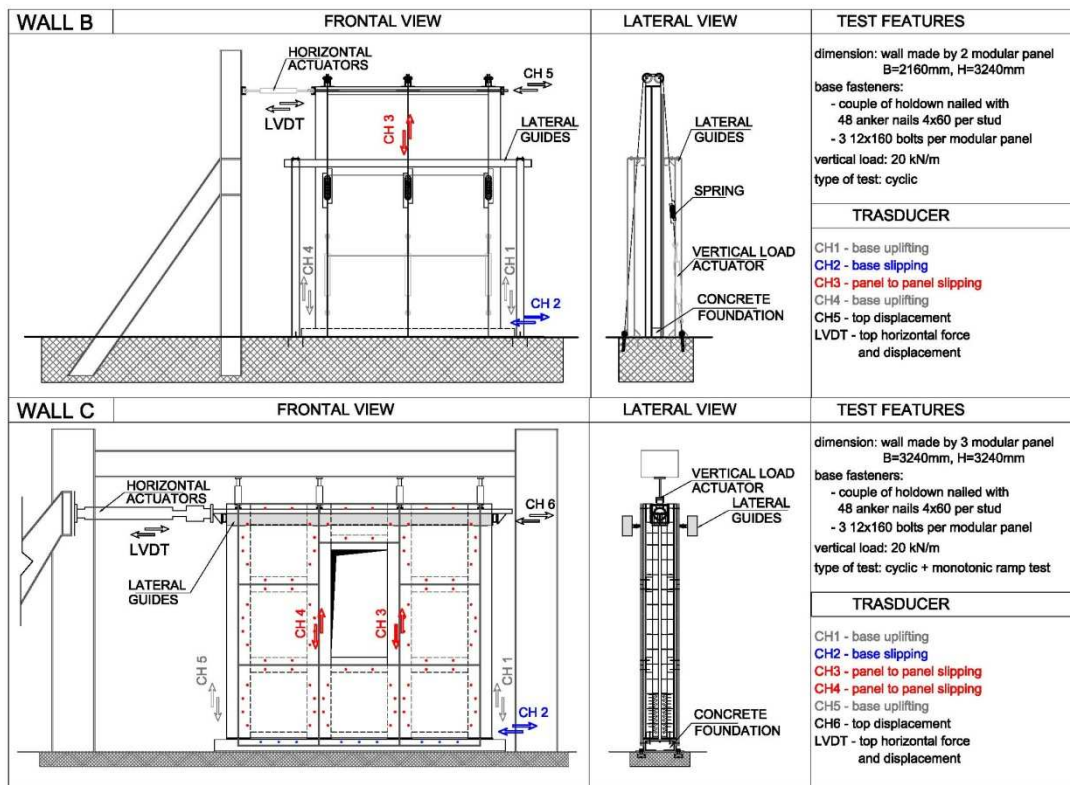


Fig. 3 Sketch of the setup, “Wall B” and “Wall C”

## 2.4 Test outcomes

The performed cyclic tests allowed to define the hysteretic cycles of the walls obtained plotting the measured top displacement and the force imposed by the actuator, Figure 3. As shown in Figure 4, the load-slip curve related to “Wall B” is asymmetric because during the test the lateral guides have shown problems in the maintenance of the unidirectional movement of the wall. Due to this problem it has not been possible to carry out the last push cycles but only those in pull. At the largest cycle amplitude admitted by the actuator system (100mm) the wall has not jet reached the failure.

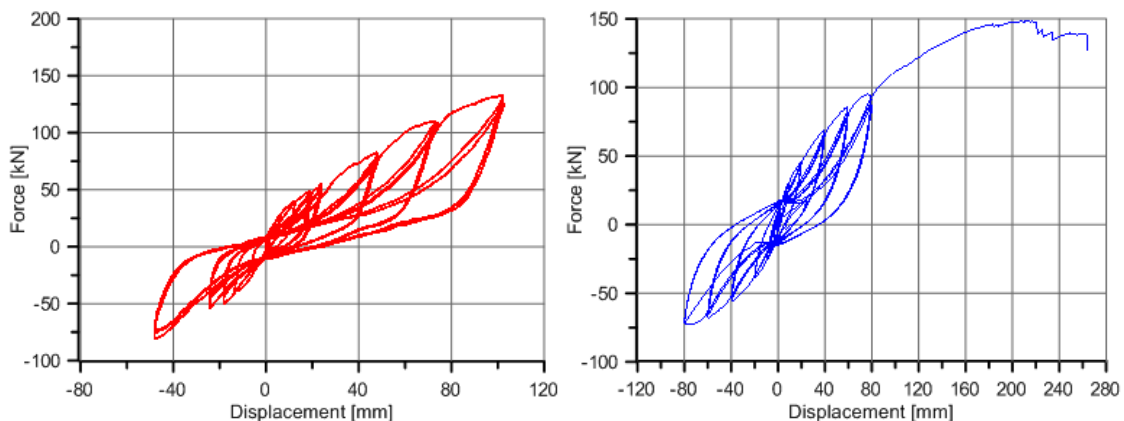


Fig. 4. Load displacement curve, cyclic test for “Wall B” (left) and “Wall C” (right)

During the cyclic test, the “Wall C” has not shown failure or relevant strength degrading phenomena. The collapse condition was achieved only with a monotonic ramp test performed at the end of the cyclic test as shown Figure 4. “Wall B” and “Wall C” present the typical hysteretic behaviour of the steel-wood and wood-wood connections characterized by the pinching phenomenon. Moreover the tested walls show a marked

hardening phase due to the use of large diameter connectors to fix the concrete bracing system to the wood frame.



Fig. 5. Wall configuration at the end of the test

#### 2.4.1 Determination of stiffness, yielding point and ductility

The yielding condition can be define according to EN 12512 [3], but in the studied case, because of the strong hardening behavior of the load-slip curve, this approach is not correct. Consequently, also the calculated ductility values results are unrepresentative of the actual displacement capacity of wall.

In this work, an alternative approach was used in order to obtain a more accurate prediction of yield conditions. The exponential approximation of the monotonic curve proposed by Folz and Filiatrault [5] was used according to (1).

$$F=(r_1 k_0 x+F_0)(1-e^{-\frac{k_0 x}{F_0}}) \quad (1)$$

where:

F = actual value of the force

x = actual value of the displacement

$k_0$  = elastic stiffness

$r_1 k_0 = \beta$  = hardening stiffness

$F_0$  = residual force

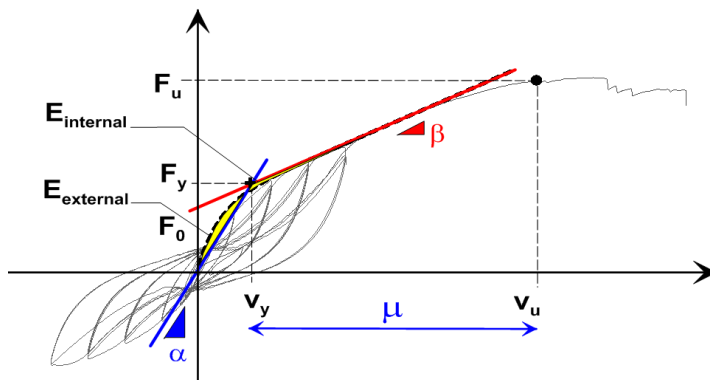


Fig. 6. Identification of yielding point and stiffness on the experimental curve

The stiffness  $\beta$  of the hardening branch and the residual force  $F_0$  are obtained fitting to the experimental curve while the elastic stiffness  $\alpha$  is obtained imposing the equality of the strain energy as depicted in Figure 6. Using an analytical expression for the monotonic

load-displacement curve approximation it is possible to evaluate the compensation area, representing the strain energy, through equation (2), (3) and (4).

$$E_{\text{internal}} = \int_0^{\chi} [(r_1 k_0 x + F_0)(1 - e^{-\frac{k_0 x}{F_0}}) - \alpha x] dx \quad (2)$$

$$E_{\text{external}} = \int_{\chi}^{\infty} [(r_1 k_0 x + F_0) e^{-\frac{k_0 x}{F_0}}] dx \quad (3)$$

The elastic stiffness  $\alpha$  is obtained imposing the equality according to Eq. 4.

$$\alpha = \frac{k_0^2}{2(k_0 + r_1 k_0)} + r_1 k_0 \quad (4)$$

Once the value of the elastic stiffness  $\alpha$  is defined the yielding condition ( $V_y$ ,  $F_y$ ) is given by the intersection between the elastic and the hardening slope. According to this approach the main outcomes in terms of strength, stiffness and ductility for the tested walls are summarised in Table 1. A comparison with the value obtained from the EN12512 [3] procedure is also given.

Table 1. Test results and interpretation according to exponential and EN 12512 approach

	WALL B		WALL C	
	Test Results		Test Results	
$K_0$ [kN/mm]	7.9		8.2	
$V_u$ [mm]	102		180	
$F_u$ [kN]	132		145	
	Exp. Approach	EN 12512	Exp. Approach	EN 12512
$\alpha$ [kN/mm]	3.3	5.5	2.6	4.5
$\beta$ [kN/mm]	1	1	0.6	0.6
$V_v$ [mm]	15.3	7.8	23.3	11.5
$F_v$ [kN]	50.9	42.8	59.8	51.7
$\mu$	6.7	13.1	7.7	15.7

The results reported in Table 1 confirm that the exponential approach gives reasonable values for the elastic stiffness and of the ductility, as opposed to the ductility values obtained with the UNI 12512 [3] approach, that are too high and inadequate to represent the actual displacement capacity of this building system.

#### 2.4.2 Wall equivalent viscous damping and impairment strength

The equivalent viscous damping,  $v_{eq}$ , is an adimensional parameter useful to summarize the hysteretic properties of a structural element. It is define according to EN 12512 [3], referring to the 3<sup>rd</sup> cycle of each ductility level, as reported in the following Table 2.

The equivalent viscous damping values decrease with the increasing of cycle amplitude. This aspect means a reduction in the dissipative capability with the increasing of the displacement due to the pinching phenomenon. However, it should be stressed that the equivalent viscous damping is always greater than 7%, confirming the good dissipative capability of this building system.

The strength degrading is a relevant parameter to identify the seismic behaviour of a building system. EC8 [2] uses this parameter to classify the dissipative capability of timber structures and imposes an impairment strength lower than 20% in order to consider a structure as ductile.

Table 2. Equivalent viscous damping values obtained from the cyclic test

Wall B				Wall C			
Cycle amplitude	Ep [kJ]	Ed [kJ]	$v_{eq}$	Cycle amplitude	Ep [kJ]	Ed [kJ]	$v_{eq}$
18mm	436.5	387	14.12%	10mm	304.6	282	14.74%
24mm	657.48	574	13.90%	20mm	911	721	12.60%
48mm	1971.6	1561	12.61%	40mm	2725.2	1928	11.27%
72mm	3965.4	2250	9.04%	60mm	5128.8	2695	8.37%
102mm	6763.62	3263	7.68%	80mm	7569.6	4030	8.48%

Table 3. Empairment strength at each cycle amplitude

Wall B		Wall C	
Cycle amplitude	Empairment strength	Cycle amplitude	Empairment strength
18mm	0.041	10mm	0.025
24mm	0.047	20mm	0.059
48mm	0.067	40mm	0.078
72mm	0.069	60mm	0.085
102mm	7.10%	80mm	9.50%

As show in Table 3 the empairment strength values are always lower than 10% confirming the good behavior of this construction system under cyclic actions and, therefore, its adequacy for use in seismic zones.

## 2.5 Comparison with design provisions according to EC5 [1]

In this section a comparison between the outcome of the experimental tests and the design provisions is given with regard to the strength and stiffness value.

The analytical lateral resistance and stiffness of each tested walls are obtained by adding the strength and stiffness values related to the single modular wall panel. The following Figure 7 reports in detail the analytical stiffness and strength of each wall. The modular panel with a window, used in the Wall C, was considered with reduced mechanical characteristics because it had only one entire square panel. Figure 7 reports the experimental load displacement curve, the exponential approximation and the proposed bi-linearization for each tested wall. The analytical estimation of the initial stiffness and of the maximum strength are also reported.

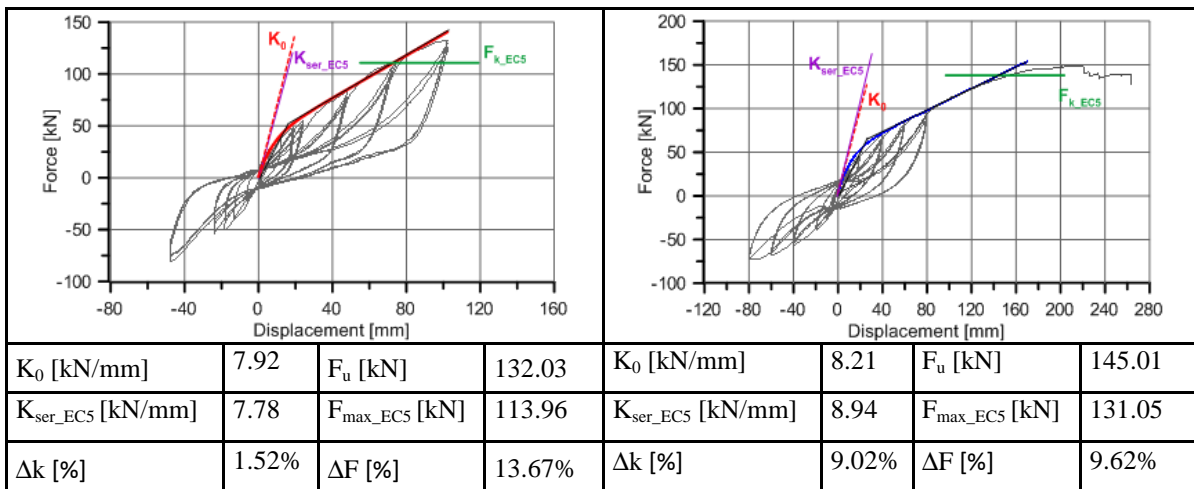


Fig. 7. Comparison between the experimental results and the code provisions

As depicted in Figure 7 the actual value of the lateral resistance is always greater than that obtained with the code provision. The difference is never greater than 15% and it is in line with the ratio between the 5% percentile and the average value of a typical normal probabilistic distribution for a wood structure. Regarding to the initial stiffness the analytical values fit very well with the experimental ones: the differences are always lower than 10%.

### 3 Numerical model of the tested modular panel

The hybrid wood-concrete buildings is characterized by four different bearing systems: bracing systems, hold-downs, base bolts and in plane vertical joints between adjacent precast modules. Regarding to hysteretic behavior, the fasteners used in this building system show a pinched load displacement response and exhibits degradation under cyclic loading. In this work the research-oriented numerical code “Open System for Earthquake Engineering Simulation” was used in order to faithfully reproduce the actual hysteretic behavior of the connectors. The nonlinear element “Pinching4” was used to reproduce the ‘pinched’ load-deformation response and degradation under cyclic loading. The analytical formulations and the damage models of this nonlinear element are described in [6].

#### 3.1 Modeling of the single connection element

The calibration of the nonlinear element able to reproduce the fasteners behaviour has been made with reference to the load-displacement curves of single connectors obtained from the experimental tests. Figure 8 shows as example the comparison between the experimental cyclic tests on base bolts, hold-down, bracing system and vertical panel to panel connection elements related to “Wall B” and the respective numerical simulations.

The proposed nonlinear numerical model shows the typical pinched behavior in the load-displacement curves, the reduction in stiffness for the reloading cycles and the strength reduction as stated in the initial hypotheses. The numerical results fit well the experimental ones also in terms of energy dissipation, with maximum differences of 12% for the hold down, 8% for the base bolt, 7% for the bracing system and 6% for the panel to panel joint.

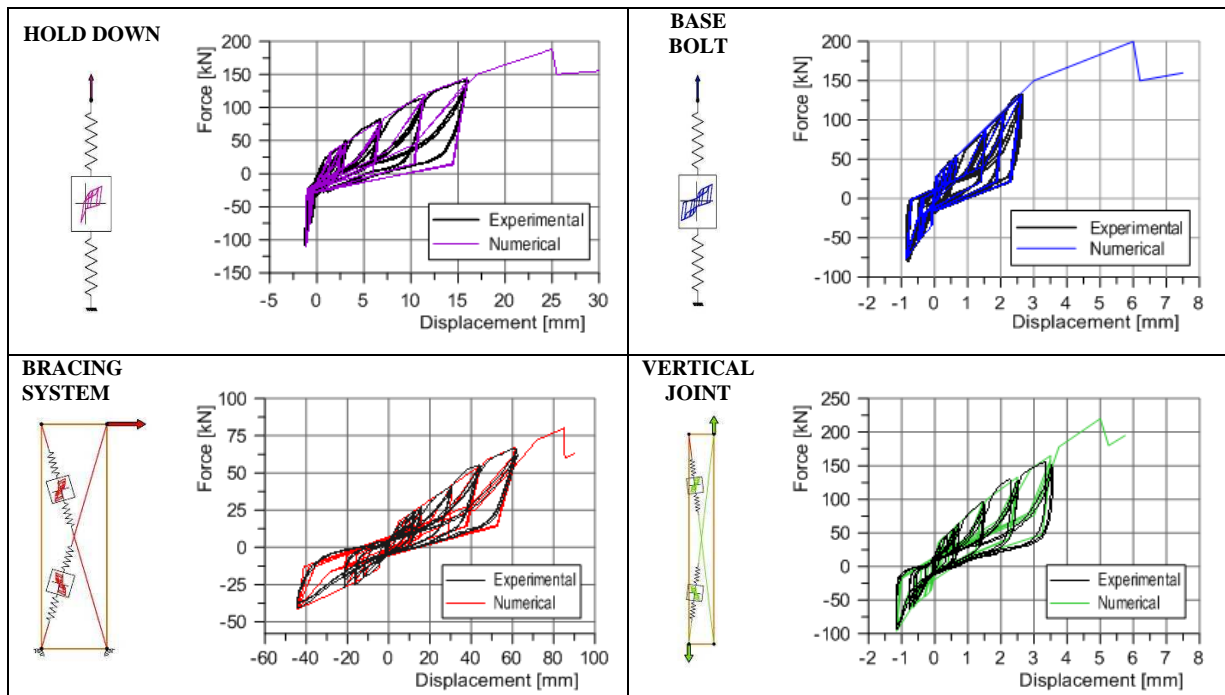


Fig. 8. Comparison between experimental results and numerical load-displacement curve

### 3.2 Numerical model of the wall,

In order to assess the wall panel-basic joints interaction and the effect of the vertical load, the complete cyclic test on “Wall B” and “Wall C” has been simulated. The numerical model is based on the hypothesis that the nonlinear behavior of the wall is concentrated in the connectors, whereas the wood frame remains in its elastic field. Therefore Finite Element Models consist of a perimeter frame made by stiff elastic truss element braced and connected to the base by the nonlinear spring defined above. The cyclic test has been simulated by imposing a horizontal displacement to the node located on the upper part of the wall. The vertical load was reproduced applying a nodal force on the top of the wall. A sketch of the numerical model used in the analysis is presented in Figure 9.

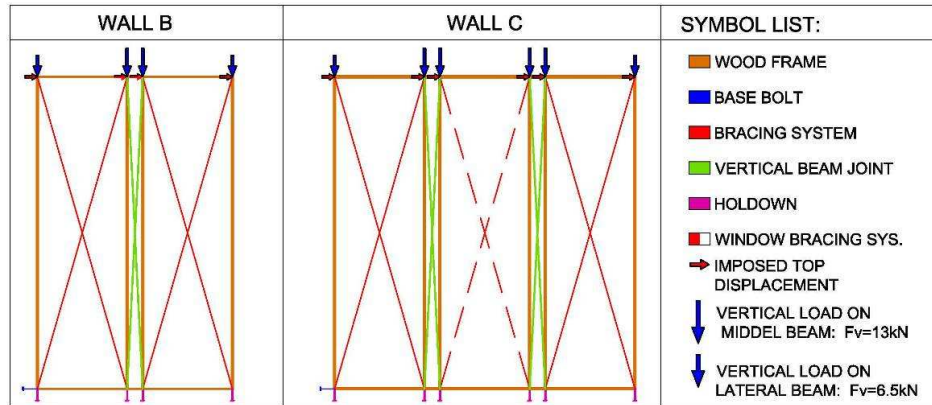


Fig. 9 FEM model “Wall B” (left) and “Wall C” (right)

The load-displacement curve, reported in Figure 10 shows the good correspondence between the results of the experimental test and the numerical simulation at each cycle.

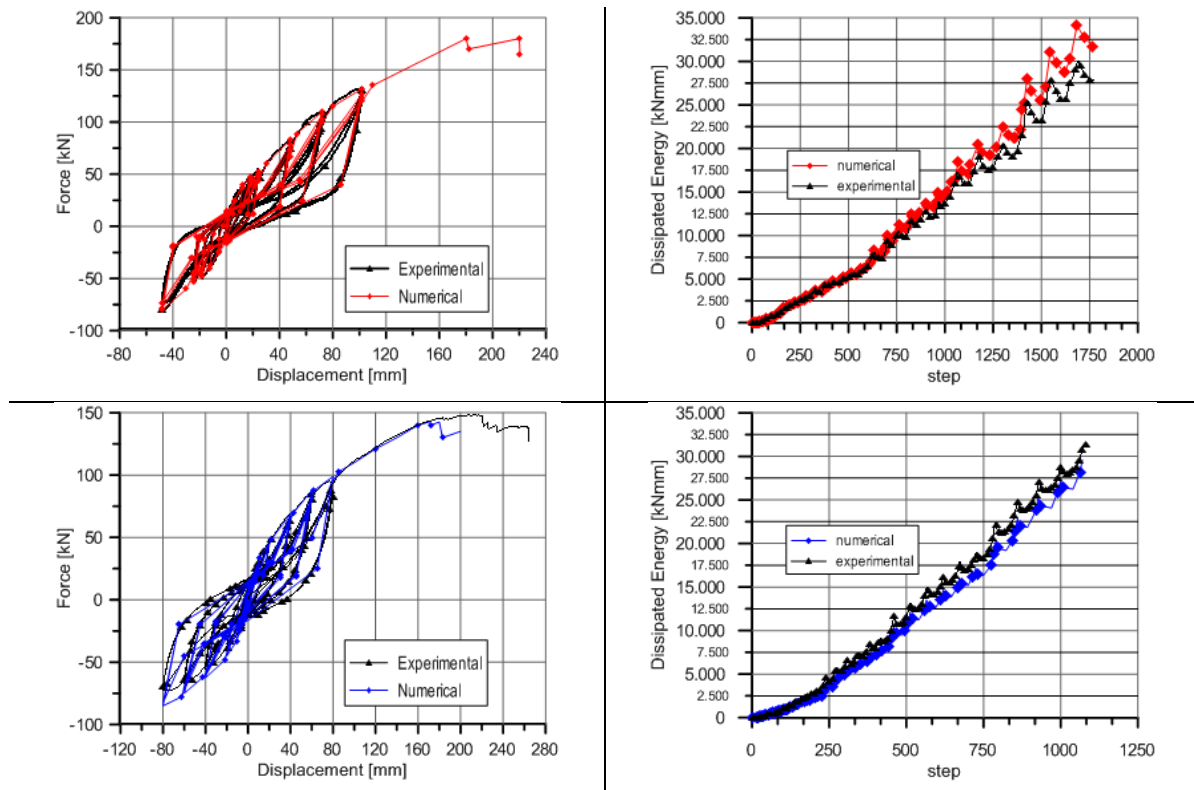


Fig. 10. Comparison between the experimental results and the FEM simulation in terms of load slip curve and dissipated energy “Wall B” (top) and “Wall C” (bottom)

The good quality of the model is further confirmed by the assessment of the dissipated energy: Figure 10 shows the difference in terms of dissipated energy per cycle between the experimental test and the numerical simulation. The correspondence is very good for each cycle amplitude, the maximum difference is 11.5% for “Wall B” and 8.5% for “Wall C”.

## 4 Assessment of the q-ductility factor

The seismic design of building using FMD method [7] requires the evaluation of the reduction factor  $q$  that resumes the post-elastic behavior and the ductility of the building. It should be noted that the definition of the  $q$ -factor is not unique since it depends on the criteria used to identify the yielding condition. This condition gives the inelastic seismic design load and, according to the code provisions, EC8 [2], it can be obtained with a properly linearization of the building response, represented through its pushover curve.

### 4.1 Case study building

In order to define the actual seismic performance of the hybrid constructive system and to make a direct comparison with crosslam one, the same three storey building tested on shaking table during SOFIE project was considered [8]. The B configuration with symmetric opening at the ground floor was investigated. The geometrical layout of this three storey building was compatible with the precast modular wood concrete panel dimension as depicted in Figure 11.



Fig. 11 Case study: modular wall panel arrangement

In this work the analyses focused on the walls placed along the X direction, which present two metre wide opening at the ground floor. Figure 11 reports the studied walls geometry, the fasteners and bracing system arrangement. Two different mass configurations were investigated in order to verify the influence of the main period of vibration on the seismic response of the building. The difference between the two case study in terms of total mass is about 25%. Table 4 reports the storey mass distribution and the eigenfrequency  $T_1$  of each studied building.

Table. 4. Different mass distribution considered

Building	1 <sup>st</sup> storey	2 <sup>nd</sup> storey	3 <sup>rd</sup> storey	Total	$T_1$
N.1	16.5t	16.5t	12.7t	45.7t	0.48 sec
N.2	10.7t	10.7t	8.4t	29.8t	0.32 sec

## 4.2 Procedure for q-factor evaluation

The procedure adopted in this work for the q-factor estimation is according to Ceccotti [8] and Pozza et a. [9].

$$q = \text{PGA}_{u\_eff.} / \text{PGA}_{design} = \text{PGA}_{u\_eff.} / \text{PGA}_{yielding} \quad (5)$$

## 4.3 Seismic design of the case study building

In this work it was assumed that the case study building was made by assembling the same modular wall panels subjected to the cyclic tests described in the previous section. The seismic design of the case studied building is based on the lateral shear resistance of the single precast modular panel and consists of the following two steps: evaluation of the base shear resistance  $F_h$  according to the outcome of the experimental test and evaluation of the maximum  $\text{PGA}_{design}$  compatible with the base shear resistance adopting a Linear Static Analysis performed considering the following common data according to Eurocode 8 [2] type 1 elastic response spectra and rock foundation (type A soil according to EN 1998-1, corresponding to  $S=1.0$ ,  $T_B=0.15\text{sec}$ ,  $T_C=0.4\text{sec}$ ,  $T_D=2.0\text{sec}$ ), behavior factor  $q=1$ , lowest bound factor for the design spectrum  $\beta=0.20$  and building importance factor  $\gamma_I=1$ .

Table 5 summarizes the outcomes of the seismic design in terms of maximum  $\text{PGA}_{design}$  values compatible with the base shear resistance of the modular precast panel.

Table 5. Seismic design parameters

Bulding test	Total mass	Fh max	Sd(T1)	$\text{PGA}_{yielding}$
N.1	45.7t	$51.8 \times 4 \times 1.1 / 1.30 = 175.3\text{kN}$	0.39g	0.18g
N.2	29.81	$51.8 \times 4 \times 1.1 / 1.30 = 175.3\text{kN}$	0.60g	0.24g

## 4.4 Seismic design of the case study building

The walls placed along the X direction with two metre wide opening at the ground floor was modelled based on the assumption that the nonlinear behavior of the wall is concentrated in the connectors whereas the wood frame remains in its elastic field. Figure 12 reports a sketch of the numerical model used for the analysis with the indication of the type and position of nonlinear springs and of the storey masses.

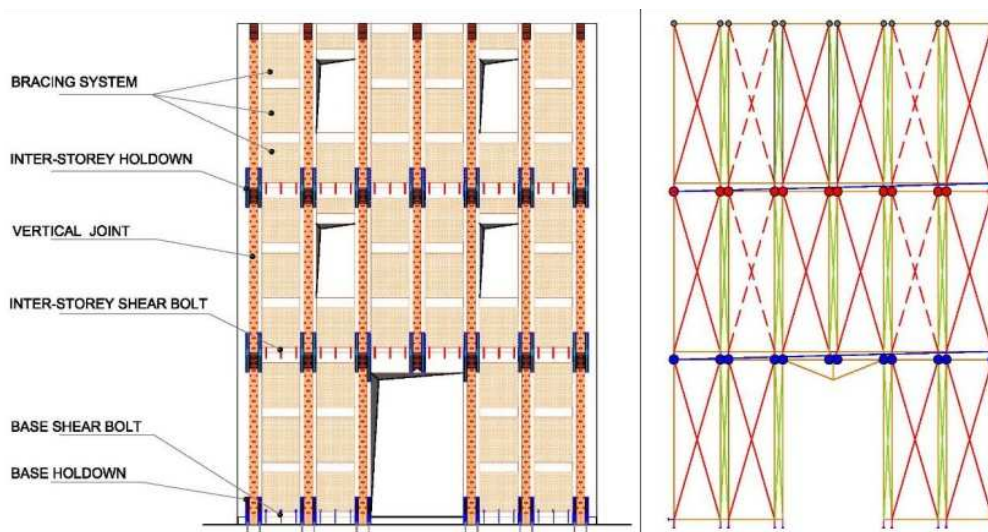


Fig. 12 Investigated wall panels: fasteners and bracing system arrangement (left) and FEM model, type and position of the nonlinear elements (right)

## 4.5 Evaluation of the q-factor

Using the numerical model above defined, several nonlinear dynamic analysis were performed to evaluate the most suitable q-ductility factor for this wood-concrete system. In order to define the influence of the frequency content of the earthquakes on the building response, a nonlinear dynamic analysis was performed considering 7 different artificially generated seismic shake, so as to meet the spectrum compatibility requirement. The dynamic equilibrium equations have been integrated with a time step of 0.001 second, by adopting an equivalent viscous damping of 2%, according to the Rayleigh model.

Both buildings that were tested have been subjected to a growing level of seismic intensity, from the peak acceleration value equal to  $PGA_{design}$  (i.e.  $PGA_{yielding}$ ) to the collapse condition ( $PGA_{u\_eff}$ ) stated as the first achievement of the ultimate displacement of the bracing system or of a base connectors. The near collapse condition was defined with the same criteria reported in [9], e.g. was assumed as an uplift of 25mm for the holddown connections and a shear displacement of the bracing system that leads to a inter storey drift equal to 100mm. Figure 13 reports the  $PGA_{u\_eff}$  that leads the building to the near collapse condition and the related q factor values for each earthquake considered and for both the case studies respectively.

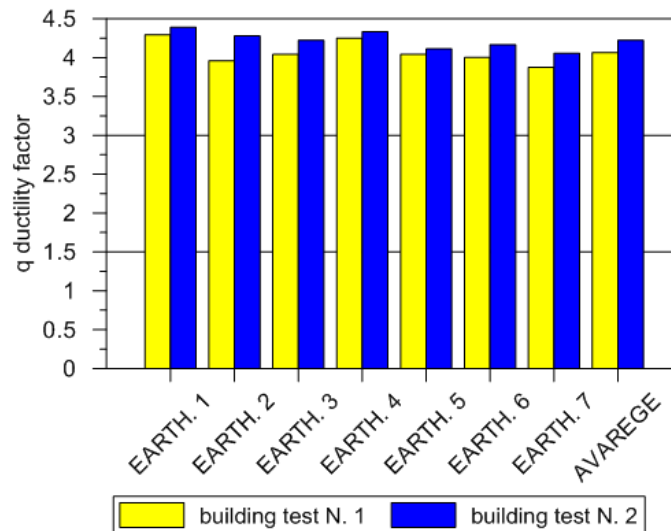


Figure 13. Values of the q-factor for the considered earthquakes

Independently from the approach used the q-ductility factors settle on a value equal to 4 confirming the good dissipative capability of this construction system.

## 5 Conclusions

In wall structures studied the ductility values are greater than 6, therefore, based on the EC8 [2] provisions this constructive system can be considered as a structure with a high level of ductility. However the design values obtained referring to the code provisions are in concordance with the outcomes from the experimental test. This confirms the adequacy of the code provisions to define the strength and stiffness of the mechanical fasteners used in this mixed wood-concrete constructive system. This constructive system doesn't belong to the standard building typologies reported on table 8.1 of EC8 [2] although it is similar to the Platform Framing technique. However the obtained q-factor value is in line with the code provision that affirm that this constructive system can be classified as high dissipative capability structure.

## 6 Acknowledgements

The research has been supported by the Polifar s.r.l. Company; the authors would like to thank the technical staff of CNR – IVALSÀ, San Michele all'Adige.

## 7 References

- [1] European Committee for Standardization (CEN). 2004. “Design of timber structures - Part 1-1 General: Common rules for buildings”, Eurocode 5, Standard EN 1995-1-1, Brussels, Belgium.
- [2] European Committee for Standardization (CEN), 2004. “Design of structures for earthquake resistance - Part 1 General rules seismic actions and rules for buildings”, Eurocode 8, Standard EN 1998-1, Brussels, Belgium.
- [3] European Committee for Standardization (CEN). EN 12512 – Timber structures – Test methods – Cyclic testing of joints made with mechanical fasteners. Brussels, Belgium, 2001.
- [4] European Committee for Standardization (CEN). EN 26891, Timber structures – Joints made with mechanical fasteners – General principles for the determination for strength and deformation characteristics. Brussels, Belgium, 1991
- [5] Folz, B., Filiatrault, A. 2004. Seismic analysis of woodframe structures. I: model formulation. *Journal of Structural engineering*, Vol 130 pp 1353-1360
- [6] Fenves G.L., 2005, Annual Workshop on Open System for Earthquake Engineering Simulation, Pacific Earthquake Engineering Research Center, UC Berkeley, <http://opensees.berkeley.edu/>.
- [7] Chopra, AK. Dynamics of structures—theory and applications to earthquake engineering. Upper Saddle River: NJ: Prentice Hall; 1995.
- [8] Ceccotti, A. New technologies for construction of medium-rise buildings in seismic regions: the XLAM case. *IABSE Struct Eng Internat* 2008;18:156–65. Tall Timber Buildings (special ed.).
- [9] Pozza, L., Scotta, R., Vitaliani, R. 2009. A non linear numerical model for the assessment of the seismic behaviour and ductility factor of X-lam timber structures. *Proceeding of international Symposium on Timber Structures*, Istanbul, Turkey, 25-27 June 2009, 151-162.



**INTERNATIONAL COUNCIL FOR RESEARCH AND INNOVATION  
IN BUILDING AND CONSTRUCTION**

**WORKING COMMISSION W18 - TIMBER STRUCTURES**

**DETERMINATION OF FAILURE MECHANISM OF CLT  
SHEAR WALLS SUBJECTED TO SEISMIC ACTION**

M Yasumura  
Shizuoka University

JAPAN

**MEETING FORTY FIVE**

**VÄXJÖ**

**SWEDEN**

**AUGUST 2012**

---

Presented by M Yasumura

B Dujic commented that the stiffness of connection rather than the load capacity of the connection might be important as the study dealt with connection. B Dujic also asked why determined the joint first then worked on the shear wall. M Yasumura stated that the work dealt with capacity first then would focus on other aspects. R Žarnić commented that energy dissipation devices could be used in this system. M Yasumura responded that this was an interesting topic but the energy dissipation should take place at a location away from failure. B Dujic commented that such a system must consider but energy dissipation and strength; couldn't ignore either.



# Determination of failure mechanism of CLT shear walls subjected to seismic action

Motoi Yasumura  
Shizuoka University, Japan

## 1 Introduction

CLT panel structures have been developed rapidly in Europe during these ten years. It has been applied to medium rise condominiums and apartment houses as well as offices, school buildings, etc. This structure may produce high performance against seismic action<sup>1)</sup> as well as permanent action because of their high shear stiffness and capacity. In seismic design, the joints connecting CLT panels to the surrounding boundaries such as vertical restrains and vertical loads dominate the mechanical properties of the structure. Therefore it is very important to determine the failure mechanism of shear walls for the seismic design of CLT structures. In this study, the failure mechanism of CLT shear walls due to the failure of vertical restrains fastening wall panel to the foundation and that of shear plates connecting two wall panels vertically was determined considering the strength distribution of fasteners. The reversed cyclic lateral loading tests of CLT shear walls connected with shear plates and steel connectors with screws showed that the design applying the reliability index ( $\beta$ ) of two predicted comparatively well the failure mechanism of CLT shear walls.

## 2 Specimen

### 2.1 Outline of shear wall specimens

Shear wall specimens of two meters width and three meters height consisted of two 90 mm thick *sugi* (*cryptomeria japonica*) CLT panels of one meter width and three meters height connected each other with steel shear plates and the screws of 5.6 mm diameters and 65 mm length (TBA-65). CLT wall panels were connected to 90 by 90 mm sill and 90mm by 120mm loading beam with screws of 8mm diameter and 180mm length (HBS-8-180) and the both edges of wall panel were connected to the steel base with steel connectors and eight or twelve screws. Considering the stiffness of the floor panels located parallel and perpendicular direction to the wall panels, rigid continuous beam (R) and flexible beam (F) which consisted of two pieces of beam separated above the vertical joints of CLT panels and connected each other with two 30 by 70mm steel rods with pin joints were prepared.

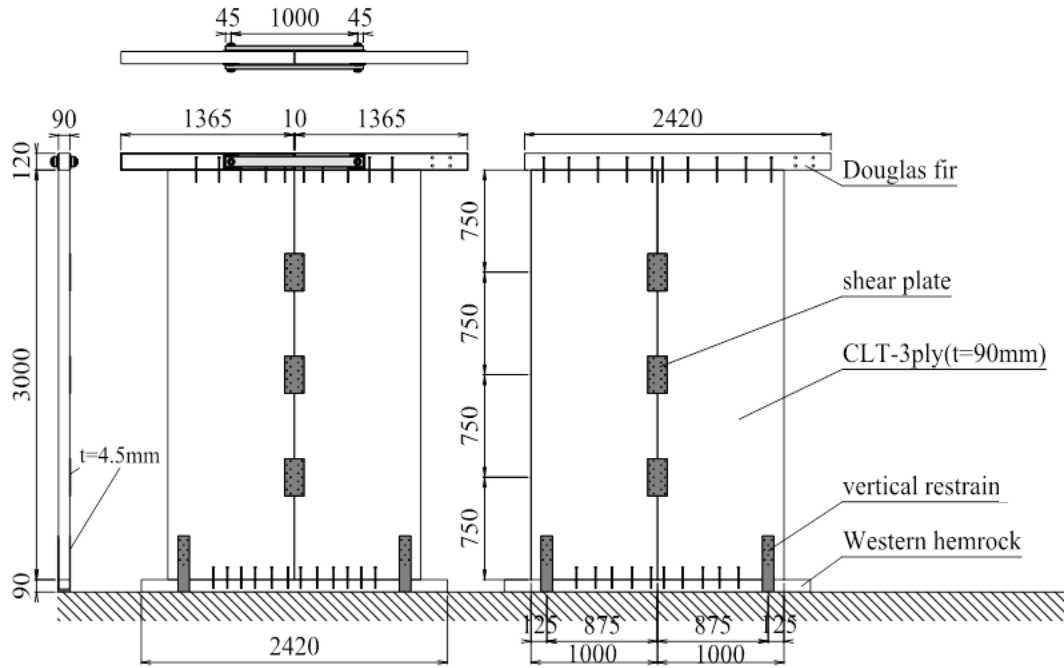


Fig.1 CLT shear wall specimens with the flexible loading beam (F) on the left and rigid loading beam (R) on the right hand

## 2.2 Determination of boundary conditions

In the case of the floor panel fixed parallel to the loading direction of the concerned wall, a rigid continuous beam was supposed at the top of the wall. Considering the vertical loads  $F_v$  (kN) per CLT panel, two failure modes was assumed; 1) the failure of vertical restrains connecting the end of wall panel to the steel base precedes the failure of shear joints of adjacent CLT panels, and 2) the failure of shear joints of adjacent CLT panels precedes the failure of vertical restrains connecting the end of wall panel to the steel base. In the case of the floor panels placed perpendicular to the loading direction to the concerned wall, it was assumed that two vertical loads were applied directly to each CLT wall panels.

### 2.1.1 Lateral resistance of shear walls with rigid or flexible beam of which failure of vertical restraint of end of wall precedes the failure of shear joints between CLT panels

In the case that the failure of the vertical restrains of end of wall panel precedes the failure of the shear joints between CLT panels, the lateral capacity of shear wall is expressed by the equation (1).

$$F_H = \frac{2 \cdot b_0}{h} \cdot F_V + \frac{b_1 + b_2}{h} \cdot T_{crt} \quad \dots (1)$$

Where,  $F_H$  : lateral resistance,  $F_v$  : vertical load per CLT panel (kN/m),  $T_{crt}$  : critical tensile strength of vertical restraint,  $h$ : height of wall panel,  $b_0$  : width of CLT panel,  $b_1$  : distance between the end of CLT panel and the centre of vertical restraint,  $b_2$  : distance between the end of CLT panel and the centre of embedding at the panel edge.

The condition in which the failure of the vertical restraint connecting the end of wall panel to the

steel base precedes the failure of shear joints between CLT panels is;

$$\bar{Z} = \bar{S} - \bar{T} - F_V \geq 0 \quad \dots (2)$$

Where,  $\bar{Z}$ : performance function,  $\bar{S}$ : capacity of shear joints between CLT panels.  $\bar{T}$ : capacity of vertical restrain,  $F_V$ : vertical load per panel.

### 2.2.2 Lateral resistance of shear walls with rigid beam of which failure of the shear joints between CLT panels precedes failure of vertical restrain at the end of wall panel

In the case that the beam connected at the top of wall is supposed to be rigid and the failure of the shear joint between adjacent CLT panels precedes the failure of the vertical restrains at the end of wall panel, the lateral resistance of shear wall is expressed by the equation (3).

$$F_H = \frac{2 \cdot b_0}{h} \cdot F_V + \frac{b_1}{h} \cdot T_{crt} + \frac{b_2}{h} \cdot S_{crt} \quad \dots (3)$$

Where,  $F_H$ : lateral resistance,  $F_V$ : vertical load per CLT panel,  $T_{crt}$ : critical tensile strength of vertical restrain,  $S_{crt}$ : critical shear strength,  $h$ : height of wall panel,  $b_0$ : width of CLT panel,  $b_1$ : distance between the end of CLT panel and the centre of vertical restrain,  $b_2$ : distance between the end of CLT panel and the centre of embedding at the panel edge.

The condition in which the failure of vertical restrain precedes is;

$$\bar{Z} = \bar{T} - \bar{S} \geq 0 \quad \dots (4)$$

Where,  $\bar{Z}$ : performance function,  $\bar{S}$ : capacity of shear joints between CLT panels.  $\bar{T}$ : capacity of vertical restrain,  $F_V$ : vertical load per panel

### 2.2.3 Lateral resistance of shear walls with flexible beam of which failure of shear joints between CLT panels precedes the failure of vertical restrain at the end of the wall

In the case that the loading beam connected at the top of wall is supposed to be flexible and the failure of the joint between the adjacent CLT panels precedes failure of the vertical restrains at the end of wall panel, the lateral resistance of shear wall is expressed by the equation (5).

$$F_H = \frac{b_0}{h} \cdot F_V + \frac{b_1}{h} \cdot T_{crt} + \frac{b_2}{h} \cdot S_{crt} \quad \dots (5)$$

Where,  $F_H$ : lateral resistance,  $F_V$ : vertical load per CLT panel,  $T_{crt}$ : critical tensile strength of vertical restrain,  $S_{crt}$ : critical shear force,  $h$ : height of wall panel,  $b_0$ : width of CLT panel,  $b_1$ : distance between the end of CLT panel and the centre of vertical restrain,  $b_2$ : distance between the end of CLT panel and the centre of embedding at the panel edge.

The condition in which the failure of vertical restrain precedes is;

$$\bar{Z} = (\bar{T} + F_V) - \bar{S} \geq 0 \quad \dots (6)$$

Where,  $\bar{Z}$ : performance function,  $\bar{S}$ : capacity of shear joints between CLT panels.  $\bar{T}$ : capacity of vertical restrain,  $F_V$ : vertical load per panel

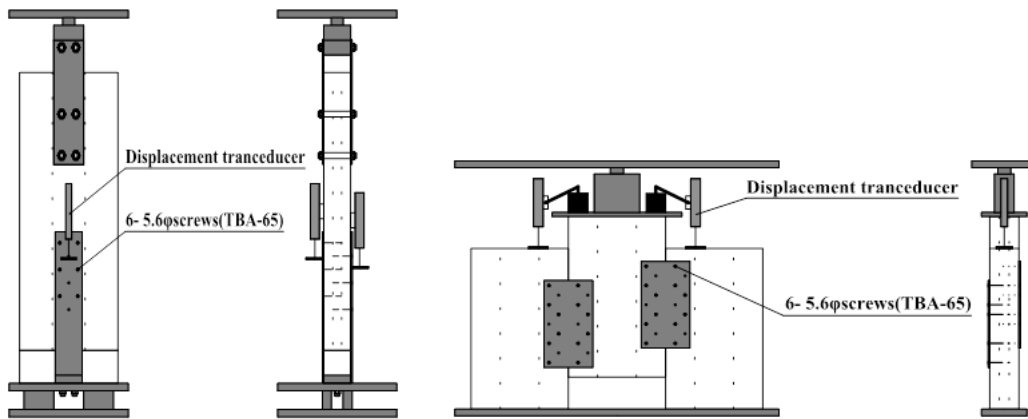


Fig.2 Experiments on vertical restrain (left) and shear plates (right)

## 2.3 Shear tests of Joints

### 2.3.1 Vertical restraints of shear walls

The end of wall panel was connected to the steel base with the vertical restrain with 8 or 12 screws of 5.6 mm diameter and 65mm length (TBA-65) as shown in Fig. 2., and this connector was tested by tension. The connector was attached to the steel base with two bolts of 16mm diameter, and 90mm thick CLT was connected to this connector through 90-by 90mm sill with 8 or 12 screws of 5.6mm diameter (TBA-65) so that the exterior lamina is parallel to the loading direction. Six specimen each for 8 and 12 screws were tested as shown in Fig. 2.

### 2.3.2 Shear plate between wall panels

Specimens with Shear plates of 4.5mm thickness and three and six screws in each side as shown in Fig.2 were prepared and were subjected to the shear forces.

### 2.3.3 Determination of number of fasteners

Fig. 3 shows the relation between the shear strength ( $P_y$  and  $P_{max}$ ) of each joint and the number of screws. It shows that the shear strength of each joint is proportional to the number of screws. Thus the average of maximum strength of all the tested joints of 6.64 kN was taken for a single fastener and they were multiplied by the number of fasteners for the average capacity of the concerned joints. Coefficient of variation (COV) of each tested joint type was however scattered because of the tested samples. Therefore the C.O.V based on all tested values of 0.102 for bearing capacity was applied to both vertical restrains and shear plates. The number of screw used for shear plates were determined by using the equations (2), (4) and (6) for each conditions with the number of screws of the vertical restrains of eight and twelve, and vertical load per CLT panel  $F_v$  of null or 15kN (30kN in total) was applied. The calculated number of screws and that used for actual tests are shown in Table 1.

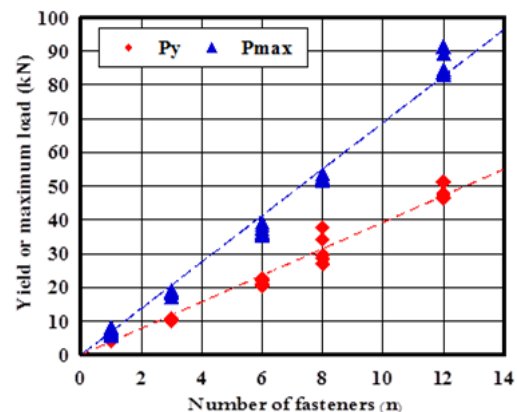


Fig.3 Relation between yield or maximum loads and number of screws

### 3 Test methods

Reversed cyclic lateral loading tests were conducted on the shear walls consisting of two CLT panels of 90mm thick, one meter width and three meters height, 90x90mm sill and 90x120mm loading beams. They were subjected to the reversed cyclic lateral loads together with the vertical loads applied to the loading beam with two hydraulic jacks which were controlled to give the constant loads of 15kN each. The reversed cyclic loads based on ISO 21581<sup>2)</sup> were applied by computer controlled actuator. For the specimen assuming flexible loading beam, the loading beam was separated at the centre of specimen to allow the free slips between two panels, and they were connected by two steel bar of 30x70mm at the centre of each panel. Horizontal and vertical displacements were measured by electric transducers.

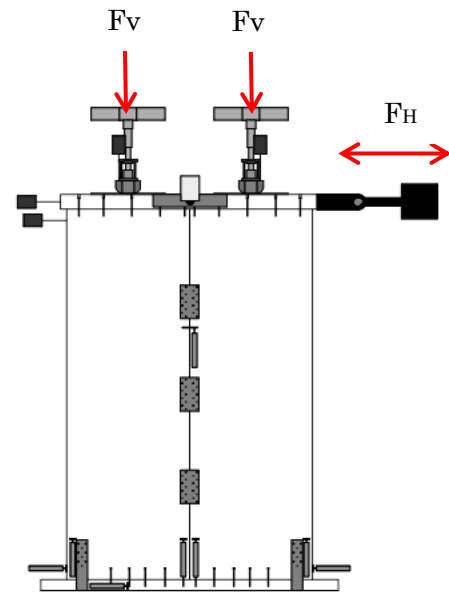


Fig. 4 Outline of lateral loading test

Table 1 Calculated number of screws of shear plates based on the failure mode

Specimen	Loading beam	Vertical load (kN/m)	Expected failure	Number of screws				
				Vertical restrain	Shear plates			Experiment
					$\beta=2.0$	$\beta=2.5$	$\beta=3.0$	
T8S7V0R	Rigid	0	Shear plate	8	6	5.5	5.1	7
T8S7V15R		15		8	6	5.5	5.1	7
T8S10V0R		0	Vertical restrain	8	10.7	11.5	12.5	10
T8S13V15R		15		8	13.4	14.4	15.5	13
T8S7V0F	Flexible	0	Shear plate	8	6	5.5	5.1	7
T8S8V15F		15		8	8	7.5	7	8
T8S11V0F		0	Vertical restrain	8	10.7	11.5	12.5	11
T8S13V15F		15		8	13.4	14.4	15.4	13
T12S11V0R	Rigid	0	Shear plate	12	9	8.3	7.7	11
T12S11V1R		15		12	9	8.3	7.7	11
T12S17V2R		0	Vertical restrain	12	16	17.2	18.7	17
T12S20V3R		15		12	18.7	20.1	21.7	20

### 4 Results and discussions

Figure 5 shows the load-displacement relationship of each specimen in reversed cyclic lateral loading tests, and Tables 2 to 4 show the yield, ultimate and maximum loads and their displacements of each specimen. Fig. 5 shows typical curves with slips as are observed in timber structures when no vertical loads were applied, but they showed hysteretical curves with pinching and constriction which may be observed in pre-stressed system when vertical constant loads were applied. They showed obvious increase of the maximum loads by applying the vertical loads. There were also the increase of the maximum loads by applying the number of screws to shear plates so that the failure of the vertical restrains will precede the failure of shear joints.

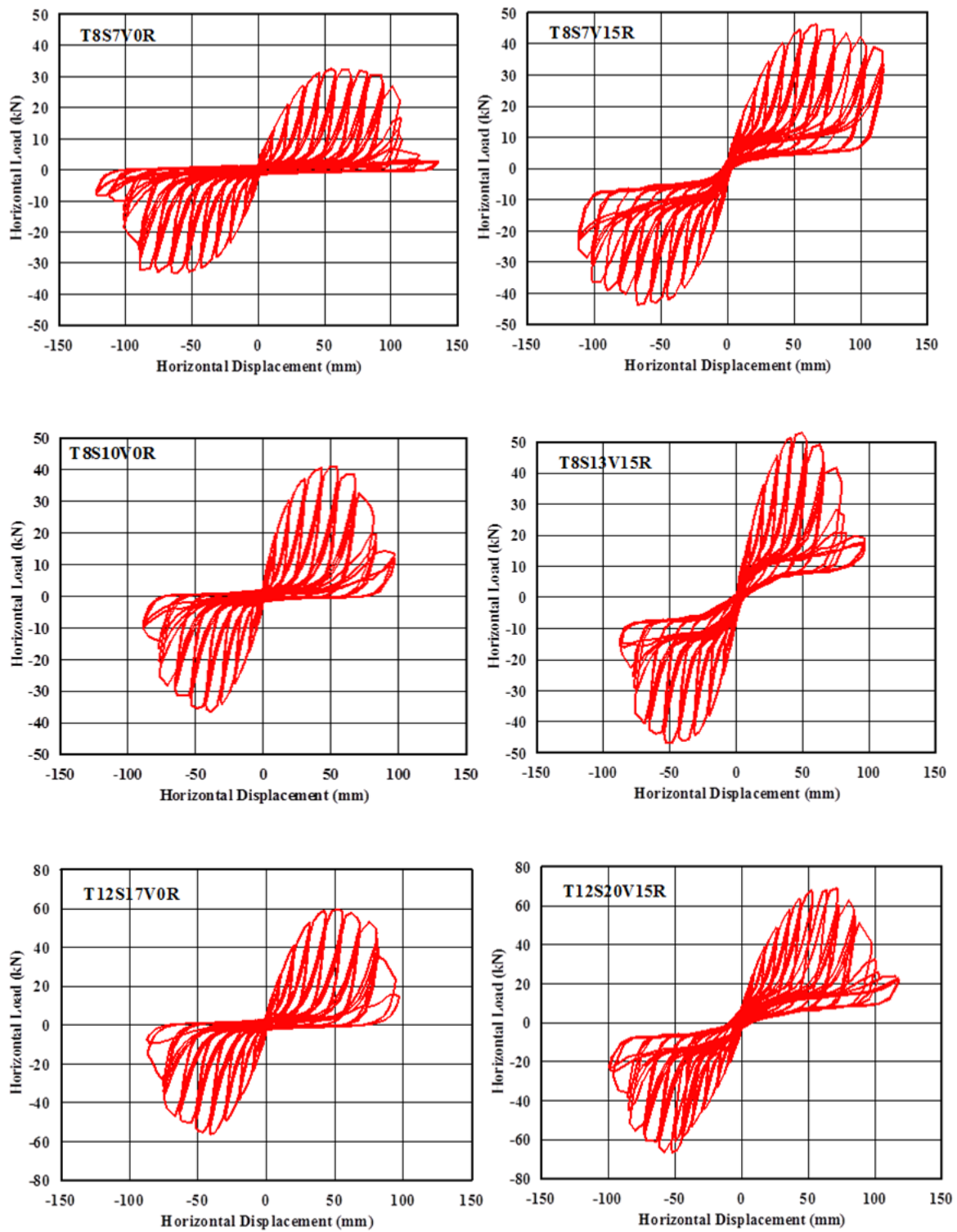


Fig. 5 Examples of Load-displacement relationships of lateral loading tests of CLT wall

Table 2 Outline of test results with rigid loading beam (8 screws for vertical restrains)

Specimen	Number of screws		Vertical Loads (kN/m)		Py	Dy	Pu	Du	Pmax	Dmax
	VR	SP			(kN)	(mm)	(kN)	(mm)	(kN)	(mm)
T8S7V0R	8	7	0	+	20.3	22.3	30.3	106.0	32.5	57.8
				-	18.4	16.6	30.8	94.7	33.2	65.5
				av.	19.4	19.5	30.6	100.4	32.9	61.7
T8S7V15R	8	7	15	+	25.6	23.6	42.1	122.4	46.3	71.9
				-	24.4	14.2	39.3	103.5	43.7	68.1
				av.	25.0	18.9	40.7	113.0	45.0	70.0
T8S10V0R	8	10	0	+	22.4	12.9	37.7	74.3	40.9	53.9
				-	18.8	13.4	33.3	68.6	36.6	42.6
				av.	20.6	13.2	35.5	71.5	38.8	48.3
T8S13V15R	8	13	15	+	30.5	17.5	48.3	73.4	53.0	55.5
				-	25.3	11.8	43.9	72.2	46.8	51.5
				av.	27.9	14.7	46.1	72.8	49.9	53.5

Table 3 Outline of test results with flexible loading beam (8 screws for vertical restrains)

Specimen	Number of screws		Vertical Loads (kN/m)		Py	Dy	Pu	Du	Pmax	Dmax
	VR	SP			(kN)	(mm)	(kN)	(mm)	(kN)	(mm)
T8S7V0F	8	7	0	+	18.3	14.1	29.7	90.0	32.7	50.1
				-	15.1	11.3	26.7	94.6	29.3	41.0
				av.	16.7	12.7	28.2	92.3	31.0	45.6
T8S8V15F	8	8	15	+	18.5	10.5	33.1	117.5	36.2	82.1
				-	21.2	14.0	32.9	96.0	34.6	61.7
				av.	19.8	12.2	33.0	106.8	35.4	71.9
T8S11V0F	8	11	0	+	21.7	17.8	33.0	110.3	35.4	75.1
				-	20.5	13.8	33.9	100.5	36.5	65.4
				av.	21.1	15.8	33.5	105.4	35.9	70.3
T8S13V15F	8	14	15	+	24.2	12.8	43.2	120.1	48.3	80.7
				-	20.0	6.2	37.3	114.6	40.4	69.0
				av.	22.1	9.5	40.2	117.4	44.3	74.9

Table 4 Outline of test results with rigid loading beam (12 screws for vertical restrains)

Specimen	Number of screws		Vertical Loads (kN/m)		Py	Dy	Pu	Du	Pmax	Dmax
	VR	SP			(kN)	(mm)	(kN)	(mm)	(kN)	(mm)
T12S11V0R	12	11	0	+	30.6	19.4	48.9	88.3	54.4	64.9
				-	31.8	21.9	48	92.2	53	76.6
				ave.	31.2	20.65	48.45	90.25	53.7	70.75
T12S11V15R	12	11	15	+	35.5	19.4	55.1	94.4	60.4	65.2
				-	30.2	13	51.5	97.5	57.4	62.7
				ave.	32.85	16.2	53.3	95.95	58.9	63.95
T12S17V0R	12	17	0	+	34.4	14.4	53.8	96.2	60.9	76.5
				-	32.5	13.9	52.4	67.5	61.8	51
				ave.	33.45	14.15	53.1	81.85	61.35	63.75
T12S20V15R	12	20	15	+	35.7	14.9	60.8	83.4	69	71.1
				-	37.7	21.9	59.6	80.3	66.8	57.9
				ave.	36.7	18.4	60.2	81.85	67.9	64.5

Fig.6 shows the deformation of wall panel in 1/200, 1/50 and 1/30 displacements. Although some slips were observed at the shear joints between two CLT panels, they determine clearly the final failure mode which was expected by the equations (2), (4) and (6), and it was proved that this procedure is appropriate to predict the failure mode of CLT wall panel. Fig.7 shows comparison between the maximum loads of each specimen and those calculated by equations (1),

(3) and (5) from the average capacity of strength of screws obtained from the joint test. The experimental results showed slightly higher values than the calculated capacity, but the calculated capacity showed comparatively good agreement with the experimental results, and it was proved that these equations are appropriate to predict the lateral resistance of CLT wall panels connected vertically by shear plates.

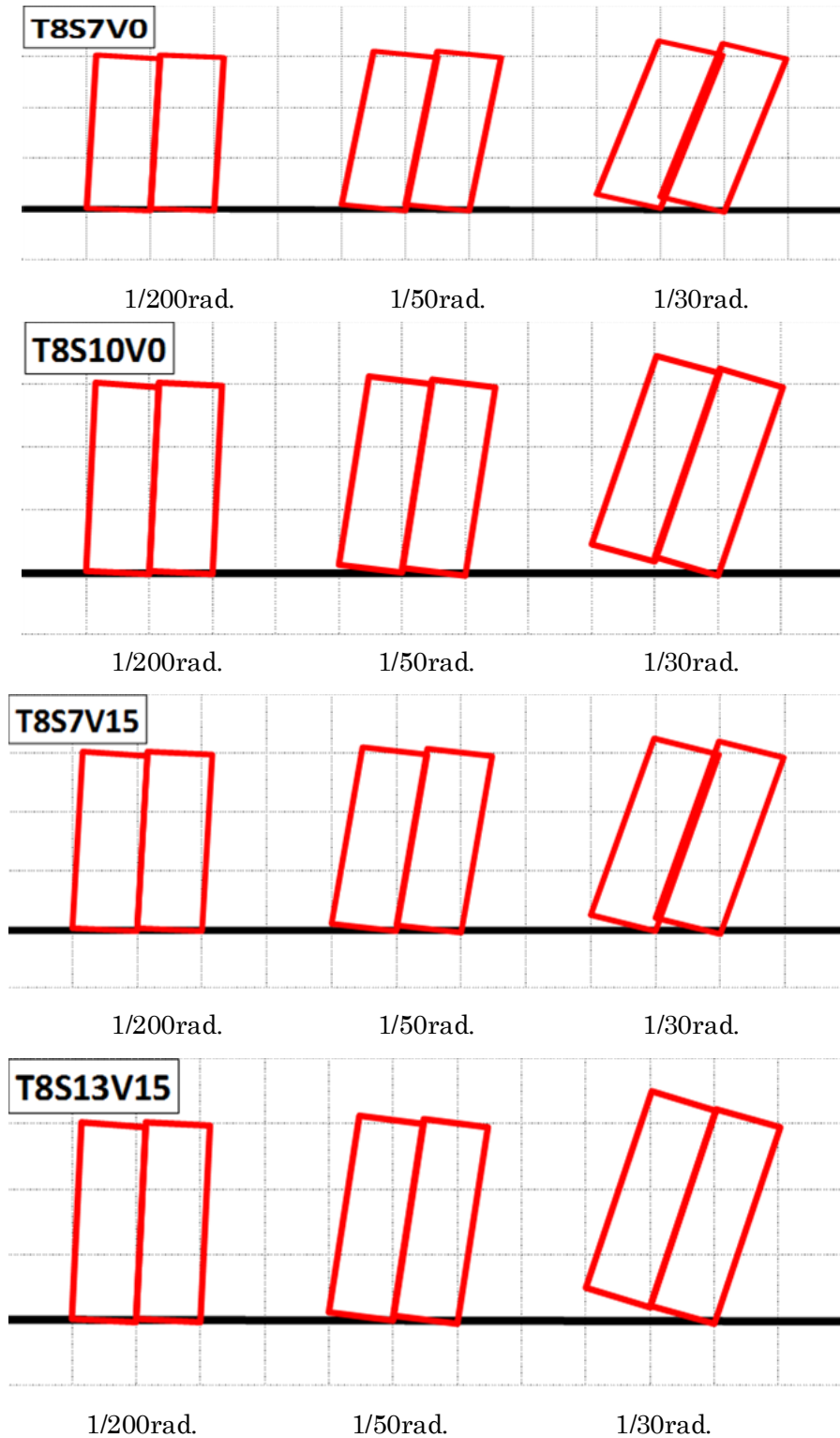


Fig.6 Deformation of each CLT panel at the shear deformation of  $1/200$ ,  $1/50$  and  $1/30$

## 5 Conclusions

It was shown that the final failure mode of CLT wall panel can be predicted by the equations (2), (4) and (6), and this procedure is appropriate to design the failure mode of CLT wall panel. The maximum strength calculated by equations (1), (3) and (5) showed comparatively good agreement with the experimental results, and it was proved that these equations are appropriate to predict the lateral resistance of CLT wall panels connected vertically by shear plates and vertical restrains at the end of wall.

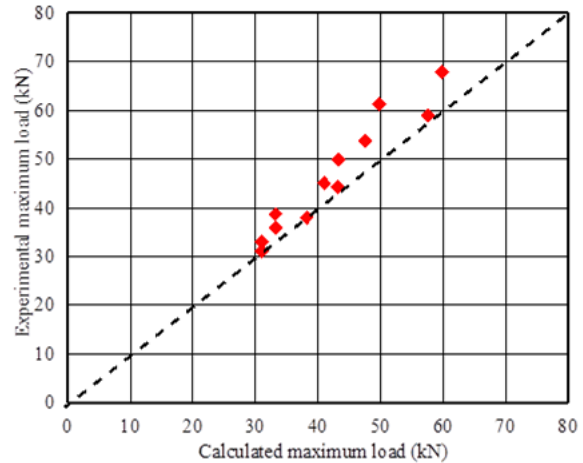


Fig.7 Comparison between experimental capacity and calculated maximum load of CLT wall panels

## Acknowledgement

The author would like to express his thanks to Mis. Yamaguchi and Mr. Ito, undergraduate students of Shizuoka University for their assistance of conducting racking tests of CLT shear walls and analysis.

## References

1. Follesa M, M P Lauriola, C Minowa, N Kawai, C Sandhaas, M Yasumura, A Ceccotti: Which Seismic Behaviour Factor for Multi-Storey Buildings made of Cross-Laminated Wooden Panels? , CIB-W18, paper 39-15-2, Florence, 2006
2. International Organization for standardization, ISO 21581: Timber structures - Static and cyclic lateral load test methods for shear walls, 2010
3. Yasumura M, E Karacabeyli: International Standard Development of Lateral Load Test Method for Shear Walls, CIB-W18, paper 40-15-5, Bled, August 2007
4. Bruno Dujic, Janez Pucelj, and Roko Zarnic, Testing of Racking Behavior of Massive Wooden Wall Panels, CIB-W18, paper 37-15-2, Edinburgh, 2004



**INTERNATIONAL COUNCIL FOR RESEARCH AND INNOVATION  
IN BUILDING AND CONSTRUCTION**

**WORKING COMMISSION W18 - TIMBER STRUCTURES**

**SEISMIC RESPONSE OF TIMBER FRAMES WITH  
LAMINATED GLASS INFILL**

V Rajčić

University of Zagreb, Faculty of Civil Engineering

CROATIA

R Žarnić

University of Ljubljana, Faculty of Civil and Geodetic Engineering

SLOVENIA

**MEETING FORTY FIVE**

**VÄXJÖ**

**SWEDEN**

**AUGUST 2012**

---

Presented by R Žarnić

B Dujic commented that the hysteresis loops indicate large residual deformation from wood crushing. R Žarnić responded that the building could be pushed back after deformation. B Dujic commented that the literature review was incomplete in this paper. R Žarnić responded that the paper described research in progress. H Blass stated that was not the interest of this working commission. C Sigrist asked about the details of how the connection looked like between the glass and the wood and received confirmation that it was based on classical window technology and they were not glued. He asked why not gluing. R Žarnić responded that the idea was not to damage the glass but to have damage in wood. F Lam commented that as a lateral load resistant system it would need to carry seismic as well as wind loads. In high winds there is a risk of projectiles that can damage the glass. R Žarnić responded that this system might not be suitable for all cases. Also he pointed out that even without glass the system had some capacity left. P Quenneville received clarification about the contact surface between the glass and wood and vertical load that there was enough surface not to damage the wood but enough to promote friction.



# Seismic response of timber frames with laminated glass infill

Vlatka Rajčić<sup>1</sup>, Roko Žarnić<sup>2</sup>

<sup>1</sup> University of Zagreb, Faculty of Civil Engineering,  
Kačićeva 26, 10000 Zagreb, Croatia, [vrajcic@grad.hr](mailto:vrajcic@grad.hr)

<sup>2</sup> Roko Žarnić, University of Ljubljana, Faculty of Civil and Geodetic Engineering,  
Jamova 2, 1000 Ljubljana, Slovenia, [roko.zarnic@fgg.uni-lj.si](mailto:roko.zarnic@fgg.uni-lj.si)

## Summary

The present paper presents an insight into on-going research of the behaviour of wooden frames infilled by glass panels. Since the research is in a relatively early stage, only typical results showing the response of tested specimens on vertical, racking and shaking loads are presented. In continuation of the research programme, the computational model will be developed, verified and validated by the experimentally obtained data on describing the behaviour of tested types of structural elements.

**Keywords:** timber-frame, laminated glass, testing, vertical load, racking, shaking

## 1 Introduction

Timber frames infilled with vertically load-bearing glass sheets represent an innovative structural element that is suitable as a load-bearing panel in prefabricated timber houses. It can be easily fixed to structural elements made of other kinds of structural materials (timber, concrete, steel) and connected to each other timber panels by simple steel fasteners. The series of tests of timber-framed glass panels started jointly at the University of Ljubljana and the University of Zagreb in order to study the load-bearing capacity of laminated glass panels and racking performance of timber-framed glass panels. In addition, dynamic shaking table tests on a full-scale box-type model made of two timber frames with glass infills exposed to real earthquake excitation has been carried out at the Institute of Earthquake Engineering and Engineering Seismology IZIIS, Skopje, Macedonia. It was a part of the Croatian-Macedonian bilateral research program, where the partner from Croatia was the University of Zagreb.

The idea of developing a new structural element based on structural glass and a simplified computational model to be used in future codes emerged from the cooperation of authors of this paper in a wide international group of experts engaged for justifying the needs for further codes related to the use of glass products in civil engineering works (Ref.1). They reported about the initial experimental work in a Workshop held in JRC ELSA in Ispra in 2010 (Ref.2).

## 2 Test specimens and test procedures

Specimens for racking testing were designed as timber frames with glass infills. Infills were made of a pair of two 10 mm sheets of toughened glass laminated together. The length of infills was 2900 mm and height 2400 mm. Two types of timber frames were

used. The first was made of cross-laminated timber and the other of glue-laminated timber. The first type of frames has corner joints fixed by a double steel bolts while the second type with single bolt and punched metal plates in each corner of timber frame. The dimensions of frame were 3220 mm in length and 2720 mm in height.

Laminated glass sheets, 1250 mm wide and 2400 high were tested to failure by vertical force (Fig. 1) to obtain data of their load-bearing capacity and deformability. Altogether three specimens were tested. Two of them were exposed to monotonous vertical load to failure and one by cyclic vertical load to failure.

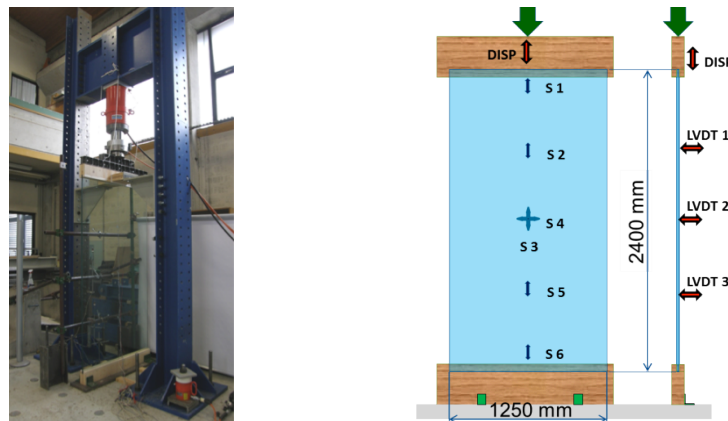


**Figure 1:** Vertical load test of laminated glass sheet and scheme of instrumentation

Glass infilled timber frames were tested by combined constant vertical load of 25 kN/m<sup>2</sup> and cyclic horizontal load (racking load) up to displacement equal to 2% of panel height. The test-setup that is installed in the laboratory of University of Ljubljana (Fig. 2) enables testing of panels exposed to three different configurations that simulate three different boundary conditions. Those are:

1. **Shear cantilever:** one of horizontal edges of panel is supported by the firm base while the other can freely translate and rotate
2. **Constrained rocking:** one of horizontal edges of panel is supported by the firm base, the other can translate and rotate as much as allowed by the ballast; ballast can translate only vertically without rotation.
3. **Shear wall:** one of horizontal edges of panel is supported by the firm base while the other can translate only in parallel with the other edge while it's rotation is fully constrained

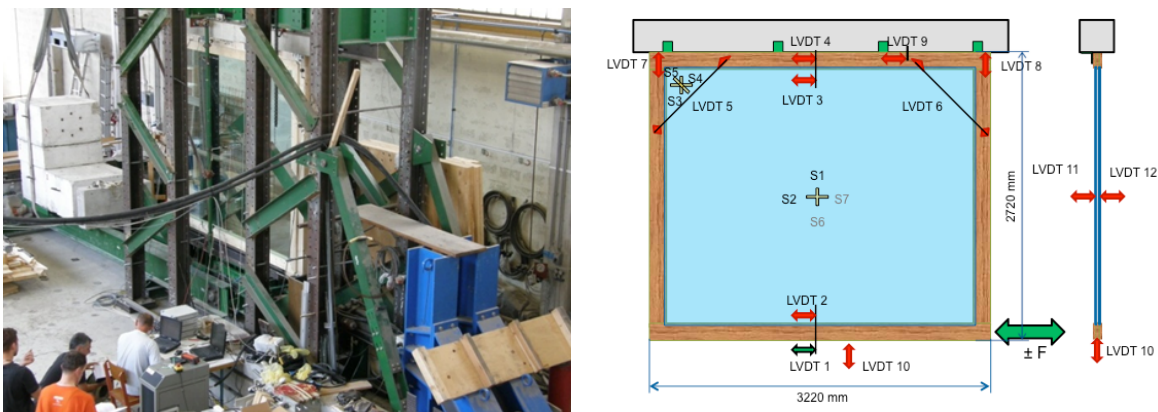


**Figure 2:** Cyclic racking test of glass-infilled timber frames and scheme of instrumentation

Glass-infilled X-laminated frames were tested with all three above described boundary conditions. Because it was found that the second boundary condition does not influence on significantly different response of tested element in comparison to the first boundary condition (Ref. 3), the frames of the second group are to be tested only by variation of two boundary conditions: shear cantilever (1) and shear wall (3). Until now only the shear cantilever tests were performed. In addition to glass infilled frames two glue-laminated frames without infill were also tested applying two boundary conditions: shear cantilever and shear wall. In those two frames joints were fixed by single bolt and punched metal plates.

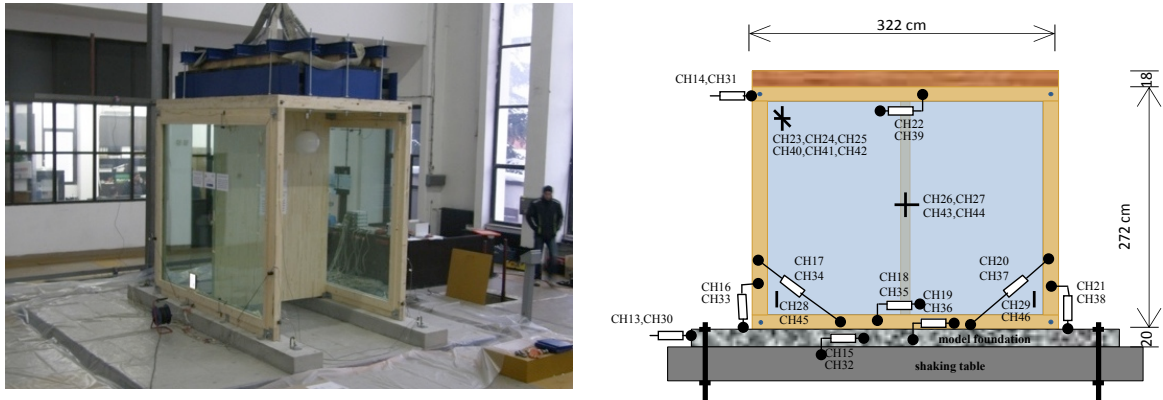


**Figure 3:** Shaking table test of box-type model and scheme of instrumentation

The objective of racking test was to obtain data for development of computational model of tested type of structural element that can be used for prediction of inelastic response of buildings made of glass-infilled timber frames on seismic action. To obtain dynamic parameters and study the phenomena of response of this type of structures on seismic action, shaking table tests were carried out (Fig. 3). The table is installed at the IZIIS Laboratory in Skopje, Macedonia. It is constructed as a pre-stressed reinforced concrete slab having 5x5 m in plan. It is used for simulation of different types of dynamic motion: random, harmonic, impulse, earthquake etc. Four vertical hydraulic actuators support it. The working frequency range of the shaking table is 0.1-80Hz, and the maximum mass of a model is limited to 40t. The max accelerations are 0.7g in horizontal and 0.5g in vertical direction, and the max displacements are 0.125m in horizontal and 0.05m in vertical direction. The shaking system controls five degrees of freedom of the table, two translations and three rotations. This three-variable control system (MTS) is capable to control displacements, velocities and accelerations, simultaneously. For earthquake generation and data acquisition modular PXI system is used

Box-type models were constructed of two glass-infilled timber frames made of simple laminated wood and corner joints fixed by single bolt and punched metal plates. The mass of 9,6 tons was added atop of model. Four types of real earthquake actions were subsequently applied to model: El Centro 1940, N-S, California, USA; Petrovac 1979 Montenegro; Kobe 1995 E-W, Japan, and Friuli 1976 E-W, recorded in Tolmezzo, Italy. The results of shaking table tests are presented in (Ref. 4).

For the seismic tests, the model was instrumented for measuring the input as well as the response at characteristic points. The both panels had the same instrumentation - 10 LVDT's and 7 SG. At the top of the model there were 4 accelerometers, one at each corner. 2 LP's were placed at the level of the foundations and 2 at the top to measure the absolute displacement of the model. Considering that the connection between the glass and the wooden frame is of crucial importance for the stability of the panel during the seismic

action, as well as the location where the energy is dissipated during the strong shaking, several LVDT's for measuring the slippages and deformation were placed at the critical points. To obtain information about the strains in the glass panels 14 strain gages were used. The total number of channels was 44, as presented on Figure 3. The real time recording of the model response was performed by 72-channel high-speed data acquisition system.

### 3 Test results

#### 3.1 Laminated glass sheets

The average loadbearing capacity of two specimens of monotonously tested laminated glass sheet was 142.1 kN/m' with mid-height horizontal displacement (buckling) of 53.7 mm. In case of cyclic vertical loading the achieved loadbearing capacity was 101.3 kN/m' and mid-height displacement 52.8 mm.

The constant vertical load applied to timber-framed glass panels induced load to laminated sheets in magnitude of approx. 12% of their load bearing capacity in the case of cyclic vertical loading. That caused only up to 10% of buckling deformation.

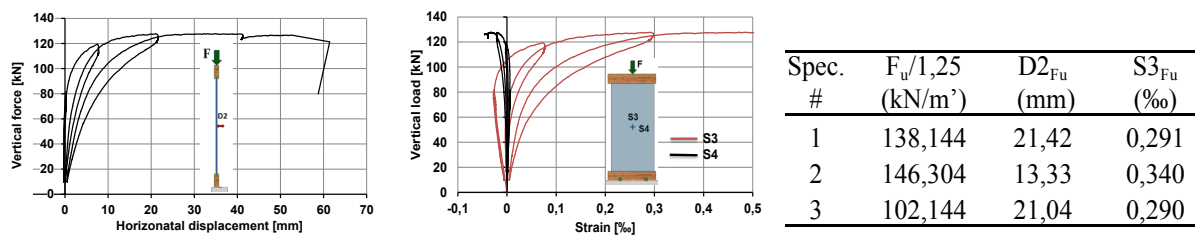


Figure 4: Response diagrams of two-layer laminated glass sheet (Spec #3) to cycled vertical load and table with main data obtained from testing of all three specimens

#### 3.2 Monotonous load test of frames with and without glass infill

Cycling testing of each specimen preceded with monotonous push test to obtain parameters needed for creation of protocol of cyclic test. In Fig. 5 are compared response diagrams for five different specimens and test arrangement (regarding boundary conditions). The main load-bearing parameters are presented in Table 1 below.

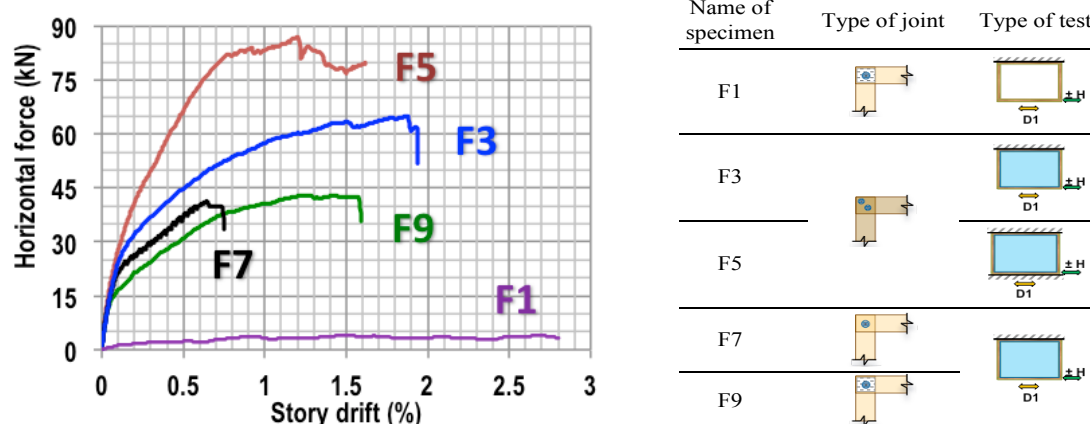


Figure 5: Comparison of diagrams of different frames with and without glass infills

As a first, the effect of glass infill on behaviour of frame itself (specimen F1) is obvious. Further on, there is a strong influence of type of frame composition. The glulam frames (F7, F9) are less resistant than X-lam frames (F3, F5). Also the effect of punched metal plates is obvious (F9). The influence of boundary conditions is well seen from the comparison of behaviour of specimen F3 and F5. In general, the observed differences were expected, but only experimental results can give the insight in their magnitude. Also it will be one of crucial set of data for development, verification and validation of complex and simplified computational model.

**Table 1:** The load-bearing characteristics of different frames with and without glass infills obtained by monotonous tests

Name of specimen	Maximal horizontal force (kN)	Corresponding story drift (%)
F1	4.0	2.66
F3	65.0	1.87
F5	87.1	1.21
F7	41.2	0.64
F9	43.0	1.24

### 3.2 Cyclic test of glue-laminated frames

The cyclic response of glue-laminated bare frame with bolted joints strengthened by punch metal plate does not much depend on boundary conditions as seen from diagrams in Fig. 6 below. Diagrams are showing only a part of response. Diagram in red is response of frame on monotonous load as is the case in all other diagrams of cyclic response in this paper. Frames were tested to the level of large deformations achieved at story drift of 7%. Damages of joints were reparable and deformed frame could be returned by horizontal pushing to the initial geometry. It is to be mentioned that the constant vertical force acting on 160/90 mm columns was 40 kN, practically equal to 10 times of value of the achieved horizontal load bearing. From the hysteresis loops calculated amount of energy dissipated by joints will enable estimation of energy dissipated by wood to glass interaction in the cases of infilled wooden frames. But due to different mechanism of response of frame joints in bare and infilled frame the frame deformation range in which comparison has sense should be defined by further analysis of test results and computational modelling.

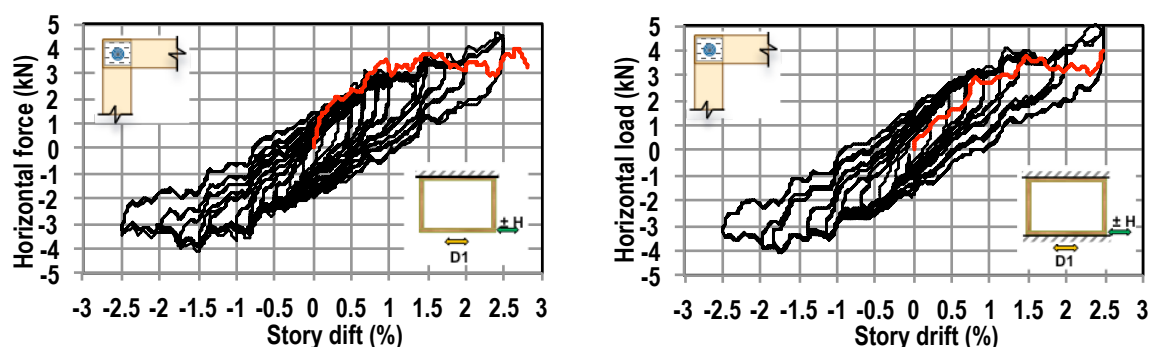


**Figure 6:** Response diagrams of glulam frames exposed to racking load with two different boundary conditions (shear cantilever and shear wall)

### 3.3 Cyclic test of frames with glass infill

Hysteretic response of tested specimens content the information on ductility of structural element, deterioration of strength due to repeating of horizontal load to equal displacement, cycle to cycle stiffness degradation and energy dissipation due to viscous damping of tested structure that passes different stages of gradual damaging of its parts. Tested type of structural elements is highly dissipative, where the main dissipation is caused by glass to wood interaction. Part of dissipation is caused by development of damages in joints and in some extends also by plastic deformations of frame anchoring elements to concrete base. Evaluation of stiffness degradation is explained in Fig. 9, and the evaluation of viscous damping in Fig. 12.

The observed differences in response of glue-laminated frames (Fig. 7) are mainly the consequence of joint configuration. The punched metal plates limited the propagation of shear damages in joints increasing their load bearing capacity and ability to dissipate energy. It reflects in the all over increase of load bearing capacity and ability to dissipate energy through the glass-wood interaction. The effect of boundary condition to response of this type of frames will be observed in the future tests, but regarding the experience gained from testing of X-laminated frames (Fig. 8) they can be of significant magnitude.

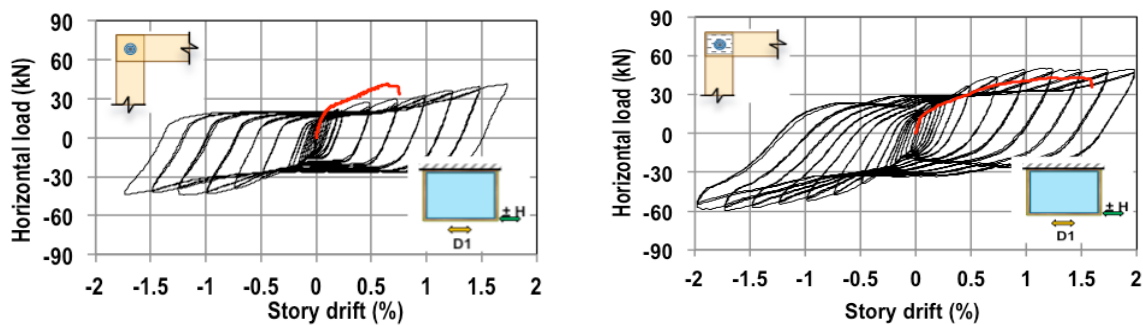


**Figure 7:** Response diagrams of glulam frames with glass infill exposed to racking load with two different joint configurations (bolted joints without and with punched metal plates)

The influence of difference in wood composition quality and joint configuration on hysteretic response of glass infilled frames is obvious from the comparison of diagrams presented in Fig. 7 and Fig. 8. From the Fig. 8 the influence of boundary condition is clearly recognisable. The same type of structural element can achieve much higher load-bearing capacity if supported firmly along the both horizontal edges (shear cantilever). In the case of tested specimens the specimen tested as shear wall has 46% higher load bearing capacity than one tested as shear cantilever. The difference is calculated as average value of maximal load achieved in opposite directions of racking.

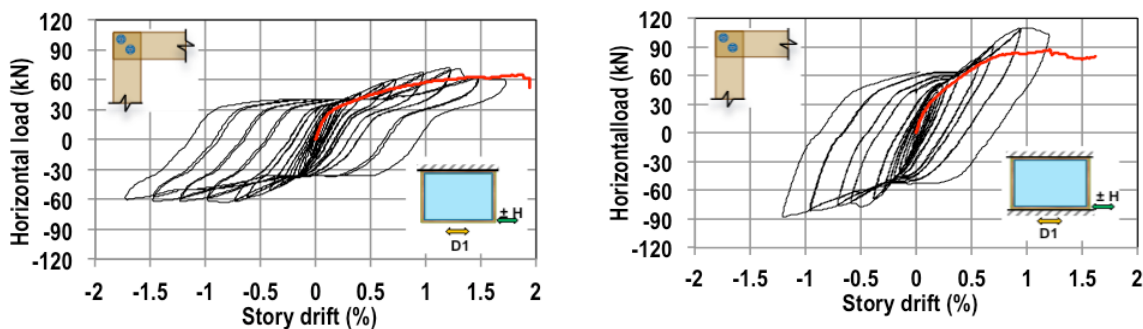


**Figure 8:** Response diagrams of X-lam frames with glass infill exposed to racking load with two different boundary conditions (shear cantilever and shear wall)

As mentioned before, one of main parameters describing the hysteresis response of structure is stiffness degradation. It can be calculated from the stiffness of the chosen loop and effective stiffness of the specimen in the early elastic stage. In the case of tested structural elements the effective stiffness ( $K_e$ ) was calculated from the inclination of the several first hysteresis loops in the elastic range of response (Fig. 9). From the coordinates of the subsequent hysteresis turning points ( $\delta_i, F_i$ ) the inclination (stiffness  $K_i$ ) of corresponding loops was calculated. The diagram of stiffness degradation can be mathematically defined by equation 1 below, where the parameter  $C_k$  is named “stiffness degradation factor”. Since its values are calculated from hysteresis response of tested specimens, it can be considered as their own, unique characteristics.  $C_k$  is very useful parameter that can be well employed in process of validation of computational models, when the experimentally obtained and calculated hysteresis responses are compared.

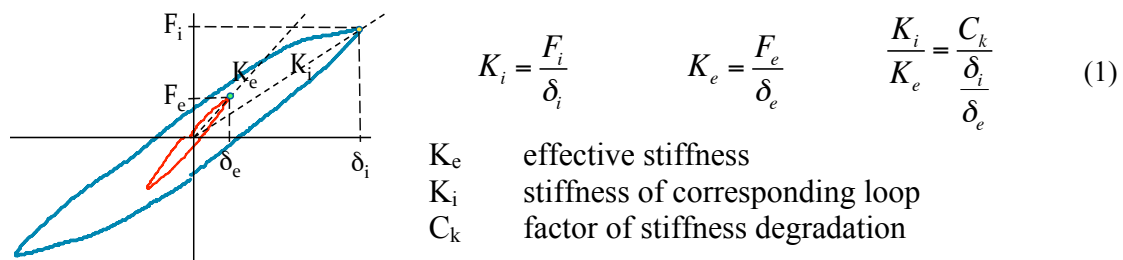


**Figure 9:** Definition of stiffness degradation factor  $C_k$

In Fig. 10 and 11 below, the experimentally obtained data on cycle-to-cycle changing of degradation factor  $C_k$  are presented. The shape of curves is of the same kind, but values depend on the own hysteretic properties of each structural element. The values of  $C_k$  show a level of structural degradation expressed by lowering of its stiffness.

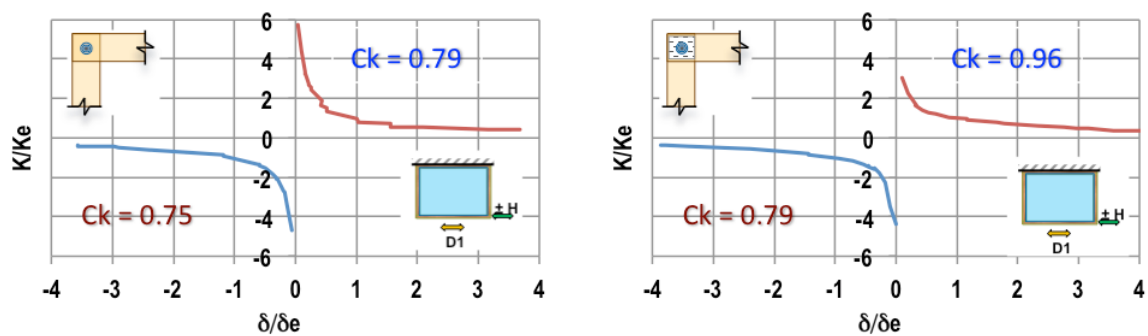


**Figure 10:** Experimentally obtained stiffness degradation factors  $C_k$  of glass infilled glulam frames

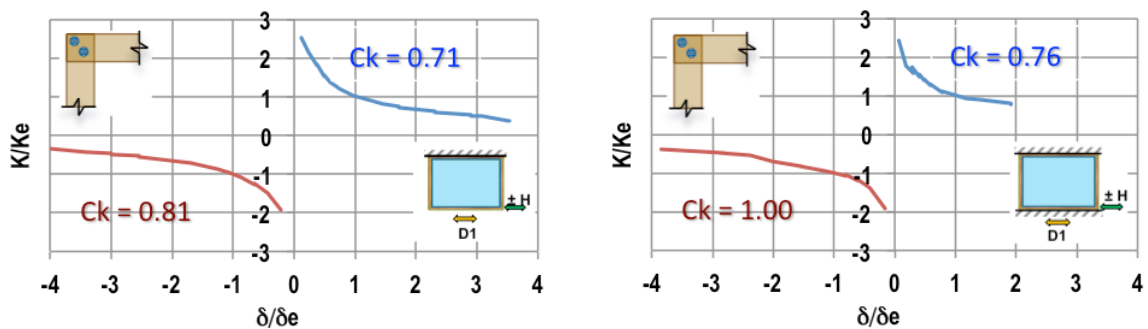


**Figure 11:** Experimentally obtained stiffness degradation factors  $C_k$  of glass infilled X-lam frames

It is obvious that due to damages of structure at certain level of deformation its stiffness at achieved equal displacement in the opposite direction of excitation is lower than when it was achieved for the first time. This "softening" effect reflects in the values of  $C_k$ , which are always lower in the direction of opposite excitation. The magnitude of differences in values of  $C_k$  shows in which extend of symmetry is development of damages in structural elements. In the case of tested types of structural elements the symmetry is much higher than in the cases of other types of structural elements as, for instance, reinforced concrete frames with masonry infills.

Another important parameter that quantifies hysteresis response of structural elements is the equivalent coefficient of viscous damping ( $\xi$ ). It can be calculated from hysteresis response as explained below and formulated by equation 2.

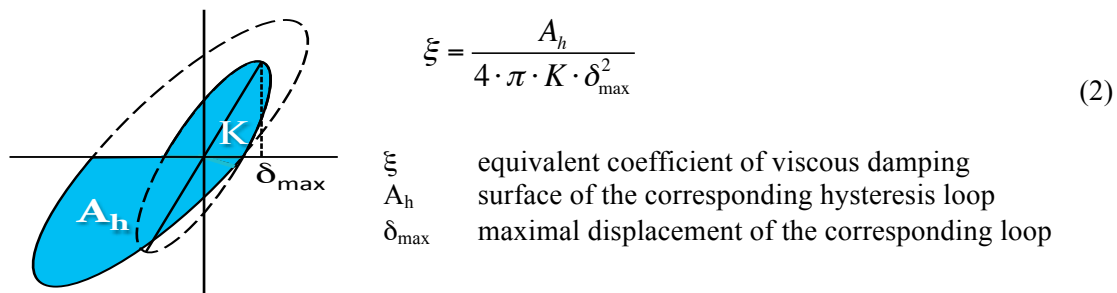


**Figure 12:** Definition of the equivalent coefficient of viscous damping  $\xi$

In figures 13 and 14 the envelopes of hysteresis loops and calculated coefficients of viscous damping are compared. The envelopes also show the amount of load bearing deterioration at repeating of deformations (three cycles to the selected displacement). In the case of X-lam frames the deterioration was insignificant, while in the case of glued laminated frames it was relatively low.

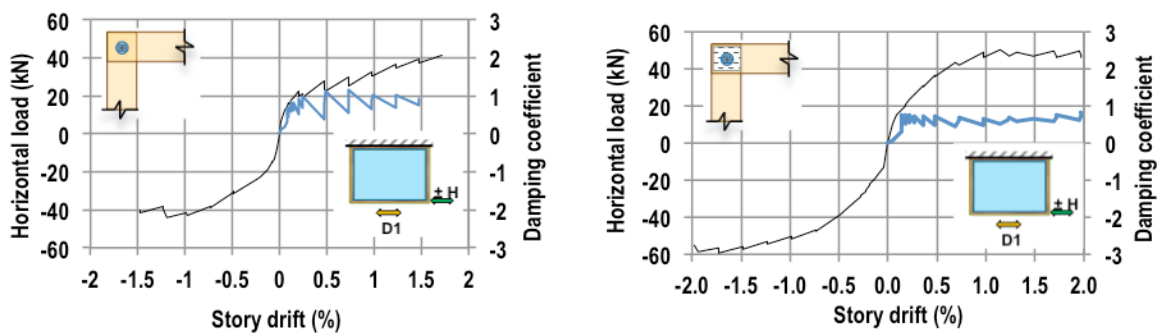


**Figure 13:** Experimentally obtained viscous damping coefficients  $\xi$  of glass infilled glulam frames

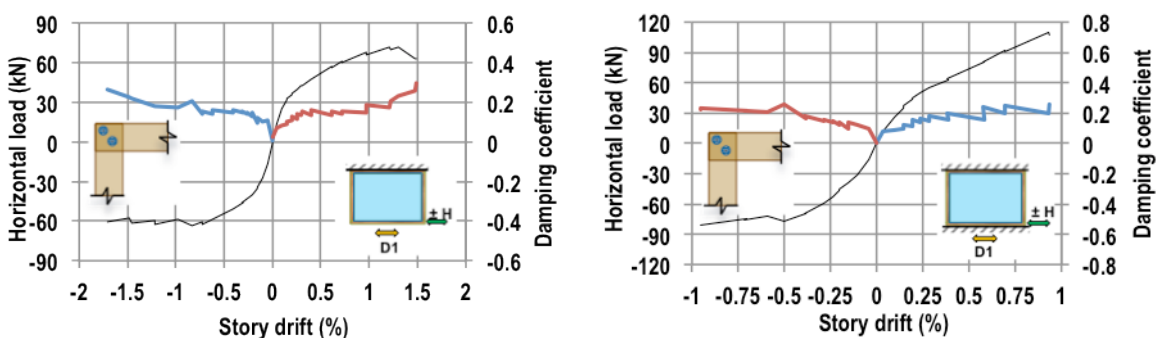


**Figure 14:** Experimentally obtained viscous damping coefficients  $\xi$  of glass infilled X-lam frames

Diagrams, showing the values of coefficients of viscous damping in relation to displacements can be observed as an illustration of hysteresis dumping in different stages of deformations of tested structure. In the case of glue-laminated frames the coefficient was in range of 0.7 in both cases of joint configuration (Fig. 13). In the case of X-lam frames the values of the coefficient were in range of 0.2. Difference of viscous damping of glue-laminated frames in comparison to X-laminated frames was governed mostly by behaviour of joints. Joints behaved differently because of both wood mechanical characteristics and type of connecting frame components.

### 3.4 Shake table test of box-type model

Before the seismic testing, the dynamic characteristics of the model were obtained by measuring the ambient vibrations at selected points and processing the records by use of the Artemis software. The seismic excitations selected for the shake-table testing of the model were four representative aelerograms recorded during the following earthquakes: El Centro ( $a_{max}=0.34g$ ), Petrovac ( $a_{max}=0.47g$ ), Kobe ( $a_{max}=0.58g$ ) and Friuli ( $a_{max}=0.31g$ ). The idea was to investigate the seismic behaviour of the model under several types of earthquake, considering their different frequency content, peak acceleration and time duration. The tests were performed in series, with increasing intensities until the damage occurrence of the model. The applied input intensities in a series were decided to be around the same percentage of the max acceleration (full scale) of the applied earthquake. The model frequencies were checked after each series of test by random excitation or by sine-sweep test. The final tests were performed by using the most unfavourable excitation, i.e. the earthquake Kobe, because it produced very intensive shaking and response of the model. The last 4 tests were performed by harmonic excitation having frequencies equal to the frequencies of the model after the seismic tests accomplishment,  $f = 4.0$  Hz and  $f = 6.0$  Hz, in order to see the effects of the resonance conditions.

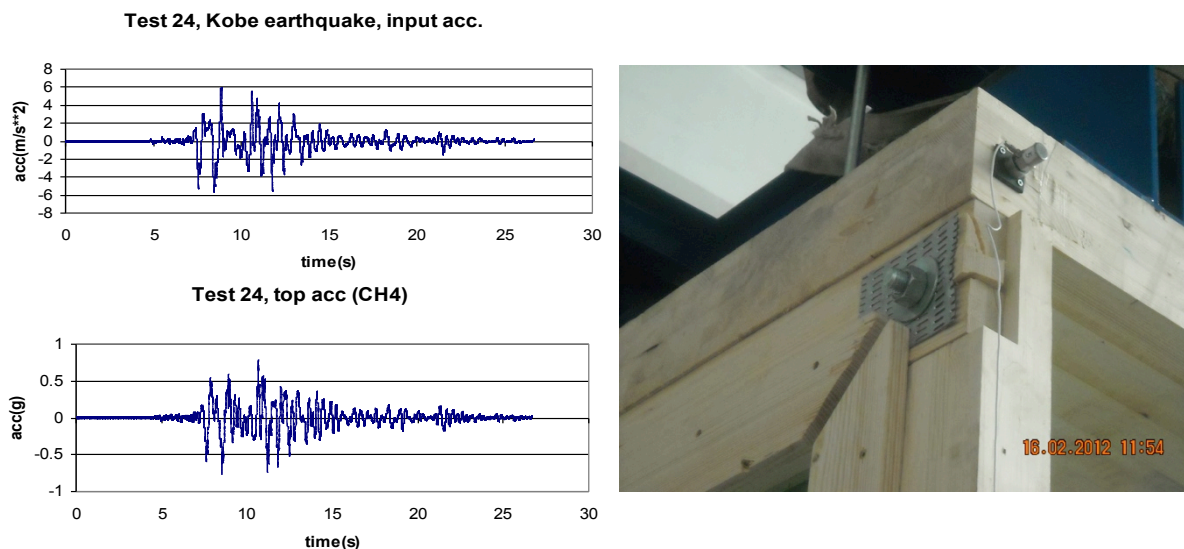


**Figure 15:** Excitation (max. input acc. = 0,6g) and response of model Kobe 1995 E-W, Japan earthquake (max. response acc. = 0.8g) and damages of upper frame joints after testing

The inelastic behaviour of model was achieved after application of full scale Kobe earthquake that was applied last in subsequent application of other three full-scale earthquakes. The damages caused by Kobe earthquake were limited to upper joints of

frame, but their extent was much lower than in the case of racking load at its ultimate stage.

The performed tests showed clearly the behaviour of the glass infilled wooden frames and failure mechanism under strong earthquake motion. It is manifested by slip of the glass along the wooden frame and permanent deformations of the wood, without any damage in the glass. The panels dissipated energy through sliding of the glass, development of damages in frame corners and activating of the still connectors that anchor frame to r. c. fundaments.

The seismic tests proved that the innovative composite panel could be considered as promising structural system, in which the load-bearing structural glass and the wood are working together, conforming to each other in beneficial manner. The dynamic tests results showed very good agreement with the results obtained during the racking tests of the panels.

## Acknowledgement

Ministry of Science, Education and Sport of Republic of Croatia, Ministry of Education and Science of Republic of Macedonia and Ministry of Education, Science, Culture and Sport of Republic of Slovenia financially supported the research. Their contribution is gratefully acknowledged.

## 3 References

1. Žarnić, R., Tsionis, G., Gutierrez, E., Pinto, A., Geradin, M., Dimova, S.. *Purpose and justification for new design standards regarding the use of glass products in civil engineering works: support to the implementation, harmonization and further development of the Eurocodes*, (JCR Scientific and Technical Reports, EUR 22856 EN). First edition. Luxembourg: Office for Official Publications of the European Communities: Joint Research Centre European Commission, 2007. 30 p.p.
2. Žarnić, R. and Rajčić, V., Cyclic response of load-bearing wood-framed glass panels, Workshop on 'Dynamics, Structural and Earthquake Engineering: Research and practice', EU JRC ELSA, Ispra, Italy, 16th July 2010 (published on ELSA web page)
3. Rajčić, V and Žarnić, R, Racking performance of wood-framed glass panels, *The future of Timber Engineering*, Final Papers, ed. Pierre Quenneville, World Conference on Timber Engineering, New Zealand, 15-19 July 2012, p. p. 57-62
4. Krstevska, L., Tashkov L., Rajcic, V. and Zarnic, R., Shaking Table Test of Innovative Composite Panel Composed of Glued Laminated Wood and Bearing Glass, Proceedings of the 15<sup>th</sup> World Conference on Earthquake Engineering, ..... September 2012, 10 p.

**INTERNATIONAL COUNCIL FOR RESEARCH AND INNOVATION  
IN BUILDING AND CONSTRUCTION**

**WORKING COMMISSION W18 - TIMBER STRUCTURES**

**MODELLING WOOD STRUCTURAL PANEL  
PORTAL FRAME RESPONSE**

T Skaggs  
Borjen Yeh

APA – The Engineered Wood Association

U.S.A.

**MEETING FORTY FIVE  
VÄXJÖ  
SWEDEN  
AUGUST 2012**

---

Presented by T Skaggs

G Doudak asked about other possible failure modes such as sill plate or header beam failures. T Skaggs responded that they were not observed except rare cases of strap failures. G Doudak asked about that testing with straps but without sheathing could be conducted to evaluate the cumulative effects. T Skaggs responded they were not done and the straps might be bending but modeled as pure moment couple. G Doudak asked if there was any limit on horizontal deformation. T Skaggs stated there was no drift limits for wind. H Larsen questioned the scientific content of the work. T Skaggs and BJ Yeh responded that the work provided engineers answers to problems that currently did not have readily available solutions. It is a justification to confirm engineering mechanics approach with data to support the case. I smith asked why there was no drift limit for wind in codes. T Skaggs clarified that drift limits or wind were more relaxed compared to seismic.



# Modelling Wood Structural Panel Portal Frame Response

Tom Skaggs and Borjen Yeh  
APA – The Engineered Wood Association, U.S.A.

## Abstract

In the 1980s, APA developed a portal frame concept, which can be site-built using standard sheathing and lumber, to create a semi-rigid moment frame. The advantage of portal frames is that they can resist relatively high lateral loads from narrow wall widths. A pair of the portal frames used for garage fronts is commonly used for prescriptive construction in the Pacific Northwest of the United States.

In the 2000s, extensive cyclic testing was conducted on this system such that design values could be determined for engineering applications. Additional prescriptive solutions were also developed, which included using the portal frames without the large holddown straps and using this portal on a raised floor system. Finally, the modern concrete codes, ACI-318 (2011), require one to consider the effects of cracked concrete on anchorage for use in areas subjected to significant seismic forces. This code requirement effectively reduced the capacities of the hold down straps in high seismic regions. Consequentially, in 2012, an additional series of full-scale wall tests were conducted by APA to confirm the effect from reduced strap capacity on the capacities of the portal frames.

A simple principle of mechanics model was developed to predict the allowable stress design capacity of wood structural panel portal frames. Model predictions are compared to test results for 17 different portal frame configurations that have been tested throughout the years. Portal frame constructions investigated in this study range from 406 to 610 mm (16 to 24 in.) wide, 2.4 to 3.0 m (8 to 10 feet) tall, sheathed with OSB or plywood, and with no holddowns or with holddowns ranging from 3.0 to 21.2 kN (670 to 4,755 lbf) capacity at the base of the wall segment. Also investigated are portal frames built on raised wood floor assemblies with variable base of wall restraint configurations.

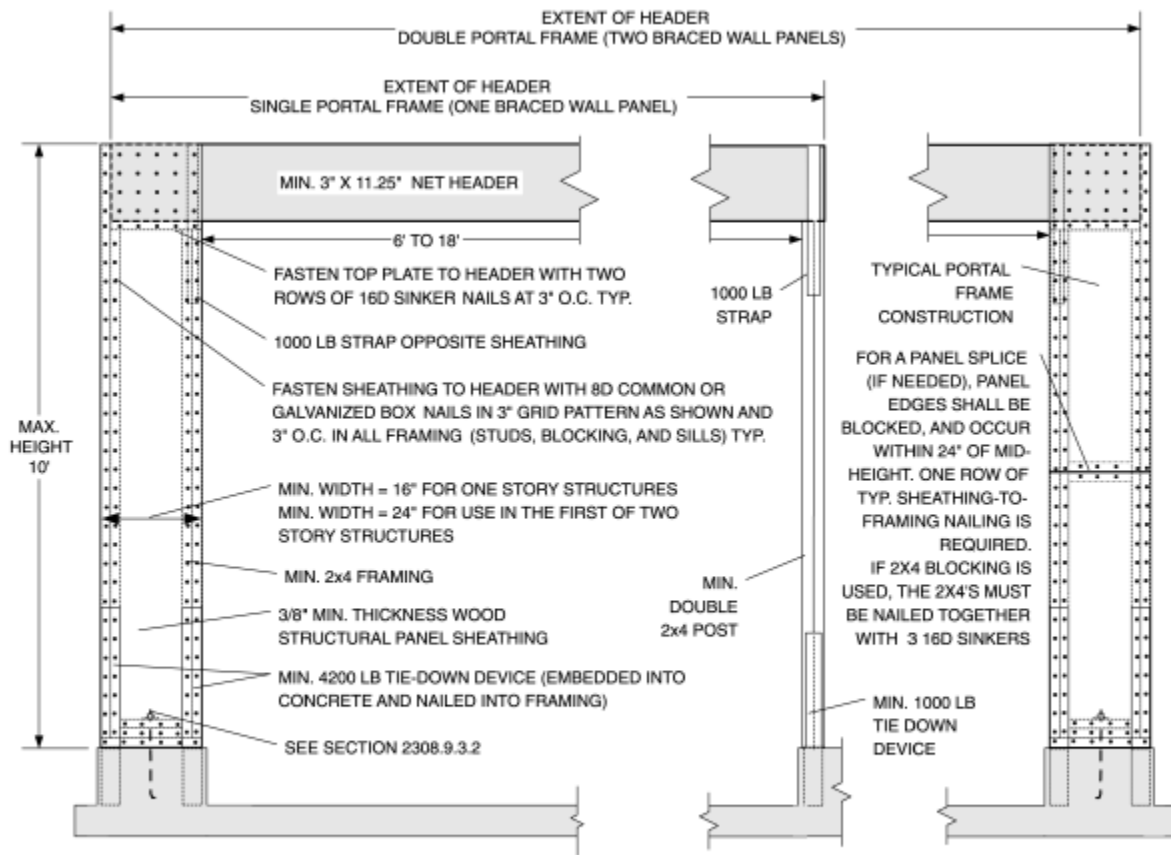
The paper provides a detailed theoretical basis for the model development as well as an expanded version of the table such that designers can reproduce these calculations for various portal frame configurations. The model predictions are compared to cyclic test data representing the 17 different wall assemblies. The average predicted allowable stress design capacity is within a few percent of the ultimate capacity divided by a factor of safety of 3.0 on average. The model is currently limited to predicting the capacity of portal frames. Additional refinements based on a database of cyclic test data might yield a suitable deflection prediction equation.

## 1. Introduction

In the 1980s, APA developed a portal frame concept, which can be site-built using standard sheathing and lumber, to create a semi-rigid moment frame, as illustrated in Figure 1. The advantage of portal frames is that they can resist relatively high lateral loads from narrow wall widths. A pair of the portal frames used for garage fronts is commonly used for prescriptive construction in the Pacific Northwest of the United States. Two widths of the portal frames, 406

mm (16 in.) and 610 mm (24 in.) and one height, 2.4 m (8 feet), were evaluated via monotonic racking tests. The general characteristics of the portal frames were as follows:

- Extended header over narrow pier
- Sheathing grid nailing in extended header to form a semi-rigid moment connection at top of pier
- Three bottom plates, which provide a semi-rigid moment connection with a grid of nails
- Hold down straps between concrete foundation and face of pier to form a semi-rigid connection.



For SI: 1 foot = 304.8 mm; 1 inch = 25.4 mm; 1 pound = 4.448 N.

**FIGURE 2308.9.3.2**  
**ALTERNATE BRACED WALL PANEL ADJACENT TO A DOOR OR WINDOW OPENING**

Figure 1. Standard portal frame detail as published in 2012 International Building Code.

In the 2000s, extensive cyclic testing was conducted on this system such that design values could be determined for engineering applications. Additional prescriptive solutions were also developed, which included using the portal frames without the large holddown straps and combining the portal frames with homes that were fully sheathed, as well as using this portal on raised floor system. Finally, the modern concrete codes, ACI-318 (2011), require one to

consider the effects of cracked concrete on anchorage for use in areas subjected to significant seismic forces. This code requirement effectively reduced the capacities of the holddown straps used for the engineered and prescriptive solutions for structures assigned a Seismic Design Category of C through E (based on the International Building Code). Consequentially, in 2012, an additional series of full-scale wall tests were conducted by APA to determine the effect from reduced strap capacity on the capacities of the portal frames.

## 2. Model Development

### 2.1 Overview

This paper presents a simple principle of mechanics model that was developed to predict the allowable stress design capacity of wood structural panel portal frames. The model treats the semi-rigid connections between the sheathing-to-header interface and the sheathing-to-sill plate interface as a fastener moment group. The tie-downs, when present, are treated as moment couples, adding to the capacity of the walls. The portal frame detail also uses a pier-to-header strap on the backside of the portal to increase out-of-plane stability. The addition of this strap is included in the model calculations. The model also accounts for shear capacity of the sheathing, the shear anchorage between the bottom plate and the foundation, and the shear nailing between the sheathing and the bottom plate of the walls. This model provides a method for one to calculate portal frame capacity for widths other than tested, as well as changing strap capacity.

The model was developed to predict the in-plane lateral racking strength,  $V$ , of a wood structural panel portal frame design. The general theory is provided in Equations 1-3 and Figure 2:

$$V = \text{Minimum of } V_{\text{moment couples}} \text{ and } V_{\text{shear strength}} \quad (1)$$

$$V_{\text{moment couples}} = (M_{\text{top}} + M_{\text{bottom}}) / H \quad (2)$$

$$V_{\text{shear strength}} = \text{Minimum of } v_{\text{panel}}, v_{\text{nails}}, \text{ and } v_{\text{base connection}} \quad (3)$$

Where:

- $M_{\text{top}}$  = Minimum of: sheathing to header fastener moment capacity plus moment capacity due to header strap, or sheathing bending strength plus the moment capacity due to header strap
- $M_{\text{bottom}}$  = Holddown (tie down) strap capacity times wall width plus sheathing to sill plate nailing moment capacity
- $H$  = Wall height
- $v_{\text{panel}}$  = Wood structural panel shear-through-thickness strength
- $v_{\text{nails}}$  = Wood structural panel-to-framing shear capacity
- $v_{\text{base connection}}$  = Shear capacity due to base of wall connections to supporting structure

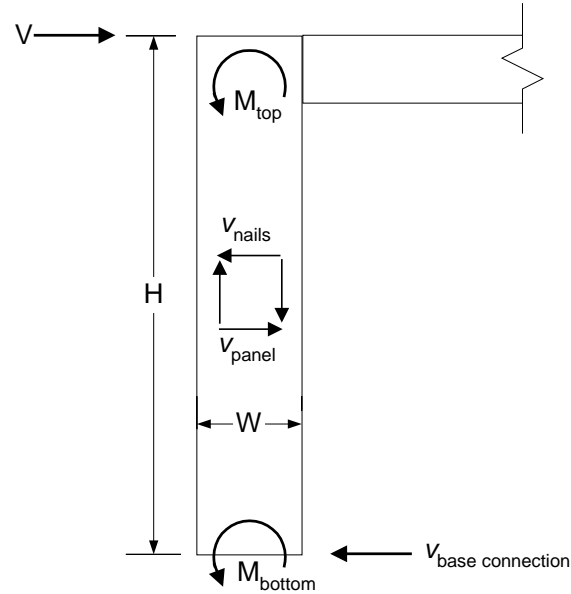


Figure 1. Principles of mechanics model to predict the strength of the wood structural panel portal frame.

## 2.2 Sheathing Fastener Moment Capacities

The fastener group moment capacities are calculated by first computing the polar moment of inertia of the fastener group. The single fastener allowable lateral load capacity is determined in accordance with the National Design Specification (NDS, 2012). Given the polar moment of inertia for the fastener group and the allowable single fastener lateral load capacity, the following formula is used to compute the allowable moment capacity of the connection:

$$M = Z'(J) / r \quad (4)$$

Where:

$Z'$  = single fastener allowable lateral load capacity per the NDS.

$J$  = polar moment of inertia

$r$  = distance to critical or average fastener.

The fastener group moment capacity can be computed using the average fastener or the critical fastener (that fastener located the furthest from the centroid of the fastener group). When using the distance to the critical fastener, the maximum moment is computed based on the assumption that the critical fastener will not exceed its allowable lateral load, and all other fasteners will be loaded to less than their allowable load.

When using the distance to the average fastener, the maximum moment is based upon a theoretical average fastener. The maximum moment of the fastener group is based on this fastener being stressed to its maximum allowable lateral load value. As a result of using the average fastener method, the moment capacity is increased at the expense of overstressing those fasteners that are further from the centroid of the fastener group than the theoretical average

fastener. Because of this, it is necessary to check the load on the critical fastener to see if the computed overload can be tolerated. Given the trend in the U.S. to going to capacity design, for this paper, the average fastener method was used.

In this paper, there are 5 different fastener moment capacity cases calculated, as shown in Figure 3. A calculation example for the “(1) Header Fastener Moment” for both critical and average distances is provided in Appendix A.

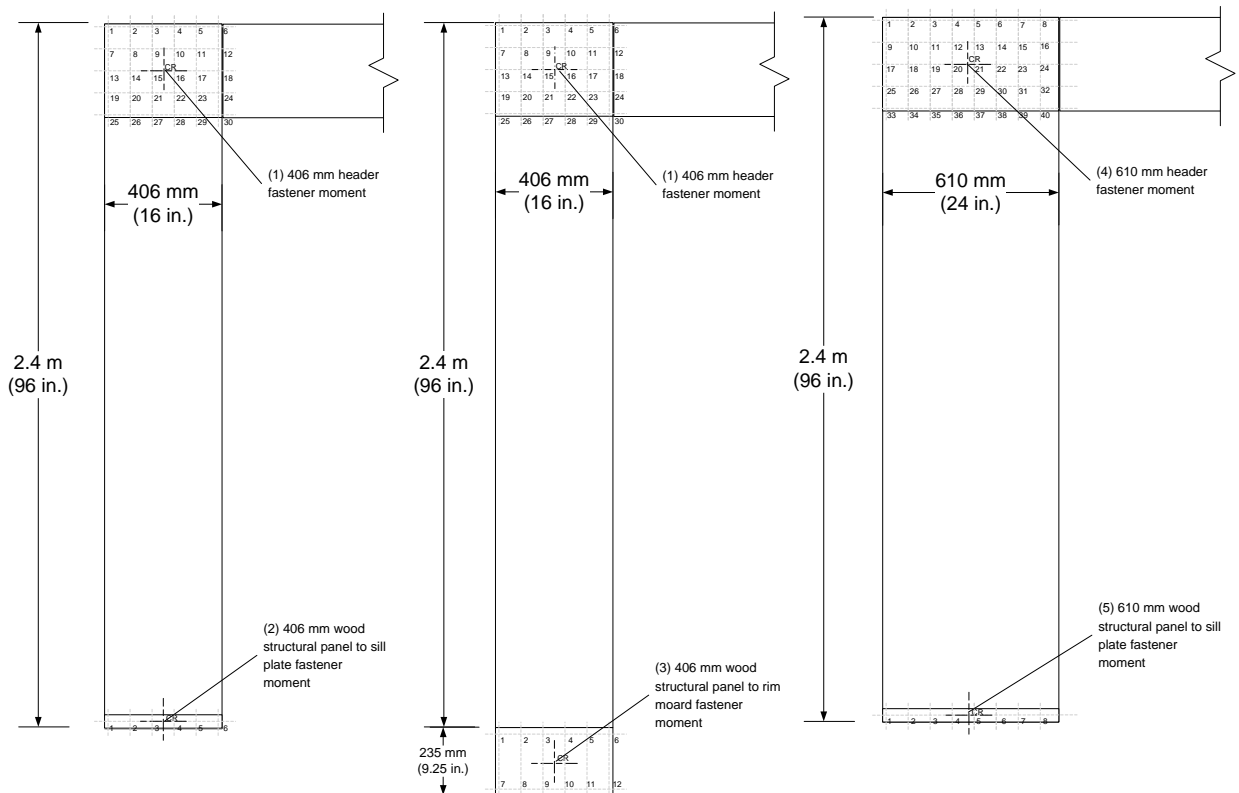


Figure 2. The five different fastener moment capacity cases

### 2.3 Calculation Procedure

The calculation procedure simply follows Equations 1 - 4. A complete example calculation for calculating the capacity of Wall #1 is provided in Appendix B. Material properties for the wood structural panels (plywood and OSB) are taken from the Plywood Design Specification (APA, 1998), Panel Design Specification, PDS (APA, 2012a), and APA Performance-Rated Rimboard (APA, 2009). The individual fastener properties, nails and anchor bolts are taken from the NDS (2012). The hold-downs (tie downs), header strap, and other framing anchors are taken from manufacturers’ catalogues at the time that the tests were conducted.

## 3. Calculation Results

The calculated results are completed for 17 different walls that have been tested at APA, as summarized in Table 1 (APA, 2002; 2003a; 2003b; 2004; 2006; 2012b; and 2012c). Following the calculation procedures previously described, Table 2 provides a summary of the calculated

values compared to the ultimate strength values divided by 3. In this report, the factor of 3 is used as the safety factor, or margin, between ultimate strength and “allowable” design value. Safety factors ranging from 2.5 to 3 have historically been used with wood shear wall assemblies, and the value of 2.8 is currently used in the product standard PS-2 (US-DOC, 2010) for wood structural panel (WSP) shear walls. All sheathing thicknesses were either 9.5 mm (3/8 in.) or 11 mm (7/16 in.), as shown in Tables 1 and 2. Note that for Wall #10, the sheathing was 9.5 mm (3/8 in.) plywood which has an effective thickness of 3.9 mm (0.155 in.), based on the provisions of Section 2.6, and published allowable bending values from the Plywood Design Specification (APA, 1998). The OSB edgewise design values were conservatively based on the values published for rimboards (APA, 2009). The shear through thickness values for both OSB and plywood were based on the Panel Design Specification (APA, 2012)

The tabulated values for the holddown capacities for Walls 1 – 10 were based on manufacturer’s literature that was current at the time of testing. For Walls 11 – 17, Simpson Strong-Tie STHD10RJ holddowns were used for all tests. The tabulated capacity of these holddowns, when all 28 nails were used, was 21.2 kN (4,755 lbf). This number was based on non-cracked concrete when used as a “mid-wall”. APA did not cast these straps into concrete, hence cracking and concrete edge distances were not considered as an issue. Additional tests of these portals were conducted by varying the strap capacity by reducing the number of nails to 20 nails and 17 nails, which was intended to simulate cracked concrete in high seismic areas. By using a simple ratio of the number of nails, the tested strap capacities were 15.1 and 12.9 kN (3,400 lbf and 2,890 lbf), respectively.

The wall series tested in Walls 1 – 10 were based on the sequential phase displacement method (SEAOSC, 1997), using a first major event (FME) equal to 30.5 mm (1.2 in). Walls 11 – 17 were tested in accordance with the CUREE protocol (ASTM, 2009), with a delta equal to 61 mm (2.4 in.).

## **4. Discussion of Results**

As shown in Table 2, the calculated results are very close to the tested results divided by a safety factor of 3 for a variety of tested boundary conditions. The predicted capacity agreed well with the tested capacities with the range of errors in predictions varied from -15% to +20%. Additional studies to this observation are being investigated. One observation is that, the wall configuration with dimensions of 610 mm x 2,440 mm (24 in. x 96 in.) was tested with four different holddown capacities (Walls 6, 13, 14 and 17). The tested lateral capacities ranged from 6.6 kN – 7.6 kN (1,476 lbf – 1,716 lbf). However, the predicted capacities ranged from 6.0 kN - 7.9 kN (1,363 lbf – 1,771 lbf). It can be observed that the wall capacities are not as sensitive to changes in strap capacity as the predictions are sensitive. This one wall configuration accounts for prediction errors ranging from -15% to +16%. It is possible that the moment at the bottom of the walls were being over-predicted, since the straps were being treated as one hundred percent effective moment couples. Due to the fact that the wood bottom plates are being subjected to compression perpendicular-to-grain, it is likely that the moment couples are indeed not fully effective. One might consider adding an empirical factor for reducing the “effectiveness” of the strap capacities, since the straps are almost certainly not one hundred percent effective. Regardless, on average, the model is providing reasonable results, and the prediction errors may not be too great for designers, especially given the large factors of safety used in adjusting the ultimate test values to allowable capacities.

Table 1. Summary of walls analyzed and APA Test Report Referenced

Wall #	Description	APA Test Report Reference
1	406 mm x 3,050 mm (16 in. x 120 in.) portal frame with 18.7 kN (4,200 lbf) hold down, 4.4 kN (1,000 lbf) header strap, 9.5 mm (3/8 in.) OSB	T2003-11: Tests 1 and 2
2	406 mm x 2,440 mm (16 in. x 96 in.) portal frame with 18.7 kN (4,200 lbf) hold down, 4.4 kN (1,000 lbf) header strap, 9.5 mm (3/8 in.) OSB	T2002-46: Test 3
3	406 mm x 2,440 mm (16 in. x 96 in.) portal frame with 18.7 kN (4,200 lbf) hold down, 10.7 kN (2,400 lbf) header strap, 9.5 mm (3/8 in.) OSB	T2002-46: Test 9
4	610 mm x 3,050 mm (24 in. x 120 in.) portal frame with 18.7 kN (4,200 lbf) hold down, 4.4 kN (1,000 lbf) header strap, 9.5 mm (3/8 in.) OSB	T2003-11: Tests 3 and 4
5	610 mm x 2,440 mm (24 in. x 96 in.) portal frame with 18.7 kN (4,200 lbf) hold down, 4.4 kN (1,000 lbf) header strap, 9.5 mm (3/8 in.) OSB	T2002-46: Test 5
6	610 mm x 2,440 mm (24 in. x 96 in.) portal frame with 18.7 kN (4,200 lbf) hold down, 10.7 kN (2,400 lbf) header strap, 9.5 mm (3/8 in.) OSB	T2002-46: Test 10
7	406 mm x 2,440 mm (16 in. x 96 in.) portal frame without hold down, 4.4 kN (1,000 lbf) header strap, 11 mm (7/16 in.) OSB	T2006-29: Test 9
8	406 mm x 2,440 mm (16 in. x 96 in.) portal frame on a raised floor with 3.0 kN (670 lbf) hold down, 4.4 kN (1,000 lbf) header strap, 9.5 mm (3/8 in.) OSB	T2004-38: Test 8
9	406 mm x 2,440 mm (16 in. x 96 in.) portal frame on a raised floor with 235 mm (9.25 in.) WSP overlap on rim board, 4.4 kN (1,000 lbf) header strap, 9.5 mm (3/8 in.) OSB	T2004-38: Test 10
10	406 mm x 2,440 mm (16 in. x 96 in.) portal frame without hold down, 4.4 kN (1,000 lbf) header strap, 9.5 mm (3/8 in.) plywood	T2006-29: Test 6
11	406 mm x 2,440 mm (16 in. x 96 in.) portal frame with 12.9 kN (2,890 lbf) hold down, 4.4 kN (1,000 lbf) header strap, 11 mm (7/16 in.) OSB	T2012-23 & T2012-24: Two replications
12	610 mm x 3,050 mm (24 in. x 120 in.) portal frame with 12.9 kN (2,890 lbf) hold down, 4.4 kN (1,000 lbf) header strap, 11 mm (7/16 in.) OSB	T2012-23 & T2012-24: Two replications
13	610 mm x 2,440 mm (24 in. x 96 in.) portal frame with 21.2 kN (4,755 lbf) hold down, 4.4 kN (1,000 lbf) header strap, 11 mm (7/16 in.) OSB	T2012P-24 Three replications
14	610 mm x 2,440 mm (24 in. x 96 in.) portal frame with 12.9 kN (2,890 lbf) hold down, 4.4 kN (1,000 lbf) header strap, 11 mm (7/16 in.) OSB	T2012P-23 Three replications
15	406 mm x 3,050 mm (16 in. x 120 in.) portal frame with 21.2 kN (4,755 lbf) hold down, 4.4 kN (1,000 lbf) header strap, 11 mm (7/16 in.) OSB	T2012P-24 Two replications
16	406 mm x 3,050 mm (16 in. x 120 in.) portal frame with 12.9 kN (2,890 lbf) hold down, 4.4 kN (1,000 lbf) header strap, 11 mm (7/16 in.) OSB	T2012P-23 Two replications
17	610 mm x 2,440 mm (24 in. x 96 in.) portal frame with 15.1 kN (3,400 lbf) hold down, 4.4 kN (1,000 lbf) header strap, 11 mm (7/16 in.) OSB	Unreported Two replications

Table 2. Summary of the calculated value and the tested values for the average fastener method.

#	Width (mm)	Height (mm)	Step 1. V based on moment couples													Step 2. V based on shear strength						Step 3.	Tested Lateral Capacity / 3 (kN)	Compared to Tested <sup>(d)</sup> %		
			M <sub>bottom</sub>				M <sub>top</sub>									V <sub>moment</sub>		V <sub>panel</sub>		V <sub>nails</sub>		V <sub>base</sub> connection (kN)			V <sub>shear</sub> strength (kN)	V <sup>(c)</sup> (kN)
			Tie down strap		WSP to Sill		Header Fastener M	Sheathing M				Header Strap			V <sub>moment</sub> couple (kN)	Shear through thickness		Nail		Z (N)	#nails/m					
			(kN)	M <sup>(a)</sup> (kN-mm)	M (kN-mm)	M <sub>bottom</sub> (kN-mm)		type	Fb (kPa)	t (mm)	M (kN-mm)	(kN)	M <sup>(b)</sup> (kN-mm)	M <sub>top</sub> (kN-mm)		Fvtv (N/mm)	V (kN)	Z (N)	V (kN)							
1	406	3048	18.7	6169	449	6618	2726	OSB	4137	9.5	1735	4.4	1638	3374	3.28	27.1	17.7	316	32.8	6.74	8.54	6.74	3.28	3.23	2%	
2	406	2438	18.7	6169	449	6618	2726	OSB	4137	9.5	1735	4.4	1638	3374	4.10	27.1	17.7	316	32.8	6.74	8.54	6.74	4.10	3.94	4%	
3	406	2438	18.7	6169	449	6618	2726	OSB	4137	9.5	1735	10.7	1735	3471	4.14	27.1	17.7	316	32.8	6.74	8.54	6.74	4.14	4.21	-2%	
4	610	3048	18.7	9965	809	10774	4458	OSB	4137	9.5	3905	4.4	2542	6447	5.65	27.1	26.5	316	32.8	10.11	8.54	8.54	5.65	5.38	5%	
5	610	2438	18.7	9965	809	10774	4458	OSB	4137	9.5	3905	4.4	2542	6447	7.06	27.1	26.5	316	32.8	10.11	8.54	8.54	7.06	7.43	-5%	
6	610	2438	18.7	9965	809	10774	4011	OSB	4137	9.5	3905	10.7	3905	7810	7.62	27.1	26.5	316	32.8	10.11	8.54	8.54	7.62	6.56	16%	
7	406	2438	0.0	0	462	462	2803	OSB	4137	11.1	2025	4.4	1638	3663	1.69	28.9	18.8	325	32.8	6.93	9.25	6.93	1.69	1.69	0%	
8	406	2438	3.0	984	0	984	2803	OSB	4137	9.5	1735	4.4	1638	3374	1.79	27.1	17.7	316	32.8	6.74	8.48	6.74	1.79	1.68	7%	
9	406	2438	0.0	0	1029	1029	2726	OSB	4137	9.5	1735	4.4	1638	3374	1.81	27.1	17.7	316	32.8	6.74	8.58	6.74	1.81	1.70	6%	
10	406	2438	0.0	0	399	399	2419	PLY	11376	3.9	1973	4.4	1638	3611	1.64	9.3	6.0	280	32.8	5.98	9.25	5.98	1.64	1.65	0%	
11	406	2438	12.9	4245	462	4707	2803	OSB	4137	11.1	2025	4.4	1638	3663	3.43	28.9	18.8	325	32.8	6.93	8.54	6.93	3.43	3.89	-12%	
12	610	3048	12.9	6857	831	7688	4584	OSB	4137	11.1	4556	4.4	2542	7098	4.85	28.9	28.2	325	32.8	10.39	8.54	8.54	4.85	5.71	-15%	
13	610	2438	21.2	11282	831	12113	4584	OSB	4137	11.1	4556	4.4	2542	7098	7.88	28.9	28.2	325	32.8	10.39	8.54	8.54	7.88	7.63	3%	
14	610	2438	12.9	6857	831	7688	4584	OSB	4137	11.1	4556	4.4	2542	7098	6.06	28.9	28.2	325	32.8	10.39	8.54	8.54	6.06	7.15	-15%	
15	406	3048	21.2	6984	462	7446	2803	OSB	4137	11.1	2025	4.4	1638	3663	3.64	28.9	18.8	325	32.8	6.93	8.54	6.93	3.64	3.05	20%	
16	406	3048	12.9	4245	462	4707	2803	OSB	4137	11.1	2025	4.4	1638	3663	2.75	28.9	18.8	325	32.8	6.93	8.54	6.93	2.75	2.76	0%	
17	610	2438	15.1	8067	831	8898	4584	OSB	4137	11.1	4556	4.4	2542	7098	6.56	28.9	28.2	325	32.8	10.39	8.54	8.54	6.56	6.92	-5%	

(a) Hold down M = strap capacity times width - 76.2 mm

(b) Header strap moment capacity = strap capacity times width - 38.1 mm, but shall not exceed sheathing moment capacity

(c) V = minimum of V based on moment couples and V based on shear strength

(d) Comparison is: (V/tested)-1 x 100%

average = 0%

## **5. Limitations**

The model presented is confirmed to be generally accurate for strength design. However, it does not include racking deflection. At present, racking deflection information can be obtained from the empirical data available in the original reports (APA, 2002; 2003a; 2003b; 2004; 2006; 2012b; and 2012c) or a deflection model could be developed. However, such a model could be rather complex.

The combined effects of vertical and lateral loads have also not been investigated in this study. It is theorized that the minimum required header stiffness “worst case” (a double 38.1 mm x 286 mm (nominal 2x12) with clear span of 5.6 m (18 ft)) provides sufficient rigidity under allowable vertical loads that it does not impart significant moment into the wall segment. On the other hand, the larger deformations associated with design lateral loads do impart moment (header fastener moment in Tables 2) into the header. Similar treatment of combined lateral and vertical loads can be seen in design information for prefabricated wood portal frame segments from Simpson Strong Tie (2012) and TrusJoist (2012).

## **6. Summary and Conclusion**

A principle of mechanics model is presented to determine the strength of wood structural panel portal frames. Details of the calculations, including complete sample calculations are provided. The analytical model compares very well to the test results for a range of portal frame constructions.

## **7. Acknowledgements**

The initial principle of mechanics model was developed by Zeno A. Martin, P.E., S.E. as a staff engineer at APA – The Engineered Wood Association.

## **8. References**

1. ACI. 2011. Building code requirements for structural concrete, ACI-318. American Concrete Institute, Farmington Hills, MI.
2. APA. 1998. Plywood design specification, Form No. Y510T. APA-The Engineered Wood Association. Tacoma, WA.
3. APA. 2002. Cyclic evaluation of APA Sturd-I-Frame for engineered design, APA Report T2002-46. APA-The Engineered Wood Association. Tacoma, WA.
4. APA. 2003a. Cyclic evaluation of APA Sturd-I-Frame with 10-ft height and lumber Header. APA Report T2003-11, APA-The Engineered Wood Association. Tacoma, WA.
5. APA. 2003b. Testing a portal frame design for use as bracing in fully sheathed structures, APA Report T2003-48. APA-The Engineered Wood Association. Tacoma, WA.
6. APA. 2004. A portal frame design on raised wood floors for use as bracing in fully sheathed structures, APA Report T2004-38. APA-The Engineered Wood Association. Tacoma, WA.
7. APA. 2006. Narrow wall bracing tests with no end restraint, APA Report T2006-29. APA-The Engineered Wood Association. Tacoma, WA.
8. APA. 2009. Performance rated rim board, Form No. W345K. APA-The Engineered Wood Association. Tacoma, WA.
9. APA. 2012a. Panel design specification (PDS), Form No. D510C, APA – The Engineered Wood Association, Tacoma, WA.

10. APA. 2012b. Bracing method PFH (portal frame with hold down) – alternative attachment – engineered values, APA Report T2012-23, APA-The Engineered Wood Association. Tacoma, WA.
11. APA. 2012c. Bracing method PFH (portal frame with hold down) – alternative attachment – prescriptive, APA Report T2012-24, APA-The Engineered Wood Association. Tacoma, WA.
12. ASTM International. 2009. Standard test methods for cyclic (reversed) load test for shear resistance of vertical elements of the lateral force resisting systems for buildings. ASTM E2126-09, West Conshohocken, PA.
13. AWC. 2012. ASD/LRFD National Design Specification (NDS) for Wood Construction, American Wood Council, Leesburg, VA.
14. ICC. 2012. International building code. International Code Council, Inc. Country Club Hills, IL.
15. SEAOSC. 1997. Standard Method of Cyclic (Reversed) Load Test for Shear Resistance of Framed Walls for Buildings. Structural Engineers Association of Southern California, Whittier, CA.
16. US-DOC. 2010. Performance standard for wood-based structural-use panels, PS 2-04, U.S. Department of Commerce, National Institute of Standards and Technology, Gaithersburg, MD.
17. Simpson Strong Tie. 2012. Wood Strong-Wall® garage portal systems on concrete foundations. webpage accessed on July, 2012.  
<http://www.strongtie.com/products/strongwall/wood-strongwall/garage-portal.asp>.
18. TrusJoist. 2012. TJ® Shear Brace, #TH-8620 Specifiers Guide.  
<http://www.woodbywy.com/literature/tj-8620.pdf>

Appendix A - A calculation example for the header fastener moment

**Fastener group moment capacity calculation (SI units)**

$Z = 325$  N/nail per NDS  
 $C_D = 1.6$   
 $Z' = 520$  N/nail  
 Width = 406.4 mm

Longest moment arm ( $r_{max}$ ) =	244 mm	
Critical fastener moment calculation =	<b>1824 kN-mm</b>	( $M = Z' \times J / r_{max}$ )
Average moment arm ( $r_{ave}$ ) =	159 mm	
Average fastener moment arm =	<b>2803 kN-mm</b>	( $M = Z' \times J / r_{ave}$ )
Load on critical fastener =	798 N	( $Z = M \times r_{max} / J$ )

Fastener	x (mm)	y (mm)	dx (mm)	dy (mm)	dx <sup>2</sup> (mm <sup>2</sup> )	dy <sup>2</sup> (mm <sup>2</sup> )	dx <sup>2</sup> +dy <sup>2</sup> (mm <sup>2</sup> )	r (mm)
1	0	305	-191	152	36290	23226	59516	244
2	76	305	-114	152	13064	23226	36290	191
3	152	305	-38	152	1452	23226	24677	157
4	229	305	38	152	1452	23226	24677	157
5	305	305	114	152	13064	23226	36290	191
6	381	305	191	152	36290	23226	59516	244
11	0	229	-191	76	36290	5806	42097	205
12	76	229	-114	76	13064	5806	18871	137
13	152	229	-38	76	1452	5806	7258	85
14	229	229	38	76	1452	5806	7258	85
15	305	229	114	76	13064	5806	18871	137
16	381	229	191	76	36290	5806	42097	205
21	0	152	-191	0	36290	0	36290	191
22	76	152	-114	0	13064	0	13064	114
23	152	152	-38	0	1452	0	1452	38
24	229	152	38	0	1452	0	1452	38
25	305	152	114	0	13064	0	13064	114
26	381	152	191	0	36290	0	36290	191
31	0	76	-191	-76	36290	5806	42097	205
32	76	76	-114	-76	13064	5806	18871	137
33	152	76	-38	-76	1452	5806	7258	85
34	229	76	38	-76	1452	5806	7258	85
35	305	76	114	-76	13064	5806	18871	137
36	381	76	191	-76	36290	5806	42097	205
41	0	0	-191	-152	36290	23226	59516	244
42	76	0	-114	-152	13064	23226	36290	191
43	152	0	-38	-152	1452	23226	24677	157
44	229	0	38	-152	1452	23226	24677	157
45	305	0	114	-152	13064	23226	36290	191
46	381	0	191	-152	36290	23226	59516	244
CR	190.5	152.4				J =	856450	

CR = center of rotation  
 dx = x distance from fastener to center of rotation  
 dy = y distance from fastener to center of rotation

Appendix B - A calculation example for the portal frame capacity

**Wood portal frame design value capacity by analysis. Example calculation for wall #1. Sheathed with 9.5 mm OSB (SI Units).**

Width = 406	mm
Height = 3048	mm
Tie <sub>down.strap</sub> = 18.7	kN, tie down strap allowable design value
M <sub>WSP.to.sill</sub> = 449	kN-mm, determined from fastener group moment capacity calculation
M <sub>header.fastener</sub> = 2726	kN-mm, determined from fastener group moment capacity calculation
Fb <sub>WSP</sub> = 4137	kPa, allowable bedding strength of OSB per APA publication W345
t = 9.5	mm, effective thickness of wood structural panel
Strap <sub>header</sub> = 4.45	kN, header strap allowable design value
F <sub>vtv</sub> = 27.1	N/mm, panel shear through the thickness from APA publication D510
Z = 316	N, from 2012 NDS Table 11Q for 8d common nails and 9.5 mm OSB
n = 32.8	number of nails per meter (based on 2 rows spaced at 76 mm o.c.)
V <sub>base.connection</sub> = 5.338·1.6	kN, value from 2012 NDS Table 11E for 15.9 mm anchor bolt bearing on 3 bottom plates. The 1.6 is the load duration factor from NDS Table 2.3.2.

**Step 1. Lateral load capacity, V, based on moment couples**

**Moment capacity at bottom of portal frame wall segment, M<sub>bottom</sub>:**

$$M_{\text{bottom}} = \text{Tie}_{\text{down.strap}} \cdot (\text{Width} - 76.2) + M_{\text{WSP.to.sill}}$$

Note: the 76.2 mm is subtracted to sum moment about tie down strap centerline.

$$M_{\text{bottom}} = 6616 \quad \text{kN-mm}$$

**Moment capacity at top of portal frame wall segment, M<sub>top</sub>:**

$$M_{\text{WSP}} = \text{Fb}_{\text{WSP}} \cdot \frac{(t \cdot \text{Width}^2)}{6 \cdot 10^6} \cdot 1.6 \quad M_{\text{WSP}} = 1728 \quad \text{kN-mm}$$

Note: the 38.1 mm is subtracted to sum moment about strap centerline.

$$M_{\text{header.strap}} = \min[\text{Strap}_{\text{header}} \cdot (\text{Width} - 38.1), M_{\text{WSP}}] \quad M_{\text{header.strap}} = 1637 \quad \text{kN-mm}$$

$$M_{\text{top}} = \min(M_{\text{WSP}}, M_{\text{header.fastener}}) + M_{\text{header.strap}} \quad M_{\text{top}} = 3365 \quad \text{kN-mm}$$

**Portal frame lateral load capacity based on moment couples, V<sub>moment couples</sub>:**

$$V_{\text{moment.couples}} = \frac{(M_{\text{bottom}} + M_{\text{top}})}{\text{Height}} \quad V_{\text{moment.couples}} = 3.27 \quad \text{kN}$$

### Step 2. Lateral load capacity, V, based on shear strength

Panel shear capacity,  $v_{\text{panel}}$ :

$$v_{\text{panel}} = \frac{F_{vtv}}{10^3} \cdot 1.6 \cdot \text{Width} \quad v_{\text{panel}} = 17.6 \quad \text{kN}$$

Nail shear capacity,  $v_{\text{nails}}$ :

$$v_{\text{nails}} = Z \cdot 1.6 \cdot n \cdot \frac{\text{Width}}{10^6} \quad v_{\text{nails}} = 6.73 \quad \text{kN}$$

Note: the 1.6 is the load duration factor from NDS Table 2.3.2.

Portal frame lateral load capacity based on shear strength,  $V_{\text{shear strength}}$ :

$$V_{\text{shear strength}} = \min(v_{\text{panel}}, v_{\text{nails}}, v_{\text{base connection}}) \quad V_{\text{shear strength}} = 6.73 \quad \text{kN}$$

### Step 3. Lateral load capacity, V, based on minimum of moment couples and shear strength

Predicted portal frame lateral load capacity:

$$V_{\text{avg}} = \min(V_{\text{moment couples}}, V_{\text{shear strength}}) \quad V = 3.27 \quad \text{kN}$$

Note: the average ultimate value based on testing / 3 = 3.22 kN APA Report T2003-11.



**INTERNATIONAL COUNCIL FOR RESEARCH AND INNOVATION  
IN BUILDING AND CONSTRUCTION**

**WORKING COMMISSION W18 - TIMBER STRUCTURES**

**SIMPLIFIED CROSS-LAMINATED TIMBER WALL MODELLING  
FOR LINEAR-ELASTIC SEISMIC ANALYSIS**

I Sustersic

B Dujic

CBD d.o.o. - Contemporary Building Design Company

SLOVENIA

**MEETING FORTY FIVE**

**VÄXJÖ**

**SWEDEN**

**AUGUST 2012**

---

Presented by I Sustersic

P Quenneville asked whether the corners would be relied upon for horizontal shear and the shear connectors were needed for wind and they should be considered along with the hold-downs. I Sustersic responded that the corners would not be relied on for shear resistance and their formulation considered every connection. R Žarnić received clarification about the contribution of the paper towards code. W Seim asked and received clarification of the spring element. He commented the bending was translated into shear in the model and asked whether uplift was considered. I Sustersic responded that the model did not consider uplift. W Seim received further clarification that the diaphragm was considered rigid in the model. W Seim stated that there was a strong statement of the potential application of the model in analysis; however, this depended on the details and limitation of the model; ie. if you were not real exact in the model one must be careful with the claims. I Sustersic agreed and stated the model must be verified.



# Simplified cross-laminated timber wall modelling for linear-elastic seismic analysis

Iztok Sustersic

CBD d.o.o. - Contemporary Building Design Company, Slovenia

Bruno Dujic

CBD d.o.o. - Contemporary Building Design Company, Slovenia

## 1 Introduction

The reference method of Eurocode 8 [1] for determining the seismic effects on a building is the modal response spectrum analysis, using a linear-elastic model of the structure and the design spectrum. A simpler lateral force method is also allowed, however it can only be used for buildings regular in plan and elevation and conditionally for buildings regular only in plan. Unfortunately for the designers a vast majority of today's buildings does not comply with such criteria. Consequently the linear modal analysis (or any type of the nonlinear methods) must be used.

One of the most important parameters when using the modal analysis is the horizontal stiffness of a building. Stiffness and mass determine the structure's vibration periods and hence the influence of an earthquake's frequency content on a structure's response. If a low-rise (only ground floor) building's vibration periods are overestimated (too long) the resulting seismic forces can yield too conservative. If the periods are underestimated (too short), the results yield on the non-conservative side. The situation is just the opposite for higher buildings where the overestimated periods yield on the non-conservative side and vice versa. Hence great care must be taken in assigning the wall's correct stiffness. More specific case studies that demonstrate the consequence of neglecting the connection stiffness are presented in Sustersic et.al. [2] and Fragiacomio et.al. [3].

In the case of crosslam the stiffness is predominantly dependent of the shear angular bracket and hold-down behaviour. However, openings in panels greatly reduce their stiffness. The influence of vertical joints between adjacent panels also needs to be taken into account.

The evolution of the proposed finite element model (if using a substitute diagonal) is presented in Figure 1, from top left to bottom right. The top left figure (*Fig. 1(i)*) shows a possible crosslam wall assembly. The left wall panel is full and the right panel has a window opening cut into it. Both panels are connected together at the adjacent sides over a

step joint and self-tapping screws. At the top and bottom the panels are attached to the floor plates with angular brackets and/or hold-downs.

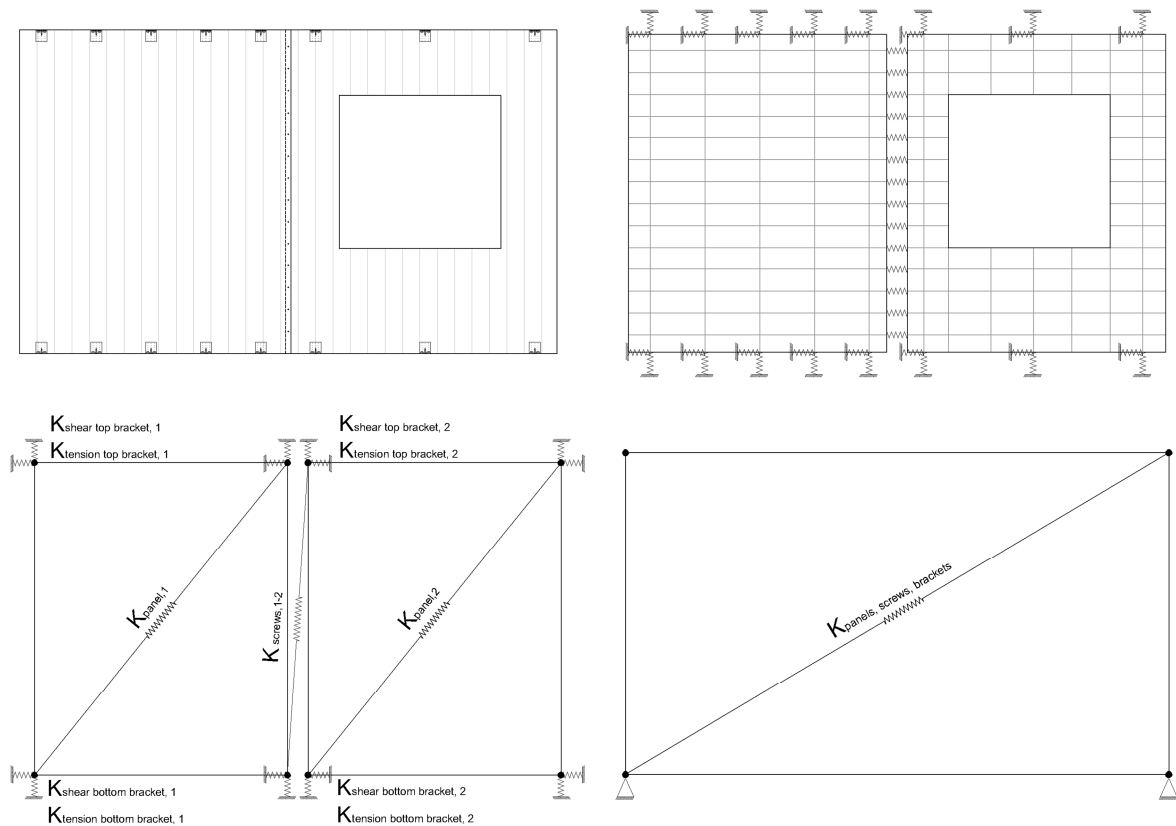


**Figure 1:** (i) Actual crosslam wall assembly (top left), (ii) a detailed finite element (FE.) model (top right), (iii) a partially simplified FE model (bottom left) and (iv) the fully simplified FE model

The top right figure (Fig. 1(ii)) shows an exact FE model where shell elements are used to model crosslam panels and springs (linear or nonlinear) are used to model the brackets. Springs are also used for modelling the screws in the step-joint between the panels. In the bottom left figure (Fig. 1(iii)) the first simplification is shown – instead of using shell elements, the crosslam panels are modelled with substitution diagonals (trusses) and individual springs used in the exact model are joined together in discrete points in the corners of the new trusses. Such a model has already been used by researchers for nonlinear dynamic analysis (NLDA), however the trusses presenting crosslam panels were modelled completely stiff [4]. The latter simplification may be tolerable to some extent for nonlinear dynamic analysis. When using linear static analysis, too stiff trusses may contribute to errors that should not be neglected [2, 3]. The bottom right figure (Fig. 1(iv)) shows the fully simplified FE model, where the influences of the crosslam panels, top and bottom brackets and vertical connections are joined together in the substitution diagonal. It must be noted, however, that such a truss simplification is mostly suitable for linear elastic design as it is practically impossible to analytically join the nonlinear hysteretic response of all the aforementioned parameters in a single element. Linear elastic design on the other hand only demands the correct stiffness. The failure mechanism is only force dependent, hence a substitute diagonal can provide enough feedback. Though technically such a simplified approach could also be used for nonlinear static analysis and displacement based design methods (i.e. the N2 method [5]) if several plastic hinges were to be incorporated in

the diagonal element.

## 2 Equations for wall horizontal stiffness

In this paper we only present equations for walls that are connected at the bottom (cantilever-like walls).

### 2.1 Crosslam panel stiffness

The stiffness of a single crosslam wall panel, connected at the bottom is calculated as:

$$k_{\text{panel}} = \frac{3E I_{\text{eff}} G A_s}{3E I_{\text{eff}} H + G A_s H^3} \quad (1)$$

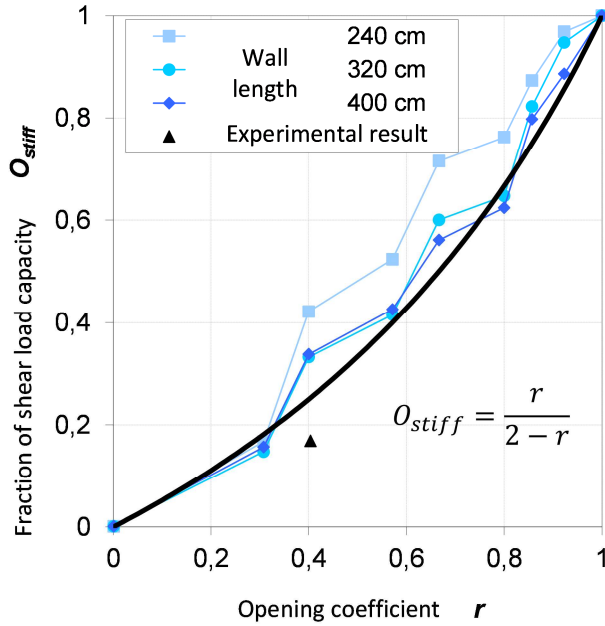


**Figure 2:** Stiffness reduction of crosslam panels based on Sugiyama's panel area ratio ( $r$ ) and stiffness reduction factors ( $O_{stiff}$ ) by Dujic

where  $E$  is the main elastic modulus parallel to grain and  $I_{\text{eff}}$  is the effective radius of gyration for a given cross section.  $G$  is the shear modulus of timber,  $A_s$  is the effective shear cross section and  $H$  is the wall height.  $I_{\text{eff}}$  is calculated according to the method proposed by Blass and Fellmoser [6]. The effective shear cross section  $A_s$  can be calculated by taking into account the full cross section of a wall if the adjacent lamellas in a layer are glued together on the narrow side as well. If not a reduction of the shear cross section is appropriate [2, 3, 7, 8]. The influence of openings can be indirectly taken into account with Sugiyama's panel area ratio ( $r$ ) [9] and stiffness reduction factors proposed by Dujic [10].

Therefore the stiffness of a panel with openings can be expressed as:

$$k_{\text{panel,eff}} = O_{stiff} k_{\text{panel}} \quad (2)$$

### 2.2 Wall connection stiffness

The bending stiffness of a panel's bottom connection can be expressed as:

$$K_{c,bend} = \frac{(\sum K_i L_i^2)}{H^2} + \frac{q_{\text{vert}} L_{\text{eff}}^2 K_n L_n}{2H^2 R_{c,n,Rd}} \quad (3)$$

where  $K_i$  is the stiffness of an individual connector,  $L_i$  is the distance of that connector from the point of rotation ( $A$ ).  $L_{\text{eff}}$  is the length of the wall panel from the point of rotation to the other end of the panel and may be estimated as  $0.9L$  to  $0.95L$  (for moderately connected and loaded panels) where  $L$  is the complete wall panel length. The vertical line load on the top of a wall is denoted by  $q_{\text{vert}}$ .  $R_{c,n,Rd}$  and  $K_n$  denote the design strength in the wall edge connection respectively. The stiffness values of connections and their strength can be derived in accordance with the Yasumura-Kawai procedure [11] if experimental

results are available. Namely, stiffness equations from Eurocode 5 [12] yield to high values.

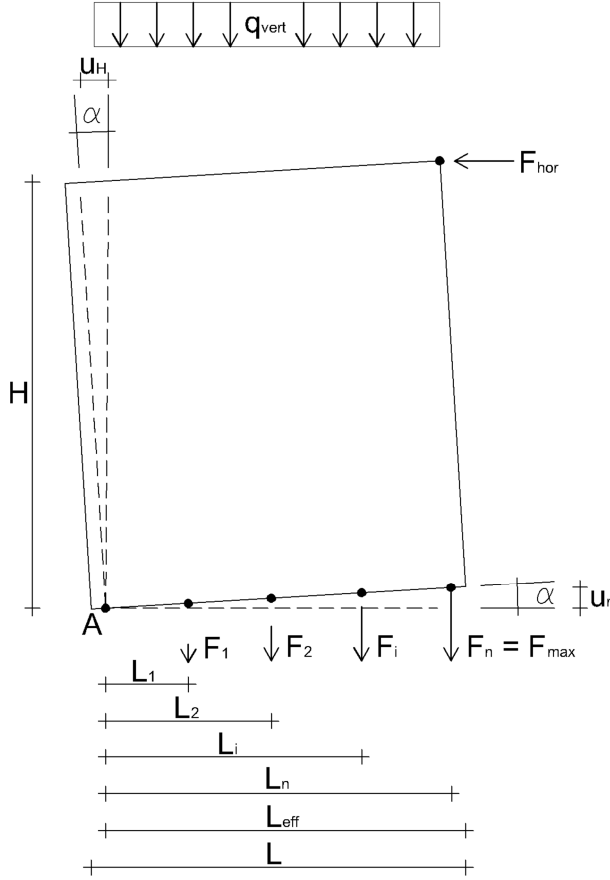


Figure 3: Equilibrium of forces on a single crosslam panel

The connection's shear stiffness is the sum of individual connectors shear stiffness ( $K_{c,i, shear}$ ) and the contribution of friction stiffness:

$$K_{c, shear} = \sum K_{c,i, shear} + \frac{q_{vert} L A_w c}{u_{slip, Rd}} \quad (4)$$

where  $u_{slip, Rd}$  is the slip of the weakest connector at the design strength according to the bilinearised response curve (at the curves' shifting point),  $c$  is the dynamic friction coefficient and  $A_w$  is the wall contact surface cross section.

The influence of screwed vertical connections between adjacent panels can also be implicitly taken into account and expressed in terms of a panels horizontal stiffness as:

$$K_{c, step} = \frac{K_{vert} L_{eff}^2}{H^2} \quad (5)$$

where  $K_{vert}$  is the sum of shear stiffness of screws in the vertical connection between two panels. However it must be noted that the upper equation is only valid up to a limited extent and for panels of approximately equal size.

### 2.3 Combined stiffness

We combine the horizontal stiffness of panels and connections into one single equation:

$$K_{wall} = \sum \left[ \left( \frac{1}{k_{panel, eff, i}} + \frac{1}{K_{c, bend, i}} + \frac{1}{K_{c, shear, i}} \right)^{-1} + K_{c, step, i} \right] \quad (6)$$

### 2.4 Case study

A crosslam wall panel setup similar to the one in Figure 1 with the exception of both walls being full (no openings) is analysed. The left panel is anchored at the bottom with 3 BMF 105 angular brackets. The right panel is attached with 5 brackets of the same type. No top connections are considered. The vertical step joint is connected with five 8 mm screws. The crosslam panels are 95 mm thick, 200 cm long (each) and 300 cm high. The bottom support is very stiff (i.e. concrete foundation). Friction is neglected and as no vertical load is applied we also presume that the rotation point (point  $A$  in Figure 3) is in the walls corner. A horizontal load of 100 kN is evenly applied along the top of the wall. The horizontal displacements at the top of the wall are compared; a precise finite element model (like in Figure 1(ii)) against the proposed simplified model (Figure 1(iv)). A relative displacement (displacement (ii) / displacement (iv)) comparison is presented in Figure 4.

The following models are compared; Case 10) where we compare the basic timber panels and hence the precision of *Equation 1*. In cases 21) and 22) the first parts of *Equations 3* and *4* checked. Case 30) displays the comparison between the step joint stiffness (*Equation 5*) if both panels are modelled stiff, however can freely pivot around their corners. Following in cases 41) and 42) *Equations 1, 3* and *4* are combined to see how their results collate with more precise FE models that consider crosslam panels along with connections. In the case 51) *Equations 1, 3, 4* and *5* are joined and the complete wall setup is compared. The last two cases again deal with the complete wall setup, however in case 52) the crosslam panels are modelled stiff and in case 53) the step joint is neglected.

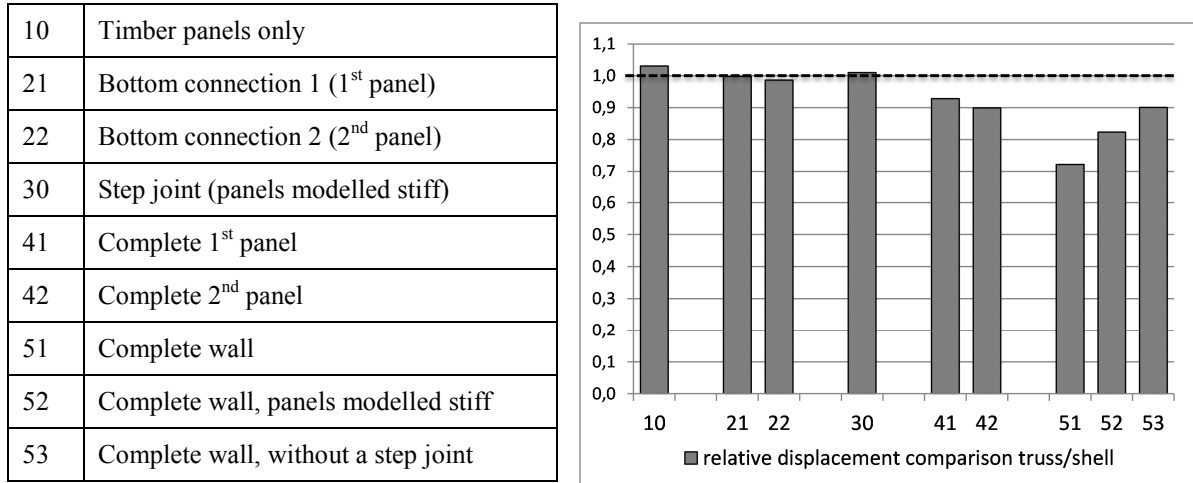


**Figure 4:** Relative displacement comparison of precise FE models (ii) and the simplified proposal (iv)

Discrepancies occur for combined stiffness (cases 42-53). The agreement between individual stiffness of panels (case 10), bottom connections (cases 21, 22) and the vertical step joint connection (case 30) is very good. However, the step joint has a significant influence on the wall assembly if the panels are not modelled stiff – compression and tension strains in individual crosslam panels occur in the vertical direction of the step joint causing a more flexible construction (case 51). That is something the proposed model does not deal with yet – additional vertical strains still need to be implemented.

### 3 Equations for wall horizontal strength

Again we only present equations for walls that are connected at the bottom (cantilever-like walls).

#### 3.1 Crosslam panel strength

The bending strength of a single crosslam wall panel, connected at the bottom:

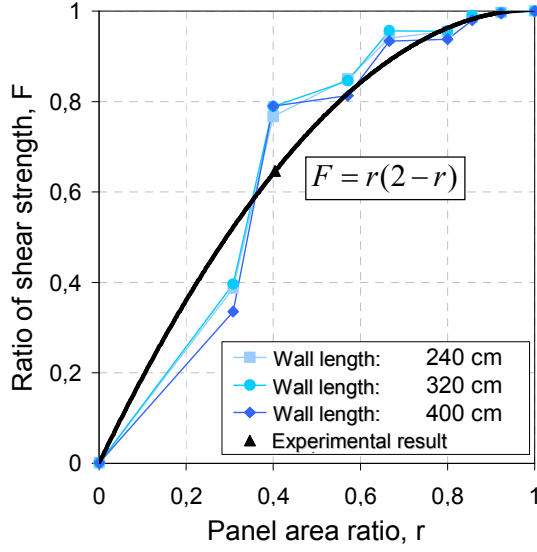
$$R_{p,bend} = \frac{W_{eff} f_{m,d}}{H} \quad (7)$$

The shear strength of the same crosslam panel is:

$$R_{p, shear} = A_s f_{v,d} \quad (8)$$

Where  $f_{m,d}$  is the design bending strength and  $f_{v,d}$  the design shear strength. The effective radius of strength  $W_{eff}$  is calculated according to Blass and Fellmoser [6]. The influence of

openings is again taken into account with the use of Sugiyama-Dujic factor for strength reduction:



$$R_{p, shear, eff} = O_{strength} R_{p, bend} \quad (9)$$

$$R_{p, shear, eff} = O_{strength} R_{p, shear} \quad (10)$$

where  $O_{strength}$  is calculated according to the formula in Dujic [10]:

$$O_{strength} = r(2 - r) \quad (11)$$

with  $r$  again being the panel ratio from Sugiyama [9].

### 3.1 Panel connection strength

The bending and shear strength of a wall panel connection in terms of horizontal strength are calculated according to *Equations 12* and *13* respectively:

$$R_{c, bend, Rd} = \frac{(\sum K_i L_i^2) R_{c, n, Rd}}{K_n L_n H} + \frac{q_{vert} L_{eff}^2}{2H} \quad (12)$$

$$R_{c, shear, Rd} = \sum R_{c, i, shear, Rd} + q_{vert} A_w c \quad (13)$$

where  $c$  is the dynamic friction coefficient and  $A_w$  is the wall contact surface cross section.

As the strength of the panel and connections are now clearly separated the overstrength factors ( $\gamma_{Rd}$ ) for steel angular brackets (Sustersic et.al [2] Fragiaco et.al [3]) can easily be incorporated and the crosslam panels can be sufficiently oversized to prevent a brittle failure in timber.

## Conclusions

In the paper we have derived equations for a simplified analysis of a crosslam structure's stiffness and strength that are suitable when performing a seismic linear elastic modal response spectrum analysis. The equations are divided into two separate categories, namely the timber panels and connections. The later enables a practical implementation of connection overstrength factors that allow the timber panels to be sufficiently oversized to prevent brittle failure. The influence of openings in timber panels is implicitly taken into account with strength and stiffness reduction factors. Through a simple case study it was demonstrated that the equations are already quite suitable for the use with single story structures with an irregular floor plan (that demands the use of a modal analysis). Further development of the method and more case studies are needed in order for the method to be completely applicable also to the multi-storey structures. However the consideration of friction in crosslam FE models is a general discussion topic that needs additional experimental evaluation.

## 8 Acknowledgements

The research support provided to the first author by the EU through the European Social Fund 'Investing in your future' is gratefully acknowledged.



## 9 References

- [1] European Committee for Standardization (CEN). Eurocode 8—Design of structures for earthquake resistance. Part 1: General rules, seismic actions and rules for buildings. prEN 1998-1; Brussels, 2003.
- [2] Sustersic I, Fragiaco M, Dujic B. 2011. Influence of connection properties on the ductility and seismic resistance of multi-storey cross-lam buildings. Meeting 44 of the Working Commission W18-Timber Structures, CIB, Alghero, Italy
- [3] Fragiaco M, Dujic B, Sustersic I. 2011. Elastic and ductile design of multi-storey crosslam massive wooden buildings under seismic actions. Engineering structures, Volume 33, Issue 11, pages 3043-3053.
- [4] Ceccotti A. New technologies for construction of medium-rise buildings in seismic regions: the XLAM case. IABSE Structural Engineering International, Special Edition on Tall Timber Buildings 2008, 18(2):156-165.
- [5] Fajfar P. A nonlinear analysis method for performance-based seismic design. Earthquake Spectra 2000; 16(3):573-592.
- [6] Blass HJ, Fellmoser P. Design of solid wood panels with cross layers. 8th World Conference on Timber Engineering, WCTE 2004, Lahti, Finland; 543-548.
- [7] Jöbstl R. A, Bogensperger TH, Schickofer G. In-plane Shear Strength of Cross laminated Timber. 2008. Meeting 41 of the Working Commission W18-Timber Structures, CIB; 2008, St. Andrews (Canada).
- [8] Moosbrugger T, Guggenberger W, Bogensperger T. Cross-Laminated Timber Wall Segments under homogeneous Shear with and without Openings. 2006. WCTE 2006 - 9th World Conference on Timber Engineering - Portland, OR, USA.
- [9] Yasumura M, Sugiyama H. Shear properties of plywood-sheathed wall panels with opening, Transactions of the Architectural Institute of Japan 1984; 338:88-96.
- [10] Dujic B, Klobcar S, Zarnic R. Influence of openings on shear capacity of wooden walls. Research report, 2005, University of Ljubljana and CBD Contemporary Building Design Ltd, Slovenia.
- [11] Yasumura M, Kawai N. Evaluation of wood framed shear walls subjected to lateral load. Meeting 39 of the Working Commission W18-Timber Structures, CIB; 1997, Vancouver (Canada), paper CIB-W18/30-15-4.
- [12] European Committee for Standardization (CEN). Eurocode 5 – Design of timber structures – Part 1-1: General rules and rules for buildings; 2004, Brussels, Belgium.



**INTERNATIONAL COUNCIL FOR RESEARCH AND INNOVATION  
IN BUILDING AND CONSTRUCTION**

**WORKING COMMISSION W18 - TIMBER STRUCTURES**

**THE REDUCED CROSS SECTION METHOD FOR TIMBER MEMBERS  
SUBJECTED TO COMPRESSION, TENSION AND BENDING IN FIRE**

M Klippel

ETH Zürich, Institute of Structural Engineering IBK, Zürich  
SWITZERLAND

J Schmid

SP Technical Research Institute of Sweden  
SWEDEN

A Frangi

ETH Zürich, Institute of Structural Engineering IBK, Zürich  
SWITZERLAND

**MEETING FORTY FIVE**

**VÄXJÖ**

**SWEDEN**

**AUGUST 2012**

---

Presented by M Klippel

S Winter asked which strength values were considered. M Klippel responded mean strength values from Eurocode were considered. S Winter asked whether solid timber or glulam. M Klippel stated it did not matter as the study considered the reduction. Also the member was considered as stub column i.e. no buckling. They will study intermediate and long columns later. S Winter commented that information on the temperature to strength relationship was weak and we had to try and make new tests and one to one scale test to establish more reliable data on temperature to strength relationship. M Klippel agreed. J Schmid clarified that on slide 20 EN1995-1-2 for small members the zero strength layer was much larger. Also as far as temperature strength curves, they were doing full scale tests. J König stated that according EC5 strength did not have to be reduced for temperature increase until after 60°C which applied to continuous heating of members e.g. in roof attic. The fire situation is transient and the EC5 provisions derived from fire tests include load duration, moisture effect etc. A Jorissen stated that EC5 had two methods i.e. also the reduced properties method. He asked if there would be agreement if the results from this study were compared to the reduced properties method. M Klippel stated that they had not yet done so. A Frangi stated that there was background information that the reduced properties method was inaccurate and should be deleted. J König stated that there would be a difference between the methods as we knew the reduced properties method was incorrect. The fire people are still working on this issue. S Winter stated that with the adoption of fire design method since the last decade there had not been reports of serious fire damage based on this method. We have to look into the design principle versus outcome. Simplicity for designer and impact to designs should be considered and one should not make the work too theoretical. The issue of the validity of the properties reduction method for small cross section versus large cross section is an issue. J Schmid responded that the likelihood of fire was not a subject of this paper. S Aicher commented that the results showed we were unsafe for stub columns. J König stated that what the safety was in case of fire was an important issue that required more studies.



# The Reduced Cross-Section Method for timber members subjected to compression, tension and bending in fire

Michael Klippel\*

Joachim Schmid\*\*

Andrea Frangi\*

\* ETH Zürich, Institute of Structural Engineering IBK, Zürich, Switzerland

\*\* SP Technical Research Institute of Sweden

## Abstract

For the design of timber members exposed to fire the “Reduced Cross-Section Method” provides a popular design method using an effective cross-section and mechanical properties at normal temperature. The method was originally developed for single span bending beams but the field of application was extended by e.g. standards and handbooks to different types of members subjected to tension, compression as well as to timber members with significantly different geometry. In this paper results of numerical simulations are presented for fire exposed timber members in tension, compression and bending. The results show that the zero-strength layer clearly depends on time of fire exposure, state of stress and dimensions of the cross-section. For members in tension, the current standard constant value for the zero-strength layer of 7 mm seems to be enough accurate while for members in compression a depth of the zero-strength layer larger than 7 mm would have been more appropriate.

## 1 Introduction

Fire reduces the cross-section as well as the stiffness and strength of the heated timber close to the burning surface. The heat-affected zone of an initially unprotected timber member below the char layer is approximately 35 to 40 mm deep [1, 2]. Within this zone, the temperature decreases from 300 °C at the char line to normal temperature (20 °C). Due to the transport of moisture (steam) from wood heated above 100 °C to the inner cooler parts of the cross-section, and condensation of steam in the cooler zones, the moisture content varies in the heat-affected zone, with a moisture peak where the temperature is near but below 100 °C [1]. The combined effect of elevated temperature and moisture affects both strength (tensile and compressive) and stiffness (modulus of elasticity). Thus, each point in the heated zone exhibits different strength and stiffness values, contrary to the situation in a steel member, where the temperature distribution is more homogeneous and therefore, strength and stiffness are approximately uniform in the whole cross-section. While for steel members the reduction of yield strength is the governing parameter, definition of failure criteria for timber members exposed to fire is more complicated. A rigorous analysis of a timber member would have to take into account the temperature and moisture gradients in the cross-section. For everyday design of fire-exposed timber structures, this would be too complex and costly, and so simplified design methods with fairly good accuracy and reliability have been developed. The most common design method is based on the concept of effective cross-section, which allows for easy-to-use

methods for the design of fire-exposed timber structures. This method is called “Reduced Cross-Section Method” (RCSM) according to EN 1995-1-2 [3] and considers the strength and stiffness reduction near the charred layer by adding an additional depth  $k_0 \cdot d_0$  (called zero-strength layer) to the notional charred layer  $d_{\text{char},n}$  (see Figure 2). It is assumed that this zero-strength layer is built up linearly with time during the first 20 minutes of fire exposure, after which it remains constant with 7 mm. This approach was originally derived for glued-laminated timber beams for which the depth of the zero-strength layer was given as 0.3 inch (7.6 mm) [4]. This method allows the designer to use strength and stiffness properties at normal temperature for the resulting effective cross-section. Thus, the temperature-dependent reduction factor for strength and stiffness is taken as  $k_{\text{mod},fi} = 1,0$  for the effective cross-section.

This paper deals with the RCSM, originally developed for glued-laminated timber beams exposed to fire on three or four sides [1]. Using appropriate values for the zero-strength layer, the RCSM can be applied for a wide range of timber members, e.g. for timber frame members in wall and floor assemblies with cavity insulation, timber I-joists and cross-laminated timber decks, as well as dowelled connections with slotted-in steel plates in tension [5, 6, 7, 8]. However, the zero-strength layer depends on different parameters and differs from the constant value given in EN 1995-1-2 [3]. This paper shows the results of numerical simulations on timber members subjected to compression, tension and bending. The results of the numerical simulations allow the calculation of the zero-strength layer and the comparison with the current approach.

## 2 Numerical simulations

To calculate the temperature distribution in the cross-section of a timber member a thermal numerical analysis was performed using two-dimensional finite element models implemented in ABAQUS [9] and SAFIR [10] respectively. The temperature development and distribution in the cross-section was then used as input for the mechanical analysis. The heat transfer to the member’s surface was modelled using temperature-independent constant values according to EN 1991-1-2 [11] for the resultant emissivity by radiation  $\epsilon_{\text{res}} = 0.8$  and the coefficient of heat transfer by convection  $\alpha_c = 25 \text{ W}/(\text{m}^2 \cdot \text{K})$ . Density, thermal conductivity and specific heat capacity of wood and charcoal vary as a function of temperature. The evaporation of water at a temperature of about 100 °C was simplified and implemented into the FE-simulation as latent heat. Mass transfer of moisture into or out of the wood was neglected since this is considered using effective relationships for specific heat and thermal conductivity [12]. In the FE-thermal analysis, charring of wood (i.e. reduction of cross-section) was taken into account by gradually changing the thermal properties of wood into those of charcoal with increasing temperature. For the FE-thermal analysis, an initial density of 450 kg/m<sup>3</sup> and an initial moisture content of 12 % were considered. The temperature-dependent relationships for the density and specific heat of wood and charcoal were implemented according to EN 1995-1-2. Cracks in the charcoal increase the heat flux due to radiation and convection. Thus, the thermal conductivity values of the char layer used in FE-thermal analyses are “effective” values rather than “real” material properties in order to take into account the increased heat flux due to cracks above about 500 °C and the degradation of the char layer at about 1000 °C [12]. For the FE-thermal analysis, the temperature-dependent relationship for the thermal conductivity of wood and charcoal was assumed according to EN 1995-1-2. The material properties of wood and charcoal used for the FE-thermal analysis were verified with a series of fire tests [13] on spruce specimens exposed to ISO-fire only on one side. The specimens had a

dimension of 225 mm × 95 mm and moisture content of about 12 %. Temperatures were measured in a depth of 6, 18, 30, 42 and 54 mm from the surface exposed to fire. Figure 1, left shows the comparison between fire tests and FE-results for the temperatures measured at different depths. Experimental and numerical results are in good agreement.

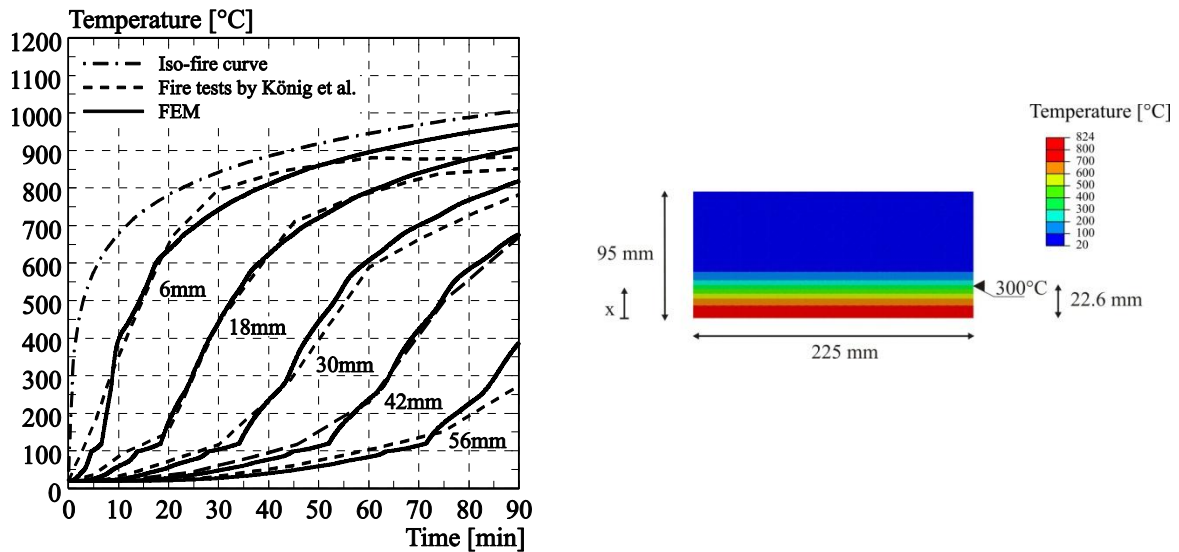


Figure 1. Comparison of measured [13] and calculated temperatures at different timber depths (left); temperature distribution in the cross-section (225 mm × 95 mm) after 30 min fire exposure (right)

For the present investigations, two-dimensional thermal analyses were performed with squared or rectangular cross-sections with width varying between 48 and 248 mm. The geometry and size of the cross-section is one of the most important parameter that influences the fire resistance. The cross-sections were exposed to standard ISO-fire according to [14] on all four sides for the members subjected to compression and tension. Whereas the members subjected to bending were exposed to fire on three sides, with the exposed side in tension (single span beams).

The temperature distribution in the cross-section was then used as an input for the mechanical analysis. Strength and stiffness mean values at normal temperature were used as input parameters, i.e. compressive, tensile and bending strengths  $f_{c,mean}$ ,  $f_{t,mean}$  and  $f_{m,mean}$  as well as  $E_{0,mean}$ . To account for the temperature-dependent material behaviour of timber, EN 1995-1-2 gives in Annex B bi-linear temperature-strength and stiffness relationships from 20 to 300 °C with breakpoints at 100 °C, also taking into account the effects of transient moisture situations and creep. Regions with temperature higher than 300 °C are not considered as the strength of timber is assumed to decrease to zero for a temperature of 300 °C [12, 15]. The 300°C isotherm is widely accepted as a rounded value for the definition of the position of the charring depth.

The mechanical analysis was performed with the help of a Visual Basic macro embedded in Excel. The cross-section's resistance for compression, tension and bending was determined for normal conditions ( $t=0$ ) and for different times of ISO-fire exposure. Knowing the temperature distribution for a defined time of fire exposure, the residual cross-section defined as the nodes of the mesh with a temperature lower than 300 °C as well as the resistance for compression, tension and bending were calculated. Failure of the member was assumed at the time when the resistance for compression, tension and bending reached 30 % of the resistance at normal temperature ( $F_{R,fi}/F_{R,20°C} = 0.3$  and

$M_{R,fi}/M_{R,20^\circ C} = 0.3$ , respectively). This value represents a typical ratio expected for the design of structural timber members.

As a basic value, the one-dimensional charring rate  $\beta_0$  is usually taken as the value observed for one-dimensional heat transfer under ISO-fire exposure in a semi-infinite timber slab. EN 1995-1-2 gives a value of  $\beta_0 = 0.65$  mm/min for softwood. In order to take into account the effects of corner roundings and fissures and to simplify the calculation of cross-sectional properties (area, section modulus and second moment of area) by assuming an equivalent rectangular residual cross-section, design codes generally define charring rates greater than the one-dimensional charring rate. The charring rate including these effects is called the notional charring rate  $\beta_n$  according to EN 1995-1-2 and for example for glued laminated timber a value of  $\beta_n = 0.7$  mm/min can be assumed, while for solid timber  $\beta_n = 0.8$  mm/min.

Figure 2 shows the definition of the notional charring depth  $d_{char,n,advanced}$  used for the present investigations. The notional charring rate  $\beta_{n,advanced}$  was calculated with the help of the residual cross-section derived from the thermal finite element and the mechanical analysis with the following equation:

$$\beta_{n,advanced} = \frac{a - \sqrt{A_{fi,advanced}}}{2 \cdot t_{Failure,advanced}} \quad (1)$$

Where  $A_{fi,advanced}$  corresponds to the residual cross-section (see Figure 2) being the area with temperatures lower than  $300^\circ C$ .

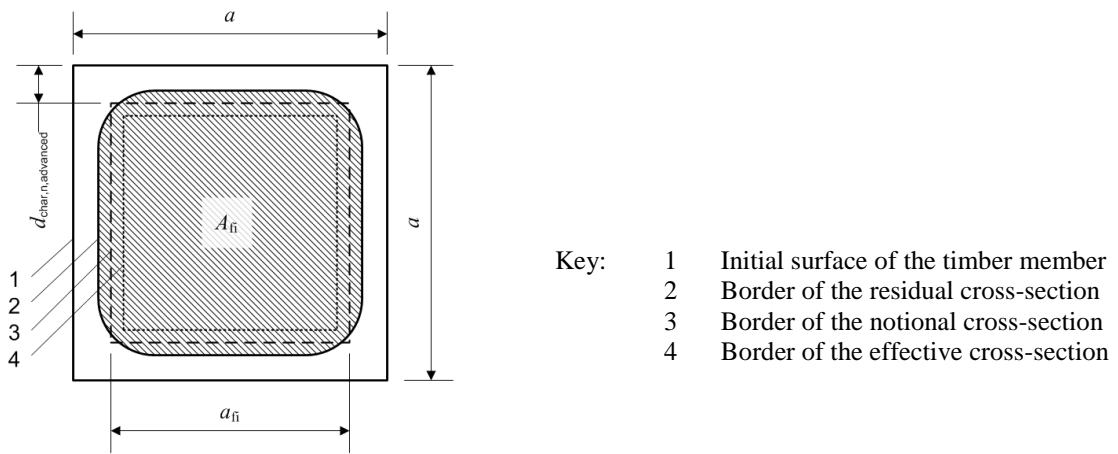


Figure 2. Definition of notional charring depth  $d_{char,n,advanced}$  as well as residual cross-section, notional cross-section and effective cross-section

The residual cross-section and consequently the charring rate have an influence on the load-carrying capacity of timber members in fire. For the investigation of the zero-strength layer  $d_0$  it is important to clearly separate the calculation models for determination of the residual cross-section and the load-carrying capacity during fire exposure. The charring rate model was discussed in detail in [16]. In the present analysis of the zero-strength layer  $d_0$ , always the advanced notional charring rate  $\beta_{n,advanced}$  is used, which considers the effects of corner roundings. In order to show the influence of different applied charring rates on the applied zero-strength layer  $d_0$  some additional calculations were performed and presented in the section 3.2.

### 3 Results and discussion

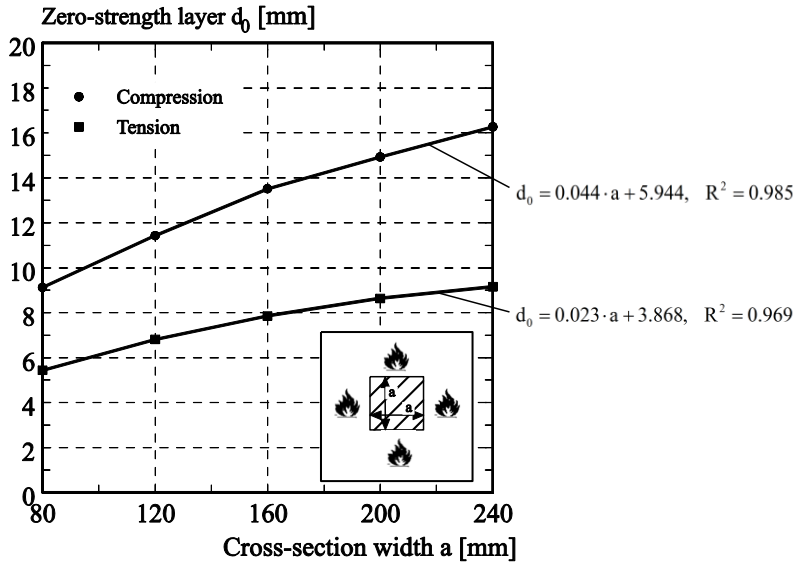
#### 3.1 Calculation of zero-strength layer $d_0$

Figure 3 shows the zero-strength layer  $d_0$  calculated back for  $F_{R,fi}/F_{R,20^\circ C} = 0.3$  with the help of equation (2) for members in compression and tension as a function of the cross-section width. The corresponding failure times defined as  $F_{R,fi}/F_{R,20^\circ C} = 0.3$  are given in Table 1. The calculation is based on the notional charring rate  $\beta_{n,advanced}$  derived from the advanced calculation as described above and the reduction factor  $k_\Theta$  given in EN 1995-1-2, Annex B depending on the state of stress.

$$F_{R,fi} = A_{fi,advanced} \cdot f_{mean} = \left[ a - 2 \cdot (\beta_{n,advanced} \cdot t_{Failure} + d_0) \right]^2 \cdot f_{mean} \quad (2)$$

Since the temperature dependent reduction of timber strength is significantly different for tension and compression (see Figure 7), the shape of the curves for the zero-strength layer is different. Further, it can be seen from the graphs in Figure 3 that the zero-strength layer for both compression and tension is different from the value according to EN 1995-1-2 where a constant value of 7 mm is given. The zero-strength value varies as a function of the cross-section width. For compression, the zero-strength value was calculated to be between around 9 mm for small cross-sections and 16 mm for larger cross-sections. For tension, values between about 6 and 9 mm were calculated. Similar values were also found in [16].

For the 80 mm wide squared cross-section, the fire resistance in compression and tension (defined as  $F_{R,fi}/F_{R,20^\circ C} = 0.3$ ) is reached after 11.5 and 15 minutes, respectively (see Table 1). According to EN 1995-1-2 [3] the zero-strength layer  $k_0 \cdot d_0$  is calculated to be about 4.0 and 5.2 mm, respectively, since  $k_0 = \min(t/20; 1)$ . Both values underestimate the zero-strength layer derived from the present advanced calculation.



a	Timber members in	
	Compr.	Tens.
[mm]	[min]	[min]
80	11.5	15.0
120	20.0	25.0
160	30.0	37.0
200	40.0	50.0
240	52.0	62.0

Table 1: Failure time  $t_R$  [min] of timber members loaded with  $0.3 \cdot F_{R,20^\circ C}$  exposed to standard fire exposure

Figure 3. Zero-strength layer  $d_0$  calculated with the advanced calculation method for compression and tension for cross-sections exposed to fire on four sides as a function of the cross-section width

Timber members subjected to compression are critical for buckling depending on their slenderness. However, it should be noted that according to EN 1995-1-2, Annex B the influence of the temperature on the stiffness is smaller than the reduction factor  $k_{\theta}$  for strength. Thus, it can be assumed that the stiffness has less influence on the load-carrying capacity than the strength. This means that the values for the zero-strength layer  $d_0$  calculated with the temperature dependent reduction of compressive strength of timber should be conservative for members subjected to buckling.

Figure 4 shows the zero-strength layer  $d_0$  for members in bending and with the exposed side in tension (tsw). The zero-strength layer depends on the time of fire exposure, see Figure 4, left.

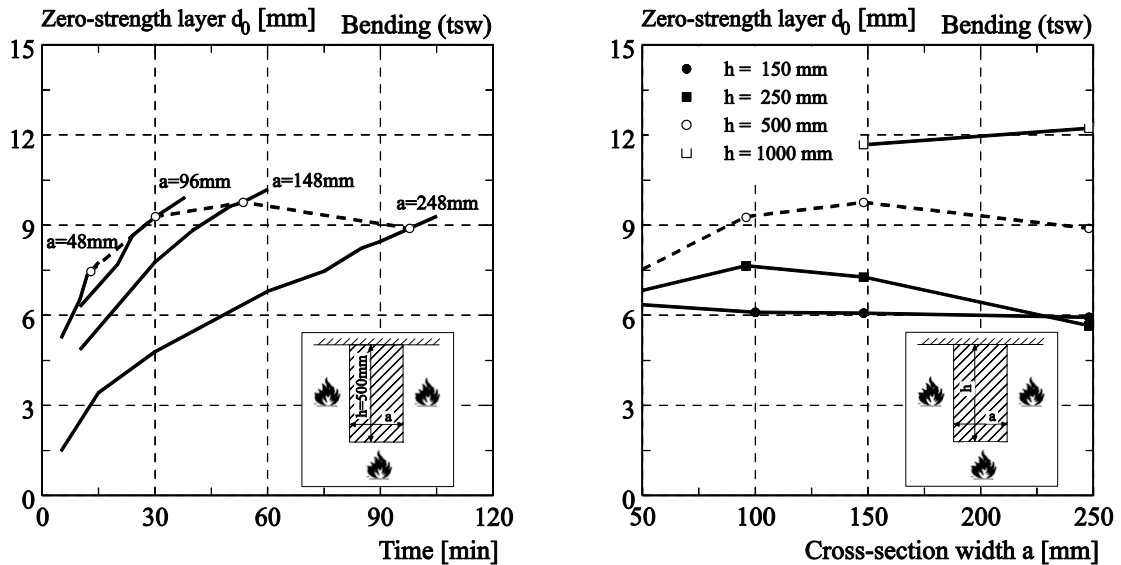


Figure 4. Zero-strength layer of a single span beam ( $h = 500$  mm) exposed to fire on three sides as a function of time of fire exposure with dots showing  $M_{R,fi}/M_{R,20^{\circ}C} = 0.3$  (left); Zero-strength layer of a single span beam exposed to fire on three sides as a function of the cross-section width for  $h = 150$  mm, 250 mm, 500 mm and 1000 mm and calculated for  $M_{R,fi}/M_{R,20^{\circ}C} = 0.3$

It is obvious that the time to failure ( $M_{R,fi}/M_{R,20^{\circ}C} = 0.3$ ) differs significantly depending on the original cross-section. Figure 4, right shows results for beams with  $h = 150$  mm to 1000 mm where the zero-strength layer varies between about 6 and 12 mm. However, for members subjected to bending and fire exposed side in compression a higher value of the zero-strength value was derived following the significantly different decrease of  $k_{\theta}$  [17]. Since the combination of elevated temperature and compression is most unfavourable in cross-sections with such conditions a higher value of the zero-strength layer was expected.

The results of the numerical simulations show that the zero-strength layer differs from the value of 7 mm given in EN 1995-1-2 and clearly depends on the time of fire exposure, the state of stress and the dimensions of the cross-section. Thus, a general constant value for the zero-strength layer may lead to a non-conservative design. For members subjected to tension, a value for the zero-strength layer  $d_0$  of 7 mm seems to be enough accurate; however, for compression a higher value would be more appropriate. It seems appropriate to describe the zero-strength layer for members in compression as a function of the dimensions of the cross-section, since the curve in Figure 3 shows a rather steep increase with increasing cross-section width. For timber members with significantly deviating geometries, e.g. I-joists, the presented conclusions may not be valid [17].

The evaluation of the zero-strength layer  $d_0$  is influenced by different assumptions. In the following sections, the influence of the assumed notional charring rate, the reduction factor  $k_\Theta$  as well as the state of stress (member in tension or compression) are discussed.

### 3.2 Influence of the assumed notional charring rate

Figure 5, left shows that with increasing cross-section width the notional charring rate  $\beta_{n,advanced}$  tends towards the value of the one-dimensional charring rate  $\beta_0$  measured by König et al. [13] in numerous fire tests to be in the order of 0.67 mm/min. This value was for simplicity rounded down to 0.65 mm/min and assumed in EN 1995-1-2. The difference of the presented curves for the charring rates (given for the time of failure for  $F_{R,fi}/F_{R,20^\circ C} = 0.3$ ) for compression and tension for small cross-sections can be explained by the difference in the fire resistance. The member subjected to compression has a lower fire resistance than the one subjected to tension and consequently the ISO-fire curve has lower temperature when failure occurs. This can be seen in Figure 5, right, that shows the development of the notional charring rate  $\beta_{n,advanced}$  for different cross-sections as a function of time of fire exposure.

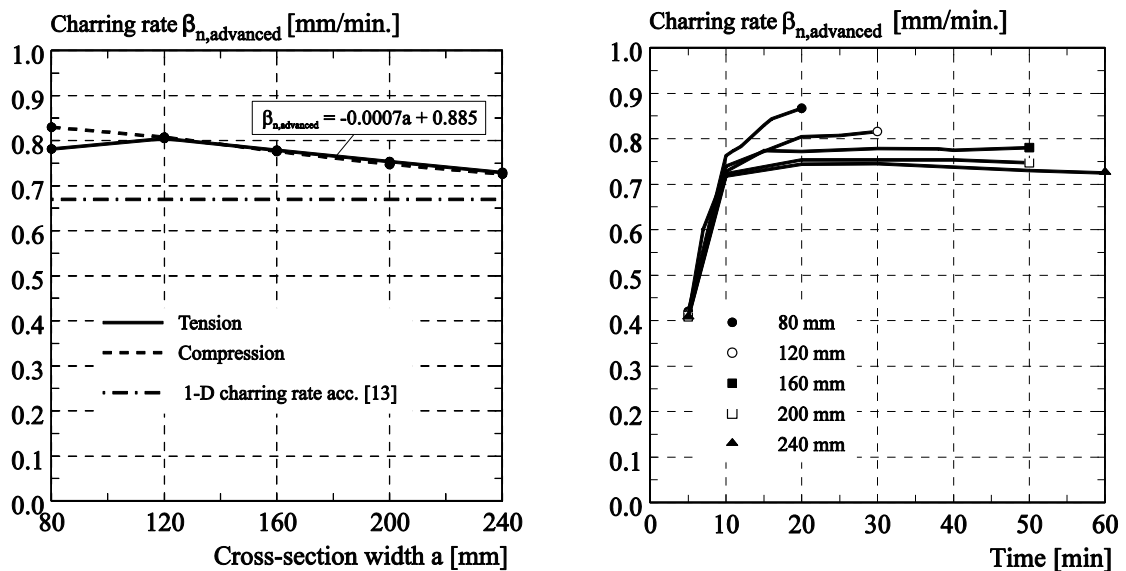


Figure 5. Comparison of the notional charring rate  $\beta_{n,advanced}$  calculated for  $F_{R,fi}/F_{R,20^\circ C} = 0.3$  as a function of the cross-section width (left); Development of the notional charring rate  $\beta_{n,advanced}$  as a function of time of fire exposure for different squared cross-sections (right)

The assumed notional charring rate influences the depth of the zero-strength layer  $d_0$ . The latter is determined comparing the load-carrying capacity of the residual cross-section with the load-carrying capacity of an effective cross-section with mechanical properties at normal temperature. If the assumed notional charring rate leads to a conservative notional cross-section, this will compensate errors of the assumed depth of the zero-strength layer. Figure 6 shows a comparison of the zero-strength layer calculated with different notional charring rates for compression and tension. The charring rate  $\beta_{n,advanced}$  was used according to the advanced calculation method described above and shown in Figure 5. Further, the zero-strength layer was calculated with the notional charring rate  $\beta_n$  of 0.7 mm/min and 0.8 mm/min being the notional charring rate of glued laminated timber and solid timber according to EN 1995-1-2. It can be seen that high values of the notional charring rate lead obviously to smaller values for the zero-strength layer  $d_0$ . For smaller cross-sections, the notional charring rate calculated with the advanced calculation and the notional charring

rate of  $\beta_n = 0.8$  mm/min gives for both compression and tension same values for the zero-strength layer.

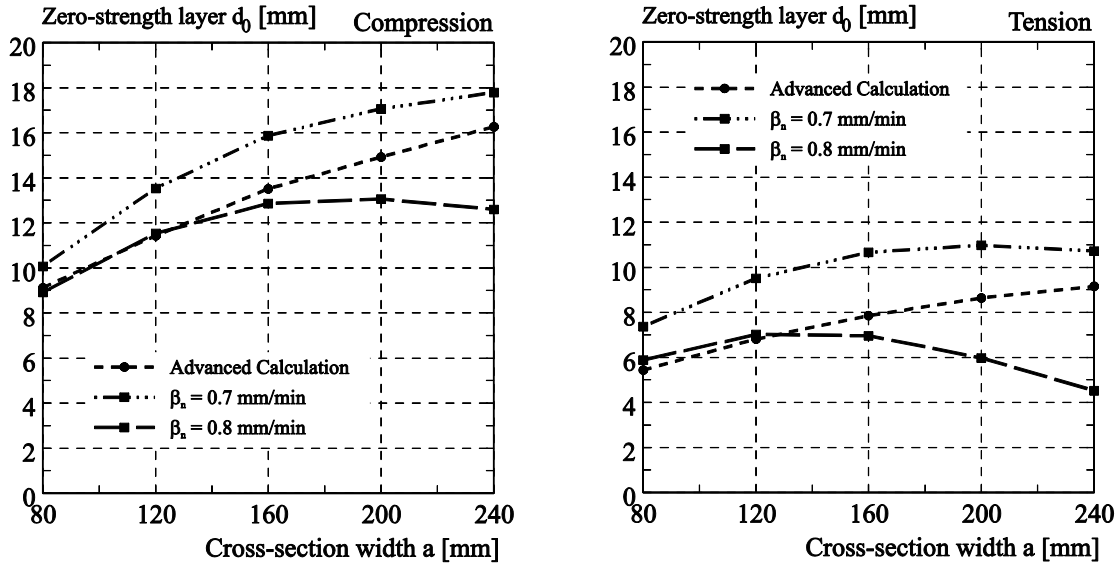


Figure 6. Comparison of zero-strength layer  $d_0$  calculated with the advanced calculation method (with  $\beta_{n,advanced}$ ) and with notional charring rates  $\beta_n$  of 0.7 and 0.8 for compression (left) and tension (right)

### 3.3 Influence of the reduction factor $k_\Theta$

Timber stiffness and strength decreases with increasing temperature. Figure 7, left shows the reduction factor  $k_\Theta$  for compressive and tensile strength according to EN 1995-1-2. The curves are given as a bi-linear relationships from 20 to 300°C with a breakpoint at 100°C and were derived by König et al. [7]. In order to investigate the influence of these curves, the reduction factor at 100°C was modified and increased by 10% for both compression and tension. In Figure 7, right the ratio between the resistance in fire and the resistance at normal temperature ( $F_{R,fi}/F_{R,20^\circ C}$ ) for compression and tension is given as a function of time of fire exposure for a cross-section of 160 mm  $\times$  160 mm. Both curves, using the reduction factor given in EN 1995-1-2 and the assumed modified increased reduction factor, gives about the same fire resistance. The difference in terms of fire resistance for this example is in the range of 2 to 3 minutes for both compression as well as tension and therefore negligible. In addition, simulations were performed with a significant increase of the reduction factor at 100°C of 20%. These simulations led to an increase of the fire resistance of about 4 minutes for both tension and compression. The main reason for this little influence is that most of the residual cross-section has low temperatures at failure, thus the influence of the temperature dependent reduction of timber strength affect only a small part of the residual cross-section.

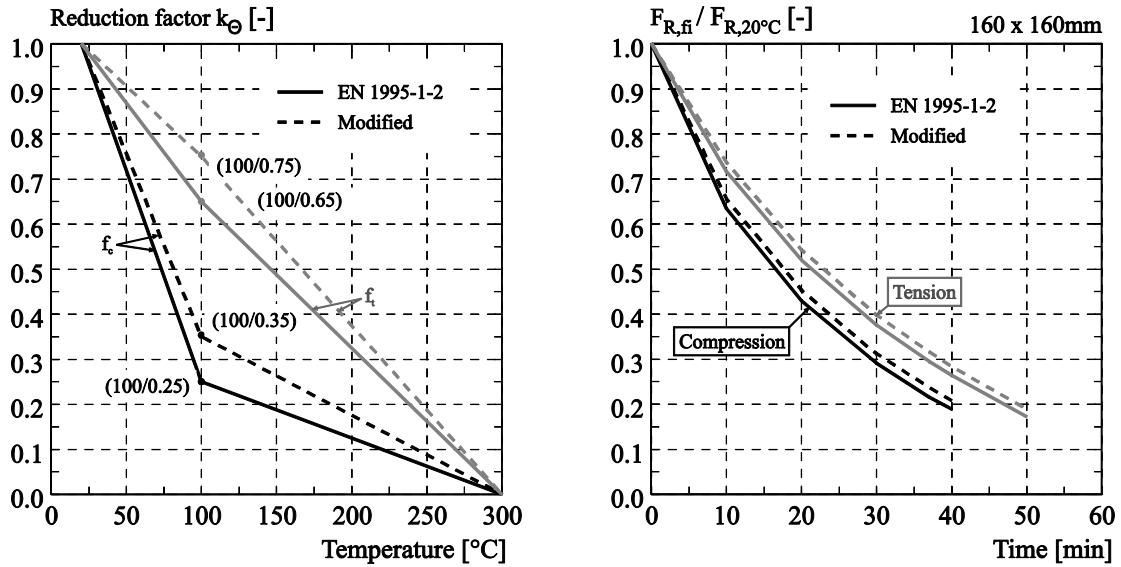


Figure 7. Reduction factors  $k_{\theta}$  for strength properties of wood according to EN 1995-1-2 and modified approach (left); Ratio  $F_{R,fi} / F_{R,20^{\circ}C}$  between the resistance in fire  $F_{R,fi}$  and the resistance  $F_{R,20^{\circ}C}$  at normal temperature as a function of time of fire exposure

Figure 8 shows a comparison of the zero-strength layer calculated with the values given in EN 1995-1-2, Annex B and the modified values (increase of 10%) as a function of the cross-section width. For the cross-sections investigated in tension and compression, the difference of the zero-strength layer is in the range of about 1 to 2 mm between both approaches. For a 20% increase, this difference is in the range of 2 to 4 mm.

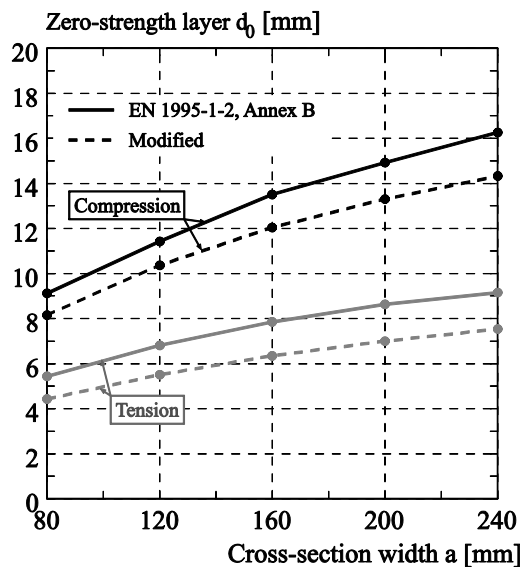


Figure 8. Influence of the reduction factor  $k_{\theta}$  on the zero-strength layer  $d_0$  as a function of the cross-section width

### 3.4 Influence of the state of stress

Figure 9 shows the temperature distribution in the cross-section of 160 mm  $\times$  160 mm after 30 minutes of fire exposure (left) and the corresponding distribution of compressive strength (right). After 30 minutes fire exposure, the inner part of the residual cross-section

still remains at very low temperature close to 20°C and therefore, compressive strength at normal temperature ( $f_{\text{mean}} = 29.4 \text{ N/mm}^2$ ) can be activated.

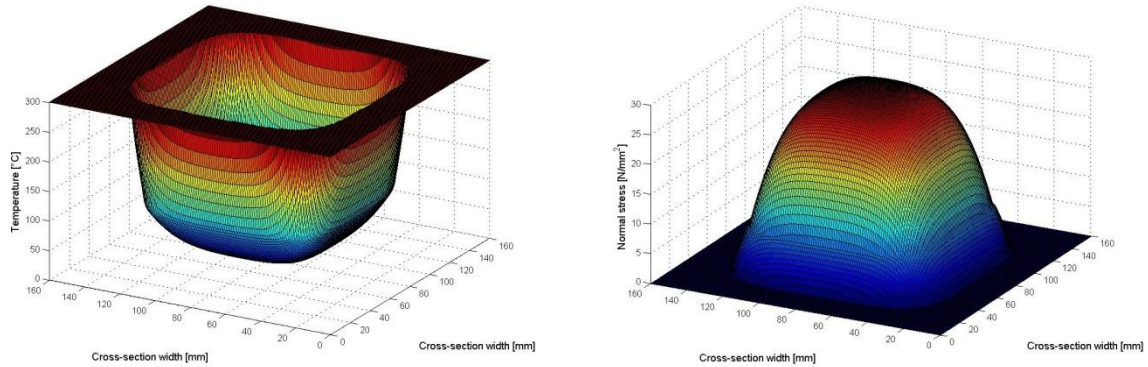


Figure 9. Temperature distribution in the cross-section (160 mm × 160 mm) (left) and corresponding distribution of the compression strength after 30 minutes of fire exposure (right)

Figure 10, left shows the ratio between the fire resistance  $F_{R,fi, \text{simple}}$  calculated with the zero-strength layer  $d_0$  of 7 mm and the fire resistance  $F_{R,fi, \text{advanced}}$  calculated with the zero-strength layer according to Figure 3 for compression and tension as a function of the cross-section width. The charring rate  $\beta_{n, \text{advanced}}$  was used for both calculations. It can be seen that for compression the resistance is overestimated by about 20 to 30%. For tension, since the calculated zero-strength layer  $d_0$  is close to the value of 7 mm given in EN 1995-1-2 (see Figure 3) also the resistance differs only slightly between the simple and advanced calculation method. This is coherent with the ratio of time to failure (defined as  $F_{R,fi}/F_{R,20^\circ\text{C}} = 0.3$ ) for the simple and advanced calculation as shown in Figure 10, right.

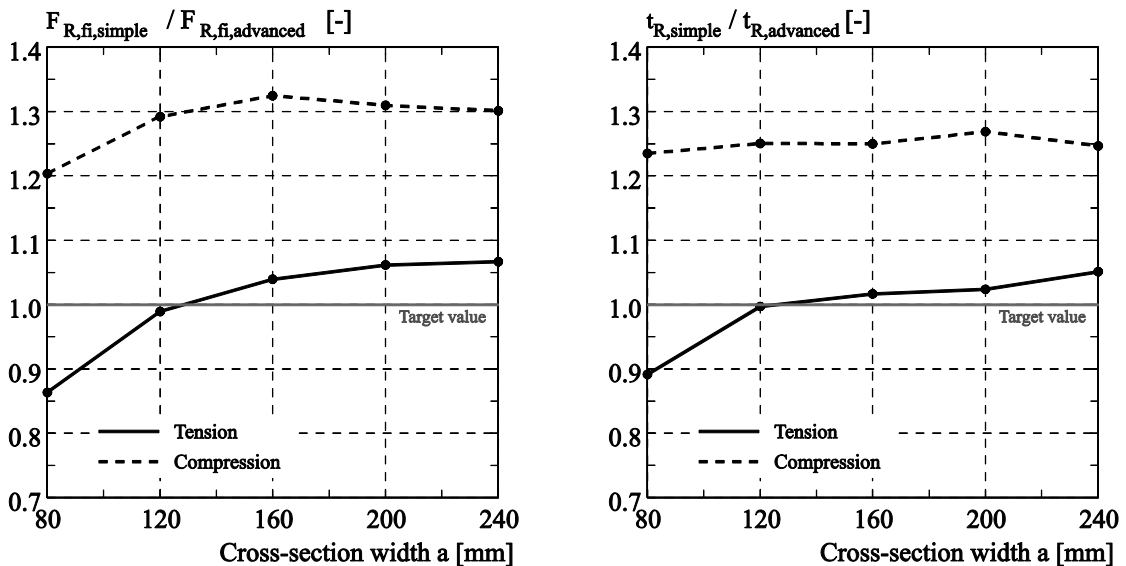


Figure 10. Ratio between fire resistance  $F_{R,fi, \text{simple}}$  calculated with the constant zero-strength layer  $d_0$  of 7 mm according to EN 1995-1-2 and  $F_{R,fi, \text{advanced}}$  calculated using the zero-strength layer  $d_0$  according to Figure 3 as a function of the cross-section width (left); Corresponding ratio between time to failure  $t_{R, \text{simple}}$  calculated with  $d_0$  of 7 mm according to EN 1995-1-2 and time to failure  $t_{R, \text{advanced}}$  calculated using  $d_0$  according to Figure 3 (right)

The resulting absolute error in the overestimation of the fire resistance using a constant value for the zero-strength layer of 7 mm for members in compression and tension is given in Figure 11 as a function of the cross-section width. The overestimation of the fire

resistance is in the order of few minutes for members in tension. For members in compression, the overestimation of the fire resistance is much higher being in the range of 24 to 32 %.

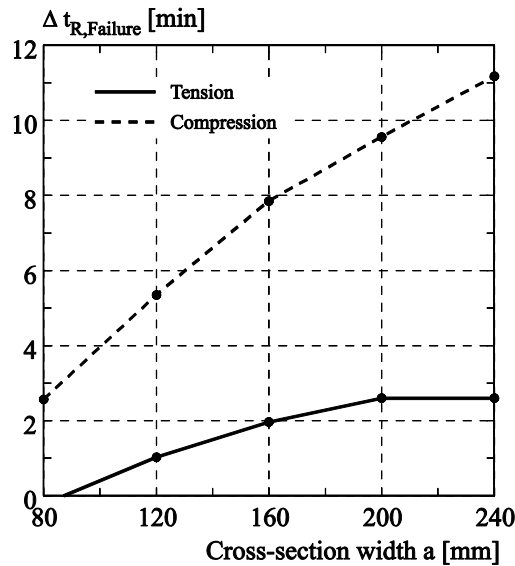


Figure 11. Absolute error (in minutes) in the overestimation of the fire resistance using a constant value for the zero-strength layer of 7 mm for members in compression and tension as a function of the cross-section width

## 4 Conclusions

For the design of timber structures in fire the “Reduced Cross-Section Method” according to EN 1995-1-2 considers the strength and stiffness reduction near the charred layer by adding an additional depth  $d_0$  (called zero-strength layer) to the charred layer.

EN 1995-1-2 gives a general constant value of  $d_0 = 7$  mm for all sizes of cross-section, state of stress and fire exposure making the calculation very easy for the designer. In this paper it is shown that for the studied cross-sections and state of stress a general constant value for the zero-strength layer is not accurate. Various parameters such as time of fire exposure, state of stress (compression, tension and bending), shape and dimensions of the cross-section have an influence on the zero-strength layer.

For members in tension and compression, the overestimation of the fire resistance was investigated in detail. For members in tension, although the calculated zero-strength layer is higher than 7 mm the overestimation is little ( $< 3$  min) and can be neglected. However, for members in compression the fire resistance is overestimated by 24 % up to 32 %. A depth of the zero-strength layer larger than 7 mm would have been more appropriate; however, the “Reduced Cross-Section Method” would not be simple anymore because it may require different values for the zero-strength layer as function of time of fire exposure and dimensions of the cross-section.

Further investigations including the analysis of experiments are planned for a better evaluation of the overall impact and influence of the assumed zero-strength layer on the design of timber structures in fire.

## 5 References

- [1] Schaffer, E.L.: *Structural fire design [microform] : wood / by E.L. Schaffer*; U.S. Dept. of Agriculture, Forest Service, Forest Products Laboratory; Madison, Wis. ; 1984;
- [2] Frangi, A., Fontana, M.: "Charring rates and temperature profiles of wood sections"; *Fire and Materials*; 27 (2); 91-102; 2003.
- [3] EN 1995-1-2:2004, Eurocode 5: *Design of timber structures – Part 1-2: General – Structural fire design. European Standard*. European Committee for Standardization. Brussels. 2004.
- [4] Schaffer, E.L., Forest Products, L.: *Strength validation and fire endurance of glued-laminated timber beams*; U.S. Dept. of Agriculture, Forest Service, Forest Products Laboratory; Madison, WI; 1986; English.
- [5] König, J., Schmid, J.: "Light Timber Frame Constructions with Solid Timber Members – Application of the Reduced Cross-section Method"; CIB W18. Meeting 43; Nelson, New Zealand; Lehrstuhl für Ingenieurholzbau, University of Karlsruhe, Karlsruhe, Germany; 2010.
- [6] Schmid, J., König, J., Köhler, J.: "Fire-exposed cross-laminated timber – Modelling and tests"; World Conf. on Timber Engineering 2010; Riva del Garda, Trentino, Italy; 2010.
- [7] König, J., Walleij, L.: "Timber Frame Assemblies Exposed to Standard and Parametric Fires – Part 2: A Design Model for Standard Fire Exposure"; Report no. I0001001; Swedish Institute for Wood Technology Research; Stockholm, Sweden; 2000.
- [8] Erchinger, C., Frangi, A., Fontana, M.: "Fire design of steel-to-timber dowelled connections"; *Engineering Structures*; 32 (2); 580-589; 2010.
- [9] Hibitt D, Karlsson D, Sorensen P: "ABAQUS v. 6.10"; Dassault Systèmes S.A.; 2010.
- [10] Franssen, J.-M.: "User's manual for SAFIR 2007. A computer program for analysis of structures"; University of Liege, Department ArGenCo, Service Structural Engineering; 2007.
- [11] EN 1991-1-2: *Actions on Structures - Part 1-2: General Actions - Actions on Structures Exposed to Fire*. CEN. Brüssel. 2002.
- [12] König, J.: "Structural fire design according to Eurocode 5—design rules and their background"; *Fire and Materials*; 29 (3); 147-163; 2005.
- [13] König, J., Walleij, L.: "One-dimensional charring of timber exposed to standard and parametric fires in initially unprotected and postprotection situation"; Trätekt Report I 9908029; Swedish Institute for Wood Technology; Stockholm, Sweden; 1999.
- [14] EN 1363-1: *Fire resistance tests - Part 1: General requirements*. CEN. Brüssel. 1999.
- [15] Hadvig, S.: "Charring of wood in building fires"; CIB-W14 Meeting; 1982.
- [16] Cachim, P., Franssen, J.-M.: "Assessment of Eurocode 5 Charring Rate Calculation Methods"; *Fire Technology*; 46 (1); 169-181; 2010.
- [17] Schmid, J., König, J.: "The Reduced Cross-Section Method for the design of timber structures exposed to fire – Background, limitations and new developments"; *Structural Engineering International*; 22 (4); 2012.

**INTERNATIONAL COUNCIL FOR RESEARCH AND INNOVATION  
IN BUILDING AND CONSTRUCTION**

**WORKING COMMISSION W18 - TIMBER STRUCTURES**

**EVALUATION OF SHEAR MODULUS OF STRUCTURAL TIMBER UTILIZING  
DYNAMIC EXCITATION AND FE ANALYSIS**

A Olsson

B Källsner

School of Engineering, Linnaeus University, Växjö

SWEDEN

**MEETING FORTY FIVE**

**VÄXJÖ**

**SWEDEN**

**AUGUST 2012**

---

Presented by A Olsson

R Görlacher asked whether the data from a 1994 CIBW18 paper with more than 1000 specimens were compared. A Olsson responded that they were not compared but would look into it. R Brandner asked whether static shear modulus rather than dynamic G should be compared. A Olsson responded that there were no test results. R Brandner stated that since there was difference between E static and E dynamic, one should also expect differences between G static and G dynamics. A Olsson agreed with R Görlacher that the ratio between E and G was not constant and grade dependent. R Steiger asked whether the mass of the accelerometer was considered. A Olsson said no but thinks he should.



# Evaluation of shear modulus of structural timber utilizing dynamic excitation and FE analysis

Anders Olsson and Bo Källsner

School of Engineering, Linnaeus University, Växjö, Sweden

**Abstract** In this study the results from dynamic excitation of 105 boards of Norway spruce in edgewise bending are evaluated with respect to shear modulus using the FE method. An advantage of the method presented here, in relation to the torsion method given in EN 408, is that the testing is very simple to carry out and also that the shear deformations take place in the same plane as the deflections due to bending occur. Although no alternative methods for evaluation of the shear modulus were applied in this study, results indicating a robustness of the suggested method are presented. According to calculations the estimated shear modulus varies considerably between different boards. The calculated mean value and standard deviation of the dynamic shear modulus is about 744 MPa and 106 MPa, respectively. No significant correlation between the estimated shear modulus and the measured static modulus of elasticity was found, but a moderate correlation between calculated shear modulus and density was identified ( $R^2 = 0.24$ ). Conclusions of the results are that dynamic excitation of boards should be considered as an alternative method for determination of shear modulus in EN 408, and a relation between the board density and the board shear modulus, rather than a relation between the board MOE and the board shear modulus, should be stated in EN 338.

## Introduction

In the European standard EN 408 (2010) two different testing methods for determination of the shear modulus of structural timber and glued laminated timber are given; the torsion method and the shear field test method. The first method is in the standard said to be particularly suitable for structural timber while the second one is recommended for laminated members. A background to the static test methods adopted in EN 408, for determination of the shear modulus, is given by Brandner et.al. (2007). Another investigation dealing with the torsion test method is given by Khokhar (2011).

Dynamic modal testing has often been used for determination of strength and stiffness properties of structural timber. Divos et al. (1998) present results from vibration testing of structural timber in both torsion and bending. They emphasize that it is difficult to compare the various shear modulus measurements because torsion and bending provide completely different shear stress distributions. This difference and the anisotropy of wood make the comparison rather complex. In addition to this may be stated that there is a large variation of the material properties in the longitudinal direction of structural timber due to the presence of knots and other inhomogeneity's. Also within a cross section there is a large variation in the material properties determined by parameters like the pith position, the annual ring width, possible compression wood etc.

The need for taking shear deformations into account when assessing bending stiffness of structural timber using dynamic modal testing has been recognized in several studies as e.g. Chui and Smith (1990). The frequencies for two modes of free bending vibration are used for

determination of modulus of elasticity and shear modulus. The analyses are based on Timoshenko's beam theory.

The authors of the present paper have in a previous investigation, Olsson et al. (2012), studied how the prediction of bending strength can be improved by using the test data from various bending modes for each board. Since this kind of analysis also gives information on the shear modulus it is reasonable to make an evaluation of the test data with respect to this material property.

### **Aim and scope**

The aim of this study is to determine the shear modulus of a number of boards utilizing resonance frequencies corresponding to edgewise bending modes and to give some measure on the uncertainty of the values. A second aim is to evaluate the correlation between the shear modulus and parameters like modulus of elasticity and density.

The investigated material consisted of 105 boards of Norway spruce from one sawmill. Only one board length and one board dimension were included. The selection of material is further described below.

### **Selection of material for evaluation**

The selection of timber for the investigation took place at the sawmill in Långasjö, Sweden, owned by the company Södra. The timber consisted of sawn boards of Norway spruce of nominal dimensions  $50 \times 150$  mm of length 3900 mm or 4500 mm. In the sampling a population with large variation in strength was aimed for. Thus boards with high and low expected strength were included. For this purpose a grading machine of type Dynagrade® was employed with settings for grading of timber to be used for roof trusses (strength class TR26) on the UK market. Both boards fulfilling (61 pieces) and boards not fulfilling the requirements (44 pieces) were selected for further investigation. A visual inspection of each board was performed in order to find the weakest section of each board according to the instructions in the European standard EN 384 (2010). This standard prescribes that the weakest section should be located in the maximum bending moment zone, i.e. between the two point loads in a four point bending test, and such bending tests were performed on the boards investigated.

All the boards were planed to dimension  $45 \times 145$  mm immediately after selection. Then the boards were cut to the length 3600 mm and placed in a climate room holding a temperature of 20 °C and 65 % RH.

### **Method**

The research involves laboratory testing of boards. Quantities measured in laboratory were the weight and dimensions of the boards, the resonance frequencies corresponding to transversal (edgewise bending) modes, the static edgewise bending stiffness (determined in two different ways, giving a local and a global measure, respectively) and the bending strength.

In addition to the laboratory work, the research also involves numerical calculations using the finite element method and common methods and algorithms for optimization and regression analysis.

#### *Dynamic excitation of boards in laboratory*

In order to resemble free-free boundary conditions each board (length 3600 mm) was suspended in rubber bands, see Fig. 1. Then an accelerometer was fastened using wax on the narrow edge at one end of the board (see the photograph to the left in Fig. 1). In the opposite end the board was

hit with an impulse hammer on the narrow edge for excitation of edgewise bending modes (see the photograph to the right in Fig. 1).

The signal from the accelerometer was transformed by a FFT-analyzer and processed using computer software delivering the resonance frequencies of the board corresponding to edgewise bending modes. The precision in measurements depends on the frequency range defined, which for the present measurements was set to 0-1000 Hz. The received precision of the detected resonance frequencies were better than  $\pm 0.25\%$ . The stiffness of the rubber bands was very low, about 400 N/m, and the weight of them was very low as well. Therefore the properties and precise position of the rubber bands (they were placed close to the nodal points of the lowest bending mode) had no significant influence on the resonance frequencies. The weight of the accelerometer including a clip, fastened as shown in Fig. 1 (left), was 13 g. This mass was not adjusted for when calculating the results presented below. The significance of it was, however, investigated and it was found that this additional mass caused an underestimation of the resonance frequencies considered of about 0.19 % to 0.25 %.



**Fig. 1** A board is suspended in rubber bands (photograph in the centre). An accelerometer is fastened at one end of the board on the narrow edge (photograph to the left). In the opposite end of the board it is hit with an impulse hammer on the narrow edge (photograph to the right).

Fig. 2 shows measured results, for board number one to five, in terms of acceleration in a logarithmic scale as function of frequency. The curves represent transversal vibrations and the peak values correspond to the resonance frequencies of the bending modes. In some cases double peaks appear, as for example for board number three slightly below 800 Hz, and it was found that if the experiment was repeated on the same board a very similar result was always achieved. The resonance frequency for each mode was identified manually and the frequency showing the highest peak within a close interval was regarded as the resonance frequency for that mode. In Fig. 2 the peaks representing resonance frequencies are marked with a small circle. (In a few cases it was not obvious what peaks should be regarded as resonance frequencies.) The six lowest resonance frequencies were identified and stored.

### *Static four-point bending test*

The local and global static bending stiffness and the bending strength of the boards were assessed using a four point bending test according to the European standard EN 408. The total span was 2610 mm long (corresponding to the depth of the board times eighteen) and the two point loads were applied 870 mm apart, each of them 870 mm from its nearest support. For such a load case the mid-span is subjected to a constant bending moment and no shear force. What was supposed to be the weakest part of each board, detected by means of visual inspection, was located within the zone with constant bending moment, i.e. between the two point loads, and was randomly located with regard to the position of the tension side of the board.

### Assessment of board density

The board density,  $\rho$ , was simply calculated as the mass of the board divided by its volume. At the time for the assessment of the board density the boards had been stored in three months in a climate room holding a temperature of 20 °C and 65 % RH. The moisture content of small parts of the wood, cut out from the boards before they were cut to 3600 mm, were determined after two months in the same climate room. At that time the mean moisture content of the small specimens was 13.6 %.

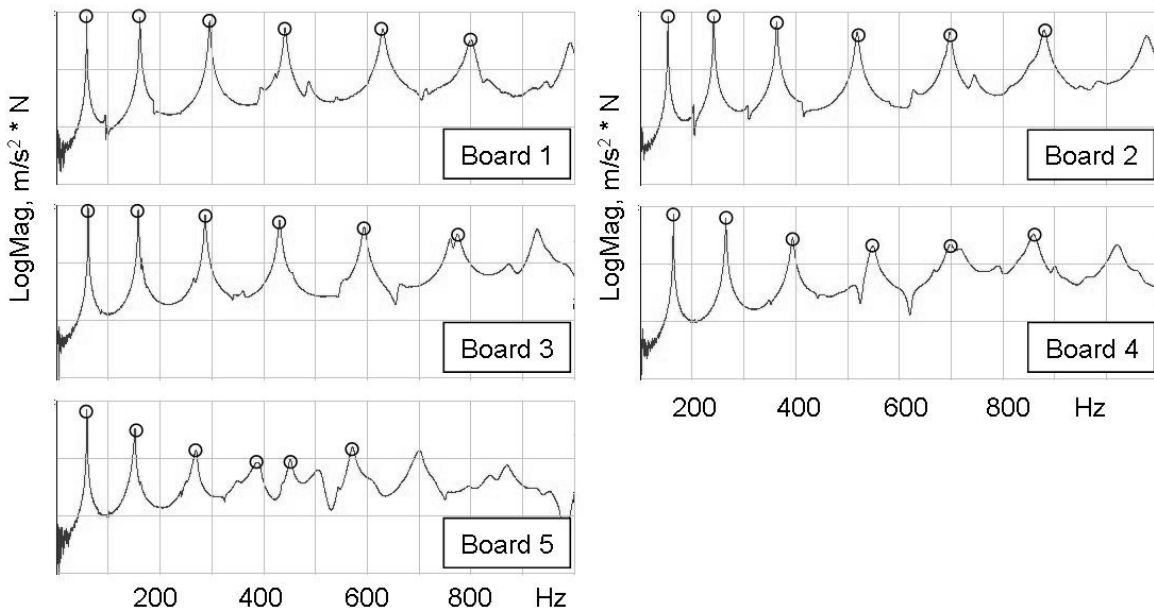


**Fig. 2** Measured transversal vibration content, in terms of acceleration (in a logarithmic scale) as function of frequency, for board number one to five.

### Finite element modelling and assessment of MOE and shear modulus

The resonance frequencies corresponding to edgewise bending modes may be utilized for calculating representative values of the board stiffness. The MOE is of course the primary stiffness parameter but also the shear modulus,  $G$ , determines the resonance frequencies corresponding to bending modes. For the lowest bending modes,  $G$  has a very low influence on the resonance frequencies, as the deformations involved in those modes contain very little shear, but higher bending modes contain significant shear deformations. Therefore, both bending stiffness and shear stiffness should be taken into account when calculating resonance frequencies using beam theory.

Timoshenko beam theory, which takes shear deformations into account, and a finite element model consisting of 40 beam elements is used for modelling the stiffness of the board. The element mass matrices of the model are, however, consistent with the Bernoulli-Euler beam theory. Eigen value analyses are performed on the model and resonance frequencies are calculated as functions of MOE and  $G$ , i.e. a large number of calculations are carried out in which different values of MOE and  $G$  are combined. Fig. 3 shows the first six calculated resonance frequencies corresponding to edgewise bending modes as functions of MOE and  $G$ , which are ranging from 5 to 25 GPa and from 0.2 to 1.6 GPa, respectively, for boards with a nominal density of  $\rho = 450 \text{ kg/m}^3$  and dimensions  $45 \times 145 \times 3600 \text{ mm}$ .

The MOE of each individual board is simply determined as the MOE giving a perfect fit between measured and calculated resonance frequency of the first mode, when G is set to 700 MPa. (As noted above, the resonance frequency corresponding to the first mode of vibration is not very sensitive to G. For example, a 10 % change in the G assumed would only result in a 0.4 % change in estimated MOE.) Then a more correct G is determined for each individual board by adjusting G in the calculation so that either a perfect agreement between measured and calculated resonance frequency is achieved for a single higher mode of vibration, or so that a best possible fit is achieved between sets of several measured and calculated resonance frequencies. In the latter case no perfect solution exists, i.e. no value of G would result in a perfect agreement between the sets of measured and calculated resonance frequencies. Instead a normalized residual vector is calculated. For example, if all higher resonance frequencies available are considered a normalized residual vector is defined as

$$\mathbf{r}_{2,3,4,5,6} = \begin{bmatrix} (f_{cb,2} - f_{b,2})/f_{b,2} \\ (f_{cb,3} - f_{b,3})/f_{b,3} \\ (f_{cb,4} - f_{b,4})/f_{b,4} \\ (f_{cb,5} - f_{b,5})/f_{b,5} \\ (f_{cb,6} - f_{b,6})/f_{b,6} \end{bmatrix} \quad (1)$$

in which  $f_{b,k}$  is the  $k^{\text{th}}$  measured resonance frequency of the board assessed and  $f_{cb,k}$  is the corresponding calculated resonance frequency using some combination of MOE and G. Then the value of G for the board assessed that minimizes the scalar value  $\sqrt{\mathbf{r}_{2,3,4,5,6}^T \mathbf{r}_{2,3,4,5,6}}$  is denoted  $G_{2,3,4,5,6}$ . Similarly,  $G_{3,5}$  is the shear modulus that minimizes  $\sqrt{\mathbf{r}_{3,5}^T \mathbf{r}_{3,5}}$ , i.e. the norm of a residual vector taking only mode three and five into account, and so on.

#### *Sensitivity to measurement errors*

For resonance frequencies corresponding to lower modes of vibration small measurement errors have comparatively large influence on the estimated shear modulus, but for higher modes of vibration the estimated shear modulus is less sensitive to errors in measured resonance frequencies. For example, in the case where a single measured resonance frequency is utilized for assessment of G, an error of 0.5 % in resonance frequency causes errors in the estimated shear modulus as follows; for  $G_2$  8.4 %, for  $G_3$  4.7 %, for  $G_4$  3.1 %, for  $G_5$  2.4 % and for  $G_6$  2.0 %. An error of 0.25 % in measured resonance frequency causes about half as large error in estimated shear modulus as a 0.5 % error does.

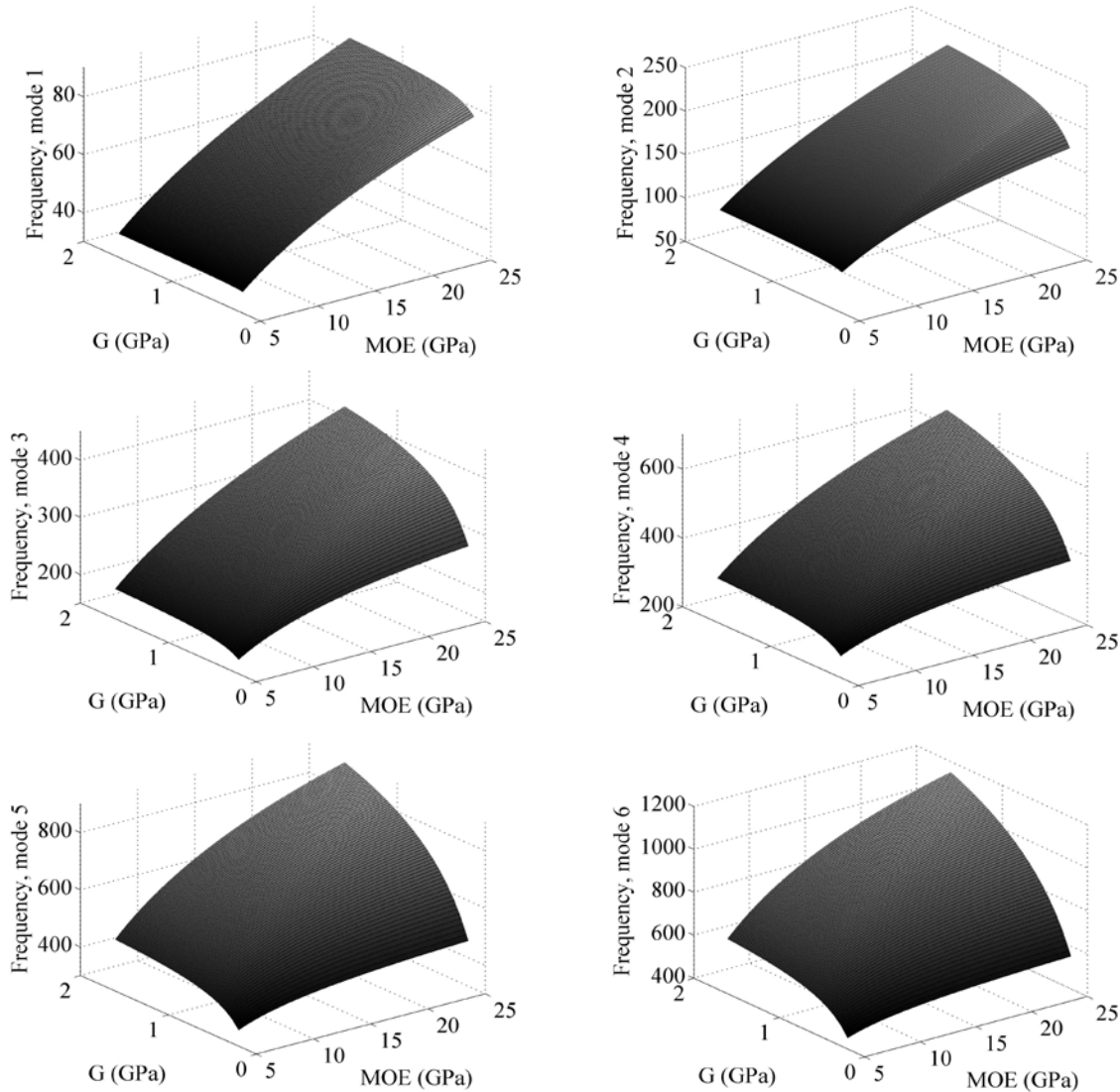


**Fig. 3** The first six resonance frequencies corresponding to bending modes as functions of MOE and G, ranging from 5 to 25 GPa and from 0.2 to 1.6 GPa, respectively, calculated using a FE-model consisting of 40 beam elements.

### Results and analysis

Table 1 shows mean values and standard deviations of different board properties. The properties presented are bending strength,  $\sigma_m$ , local and global modulus of elasticity,  $E_m$  and  $E_{m,g}$ , respectively, dynamic MOE assessed on basis of the first edgewise bending resonance frequency,  $E_{b,1}$ , the board density,  $\rho$ , and the shear modulus assessed on basis of different sets of resonance frequencies as described above. The properties  $\sigma_m$ ,  $E_m$ ,  $E_{m,g}$  and  $\rho$  are similar to what have been reported in other studies on Norway spruce and these results are not further discussed here. Regarding the shear modulus the mean value is rather stable and it does not differ very much depending on which resonance frequencies that are considered when the shear modulus is assessed. The standard deviation differs more between the different shear stiffness properties assessed, but all of them, except  $G_3$  which is based on a single, rather low bending mode, is in the range of 103-123 MPa. Thus the coefficient of variation for G is in the order of 14-17 %. This can be compared with the coefficient of variation for the MOE which is in the order of 21-25 %

according to the results presented in Table 1. The ratio between the mean values of MOE and  $G$  is in the order of 15-17.

**Table 1** Mean values and standard deviations for different properties of the 105 boards.

	Mean value		Standard dev.	
$\sigma_m$	38.4	MPa	12.9	MPa
$E_m$	11.0	GPa	2.8	GPa
$E_{m,g}$	10.6	GPa	2.3	GPa
$E_{b,1}$	12.7	GPa	2.7	GPa
$\rho$	472	kg/m <sup>3</sup>	52	kg/m <sup>3</sup>
$G_{2,3,4,5,6}$	744	MPa	106	MPa
$G_{2,4,6}$	745	MPa	102	MPa
$G_{3,5}$	744	MPa	122	MPa
$G_3$	749	MPa	178	MPa
$G_4$	731	MPa	123	MPa
$G_5$	745	MPa	121	MPa
$G_6$	752	MPa	103	MPa

Table 2 shows coefficients of determination between different estimates of the shear stiffness, i.e. shear stiffness calculated on basis of different single resonance frequencies or sets of resonance frequencies. It is reasonable to expect that  $G_{2,3,4,5,6}$ , which is based on all the resonance frequencies available except the first one, should give the best estimate of the true shear stiffness of the beam. In Table 2, however, only coefficients of determination between estimates that are based on different resonance frequencies are displayed, and therefore three resonance frequencies at the most are utilized in the shear modulus estimates presented here. The highest coefficient of determination presented is  $R^2=0.77$  which is valid for  $G_{2,4,6}$  vs  $G_{3,5}$ , but high correlation is found also when comparing a shear stiffness estimate based on a single high resonance frequency with an estimate based on several resonance frequencies, e.g.  $G_5$  vs  $G_{2,4,6}$  and  $G_6$  vs  $G_{3,5}$ . Fig. 4 shows a scatter plot with  $G_{3,5}$  and  $G_{2,4,6}$  on the x-label and y-label, respectively. Also the coefficient of determination, the equation for the line of regressions, and the standard error of estimate (SEE) are displayed in Fig. 4. Even though the two estimates are based only upon two and three resonance frequencies, respectively, they correlate well and the SEE is small in comparison with the standard deviations of the shear modulus estimates displayed in Table 1.

**Table 2** Coefficients of determination between different estimates of the shear stiffness, i.e. shear stiffness calculated on basis of different single resonance frequencies or sets of resonance frequencies.

$R^2$	$G_{2,4,6}$	$G_{3,5}$	$G_3$	$G_4$	$G_5$	$G_6$
$G_{2,4,6}$	1	0.77	0.56		0.71	
$G_{3,5}$	0.77	1		0.57		0.69
$G_3$			1	0.53	0.45	0.43
$G_4$		0.57	0.53	1	0.48	0.50
$G_5$	0.71		0.45	0.48	1	0.67
$G_6$		0.69	0.53	0.50	0.67	1

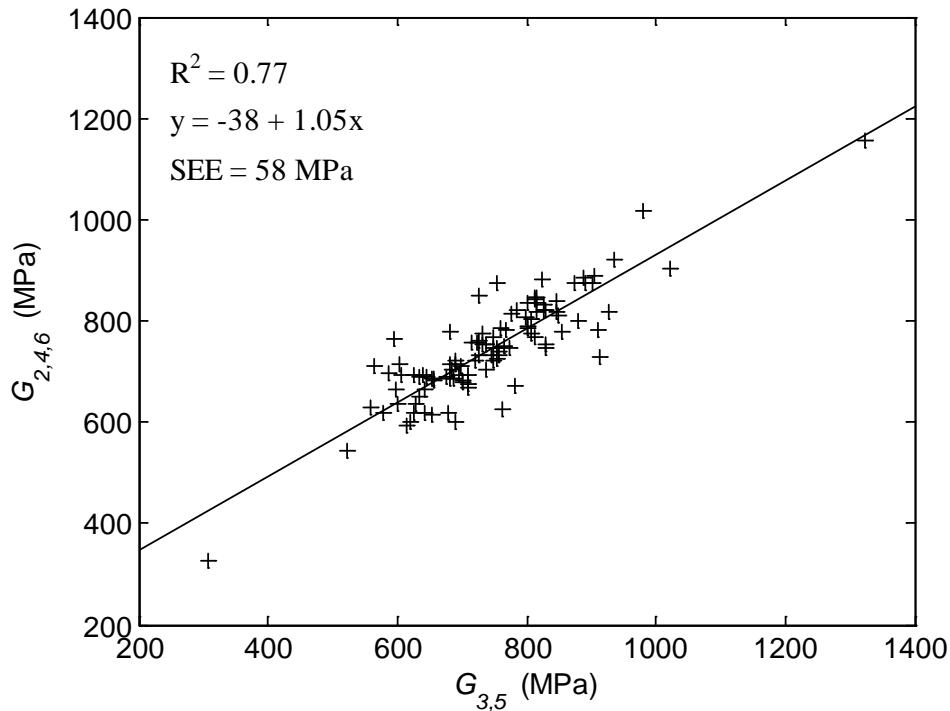


**Fig. 4** Scatter plot, coefficient of determination, equation of regression line, and standard error of estimate for  $G_{3,5}$  vs  $G_{2,4,6}$ .

A wooden board does not consist of a homogeneous material, and it should be emphasized that when talking about a board shear modulus or a board MOE, what is meant is actually some kind of average properties of the board material. As different estimates of the shear modulus, e.g.  $G_4$  and  $G_5$ , are based on resonance frequencies corresponding to different modes of vibration, involving more or less shear in different parts of the board, different values would be received for these different estimates even if there were no measurement uncertainties at all present. Large knots, for example, result in deviant local shear stiffness where the knots are located and as one mode of vibration may have a nodal point in that position while another mode is subjected to maximum shear in the same position, they would result in different estimates of the board shear modulus. An estimate based on several modes, like  $G_{2,3,4,5,6}$ , should, however, represent the average board shear modulus well.

Figs. 5-8 show scatter plots, coefficients of determination, equations of regression lines, and the standard errors of estimate for  $G_{2,3,4,5,6}$  vs  $\rho$ ,  $E_m$ ,  $E_{m,g}$  and  $\sigma_m$ , respectively. According to the results there is a clear, though not very strong, positive correlation between board density and board shear modulus,  $R^2 = 0.24$ . Between the board MOE and the board shear modulus there is, however, no significant correlation at all, neither for  $E_m$  vs  $G_{2,3,4,5,6}$  or for  $E_{m,g}$  vs  $G_{2,3,4,5,6}$ . This result thus contradicts the linear relation between MOE and shear modulus that is prescribed in EN 338 (2009), saying that the shear modulus should be set to the mean MOE of the strength class divided by 16. However, the results obtained are consistent with those presented by Görlacher and Kürth (1994) who investigated the shear stiffness of 15 cm long pieces of timber using torsional vibration and by those presented by Khokhar (2011) who used static torsion tests on boards of dimension  $45 \times 100$  mm for evaluation of shear modulus. Finally, the results here indicate that there is no significant correlation between the bending strength of the board and the board shear modulus.

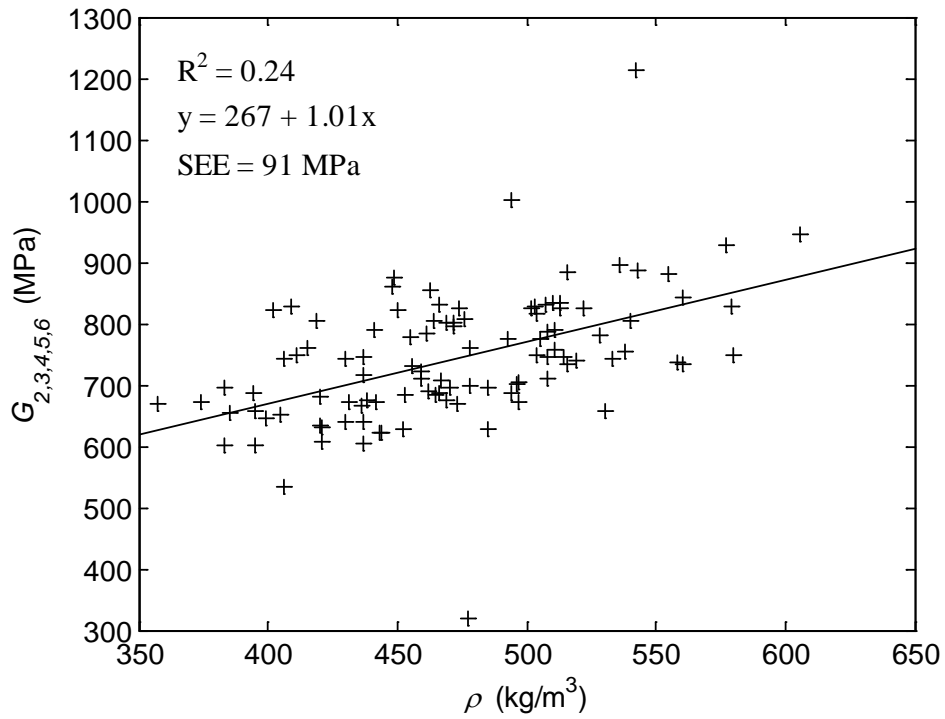


**Fig. 5** Scatter plot, coefficient of determination, equation of regression line, and standard error of estimate for  $\rho$  vs  $G_{2,3,4,5,6}$ .

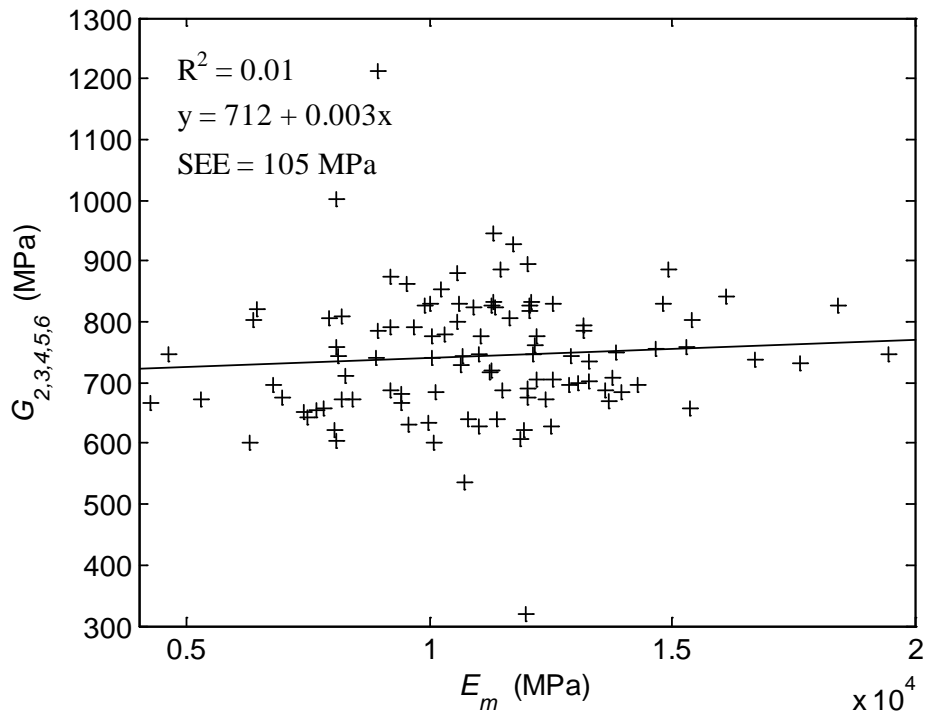


**Fig. 6** Scatter plot, coefficient of determination, equation of regression line, and standard error of estimate for  $E_m$  vs  $G_{2,3,4,5,6}$ .

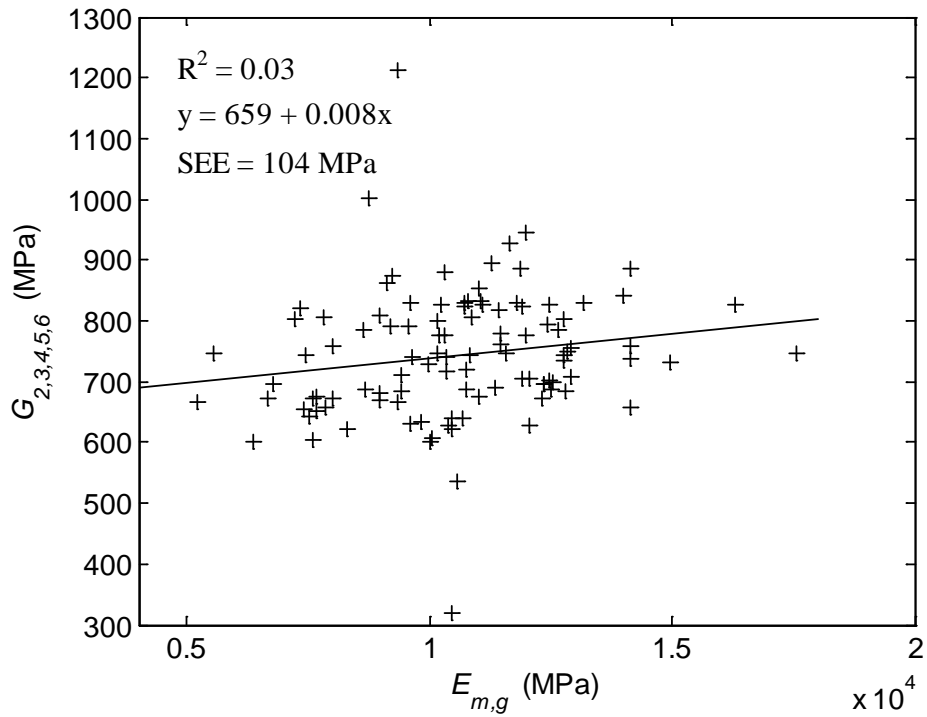


**Fig. 7** Scatter plot, coefficient of determination, equation of regression line, and standard error of estimate for  $E_{m,g}$  vs  $G_{2,3,4,5,6}$ .

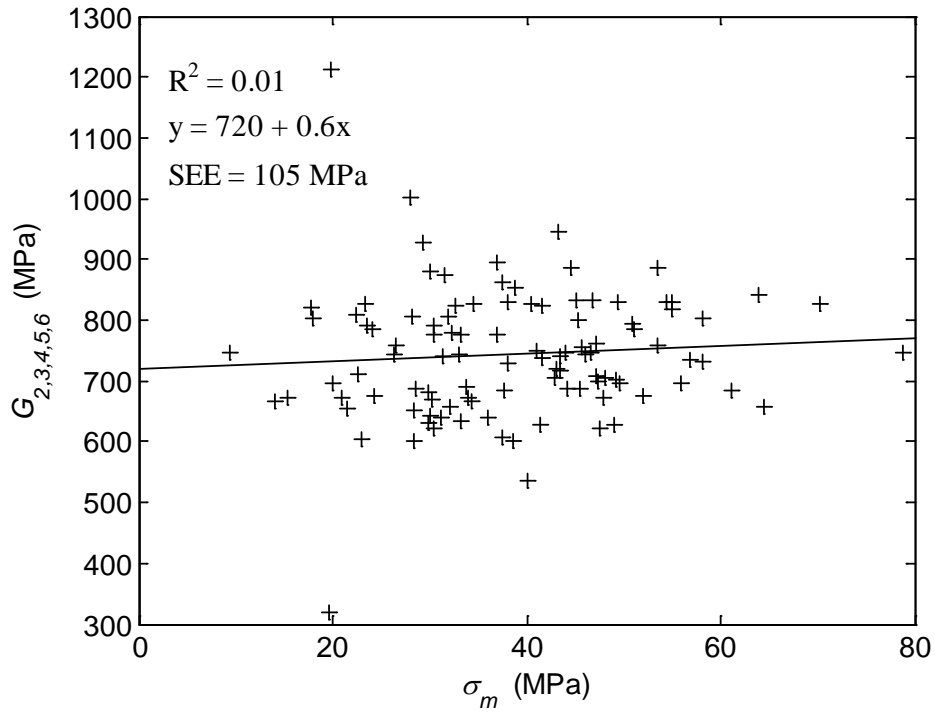


**Fig. 8** Scatter plot, coefficient of determination, equation of regression line, and standard error of estimate for  $\sigma_m$  vs  $G_{2,3,4,5,6}$ .

## Discussion and conclusions

A method for evaluation of shear modulus for wooden boards on basis of resonance frequencies corresponding to edgewise bending modes is suggested. Although the shear modulus of the boards included in the study, 105 boards of Norway spruce with dimensions  $45 \times 145 \times 3600$  mm, were not evaluated using any alternative method, comparisons of results when utilizing different sets of resonance frequencies indicate that the method is reliable when resonance frequencies corresponding to several modes of vibration are utilized. Important advantages of the method is that the testing is very simple to carry out and also that the shear deformations that occur during this kind of testing take place in the same plane as the deflections due to bending.

When investigating how the board shear modulus assessed using the suggested method correlates with properties like board density, MOE and bending strength it was found that the only property that correlates significantly with the board shear modulus is the board density,  $R^2 = 0.24$ . Local or global MOE do not seem to correlate at all with the board shear modulus. On the other hand, studies have shown, e.g. Khokhar (2011), that for clear wood, MOE and shear modulus correlates significantly. A reasonable explanation to the results presented here is thus that though a high MOE in clear wood also means that the clear wood shear modulus is high, the presence of knots leads to a low board MOE at the same time as they contribute to an increased board shear modulus. This means that two effects may cancel each other. A conclusion of the results presented herein is that EN 338 should prescribe the application of a relation between the board density and the board shear modulus, rather than a relation between the board MOE and the board shear modulus.

The results regarding correlation between MOE and G of boards are in agreement with what was found by Görlacher and Kürth (1994) and Khokhar (2011) who used dynamic and static torsion tests respectively for evaluation of shear modulus. Chui (1991), however, who tried to evaluate shear modulus on wooden members,  $40 \times 40 \times 640$  mm in dimension, with and without single knots, using dynamic excitation of bending modes, got results indicating that knots may have a strong negative influence on the shear modulus.

## Some notations

$\sigma_m$	bending strength
$\rho$	board (average) density
MOE	Abbreviation/General notation for modulus of elasticity
$E_m$	local MOE assessed by static bending
$E_{m,g}$	global MOE assessed by static bending
$f_{b,k}$	res. freq. of bending mode $k$
$E_{b,k}$	MOE calc. on basis of $f_{b,k}$
G	General notation for shear modulus
$G_k$	Shear modulus calc. on basis of the resonance freq. of the $k$ :th mode of vibration
$G_{3,5}$	Shear modulus calc. on basis of the resonance freq. of mode 3 and 5
$G_{2,4,6}$	Shear modulus calc. on basis of the resonance freq. of mode 2, 4 and 6
$G_{2,3,4,5,6}$	Shear modulus calc. on basis of the resonance freq. of mode 2, 3, 4, 5 and 6

## References

Brandner, R., Gehri, E., Bogensperger, T., Schickhofer, G. (2007) Determination of modulus of shear and elasticity of glued laminated timber and related examinations, Proceedings of CIB W18, paper 40-12-2, Bled.

Chui Y.H., Smith I. (1990) Influence of rotary inertia and shear deformation and support condition on natural frequencies of wooden beams. *Wood Sci. Technol.* 24: 233-245.

Chui Y.H. (1991) Simultaneous evaluation of bending and shear moduli of wood and the influence of knots on these parameters. *Wood Sci. Technol.* 25: 125-134.

Divos F., Tanaka T., Nagao H., Kato H. (1998) Determination of shear modulus on construction size timber. *Wood Sci. Technol.* 32: 393-402.

EN 338 (2009) Structural timber – Strength classes.

EN 384 (2010) Structural timber – Determination of characteristic values of mechanical properties and density.

EN 408 (2010) Timber structures – Structural timber and glued laminated timber – Determination of some physical and mechanical properties.

Görlacher R., Kürth J. (1994) Determination of shear modulus, Proceedings of CIB W18, paper 27-10-1, Sydney.

Khokhar A.M. (2011) The evaluation of shear properties of timber beams using torsion test method. PhD thesis, Edinburgh Napier University, UK.

Olsson A., Oscarsson J., Johansson M., Källsner B. (2012) Prediction of timber bending strength on basis of bending stiffness and material homogeneity assessed from dynamic excitation. *Wood Sci. Technol.* 46: 667-683.

**INTERNATIONAL COUNCIL FOR RESEARCH AND INNOVATION  
IN BUILDING AND CONSTRUCTION**

**WORKING COMMISSION W18 - TIMBER STRUCTURES**

**ASSESSMENT OF SELECTED EUROCODE BASED DESIGN EQUATIONS IN  
REGARD TO STRUCTURAL RELIABILITY**

J Köhler

Department of Structural Engineering, NTNU, Trondheim  
NORWAY

R Steiger

Empa, Structural Engineering Research Laboratory, Duebendorf

G Fink

R Jockwer

Swiss Federal Institute of Technology, Zurich  
SWITZERLAND

**MEETING FORTY FIVE**

**VÄXJÖ**

**SWEDEN**

**AUGUST 2012**

---

Presented by J Köhler

T Poutanen received clarification that the Beta values calculated in the paper are based on one year maximum snow load. He commented that the Eurocode is based on snow load with a 50 year return period. He also commented that loads were combined independently. J Köhler responded that this issue was covered extensively in the past year and would further discuss with T Poutanen during break. J Munch Andersen questioned the calculations based on "optimized" beta values of finding the partial safety factors from minimization of error between calculated and target beta. One should look into cases that lied below the target beta. J Köhler agreed that it could be done and perhaps with consideration weighing different cases. J König commented that the EN1990 noted that the target beta was based on assuming normally distributed loads. External loads that are based on Gumbel distribution will give different results. J Köhler responded that different load models were also considered. S Aicher stated that target beta of 4.7 was used in the Eurocode and asked whether the results were showing that the partial safety factors in the code were too low. He also asked whether the difference was due to the use of Gumbel distribution only. J Köhler stated that the choice of Weibull distribution for the resistance might also make a difference as beta values were sensitive to the lower tail of the distribution. U Kuhlmann stated that one should consider different target beta for different failure modes, and stiffness dependence should also be considered where not only simple structures are studied. J Köhler agreed. J Munch Andersen commented that it didn't make sense to use different distributions for different strengths and compare the results. J Köhler agreed. T. Poutanen further commented that target beta values for one year and 50 year were 4.7 and 3.6, respectively. F Lam received confirmation that the resistance distributions were not based on real data. He commented that in Canada by fitting to the lower tails of the strength data more consistent results were obtained where the beta values were less sensitive to the choice of strength distribution. S Winter commented that more transparent strength data were needed; e.g. new material strength data in the code is based on test data and also may consider test data from worldwide sources. J Köhler commented different partial safety factors for different strengths might add complications to design and agreed on the need to use transparent test data. S. Aicher commented that the partial safety factors would always reflect the COV of the material; therefore, one should have groupings with COV.



# Assessment of selected Eurocode based design equations in regard to structural reliability

Jochen Kohler

Department of Structural Engineering, NTNU, Trondheim, Norway

René Steiger

Empa, Materials Science and Technology, Structural Engineering Research Laboratory  
Duebendorf, Switzerland

Gerhard Fink

Swiss Federal Institute of Technology  
Zurich, Switzerland

Robert Jockwer

Swiss Federal Institute of Technology  
Zurich, Switzerland

## 1 Introduction

A large proportion of the societal wealth is invested in the continuous development and maintenance of the built infrastructure. It is therefore essential that decisions in this regard are made on a rational basis. A structural design code should be such a rationale that facilitates design solutions that balance expected adverse consequences (e.g. in case of failure or deterioration) with investments into more safety (e.g. larger cross-sections). Structural design codes are therefore calibrated on the basis of associated risks or, simplified, on the basis of associated failure probability. In this paper it is focused on the latter.

Reliability based code calibration has been formulated by several researchers, see e.g. Ravindra and Galambos [1], Ellingwood et al. [2] and Rosenblueth and Esteva [3] and has already been implemented in several design codes, see e.g. OHBDC [4], NBCC [5], and more recently the Eurocodes [6]. However, the safety format of e.g. Eurocode 5 [7] still relies on a large extent on experience and engineering judgement. In the present paper, some selected design situations are assessed in regard to the reliability of the corresponding Eurocode 5 design solutions. A possible modification of the resistance related partial safety factor  $\gamma_M$  is discussed in the light of practical usability of the safety format.

## 2 Basic principles of reliability based code calibration

Modern design codes are based on the so-called load and resistance factor design (LRFD) format. In the present paper selected situations are evaluated where timber structural elements are subjected to

two main loads (one constant and the other variable over time) as e.g. it is typical for roof structures (self-weight + ballast and snow load) or joists supporting ceilings/floors (self-weight + ballast and imposed load). For this case a LRFD equation could be written as:

$$z \frac{R_k}{\gamma_m} - \gamma_G G_k - \gamma_Q Q_k = 0 \quad (1)$$

$R_k$  is the characteristic value of the resistance,  $G_k$  is the characteristic value of the permanent load (self-weight + ballast),  $Q_k$  is the characteristic value of the load variable over time (snow load, imposed load),  $\gamma_m, \gamma_G, \gamma_Q$  are the corresponding partial safety factors for the resistance and for the load.  $z$  is the so-called design variable, i.e. it is defined by the chosen dimensions of the structural component.

The characteristic values for the resistance and the loads are conventionally defined as certain fractile values of the probability distributions of the random variables representing resistance and load, respectively. Within the Eurocodes,  $R_k$  corresponds to the 5% fractile value of the random resistance  $R$  [7],  $G_k$  to a 50% fractile value (or median value) of the random load constant in time  $G$  [6].  $Q_k$  is the 98% fractile value of the random yearly maxima of the variable load  $Q$  [6]. Based on this conventional choice of  $R_k, G_k$  and  $Q_k$  the corresponding partial safety factors can be calibrated to provide design solutions ( $z$ ) with an acceptable failure probability. The failure probability  $P_F$  is expressed as:

$$P_F = \Pr\{g(X, R, G, Q) < 0\}$$

with

$$g(X, R, G, Q) = z^* X R - G - Q \quad (2)$$

$g(\cdot)$  is the Limit State Equation.  $R, G$  and  $Q$  are resistance and loads represented as random variables.  $z^* = z(\gamma_m, \gamma_G, \gamma_Q)$  is the design solution identified with Equation (1) as a function of the selected partial safety factors.  $X$  is the model uncertainty.

It is common to express structural reliability with the so called reliability index  $\beta$ , which is defined as:

$$\beta = -\Phi^{-1}(P_F) \quad (3)$$

where  $\Phi$  is the standard normal operator.

In general, different design situations are relevant in terms of contributions of the permanent and variable load. With the following modification of Equations (1) and (2) this can be taken account of:

$$z_i \frac{\hat{R}_k}{\gamma_m} - \gamma_G \alpha_i \hat{G}_k - \gamma_Q (1 - \alpha_i) \hat{Q}_k = 0 \quad (4)$$

$$g_i(X, \hat{R}, \hat{G}, \hat{Q}) = z_i^* X \hat{R} - \alpha_i \hat{G} - (1 - \alpha_i) \hat{Q} = 0 \quad (5)$$

Here,  $\alpha_i$  might take values between and including 0 and 1, representing different relative contributions of permanent and variable load. The hat “^” indicates that the variables  $R, G$  and  $Q$  are normalized to a mean value of 1, resulting in  $\hat{R}, \hat{G}$  and  $\hat{Q}$ . With, e.g.,  $\alpha = [0, 0.1, 0.2, \dots, 1.0]$  11 different design situations are numerically represented.

The partial safety factors  $\boldsymbol{\gamma} = \gamma_m, \gamma_G, \gamma_Q$  can be calibrated by solving the following optimisation problem:

$$\min_{\gamma} \left[ \sum_{j=1}^L (\beta_{target} - \beta_j)^2 \right] \quad (6)$$

for the mentioned  $L = 11$  different design situations  $\alpha=0, 0.1, 0.2, \dots, 1.0$ .

$\beta_{target}$  represents the general requirement to the safety of the structure. In Table 1 target failure probabilities and corresponding target reliability indices are given for ultimate limit states based on the recommendations of JCSS [8]. Note that the values given correspond to a year reference period and the stochastic models recommended in JCSS [8].

*Table 1: Target reliability indices  $\beta$  (and associated target failure probabilities) related to a one-year reference period and ultimate limit states (JCSS [9]).*

Relative cost of safety measure	Minor consequences of failure	Moderate consequences of failure	Large consequences of failure
High	$\beta=3.1$ ( $p_f \approx 10^{-3}$ )	$\beta=3.3$ ( $p_f \approx 5 \cdot 10^{-4}$ )	$\beta=3.7$ ( $p_f \approx 10^{-4}$ )
Normal	$\beta=3.7$ ( $p_f \approx 10^{-4}$ )	$\beta=4.2$ ( $p_f \approx 10^{-5}$ )	$\beta=4.4$ ( $p_f \approx 5 \cdot 10^{-5}$ )
Low	$\beta=4.2$ ( $p_f \approx 10^{-5}$ )	$\beta=4.4$ ( $p_f \approx 10^{-5}$ )	$\beta=4.7$ ( $p_f \approx 10^{-6}$ )

The value for the most common design situation is indicated with grey shading in Table 1 ( $\beta_{target} = 4.2$ ). Guidelines for the classifications in this table can be found in the probabilistic model code, JCSS [8].

### 3 Example

The design equation for a beam subjected to bending can be calibrated according to the procedure described in chapter 2. The chosen formulations for the variables in Equations (4) and (5) are taken from the JCSS Probabilistic Model Code (PMC) [8, 9] and summarized in Table 2.

*Table 2: Chosen representation of the model uncertainty  $X$ , the bending strength  $R$ , the permanent load  $G$  and the variable load  $Q$  (assumptions according to the JCSS Probabilistic Model Code (PMC) [8] and EN 1990 [6]).*

	$X$	$R$	$G$	$Q$
Mean value	1	1	1	1
Standard deviation	0.1	0.25	0.1	0.4
Distribution type	Lognormal	Lognormal	Normal	Gumbel
Fractile	–	0.05	0.5	0.98
Characteristic value	–	0.647	1	2.037

A load range of  $\alpha = [0.1, 0.2, \dots, 0.8]$  was chosen, i.e. the unrealistic design situations with less than 10% and more than 80% permanent load were excluded from the optimisation (Figure 1). The software CodeCal [10] was used to perform the calculations.

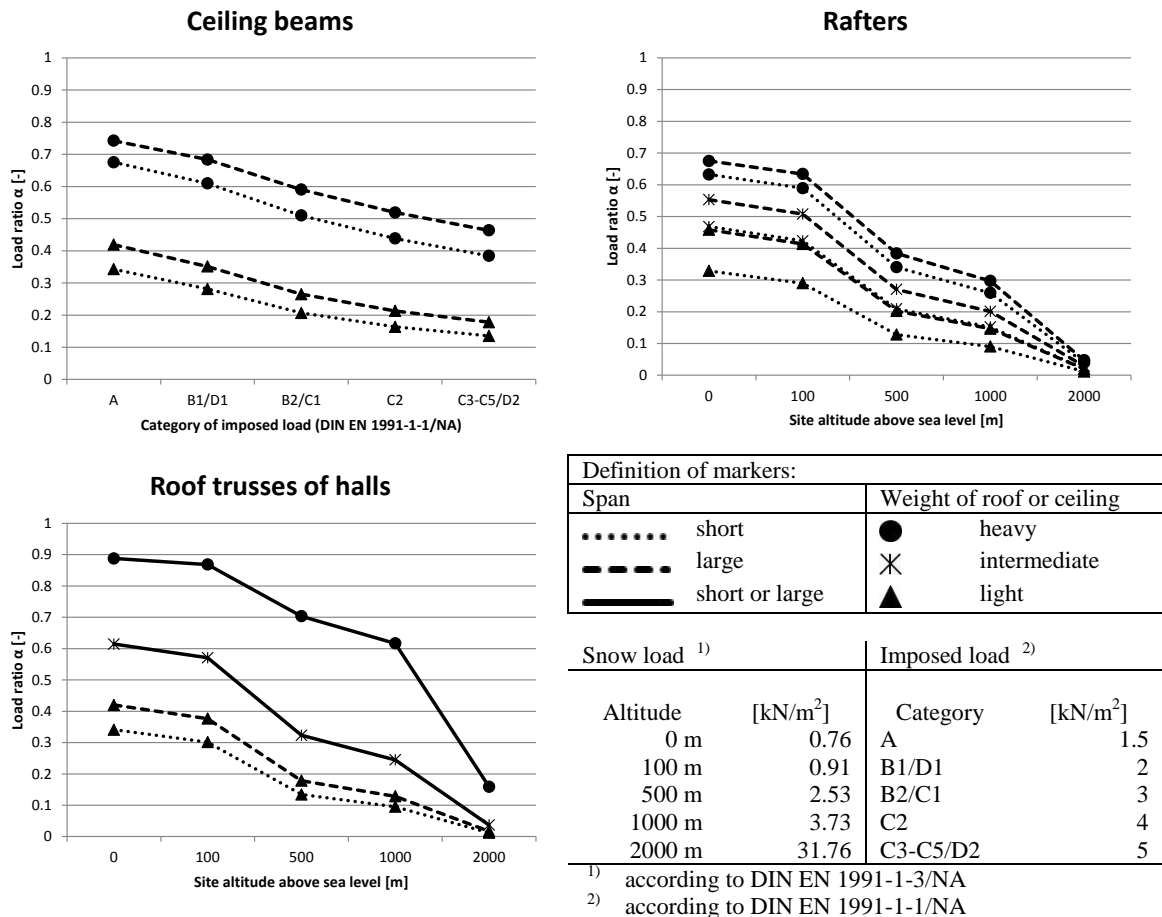


Figure 1: Load ratio  $\alpha$  (permanent load / variable load) for ceiling beams, rafters and roof trusses of halls in function of their span, the type of construction of the roof / ceiling, the imposed load (on ceilings) or the snow load (on roofs).

In Figure 2 the target reliability index of  $\beta = 4.2$  (red line) [6] is compared with the design solutions for structural solid timber obtained according to the recommended values in the current version of the Eurocodes [6, 7]; i.e.  $\gamma_m = 1.3, \gamma_G = 1.35, \gamma_Q = 1.5$  represented by the line with squares. It can be observed that the reliability indices of the design solutions according to the Eurocodes tend to be too low compared to the target reliability index, especially for small alphas. The line with the diamonds is obtained when all partial safety factors are subject to optimisation. The resulting set of partial safety factors is  $\gamma_m = 1.29, \gamma_G = 1.3, \gamma_Q = 1.57$ . However, it is the philosophy of the Eurocodes that the partial safety factors for the loads are material independent [6]; therefore it is reasonable to fix  $\gamma_G$  and  $\gamma_Q$  and to perform the optimisation only subject to  $\gamma_m$ . The line with the circles in Figure 2 is representing the corresponding result ( $\gamma_m = 1.33$ ). An enhancement in reaching the target reliability level can be observed for both calibrated solutions.

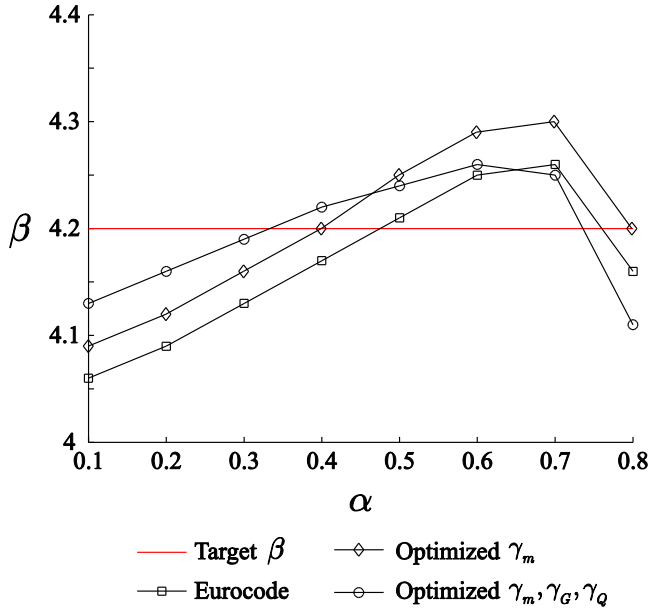


Figure 2: Reliability index  $\beta$  for different design situations alpha for solid timber in bending. The three black lines represent different sets of partial safety factors. The target reliability index  $\beta_{target}$  equals 4.2 (red line).

## 4 Comparison of design solutions of different ultimate limit states for structural solid timber

In the following the design solutions for different ultimate limit states are analysed for structural elements made from solid timber; i.e. uniaxial bending, tension parallel to the grain, tension perpendicular to the grain, compression parallel to the grain, compression perpendicular to the grain and shear.

Modification factors ( $k_{mod}$ , etc.) that are introduced to Eurocode 5 to account for e.g. moisture content, duration of load or size effects are not considered in this study, i.e. have been set to unity.

In the Eurocodes the same design equation (Equation (1)) and the same set of partial safety factors ( $\gamma_m = 1.3, \gamma_G = 1.35, \gamma_Q = 1.5$ ) is used for all considered design situations. However, structural timber shows different material behaviour for different load types (see e.g. Köhler [11]). In Table 3 the distribution functions and the coefficients of variation  $COV$ , to describe the resistance of structural solid timber for the different load types, are listed in accordance with the JCSS PMC [8]. This statistical representation of timber strength properties in the PMC had been subject of a collection of available experimental data and of extensive discussions along COST Action E24 “Reliability of Analysis of Timber Structures” [12].

Under the assumption that the resistance of structural solid timber for different loading modes can be represented as suggested by the JCSS PMC (Table 3) the reliability indices  $\beta$  for different design situations alpha were calculated for the prescribed set of partial safety factors ( $\gamma_m = 1.3, \gamma_G = 1.35, \gamma_Q = 1.5$ ). The results are shown in Figure 3 (left) and Table 4.

A comparison of the target and the actual reliability indices shows a relatively good agreement for uniaxial bending (as already presented in the initial example above) and for shear (exactly the same results as for bending due to similar assumptions for the statistical representation of the material resistance in bending and shear). There, the mean value of the calculated reliability index is

$\beta = 4.17$  which corresponds to a probability of failure  $P_F = 1.55 \cdot 10^{-5}$ . For the ultimate limit state design in tension parallel to the grain and in compression parallel to grain the differences between the target and the actual reliability indices are significantly larger; i.e.  $\beta = 4.01$  and  $\beta = 4.32$ , respectively.

However, the calculated reliability indices for the ultimate limit state design in tension perpendicular to the grain and in compression perpendicular to grain are significantly different to those recommended by the JCSS PMC and by Eurocode 0. For compression perpendicular to the grain the present version of the Eurocode delivers design solutions that are too safe; i.e. the probability of failure is only one third of the value recommended by the JCSS. More problematic is the ultimate limit state design for tension perpendicular to the grain. Here, the Eurocode delivers design solutions that are not safe enough; i.e. the estimated probability of failure is order of magnitudes larger than the recommended. However, tension perpendicular to the grain is certainly a failure mode that is not sufficiently covered by the level of detail applied in the present analysis. The characteristic values prescribed in the EN 338 are of nominal character, i.e. a certain degree of conservatism is included due to the sensitivity of the failure mode to several aspects, e.g. moisture induced stresses, volume effects, deviation of test procedures to structural conditions, etc. It is also interesting to see that the chosen COV for tension perpendicular to the grain is similar to the COV for bending and shear. The large difference in regard to reliability indices is due to the different distribution type that is chosen to represent tension perpendicular to the grain.

*Table 3: Distribution type and coefficients of variation for different ultimate limit states for structural solid timber: assumptions according to the JCSS PMC [8].*

Ultimate limit state	Distribution type	COV
Bending	Lognormal	0.25
Tension parallel to the grain	Lognormal	0.30
Tension perpendicular to the grain	2-p Weibull	0.25
Compression parallel to the grain	Lognormal	0.20
Compression perpendicular to the grain	Normal	0.10
Shear	Lognormal	0.25

As described above, the philosophy of the Eurocodes [6] is that the partial safety factors for the loads are material independent. In the following the partial safety factor for the resistance  $\gamma_m$  is calibrated for the different limit states. For the calibration the partial safety factors for the loads are assumed constant with  $\gamma_G = 1.35$  and  $\gamma_Q = 1.5$ . The calibrated partial safety factors for the resistance  $\gamma_m$  are listed in Table 4. In Figure 3 (right) the reliability indices  $\beta$  calculated with the optimised  $\gamma_m$  for different design situations alpha are illustrated.

*Table 4: Calibrated partial safety factors for the resistance (for constant  $\gamma_G = 1.35$  and  $\gamma_Q = 1.50$ ).*

Ultimate limit state	$\gamma_m$
Bending	1.33
Tension parallel to the grain	1.40
Tension perp. to the grain	<b>3.05</b>
Compression parallel to the grain	1.24
Compression perp. to the grain	<b>1.20</b>
Shear	1.33

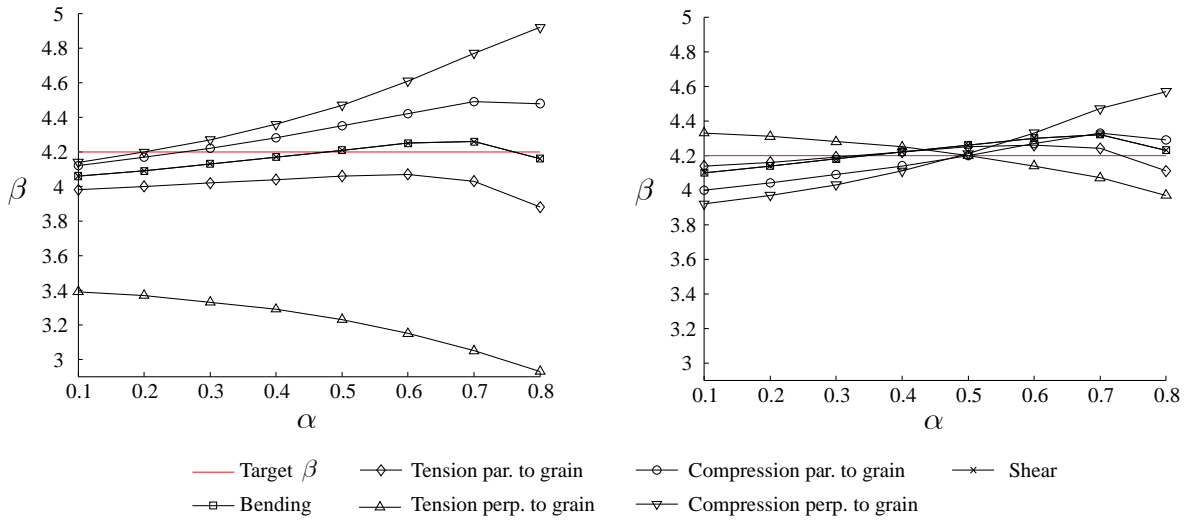


Figure 3: Reliability index  $\beta$  for different design situations  $\alpha$ . The different lines represent different ultimate limit states. Left: Calculated according to Eurocode. Right: Calculated with the optimised partial safety factor for the resistance  $\gamma_m$  (given in Table 4).

Table 5: Reliability index (mean value, minimum and maximum) and the associated probability of failure  $P_F$  for resistance for different ultimate limit states for structural solid timber calculated with the partial safety factors given in the Eurocodes [6, 7]

Ultimate limit state	$\beta$			$P_F$
	Mean value	Min. value	Max. value	For the mean value of $\beta$
Bending	4.17	4.06	4.26	$1.55 \cdot 10^{-5}$
Tension parallel to the grain	4.01	<b>3.88</b>	4.07	$3.04 \cdot 10^{-5}$
Tension perpendicular to the grain	<b>3.22</b>	<b>2.93</b>	<b>3.39</b>	$6.43 \cdot 10^{-4}$
Compression parallel to the grain	4.32	4.12	4.49	$7.94 \cdot 10^{-6}$
Compression perpendicular to the grain	4.47	4.14	4.92	$3.96 \cdot 10^{-6}$
Shear	4.17	4.06	4.26	$1.55 \cdot 10^{-5}$

## 5 Comparison of design situations of structural solid timber and glued-laminated timber in bending

For glued-laminated timber (glulam) in bending the design equation for a beam can similarly be calibrated according to the procedure described in chapter 2. The recommended partial safety factors are  $\gamma_m = 1.25$ ,  $\gamma_G = 1.35$  and  $\gamma_Q = 1.5$  [6, 7]. Furthermore, it is assumed that the bending resistance can be represented by a lognormal distribution and a coefficient of variation  $COV=0.15$  according to the JCSS PMC [8].

In Figure 4 (left) the reliability indices  $\beta$  for structural solid timber and glulam for different design situations  $\alpha$  are illustrated. It can be observed that the reliability indices of the design situations for glulam according to the Eurocodes tend to be too high, especially for large  $\alpha$ s.

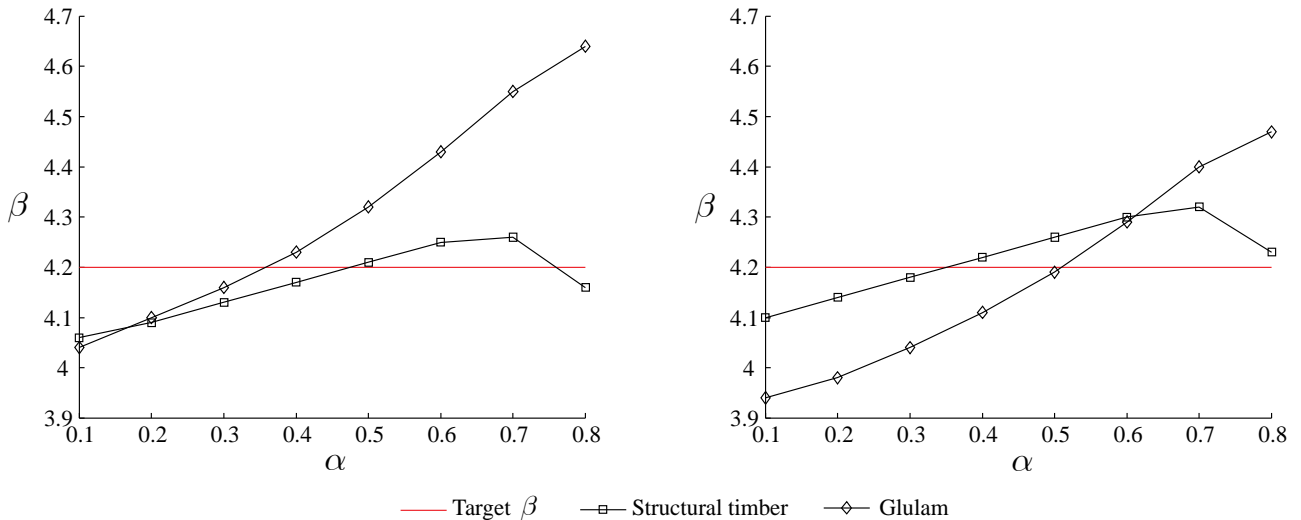


Figure 4 Reliability index  $\beta$  for different design situations alpha. The different lines represent the ultimate limit state in bending of structural solid timber and glulam. Left: Calculated according to the Eurocodes. Right: Calculated with the optimised partial safety factor for the resistance  $\gamma_m$ .

In the following the partial safety factor for the resistance of glulam subjected to bending is calibrated to  $\gamma_m = 1.20$ . In Figure 4 (right) the reliability indices  $\beta$  for different design situations alpha are illustrated. Glulam shows a significantly larger scatter of the reliability index for different design situations than solid timber. This results from the smaller variation of the bending strength.

For the ultimate limit states tension parallel to the grain, compression parallel to the grain and shear the tendencies compared to uniaxial bending as observed for solid timber are qualitatively the same for glulam due to the same relations of coefficients of variation between the different ultimate limit states assumed in JCSS PMC [8]. However for tension perpendicular to the grain the estimated probability of failure is even larger as for structural solid timber. For compression perpendicular to the grain the probability of failure is lower than the target.

## 6 Conclusions

From the assessment of the current design format of Eurocode 5 in regard to the reliability of the design solutions obtained by following the prescriptions in the code, it results that the safety level is rather different and very much dependent on:

- the failure mode (i.e. bending, tension, shear etc.).
- the importance of different load effects (constant and variable load, represented by the factor  $\alpha$  in the present study).

While the latter dependence is also observed for other building materials, the large dependence on the failure modes is a timber specific phenomenon. The load bearing capacity of structural solid timber and timber based materials as e.g. glued laminated timber is very much dependent on the loading mode. This results in rather different magnitudes and stochastic properties of the different load bearing capacities. This matter of fact is contrasted by the use of partial safety factors for the material related load bearing capacity, e.g.  $\gamma_M = 1.3$  for solid timber.

The results as presented in this paper suggest a differentiated treatment of different failure modes in terms of different partial safety factors applied to different failure modes. This would enhance the consistency of the design format in regard to the structural reliability presented by the corresponding design solutions. However, such a development would add more complexity to the code and would not match the recent aim towards clarity and user friendliness of the Eurocodes [13].

A veritable alternative or a valuable extension respectively would be the presentation of “capacity values” in Eurocode 5, i.e. the characteristic values as presented in EN 338 (for solid timber) or EN 14080 (for glulam) multiplied with the failure mode specific partial safety factor. This has e.g. been done in Swiss code for the design of timber structures SIA 265 [14] where also duration of load effects are included into the simplified representation of capacity values.

## 7 References

1. Ravindra, M. and T.V. Galambos, *Load and resistance factor design for steel*. ASCE, Journal of the Structural Division, 1978. **104**(9): p. 1337-1353.
2. Ellingwood, B., et al., *Probability Based Load Criteria: Load Factors and Load Combinations*. ASCE, Journal of the Structural Division, 1982. **108**(5): p. 978-997.
3. Rosenblueth, E. and L. Esteva, *Reliability basis for some Mexican codes*. ACI Publication, 1972. **31**: p. 1-42.
4. OHBDC, (*Ontario Highway Bridge Design Code*), Ontario Ministry of Transportation and Communication, Ontario. 1983.
5. NBCC, (*National Building Code of Canada*), National Research Council of Canada. 1980.
6. CEN, *EN 1990: Basis of structural design*. 2002, European Committee for Standardization: Brussels.
7. CEN, *EN 1995-1-1, Eurocode 5: Design of timber structures; part 1-1: general rules and rules for buildings*. 2004, European Committee for Standardization: Brussels.
8. JCSS Probabilistic Model Code. *Probabilistic Model Code Part III - Resistance Models (3.05 Timber)*. 2006.
9. Köhler, J., J.D. Sørensen, and M.H. Faber, *Probabilistic modeling of timber structures*. Structural Safety, 2007. **29**(4): p. 255-267.
10. JCSS, *CodeCal - Reliability Based Code Calibration*. 2004, <http://www.jcss.ethz.ch/CodeCal/CodeCal.html>.
11. Köhler, J., *Reliability of Timber Structures*, in *Department of Civil, Environmental and Geomatic Engineering*. 2006, ETH Zurich: Zurich. p. 237.
12. COST Action E 24. *Reliability of timber structures. Several meetings and Publications, Internet Publication: <http://www.km.fgg.uni-lj.si/coste24/coste24.htm>*. 2005.
13. Dietsch, P. and S. Winter, *Eurocode 5-Future Developments towards a More Comprehensive Code on Timber Structures*. Structural Engineering International, 2012. **22**(2): p. 223-231.
14. Schweizerischer Ingenieur- und Architekten-Verein SIA, *SIA 265: Timber Structures*. 2003: SIA, Zürich, Switzerland.



**INTERNATIONAL COUNCIL FOR RESEARCH AND INNOVATION  
IN BUILDING AND CONSTRUCTION**

**WORKING COMMISSION W18 - TIMBER STRUCTURES**

**NOTES**

Block Shear - **H J Larsen**

Single Shearing Properties on Various Types of Screwed Joints Tested According to ISO16670 - **K Kobayashi, M Yasumura**

Failure Criteria for Post-tensioned Timber Beams - **W van Beerschoten, A Palermo, D Carradine, A Buchanan**

Some comments on CIB-W18 paper 45-102-1 by J. Köhler, R. Steiger, G. Fink and R. Jockwer - **T Poutanen**

The withdrawal strength of 8 threaded nails types - **J Munch-Andersen, S Svensson**

Simulation of Bottom Rail Fracture in Partially Anchored Shear Walls Using XFEM - **J Vessby, E Serrano, A Olsson, U A Girhammar, B Källsner**

Some Comments on the Sugiyama Opening Coefficient method and lower-bound solutions for shear walls - **J L Jensen, Xi'an Jiaotong, B Källsner, P Quenneville, U A Girhammar**

A note on surface scanning and stress grading based on fracture mechanics - **H Petersson**

**MEETING FORTY FIVE**

**VÄXJÖ**

**SWEDEN**

**AUGUST 2012**



# Block shear

H. J. LARSEN

Denmark

## 1 Introduction

When a member is loaded by a group of mechanical fasteners close to the end, there is a risk of failure because a plug or a block with depth  $t$  is torn out, see Figure 1.

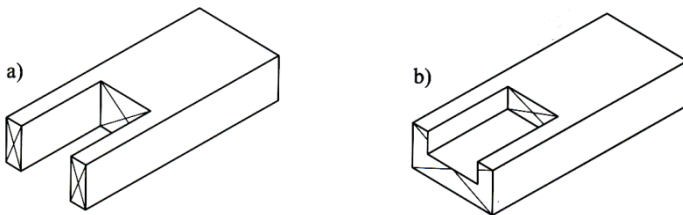


Figure 1. a) Plug shear. b) Block shear.

The most comprehensive treatment of plug/block shear may be found in [1].

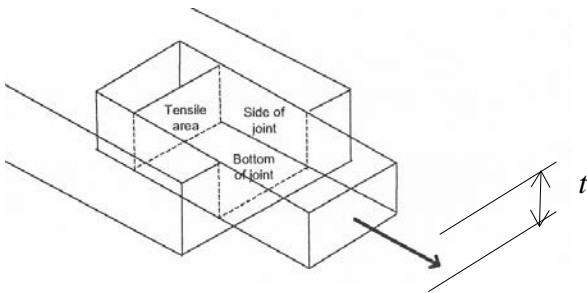


Figure 2. Definition of plug faces and belonging stresses. From [1].

According to [1] the sequence of failures, see figure 2, is as follows:

1. A crack develops internally along one side of the joint. The failure is initiated at the nail farthest from the free end.
2. The crack reaches the free end and is visible on the edge. A similar crack develops along the other side of the joint.
3. The end face fails in tension.
4. The final failure occurs when a shear crack along the bottom face joins the two side cracks.

The load-deformation properties in tension and shear are very different – failure in tension takes place long before failure in shear – and their contributions cannot be added.

Consequently, the load-carrying capacity  $R$  corresponds to the minimum of:

1. Failure of the nails
2. Tensile failure at the end face of the block
3. Shear failure at the bottom surface of the block.

In contradiction to the observations, the design according to [2] is based on the assumption that the two side cracks and the bottom crack form simultaneously.

The purpose of this Research Note is to investigate whether this assumption can be substantiated by tests.

## 2 Test results

Helena Johnsson's test results reported in [1] are summarised in the following. The nail patterns tested are shown in figure 3; details of specimen characteristics are given in Table 1.

Table 1. Specimen characteristics.

	number of rows $n_{rows}$	number of columns $n_{columns}$	number of nails $n$	spacing parallel $d$	spacing perp $d$	end distance mm
DUCT	4	5	20	15	7	83
RECTS	14	5	59	7	3,5	66
RECTL	25	10	143	7	3,5	80
RECTX	29	10	276	7	3,5	60
GRPS	16	10	143	7	3,5	56
GRPL	16	10	143	7	3,5	56
GRPX	16	4	143	7	3,5	56
NORMS	10	7	35	10	5	60
NORML	11	8	72	10	5	60
NORMX	21	10	157	10	5	60
SPREAD	15	10	143	10	5	56
TENSS	3	7	21	7	3,5	60
TENSL	4	17	66	7	3,5	60

## 3 Conclusions

It is obvious that the assumption that both the bottom and the sides of the failure block are active is not supported by tests.

## 4 Litterature

- [1] Johnsson, H. Plug Shear Failure in Nailed Timber Connections. Doctoral Thesis Luleå University of Technology, 2004.
- [3] EN 338. European Standard. Structural timber - Strength classes. 2009.





# Single shearing properties on various types of screwed joints tested according to ISO16670

Kenji Kobayashi, Motoi Yasumura  
Faculty of Agriculture, Shizuoka University, Japan

## 1 Introduction

Screws are used gradually for timber structures in Japan. Screws are often used after heat treatment such as quenching and tempering to improve their strength. Conditions of heat treatment or shapes of screw sometimes cause brittle failure of screws, so it is important to confirm a ductility of a screw. According to EN 14592, screws shall be bent up to a bending angle of  $\alpha = 45/d^{0.7} + 10$  degrees ( $d$ = outer thread diameter) without any cracks.

On the other hand, some kinds of joints are subjected to seismic (repetitive) action. Therefore, brittleness under cyclic loading should be taken into account to evaluate shear property of screw joints which resist seismic action.

This note introduces examples about results of reversed cyclic loading tests on various types of single shear joints with screws conducted according to ISO16670.

## 2 Test specimen

Combinations of materials and fasteners are shown in Table 1. Test type A and B are plywood-to-timber joints with wood screws (the result of shear wall tests of the same specification has been reported in 44<sup>th</sup> CIB-W18 meeting). Test type C is Steel-to-timber joints with lag screws. In test type D, cross laminated timber (CLT) made of Japanese Cedar was used for test specimen.

All fasteners used for the tests can be deformed more than required angles by three-point bending tests (wood screws with  $d=4.5\text{mm}$  and  $l=32\text{mm}$  were not tested because they were too short for three point bending test). The loading protocol is determined by ISO 16670, shown in Figure 1. Ultimate displacement  $D_u$  of each type was determined from monotonic test results. In case of  $D_u > 25\text{mm}$ , it was regarded as  $D_u = 25\text{mm}$  to determine cyclic displacement.

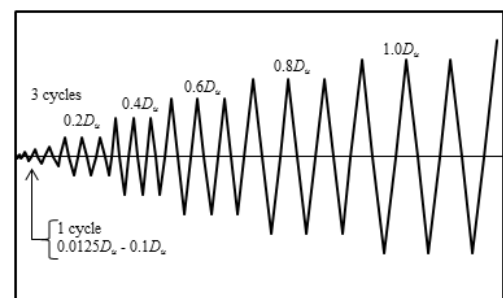


Figure 1 Loading protocol of ISO 16670

Table 1 Combinations of materials and fasteners

Test Type	Main member	Side member	Fastener		
			Type of fastener	Diameter	Length
A	Sawn timber (Japanese Cedar)	Plywood with 9mm thick (Pine)	Wood screw (WS)	4.5mm	32mm
B	Sawn timber (Japanese Cedar)	Plywood with 9mm thick (Pine)	Wood screw (WS)	4.5mm	50mm
C	Glulam (European Pine)	Steel plate with 9mm thick	Lag screw (LS)	12mm	90mm
D	CLT (Japanese Cedar)	CLT with 90mm thick (Japanese Cedar)	Self-Tapping Screw (STS)	8mm	180mm

### 3 Test Results

Pictures of screws after the test are shown in Figure 2. A fracture of screw occurred at the point of plastic hinge. These brittle failures were observed mainly at reversed cyclic loading tests. On the other hand, screw withdrawal (in all types), head embedment (in type B and D) and head pull-through (in type B) were mainly observed at monotonic tests. In type A, no plastic hinges were observed after the test of both monotonic and cyclic loading.

Examples of load displacement curve of each test types were shown in Figure 3.

Except for type A, monotonic loading test results showed higher performance than cyclic loading test results in each test type. Especially, ductile behavior was observed at monotonic loading test. In type D, while ultimate displacement was more than 80mm in monotonic test, it was about 20mm in reversed cyclic test. In type A, envelope curves were relatively similar between monotonic and cyclic loading.

Maximum load  $P_{max}$ , ultimate displacement  $D_u$  and total energy dissipation  $E_{total}$  (include hysteresis loop) were shown in Table 2. Each value was determined from load displacement curves at positive direction.  $P_{max}$  values did not decrease so much by

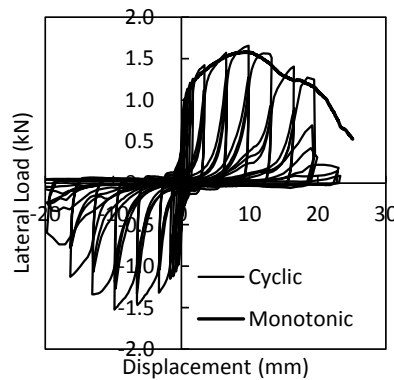


(C) Lag screws

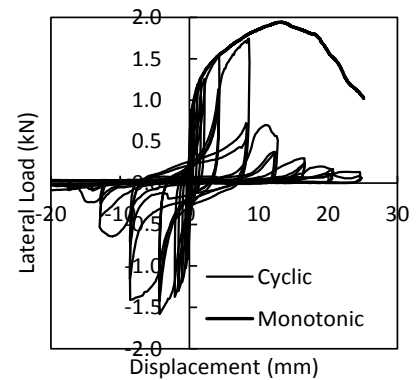


(D) Self tapping screw

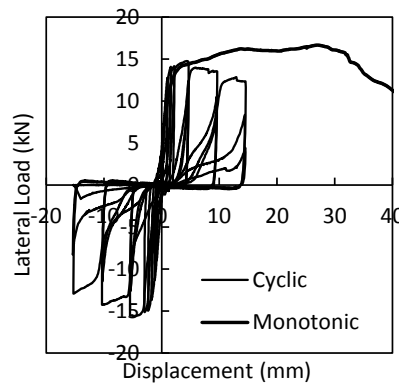
Figure 2 Pictures of screws after the test



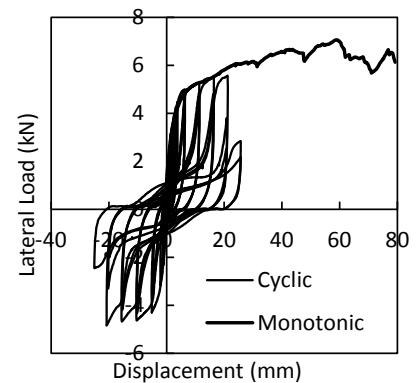
(A) Plywood-to-timber joint with wood screw 4.5x32mm



(B) Plywood-to-timber joint with wood screw 4.5x50mm



(C) Steel-to-timber joint with lag screw



(D) CLT-to-CLT joint with self-tapping screw

Figure 3 Load displacement curves of single shearing test

cyclic loading for all types. In type A,  $E_{total}$  value of cyclic loading test result was larger than that of monotonic test. It is because of hysteretic energy dissipation.  $D_u$  and  $E_{total}$  values of cyclic loading were much smaller than that of monotonic tests.

A fracture of screw did not occur before yielding at cyclic loading. Therefore, the requirement of EN 14592 is valid to keep a certain load-bearing capacity. But even in type D, a fracture of screw could not prevent nevertheless the fasteners could bend more than 90 degrees. Of course it is possible to consider that type D has enough ductility (for example, if a deformation limit of the joint is 15mm, the joint will work in the range of the deformation limit). It depends on the role of joints. If a joint is expected to dissipate seismic energy, both deformation and energy dissipation should be taken into account to design rules.

*Table 2 Comparison of test results*

Type	Loading Schedule	$P_{max}$ (kN)		$D_u$ (mm)		$E_{total}$ (kNmm)	
		ave.	(s.d.)	ave.	(s.d.)	ave.	(s.d.)
A (WS4532)	Cyc.	1.61	(0.17)	14.8	(3.80)	56.78	(16.32)
	Mono.	1.59	(0.16)	17.3	(2.90)	43.27	(4.52)
	Cyc./Mono.	<b>1.01</b>		<b>0.86</b>		<b>1.31</b>	
B (WS4550)	Cyc.	2.09	(0.21)	8.80	(1.60)	29.53	(2.09)
	Mono.	2.18	(0.36)	19.4	(4.60)	84.57	(7.19)
	Cyc./Mono.	<b>0.96</b>		<b>0.45</b>		<b>0.35</b>	
C (LS_D12L90)	Cyc.	15.8	(0.92)	14.6	(1.02)	364.4	(39.57)
	Mono.	17.1	(1.06)	32.5	(7.01)	487	(120)
	Cyc./Mono.	<b>0.9</b>		<b>0.5</b>		<b>0.7</b>	
D (STS_D8L180)	Cyc.	6.48	(1.14)	25.2	(3.82)	357	(89.2)
	Mono.	7.98	(0.80)	75.6	(7.34)	484	(39.4)
	Cyc./Mono.	<b>0.81</b>		<b>0.33</b>		<b>0.74</b>	

#### 4 Conclusions

In this study, reversed cyclic loading tests on various types of single shear joints with screws were conducted according to ISO16670 and compared to the results of monotonic loading tests. As a result, a fracture of screw occurred by cyclic loading nevertheless the fasteners could bend more than 90 degrees. In case that the joint is required to resist seismic action, both deformation and energy dissipation should be taken into account to design rules.

#### 5 References

- 1) EN 14592:2009. Timber structures - Dowel type fasteners – Requirements
- 2) ISO 16670:2003. Timber structures - Joints made with mechanical fasteners - Quasi-static reversed-cyclic test method.
- 3) Kobayashi K, Yasumura M. Evaluation of plywood sheathed shear walls with screwed joints tested according to ISO 21581. Proceedings of the 44th CIB-W18 meeting, paper 44-15-8, Alghero, Italy.



# Failure Criteria for Post-tensioned Timber Beams

Wouter van Beerschoten, Alessandro Palermo, David Carradine, Andrew Buchanan  
University of Canterbury, New Zealand

## 1 Introduction

Post-tensioned timber box beams can create long spans necessary for large open spaces in commercial and office buildings. Engineered wood products, like Glulam and Laminated Veneer Lumber (LVL), make it possible to use large timber hollow sections in combination with unbonded post-tensioning tendons [1], in either straight or draped profiles (Figure 1). Beams can be manufactured and stressed off-site, similar to precast concrete beams.

Design of long span timber beams is often governed by deflection criteria, resulting in an underutilization of the strength of timber. This can be partly resolved by adding a precamber during construction of Glulam beams, but this is difficult for LVL beams. Similar to typical applications in prestressed concrete elements, the use of post-tensioning can induce a precamber resulting in decreased deflections.

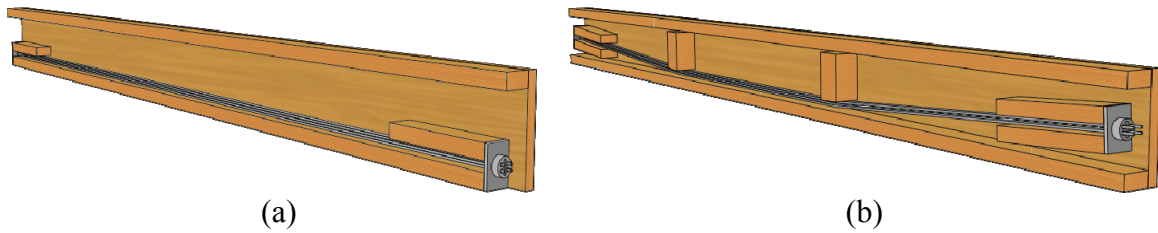


**Figure 1.** Longitudinal section of timber box beams with (a) straight post-tensioning and (b) draped post-tensioning tendons.

Four LVL box beams with and without post-tensioning have been tested till failure. This paper describes the results and proposes failure criteria for ultimate limit state design of long-span post-tensioned timber box beams.

## 2 Experimental testing

Testing was performed as a four point bending test with a 9.2m span (Figure 2). All beams were designed to have a similar load carrying capacity. Beam 1 does not have post-tensioning. Beam 2 has straight tendons down the bottom. Beam 3 and 4 both have draped tendons, but are designed to have a different failure mechanism. One end of each beam was supported by a pin and the other end by a roller support. Two hydraulic actuators were used which were programmed to apply equal loads. The box beams were made of LVL 11, with characteristic properties as shown in Table 1. Section properties of the four box beams are shown in Table 2. Initial post-tensioning (PT) forces and tendon profiles are also shown. Furthermore, design compression and bending capacities, based on NZS3603 [2], are given. These values are based on Equations 1 and 2.

$$\phi N_n = \phi \cdot k_1 \cdot A \cdot f_c \quad (\text{Eq. 1})$$

$$\phi M_n = \phi \cdot k_1 \cdot k_{24} \cdot Z \cdot f_b \quad (\text{Eq. 2})$$

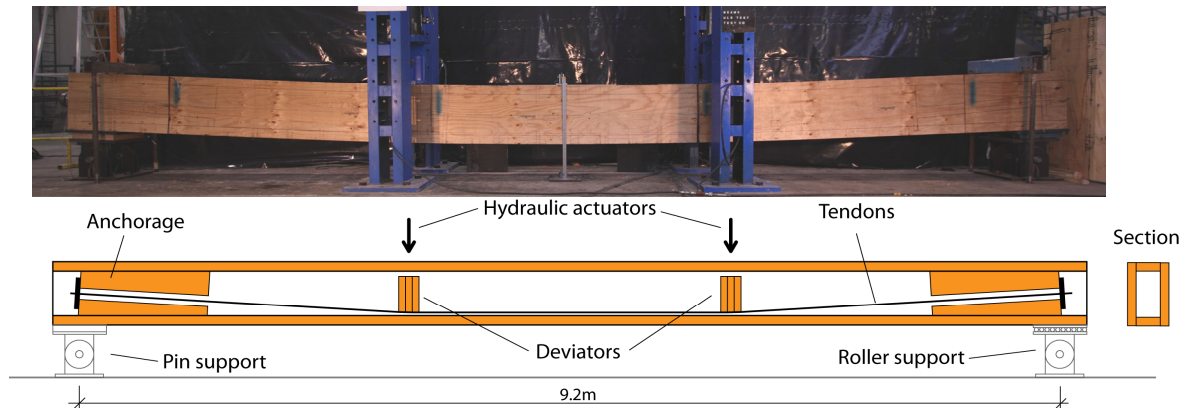
where the strength reduction factor  $\phi = 0.9$ , the load duration factor  $k_1 = 0.8$  and the size factor  $k_{24} = 0.7$  (for  $h=760\text{mm}$ ) or  $0.73$  (for  $h=610\text{mm}$ ).

**Table 1.** Characteristic material properties [3]

Type	Bending $f_b$ [MPa]	Compression parallel $f_c$ [MPa]	Tension parallel $f_t$ [MPa]	Compression perpendicular $f_{c,90}$ [MPa]	Shear strength $f_s$ [MPa]	Modulus of elasticity $MoE$ [GPa]
LVL 11	48.0	45.0	30.0	12.0	6.0	11.0

**Table 2.** Specimen details of tested beams

Beam No.	Height [mm]	Width [mm]	T top flange [mm]	T bottom flange [mm]	T webs [mm]	Initial PT force [kN]	Tendon profile	$\phi N_n$ [kN]	$\phi M_n$ [kNm]
1	760	426	90	90	63	-	-	4852	682
2	610	426	90	90	63	910	straight	4240	500
3	610	426	90	90	63	910	draped	4240	500
4	610	426	180	90	63	910	draped	5115	506

**Figure 2.** Picture and schematics of typical beam test setup (for beam with draped tendon)

### 3 Results

Figure 3(a) shows the load deflection graphs for the four beams. Beam 1, without post-tensioning showed very linear behaviour until sudden brittle failure at the bottom of the beam at 695kN loading. The higher stiffness in comparison with the other beams was due to larger section height. Beam 2 started with a precamber of just over 20mm and failed under 536kN load. This was a shear failure in one of the webs due to damage which occurred during initial stressing. Therefore the real section capacity is most likely greater. Beam 3 started with a similar precamber as Beam 2. At around 550kN the top flange started to fail in compression, followed by a load increase until tensile failure at the bottom was reached under a load of 726kN. Beam 4 also had just over 20mm precamber and showed a brittle tension failure under 837kN load.

Strain profiles at mid-span were measured using several strain gauges, located at top and bottom of both flanges and at neutral axis height. Figure 3(b) shows the stresses, derived from the strain measurements, under final failure load. The design bending strength limit ( $k_{24} \times f_b$ ) is also shown. When analyzing results at centroid of the beam it can be seen that Beam 1 was close to zero stress. Beam 2 and Beam 4 had a stress of 6.8 and 7.8MPa, respectively. Beam 3 started to show plastic behaviour in compression resulting in lowering of the neutral axis and thus an increased stress of 13.2MPa at beam mid-height. The maximum tensile stress for all beams, except for Beam 2 which failed prematurely, was between 44 and 49MPa.

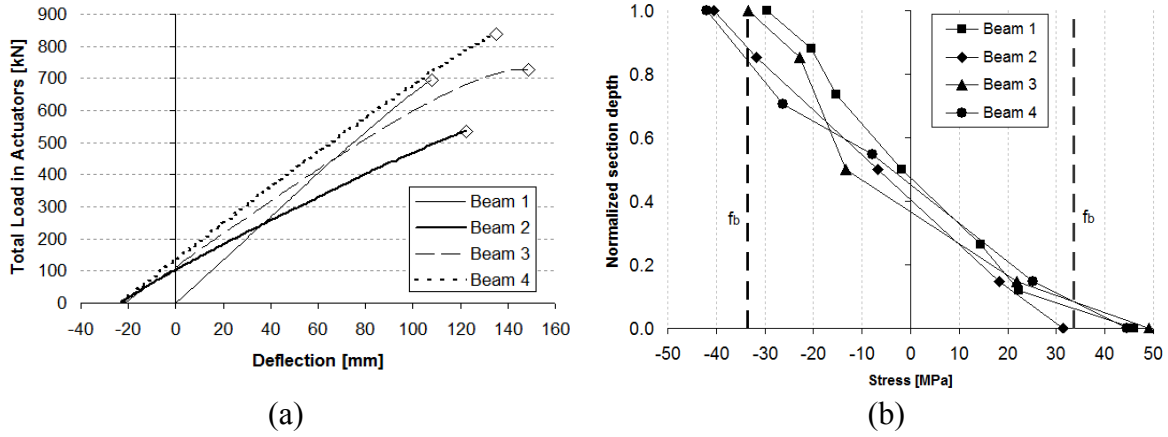


**Figure 3.** (a) Load-deflection graph and (b) strain profile at mid-span at failure load

## 4 Analysis

To calculate the load carrying capacity of the beams, two methods of design are possible:

- 1) based on combination of bending strength and compressive strength as per NZS, and
- 2) based on tension and compression capacity of top and bottom flange.

Method 1 assumes the compression demand ( $N^*$ ) is known based on summation of initial post-tensioning force and amount of tendon elongation [4], allowing the ratio of compression demand over compression strength ( $\phi N_n$ ) to be calculated. Next, using Equation 3, the ratio of bending demand ( $M^*$ ) over bending strength ( $\phi M_n$ ) can be calculated. This allows evaluation of acceptable bending demand according to this design limit.

$$\frac{N^*}{\phi N_n} + \frac{M^*}{\phi M_n} < 1 \quad (\text{Eq. 3})$$

The ratio of actual bending capacity ( $M_{\text{failure}}$ ), based on experimental testing, over allowable bending demand ( $M^*$ ) can be calculated. This ratio, calculated in Table 3, can be seen as the design safety factor and should be higher than one to ensure a safe design, but not so much higher that the design becomes uneconomical. From Table 3 it can be seen that for the four tested beams this method gives very different factors of safety, ranging from 1.56 to 2.76.

**Table 3.** Design values based on NZS3603 (Method 1) and test value comparisons

Beam	$N^*$ [kN]	$\phi N_n$ [kN]	$N^*/\phi N_n$	$M^*/\phi M_n$	$\phi M_n$ [kNm]	$M^*$ [kNm]	$M_{\text{failure}}$ [kNm]	$M_{\text{failure}}/M^*$
1	0	4852	0.00	1.00	682	682	1061	1.56
2	979	4240	0.23	0.77	500	385	763	1.98
3	1071	4240	0.25	0.75	500	374	939	2.51
4	1080	5115	0.21	0.79	506	399	1100	2.76

Method 2 evaluates the compression and tensile stresses in top and bottom flanges, ignoring bending stresses in the webs, similar to what is done for plywood box beams. The stress at the neutral axis is determined based on the compressive force. Stresses at top and bottom are limited by compressive and tensile strength. Integration of these stresses over the area of the flanges and multiplied by their internal lever arm to the neutral axis gives the bending moment capacity of the section ( $M_n$ ), as is shown in Figure 4. Resulting bending moments should be multiplied by the  $k_1$  and  $\phi$  factors in order to get the design

bending moment capacity ( $\phi M_n$ ). Failure bending moment ( $M_{failure}$ ) divided by bending moment capacity ( $\phi M_n$ ) gives the factor of safety. This procedure is shown in Table 4. It can be seen that for all beams tested the factor of safety is consistent at just over two, except for Beam 2 which failed prematurely.

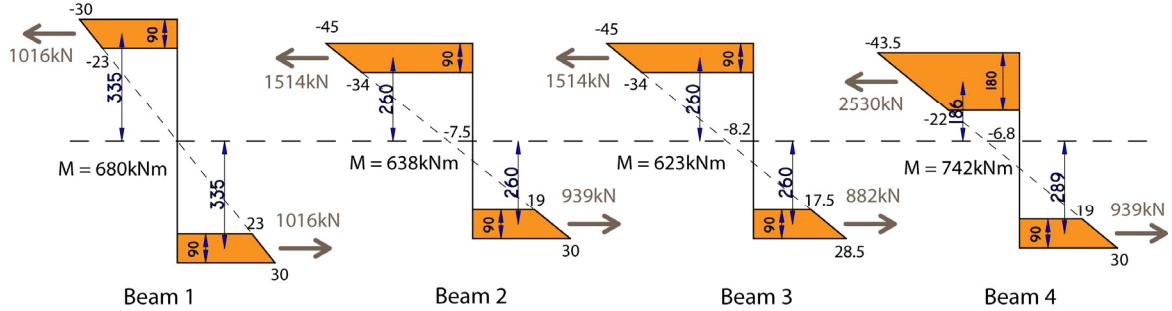


**Figure 4.** Stress integration over the flanges for determination of bending moment capacity

**Table 4.** Design values based on Method 2 and test value comparisons

Beam	$\sigma_{compr}$ [MPa]	$\sigma_{top}$ [MPa]	$\sigma_{bottom}$ [MPa]	$M_n$ [kNm]	$\phi M_n$ [kNm]	$M_{failure}$ [kNm]	$M_{failure}/\phi M_n$
1	0	-30	<b>30</b> <sup>1</sup>	680	490	1061	2.17
2	-7.5	<b>-45</b> <sup>1</sup>	<b>30</b> <sup>1</sup>	638	459	763	1.66
3	-8.2	<b>-45</b> <sup>1</sup>	28.5	623	449	939	2.09
4	-6.8	-43.5	<b>30</b> <sup>1</sup>	742	534	1100	2.06

<sup>1</sup> bold figures indicate values governing the design

When comparing the factors of safety found using the two methods it can be seen that Method 2 gives more consistent results. It also allows predicting whether the section strength is governed by compression or tensile capacity. Therefore this method is preferred over Method 1.

## 5 Conclusions

Experimental testing of four LVL box beams with and without post-tensioning has provided data on ultimate strength. Two different design methods to predict the load carrying capacity have been evaluated. It has been shown that the current design method, based on NZS3603, gives variable levels of safety. An alternative method, evaluating maximum tensile and compression strength gives much more consistent levels of safety. This method also indicates if the section strength is governed by tensile or compression capacity. As only four beams have been tested, further numerical modelling will be performed to validate the design method.

## References

- [1] A. Buchanan, A. Palermo, D. Carradine, and S. Pampanin, "Post-Tensioned Timber Frame Buildings," *The Structural Engineer*, vol. 89, September 2011.
- [2] Standards New Zealand, *Timber structures standard*, NZS 3603:1993, Wellington, New Zealand, 1993.
- [3] Nelson Pine, "Nelson Pine LVL 11 Brochure," ed. Nelson, 2010, p. 8.
- [4] A. Palermo, S. Pampanin, D. Carradine, A. Buchanan, B. Lago, C. Dibenedetto, S. Giorgini, and P. Ronca, "Enhanced performance of longitudinally post-tensioned long-span LVL beams," 11th WCTE, Trentino, Italy, 2010.

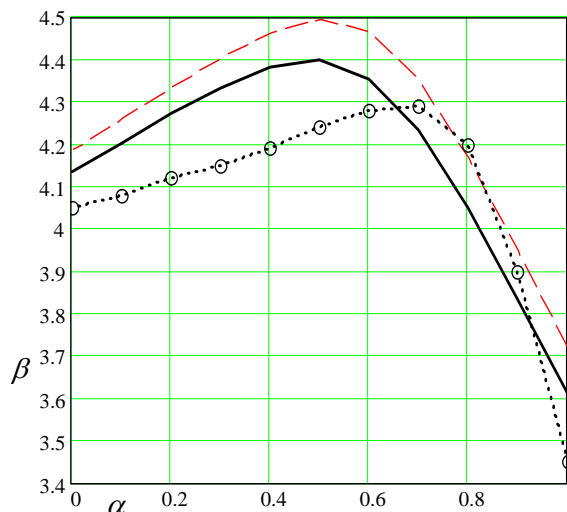
Some comments on CIB-W18 paper 45-102-1 by J. Köhler, R. Steiger, G. Fink and R. Jockwer

T. Poutanen<sup>1</sup>

1. In the paper, the reliability calculation is based on one-year reliability and the safety factors of this calculation are compared with Eurocode safety factors. However, Eurocode safety factors are based on 50-year reference and working time. It is wrong to compare one-year and 50-year safety factors.
2. In the paper, the target one-year reliability is  $\beta_1= 4.2$ . However, in Eurocode one-year reliability is  $\beta_1= 4.7$ . Eurocode safety factors are based on reliability  $\beta_{50}= 3.826$ . For this reason the calculation includes a safe error ca 15...20 % which counterbalances the unsafe error of independent load combination and therefore the calculated safety factors are approximately equal to the current Eurocode safety factors.
3. The reliability model of the paper is based on the dependent load combination model of Eurocode 6.10. However, the loads are combined independently. If loads are combined independently the independent load combination model should be applied consistently and the independent combination model of Eurocode, either 6.10a,b or 6.10a,mod should be used.
4. The paper does not include reliability values without model uncertainty. If these values were included, we could see the apparent error of the current uncertainty calculation: the uncertainty effect is unrealistically little, 10 % uncertainty decreases reliability index 1...3 %, see Figure, red dashed line and Table,  $\beta_{U=0}, U=0.1/U=0$  below.
5. Numerical reliability calculations are difficult and it is common that these calculations involve inaccuracies. The paper includes apparent numerical calculation error  $\pm 4$  %, see Figure and Table below with the calculation comparison of the paper and by Poutanen.

$$\gamma_G = 1.35, \gamma_Q = 1.5, \gamma_M = 1.313, COV_{G,normal} = 0.1, COV_{Q,Gumbel} = 0.4, COV_{U,lognormal} = 0.1, \alpha = G/G+Q$$

$\alpha$ G/G+Q	$\beta$ Poutanen	$\beta$ Paper	Paper/ Poutanen	$\beta, U=0$ Poutanen	$U=0.1/U=0$
0,0	4,136	4,05	0,98	4,185	0,99
0,1	4,204	4,08	0,97	4,259	0,99
0,2	4,271	4,12	0,96	4,333	0,99
0,3	4,334	4,15	0,96	4,405	0,98
0,4	4,382	4,19	0,96	4,465	0,98
0,5	4,398	4,24	0,96	4,495	0,98
0,6	4,355	4,28	0,98	4,467	0,97
0,7	4,234	4,29	1,01	4,355	0,97
0,8	4,051	4,20	1,04	4,172	0,97
0,9	3,836	3,90	1,02	3,952	0,97
1,0	3,610	3,45	0,96	3,720	0,97



solid line - Poutanen; dotted circled line - paper;  
dashed line - Poutanen  $COV_U = 0$

<sup>1</sup> Tampere University of Technology, P.O. Box 600, FIN 33101 Tampere, FINLAND, tuomo.poutanen@tut.fi

# Dependent load combination in structural design

T. Poutanen<sup>1</sup>

## Introduction

Permanent loads,  $G-G$ , are independent and combined in current codes always dependently. A permanent load and a variable load,  $G-Q$ , are independent during one year but dependent in 50 years and combined in the failure state sometimes independently and sometimes dependently but in the serviceability state always dependently. Variable loads,  $Q-Q$ , are combined usually semi-dependently but sometimes dependently. A universal theory on the load combination was lacking.

However, regardless of whether the loads are independent or dependent the structural loads must always be combined dependently i.e. by adding up the loads in the partial load fractiles to obtain the combination load value of the related fractile.

## Arguments for the dependent load combination

Several arguments alone stipulate the dependent combination e.g.: extreme distribution, maximum load rule, equality equation, Hook's law, linearity and load losing.

In the structural design the distributions must be the extreme distributions: either the highest loads or the least strengths of a specific probability. The combination distribution must be the extreme distribution, too, i.e. the extreme of the extremes. The independent combination is the sum of the extremes when the maximum load rule is wrongly ignored.

The basic design equation of the structural design with the permanent load  $G$ , the variable load  $Q$  and the material property  $M$  is

$$\gamma_G \cdot G + \gamma_Q \cdot Q \leq \frac{M}{\gamma_M} \quad (1)$$

The equality equation makes a definite correlation between  $G$  and  $Q$  in the combination though  $G$  and  $Q$  were independent as  $M$  is constant regarding the loads.

One realization of the independent load combination is the combination rule 6.10a,mod of Eurocode. In this load combination with low permanent load when the variable load increases no effect occurs contrary to the linearity and Hook's law.

The independent combination actually contradicts the linearity and the Hook's law and includes a load losing: Assume the target reliability is 0.98, the loads  $G$  and  $Q$  have normal distribution, and act in a tension bar,  $A = 1000 \text{ mm}^2$ . We see in Table 1 and the load case 5 with the independent combination that ca 10 % load vanishes in the combination; the linearity and Hook's law are not valid.

Table 1. Five load cases of  $G$  and  $Q$ . The load case 5 shows that the independent combination results in a load losing of ca 10 %, the linearity and the Hook's law are not valid.

load case	load [kN]		stress [N/mm <sup>2</sup> ]	
	$G$	$Q$	depend.	independ.
1	1	0	1	1
2	0	1	1	1
3	0.2	0	0.2	0.2
4	0	0.2	0.2	0.2
5	0.2	0.2	0.4	0.37

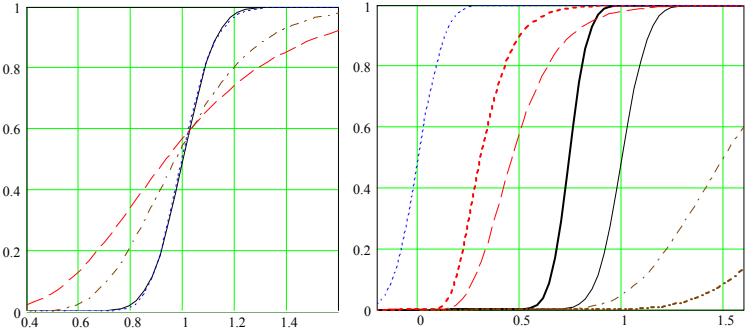
---

<sup>1</sup> Tampere University of Technology  
P.O. Box 600, FIN 33101 Tampere, FINLAND  
p: +358408490900, f: +358331152811, e: tuomo.poutanen@tut.fi

## New method for reliability calculation

I presented in CIB-W18/42 [1] a new method for reliability calculation. In CIB-W18/44 [3] J. Köhler argued my claim of dependent load combination and presented the current method. The methods are compared by using Köhler's example. The new method has some advantages: It calculates the independent and the dependent safety factors without an interphase and without  $\beta$ - and  $P_f$ -bias.

Figure 1, Distribution fitting in the current method, left, the distribution means are set at the design point [3] and in the new one, right, the distributions have their actual location in reference to each other. Permanent load: continuous black line; variable load: red dashed line; model uncertainty: blue dotted line; material property: brown dash-dotted line. Thick lines denote the corresponding failure distributions.



In the current calculation, the basic design equation 1 is converted to a particular limit state equation [3] and a special computer program is needed. The output is the reliability,  $\beta$  or  $P_f$ . To obtain appropriate safety factors trial and error or a further computer program is needed<sup>2</sup>. Neither such equations nor computer programs are needed in the new method as the design equation 1 is converted explicitly to the reliability equation<sup>3</sup> and the method results in the arrangement of safety factors corresponding to the target reliability.

$$1 - \int_0^{\infty} \int_{-\infty}^{\infty} FQ \left( x - r, \frac{\mu_Q \cdot \alpha}{\gamma_Q \cdot \gamma_M}, \frac{\sigma_Q \cdot \alpha \cdot \kappa}{\gamma_Q \cdot \gamma_M} \right) \cdot fN \left[ r, \frac{1 - \alpha}{\gamma_G \cdot \gamma_M}, \frac{\sigma_G \cdot (1 - \alpha) \cdot \kappa}{\gamma_G \cdot \gamma_M} \right] \cdot dr \cdot fL(x, \mu_M, \sigma_M) dx = P_f \quad (2)$$

$FG$  is the cumulative distribution of the variable load,  $fN$  and  $fL$  are the density distributions of the permanent load and the material property,  $\alpha$  is the proportion of the variable load in the total load,  $P_f$  is the failure probability,  $\kappa$  is the dependence factor<sup>4</sup>. According to equation 2, the reliability can be set in the action, in the resistance or in both, and the option  $\gamma_G = \gamma_Q = 1$  is always possible, for instance.  $fL$  can be replaced by test or quality control data when  $fL$  is not needed i.e. the error induced from the distribution fitting is avoided. Analogously,  $FG$  and  $fN$  can be replaced by the load data.

Currently, the uncertainty is considered in the resistance by using the lognormal function and the independent combination. The reference is either the design point or the distribution mean<sup>5</sup>. Both options result in an unrealistically low effect. Other alternatives are: the uncertainty in the action instead of the resistance. It is obvious that the uncertainty distribution is closer to the normal than the lognormal function. In any case, the uncertainty must be combined dependently as it acts like a load. Figure 2 shows the results of the basic options. Eurocodes have the material factor  $\gamma_M \approx 1.35$  for the sawn timber  $V_M = 0.25$ ,  $\beta = 3.826$ , approximately corresponding to the dependent calculation,  $\gamma_M \approx 1.4$ . The independent calculation results in  $\gamma_M \approx 1.15$  respectively.

Besides the model uncertainty, we should consider the variability and error induced by design, execution, use. The total effect may be called “uncertainty” or “miscellaneous variation”. In order to have the balanced reliability between the metal and the timber we should have  $V_U = 0.1 \dots 0.15$ . In the current codes,  $V_U = 0 \dots 0.1$ , metal structures fail by a minor error [4].

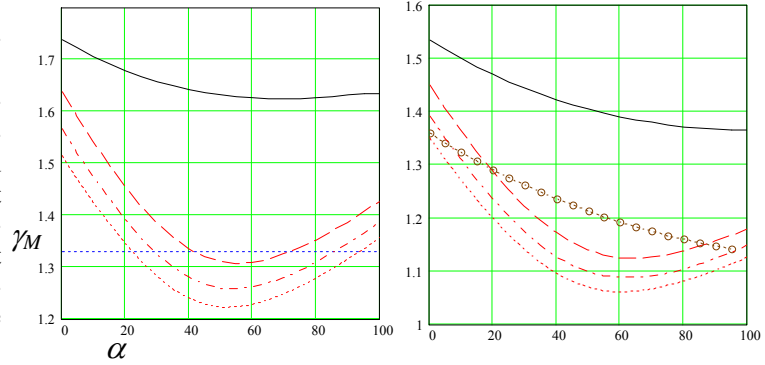
<sup>2</sup> Current methods for deriving  $\gamma_M$  from  $\beta$  or  $P_f$  are questionable and include a bias as  $\gamma_M - \beta$  and  $\gamma_M - P_f$  relation are assumed linear and the same for all loads.

<sup>3</sup> We may write this equation in many other ways analogously to the design equation 1.

<sup>4</sup> The result is the same as obtained from the Ferry Borges - Castanheta's model, if  $\kappa = 1$ .

<sup>5</sup> This is questionable as the uncertainty is a function of the current material.

Figure 2, Material safety factors  $\gamma_M$  calculated in Köhler's example [3],  $V_M = 0.25$ ,  $V_U = 0.1$ ,  $\beta = 4.265$ , left; Eurocode reliability,  $\beta = 3.826$ , right.  $\alpha$  is the proportion of the variable load in the total load [%]. Independent combination without model uncertainty: red dotted line; independent load combination, independent model uncertainty calculated with log-normal function, the design point is the reference: red dash-dotted line;



the same as the previous one but the uncertainty reference is the distribution mean: dashed line; dependent load combination, dependent model uncertainty calculated in the action with normal function: black continuous line; the same as the previous one but  $\beta = 3.4$ : red o-line. The horizontal blue dotted line denotes the safety factor  $\gamma_M = 1.33$  according to Köhler, my calculation is  $\gamma_M = 1.65$  correspondingly.

## Conclusions

Loads are always combined dependently; it is the consistent and the universal load combination.

Combination rules with two permanent load factors e.g. rules 6.10a,b and 6.10a,mod of Eurocode are based on the independent load combination. These rules should be deleted.

The current reliability model is up to 20 % unsafe in comparison with the target reliability due to the independent and semi-dependent load combination. The current uncertainty calculation increases the unsafe error further. The actual maximum unsafe error of current codes apparently is ca 15 % as the safety factors are higher than those obtained from the reliability model. On the other hand, the current codes have an excess safe error of ca 50 % in some load cases due to the constant design point value,  $dp_Q$ , for all variable loads and the constant material factor  $\gamma_M$  for all  $G-Q$  load combinations.

The variable loads are combined dependently, too when the distributions are altered in a way the loads are simultaneous. A combination factor  $\psi_0$  is induced from this distribution alteration. Some variable loads, e.g. the snow load (combined to any load) and the imposed load (combined to each other) have no combination factors,  $\psi_0 = 1$ .

A common misunderstanding is that each load and material should have a safety factor in the failure design. However, the reliability can be set in the action, in the resistance or in both. If we set  $\gamma_G = \gamma_Q = 1$ , the design equations and the current limit state design concept remain intact and the reliability accuracy is as good as in the current codes. If we set  $\gamma_G = \gamma_Q = 1$ ,  $dp_Q$  variable and  $\gamma_M$  semi-variable (constant in normal load cases) we obtain a code which is much more accurate (the reliability error is ca 0...10 %) and the design work less than in any code,  $\gamma_G \neq \gamma_Q \neq 1$ ,  $dp_Q$  constant and  $\gamma_M$  constant (the reliability error is ca -20...50 %).

The target reliability of Eurocode,  $\beta = 3.826$ , is high and the reliability error of 20 % cannot be observed by failures in the actual construction, maybe except for metal structures [4].

## References

- [1] Poutanen T., (2009) Calculation of partial safety factors, CIB-W18/42-1-1<sup>6</sup>
- [2] Poutanen T., (2010) Dependent versus independent loads in structural design CIB-W18/42-101-1<sup>7</sup>
- [3] Köhler J., (2011), Reliability Based Code Calibration – note on basic principles and possible misunderstandings, CIB-W18/44
- [4] [www.tut.fi/rtek/poutanen/en](http://www.tut.fi/rtek/poutanen/en)

<sup>6</sup> This paper was not published in the proceedings; however the paper discloses a new and correct reliability theory and a simple method for safety factor calculation.

<sup>7</sup> This paper makes distinction between dependent and correlated loads; however such distinction is irrelevant.

# The withdrawal strength of 8 threaded nails types

Jørgen Munch-Andersen, Danish Timber Information

Staffan Svensson, Dept. of Civil Eng., Technical University of Denmark

## Introduction

8 types of threaded nails with nominal diameter 3,1 mm and length about 90 mm have been nailed approximately 30 to 40 mm into 10 different boards by a pneumatic hammer. 3 nails of each type are used in each board, so a total of 240 nails are withdrawn, give or take a few. One nail type was twisted, all the other 7 were ring sharked and very similar in appearance.

The purpose of the study is to investigate if there is a difference between the real withdrawal strengths  $f_{ax}$  or if the difference between the declared values in the CE-marking are a matter of uncertainties during the ITT tests used to establish the declared value. Some of the factors that might influence the ITT-results are discussed in [1].

## Model and estimates

The following model is used to estimate the mean value of withdrawal capacity:

$$F_{ax,est} = d f_{ax} k_{nail} k_{board} l_{ef}$$

where

$F_{ax,est}$  is the estimated withdrawal capacity

$d f_{ax}$  is the estimated withdrawal capacity per unit penetration length (equal to nominal nail diameter  $d$  times withdrawal parameter  $f_{ax}$ )

$k_{nail}$  is a nail factor estimated for each of the 8 nail types, average =1

$k_{board}$  is a board factor estimated for each of the 10 boards, average =1

$l_{ef}$  is the measured penetration depth excluding the point length (1,5  $d$ )

The estimates are, as in [1] and in accordance with Eurocode 0, Annex D for LogNormally distributed strengths, chosen in order to minimize the variation of the error

$$\Delta = \ln \frac{F_{ax,obs}}{F_{ax,est}}$$

The basic estimate for the withdrawal strength becomes  $d f_{ax} = 48,1$  N/mm (= 3,1 mm · 15,5 MPa). The coefficient of variation on  $F_{ax,est}$  is  $V = 0,105$ . It is equal to the standard deviation of  $\Delta$ . The deviations between the estimate and the observed values are shown in Figure 1.

$k_{nail}$  represents the systematic difference between the withdrawal parameters for the nails. The estimates are given in Table 1.

$k_{board}$  represents the systematic difference related to the boards and include the effect of the density. The estimates are given in Table 2.

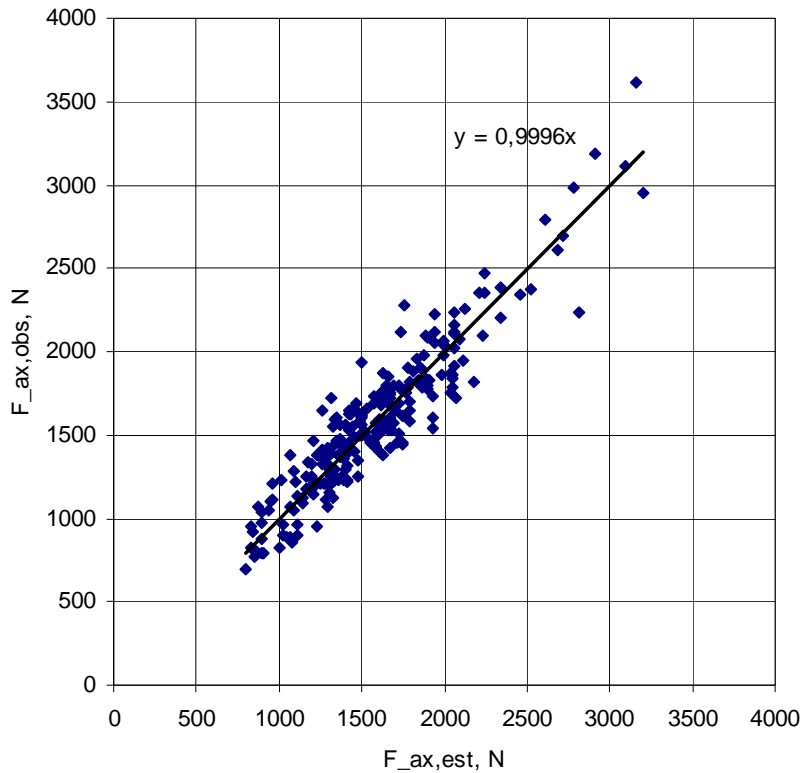


Figure 1. The estimated versus the observed values of the withdrawal capacity  $F_{ax}$ .  $d.f_{ax}$  is chosen such that the slope becomes 1.

Table 1. Estimated nail factors.

Nail no	1	2	3	4	5	6	7	8
$k_{nail}$	1,25	0,68	0,93	0,96	1,02	1,16	1,04	1,01

Note: Nail no 2 is twisted. No 4 is similar to no 3, but uncoated. No 1 and no 8 appears to be identical, but originates from two different suppliers.

Table 2. Estimated board factors.

Board no	2	3	4	5	6	7	8	9	10	11
$k_{board}$	0,87	0,73	0,87	0,68	0,68	1,03	1,33	1,19	1,03	1,60
Density, $kg/m^3$	396	396	420	407	398	436	482	490	414	555

Note: Board no 6 consists of two parts with densities  $391 kg/m^3$  and  $405 kg/m^3$ .

## Discussion

Figure 2 demonstrates that the major part of the board factor can be related to the density of the boards. It was expected that  $F_{ax}$  would increase linearly with the density for ring sharked nails, but the figure shows that the best estimate would be obtained using a power above 2 on the density.

Figure 3 shows the "individual nail factor" for each tested nail after correction with the board factor. For each nail type the mean value of the individual factors become equal to the nail factor given in table 1.

If the individual factors for two nail types overlap significantly a statistical test will tell that they cannot be assumed to be different. It is obvious that Nail type 3, 4, 5, 7 and 8 cannot be assumed to be different. The nail factors for this group range from 0,93 to 1,04, a difference similar to the coefficient of variation, 10,5%. The difference ought to be twice the coefficient of variation to be significant.

There is a clear difference between this group and Nail type 1 and 2. Nail type 6 might also be different, but not very convincing.

It is not surprising that Nail type 2, the twisted nail, has a lower capacity than the other nails. For the ring sharked nails type 1 and 6 seems to be better than the rest, but the fact that Nail type 1 and 8 originates from the same factory demonstrates that the observed statistically significant difference can be caused by variations in the production process, i.e. if the tool used to shape the nails is new or nearly worn out. With that in mind the tested ring sharked nails can be assumed to have similar withdrawal load bearing capacities.

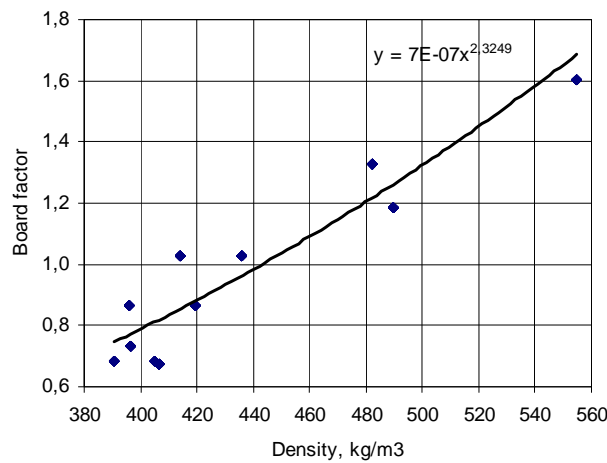


Figure 2. The board factor as a function of density. It is to a large extent proportional to the density raised to power 2,3.

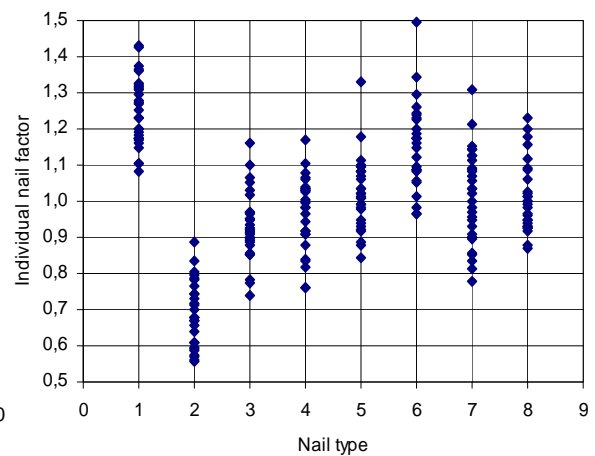


Figure 3. The "individual nail factor" for each tested nail after correction with the board factor.

## Acknowledgment

The tests on which this note is based are carried out by Mads Wendt-Larsen and Jonas Madsen as part of their diploma work for obtaining the BSc(Eng) degree at the Technical University of Denmark.

## References

- [1] Munch-Andersen, J, Sørensen, J D & Sørensen, F: Estimation of load-bearing capacity of timber connections. Proc. of CIB-W18 Timber Structures (Paper 43-21-1). Nelson, New Zealand. 2010.



# Simulation of bottom rail fracture in partially anchored shear walls using XFEM

Johan Vessby<sup>1</sup>, Erik Serrano<sup>1</sup>, Anders Olsson<sup>1</sup>, Ulf Arne Girhammar<sup>2</sup>, Bo Källsner<sup>1</sup>

<sup>1</sup>Linnæus University, Växjö, Sweden.

<sup>2</sup>Luleå University of Technology, Luleå, Sweden.

## 1 Background, aim and scope

A recent development in the design of medium-rise timber structures relates to the use of plastic design approaches that include three-dimensional effects, see e.g. Källsner and Girhammar (2009) and Källsner et.al. (2010). Among the benefits included with such an approach are that *partially* anchored walls may be used as stabilising elements and that lateral walls connected to stabilising walls may be used as anchorage to counteract the considerable uplifting forces that may occur, see Figure 1. On the one hand this design philosophy predicts an enhanced performance of the timber building; on the other hand it may introduce uplifting forces in the bottom rail anchored to the floor or foundation. Thus, the risk of splitting failure in the bottom rail must be assessed, since if such brittle failure occurs, the plastic design philosophy may be questioned, see e.g. Girhammar and Källsner (2009). Bearing in mind that the failure modes are dominated by fracture perpendicular to the fibre direction, fracture mechanics is an appealing technique to utilize in analysing the phenomenon.

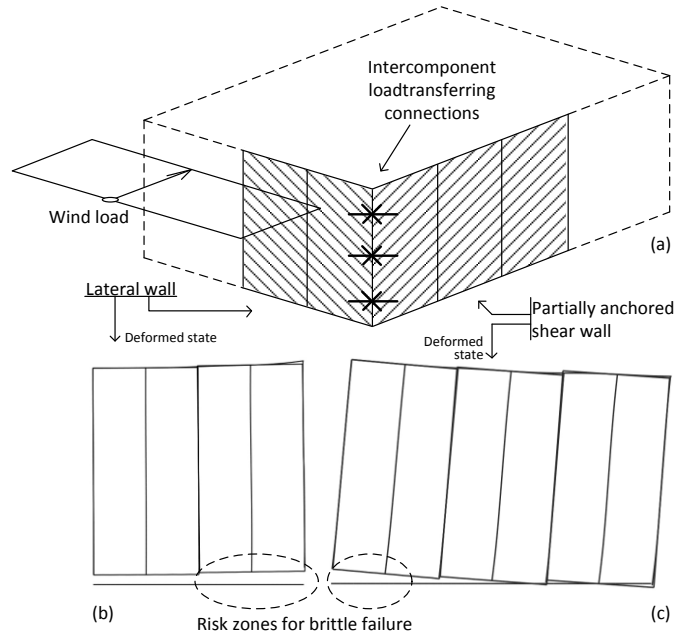


Figure 1. (a) Part of a storey in a timber framed building where the shear wall is interconnected to the lateral wall. The deformed state of the (b) lateral and (c) partially anchored shear wall is shown and the risk zones for brittle failure are indicated.

In previously performed studies, see Serrano et al. (2011 a,b), linear elastic fracture mechanics (LEFM) was used for analysing the crack propagation with an analytical closed form expression (eq. 1) as well as by using two-dimensional plane strain finite element models, see Figure 2(b).

$$P_C = lh \sqrt{\frac{2GG_C/b_e}{12\frac{G_C}{E}\left(\frac{b_e}{h}\right)^2 + \beta_s}} \quad \text{eq. 1}$$

The aim of the current study is to analyse the vertical crack, which may occur in the rail, with respect to size and location of the washer. In the current study the analyses are performed using the *extended finite element method* (XFEM) which includes the possibility for cracks to propagate through finite elements i.e. without the need to define a crack path *a priori* or perform remeshing during analyses. Examples of XFEM models in 2 as well as 3 dimensions are shown in Figure 2(c) and (d). Based on the results of the models, the previously suggested closed form expression may be further verified for possible implementation in Eurocode 5. The evaluation is limited to walls with sheathing fastened to one side only and to a bottom rail with the dimensions 45 · 120 mm, see Figure 2(a).

## 2 Crack growth using XFEM

The extended finite element method was first introduced by Belytschko and Black (1999) and has since then become increasingly used for simulating discontinuous phenomena such as fracture in 2D as well as in 3D. The fundamental idea is to enrich the approximating functions within a specified region with a step function that allows for the presence of displacement discontinuities. Lately the technique has been implemented into various commercial software such as the general purpose finite element software ABAQUS. The main advantages using XFEM in simulating fracture is that the crack propagation path does not need to be defined prior to the analysis itself but is instead arbitrary and solution-dependent. This implies that the crack propagates inside elements and across element boundaries rather than along predefined element edges.

In the current study XFEM was used for modelling the rail in two dimensions (plain strain), but a simplified analysis was also performed in three dimensions, see Figure 2. The result in terms of ultimate load capacity will depend heavily on the *location* of the crack, i.e. also on the location of initial crack formation. In the analyses a crack may either develop at any location that fulfils a certain crack initiation criterion, e.g. a maximal principle stress, or at a predefined location. In the current analyses the crack initiation is defined by the location of the maximum stress component  $S_{xx}$  in an elastic reference model loaded by  $P=5$  kN, cf. Figure 3.

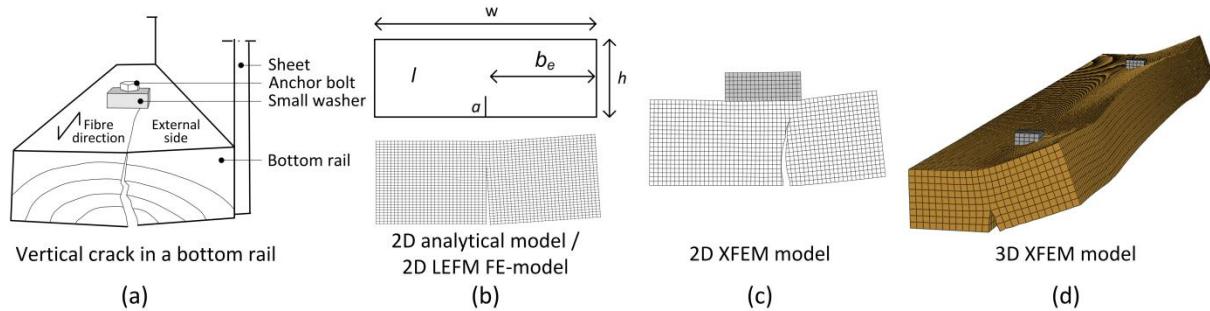


Figure 2. Vertical and horizontal crack (a) illustrated schematically and as calculated using three different models, i.e. (b) an analytical model, (c) a XFEM model and (d) an XFEM model. The 3D XFEM model is used to verify the previously suggested 2D models.

## 3 Geometry and material properties

Some of the conclusions in previous studies have been that further investigation is needed aiming at clarifying the importance of some critical parameters, see e.g. Serrano et al. (2011 a,b) and Caprolu et al. (2012). Of the parameters identified, the effect of the size and position of the washer will be further elaborated on herein. Note that the placement of the washer may vary for different washer widths and edge distances. Dimensions of the studied rail as well as notations and material parameters used for the analysis are defined in Figure 3 and in Table 1. In the contact between rail and washer a penalty formulation was used for the normal direction of the contact and friction was neglected (contact property I). The same applied for the contact region between rail and substrate, but here the default value of friction was set to  $\mu=0.2$  in accordance with EN 1995-2:2004 (E) (contact property II). In the orthotropic material model used, the pith was assumed to be located 5 mm below the bottom surface of the rail, at half its width.

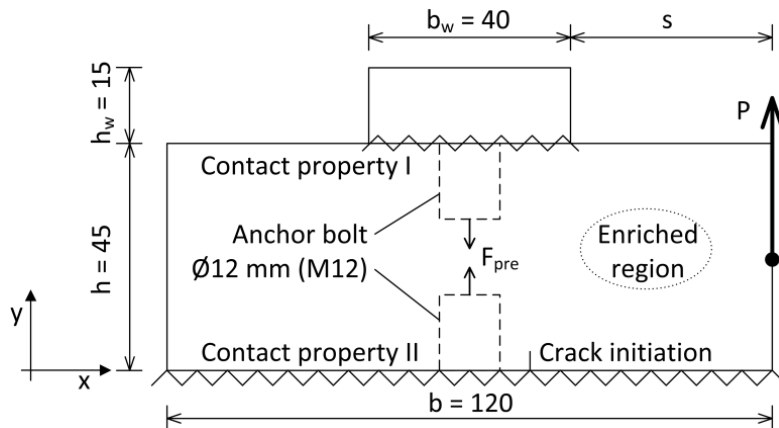


Figure 3. Dimensions and notations used in the analysis of the bottom rail.

Table 1. Material data and values of studied parameters used in the analyses.

$E_r$ (MOE, radial)	600 MPa (500 MPa in analytical (beam) model)	$\nu_{rt}$ (Poisson's ratios)	0.5
$E_t$ (MOE, tangential)	500 MPa (500 MPa in analytical (beam) model)	$f_{t,90}$ (tension perp.)	2.5 MPa
$G_{rt}$ (Shear modulus)	50 MPa	$G_C$ (fracture energy)	300 J/m <sup>2</sup>
Pretension force, $F_{pre}$			15 kN
Friction between rail and substrate, $\mu$			0.2
Width of washer, $b_w$			40, 50, 60, 80 mm
Edge distance, $s$			25,30, 40, 50, 60mm ( $b_w+s$ never exceeds 120 mm)
Length of rail, $l$			900 mm
Height of rail, $h$			45 mm
Length of cantilever beam in analytical eq., $b_e$			$s$
Shear correction factor, $\beta_s$			1.2

## 4 Results

In Figure 4 the critical load,  $P_c$ , is shown for the four studied widths of the washer,  $b_w$ , as a function of the distance between the washer edge and the rail edge,  $s$ . The results show that the size of the washer does not affect the critical load significantly, but the distance  $s$  may increase the capacity from around 15 kN to around 30 kN if decreased from  $s=60$  to  $s=25$  mm. As a comparison the critical load obtained using the analytical model is plotted; a reasonable agreement is achieved.

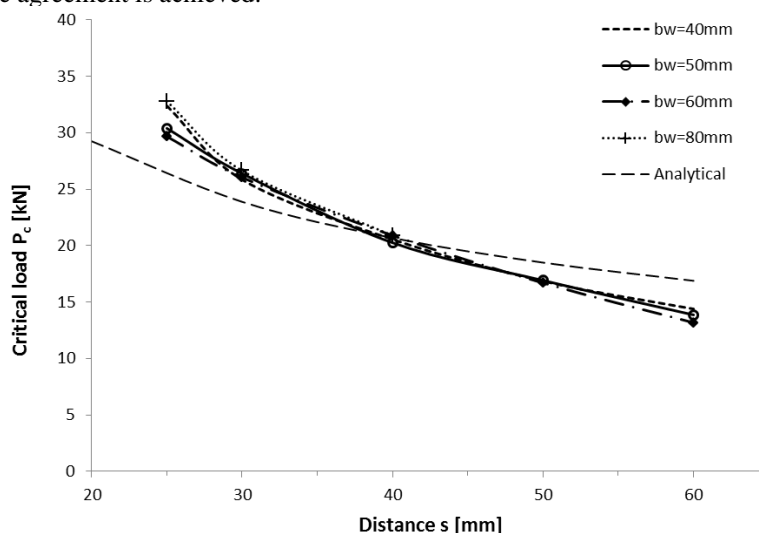


Figure 4. Critical load,  $P_c$ , for four different washer sizes ( $b_w=40, 50, 60$  and  $80$  mm) and analytical model as a function of distance  $s$  between washer edge and loaded rail edge.

## 5 Conclusions

In the study performed the capacity in the bottom rail in partially anchored shear walls has been examined for different washer sizes and different edge distances using the extended finite element model. Reasonably good agreement was achieved between the various simulations performed and the previously suggested analytical solution. Furthermore, the simulations show that the size of the washer is not a primary parameter, but rather the distance from the washer edge to the loaded rail edge.

## 6 References

- Caprolu, G., Källsner, B., Girhammar, U.A., Vessby, J. (2012). "Analytical and experimental evaluation of the capacity of the bottom rail in partially anchored timber shear walls", Proc. World conference on timber engineering, Auckland 2012, New Zealand.
- Eurocode 5 – Design of timber structures, Part 2: Bridges, EN 1995-2:2004 (E).
- Girhammar, U.A., Källsner, B. (2009). "Design aspects on anchoring the bottom rail in partially anchored wood-framed shear walls", Proc. CIB-W18 meeting, Dübendorf, Switzerland, 2009.
- Källsner, B., Girhammar, U.A., Vessby, J. (2010). "Some design aspects on anchoring of timber frame shear walls by transverse walls" Proc. World conference on timber engineering, Riva del Garda, Italy.
- Källsner, B., Girhammar, U.A., "Plastic models for analysis of fully anchored light-frame timber shear walls", Engineering Structures, 31(9), 2171-2181 (2009).
- Serrano, E., Vessby, J., Olsson, A., Girhammar, U.A., Källsner, B. (2011). "Design of Bottom Rails in Partially Anchored Shear Walls Using Fracture Mechanics" Proc. CIB-W18 meeting, Alghero, Italy, paper 44-15-4.
- Serrano, E., Vessby, J., Olsson, A. (2011). "Modeling of Fracture in the Sill-Plate in Partially Anchored Shear Walls", Journal of Structural Engineering doi:10.1061/(ASCE)ST.1943-541X.0000548.



# Some comments on the Sugiyama opening coefficient method and lower-bound solutions for shear walls

Jørgen L. Jensen, Xi'an Jiaotong-Liverpool University, China

Bo Källsner, Linnæus University and SP, Sweden

Pierre Quenneville, The University of Auckland, New Zealand

Ulf Arne Girhammar, Luleå University of Technology, Sweden

## Note

The Sugiyama opening coefficient method has hitherto been considered an empirical method for estimation of the failure load of a shear wall with an opening. Sugiyama allegedly never explained how he arrived at his opening coefficient, but just a look at the equation makes it clear that some kind of derivation based on mechanics must lie behind it. Yasumura [1] presents for the first time a model based on mechanics, which leads to Sugiyama's opening coefficient, and which most probably is the way used by Sugiyama. The present note reviews the derivation given by Yasumura [1] and compares it with a lower-bound solution named the Stringer Method. The Stringer Method is used for design of the reinforcement around holes in concrete walls [2].

Yasumura [1] considers a fully restrained shear wall with an opening as shown in Fig. 1. Sugiyama's opening coefficient method is given by Eq. (1).

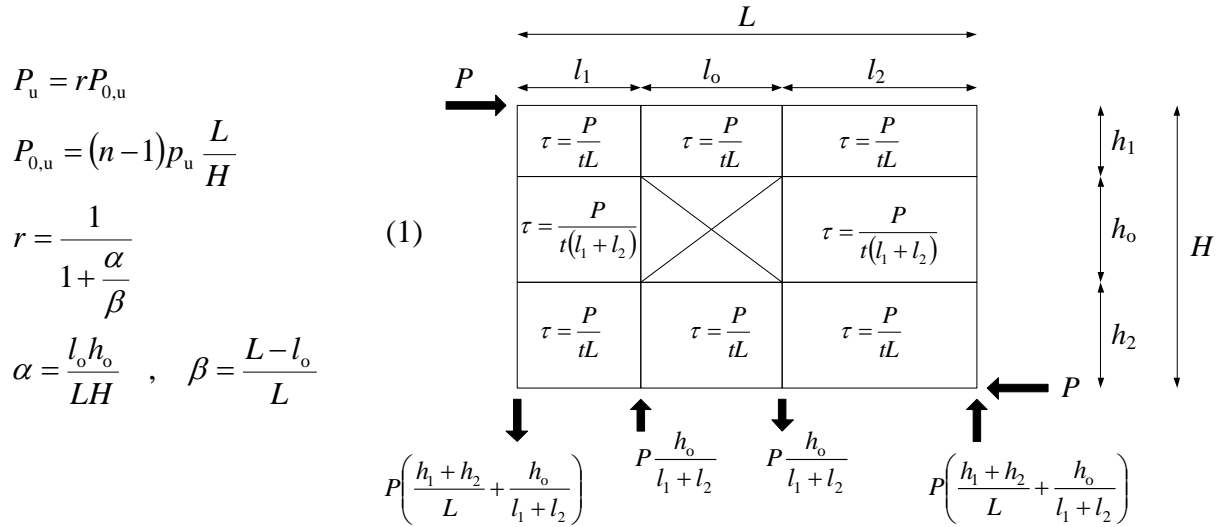


**Fig. 1** Assumed shear stresses and support loads

In Eq. (1) and Fig. 1,  $t$  is the thickness of the panel,  $\tau$  is the shear stress,  $n$  is the number of fasteners along one of the outer vertical perimeters,  $p_u$  is the shear failure load per fastener,  $P_u$  is the ultimate value of the applied load,  $P$  and  $P_{0,u}$  is the ultimate load for a corresponding shear wall without opening. Other geometrical parameters are defined in Fig.1 and Eq. (1).

It is very interesting to notice that Eq. (1) only depends on the size of the opening, i.e.  $l_o$  and  $h_o$ , but not on the location of the opening, i.e.  $l_1, l_2, h_1, h_2$ .

The external load,  $P$ , and the supports constitute a system in equilibrium, and horizontal or vertical cuts anywhere in the shear wall lead to shear stresses in equilibrium with the loads.

Yasumura [1] explains Sugiyama's opening coefficient,  $r$ , in the following way: The total shear force that can be taken by the  $n$  fasteners along the outer vertical perimeter is  $(n-1)p_u$ . (It seems that the outermost two fasteners are assumed to have half the capacity of the inner fasteners). Failure therefore occurs when the maximum support load equals  $(n-1)p_u$ , i.e.  $P_u((h_1+h_2)/L+h_o/(l_1+l_2)) = (n-1)p_u$ , from which  $P_u$  may be calculated and Eq. (1) obtained.

In the framework of limit analysis it may be shown that any system of load and supports that satisfy the equilibrium conditions cannot cause failure if the stress in all points of the considered body is within the yield surface. Such a solution is termed a lower-bound solution since the failure load obtained is lower than or equal to the exact solution.

A special case of a shear wall is considered as shown in Fig. 2. Here all areas are quadratic and of the same size. Three different distributions of the shear stresses and the supports are considered. All systems satisfy the equilibrium conditions and do therefore qualify for lower-bound solutions as long as it has been ensured that the shear stress in no point exceeds the shear strength. The exercise when using the lower-bound technique is to find the system that leads to the maximum possible failure load.

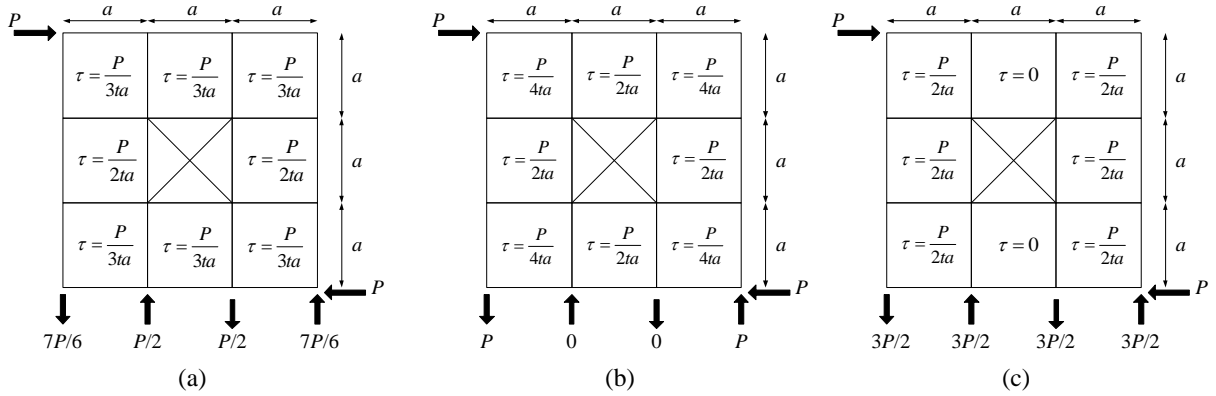


**Fig. 2** Example of three different valid lower-bound solutions

The system shown in Fig. 2 (a) is the one used by Sugiyama [1]. The system shown in Fig. 2 (c) is the segmented shear wall approach. The system shown in Fig. 2 (b) has zero loads at the internal supports, i.e. in effect a partially restrained shear wall.

It is usually not economically feasible to use different fastener spacing in the different areas of the shear wall. Since the lower-bound theorem requires that the stress in no point exceeds the shear strength, the fastener spacing must be derived from the area with highest shear stress if the same fastener spacing is used in all areas of the wall. All three systems shown in Fig. 2 thus lead to the same solution since the maximum shear stress in all cases is  $\tau = P/(2ta)$ . Other valid systems of shear stress distributions and corresponding support loads are possible for a wall as the one shown in Fig. 2, but no system can ever lead to a lower maximum shear stress than  $\tau = P/(2ta)$ . It can therefore be concluded that a proper lower-bound solution for a wall as considered here can never lead to a better solution than the solution given by the simple segmented shear wall approach.

The method used by Yasumura [1] to explain Sugiyama's opening coefficient does not qualify for a lower-bound solution since the shear stress in the area with the highest shear stress exceeds the shear strength. It is further noticed that if the (yield-condition-violating) approach of distributing the maximum vertical support load equally on all the fasteners along a vertical perimeter, as done by Yasumura [1], is applied to the systems shown in Fig. 2, then the system in Fig. 2 (b) leads to a higher failure load than Sugiyama's system, i.e. the shear stress distribution considered by Sugiyama is not the optimum one.

Further, the systems of shear stresses and support loads as considered here and in [1] satisfy the equilibrium equations if making vertical or horizontal cuts through the wall. However, the systems can in general not exist without tension and compression STRINGERS. If the shear stresses in two neighbouring areas are different, then a tensile or compression stringer is needed to ensure equilibrium. The Stringer Method is exactly used for determination of the necessary reinforcement around holes in concrete walls. The problem considered in Fig. 2 can be found treated in [2], where as well practical applications as the theoretical basis for the Stringer Method can be found. Figure 3 shows the tension and compression stringers in a wall as considered in Fig. 2 (b). An exploded view of the wall is used in Fig. 3, but the stringers are of course assumed to be continuous. The magnitudes of the tension and compression forces in the stringers are found by simple equilibrium. Fig. 3 shows that tension stringers are needed at the upper left corner and the lower right corner of the opening. These corners are crucial in the practical design, and the stringer method can quantify the tensile forces.

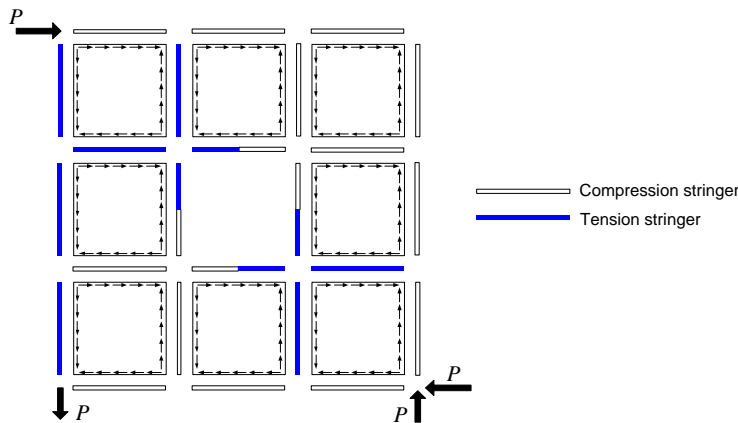


**Fig. 3** Necessary tension and compression stringers in shear wall according to Fig. 2 (b)

## Acknowledgement

The research presented in this paper was funded by the European Union's Structural Funds – The Regional Fund.

## References

1. Yasumura M (2010) Influence of the boundary conditions on the racking strength of shear walls with an opening. In: Proceedings of the International Council for Research and Innovation in Building and Construction, Working Commission W18, Meeting Forty-Three, Nelson, New Zealand, paper 43-15-1.
2. Nielsen MP (2011) Limit Analysis and Concrete Plasticity. CRC Press, Boca Raton. 3<sup>rd</sup> edition.



# A note on surface scanning and stress grading based on fracture mechanics

Hans Petersson

School of Technology, Linnaeus University  
SE-351 95 Växjö, Sweden

## Introduction

In the research on better utilization of wood as a raw material, improved sorting techniques for structural applications are of key importance. The technique to be applied is partly dependent on the wood species used for the wood products. As the northern European sawmill industry mostly is using spruce and pine for their sawn products, these species are of primary importance.

The behaviour of wood depends on a large number of internal properties such as wood density, grain angle distribution, annual ring pattern, compression wood, pith location and occurrence of knots. This means that results from the grading techniques used today, not considering many of these properties, leads to a material characterization that is not optimal for practical use.

The most important parameter for a good prediction of timber strength is the distribution of the grain angle (L-direction) as wood is strongly anisotropic, but also the radial (R-) and tangential (T-) directions need to be well defined. The spatial description of the orientation of the L-R-T-axes is thus a key issue.

The material parameters needed for modelling phenomena as elasticity and fracture are best described with reference to the L-R-T-axes. How these material parameters are varying in wood and around knots is strongly dependent on the tree growth conditions. Also the strong property variation in the radial direction due to varying growth conditions has to be considered. The problem of finding the main material directions and material characterization with respect to the radial direction are treated in [1].

A problem of using fracture mechanics for stress grading has until now been to find out how the slope of grain varies, especially around knots. Another problem has been to define how the longitudinal E-modulus varies over the cross section. This important stiffness parameter is strongly related to the growth conditions and annual ring widths. A model for the cross sectional variation of the E-modulus was presented in [1].

## Scanning

The tool developed for obtaining a continuous description of the grain angle distribution seems to be most valuable in fracture analysis of wood and wooden structures. This means that a good description of knot locations and fibre angle disturbances around the knots is needed. The applied technique will be illustrated by presenting some results from a study of sawn and planed boards. Some illustrating results from the scanning procedure are shown below in Figures 1 and 2.

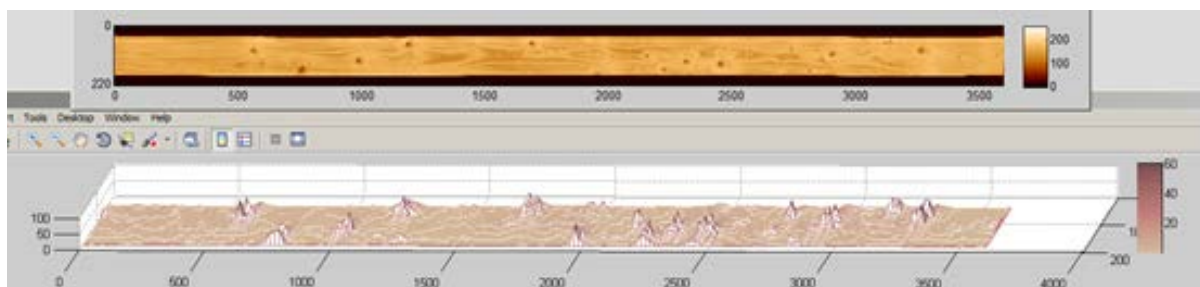


Figure 1: Absolute value of fibre angle obtained from laser scanning of a board face, used for characterising the influence of knots



Figure 2: Fibre angle lines at outer face of a timber board obtained from laser scanning

### Strength prediction based on fracture mechanics

The usefulness of fracture mechanics applying a fracture energy approach in strength analysis of notched timber beams has been shown in a number of papers by Gustafsson and others, the first paper published already in 1988 [2]. Extensive testing was later performed for determination of the most needed material parameters, especially the fracture energy for the case of wood subjected to tension perpendicular to grain, see for example [3] for some early presented results. In [4] a theory based on linear fracture analysis was outlined that could be used both for more general finite element analysis and for deriving simple hand-calculation formulae. A number of load cases were studied where the strength of statically determined and cracked timber beams, loaded by moments, shear forces and normal forces were determined. Such formulae could be of use in timber grading if the cracking paths are known.

In order to introduce a fracture mechanics approach for strength grading of timber results from an experimental test series consisting of 105 boards (45\*145 mm<sup>2</sup>) will be used. These boards were tested in accordance to EN 408 using standard four point bending.

The failure bending moment  $M_c$  is first replaced by a formal failure stress  $f_m = \sigma_c$ , where

$$\sigma_c = 6 M_c / b h^2 \quad (1)$$

For a case where the longitudinal E-modulus is constant the bending stiffness is  $E b h^3 / 12$ . The square of the failure stress can according to fracture mechanics, for a crack propagating lengthwise, be written as

$$(\sigma_c)^2 = 6 b_c G_c E \kappa / (b h) \quad (2)$$

Here  $b_c G_c$  is the fracture energy per unit length with  $b_c$  as the crack width,  $b h$  is the cross sectional area and the parameter  $\kappa$  depends on how the cracking plane splits the cross section into two parts.

The sizes and locations of the most dangerous knots has a strong influence on where the final crack failure will occur and in which subregions the failure criterion according to Eq. (2) has to be applied. The knot location has a strong influence on the parameter  $\kappa$ , which in many cases can be defined as a ratio at the crack tip between the difference in beam compliance after and before cracking and the beam compliance before cracking. The parameter  $\kappa$  depends further on whether the crack path starts from the tension edge of the beam tested or whether the failure crack propagates internally (whether the sectional forces of the split beam parts are statically determined or not).

Equation (2) can be generalised taking an arbitrary variation of the E-modulus over the cross section into account. In the following, however, the approximative value of E determined as the global static edgewise MOE (neglecting shear deformations) will be used. This means that a statistical relation based on Eq. (2) between the energy quantity  $0.5(\sigma_c)^2/E$  and the failure stress can easily be found for the test series studied. The relation is almost linear with a high  $R^2$ -value.

According to Eq. (2) the energy quantity  $(\sigma_c)^2/E$  can be replaced by the fracture variable F,

$$F = 6(b_c G_c / b) \kappa / h \quad (4)$$

This results in the simple expression

$$(\sigma_c)^2 = E F \quad (5)$$

which means that the failure stress  $\sigma_c$  is the square root of the product of E and F.

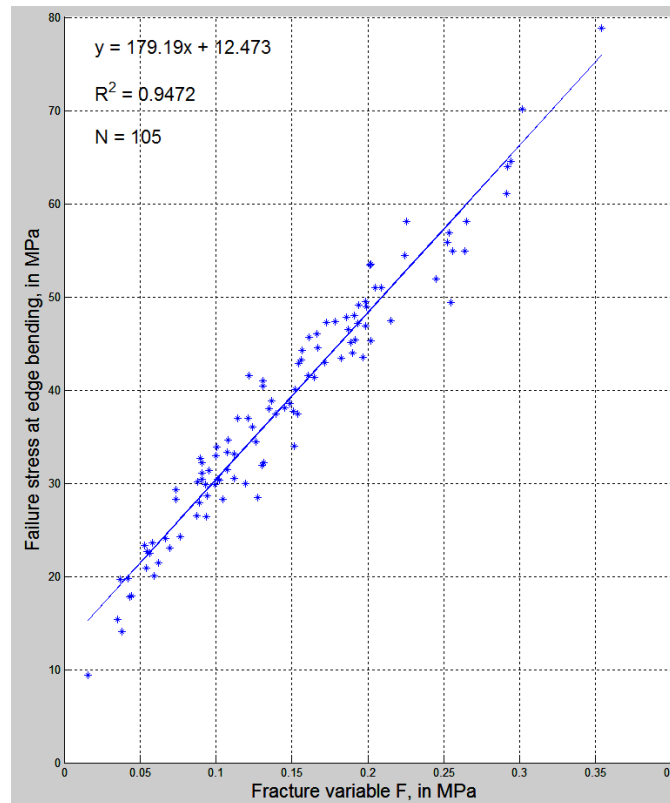


Figure 3 Relation between the failure stress and fracture variable F according to test series of 105 boards. The global static edgewise MOE neglecting shear deformations is used as stiffness variable.

Eq. (4) tells us that besides the E-modulus the fracture energy  $b_c G_c$  per unit length, the beam height  $h$  and the fracture parameter  $\kappa$  are parameters that have to be considered. In Figure 3(b) the failure stress  $\sigma_c$  in the test series studied is expressed as a function of the fracture variable F. The experimentally obtained values of  $\sigma_c$  and E (approximated by the global MOE) give us the needed experimental values of F, where  $F = (\sigma_c)^2/E$ .

Which value to be chosen for  $G_c$  is dependent on the stress state at the crack tip. Usually the value to be chosen is between around  $300 \text{ Nm/m}^2$  for a pure tension (opening) mode and a three to four times larger value for a pure shear mode.

## Concluding remarks

An approach for strength prediction based on fracture mechanics has been suggested in this note. According to the model the square of the failure stress  $\sigma_c$  should be equal to the product of the stiffness here represented by the E-modulus  $E$  and the fracture variable  $F$  according to Eq. (5).

For determining a proper values of  $F$  a simple hand calculation might be sufficient, otherwise a finite element analysis has to be employed. The accuracy of the results that will be obtained will very much depend on how well the fibre angle around knots the can be predicted. The surface scanning approach using both optical and laser techniques is promising but can be further developed by using two fibre angles instead of one for defining the fibre directions.

The experimental test series consisting of 105 boards had quite a normal strength distribution as can be seen from Figure 4 (a) where the failure stress is plotted as a function of the E-modulus determined from the lowest axial eigenmode and the mean density. In Figure 4 (b) the E-modulus is set equal to the global MOE determined from the measured mid-deflection at edgewise bending. The obtained  $R^2$ -value is substantially improved in Figure 4 (b) in comparison with Figure 4(a).

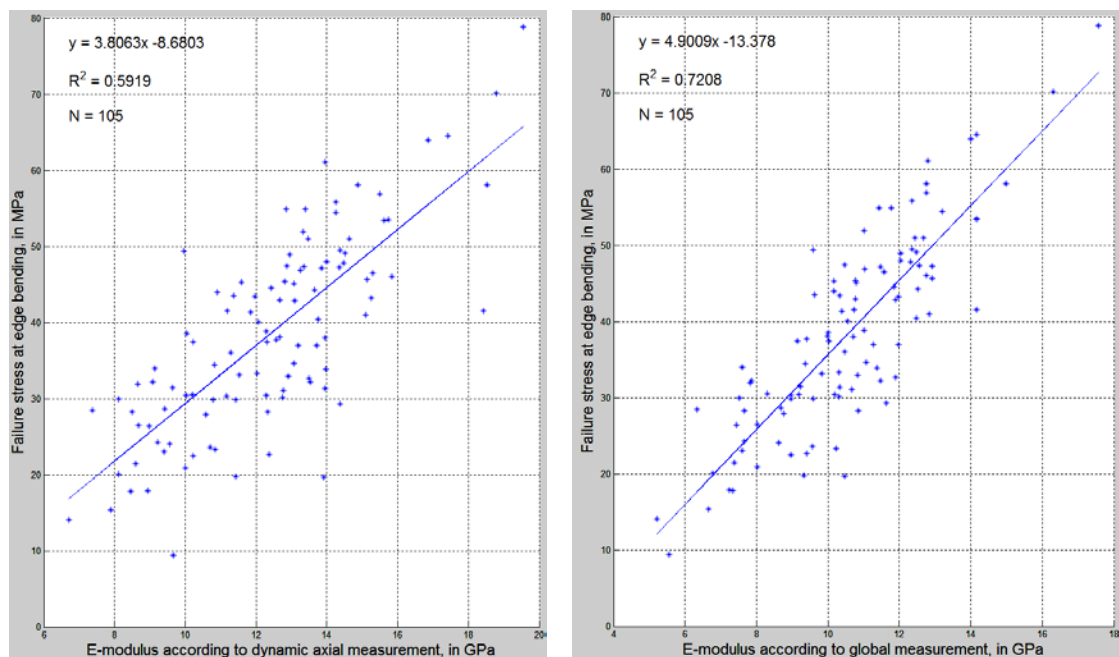


Figure 4 (a) Relation between failure stress and E-modulus determined from axial eigenmode.  
(b) Relation between failure stress and global MOE.

## References

- [1] Petersson H.: Use of optical and laser scanning techniques as tools for obtaining improved FE-input data for strength and shape stability analysis of wood and timber, IV European Conference on Computational Mechanics, Paris, May 2010
- [2] Gustafsson P. G.: A study of strength of notched beams. Paper 21-10-1, CIB-W18A meeting, Vancouver 1988
- [3] Larsen H. J. and Gustafsson P. G.: The fracture energy of wood in tension perpendicular to the grain. Paper 21-10-1, CIB-W18A meeting, Lisbon 1990
- [4] Petersson H.: On design criteria for tension perpendicular to grain. CIB-W18A meeting, Åhus Sweden 1992